2nd International Conference on Multidisciplinary Sciences and Technological Developments (ICMUSTED 2025)

PROCEEDINGS BOOK

December 12-15, 2025

Bayburt, Türkiye

ISBN: 978-625-7960-84-7

2nd International Conference on Multidisciplinary Sciences and Technological Developments (ICMUSTED 2025)

Onsite – Online (Hybrid) Conference

December 12-15, 2025 | Bayburt, Türkiye

Editor-in-Chief

Yunus Kaya

Editors

Erman Kadir Oztekin

Hamdullah Ozturk

Intan Helina Hasan

Nurhafizah Hasim

Selahattin Kosunalp

Umit Yildirim

ISBN: 978-625-7960-84-7

December 2025

Papers reviewed by at least two reviewers presented at the 2nd International Conference on Multidisciplinary Sciences and Technological Developments (ICMUSTED 2025) are included in this proceedings book. The full responsibility for all papers presented at the ICMUSTED 2025 and published in this proceedings book belongs solely with the respective authors of the papers.

ISBN: 978-625-7960-84-7
Publication Date: 19.12.2025

Dear Participants,

We would like to thank all of you for your participation and interest in the 2nd International Conference on Multidisciplinary Sciences and Technological Developments (ICMUSTED 2025), which was held as Onsite/Online (Hybrid) in Bayburt, Türkiye on December 12-15, 2025.

The aim of ICMUSTED 2025 is to provide an international forum for researchers, academics, people in industry, and students to consider the latest research results and to present and discuss their ideas, theories, technologies, systems, tools, applications, work in progress. In this regard, participants will experience all theoretical and practical problems and technological developments that arise in multidisciplinary topics.

Onsite and online presentations were made by invited speakers and other participants within the scope of the ICMUSTED 2025. ICMUSTED 2025, where 195 oral presentations prepared by 475 participants from 25 different countries, took place and opened a direction to new cooperation opportunities.

Therefore, we would like to thank the invited speaker and all other participants, the members of the scientific committee, the session chairs, and all those who contributed to make this conference a great success.

Hope to see you at the next ICMUSTED.

Best Regards,

On behalf of the ICMUSTED 2025 Organizing Committe
Organizing Committee Chairman
Assoc. Prof. Dr. Yunus Kaya

COMMITTEES

Organizing Committee

Conference Chairman

Assoc. Prof. Dr. Yunus Kaya, Bayburt University, Türkiye

Members

Prof. Dr. Jorge Montanari, National University of Hurlingham, Argentina
Assoc. Prof. Dr. Emre Tekce, Bayburt University, Türkiye
Assoc. Prof. Dr. Mehmet Uyar, Bayburt University, Türkiye
Assoc. Prof. Dr. Mustafa Ozdemir, Bayburt University, Türkiye
Assoc. Prof. Dr. Selahattin Kosunalp, Bandirma Onyedi Eylul University, Türkiye
Assoc. Prof. Dr. Umit Yildirim, Bayburt University, Türkiye
Asst. Prof. Dr. Erman Kadir Oztekin, Bayburt University, Türkiye
Asst. Prof. Dr. Hamdullah Ozturk, Gaziantep Islam Science and Technology University, Türkiye
Dr. Intan Helina Hasan, Universiti Putra Malaysia, Malaysia
Dr. Nurhafizah Hasim, Universiti Teknologi Malaysia, Malaysia

Secretary

Asst. Prof. Dr. Meltem Kizilca Coruh, Ataturk University, Türkiye
Asst. Prof. Dr. Sebahat Oztekin, Ataturk University, Türkiye

Scientific Committee

Prof. Dr. Ahmet Cansiz, Istanbul Technical University, Türkiye
Prof. Dr. Alyani Ismail, Universiti Putra Malaysia, Malaysia
Prof. Dr. Grigor Yordanov Mihaylov, University of Telecommunications and Post, Bulgaria
Prof. Dr. Halim Kovaci, Ataturk University, Türkiye
Prof. Dr. Jorge Montanari, National University of Hurlingham, Argentina
Prof. Dr. Mehmet Ertugrul, Karadeniz Technical University, Türkiye
Prof. Dr. Mohd Nizar Hamidon, Universiti Putra Malaysia, Malaysia
Prof. Dr. Teodor Iliev, University of Ruse “Angel Kanchev”, Bulgaria
Prof. Dr. Ugur Cem Hasar, Gaziantep University, Türkiye
Prof. Dr. Zehra Can, Bayburt University, Türkiye
Assoc. Prof. Dr. Adem Korkmaz, Bandirma Onyedi Eylul University, Türkiye
Assoc. Prof. Dr. Bora Goktas, Bayburt University, Türkiye
Assoc. Prof. Dr. Emre Tekce, Bayburt University, Türkiye
Assoc. Prof. Dr. Fatih Yilmaz, Bayburt University, Türkiye
Assoc. Prof. Dr. Gokhan Komur, Bayburt University, Türkiye
Assoc. Prof. Dr. Gokhan Ozturk, Ataturk University, Türkiye
Assoc. Prof. Dr. Kubilay Demir, AISOFT Software Corporation, Türkiye
Assoc. Prof. Dr. Mehmet Uyar, Bayburt University, Türkiye
Assoc. Prof. Dr. Mustafa Ozdemir, Bayburt University, Türkiye
Assoc. Prof. Dr. Mustafa Tolga Yurtcan, Ataturk University, Türkiye
Assoc. Prof. Dr. Ruhsen Aldemir Engin, Kafkas University, Türkiye
Assoc. Prof. Dr. Samsuri Abdullah, Universiti Malaysia Terengganu, Malaysia
Assoc. Prof. Dr. Selahattin Kosunalp, Bandirma Onyedi Eylul University, Türkiye
Assoc. Prof. Dr. Umit Yildirim, Bayburt University, Türkiye

Assoc. Prof. Dr. Yunus Kaya, Bayburt University, Türkiye
Assoc. Prof. Dr. Yusuf Esmer, Bayburt University, Türkiye
Asst. Prof. Dr. Duygu Tekin, Bayburt University, Türkiye
Asst. Prof. Dr. Erdal Igman, Bayburt University, Türkiye
Asst. Prof. Dr. Erman Kadir Oztekin, Bayburt University, Türkiye
Asst. Prof. Dr. Hamdullah Ozturk, Gaziantep Islam Science and Technology University, Türkiye
Asst. Prof. Dr. Ibrahim Cengiz, Ataturk University, Türkiye
Asst. Prof. Dr. Latif Akcay, Erzurum Technical University, Türkiye
Asst. Prof. Dr. Meltem Kizilca Coruh, Ataturk University, Türkiye
Asst. Prof. Dr. Mustafa Alptekin Engin, Bayburt University, Türkiye
Asst. Prof. Dr. Ramazan Simsek, Bayburt University, Türkiye
Asst. Prof. Dr. Sebahat Oztekin, Ataturk University, Türkiye
Asst. Prof. Dr. Zeynep Ozturk, Erzurum Technical University, Türkiye
Dr. Hafize Hasar, Gaziantep Directorate of Provincial Agriculture and Forestry, Türkiye
Dr. Intan Helina Hasan, Universiti Putra Malaysia, Malaysia
Dr. Lawal Mohammed Bello, Bayero University Kano, Nigeria
Dr. Norhazren Izatie Mohd, Universiti Teknologi Malaysia, Malaysia
Dr. Nurhafizah Hasim, Universiti Teknologi Malaysia, Malaysia

TOPICS

Agriculture, Forestry, and Aquaculture
Architecture, Planning, and Design
Education Sciences
Engineering
Fine Arts
Health Sciences
Law
Philology (Language and Literature)
Research & Development and Technological Developments
Science and Mathematics
Social, Humanities, and Administrative Sciences
Sport Sciences
Theology

INVITED SPEAKER

Assoc. Prof. Dr. Samsuri Abdullah
Universiti Malaysia Terengganu (Terengganu, Malaysia)

Samsuri Abdullah is an Associate Professor at Universiti Malaysia Terengganu (UMT), Malaysia. He has been teaching environmental technology since 2018 and was promoted to Associate Professor in 2022. He obtained his Bachelor of Technology (Environment) with First Class Honours in 2014 and completed a fast-track PhD in Environmental Technology and Management in 2017, specializing in air quality. His research focuses on ambient and indoor air quality, as well as noise pollution. Samsuri has published 162 works, including journal articles, book chapters, conference papers, and a technical report. He has led or co-led 20 research projects with total funding of approximately MYR 1.4 million and has conducted data analysis workshops for applied sciences. He is also involved in consultancy projects with Tenaga Nasional Berhad Research and Enviro Excel Tech Sdn. Bhd. At UMT, he contributes to sustainability initiatives related to the Times Higher Education (THE) Impact Rankings and the UI GreenMetric World University Rankings. Currently, he serves as the Coordinator for the Undergraduate Final Year Project Dissertation, overseeing academic quality and research supervision at the faculty level.

ICMUSTED 2025 PROGRAM

Friday, December 12, 2025

Conference Opening

Conference Hall (Bayburt Teacher's House, Bayburt)

09:30 – 10:00	Registration and Tea/Coffee Service	
10:00 – 10:45	Opening Ceremony	Asst. Prof. Dr. Erman Kadir Oztekin – On Behalf of the Organizing Committee
	Opening Session	Air Quality and Sustainable Development: The Role of Machine Learning in Shaping Future Cities Invited Speaker – Assoc. Prof. Dr. Samsuri Abdullah

Onsite Session

Conference Hall (Bayburt Teacher's House, Bayburt)

Onsite Session – 1 (in Turkish) Head of Session: Asst. Prof. Dr. Erman Kadir Oztekin	
10:45 – 12:00	A Modified Two-Sided Approximation Method for a Special Boundary Value Problem with Delayed Arguments *Arzu Aykut*[*]*, Fulya Koc Simsek*
	AI-Based Intelligent Document Classification in the Logistics Sector *Selcuk Zereyalp*[*]*, Kemal Sogukcesme, Bahadir Fatih Yildirim*
	History of Mobile Communication from 1G to 6G *Hanifi Turgut, Tevhit Karacali, Tarik Bugra Ala*[*]
	Design and Analysis of Metamaterial Absorber for Microwave X-Band Applications *Yunus Kaya*[*]*, Mehmet Ertugrul*
	Multi-Band and Inexpensive Linear and Circular Polarization Converter Using a Single-Layer Reflective Metasurface *Yunus Kaya*[*]*, Ugur Cem Hasar*
12:00 – 13:15	Lunch (Bayburt Teacher's House)

Online Sessions

Virtual Hall

Online Session – 1 (in Turkish) Head of Session: Asst. Prof. Dr. Duygu Tekin	
13:15 – 14:45	Design, Prototype Production, and Testing of a 12(16) MVA 115/6.3 kV Power Transformer with Twin-Wire Transposed High-Voltage Winding for Loss Reduction *Zuhal Isikli*[*]

	Design, Manufacturing, and Testing of a 60 Hz Frequency Distrubition Transformer *Nadya Atakan*[*]
	Forecasting Daily Mean Temperature in Izmir Using Machine Learning Algorithms *Pelin Coskun*[*], *Onur Ugurlu, Orhan Er*
	Performance Evaluation of a Luenberger Observer for Sensorless FOC of BLDC Motor *Beytullah Gokoglan*[*], *Mustafa Tumbek*
	Electric Vehicle Charging Scheduling: Time Shift *Cengizhan Abay*[*], *Hanife Apaydin Ozkan*
	Design, Prototype Production, and Testing of a Low-Impedance High Short-Circuit Current 18 MVA 33/33 kV Power Transformer *Bugra Akpinar*[*]
	Fire Safety in Electric Vehicles: An Assessment of Battery Risks, Intervention Techniques, and Policy Recommendations *Mehmet Akif Er, Omer Kaya*[*]
14:45 – 15:00	Break
Online Session – 2 (in Turkish) Head of Session: Asst. Prof. Dr. Duygu Tekin	
15:00 – 16:30	Use of Aggregates Produced from Waste Concrete Samples of Different Strength Classes in Concrete *Melek Demirtas, Omer Ozmen, Rahman Cankaya, Omer Can*[*]
	Numerical Modelling of Moisture Loss and Oil Uptake in Noodle Strips During Deep-Fat Frying Using Finite Difference and Finite Element Methods *Serpil Pekdogan Goztok*[*], *Cihat Guner, Hakan Basdogan, Omer Said Toker*
	Investigation of the Usability of Bayburt Yellow Tuff in Structural Lightweight Concrete Production *Omer Bayrak*[*], *Emin Erdem*
	Use of Bayburt White Tuff as Cement Substitute Material *Omer Bayrak*[*], *Emin Erdem*
	Investigation of Parameters Affecting Pedestrian Crossing Speeds: Empirical Findings from Türkiye *Mehmet Burhan Sume*[*], *Erdem Dogan*
	Performance Properties of Lightweight Aggregate Hybrid Foam Concretes *Selcuk Memis*[*]
	The Role of Biodiesel Addition in Reducing Vapor Pressure in Gasoline–Methanol–Ethanol Ternary Blends

	Abdulvahap Cakmak[*]
	Shunt Reactor (without Tap Changer) Design, Manufacturing, and Testing *Ali Tas*[*]
16:30 – 16:45	Break
Online Session – 3 (in Turkish) Head of Session: Asst. Prof. Dr. Ramazan Simsek	
16:45 – 18:15	Use of Bayburt Green-Spotted White Tuff in the Production of Structural Lightweight Concrete *Omer Bayrak*[*], *Emin Erdem*
	Investigation of the Suitability of Waste Concrete Paving Blocks as Aggregate in Concrete *Melisa Kayrak, Arda Sahin, N. Sebnem Karahan, Omer Can*[*]
	Spintronics: The Future of Electronics – A Comprehensive Overview of Dilute Magnetic Semiconductors *Muhammet Arucu*[*]
	Investigation of Photon and Neutron Interaction Probabilities of Some Selected High Entropy Alloys *Bunyamin Alim*[*], *Erdem Sakar*
	Structural and Gamma-Ray Absorption Properties of Newly Developed Ni_3Al Based Superalloys *Merve Durdag, Bunyamin Alim, Erdem Sakar*[*]
	Convergence Analysis for Parallel Iteration Methods *Yasin Berkay Can*[*], *Nazli Kadioglu Karaca, Isa Yildirim*
	On Nearness Ideals of Nearness Semigroups *Mehmet Ali Ozturk, Ozlem Tekin*[*]
18:15 – 18:30	Break
Online Session – 4 (in Turkish) Head of Session: Assoc. Prof. Dr. Mehmet Uyar	
18:30 – 20:00	Investigation of Temperature Changes During the Composting of Pomegranate Processing Solid Wastes with the Addition of Bioactivator *Kemal Suluk, Fevzi Sevik*[*], *Barbaros S. Kumbul, Kamil Ekinci*
	Effect of Different Reactor Sizes on Mass and Volume Changes in the Composting Process *Fevzi Sevik*[*], *Kemal Suluk, Barbaros S. Kumbul, Kamil Ekinci*
	Fungal Intoxications *Nesrin Cakici*[*], *Meltem Asik*
	The Trifid Incisive (Nasopalatine) Canal: A Rare Variation of the Maxilla

	Burhan Yarar[*], *Melike Tasci*
	FELVERA: Development of an Web and Mobile Application for Animal Welfare *Numan Tugrul Ertugrul, Irem Baysal*[*], *Semanur Cicek, Vildan Sozen, Zuhal Aslan Akyol*
	Smart Platform for Book Swapping, Sales, and Social Interaction *Numan Tugrul Ertugrul, Samet Sargin*[*], *Mehmet Yasa, Umut Temel, Zuhal Aslan Akyol*
	Library Automation System with Automatic Penalty and Email Notification Module *Zuhal Aslan Akyol, Numan Tugrul Ertugrul, Osman Mert Ergin*[*]
	AI-Based Risk Prediction Model for Airport Ground Operations *Onur Arslan*[*]
20:00 – 20:15	Break
Online Session – 5 (in Turkish) Head of Session: Assoc. Prof. Dr. Mehmet Uyar	
20:15 – 21:45	Solo Travel Research: A Bibliometric Analysis *Yeliz Guler*[*]
	Determining Green Transformation Strategies in Businesses Using the SWARA Method *Sadrettin Codur, Ahmet Cem Esenlikci*[*]
	Psychological Factors Influencing University Students' Trust in AI-Based Learning Assistants *Ezgi Dagtekin, Ercan Erkalkan*[*]
	A Multi-Objective Optimization Approach for Airport Ground Handling and Resource Management Operations *Seckin Unver*[*], *Merve Gozde Sayin*
	Digitalization in Literature, Ergodic Literature, and Hypertexts: An Example from German *Harun Gocerler*[*]
	Andrzej Wajda: A Political Critique of Danton (1983) *Ismail Tasar*[*]
	Designing Adaptive Conceptual Stories via Artificial Intelligence for Science and Mathematics Learning *Ilhan Polat*[*]
	Evaluating the Basic Life Skills Activity Book: Alignment with Life Skills Course Outcomes and the 21st Century Skills Framework *Ilhan Polat*[*], *Mehmet Akif Ersoz*

Saturday, December 13, 2025

Online Sessions

Virtual Hall

Online Session – 6 (in English) Head of Session: Dr. Nurhafizah Hasim	
09:00 – 10:30	EfficientNet with Data Augmentation for Potato Disease Detection and Sustainable Agriculture *Mansouria Sekkal*[*]*, Badir Benkrelifa Lahouaria*
	AI-Powered MRI Analysis for Early and Accurate Medical Diagnosis *Mansouria Sekkal*[*]*, Badir Benkrelifa Lahouaria*
	Alginate/Chitosan-Based Nanostructures as Sustainable Nanopriming Agents for Wheat Seeds *Arruje Hameed*[*]*, Muhammad Mujahid, Tahir Farooq, Amjad Hameed*
	A Natural Ally Against Pine Aphids: *Pauesia Silana* as a Key Biocontrol Agent of *Cinara Maghrebica* *Leila Bourouba*[*]
	Antagonistic Yeasts as Biocontrol Agents Against Phytopathogenic Fungi *Kheira Hiba Benghaffor*[*]*, Hadri Zouheyr*
	Morphological and Cultural Characterization of *Verticillium Dahliae Kleb.*, the Causal Agent of Verticillium Wilt in Olive (*Olea Europaea L.*) *Saliha Ogab*[*]*, Houria Chaalal, Tahar Maza, Fatima Zohra Zoudji*
	Role of Edible Coating on Post-Harvest Management of Fruits and Vegetables *Tusneem Kausar*[*]*, Ashiq Hussain*
10:30 – 10:45	Break
Online Session – 7 (in English) Head of Session: Dr. Nurhafizah Hasim	
10:45 – 12:15	Comparison the Values of Reverse Harmonic Index of Two Types Hexagonal Cactus Chain Graphs *Mukaddes Okten Turaci*[*]
	Chitosan-Modified Silver-Doped Phosphate Glass: Physical, Structural, and Mechanical Improvements *Siti Norfariza Farhana Binti Mohd Razak, Nurhafizah Binti Hasim*[*]*, Nur Hidayah Binti Ahmad, Norshahirah Binti Mohamad Saidi, Mohd Fuad Bin Mohamad*
	Methylammonium Iodide Doped CMC Electrolyte: A Safer and Environmentally Friendly Solution for Sustainable Power Storage *Na'imah Husna Nasaruddin, Nur Hidayah Ahmad*[*]
	A Green Laser Ablation Approach to Ag/*Cinnamon Cassia* Nanohybrid for Sensitive Colorimetric Glucose Sensing Applications *Fitriyatun Naldiyah, Wulandari Dwi Lestari, Adeka Delvis Tama, Muhammad*

	Dimas Adytia Airlangga, Nurul Hidayat[*]
	Composition-Dependent Thermal, Mechanical, and Electrical Responses of CMC–CA–Glycerol Biopolymeric Films *Noorul Ain Binti Kamal Ariffin, Nurhafizah Binti Hasim*[*]
	High-Sensitivity Atrazine Sensor Using Aluminum Plasmonics and Molecular Imprinting *Mohamed Esseddik Ouardi*[*]*, Kada Abdelhafid Meradi, Fatima Tayeboun*
	Tailoring the Structural, Electrical, and Magnetic Properties of $Ni_{0.35}Zn_{0.25}Cd_{0.4}Fe_{1.97}Ce_{0.03}O_4$/GNPs Composites *Muhammad Ajaz Un Nabi*[*]
12:15 – 12:30	Break
Online Session – 8 (in English) Head of Session: Dr. Nurhafizah Hasim	
12:30 – 14:00	Cadmium Sulfide Thin Film-based Photodetector: Fabrication and Photoresponse Evaluation *Erman Erdogan*[*]
	Experimental Evidence of Thermally Activated Transport at the Mobility Edge in 4H Silicon Carbide Metal-Oxide-Semiconductor Field Effect Transistor *Sabrina Meguellati*[*]*, Mustapha Sarra*
	Normalized Differential Conduction Analysis of Temperature-Dependent Gate Conduction in 4H-SiC MOS Capacitor *Sabrina Meguellati*[*]*, Mustapha Sarra*
	Tailoring Phosphate Glass Performance: Structural, Mechanical, and Optical Enhancement via Chitosan Doping *Nurhafizah Hasim*[*]
	Effect of Incorporating Graphene Oxide Nanoparticles on Ion Mobility in Deep Eutectic Polymer Electrolyte *Siti Norfazleen Farhana Binti Mohd Razak, Norshahirah Binti Mohamad Saidi*[*]
	Composability of Nanofillers Carboxymethyl Cellulose Doped Ammonium Thiocyanate for Bioplastic Packaging *Hazwani Nadirah Zamri, Nur Hidayah Ahmad*[*]
	Study of the Dynamic of Benthic Diatom Communities in Response to Water Fluctuations Along Specific Rivers in Skikda Province, North East Algeria *Hadjer Kaddeche*[*]
14:00 – 14:15	Break
Online Session – 9 (in English) Head of Session: Dr. Nurhafizah Hasim	
14:15 – 15:45	Discharge Prediction Using Artificial Neural Networks: A Case Study for the

	Enoree River, South Carolina, USA *Betul Mete*, *Sinan Nacar, Adem Bayram*
	Stream Water Quality Assessment in a Dammed Watershed: A Case Study from North East Türkiye *Adem Bayram, Betul Mete**
	Influence of Single-Layer Tile Waste Sand on Concrete Properties *Yasmine Mohamed Bouteben*, *Leila Kherraf*
	Optimization of Unconfined Compressive Strength in Stabilized Soils Using Taguchi L9 Design *Fadila Benayoun*, *Moufida Moussaoui, Souhila Rehab Bekkouche*
	Enhancing Facility Layout Design: An Integrated AHP–NLP Approach *Muhammad Waqas Aslam, Zeqiang Zhang**
	Study of Earthquake Ground Motion Duration Recorded in Soft Soils *Issam Aouari*, *Aicha Rouabeh, Benahmed Baizid, Rachid Bakhti*
	Approaches to Enhancing Energy Efficiency Through Building Envelope Insulation in Algeria *Sadia Laidi*, *Sidi Mohamed Karim El Hassar, Achour Mahrane, Rabah Sellami, Ilyas Khelifa Kerfah*
15:45 – 16:00	Break
Online Session – 10 (in English) Head of Session: Dr. Nurhafizah Hasim	
16:00 – 17:30	Utilising Graph Neural Networks for Research Paper Category Prediction and Similarity Search *Bengisu Sahin*, *Sedanur Ozer, Emrah Inan*
	Leveraging Large Language Models for Event Detection in Water Resources Literature *Bengisu Sahin*, *Ozge Yaren Turkseven, Emrah Inan*
	Degradation Behavior of PET Polymers: Mechanical and FTIR Insights *Ivana Salopek Čubrić*, *Goran Čubrić*
	Structural Performance of Hybrid Composite Patch Repairs in Double Lap Configurations with Unidirectional and Woven Fiber Reinforcements *Faycal Mili*, *Walid Halloufi, Sarah Guenifa*
	Solar-Powered Pneumatic Water Pump: A Sustainable Solution for Water Supply in Off-Grid Areas *Shoukat Mugheri*, *Touqeer Aslam, Mazhar Ali, Muhammad Kaleem, Umair Mehmood, Ayaz Ali, Ammar Asghar*
	Optimizing the Effect of Cow Dung on Swelling Soil *Marwa Feligha*, *Souhila Rehab Bekkouche, Fadila Benayoun, Fatima Zohra*

	Benamara
	Structural Properties of Ni-Doped ZnO Thin Films Investigated by XRD, AFM, and Profilometry *Maya Hanane Rezoug*[*], *Chewki Zegadi, Abdelkader Nouri, Nasr-Eddine Hamdadou, M'hamed Guezzoul*
17:30 – 17:45	Break
Online Session – 11 (in English) Head of Session: Dr. Nurhafizah Hasim	
17:45 – 19:15	Immobilized Microalgae for Sustainable Soilless Agriculture in the Green Transition *Burcu Simsek Uygun, Gizem Demirel*[*]
	Implementation of Open Science Framework for Materials Engineering *Elisabeth Viviana Lucero Baldevenites*[*], *Jose Rogelio Fung Corro, Yorlenis Martínez*
	Separation of Toluene – Cyclohexane Mixture Using Intensified Extraction Process by Imidazolium-Based Ionic Liquids *Mohammed Djamel Eddine Allali*[*], *Hassiba Benyounes, Nesrine Amiri*
	Study of the Effectiveness of Steel Shavings as a Foaming Agent for the Production of Foams Glass *Fayrouz Benhaoua*[*], *Djalila Aoufi, Nacira Stiti, Mehdia Toubane, Djedjiga Bousalah*
	Electromagnetic Frequency and Time Reaction in Electromechanical Systems Under Low Energy Mechanical Faults *Azeddine Ratni*[*], *Ali Damou, Djamel Benazzouz, Mohamed Tsebia*
	Microstructural and Electrochemical Assessment of Co–Cr Dental Alloys in Ringer Solution *Alberto Daniel Rico-Cano, Adriana Saceleanu, Anca Fratila, Julia Claudia Mirza-Rosca*[*]
	Electrospinning of Polyacrylonitrile-Nanocellulose Composites Reinforced with Carbon Materials for Advanced Fiber Performance *Mohd Ali Mat Nong*[*], *Juraina Md Yusof, Suzila Sabil, Mohd Hafizuddin Ab Ghani, Che Azurahanim Che Abdullah*
19:15 – 19:30	Break
Online Session – 12 (in English) Head of Session: Asst. Prof. Dr. Latif Akcay	
19:30 – 21:00	Hybrid Voltage Regulation Strategy Combining AVR and Microgrid Coordination for Enhanced Power System Stability *Fazia Ahcene*[*], *Hamid Bentarzi, Mohammed Tsebia, Djamila Talah*

	Next-Generation Deep Learning Architectures for Satellite Image Classification: Integrating Capsule Networks with CNNs and Transformers *Boucif Beddad*[*]*, Samiha Mezrar, Postaire Jack-Gerard*
	Harvesting Waste Kinetic Energy from Vehicle Suspensions for Enhanced Mileage and Power Generation *Touqeer Aslam*[*]*, Shoukat Ali Mugheri, Ali Azam, Manthar Ali, Abbas Raza*
	Development of an Algorithm for Determining the Characteristics of the Ejection System *Oleksandr Panevnyk*[*]
	Virtual Students in Programming Fundamentals: Comparing Large Language Models with Vocational Computer Programming Students in Classical Exams *Selma Bulut, Adem Korkmaz*[*]
	AI-Based Anomaly Detection in Agricultural Farms Using Drone Data and Deep Learning *Berrimi Fella*[*]
	Bone Fracture Classification Analysis Base Machine Learning Algorithms *Ei Phyu Sin Win*[*]
	Large Language Model–Assisted Hardware Design: Insights from the Ascon-128 Implementation *Latif Akcay*[*]

Sunday, December 14, 2025

Online Sessions

Virtual Hall

Online Session – 13 (in English) Head of Session: Dr. Nurhafizah Hasim	
09:00 – 10:30	Indoor Particulate Matter Levels in the Department of Environmental Engineering at Eskisehir Technical University, Türkiye *Melike Cengel, Ozlem Ozden Uzmez*[*]
	Seismic Earth Pressures on Retaining Walls: A Comprehensive Review of Analytical, Numerical, and Experimental Approaches *Ayman Gharbi*[*]*, Fadoua Elkhannoussi, Bouraida Elyamouni, Abdellatif Khamlichi*
	Numerical Evaluation of Seismic Performance in Earth Dams: The Case of Fontaine Gazelles Dam, Biskra, Algeria *Alaoua Bouaicha*[*]*, Aissam Gaagai, Mosbah Ben Said, Ali Hachemi*
	Influence of Carbonation on Reinforced Concrete Structures in Southern Algeria *Ben Ammar Ben Khadda*[*]

	Numerical Study to the Enhancement of Pressure Distribution within the Alveolus of an Aerostaic Bearing *Faiza Ghezali*[*]
	A Comparative Finite Element Analysis of Static Coil Geometries for Electromagnetic Eddy Current Separation *Amir Merahi*[*], *Kaouther Boutarfa, Adel Benabboun, Meriem Boumehed*
	Contribution to the Recovery of Paint Sludge in Wastewater Treatment *Aicha Metali*[*], *Mounir Ziati, Ikram Rebiai, Khedidja Bachi*
10:30 – 10:45	Break
Online Session – 14 (in English) Head of Session: Dr. Nurhafizah Hasim	
10:45 – 12:15	Microservice Transformation for Infrastructure Modernization of Payment and Electronic Money Institutions *Ahmet Ulker, Cansu Barisici, Eren Capraz, Ilker Ogutcu, Mehmet Bulent Muslu, Zafer Golgeli, Ceren Ulus, M. Fatih Akay*[*]
	Experimental Investigation of Concrete by Using Marble Waste as Replacement of Fine Aggregate *Hassaan Amjad*[*], *Faisal Ahmed, Allah Noor*
	Investigating the Properties Ultra High-Performance Concrete Using Silica Fume and Ground Granulated Blast Furnace Slag *Hassaan Amjad*[*], *Waseem Asghar, Dawood Jan*
	Production of Bioethanol Using Lower-Quality Algerian Sugar Dates Box-Behnken *Kaouther Zeghida*[*], *Sarra Guilane, Leila Benmansour*
	Artificial Intelligence Control of Active and Reactive Power for a Three-Level NPC Inverter Connected to Grid Utility *Ghrissi Tahri*[*], *Fatima Tahri, Ali Tahri*
	Mechanical Properties of Concrete Reinforced with Steel Fiber *Noshad Ali*[*], *Waqar Ali, Muhammad Hessib*
	Influx of Different Growth Geometries on Titanium Thin Film for Medical Applications *Matteo Bertapelle, Joel Borges, Julia Claudia Mirza Rosca, Filipe Vaz*[*]
12:15 – 12:30	Break
Online Session – 15 (in English) Head of Session: Dr. Nurhafizah Hasim	
12:30 – 14:00	Universal Design of Apparel Labels for People with Visual Impairment *Ilkay Ozsev Yuksek*[*], *Busra Ozdemir, Izel Kabaagac, Pelin Altay, Sukriye Yuksel Filiz, Nevin Cigdem Gursoy*

	Systematic Study of Design and Operating Parameters in Forced Circulation Solar Water Heaters *Ahmed Remlaoui*[*], *Driss Nehari*
	Comparative Study of the Corrosion Resistance of Magnesium and Zinc in Simulated Body Fluid *Cristina Jimenez-Marcos, Francisco Miguel Sanchez-Sosa, Julia Claudia Mirza-Rosca, Ionelia Voiculescu*[*], *Victor Geanta*
	Numerical Investigation of the Behavior of Strip Footings under Eccentric Loading in Non-Homogeneous Clay Soils *Nassima Zatar*[*], *Alaoua Bouaicha*
	Oxidation Behaviors of Nickel-Based Superalloys at 1050 °C *Saida Bouyegh*[*], *Samira Tlili*
	Recent Progress on Nanomaterial Application for Improving Water-Based Drilling Fluid *Siti Zulaika Razali*[*], *Norizah Abdul Rahman, Mohd Hafizuddin Ab Ghani, Siti Hajar Othman, Tan Sin Tee, Robiah Yunus, Umer Rashid*
	Valorization of Coal Bottom Ash in Sustainable Lightweight Self-Compacting Concrete *Ibtissam Boulahya*[*], *Abedlkadir Makkani*
14:00 – 14:15	Break
Online Session – 16 (in English) Head of Session: Asst. Prof. Dr. Sebahat Oztekin	
14:15 – 15:45	Teaching Strategies, Methods, and Techniques Used by Science Teachers *Ulas Kubat*[*]
	The Impact of Out-Door Learning Environments on the Attainment of Objectives in the Teaching-Learning Process *Ulas Kubat*[*], *Matthew Price*
	Use of Artificial Intelligence by Nursing Students: What Impact on Research Integrity? *Imane Bettane*[*], *Mohammed-Yassine Takzima, Amine Mohamed, Asma Sbai, Latifa Adarmouch*
	Valorization of Waste Rosehip Seeds – A Green and Novel Procedure *Abdulkadir Keskin, Betul Akhoroz, Gulin Amasya, Zerrin Sezgin Bayindir, Zekiye Goksel, Seda Kayahan, Yasin Ozdemir, Serpil Takac, Ayse Ezgi Unlu*[*]
	Exploring the Determinants of Green Innovation Adoption Among SMEs in Albania *Anxhela Bakiasi*[*], *Oljam Dervishi, Merzai Bakiasi*
	A Comparative Analysis of Drought Indices Using Remote Sensing and

	Geospatial Data Processing *Amar Benlakhdar*, *Abdelmoutia Telli, Nourelhouda Dekhili*
	Environmentally Friendly Synthesis, Structural Characterization, Computational Analysis, and Biological Assessment of Benzodiazepine Derivatives *Samir Hmaimou*, *Marouane Ait Lahcen, Wiam Lahrich, Mohamed Adardour, Mohamed Maatallah, Abdesselam Baouid*
15:45 – 16:00	Break
Online Session – 17 (in English) Head of Session: Asst. Prof. Dr. Sebahat Oztekin	
16:00 – 17:30	Enhancing Diesel Desulfurization via Oxidation over Modified USY Zeolite Catalyst *Louiza Aichaoui*, *Soraya Aidene, Boudjema Hamada*
	Volatile Composition and Antioxidant activity of Blue Safflower Oil *Yasmine Ouali*, *Nacera Dahmani-Hamzaoui, Zahia Ghouila*
	Formulation and Characterization of an Ointment Based on Hot Pepper Vegetable Oil *Saida Touzouirt*, *Selma Kadja, Sylia Badja*
	Nanoencapsulation of Eucalyptus Oil for *Aedes Aegypti* Repellents *Laura Astorga*, *Gisela Romero, Marina Turrado, Emiliano Nicodemo, Jorge Montanari*
	Antimicrobial Evaluation and Phytochemical Analysis of *Asphodelus Microcarpus* Extract *Azziza Chabane Chaouch*, *Farid Benkaci-Ali, Samira Tata*
	Coagulation-Flocculation of Humic Substances: Effectiveness of Aluminum Sulfate and the Role of Sulfate and Phosphate Salts *Lynda Hecini*, *Fedia Bekiri, Naima Bacha, Wahida Kherifi*
	Citric Acid-Crosslinked CMC Bioplastics: Tuning Flexibility, Strength, and Biodegradation for Sustainable Food Packaging *Nur Alya Maisarah Binti Mohamad, Nurhafizah Binti Hasim*
17:30 – 17:45	Break
Online Session – 18 (in English) Head of Session: Dr. Nurhafizah Hasim	
17:45 – 19:15	On the Thermodynamic Stability of Some Metal Complexes within the Framework of a Density Functional Theory Approach Investigation *Boulanouar Messaoudi*, *Baian Alkassas*
	Inverse Partial Least Squares Regression for the Prediction and Optimization of Carboxyl Group Content in Graphene Oxide *Soraya Aidene*, *Abdelsattar Osama Elemam Abdelhalim*

	Biofunctionalized Gold Nanocomposites from *Spatholobus Litoralis* for High-Sensitivity Refractive Index Sensing *Firdausi Nuzulah, Sumini Sumini, Titin Syufairoh, Shelgiana Hayu Krisnanda, Nurul Hidayat*[*]
	Mercury Sensing in Fish via Gold-Based SPR and Chitosan Composite Functionalization *Kada Abdelhafid Meradi*[*]*, Mohamed Esseddik Ouardi, Fatima Tayeboun*
	Enhancing the Thermal Stability of Deep Eutectic Polymer Electrolytes Through Nanoparticle Incorporation *Hazimah Binti Hazman, Norshahirah Binti Mohamad Saidi*[*]
	Comparative Green Synthesis of Zinc Nanoparticles via Pulsed Laser Ablation in Different Liquid Mediums *Nur Nadirah Binti Mohd Nor, Fairuz Diyana Binti Ismail*[*]*, Maisarah Binti Duralim*
	Study of Electrical Conductivity in Deep Eutectic Solvent Based on Hydrogen Bond Donor and Hydrogen Bond Acceptor Combinations *Farhan Shazwan Shah Shahbani*[*]*, Norshahirah Mohamad Saidi, Nurhafizah Hasim, Nur Hidayah Ahmad, Muhammad Amirul Aizat Mohd Abdah*
19:15 – 19:30	Break
Online Session – 19 (in English) Head of Session: Asst. Prof. Dr. Latif Akcay	
19:30 – 21:00	Grid-Connected Photovoltaic System with a Three-Level NPC Inverter for Power Quality Enhancement *Fatima Tahri*[*]*, Ghrissi Tahri, Ali Tahri*
	Dynamic Energy Management of Smart Microgrids Considering Renewable Variability *Mohammed Tsebia*[*]*, Hamid Bentarzi, Fazia Ahcene, Djamila Talah, Azeddine Ratni*
	Inexpensive, Thin, and Dual-Band Metamaterial Absorber with Inner-Nested Split Ring Resonators *Yunus Kaya*[*]*, Ugur Cem Hasar, Mehmet Ertugrul*
	Discriminating Natural Modes from Defect Signatures in Rolling Bearings Through Hybrid Vibration Modelling *Azeddine Ratni*[*]*, Ali Damou, Djamel Benazzouz, Mohamed Tsebia*
	Quantitative Structure–Toxicity Relationship Prediction of Ionic Liquid Toxicity Using an GWO-Optimized Support Vector Machine *Hayet Abdellatif*[*]*, Maamer Laidi, Cherif Si-Moussa, Widad Benmouloud, Imane Euldji*
	Bibliometric Analysis of AI-Driven Energy Harvesting and Prediction in

	Resource-Constrained IoT and Edge Systems *Sami Acik, Selahattin Kosunalp*, Mustafa Tasci*
	Numerical Analysis of the Seismic Bearing Capacity of Offshore Shallow Skirted Foundations on Sand Using the Pseudo-Static Approach *Alaoua Bouaicha**
	Leveraging Large Language Models for Transport-Triggered Architecture Processor Design *Latif Akcay**

Monday, December 15, 2025

Online Sessions

Virtual Hall

Online Session – 20 (in English) Head of Session: Dr. Intan Helina Hasan	
09:00 – 10:30	Evaluating the Role of Plant Growth-Promoting Rhizobacteria Strains in Boosting the Nutritional Quality of *Trifolium Alexandrinum* *Yousra Debbah*, Mohamed Bencherchali, Saida Messgo-Moumene*
	Sustainable Utilization of *Mentha Pulegium* by-Products: From Cellulose Microfibers to Fermentable Sugars *Fatma Bhiri*, Feriel Lessig, Amir Bouallegue, Samira Abidi, Aida Ben Hassen Trabelsi*
	Unlocking Aromatic Potential: Tripartite Rhizosphere Interactions Steer Metabolism for Stable Essential Oil Biosynthesis in Citronella Grass *Ferota Larasati*, Sudiarso Sudiarso, Nunun Barunawati*
	Potential of Plant Waste Ash Supplemented Culture Media for in Vitro Microtuber Induction in *Solanum Tuberosum* L. *Amina Belguendouz*, Benamar Benmahioul*
	Effects of Activated Charcoal Supplementation on in Vitro Microtuber Production and Quality in Potato *Amina Belguendouz*, Benamar Benmahioul*
	Lignocellulosic Biomass Valorization for Biogas Production *Samira Abidi*, Arwa Masrouhi, Fatma Bhiri, Aida Ben Hassen Trabelsi*
	Nanoencapsulation of Polyphenols from Native *Schinus Molle* and Non-Native Fruits for Sustainable Plant Growth Promotion *Matias Aguilar*, Jorge Montanari, Luciano Gabbarini*
10:30 – 10:45	Break
Online Session – 21 (in English) Head of Session: Dr. Siti Zulaika Razali	

10:45 – 12:15	Nurses' Perceptions of Spirituality and Spiritual Care: A Cross-Sectional Study in Kabul, Afghanistan *Farzana Mortazavi, Hatice Sutcu**
	The Knowledge and Attitudes of Iranian Nurses About Pain Management *Elahe Mohammadian, Hatice Sutcu*, Fatemeh Bahramnezhad*
	Exploring the Interplay Between Sulpiride and Physical Activity: Health Sciences Perspectives *Hassina Fisli*, Mohamed Lyamine Chelaghmia*
	Personalized Nutrition and Food Design *Ali Khalfa*, Azzeddine Senouci, Djahira Hamed, Mounir Chihab, Sofiane Bouazza, Bensalah Fatima, Farid Bennabi*
	Antibacterial Activity of Lactic Acid Bacteria Strains on Uropathogens *Djamila Amamra*, Fadela Chougrani, Mansouria Belhocine, Abdelkader El-Amine Dahou*
	Synthesis, Structural Elucidation, and Molecular Modeling Studies of 1,2,4-Triazolo-1,5-Benzodiazepine Diastereoisomers as Promising Anti-Ebola Candidates *Marouane Ait Lahcen*, Nouhaila Ait Lahcen, Saad Zekri, Samir Hmaimou, Mohamed Adardour, Ismail Hdoufane, Driss Cherqaoui, Abdesselam Baouid*
	Detection of Multi-Drug-Resistant Extended Spectrum β-Lactamase Producing *Enterobacteriaceae* in Patients with Urinary Tract Infection *Anfal Kara*, Naouel Boussoualim, Feryal Belfihadj, Meriem Elkolli*
12:15 – 12:30	Break
Online Session – 22 (in English) Head of Session: Dr. Intan Helina Hasan	
12:30 – 14:00	Examining the Satisfaction Levels of Patients with Nursing Care in the Internal Medicine Ward *Cigdem Koc, Halise Coskun**
	Impact of Child-Centered Empowerment on Lifestyle Behaviors in Children with Leukemia *Pouran Varvani Farahani*, Candan Ozturk, Aziz Eghbali, Atefeh Rezapoor*
	Identification of Potent Sulfonamide Derivatives Targeting MMP2 Through Pharmacophore Ligand-Based Modeling *Saad Zekri*, Nouhaila Ait Lahcen, Adnane Ait Lahcen, Wissal Liman, Ismail Hdoufane, Driss Cherqaoui*
	Valorization of Moroccan Medicinal Biodiversity as a Source of Novel Antileishmanial Agents *Mohammed-Yassine Takzima*, Mohamed Echchakery, Mohamed Hafidi, Loubna El Fels*

	Epidemiological Profile and Phenotypic Characterization of Aminoglycoside-Resistant Clinical Strains in the Setif Region *Iman Krache*[*], *Anfal Kara, Naouel Boussoualim, Zineb Daoudi, Noussaiba Douadi, Fatma Gridi*
	Anti-Bacterial and Anti-Inflammatory Activities of the Mucus of the Snail *Helix Aspersa* Muller *Imene Yahla*[*]
	Computer-Aided Drug Discovery of Novel Ebola Virus Glycoprotein Inhibitors: Integrating QSAR, Fragment-Based Design, and Molecular Dynamics *Nouhaila Ait Lahcen*[*], *Wissal Liman, Saad Zekri, Mehdi Oubahmane, Ismail Hdoufane, Mohammed Mater Alanazi, Mohamed Maatallah, Driss Cherqaoui*
14:00 – 14:15	Break
Online Session – 23 (in English) Head of Session: Asst. Prof. Dr. Sebahat Oztekin	
14:15 – 15:45	Biopolymeric Films of HEC/PAADDA Crosslinked with Glutaraldehyde as Controlled Release Systems of Tannic Acid for Antitumoral and Wound Healing Applications *Isabela Viudes Rossatto Ferrarezi*[*], *Ingrid Cristine de Sousa Everton, Júlia Monteiro Fernandes, Luca Kiichi Suzuki Trancolin, Lucas Gomes Nascimento, Marcos Elias da Silva Almeida, Maria Carolina Rodrigues Garcia, Mariana Aparecida Vieira, Weslley Aparecido Vicente Luiz, William Capellari Fumegali*
	Infertility Among Women in Tebessa (Northeastern Algeria): Anthropometric and Biological Risk Determinants *Khalida Abla*[*], *Nassima Toumi-Halaimia, Sawssane Ziani, Ines Benamer, Asma Kraidia*
	Impact of Traditional Phytotherapy on Hematological Parameters and Chemotherapy Tolerance in Breast Cancer Patients: A Case-Control Study in Tebessa, Algeria *Khalida Abla*[*], *Nassima Toumi-Halaimia, Sawssane Ziani*
	Effects of Twin Hearts Meditation Versus Mandala Coloring on Practical Examination Anxiety in Undergraduate Nursing Students *Pouran Varvani Farahani*[*], *Samineh Esmailzadeh, Precious Chisom Uzoeghelu, Hatice Sutcu*
	Body Image Perception Among Women After Mastectomy *Mohamed Khalyfa*[*], *Mohammed-Yassine Takzima, Imane Bettane, Youssef El Allam, Aya Ait Benaim*
	In Silico Prediction of the Biological Activity of New Oxazole Derivatives *Nadia Hadhoum*[*], *Nassim Haddouche, Yasmine Hannachi, Sabine Herbi*
	Circular Economic Model in the Hotel Industry for the Optimization of Solid and

	Recyclable Waste: Case Study of the City of Essaouira, Morocco *Assala Loukili*[*], *Mohamed Hafidi, El Hassan El Mouden, Abdallah Nassour, Nour-El Houda Chaher, Loubna El Fels*
15:45 – 16:00	Break
Online Session – 24 (in English) Head of Session: Dr. Mohd Hafizuddin Ab Ghani	
16:00 – 17:30	Food Safety and Microbial Control *Ali Khalfa*[*], *Azzeddine Senouci, Djahira Hamed, Mounir Chihab, Sofiane Bouazza, Bensalah Fatima, Farid Bennabi*
	Knowledge of Leishmaniasis: A Comparative Review of Morocco and Ethiopia *Mohammed-Yassine Takzima*[*], *Mohamed Echchakery, Mohamed Hafidi, Loubna El Fels*
	Chemical Profiling and Neuroprotective Activity in Elaeagnaceae Leaves *Rayene Bouaita*[*], *Randa Djemil, Samira Bouahlit, Saber Boutellaa, Chourouk Babouche, Zineb Bouamrane*
	Nickel Sulfate Induced Hepatotoxicity Mediated Through Reactive Oxygen Species Generation and Impairing the Antioxidant Defense in Albino Rats *Mohamed Khiari*[*], *Youcef Bougoutaia, Nadjette Bourafa, Zine Kechrid*
	A Green Nanotechnology Approach: Rice Husk-Derived Carbon Quantum Dots (CQDs) for Sustainable Applications *Mohd Hafizuddin Ab Ghani*[*], *Siti Hajar Othman, Siti Zulaika Razali, Mohd Ali Mat Nong, Josephine Liew Ying Chyi, Nishata Royan Rajendran Royan, Chen Ruey Shan, Johari Abdu Rahim*
	Biochar Amendment and PGPR Inoculation Improve Growth, Nutrient Uptake, and Soil Fertility in Millet *Asma Dahani*[*], *Elmostapha Outamamat, Khalid Oufdou, Loubna El Fels*
	Mapping the Physico-Chemical and Microbiological Characteristics of Olive Mill Wastewater Across Morocco: Advancing a Waste-to-Resource Circular Strategy *Oumaima Dahbane*[*], *Mohamed Hafidi, Mohammed Rhazi, Youness Bouhia*
17:30 – 17:45	Break
Online Session – 25 (in English) Head of Session: Asst. Prof. Dr. Mustafa Alptekin Engin	
17:45 – 19:15	Key Scoring Models Used for Performance Evaluation of Employees: A Systemic Review and Its Applicability in the Albanian Banking Sector *Sllavka Kurti, Katerina Vasili*[*]
	Albania's Perspective in Fighting High-Level Corruption Compared to Bulgaria, Before the Technical Closing of EU Accession Negotiations *Anila Shehi*[*]

	Exploratory Factor Analysis of Mobile Application Usage Among Youth Associations in Malaysia *Mohd Hazlami Jusoh*, Noor Aisyah Abdul Aziz, Mohd Yusri Ibrahim*
	Understanding the Role of AI Literacy in Work Engagement: The Mediating Effects of Job Crafting and Job Insecurity, and the Moderating Role of Regulatory Focus *Ali Jan Shayiq*, Ipek Mete Tonge*
	Scientific Integrity in the Era of Artificial Intelligence: Current Knowledge and Challenges for Nursing Education – A Narrative Review *Imane Bettane, Mohammed-Yassine Takzima*, Mohamed Khalyfa*
	The Challenges Encountered by Science Teachers in Utilizing Laboratory Facilities *Ulas Kubat**
	The Chronotopes of Racialized Experience in Toni Morrison's *The Bluest Eye* *Tulay Dagoglu**
	Challenge of Ancient Regimes Toward the Republic: Example of Napoleon Bonaparte *Erdal Aydin**
19:15 – 19:30	Break
Online Session – 26 (in English) Head of Session: Asst. Prof. Dr. Mustafa Alptekin Engin	
19:30 – 21:00	Structural, Photocatalytic, and Dielectric Properties of ZnO-Phosphate Glass-Ceramics *Chaima Assamadi*, Nourdine El Binna, Mohamed El Masloumi, Abdelaziz El Abiad, Hakima Aouad*
	Structural and Optical Characterization of Cellulose Acetate/ZnO Nanocomposite Films *Asmaa Bessaad*, Badreddine Toubal*
	Wide-Angle Quad-Band Metamaterial-Based Absorber Operating in Microwave Bands *Yunus Kaya*, Ugur Cem Hasar*
	Enhanced Activation of Peroxymonosulfate by a Mixed Oxide Co_2O_4-Fe_2O_3 for Sunset Yellow Dye Removal *Djedjiga Bousalah*, Hanane Zazoua, Amel Boudjemaa, Khaldoun Bachari, Nahed Dokhan, Mohamed Zine Messaoud-Boureghda, Fayrouz Benhaoua*
	Applications of MEMS Sensors and Micropneumatics in Automated Systems *Goran Čubrić*, Ivana Salopek Čubrić*
	First-Principles Investigation of ABX3 Perovskites: Structural and Functional

	Properties for Spintronic Applications *Saadiya Benatmane*[*]
	Multimodal Large Language Models and Image Processing: A Bibliometric and Network Analysis for the Period 2023–2025 *Adem Korkmaz*[*]*, Selma Bulut*
	Exploring the Thermoelectric Potential of Perchalcogenoborates via DFT-Based Analysis *Fatima Garadi*[*]*, Ahmed Al-Amin Ben Kamri, Ben Messaoud Chikh Lakdar*

[*] : Corresponding Author

_ : Presenter

Summary of Sessions

Friday, December 12, 2025	
Conference Hall	*Virtual Hall*
Opening Session Onsite Session – 1	Online Session – 1 Online Session – 2 Online Session – 3 Online Session – 4 Online Session – 5

Saturday, December 13, 2025	**Sunday, December 14, 2025**	**Monday, December 15, 2025**
Virtual Hall	*Virtual Hall*	*Virtual Hall*
Online Session – 6	Online Session – 13	Online Session – 20
Online Session – 7	Online Session – 14	Online Session – 21
Online Session – 8	Online Session – 15	Online Session – 22
Online Session – 9	Online Session – 16	Online Session – 23
Online Session – 10	Online Session – 17	Online Session – 24
Online Session – 11	Online Session – 18	Online Session – 25
Online Session – 12	Online Session – 19	Online Session – 26

CONTENTS

Invited Speaker

Oral Presentations

2nd International Conference on Multidisciplinary Sciences and Technological Developments (ICMUSTED 2025)

December 12-15, 2025

Air Quality and Sustainable Development: The Role of Machine Learning in Shaping Future Cities

Samsuri Abdullah[1]

[1]Faculty of Ocean Engineering Technology, Universiti Malaysia Terengganu, Malaysia
Corresponding author: Samsuri Abdullah (e-mail: samsuri@umt.edu.myc)

Abstract

Air pollution remains a critical environmental and public health issue, contributing significantly to premature mortality, respiratory and cardiovascular diseases and climate forcing. According to the World Health Organization, over 90% of the global population is exposed to air pollutant concentrations exceeding recommended limits, underscoring its relevance to the sustainable development goals (SDGs). Traditional air quality management strategies, while valuable, are often limited by sparse monitoring networks, delayed reporting, and the complexity of atmospheric interactions among precursors, pollutants and meteorological variables. This study examines the role of machine learning (ML) as an emerging approach for advancing air quality prediction and management within the framework of sustainable urban development. By leveraging nonlinear algorithms, ML models can capture intricate relationships among emissions, meteorological drivers and urban activities, enabling short and long-term forecasts with improved accuracy compared to conventional statistical techniques. Furthermore, the integration of ML-based predictions into urban planning and policy frameworks presents opportunities to strengthen SDG 3 (good health and well-being), SDG 11 (sustainable cities and communities), and SDG 13 (climate action). Key challenges remain, including data heterogeneity, model interpretability and the need for interdisciplinary collaboration to translate computational outputs into actionable policy. The study presents recent methodological advances, case studies and future research directions, highlighting how machine learning can serve as a scientific and technological pathway toward cleaner air and more sustainable cities.

Keywords: Air quality, Machine learning, Sustainable development goals, Urban sustainability, Predictive modeling

2nd International Conference on Multidisciplinary Sciences and Technological Developments (ICMUSTED 2025)

December 12-15, 2025

A Modified Two-Sided Approximation Method for a Special Boundary Value Problem with Delayed Arguments

Arzu Aykut[1], Fulya Koc Simsek[1]

[1]Department of Mathematics, Faculty of Science, Ataturk University, Erzurum, Türkiye
Corresponding author: Arzu Aykut (e-mail: aaykut@atauni.edu.tr)

Abstract

In this study, the considered boundary value problem is analyzed by transforming it into an equivalent integral form using analytical methods. This transformation yields a Fredholm-Volterra type integral equation that effectively represents the delayed characteristics of the original system. The corresponding Fredholm operator contains a degenerate kernel, which allows for reduced complexity and supports the use of iterative approximation schemes. The modified two-sided convergence method is applied to find the solution of the obtained integral equation. This approach produces two sets of approximations, serving as lower and upper bounds, that monotonically converge to the exact solution. The method is particularly advantageous for delayed type problems by providing guaranteed stability and convergence under appropriate kernel conditions. The primary objective of the research is to verify the efficiency and reliability of the simple two-sided convergence method in solving this class of boundary value problems. Finally, a numerical example is given to confirm the theoretical analysis, with the approximate solutions compared against the exact analytical results. All numerical computations were performed using Maple to ensure high precision.

Keywords: Boundary value problem, Fredholm-Volterra integral equation, Differential equation with retarded argument

AI-Based Intelligent Document Classification in the Logistics Sector

Selcuk Zereyalp[1], Kemal Sogukcesme[1], Bahadir Fatih Yildirim[2]

[1]Sertrans Logistics, Istanbul, Türkiye
[2]Istanbul University, Istanbul, Türkiye
Corresponding author: Selcuk Zereyalp (e-mail: selcuk.zereyalp@sertrans.com.tr)

Abstract

This study presents an artificial intelligence (AI)-based intelligent document classification system designed specifically for the logistics sector. The proposed system integrates deep learning, natural language processing (NLP), and document visual analysis (document AI) to automatically classify and manage various document types such as ATR, CMR, commercial invoice, proforma invoice, customs declaration, and transit (T1/T2) forms. The architecture employs the advanced LayoutLMv3 model, which processes textual, visual, and layout information simultaneously to achieve high accuracy in classification tasks. By combining optical character recognition (OCR)-extracted text and document layout embeddings, the system enables precise categorization even for scanned or unstructured documents. Active learning mechanisms continuously improve classification performance through user feedback. The system ensures full automation, multilingual support, and data security while maintaining flexibility for new document types. Through this multimodal AI approach, document management in logistics operations becomes faster, more reliable, and highly adaptable to real-world business needs.

Keywords: Artificial intelligence, Document classification, Logistics, NLP, LayoutLMv3

History of Mobile Communication from 1G to 6G

Hanifi Turgut[1], Tevhit Karacali[2], Tarik Bugra Ala[2]

[1]Department of Electrical and Communications Engineering, Kocaeli University, Kocaeli, Türkiye
[2]Department of Electrical and Electronics Engineering, Ataturk University, Erzurum, Türkiye
Corresponding author: Tarık Bugra Ala (e-mail: tbugratk@gmail.com)

Abstract

This study analyzes the evolution of mobile communication technologies from the first generation (1G) to the sixth generation (6G) within the framework of fundamental engineering principles and performance metrics. Utilizing a qualitative literature review approach, the research focuses on the development, emergence requirements, architectural solutions, challenges, and legacies of each generation. Instead of experimental implementation, the study examines technical reports from standardization bodies like International Telecommunication Union (ITU) and Third Generation Partnership Project (3GPP), industry documents, and peer-reviewed academic papers to comparatively evaluate the technical characteristics and performance objectives of each era. The findings reveal that the evolution in mobile communications represents not only an increase in speed and capacity but also a profound transformation from hardware based structures to software driven systems. Ultimately, the study demonstrates a clear shift from hardware-centric to software- and intelligence-oriented paradigms, concluding that the success of future mobile networks (6G and beyond) will depend on factors surpassing mere technical excellence, such as speeds at the terabits per second (Tbps) level and microsecond latency, but rather on criteria like sustainability, trustworthiness, and native artificial intelligence (AI) integration.

Keywords: Mobile communication, Intergenerational comparison, Technological evolution, Network architecture, Efficiency

1. INTRODUCTION

Mobile communication systems have become an indispensable part of modern life since the last quarter of the 20th century and have entered a continuously evolving technological transformation process [1, 2]. This process has profoundly influenced not only individuals' communication habits but also the global economy, industry, and social structures. At the core of this evolution lies the engineering challenge of pushing the theoretical capacity limits of a communication channel, first formulated by Claude Shannon (1948) [3].

Each new generation has sought to surpass these fundamental limits by discovering wider bandwidths (B) and improving the signal-to-noise ratio (S/N) through more efficient technologies [2]. This technological journey began with first generation (1G), where the systematically organized cellular structure was introduced commercially and analog voice transmission marked the starting point. The subsequent digital-based second generation (2G) systems digitized voice using the principles of the Nyquist theorem, thereby offering enhanced data security, short message service (SMS), and higher capacity [4, 5].

The true data revolution began with third generation (3G), which unlocked mobile internet access and enabled data rates in the megabits per second (Mbps) range, largely thanks to wideband code division multiple access (WCDMA) technology. Building on this foundation, fourth generation (4G; long-term evolution (LTE) fully transitioned to an all-internet protocol (IP) architecture based on orthogonal frequency-division multiple access (OFDMA), reducing latency to under 10 milliseconds and inaugurating the era of mobile broadband. Today, fifth generation (5G) provides peak speeds of up to 20 gigabits per second (Gbps) and represents a fundamental architectural shift, integrating diverse service requirements. These include ultra-low latency of 1 millisecond (URLLC) and massive connectivity for up to one million devices per square kilometer (mMTC), all within a single, flexible infrastructure. This leap is enabled by key technologies including virtualization (network functions virtualization (NFV) / software-defined networking (SDN)) and network slicing [6, 7].

This rapid and multilayered evolution in mobile communication technologies has created a need for detailed and evidence-based analysis [8]. In this context, this study examines the intergenerational development of mobile communication technologies from a comparative perspective, grounded in fundamental engineering principles and

quantitative performance metrics (data rate, latency, spectral efficiency, etc.). The aim is not only to describe the innovations introduced by each generation but also to reveal the technical necessities behind these innovations and how they overcame the limitations of previous generations using concrete data. This study is based on reliable sources published by international standardization bodies (International Telecommunication Union (ITU), Third Generation Partnership Project (3GPP)), technical reports from technology manufacturers, and peer-reviewed academic literature. Although it does not include experimental work due to its review-based nature, it provides a comparative and systematic analysis by synthesizing theoretical targets and measured performance data from the literature.

2. MATERIAL AND METHOD

This study is a systematic literature review and technical analysis examining the evolution of mobile communication technologies from 1G to sixth generation (6G) comprehensively [2, 4]. The main objective of the research is to present the motivation for the emergence, technological foundation, and architectural transformations of each generation in a chronological framework, and to compare the results of this evolution through key performance indicators (KPIs).

2.1. Literature Review and Data Collection

The data material for the study was obtained from academic databases (The Institute of Electrical and Electronics Engineers (IEEE) Xplore, Google Scholar) containing fundamental and current developments in the mobile communication field, as well as publications from official standard and regulatory bodies. The primary sources include:

- Standard Bodies and Reports: International Mobile Telecommunication (IMT)-2000 and IMT-Advanced vision reports from the International Telecommunication Union Radiocommunication Sector (ITU-R) [7], technical specifications from the 3GPP [9–13], and sectoral data reports from the Information and Communication Technologies Authority (BTK in Turkish) [14–16].
- Academic Publications: Foundational, high-impact journal articles, conference papers, and technical reports detailing the core architecture, key technologies, and future visions in high-impact journals [1, 2].
- The search was limited to core publications that explicitly detail the fundamental architecture, key technologies (code division multiple access (CDMA), OFDMA, multiple input, multiple output (MIMO), Terahertz (THz)), and performance indicators for each mobile generation (1G, 2G, 3G, 4G, 5G, and 6G).

2.2. Analysis Approach

The collected data was analyzed and synthesized across three main axes to provide a holistic perspective throughout the paper:

- Chronological and Motivational Review: The impetus for the emergence of each generation and the fundamental limitations triggering the transition were identified.
- Architectural and Technological Evolution: The shift from circuit-switched structures to fully packet-switched and flattened architectures was examined through the core architectural components of each generation.
- Comparative Performance Analysis: Inter-generational changes in KPIs such as latency, spectral efficiency, and spectrum utilization were compared using figures and tables.

3. RESULTS

3.1. 1G Systems and the Birth of Cellular Architecture

1G, the first generation of wireless communication technology, is an analog telecommunication system introduced in the 1980s. The world's first cellular system was introduced in Tokyo, Japan, by Nippon telephone and telegraph (NTT) in 1979. Two years later, the cellular era reached Europe, and the two most popular analog systems became Nordic mobile telephones (NMTs) and total access communication systems (TACS). Subsequently, the advanced mobile phone systems (AMPS) technology was introduced; however, these technologies, particularly AMPS, encountered various problems and limitations such as poor voice quality, capacity constraints, and limited security measures [1, 4, 17].

3.1.1. 1G Technology and System Architecture

The cellular network model depicted in Figure 1 explained is the network structure that forms the foundation of mobile communication technologies and enables user equipments (UEs) to communicate with core networks without any location constraints. Young's work [18] addresses the working principle of this system, explaining that the service area is divided into hexagonal-shaped cells, and the mobile telephone switching office (MTSO), located at the center of the system, is the hub that manages location information and call details, simultaneously implements billing and charging services, and controls the cell sites.

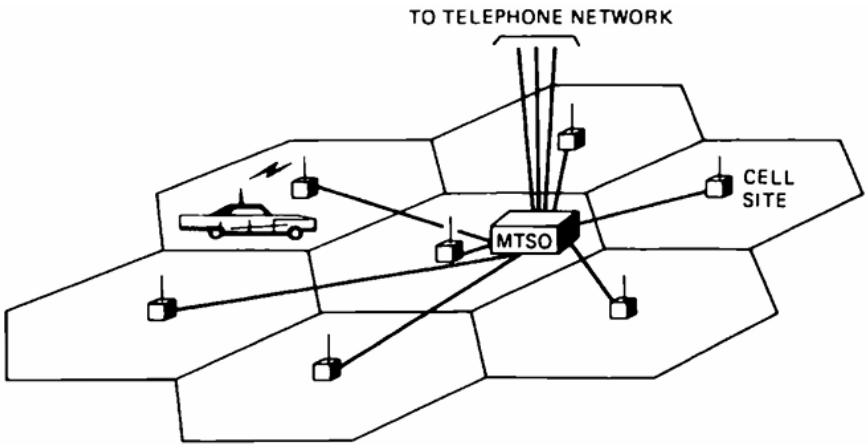

Figure 1. 1G architecture [19]

3.1.2. Global Standards and Comparative Analysis

Firstly, the NTT standard was launched in Tokyo in 1979. It quickly became the country's first national 1G network. On the other hand, the NMT system, an analog standard, was initiated by public telephone operators in Finland, Sweden, Norway, and Denmark, creating the world's first multinational standardized mobile telephone system. The two most popular systems in Europe were the NMTs and TACS. Apart from NMT and TACS, other analog systems were also introduced across Europe in the 1980s. Each of these systems had capabilities such as handoff and roaming; however, the biggest disadvantage of this era was that the cellular networks did not operate internationally [1, 19].

3.2. 2G Mobile Communication Services

3.2.1. The Advent and Motivation of 2G Technology

2G was introduced in the early 1990s, and the dominant 2G standard became the global system for mobile communications (GSM). GSM was first launched in Finland in 1991 with the aims of supporting roaming across national borders and having a higher capacity compared to 1G. While initially used only for voice transmission, it was later also utilized for data communication, such as the SMS and internet access [20, 21].

In essence, 2G is the first digital mobile communication technology developed to overcome the limitations of 1G, primarily the restriction on international roaming and the constraints imposed by its analog structure [21]. This transition from analog to digital was made possible by advancements in Metal-Oxide Semiconductor Field-Effect transistor (MOSFET) technology [1].

3.2.2. Core 2G Architecture: GSM

Within each cell, there are stations called base transceiver station (BTS) that allow users to access the network. Control centers, called base station controller (BSC), are connected to the mobile switching center (MSC), which facilitates call establishment. This center ensures the establishment and termination of all telephone calls [22].

The first GSM systems utilized the 900 MHz band and a 25 MHz frequency spectrum [23]. Frequency division multiple access (FDMA) was used to divide the available bandwidth into 124 carrier frequencies, each of which was 200 kHz. Subsequently, each frequency was divided into eight time slots using time division multiple access (TDMA), which allowed the same frequency to accommodate eight different simultaneous calls [21].

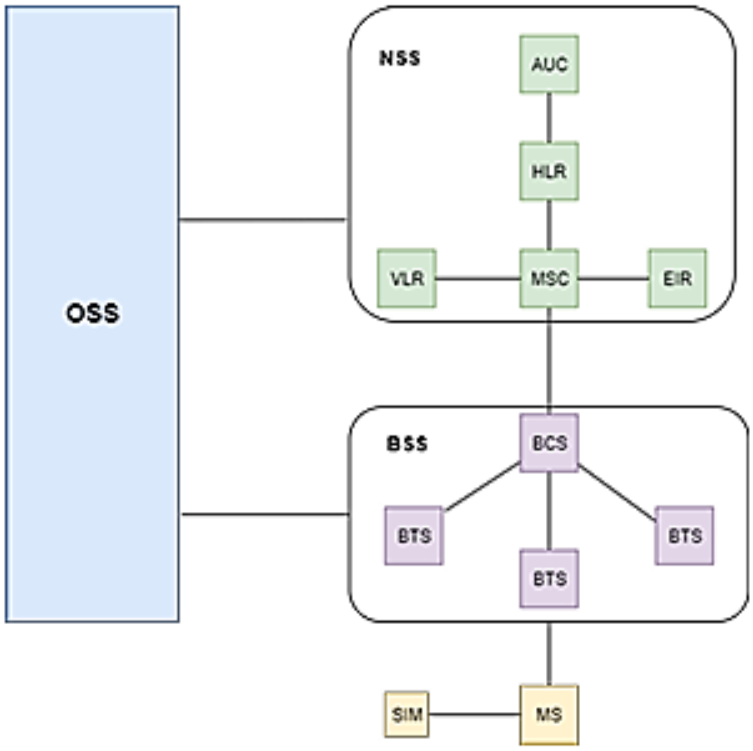

Figure 2. GSM architecture [1]

3.2.3. Data Rate and Content Limitations (Performance Issues)

All 2G systems are voice-centric. While GSM includes SMS in addition to voice, it actually supports data transfer over voice channels; however, it typically does so at slow speeds, such as 9.6 kb/s or 14.4 kb/s. Consequently, voice remained the dominant service in the 2G world; as a result, 2G eventually failed to meet changing demands [24, 25].

3.2.4. The Evolution of 2G: High-Speed Circuit-Switched Data (HSCSD), 2.5G (General Packet Radio Service (GPRS)), and 2.75G (Enhanced Data rates for Global Evolution (EDGE))

HSCSD is an application designed to increase 2G's speed by combining time slots and utilize the existing structure for bursty internet data. A maximum data rate of 14.4 kbit/s could be transferred over a single existing time slot. HSCSD could combine and allocate multiple channels to the user, and thus it was calculated that speeds up to 115.2 kbit/s could be reached with the use of 8 channels; however, this remained theoretical because the MSC could only allow speeds up to a maximum of 64 kbit/s for each connection. In practical application, it was limited to a speed of 57.6 kbit/s using 4 channels [21, 22].

3.2.5. GPRS and the Packet Switching Revolution

The GPRS system served as a bridge between third-generation and second-generation technologies and was named as a packet-switched radio service. This sub-version utilized Packet Switching, meaning it added IP support to the existing GSM infrastructure [22].

With 2.5G also proving insufficient, the system moved away from the currently used Gaussian minimum shift keying (GMSK) modulation technique to a more efficient one: 8-phase shift keying (8PSK). However, the biggest innovation in this regard was the adoption of the adaptive modulation and coding (AMC) technique. With this technique, the appropriate modulation scheme is used according to the channel conditions: 8PSK, which is very sensitive to noise, is preferred under good channel conditions; but if suitable conditions are not met and the noise is high, the system automatically switches to GMSK, which is more noise-resistant but less spectrally efficient than 8PSK [4].

This evolution of 2G extending to 2.75G is essentially a story of an architecture, originally designed for voice calls and messaging, attempting to adapt to the different nature of data traffic brought by the internet. However,

regardless of the efforts made, the progress of mobile communication and the increasing data demands of users could not be halted.

3.3. 3G Mobile Communication Systems

3.3.1. The Global Standards Quest and 3G's Objectives

Initial plans made for 3G in the 1980s were for video conferencing applications using mobile phones. The 3G concept evolved when it was understood that the true focus was the internet. In response to this data demand, the ITU created an international standard for 3G in the 90s. This standard was named IMT-2000; a minimum speed target of 200 kbit/s was set [5, 26].

However, just like with 2G, a kind of standards war broke out for 3G. While European and Japanese GSM operators supported the WCDMA standard, which was the natural evolution of the GSM infrastructure, operators in North America began using the CDMA2000 standard, based on their own 2G evolution. China, meanwhile, developed its own standard, time division - synchronous code division multiple access (TD-SCDMA) [27, 28].

Table 1. The evolution of 3G [28]

No	Generation	3G	3.5G	3.75G
1	Year	2000	2003	2003
2	Frequency	1.6–2 GHz	1.6–2.5 GHz	1.6–2.5 GHz
3	Technology	FDD/TDD	GSM/2GPP	GSM/3GPP
4	Service	Voice and Data	Voice and Data	High Speed Internet and Multimedia

FDD: Frequency division duplex and TDD: Time division duplex

Due to this mixed market and commercial competition, a global standard still could not be adopted. As Mendes et al. pointed out: It was harder to agree on frequency bands for IMT-2000, and the resulting compromise included five different radio standards and three separate frequency bands. This situation caused 3G to be born in the form of various standards [24].

3.3.2. The GSM Path and Evolution: From WCDMA to High Speed Packet Access Plus (HSPA+)

As mentioned, the gateway to 3G for Europe and Asia was universal mobile telecommunications system (UMTS), which emerged from the evolution of GSM. The UMTS system was built upon the packet-switched foundations of 2.5G. In this improved architecture, the node B replaced the BTS of 2G, and the radio network controller (RNC) replaced the BSC [20].

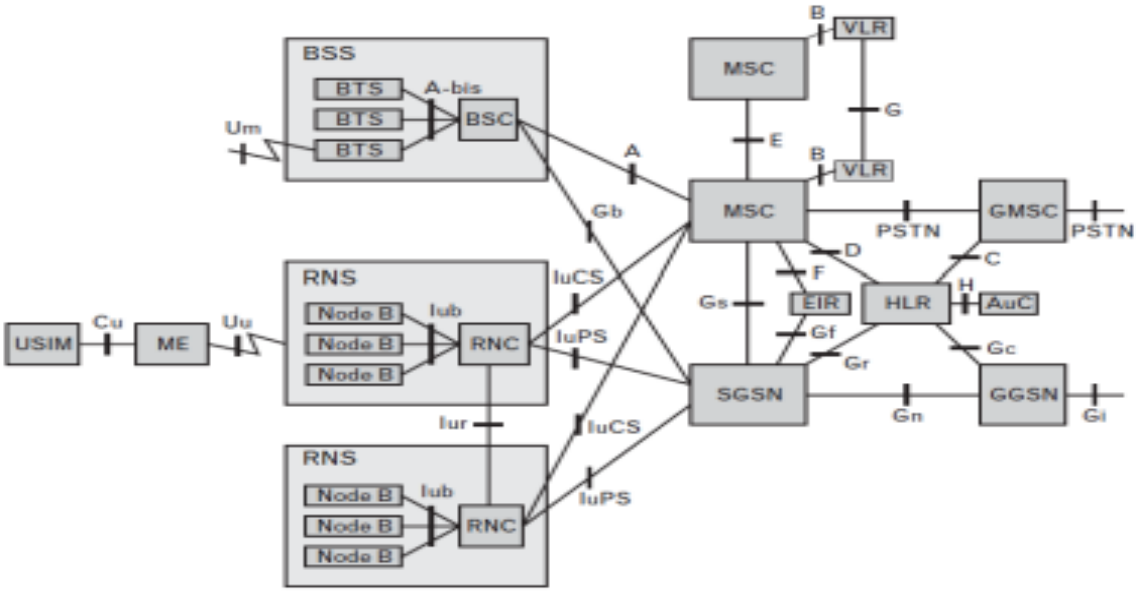

Figure 3. UMTS architecture [29]

3.3.3. UMTS Radio Layer Details (Physical Layer)

The main air interface of UMTS is WCDMA, which is referred to as universal terrestrial radio access (UTRA). The operation of the UTRA network (UTRAN) is asynchronous, and both FDD and TDD modes can be configured to achieve data rates up to 2 Mbps. The WCDMA carrier spacing is approximately 5 MHz, with a chip rate of 3.84 Mcps and a frame length of 10 ms.

WCDMA utilizes the radio spectrum efficiently because the CDMA technique allows all base stations to use the same frequency. Furthermore, WCDMA has additional advantages such as high transfer speed, increased system capacity through statistical multiplexing, and improved communication quality [24, 30].

3.3.4. Core UMTS and Speed Tiers

The initial trials of UMTS were designed to offer speeds that varied according to the user. Data rates targeting up to 144 kbps for a user traveling in a vehicle, 384 Kbps for a pedestrian, and up to 2 Mbps for a stationary, indoor user were targeted [26].

Higher data rates (such as 2 Mbps) utilize more complex modulation and coding schemes that require flawless signal transmission. These complex schemes are more sensitive to signal distortions that occur while moving at high speeds. This is why system engineers were driven to implement this tiered speed format.

3.3.5. Factors Triggering 4G and the Advent of a New Era

The new consumption perception initiated by 3G exceeded its scope and gave rise to the need for a new technology. 4G, which would address these needs, does not just mean fast internet; it also means a technology capable of providing smart, ubiquitous, seamless, and personalized service.

Jiang and Han stated that the exponential growth in data traffic was fueled by the increase in mobile broadband traffic [2]. Furthermore, Ekström expressed that both the number of mobile broadband subscribers and the traffic volume per subscriber were increasing rapidly [18]; however, this created a major challenge for cellular networks, which were primarily designed for voice communication.

The goal of 4G was precisely to overcome this major challenge: the necessity for cellular networks to operate both a packet-switched network for data delivery and a circuit-switched network for voice calls. With 4G, the inefficient, complex, and dual-network structure of 3G was ended, and a transition to an all-packet-switched network architecture was made.

3.3.6. Establishing Official Standards for True 4G: IMT-Advanced

The ITU-R group outlined the basic technical requirements for the 4G system in a report published in 2008. However, it was understood that Release 8, which we call LTE and which was the initial equivalent of 4G, could not fully meet these requirements. For instance, the expected peak data rates of 1 Gbps for low mobility and 100 Mbps for high mobility were not entirely satisfied [2].

As a result of this situation, Release 10, known as LTE-Advanced, began to be developed by 3GPP and was approved as an IMT-Advanced technology in November 2010 [31, 32].

3.4. 4G Market: LTE, HSPA+, and the Rival Worldwide Interoperability for Microwave Access (WiMAX)

3.4.1. The Two Main Market Rivals: LTE and WiMAX

The market journey of 4G, similar to previous generation technologies, began once again with standards competition. As Khan et al. pointed out, while operators were trying to decide on the best standard for long-term investment, there were two distinct standards: WiMAX, which had a technological head start, on one side, and LTE, which offered a clean transition from 3G, on the other [25].

As also noted by Jiang and Han, WiMAX was commercialized earlier than LTE and enjoyed a period of performance superiority between 2005 and 2009; it was at the forefront of adopting MIMO and OFDM technologies [2].

The biggest reason for LTE gaining market dominance was its ability to offer a smooth transition from dominant standards like GSM and WCDMA, meaning it was an evolution of the previous technology. On the other hand, WiMAX was referred to as a disruptive technology serving small users. Ultimately, major mobile operators such as Verizon, Vodafone, China Mobile, NTT, and Deutsche Telekom chose to seamlessly upgrade their existing 3G infrastructures to LTE rather than taking on the risk and high cost of a disruptive standard [2].

3.4.2. LTE Architecture (Release 8)

LTE is a disruptive and pioneering standard, designed without regard for backward compatibility constraints. The system design has been simplified and significantly flattened to reduce latency.

One of the most concrete examples of this flat architecture is that while 3G had a central RNC managing the node B (the 3G base station), this structure was eliminated with LTE Release 8. The station, now called the evolved node B (eNodeB) is much smarter and makes decisions regarding resource management and handover internally. This allows decisions to be made faster, without intermediate processing [2].

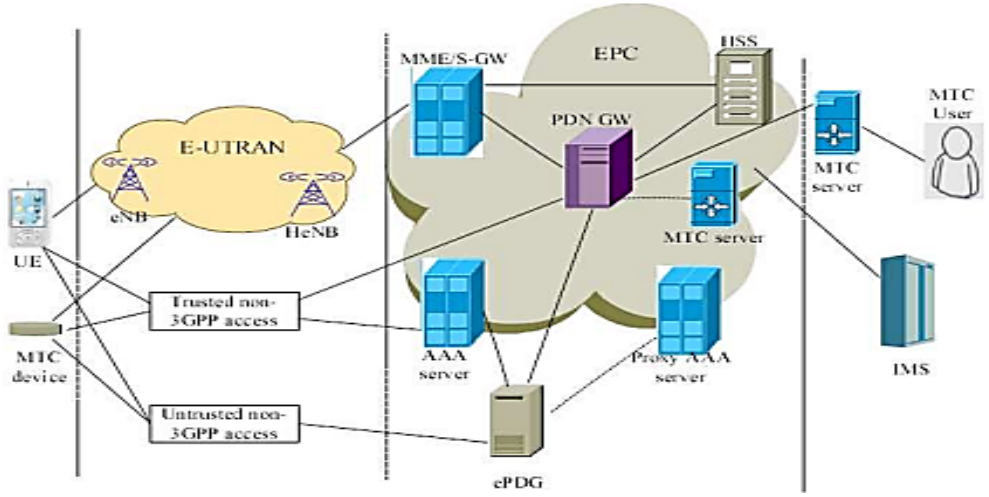

Figure 4. LTE architecture [33]

Guo et al. stated that the LTE architecture, known as evolved packet system (EPS), consists of two main parts: the evolved universal terrestrial radio access network (E-UTRAN) and the EPC [34]. They summarized the EPC architecture as follows:

- Mobility Management Entity (MME): The MME controls the control plane signaling between the user and the EPC.
- Serving Gateway (S-GW): The S-GW is responsible for routing and forwarding data packets between the users and the eNodeB. It is also responsible for acting as the mobility anchor...
- Packet Data Network Gateway (PDN-GW): The PDN-GW serves as an interconnection point between the EPC and external packet data networks.
- Home Subscriber Server (HSS): The HSS is a database that contains all relevant user and subscriber-related information.

3.4.3. The Journey to True 4G, LTE-Advanced, and Beyond

It was understood that LTE, upon the release of Release 8, could not fully meet the targets set by IMT. The expected peak data rates of 1 Gbps for low mobility and 100 Mbps for high mobility were not entirely satisfied. To reach these targets, the LTE-Advanced 4G technology was officially approved [32].

3.4.4. Technologies Enabling LTE-Advanced to be True 4G

i. Carrier Aggregation (CA): LTE-Advanced allows up to five component carriers with different bandwidths to be combined (Carrier Aggregation) in order to achieve a bandwidth of 100 MHz for a single terminal. However, the cost of using this feature is that the combination of different frequencies in the same device leads to engineering problems, such as the device's own signal interfering with itself [35].

ii. Advanced MIMO (eMIMO) and Multi-User MIMO (MU-MIMO): Analogically speaking, lanes were added to the data highway expanded by carrier aggregation using the eMIMO technique, allowing for more data flow simultaneously. Eluwole et al. stated that this enhancement offers more layers to a single user with single-user MIMO (SU-MIMO) and also allows different layers to be assigned simultaneously with MU-MIMO [36]. They also noted that switching between SU-MIMO and MU-MIMO is much more advantageous than using only single-user MIMO [36].

3.5. 5G Mobile Communication Systems

3.5.1. From the Limits of 4G to the 5G Vision (IMT-2020)

We are witnessing an exponential increase in the amount of mobile traffic. Saghezchi et al. noted that mobile data traffic doubled between 2010 and 2011 [6]. Furthermore, this increase is projected to be about 20,000 times from 2010 to 2030 [40]. The surge is primarily driven by the rise in mobile device usage and mobile video consumption, alongside the changes in consumption habits mentioned for 4G [6].

One of the biggest factors is that the expected end-to-end latency for 5G is one-tenth of 4G's [36]. As stated in both references [7] and [36], 5G's user plane latency will be even lower than 1 ms. This low latency makes it possible to handle demanding services and applications—such as autonomous cars, augmented reality, or ultra-high-resolution multimedia streaming—that push the limits of 4G and require 100% reliability, as also indicated by reference [37], unlike 4G.

3.5.2. Three Core Use Cases Shaping 5G

i. Enhanced Mobile Broadband (eMBB): This is a higher stage of the mobile broadband technology offered by 4G. The International Telecommunication Union Radiocommunication Sector noted that it offers high speeds at Gbps levels for users and can be utilized for applications such as ultra-high-definition video streaming, 3D video, augmented reality, virtual reality, and cloud-based gaming [7].

ii. URLLC: One of 5G's most revolutionary promises, URLLC is a technology that provides extremely low end-to-end latency for applications requiring ultra-high reliability, where interruption or delay is unacceptable. It is critical for applications such as industrial automation and control, autonomous vehicles, and intelligent transportation systems [7].

iii. mMTC: This is associated with communicating with a massive number of connected devices that perform low-volume data transmission and are not delay-sensitive. References [36] and [37] mentioned a target of 1 million devices per km^2 and noted that latency tolerance is high; they also mentioned that network slicing is essential for separating mMTC traffic from other traffic types. It is critical for applications such as smart cities, smart buildings, smart agriculture, and smart meters [38].

3.5.3. 5G's Core Technological Pillars and Architecture

i. New Radio (NR) and Spectrum Utilization: The first 5G NR specifications were approved by 3GPP in December 2017, paving the way for trial experiments and commercial deployment [39].

Reference [38] explained that 5G NR's flexible frame structure is designed to meet the diverse requirements (such as low latency, high speed, and efficiency) of 5G services like eMBB, URLLC, and mMTC, compared to the more rigid structure of 4G LTE. Reference [37] stated that the interoperability of the 4G RAN architecture with the new radio access technology is an important design requirement.

ii. 5G Core Network (5GC): The Center of Flexibility and Intelligence: In 5G, network functions are partitioned based on their services and communicate with each other via a service-based interface [40]:

- Core Access and Mobility Management Function (AMF): It has functions such as access, authentication and authorization, registration management, mobility management, session management function (SMF) selection, and arrangement of network slice selection [36, 41].
- SMF: It is responsible for session management, IP allocation for users, enforcement of user subscription policies, and control of quality of service (QoS) [41, 42].

- User Plane Function (UPF): It is responsible for functions such as packet routing and forwarding, packet inspection of traffic, and traffic usage reporting [36]. It is stated that it is geographically located closer to end-users to reduce latency [41].
- Authentication Server Function (AUSF): It is the authentication server function; it enables the AMF to verify the UE [43].
- Policy Control Function (PCF): The PCF generates and decides the control framework for policies and decisions; that is, it provides the policy frameworks for roaming, network slicing, mobility management, session management, and QoS support [36, 40].
- Unified Data Management (UDM): It contains data related to the HSS; meaning it stores user subscription information; it also performs tasks such as authentication, credential handling, and user identity management [41]. It is the functional unit that takes over the main tasks of the 4G HSS for 5G. It holds and manages the subscriber's data.

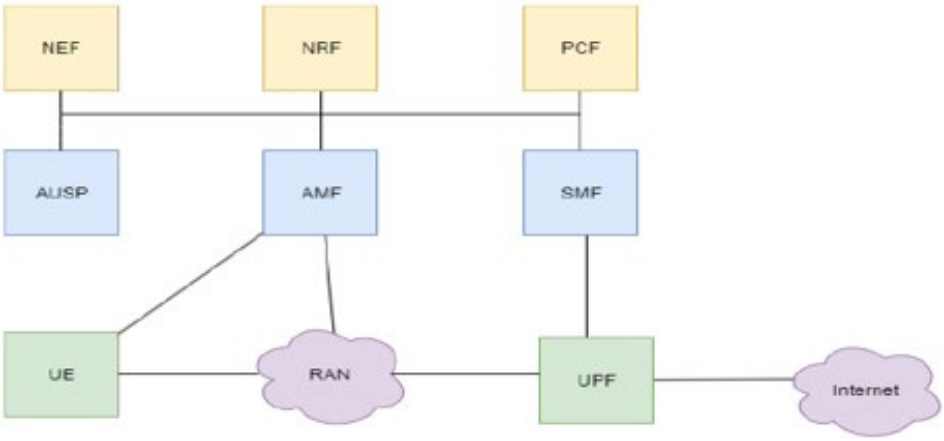

Figure 5. 5G core network [1]

3.5.4 Deployment Architectures: Standalone (SA) and Non-Standalone (NSA) Architecture

In a typical 5G NSA mode, the next generation node B (gNodeB) connects directly to the EPC via the user plane, without the need to use the next generation core (NGC), i.e., the 5G core network. Thus, the gNodeB serves as a secondary service function to boost throughput and capacity, while the eNodeB connects to the EPC to execute control plane functions. Operators can choose to leverage their existing 4G deployments by combining LTE and 5G NR to offer 5G cellular services [43].

i. SA Architecture: The 5G SA model provides both user plane and control plane functions through its connection established between the NGC and the gNodeB, and it is the ultimate long-term goal for 5G deployment across operators. It will also play a key role in fully realizing true 5G capabilities.

Consequently, NSA deployment provides a fast start for operators, while SA will deliver the full 5G experience. At the same time, the SA architecture is mandatory to support all of 5G's advanced capabilities, such as URLLC, massive connectivity (mMTC), and especially network slicing. Therefore, it is a mandatory goal that must be reached to unleash 5G's true potential.

3.6. 6G's Core Use Cases and Objectives

3.6.1. Performance Targets and KPI

Compared to 5G, 6G networks are expected to provide higher spectral, energy, and cost efficiency, higher data rates, 10 times lower latency, 100 times higher connection density, more intelligence for full automation, sub-centimeter geographical location accuracy, near 100% coverage, and time synchronization with sub-millisecond latency [44]. Furthermore, Jiang et al. specified these criteria numerically, projecting the peak data rate to reach up to 1 Tbps (ten times that of 5G), the user experienced data rate to reach 1 Gbps or more (ten times that of 5G), and latency to be reduced to 100 or even 10 μs [45]. They also projected the connection density to be improved by a factor of 10, reaching 10^7 devices per km^2.

i. Core Use Cases: In November 2023, the ITU approved the IMT-2030 objectives. References [2] and [48] addressed three new use cases for 6G with these objectives: Ubiquitous Mobile Broadband (uMBB), Ultra-reliable

low-latency broadband communications (ULBC), and massive ultra-reliable low-latency communications (mULC).

3.6.2. New Scenarios Specific to 6G

i. Integrated Sensing and Communication (ISAC): This is a revolutionary approach made possible by the presence of sensing capabilities. This can include pilot signal training, beam alignment and tracking, interference coordination, proactive resource management, and others [46]. The networks we currently use only "talk," meaning they carry data via signals; however, in 6G, much like a radar system, the radio waves will return to the base station after interacting with surrounding objects, and the network will be able to create a physical map of its environment through these returning signals. In other words, the network will become capable of seeing and sensing, in addition to just talking.

ii. Artificial Intelligence (AI) and Communication: The network, thanks to AI, is not only able to transmit data but also to recognize and understand it, allowing it to behave appropriately for changing conditions and send specialized signals to each receiver and each channel:

- Semantic Communication: Instead of a security camera transmitting the video of an "empty hallway for hours" as is, the network understands the meaning of the video and transmits only the information that "a person passed through the corridor," thereby achieving a bandwidth saving of over 99% [47].
- AI-Driven Air Interface: When the network sends data to a device, it learns how noisy the channel is. Instead of transmitting a standard signal, it sends the most efficient signal, "designed by itself," specifically for the current conditions. It essentially learns to speak to each device in its own language [48].

This means the network now operates not through static rules, but by learning and adapting.

iii. Key Technologies That Will Enable 6G: Undoubtedly, the revolutionary capabilities and advancements promised by 6G will not be possible with a single technology, but with the presence of multiple technologies working in an integrated manner.

iv. New Spectrum Technologies (THz and Visible Light Communication (VLC)): The THz band is regarded as one of the most critical technologies required to meet the exponential growth in data volume. The necessity for the THz band stems from four key advantages: its contiguous bandwidth of up to hundreds of Gigahertz (HHz), symbol duration at the picosecond level, the ability to integrate thousands of sub-millimeter length antennas, and the ease of co-existence with other regulated and standardized spectrums. Complementing this, VLC operates in the vast 400–800 THz range. This spectrum is entirely unlicensed and vacant, making it thousands of times larger than the radio spectrum and offering immense potential for reaching Tbps speeds [49].

v. Network Architecture (Space-Air-Ground Integrated Network (SAGSIN) and Zero-Touch Network and Service Management (ZSM)): We previously mentioned the SAGSIN, which integrates satellite-air-ground-sea networks. When the question of how such a large and complex network will be managed comes up, ZSM emerges [50]. The main goal of the ZSM concept is to create a network system that can configure, monitor, heal, and optimize itself without human intervention.

vi. Evaluation of the 6G Vision and Future Impacts: Hexa-X introduced key value indicator (KVI) metrics, which aim to make new key metrics like sustainability, inclusiveness, and trustworthiness the main theme instead of traditional KPI metrics, and also seek to measure success based on the question, "how beneficial is it to society?" [8]. Considering these metric changes, we can draw some conclusions about the 6G vision. Up to 6G, technology-focused goals were set, and success was measured by achieving these engineering targets; the benefit of these achievements to society and the environment was considered an indirect benefit. However, upon reaching 6G, the metrics are now directly related to the environment and society; thus, the approach can be said to be human- and value-centric.

3.7. Comparative Technical Analysis Across Generations

With 2G, it was realized how critical low bands (1 GHz) are in meeting the requirements for coverage and penetration, and this trend continued throughout 3G and 4G. However, the increasing data demand from 4G onwards showed that mid-bands (1–6 GHz) are ideally positioned in terms of the capacity–coverage balance, and these bands became central to mobile broadband services.

With 5G, a multi-layer spectrum approach was adopted for the first time; low bands began to be used for coverage, mid-bands for capacity, and high bands (mmWave) for ultra-high data speeds. This multi-layer architecture created an infrastructural transition to the future 6G networks as well.

In 6G studies, the spectrum map is expanding further. While the existing low and mid-bands are preserved with increased efficiency, the sub-THz (92–300 GHz) range is predicted to be mandatory for connections capable of reaching 1 Tbps levels. This indicates that the spectrum will no longer be merely segmented, but the unified operation of multiple frequency layers will become a core capability.

Table 2. Evolution of spectrum grouping from 1G to 6G [1]

Generation	Spectrum Range	Basic Spectrum Grouping
1G	800–900 MHz	Low Band
2G (GSM/GPRS/EDGE)	800–900 MHz	Low Band
3G	2 GHz	Low-Mid Band
4G	1–6 GHz	Düşük-Orta Bant
5G (NR/IMT-2020)	Below 2 GHz, 3–6 GHz, above 24 GHz	Multi-Layered Approach
6G	Sub-1 GHz, 1–24 GHz, and 24–300 GHz	Multilayer Approach with Sub-THz

The data in the graph concretely reveals the mobile networks' transition from human-centric communication to machine-centric critical communication. While 4G LTE networks were optimized for the 30-50 ms band, which is sufficient for human perception, the 5G and 6G vision targets sub 1 ms latency required for the Tactile nternet and collaborative robots (cobots). The 1 ms end-to-end (E2E) target specified in the table validates the necessity of a new cyber-physical system (CPS) infrastructure where physical transmission limits are pushed, and processing and transmission times are minimized.

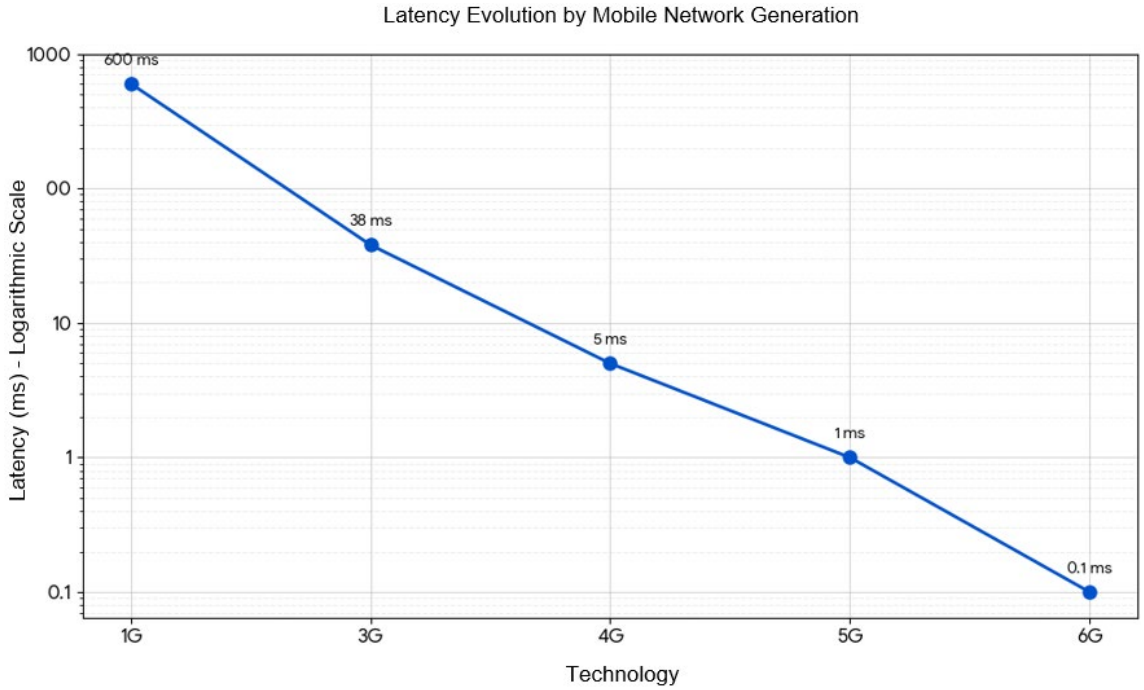

Figure 6. Evolution of latency across mobile network generations

When examining the evolution of mobile communication technologies, the increase in spectral efficiency is observed to follow an exponential trend alongside technological leaps, rather than a linear one. Notably, the efficiency leap initiated by the integration of OFDM and MIMO technologies during the transition from 3G to 4G is being maximized in 5G and the targeted 6G standards through Massive MIMO and Terahertz (THz) communication techniques. As seen in the graph, the value of 100 bit/s/Hz targeted under the IMT-2030 (6G) vision represents an approximately 200-fold increase in capacity compared to early digital networks (2G). This confirms that future networks will evolve into a "hyper-connected" structure, capable of accommodating significantly more devices within the same bandwidth, not just providing higher speeds.

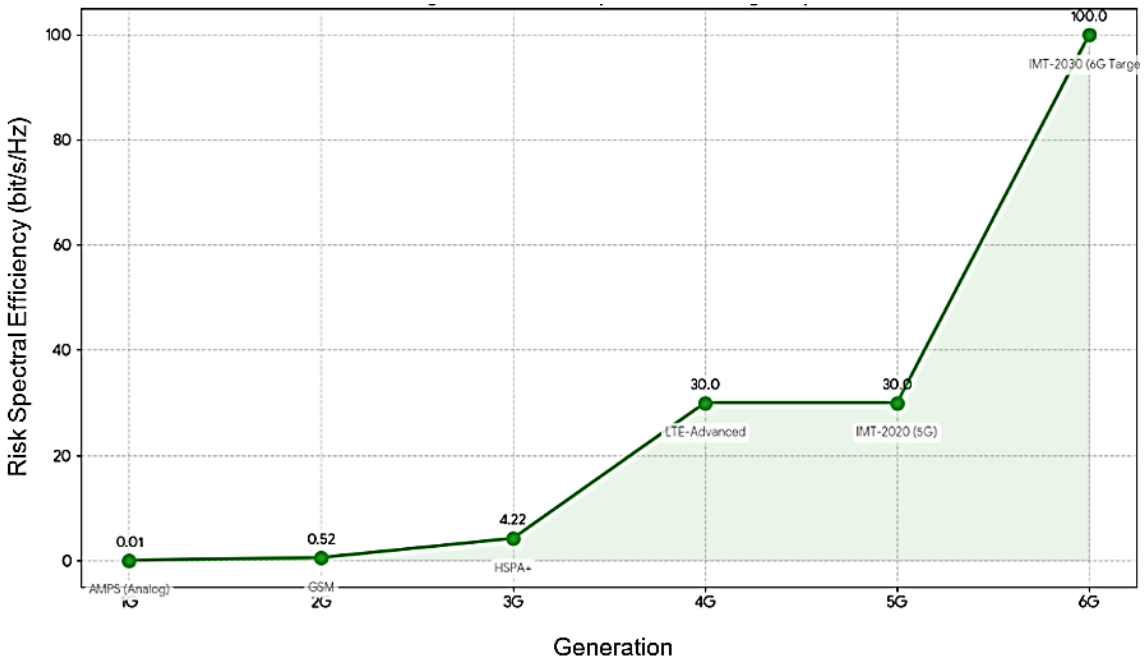

Figure 7. Spectral efficiency in mobile network generations [5, 25, 26]

When examining the average monthly data consumption per subscriber in Türkiye in light of BTK data, it is evident that demand is increasing at an exponential rate. The average consumption, which was only 1.4 GB in 2015 before the 4.5G era, began an upward trend with the widespread adoption of 4.5G in 2016 and reached 16.8 GB as of 2024.

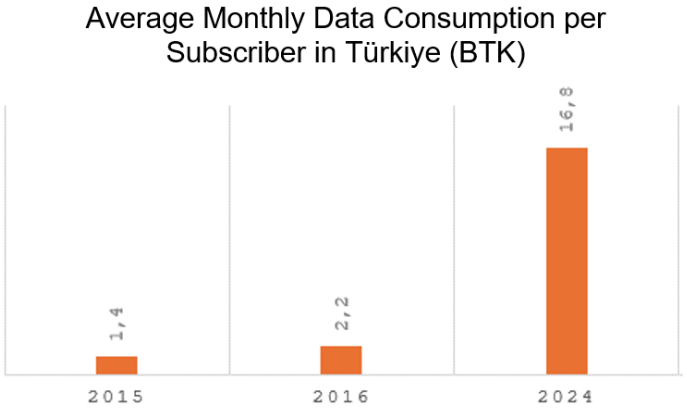

Figure 8. Monthly average data consumption per subscriber in Türkiye [27–29]

The 12-fold increase in data consumption observed during this approximately 9-year period is the most concrete indicator of why existing spectr cum resources must be used more efficiently. This situation proves that new-generation technologies (5G and 6G) that will enhance spectral efficiency are not a luxury but a necessity for network sustainability.

4. CONCLUSION

The evolution of mobile communication technologies from 1G to the emerging vision of 6G reflects a steady transition from analog, hardware-driven systems to software-defined, fully IP-based and increasingly intelligent architectures. While the early generations focused mainly on voice transmission and basic mobility, the shift to packet-based data with 3G matured significantly in 4G/LTE, where a simplified, flat architecture enabled high speeds and low latency as standard features. With 5G, mobile networks have moved beyond being merely faster systems and have become flexible platforms capable of supporting diverse service types through features such as network slicing and virtualization.

Expectations for 6G go even further and aim to redefine the role of communication networks themselves. In addition to targeting terabit-class data rates and microsecond-level latency, 6G envisions networks that can sense their environment (ISAC), self-optimize through native AI, and seamlessly integrate the physical and digital worlds. This perspective marks a shift toward an era in which the success of mobile communication is measured not only by technical performance but also by criteria such as sustainability, reliability, and human-centered value.

References

[1] E. Zontou, "Unveiling the evolution of mobile networks: From 1G to 7G," *arXiv*, Oct. 2023. doi: 10.48550/arXiv.2310.19195

[2] W. Jiang and B. Han, *Cellular Communication Networks and Standards*, Springer, 2024.

[3] C. E. Shannon, "A Mathematical Theory of Communication," *Bell System Technical Journal*, vol. 27, no. 3, pp. 379–423, 1948.

[4] M. H. Mahmud, "Cellular mobile technologies (1G to 5G) and massive MIMO," *Int. J. Sci. Res.*, vol. 8, no. 7, pp. 929–937, 2019. doi: 10.21275/ART20199494

[5] J. A. del Peral-Rosado, R. Raulefs, J. A. López-Salcedo, and G. Seco-Granados, "Survey of cellular mobile radio localization methods: From 1G to 5G," *IEEE Commun. Surveys Tuts.*, vol. 20, no. 2, pp. 1124–1148, 2017. doi: 10.1109/COMST.2017.2785181

[6] F. B. Saghezchi, J. Rodriguez, S. Mumtaz, A. Radwan, W. C. Y. Lee, B. Ai, et al., "Drivers for 5G," in *Fundamentals of 5G Mobile Networks*, J. Rodriguez, Ed.: Wiley, 2015, pp. 1–27.

[7] ITU-R, *Recommendation ITU-R M.2083–0: IMT Vision*, 2015.

[8] M. A. Uusitalo, P. Rugeland, M. R. Boldi, E. C. Strinati; P. Demestichas, and M. Ericson, "6G vision, value, use cases and technologies from european 6G flagship project hexa-X," *IEEE Access*, vol. 9, pp. 160004–160020, 2021.

[9] *ETSI TS 125 101 V10.1.0: Universal mobile telecommunications system (UMTS); user equipment (UE) radio transmission and reception (FDD) (3GPP TS 25.101 version 10.1.0 Release 10)*, ETSI Standard, May 2011.

[10] *ETSI TS 145 005 V15.1.0: Digital cellular telecommunications system (Phase 2+) (GSM); GSM/EDGE Radio transmission and reception (3GPP TS 45.005 version 15.1.0 Release 15)*, ETSI Standard, Oct. 2018.

[11] *ETSI TS 145 001 V17.0.0: Digital cellular telecommunications system (Phase 2+) (GSM); GSM/EDGE Physical layer on the radio path; General description (3GPP TS 45.001 version 17.0.0 Release 17)*, ETSI Standard, May 2022.

[12] ETSI TR 125 912 V18.0.0 (2024-05) Universal Mobile Telecommunications System (UMTS); LTE; Feasibility study for evolved Universal Terrestrial Radio Access (UTRA) and Universal Terrestrial Radio Access Network (UTRAN) (3GPP TR 25.912 version 18.0.0 Release 18)

[13] *3GPP TS 23.060 V7.11.0: General Packet Radio Service (GPRS); Service description; Stage 2 (Release 7)*, Technical Specification, June 2011.

[14] Bilgi Teknolojileri ve Haberlesme Kurumu (Sektorel Rekabet Bolumu). (2015). *Elektronik haberlesme sektoru 3 aylik veriler raporu: 2015 – 1. ceyrek* [Online]. Available: https://www.bthk.org

[15] Bilgi Teknolojileri ve Haberlesme Kurumu (Sektorel Rekabet Bolumu). (2016). *Elektronik haberlesme sektoru 3 aylik veriler raporu: 2016 – 1. ceyrek* [Online]. Available: https://www.bthk.org

[16] Bilgi Teknolojileri ve Haberlesme Kurumu (Sektorel Rekabet Bolumu). (2024). *Elektronik haberlesme sektoru 3 aylik veriler raporu: 2024 – 3. ceyrek* [Online]. Available: https://www.bthk.org

[17] B. I. Bakare and E. E. Bassey, "A comparative study of the evolution of wireless communication technologies from the first generation (1G) to the fourth generation (4G)," *Int. J. Electron. Commun. Comput. Eng.*, vol. 12, no. 3, Jul. 2021.

[18] W. R. Young, "Advanced mobile phone service: Introduction, background, and objectives," *Bell Syst. Tech. J.*, vol. 58, no. 1, pp. 1–14, 1979.

[19] J. Lehenkari and R. Miettinen, "Standardisation in the construction of a large technological system: The case of the nordic mobile telephone system," *Telecommun. Policy*, vol. 26, no. 3, pp. 109–127, 2002. doi: 10.1016/S0308-5961(02)00004-6

[20] D. Forsberg, G. Horn, W.-D. Moeller, and V. Niemi, *LTE Security*, 2nd ed. Chichester, U.K.: Wiley, 2013.

[21] H. Soy, O. Ozdemir, and M. Bayrak, "Future generation mobile communication systems: 3G, 4G and beyond," in *Academic Informatics 2012 Proceedings*, Usak, Türkiye, Feb. 2012, pp. 211–218.

[22] A. Dinckan, "Security in GPRS systems," M.S. thesis, Yildiz Technical University, Istanbul, Türkiye, 2006.

[23] A. Matam, "A survey on evolution of wireless technologies and the use of wireless technologies in tele audiology," *Int. Res. J. Eng. Sci. Technol. Innov.*, vol. 7, no. 5, pp. 1–2, 2021.

[24] P. M. Mendes, T. Sousa, V. Pereira, and E. Monteiro, "Evaluation of mobile communications: From voice calls to ubiquitous multimedia group communications," in *Proc. Performance Modeling and Evaluation of Heterogeneous Networks Conf.*, 2004.

[25] A. H. Khan, M. A. Qadeer, J. A. Ansari, and S. Waheed, "4G as a next generation wireless network," in *Proc. ICFCC*, 2009, pp. 334–338. doi: 10.1109/ICFCC.2009.108.
[26] T. J. Seymour and A. Shaheen, "History of wireless communication," *Rev. Bus. Inf. Syst.*, vol. 15, no. 2, pp. 37–42, 2011. doi: 10.19030/rbis.v15i2.4202
[27] L. J. Vora, "Evolution of mobile generation technology: 1G to 5G and review of upcoming wireless technology 5G," *Int. J. Mod. Trends Eng. Res.*, vol. 2, no. 10, pp. 281–290, 2015.
[28] R. Patel and V. Sah, "Evolution & envisage of mobile network," *Int. J. Sci. Eng. Technol. Res.*, vol. 3, no. 1, pp. 136–143, 2014.
[29] Kornelakis, "Implementation and testing of the 3GPP PCC architecture in a 4G-LTE lab environment," M.S. thesis, Univ. of Piraeus, 2016.
[30] J. Agrawal, R. Patel, P. Mor, P. Dubey, and J. M. Keller, "Evolution of mobile communication network: From 1G to 4G," *Int. J. Multidiscip. Current Res.*, vol. 3, pp. 1100–1104, 2015.
[31] D. Xenakis, N. Passas, L. Merakos, and C. Verikoukis, "Mobility management for femtocells in LTE-advanced," *IEEE Commun. Surveys Tuts.*, vol. 16, no. 1, pp. 64–91, 2014.
[32] J. Zhang, S. L. Ariyavisitakul, and M. Tao, "LTE-advanced and 4G wireless communications," *IEEE Commun. Mag.*, vol. 50, no. 2, pp. 102–103, 2012.
[33] P. Kanani, K. Shah, and V. Kaul, "A survey on evolution of mobile networks: 1G to 4G," *Int. J. Eng. Sci. Res. Technol.*, vol. 3, no. 2, pp. 803–810, 2014.
[34] E. Guo, J. Lin, and Y. Zhang, "The performance analysis of LTE network," ENSC 427 Project, Simon Fraser Univ., 2014.
[35] S. Sadjina, C. Motz, T. Paireder, M. Huemer, and H. Pretl, "A survey of self-interference in LTE-advanced and 5G NR transceivers," *IEEE Trans. Microw. Theory Tech.*, 2020.
[36] O. T. Eluwole, N. Udoh, M. Ojo, C. Okoro, and A. J. Akinyoade, "From 1G to 5G, what next?," *IAENG Int. J. Comput. Sci.*, vol. 45, no. 3, 2018.
[37] D. Jiang and G. Liu, "An overview of 5G requirements," in *5G Mobile Communications*, Springer, 2017.
[38] S. Akhila and Hemavathi, "5G ultra-reliable low-latency communication," B.M.S. College of Engineering, 2023.
[39] Y. Huo, X. Dong, W. Xu, and M. Yuen, "Cellular and WiFi co-design for 5G user equipment," in *Proc. 5GWF*, 2018.
[40] D. S. Duhan, J. K. Verma, Manoj, and U. Shrivastava, "A study on 5G technology," in *Proc. ComPE*, 2021.
[41] S. Behrad, E. Bertin, and N. Crespi, "A survey on authentication and access control for mobile networks," *Ann. Telecommun.*, vol. 74, pp. 593–603, 2019.
[42] J. Lee, S.-J. Moon, B. Bae, and J. Lee, "Local area data network for 5G system architecture," in *Proc. 5GWF*, 2018.
[43] C. S. Choudhari, "Deployment of 5G core for 5G private networks," in *Proc. I4Tech*, 2022.
[44] X. Wang, S. Mao, and M. X. Gong, "A survey of LTE Wi-Fi coexistence in unlicensed bands," *GetMobile*, vol. 20, no. 3, pp. 17–23, 2016.
[45] W. Jiang, B. Han, M. A. Habibi, and H. D. Schotten, "The road towards 6G: A comprehensive survey," *IEEE Open J. Commun. Soc.*, vol. 2, pp. 334–366, 2021.
[46] M. Malatji, "A strategic overview of 5G/6G networks," in *Proc. ICEET*, 2024.
[47] Z. Qin, X. Tao, J. Lu, W. Tong, and G. Y. Li, "Semantic communications: Principles and challenges," *arXiv*, 2022. doi: https://doi.org/10.48550/arXiv.2201.0138
[48] J. Hoydis, F. A. Aoudia, A. Valcarce, and H. Viswanathan, "Toward a 6G AI-native air interface," *IEEE Commun. Mag.*, vol. 59, no. 5, pp. 76–81, 2021.
[49] N. Chi, Y. Zhou, Y. Wei, and F. Hu, "Visible light communication in 6G," *IEEE Veh. Technol. Mag.*, vol. 15, no. 4, pp. 93–102, 2020.
[50] M. Liyanage, Q.-V. Pham, K. Dev, S. Bhattacharya, P. K. R. Maddikunta, T. R. Gadekallu, et al. "A survey on zero touch network and service management," *J. Netw. Comput. Appl.*, vol. 203, art. no. 103362, 2022.

2nd International Conference on Multidisciplinary Sciences and Technological Developments (ICMUSTED 2025)

December 12-15, 2025

Design and Analysis of Metamaterial Absorber for Microwave X-Band Applications

Yunus Kaya[1], Mehmet Ertugrul[2]

[1]Department of Electronics and Automation, Bayburt University, 69010 Bayburt, Türkiye
[2]Department of Metallurgy and Materials Engineering, Karadeniz Technical University, 61080 Trabzon, Türkiye
Corresponding author: Yunus Kaya (e-mail: ykaya@bayburt.edu.tr)

Abstract

In this study, a new metamaterial (MM) absorber has been designed for microwave X-band (8–12 GHz frequency range) applications. The suggested MM absorber structure consists of a uniquely designed copper metasurface, an FR-4 dielectric substrate, and a copper ground plane. The simulations performed show that the suggested MM absorber provides a 99.97% absorption rate at a frequency of 10.293 GHz under normal incidence (0°). In addition, the FR-4 dielectric substrate used in the suggested MM absorber is quite thin, with a thickness of 0.7 mm. The suggested MM absorber design, with its compact design and simulated strong absorption performance, will find an important place in many microwave X-band applications, from radar systems to stealth technology and communication devices.

Keywords: Metamaterial, Absorption, X-band

1. INTRODUCTION

The Salisbury screen absorber, developed by Salisbury in 1952, was the first simple planar absorber [1]. Following the Salisbury screens, a wide variety of absorber structures have been developed to meet various operational requirements, including Jaumann layers and Dallenbach layers [2]. Today, the concept of electromagnetic (EM) metamaterial (MM) absorbers, which do not exist in nature and are artificially designed and manufactured, has been developed due to reasons such as their thin structures, simple designs, and wide operating bandwidths [3, 4]. These MM absorbers are widely used in wireless communications, radar cross section (RCS) reduction, EM compatibility, and EM interference [3, 5–7].

Following the publication of an excellent MM absorber study by Landy et al., which achieved good microwave absorption by reducing the reflection ratio of incoming microwaves using the absorber's dielectric and ohmic losses, MM-based absorber designs were rapidly designed and produced [5, 7–9]. In this study, an MM absorber is suggested for microwave X-band (8–12 GHz frequency range) applications. The suggested absorber consists of a 0.7 mm thick FR-4 substrate, a ring on the substrate, a '+' shaped resonator inside the ring, and a metasurface (MS) design consisting of square resonators at the four ends of the resonator, as well as a ground plane behind the substrate. Detailed information about the design and a summary of absorption theory are provided in Section 2. Additionally, the suggested MM absorber design and simulations in the microwave X-band were performed using the Computer Simulation Technology (CST) Microwave Studio EM simulation program, and the performance data for these simulations are provided in Section 3. A summary of the results of our study is provided in Section 4.

2. MATERIAL AND METHOD

This section first provides detailed information about the suggested MM absorber structure and geometry, and then summarizes the absorption theory using the absorption equation.

2.1. Suggested Absorber Structure

The three-dimensional (3D), front, and side views of the suggested absorber geometry for microwave X-band applications are shown in Figures 1(a)–1(c). The suggested MM absorber, which consists of copper (with electrical conductivity $\sigma = 5.8\times10^7$ S/m) MS design, thin (0.7 mm thick) FR-4 dielectric substrate (with a relative dielectric constant $\varepsilon_r = 4.3$ and loss tangent $\tan\delta = 0.025$) and copper ground plane, was configured by means of CST Microwave Studio EM simulation program. MS consists of a ring, a '+' shaped resonator within this ring, and a

square resonator at each of the four ends of the resonator. The lengths of the suggested MM absorber design geometry shown in Figure 1 are summarized in Table 1.

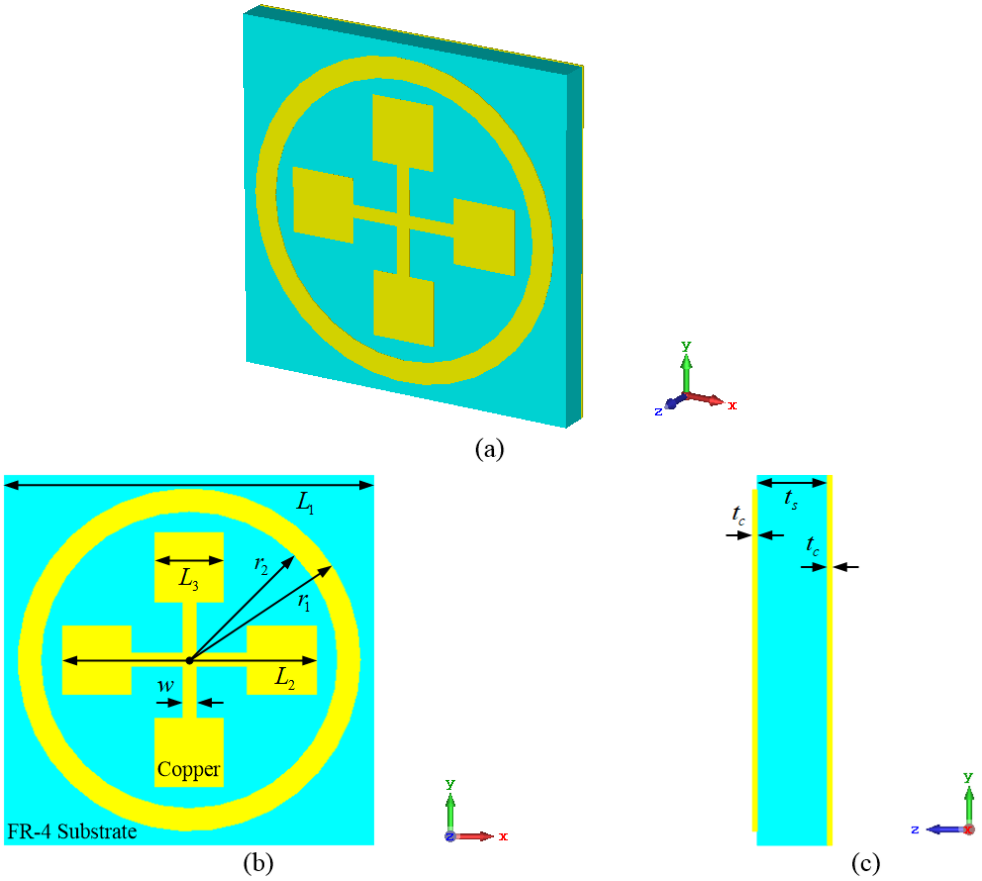

Figure 1. The suggested absorber's (a) 3D, (b) front, and (c) side views

Table 1. Lengths of the design geometry of the suggested absorber

r_1	r_2	L_1	L_2	L_3	w	t_s	t_c
3.7 mm	3.2 mm	8 mm	5.5 mm	1.5 mm	0.3 mm	0.7 mm	35 µm

2.2. Absorption Equation

When an EM wave reaches a surface, it is both transmitted and reflected from the surface. The absorbed power $\left(A(\omega)\right)$ is calculated as follows, where the power of the reflected wave is denoted as $R(\omega)$ and the power of the transmitted wave is denoted as $T(\omega)$ [4, 5, 8].

$$A(\omega) = 1 - R(\omega) - T(\omega) \tag{1}$$

As can be seen from Equation (1), for maximum absorption (i.e., 100%), the reflected and transmitted power must approach zero. $R(\omega) = \left|S_{11}(\omega)\right|^2$ and $T(\omega) = \left|S_{21}(\omega)\right|^2$, where $S_{11}(\omega)$ and $S_{21}(\omega)$ are the reflection and transmission scattering (*S*-) parameters, respectively [5]. Here, |*| indicates the magnitude of '*'. Accordingly, the expression of the absorbed power in Equation (1) can be written in the form of *S*-parameters as follows.

$$A(\omega) = 1 - \left|S_{11}(\omega)\right|^2 - \left|S_{21}(\omega)\right|^2 \tag{2}$$

In our suggested design in Figure 1, a unique MS shape was created on the front part of the substrate, while the back part was grounded with a copper plate. Therefore, the $S_{21}(\omega)$ parameter in Equation (2) can be neglected [7, 10].

3. PERFORMANCE OF THE SUGGESTED ABSORBER

In order to evaluate the absorption performance of the MM absorber suggested in Figure 1, simulations were carried out using the CST Microwave Studio EM simulation program by selecting the boundary conditions as 'unit cell' along the *x*- and *y*-axes and 'open (add space)' along the *z*-axis, applying floquet ports according to the *z*-direction, and selecting the tetrahedral mesh type in the frequency domain. The amplitudes of the reflection, transmission, and absorption parameters ($|S_{11}(\omega)|$, $|S_{21}(\omega)|$, and $A(\omega)$, respectively) obtained from simulations performed at microwave X-band frequencies under normal incidence (0°) are plotted together in Figure 2.

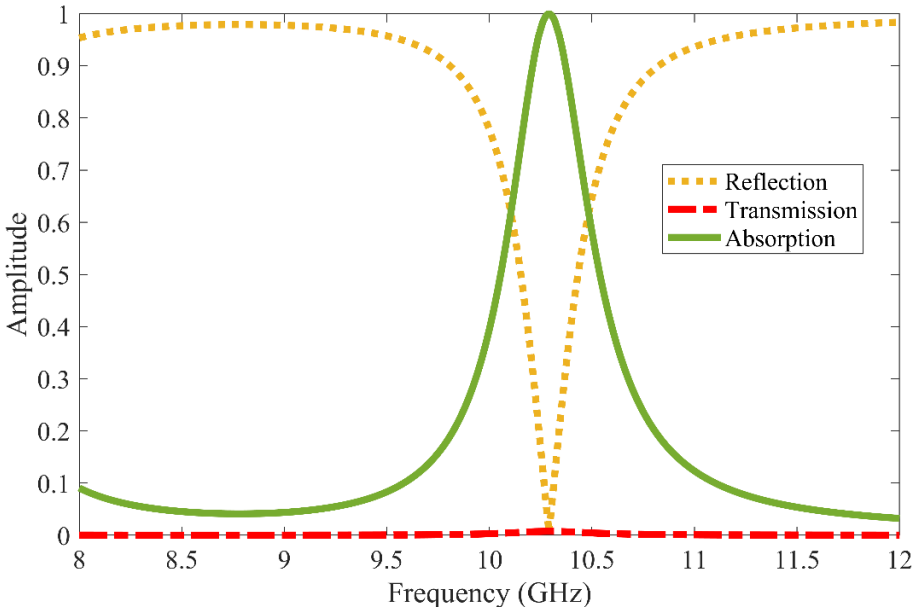

Figure 2. Reflection $\left(|S_{11}(\omega)|\right)$, transmission $\left(|S_{21}(\omega)|\right)$, and absorption ($A(\omega)$) amplitudes of the suggested MM absorber

When Figure 2 is examined, it is seen that the transmission in the microwave X-band is almost zero at all frequency points, whereas the reflection is approximately zero at 10.293 GHz and the absorption at this frequency point is 0.9997 (i.e., 99.97% absorption rate). In future studies, additions, deductions, resizing, etc. can be made to the MS, or optimization techniques can be used to improve the absorber's performance (absorption bandwidth, number of resonance frequencies, etc.). Additionally, the suggested MM absorber can be verified with real-time measurements in subsequent stages.

4. CONCLUSION

In this study, a new MM absorber characterized by a single resonance peak (at 10.293 GHz) in the microwave X-band under normal incidence (0°) and offering strong absorption performance (with a 99.97% absorption rate) was designed and its performance analyzed. A new MS structure designed on inexpensive and readily accessible FR-4 substrate and an MM absorber consisting of a copper ground plane behind the FR-4 substrate can be used in microwave X-band applications with its strong absorption performance and thin structure.

References

[1] J. M. Woo, M. S. Kim, H. W. Kim, and J. H. Jang, "Graphene based salisbury screen for terahertz absorber," *Appl. Phys. Lett.*, vol. 104, no. 8, art. no. 081106, Feb. 2014.

[2] B. A. Munk, *Frequency Selective Surfaces: Theory and Design*, John Wiley & Sons, 2000.

[3] A. T. Matei, A. I. Visan, and G. F. Popescu-Pelin, "Design and processing of metamaterials," *Cryst.*, vol. 15, no. 4, art. no. 374, Apr. 2025.

[4] M. R. Soheilifar, R. A. Sadeghzadeh, and H. Gobadi, "Design and fabrication of a metamaterial absorber in the microwave range," *Microwave Opt. Technol. Lett.*, vol. 56, no. 8, pp. 1748–1752, Aug. 2014.

[5] K. H. M. Naik, A. K. Singh, and D. R. Krishna, "Ultrathin wideband low profile circuit analog metamaterial absorber," *Microwave Opt. Technol. Lett.*, vol. 66, no. 7, art. no. e34247, Jul. 2024.

[6] H. Zhai, K. Zhang, S. Yang, and D. Feng, “A low-profile dual-band dual-polarized antenna with an AMC surface for WLAN applications,” *IEEE Antennas Wirel. Propag. Lett.*, vol. 16, pp. 2692–2695, 2017.
[7] P. P. Zuo, T. W. Li, M. J. Wang, H. X. Zheng, and E. P. Li, “Miniaturized polarization ınsensitive metamaterial absorber applied on EMI suppression,” *IEEE Access*, vol. 8, pp. 6583–6590, 2020.
[8] N. I. Landy, S. Sajuyigbe, J. J. Mock, D. R. Smith, and W. J. Padilla, “Perfect metamaterial absorber,” *Phys. Rev. Lett.*, vol. 100, no. 20, art. no. 207402, May. 2008.
[9] Y. Zhang, X. Wang, S. H. Yang, J. Y. Zhang, Y. Z. Gao, and Z. Li, “Ultrabroadband microwave metamaterial absorber with dielectric lossy layer,” *Sci. Rep.*, vol. 15, no. 1, art. no. 12547, Apr. 2025.
[10] Y. Ra’di, C. R. Simovski, and S. A. Tretyakov, “Thin perfect absorbers for electromagnetic waves: Theory, design, and realizations,” *Phys. Rev. Appl.*, vol. 3, no. 3, art. no. 037001, Mar. 2015.

2nd International Conference on Multidisciplinary Sciences and Technological Developments (ICMUSTED 2025)

December 12-15, 2025

Multi-Band and Inexpensive Linear and Circular Polarization Converter Using a Single-Layer Reflective Metasurface

Yunus Kaya[1], Ugur Cem Hasar[2]

[1]Department of Electronics and Automation, Bayburt University, 69010 Bayburt, Türkiye
[2]Department of Electrical and Electronics Engineering, Gaziantep University, 27310 Gaziantep, Türkiye
Corresponding author: Yunus Kaya (e-mail: ykaya@bayburt.edu.tr)

Abstract

This paper presents a multi-functional reflective metasurface (MS)-based polarization converter (PC) design. The design is suggested as a single-layer structure consisting of a 1.6 mm thick, inexpensive, and readily available FR-4 substrate in the middle, a copper MS design on top, and a copper ground plane on the bottom. The MS-based PC was designed in CST Microwave Studio, and simulations were performed in microwave S-, C-, X-, Ku-, and K-bands (2–4 GHz, 4–8 GHz, 8–12 GHz, 12–18 GHz, and 18–27 GHz, respectively, for a total frequency range of 2–27 GHz). Based on the calculations and analyses performed according to the simulation results, the suggested PC exhibits linear polarization (LP) conversion with a polarization conversion ratio (PCR) value of over 90% at 4.62 GHz in the microwave C-band, in the frequency ranges of 9.63–10.11 GHz and 11.04–11.58 GHz in the microwave X-band, in the frequency range of 14.52–15.36 GHz in the microwave Ku-band, and in the frequency ranges of 19.26–19.74 GHz and 23.58–24.18 GHz in the microwave K-band, adn also demonstrates circular polarization (CP) conversion in the frequency range of 20.87–22.21 GHz in the microwave K-band and in the frequency ranges of 12.25–13.63 GHz and 26.06–26.08 GHz in the microwave Ku-band. The suggested MS-based PC is suitable for use in technologies such as stealth, sensing, sensor, communication with its operation in microwave C-, X-, Ku-, and K-bands, multi-function (both LP and CP conversion feature), LP conversion in five frequency bands (and also at one frequency point), and CP conversion in three frequency bands with high efficiency.

Keywords: Metasurface, Polarization converter, Linear, Circular, Multi-band

1. INTRODUCTION

Polarization, which plays an important role in electromagnetic (EM) waves, indicates the direction of the oscillating electric field in a plane perpendicular to the wave's propagation [1]. Manipulating the polarization of an EM wave plays an important role in many applications, such as EM stealth, detection, antenna gain enhancement, and radar cross-section reduction [2, 3]. Traditional materials formed naturally exhibit polarization modulation due to their structure, but their use, especially in practical and miniaturized applications, is limited by high power losses, limited bandwidths, and large volumes [4]. Metasurfaces (MSs), which are two-dimensional planar versions of metamaterials designed artificially and attracting the attention of many researchers today due to their extraordinary properties, are widely used in the design of compactly designed polarization converters (PCs) [4, 5].

Researchers have developed PCs that operate at various frequency ranges, such as microwave [2], terahertz [6], visible [7], and infrared [8] frequencies. In recent years, multi-functional PCs have been suggested rather than PCs that exhibit only linear polarization (LP) or only circular polarization (CP) conversion [9]. Additionally, many researchers have developed MSs that can change the polarization of the incident EM wave in transmission or reflection type. Transmissive type PCs are manufactured with a multi-level structure compared to reflective types [10]. Therefore, their production processes are more difficult compared to reflective types. Because of this,, reflection type PCs are generally preferred because higher efficiency can be achieved thanks to the full reflection of incident EM waves [11]. Reflective PCs are manufactured on metal-supported dielectric layers that have a significant effect at the resonance frequency and also restrict the transmission of EM waves [12].

In this paper, single-layer, multi-band PC using a reflective type new MS is suggested that exhibits both LP (in five frequency bands (and also at one frequency point)) and CP (in three frequency bands) characteristics. The suggested PC was designed in CST Microwave Studio (MWS), simulations were performed in the 2–27 GHz frequency range, and the PC's performance was evaluated based on the obtained data.

2. UNIT CELL DESIGN

Figure 1 shows the suggested single-layer reflective MS unit cell for multi-band linear and circular polarization in three-dimensional (3D). The unit cell design consists of an inexpensive and readily available FR-4 substrate in the middle, with a thickness of t_s = 1.6 mm, a relative dielectric constant ε_r = 4.3, a loss tangent tanδ = 0.025, a square shape, and a side length of L_1 = 10 mm. The top MS pattern and bottom metallic ground plane (which completely reflects EM waves) are selected from copper with a conductivity of $\sigma = 5.8\times10^7$ S/m and a thickness of t_c = 35 µm. For the MS pattern, a square patch with a side length of L_2 = 5.5 mm was inserted into a circular ring with an outer radius of r_1 = 4.9 mm and an inner radius of r_2 = 4.4 mm, and a square cavity with a side length of L_3 = 1.5 mm was remove from the center of this patch. Subsequently, a patch with a width of g = 0.5 mm, passing through the center of the copper structure and rotated 45° clockwise with respect to the y-axis, was remove from this copper structure created at the front, and finally the suggested MS was formed. All these dimensional parameters in the design were determined by optimization.

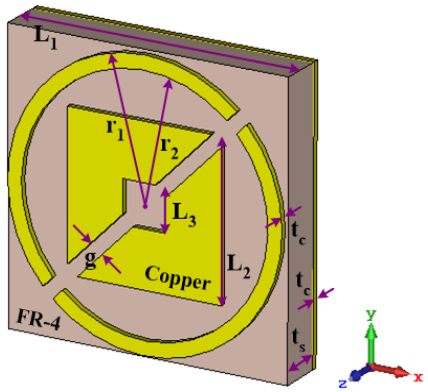

Figure 1. 3D representation of a suggested single-layer reflective MS unit cell for multi-band linear and circular PCs

3. SIMULATIONS AND PERFORMANCE ANALYSIS

Simulations for the suggested multi-band PC design and numerical analysis were performed using CST MWS, an EM field simulation software. In CST MWS, boundary conditions are defined as unit cells in the x- and y-planes, while a Floquet port is used for excitation in the z-direction.

For a y-polarized (transverse magnetic (TM) mod) incident wave, the co- and cross-polarized reflection coefficients (r_{yy} and r_{xy}, respectively) are defined as follows [2, 6, 9, 12].

$$r_{yy} = \frac{E_{ry}}{E_{iy}} \text{ and } r_{xy} = \frac{E_{rx}}{E_{iy}} \tag{1}$$

Here, E represents the electric field, while 'r' and 'i' represent the reflected and incident electromagnetic waves, respectively. Polarization conversion ratio (PCR) is used to evaluate the LP conversion performance of a PC. For an incident wave in TM mode, the PCR value is calculated using the following formula [2, 6, 9–12].

$$PCR = \frac{\left|r_{xy}\right|^2}{\left|r_{xy}\right|^2 + \left|r_{yy}\right|^2} \tag{2}$$

Generally, an amplitude greater than 80% $\left(\left|r_{yy}\right| < 0.8\right)$ or a magnitude less than −10 dB (r_{yy} < −10 dB) is considered effective for the co-polarized reflection coefficient. In addition, an efficient performance requirement for the cross- polarized reflection coefficient is 0 dB < r_{xy} < −3 dB [12]. The CP conversion capacity of a PC is calculated as follows using the normalized ellipticity (e) value [9−11].

$$e = \frac{2\left|r_{xy}\right|\left|r_{yy}\right|\sin(\Delta\phi)}{\left|r_{xy}\right|^2 + \left|r_{yy}\right|^2} \tag{3}$$

Here, $\Delta\phi = \phi_{xy} - \phi_{yy}$, where ϕ_{yy} and ϕ_{xy} are the phases of the co- and cross-polarized reflection coefficients, respectively. If e = +1, it means $|r_{xy}| = |r_{yy}|$ and $\Delta\phi = +90°$ and the TM mode incident wave exhibits right-handed CP (RHCP) characteristics [6, 9−11]. If e = −1, then $|r_{xy}| = |r_{yy}|$ and $\Delta\phi = -90°$, and the TM mode incident wave exhibits left-handed CP (LHCP) characteristics [6, 9−11]. The effect of both the amplitude and the phase difference of the reflected waves is calculated using the axial ratio (AR) formula given below [9−11].

$$AR = \sqrt{\frac{|r_{xy}|^2 + |r_{yy}|^2 + \sqrt{|r_{xy}|^4 + |r_{yy}|^4 + 2|r_{xy}|^2 |r_{yy}|^2 \cos(2\Delta\phi)}}{|r_{xy}|^2 + |r_{yy}|^2 - \sqrt{|r_{xy}|^4 + |r_{yy}|^4 + 2|r_{xy}|^2 |r_{yy}|^2 \cos(2\Delta\phi)}}} \quad (4)$$

The AR value is used to calculate the efficiency of CP. In the CP condition, i.e., when $\Delta\phi = \pm 90°$ and $|r_{xy}| = |r_{yy}|$, the AR value is equal to 1.

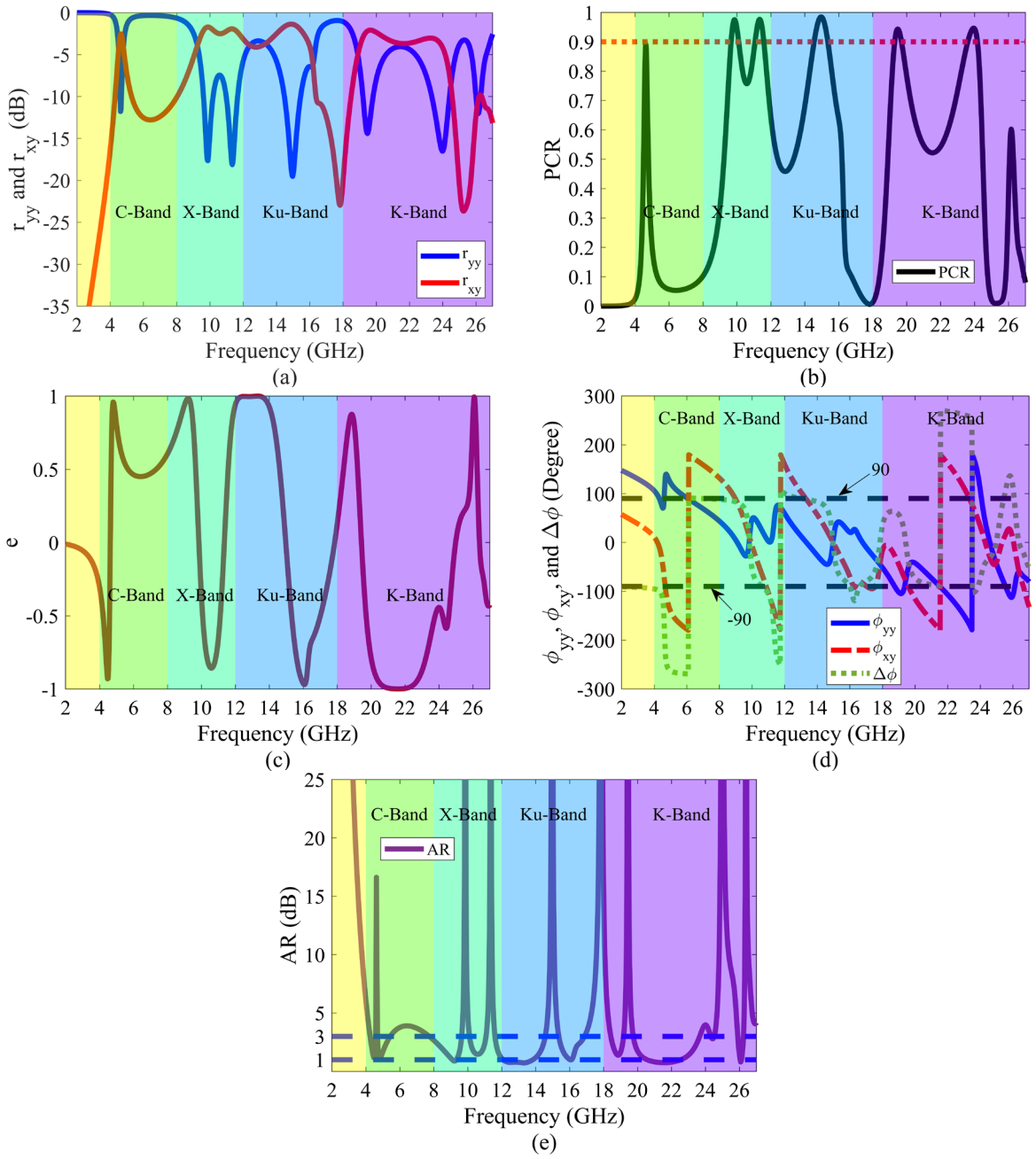

Figure 2. (a) Reflection coefficients in dB, (b) PCR values, (c) e values, (d) phases and phase differences of reflection coefficients and (e) AR values of the suggested PC in the frequency range of 2–27 GHz

To evaluate the performance of the suggested PC, the reflection coefficients, PCR values, e values, phases and phase differences of the reflection coefficients, and AR values obtained based on simulations performed in CST MWS in microwave S-, C-, X-, Ku- and K-bands (2–4 GHz, 4–8 GHz, 8–12 GHz, 12–18 GHz, and 18–27 GHz, respectively, for a total frequency range of 2–27 GHz) for the TM mode wave under normal incidence (0°) are plotted against frequency in Figure 2(a)–2(e), respectively.

When Figure 2(a)–2(e) is examined, the following conclusions can be reached. Firstly, from Figure 2(a), it can be seen that ryy is less than –10 dB at 4.62 GHz (C-band), 9.87 GHz (X-band), 11.34 GHz (X-band), 14.97 GHz (Ku-band), 19.47 GHz (K-band), 24 GHz (K-band), and 26.13 GHz (K-band), and rxy is greater than –3 dB at all resonance frequencies except the 26.13 GHz resonance frequency. Secondly, from Figure 2(b), it is determined that the PCR values are over 90% in the frequency ranges of 4.62 GHz (C-band), 9.63−10.11 GHz and 11.04−11.58 GHz (X-band), 14.52−15.36 GHz (Ku-band), 19.26−19.74 GHz, and 23.58−24.18 GHz (K-band). In other words, a y-polarized incident wave at these frequencies is reflected as an x-polarized wave over 90% and LP conversion is achieved. Thirdly, in the frequency ranges of 12.25−13.63 GHz and 26.06−26.08 GHz (Ku-band), it can be seen from Figure 2(c) that e = +1, from Figure 2(d) that $\Delta\phi$ is around +90°, and from Figure 2(e) that AR < 1 dB. Therefore, the suggested PC shows RHCP feature in the frequency ranges of 12.25–13.63 GHz and 26.06–26.08 GHz. Fourthly, in the frequency range of 20.87−22.21 GHz (K-band), it is seen from Figure 2(c) that e = −1, from Figure 2(d) that $\Delta\phi$ is around −90°, and from Figure 2(e) that AR < 1 dB. Therefore, the suggested PC shows LHCP feature in the frequency range of 20.87−22.21 GHz.

4. CONCLUSION

In summary, in this study, a single-layer, multi-band, and multi-functional (both LP and CP conversion) reflective MS-based PC operating in microwave C-, X-, Ku-, and K-bands was designed. The suggested PC, designed on an inexpensive and easily accessible 1.6 mm thick FR-4 substrate, was simulated in the CST MWS and its performance was evaluated. The suggested PC design achieves LP conversion in five frequency bands (and also at one frequency point) with high PCR values exceeding 90%, and CP conversion in three frequency bands (two exhibiting RHCP characteristics while one exhibiting LHCP characteristics) with high efficiency in terms of e and AR values. The PC suggested in this study shows promising prospects in applications such as radar systems, sensing technologies, and wireless communications.

References

[1] M. Beruete, M. Navarro-Cia, M. Sorolla, and I. Campillo, “Polarization selection with stacked hole array metamaterial,” *J. Appl. Phys.*, vol. 103, no. 5, art. no. 053102, Mar. 2008.

[2] X. Wang, X. Y. Tong, J. L. Wang, A. Saer, J. Wang, and X. Y. Han, “A polarization conversion metasurface for reducing radar cross section and enhancing radiation performance of circularly polarized array antennas,” *Opt. Commun.*, vol. 556, art. no. 130269, Apr. 2024.

[3] J. K. Huang, J. P. Yin, Z. M. Xu, and Y. Z. Li, “Polarization scattering regions: A useful tool for polarization characteristic description,” *Remote Sens.*, vol. 17, no. 2, art. no. 306, Jan. 2025.

[4] J. B. Sun and J. Zhou, “Metamaterials: The art in materials science,” *Eng.*, vol. 44, pp. 145–161, Jan. 2025.

[5] A. Adnan, A. Mitra, and B. Aissa, “Metamaterials and metasurfaces: A review from the perspectives of materials, mechanisms and advanced metadevices,” *Nanomater.*, vol. 12, no. 6, art. no. 1027, Mar. 2022.

[6] R. M. H. Bilal, M. A. Baqir, P. K. Choudhury, M. M. Ali, and A. A. Rahim, “On the specially designed fractal metasurface-based dual-polarization converter in the THz regime,” *Results Phys.*, vol. 19, art. no. 103358, Dec. 2020.

[7] Q. Ma, W. Gao, Q. Xiao, L. S. Ding, T. Y. Gao, Y. J. Zhou, et al., “Directly wireless communication of human minds via non-invasive brain-computer-metasurface platform,” *Elıght*, vol. 2, no. 1, art. no. 11, Jun. 2022.

[8] D. D. Wen, F. Y. Yue, G. X. Li, G. X. Zheng, K. L. Chan, S. M. Chen, et al., “Helicity multiplexed broadband metasurface holograms,” *Nat. Commun.*, vol. 6, art. no. 8241, Sep. 2015.

[9] J. Zafar, H. Z. Khan, A. Jabbar, J. R. Kazim, M. Ur Rehman, A. M. Siddiqui, et al., “Multi-band reflective metasurface for efficient linear and circular polarization conversion,” *Opt. Quantum Electron.*, vol. 57, art. no. 149, 2025.

[10] M. I. Khan, Y. X. Chen, B. Hu, N.Ullah, S. H. R. Bukhari, and S. Iqbal, “Multiband linear and circular polarization rotating metasurface based on multiple plasmonic resonances for C, X and K band applications,” *Sci. Rep.*, vol. 10, no. 1, art. no. 17981, Oct. 2020.

[11] R. Dutta, J. Ghosh, Z. B. Yang, and X. Q. Zhang, “Multi-band multi-functional metasurface-based reflective polarization converter for linear and circular polarizations,” *IEEE Access*, vol. 9, pp. 152738–152748, 2021.
[12] S. Hafeez, J. G. Yu, F. A. Umrani, W. Yun, and M. Ishfaq, “A multiband and multifunctional metasurface for linear and circular polarization conversion in reflection modes,” *Cryst.*, vol. 14, no. 3, art. no. 266, Mar. 2024.

Design, Prototype Production, and Testing of a 12(16) MVA 115/6.3 kV Power Transformer with Twin-Wire Transposed High-Voltage Winding for Loss Reduction

Zuhal Isikli[1]

[1]R&D Department, Beta Enerji ve Teknoloji A.S., Adana, Türkiye
Corresponding author: Zuhal Isikli (e-mail: zuhal.isikli@betaenerji.com)

Abstract

Power transformers are essential devices that enable the safe and efficient transmission of electrical energy. Their design critically affects efficiency, durability, and thermal performance. In high-voltage windings, electromagnetic imbalances and localized heating can negatively impact transformer performance. In this context, the use of twin-wire transposed windings in 12(16) MVA 115/6.3 kV power transformers represents an innovative approach to balance current distribution and reduce energy losses. Combined with disk-type winding structures, this method ensures uniform thermal distribution, enhancing thermal performance while minimizing electrical and mechanical stresses within the windings. The project aims to develop a transformer design capable of reliable and efficient operation under harsh ambient temperatures (+55 °C), while providing ease of manufacturing and assembly and maintaining cost-effectiveness. By implementing the twin-wire transposition technique, current circulation due to proximity and skin effects is reduced, and electromagnetic imbalances are minimized. This approach improves energy efficiency, maintains stable operation under high thermal stress, and provides a practical alternative to more complex designs. Overall, the design achieves a balance between performance, reliability, and economic feasibility, offering a solution suitable for demanding operating conditions. The expected outcomes include reduced winding losses, improved mechanical strength, better thermal stability, and a simplified production process compared to conventional designs, contributing to enhanced transformer performance and system-level efficiency.

Keywords: Twin-wire transposition, Power transformer, Disk winding, Thermal stability

Design, Manufacturing, and Testing of a 60 Hz Frequency Distrubition Transformer

Nadya Atakan[1]

[1]R&D Department, Beta Enerji ve Teknoloji A.S., Adana, Türkiye
Corresponding author: Nadya Atakan (e-mail: nadya.atakan@betaenerji.com)

Abstract

This study covers the design, manufacturing, and testing processes of a 1600 kVA distribution transformer with voltage levels of 0.48/0.69 kV, developed based on design criteria specific to a 60 Hz grid frequency. The higher efficiency of transformers operating at 60 Hz serves as a key motivation for this work. The higher operating frequency allows for a reduction in core size, which in turn decreases both hysteresis and eddy current losses. Therefore, frequency-based optimization strategies have been applied in determining the core material, lamination thickness, and magnetic circuit cross-section. In general, the effects of 60 Hz frequency on core and winding design are analyzed in detail, with design criteria such as minimizing loss components, improving thermal performance, and maintaining mechanical strength integrated into the design process. The project aims not only to enhance energy efficiency but also to develop optimal magnetic circuit and winding configurations that ensure the transformer's long-term and reliable operation. As a result, this study aims to present a 60 Hz-compatible distribution transformer design that is low-loss, thermally efficient, and mechanically balanced.

Keywords: Distribution transformer, 60 Hz frequency, Energy efficiency

2nd International Conference on Multidisciplinary Sciences and Technological Developments (ICMUSTED 2025)

December 12-15, 2025

Forecasting Daily Mean Temperature in Izmir Using Machine Learning Algorithms

Pelin Coskun[1], Onur Ugurlu[2], Orhan Er[2]

[1]Department of Smart Systems Engineering, Izmir Bakircay University, Izmir, Türkiye
[2]Department of Computer Engineering, Izmir Bakircay University, Izmir, Türkiye
Corresponding author: Pelin Coskun (e-mail: pelin97coskun@gmail.com)

Abstract

This study focuses on forecasting daily mean temperatures for Izmir, Turkey, using machine learning (ML) algorithms over the period 2014–2023. Three regression-based models—support vector regression (SVR), random forest (RF), and extreme gradient boosting (XGBoost)—were trained and evaluated using daily temperature data obtained from the Turkish State Meteorological Service. Model performances were compared using the mean absolute error (MAE) and coefficient of determination (R^2) metrics. According to the results, the RF model achieved the highest predictive accuracy with an R^2 of 0.89 and an MAE of 1.37 °C, outperforming both SVR and XGBoost. These findings indicate that ensemble-based approaches, particularly RF, can effectively capture the nonlinear temperature dynamics of İzmir's complex coastal climate and provide reliable short-term forecasts.

Keywords: Temperature forecasting, Machine learning (ML), Random forest (RF), Support vector regression (SVR), Extreme gradient boosting (XGBoost)

1. INTRODUCTION

The impacts of global warming and climate change have become increasingly apparent in recent decades, creating significant challenges for environmental balance, economic development, and public health. One of the most prominent indicators of these changes is the persistent increase in surface air temperatures, which affects multiple sectors including agriculture, energy, transportation, and healthcare. Accurate temperature prediction is therefore essential for effective resource management, strategic planning, and early mitigation of extreme weather events.

Temperature variability is a fundamental element of the climate system with wide-ranging consequences. Monitoring how mean temperatures change over time allows both researchers and policymakers to identify short-term variations as well as long-term climatic tendencies. In countries such as Turkey—characterized by complex topography and diverse climatic zones—temperature modeling requires not only traditional statistical tools but also advanced data-driven approaches capable of capturing nonlinear relationships.

In recent years, machine learning (ML) techniques have increasingly been utilized to model and forecast temperature dynamics using extensive meteorological datasets. Several studies in Turkey have explored ML-based modeling of meteorological parameters. Yilmaz et al. estimated long-term monthly average temperatures (1981–2020) through spatial interpolation techniques such as inverse distance weighting, kriging, and radial basis function, using observations from 81 meteorological stations [1]. Their results indicated that interpolation-based models can effectively represent spatial temperature distributions, wit. Similarly, Coskun examined potential water shortages in Bursa under different climate and population growth scenarios using ML methods [2]. The findings highlighted the value of ML models in evaluating climate-induced water scarcity. Bilgic and Elbir employed Sentinel-5P satellite data together with a random forest (RF) model to estimate hourly NO_2 concentrations over Izmir [3]. By integrating meteorological and remote sensing variables, they achieved improved prediction accuracy, demonstrating the capability of ML-based models in environmental applications.

In the present study, daily mean temperature data from the Turkish State Meteorological Service covering the period 2014–2023 were used to evaluate the predictive performance of different ML algorithms. Support vector regression (SVR), RF, and extreme gradient boosting (XGBoost) models were implemented to forecast daily temperature averages. Model accuracy was assessed through common statistical metrics, including mean absolute error (MAE) and the coefficient of determination (R^2). The findings showed that the RF model achieved the best predictive results with an R^2 of 0.894, outperforming both SVR (R^2 = 0.835) and XGBoost (R^2 = 0.857). This outcome suggests that ensemble-based learning algorithms, particularly RF, can effectively capture nonlinear

patterns in temperature data and provide reliable forecasts for regions with diverse climatic characteristics such as Turkey.

2. MATERIAL AND METHOD

ML, a core field of artificial intelligence, allows computer systems to learn from data and make predictions without explicit rule-based programming. By uncovering hidden relationships and patterns in large datasets, ML algorithms can model complex systems and forecast future trends. These techniques are widely used across domains such as meteorology, healthcare, finance, and industrial automation.

The objective of this study is to forecast daily mean temperatures using regression-based ML algorithms. Three models were implemented: SVR, RF, and XGBoost. These algorithms were selected for their capability to capture nonlinear relationships and handle noisy meteorological data. All models were trained and evaluated on the same dataset to ensure fair comparison, and their performances were measured using MAE and the R^2.

SVR is a kernel-based supervised learning algorithm that aims to identify a regression function capable of approximating the target variable within a specified tolerance margin [4]. Instead of minimizing the total error, SVR focuses on fitting as many data points as possible within this margin, thereby preventing overfitting and enhancing generalization. The algorithm relies on the concept of support vectors—data points that lie closest to the regression boundary—which play a decisive role in defining the predictive function. By employing nonlinear kernel transformations such as radial basis function, polynomial, or sigmoid kernels, SVR can project input variables into higher-dimensional feature spaces where complex and nonlinear relationships become more easily separable. This property makes SVR particularly effective for meteorological forecasting tasks, where temperature patterns often exhibit nonlinear dependencies influenced by atmospheric dynamics, topographic variations, and seasonal transitions.

RF, developed by Breiman, is an ensemble-based learning technique that combines multiple decision trees to generate a more accurate and stable prediction model [5]. Each tree in the ensemble is trained using a random subset of the training data and a random selection of input features—a process known as bootstrap aggregation or bagging. This randomization ensures model diversity, minimizes variance, and reduces the likelihood of overfitting. The final prediction in regression tasks is obtained by averaging the outputs of all trees, which significantly enhances robustness against noisy observations and outliers. RF can effectively capture nonlinear patterns and interactions among predictors without the need for explicit feature scaling or transformation. Its simplicity, interpretability through feature importance analysis, and computational efficiency have made it one of the most widely used algorithms in environmental and climate-related modeling.

XGBoost, short for extreme gradient boosting, is an advanced implementation of the gradient boosting framework designed for both efficiency and scalability [6]. Unlike RF, which builds trees independently in parallel, XGBoost constructs them sequentially, where each subsequent tree attempts to correct the errors of its predecessors. This additive learning process minimizes a differentiable loss function through gradient descent optimization, progressively refining prediction accuracy. XGBoost incorporates several improvements over traditional gradient boosting, such as regularization terms (L1 and L2) to prevent overfitting, tree pruning strategies for optimal complexity, and efficient handling of missing data. In meteorological applications, XGBoost has proven effective in identifying subtle temporal patterns and complex variable interactions, especially when atmospheric data exhibit heterogeneity or noise.

3. RESULTS

The predictive performance of the three ML models was assessed using two key metrics: The R^2 and the MAE. The comparative results are summarized in Table 1.

Table 1. Performance comparison of ML algorithms

	MAE	R^2
SVR	2.16	0.84
RF	1.32	0.89
XGB	1.96	0.86

As presented in Table 1, the RF achieved the best overall accuracy, with an R^2 value of 0.894 and an MAE of 1.37 °C, surpassing both SVR and XGBoost. The SVR yielded an R^2 of 0.835 and an MAE of 2.16 °C, while XGBoost

reached an R^2 of 0.857 and an MAE of 1.96 °C. The RF model was optimized with 300 estimators, a minimum samples split of 5, and a minimum leaf size of 2, which improved generalization and reduced bias. Similarly, the XGBoost model performed best with 200 estimators, max_depth = 3, and a learning rate of 0.2. The consistent superiority of the RF suggests that bagging-based ensemble methods capture nonlinear dependencies and complex temporal relationships more effectively than kernel-based (SVR) or boosting-based (XGBoost) algorithms.

Overall, the combination of high R^2 and low MAE values demonstrates that the RF algorithm provides the most reliable and stable temperature forecasts for the 2014–2023 period.

4. CONCLUSION

The results reveal that ML algorithms can effectively model and predict daily temperature variations in Izmir, a city that exhibits strong coastal influences, land–sea interactions, and distinct microclimatic conditions. The application of data-driven regression models to a decade of meteorological observations demonstrated that nonlinear approaches outperform traditional linear techniques in representing temporal temperature dynamics. Among the tested algorithms, the RF algorithm achieved the most accurate results, which can be attributed to its ensemble-based architecture that aggregates multiple decision trees to minimize variance and reduce overfitting. This structure allows the model to recognize complex interactions between temporal and climatic variables—patterns that are often missed by single-model or kernel-based methods such as SVR.

The strong predictive capability of RF, indicated by its high R^2 and low MAE values, highlights its suitability for handling heterogeneous meteorological data with seasonal fluctuations and noise. The findings suggest that ensemble learning algorithms, when properly tuned, can provide robust and generalizable temperature forecasts even in regions with rapidly changing atmospheric conditions. The XGBoost algorithm also performed reasonably well, showing that gradient boosting can serve as a competitive alternative in applications requiring fast computation and high scalability. However, its tendency to overfit under certain parameter configurations emphasizes the importance of careful model calibration.

Overall, this study demonstrates that ML-based methods can play a key role in enhancing the accuracy of regional temperature forecasting systems. For Izmir, such predictive capabilities are particularly valuable for urban heat management, energy demand planning, and agricultural scheduling, as well as for supporting municipal climate adaptation strategies. Future research may focus on integrating additional climatic and environmental parameters—such as humidity, wind speed, solar radiation, and atmospheric pressure—to improve model precision and extend the framework toward multivariate climate prediction. Furthermore, exploring deep learning architectures like long short-term memory (LSTM) or hybrid ensemble models could provide new insights into the temporal dependencies of temperature behavior and contribute to more resilient and adaptive forecasting systems for coastal regions.

References

[1] C. B. Yilmaz, H. Bodu, E. S. Yuce, V. Demir, and M. F. Sevimli, “Estimation of long-term average temperature (°C) values of Turkey using three different interpolation methods,” *Geomatik*, vol. 8, no. 1, pp. 9–17, 2023.

[2] S. Coskun, “2022 Investigation of climatic conditions of Bursa in terms of climate, climate and population scenarios using machine learning,” M.Sc. thesis, Bursa Uludag University, Turkey.

[3] E. Bilgic and T. Elbir, “Estimation of hourly NO2 concentrations in Izmir atmosphere using sentinel-5P satellite data and machine learning method,” *Karaelmas Journal of Science and Engineering*, vol. 15, no. 1, pp. 175–194, 2025.

[4] M. Awad and R. Khanna, “Support vector regression,” in *Efficient Learning Machines: Theories, Concepts, and Applications for Engineers and System Designers*, Berkeley, CA: Apress. 2015, pp. 67–80.

[5] L. Breiman, “Random forests,” *Machine Learning*, vol. 45, no. 1, pp. 5–32, 2001.

[6] T. Chen and C. Guestrin, “XGBoost: A scalable tree boosting system,” in *22nd ACM SIGKDD International Conference on Knowledge Discovery and Data Mining*, San Francisco, CA, USA, Aug. 2016, pp. 785–794.

2nd International Conference on Multidisciplinary Sciences and Technological Developments (ICMUSTED 2025)

December 12-15, 2025

Performance Evaluation of a Luenberger Observer for Sensorless FOC of BLDC Motor

Beytullah Gokoglan[1], Mustafa Tumbek[1]

[1]Department of Electrical and Electronics Engineering, Pamukkale University, Denizli, Türkiye
Corresponding author: Beytullah Gokoglan (e-mail: bgokoglan@pau.edu.tr)

Abstract

Brushless direct current (BLDC) motors are widely employed in applications ranging from electric vehicles to robotic systems due to their high efficiency, broad speed operating range, and maintenance-free structure. In field-oriented control (FOC), accurate estimation of rotor position and speed is vital for achieving high-performance torque and speed regulation. Although sensor-based methods offer high accuracy, they also introduce drawbacks such as increased cost, wiring complexity, susceptibility to faults, and sensitivity to environmental conditions. For these reasons, sensorless control strategies have become increasingly attractive in practical applications. This study examines a Luenberger observer-based FOC method for the sensorless control of BLDC motors. The Luenberger observer is preferred because its model-based structure requires low computational effort, allows straightforward implementation on control hardware, and enables explicit assessment of closed-loop stability. The mathematical model of the motor is formulated, and the observer equations required for rotor position and speed estimation are derived. MATLAB/Simulink simulations are conducted to evaluate observer performance under different speed and load conditions. At nominal speed, the rotor position mean absolute error (MAE) is 28.06° under load and 29.26° without load, with corresponding speed ripple values of 0.81% and 0.54%. In the low-speed region, the MAE is 4.99° with 3.77% speed ripple under load, and 2.16° with 9.78% ripple under no-load conditions. Under a parameter variation scenario in which stator resistance is increased by 50%, the MAE rises to 28.96° and the speed ripple to 2.06%, indicating a clear sensitivity to model uncertainties. Overall, the results demonstrate that the Luenberger observer achieves high estimation accuracy at low speeds and light loads, while its performance degrades at nominal speed and under parameter deviations. These results highlight both the strengths and limitations of the Luenberger observer and contribute meaningful insights to the literature on sensorless motor control.

Keywords: Sensorless motor control, Luenbeger observations, Field-oriented control, Brushless direct current motors

Electric Vehicle Charging Scheduling: Time Shift

Cengizhan Abay[1], Hanife Apaydin Ozkan[1]

[1]Department of Electrical and Electronics Engineering, Eskisehir Technical University, Eskisehir, Türkiye
Corresponding author: Cengizhan Abay (e-mail: cengizhanabay@gmail.com)

Abstract

Global adoption of electric vehicles (EVs) plays a critical role in achieving sustainable transportation goals. However, uncontrolled EV charging creates severe load imbalances, peak demand spikes, and voltage drops on existing power grids, particularly in residential and commercial areas. This compromises grid stability and requires additional investment in infrastructure capacity. To address these challenges, dynamic scheduling of EV charging is crucial. The main challenge of this work is to balance two conflicting objectives through optimization: first, to minimize the grid peak load, and second, to ensure timely charging. To this end, we propose a scheduling framework that takes into account EV arrival and departure times and hourly stochastic energy changes. The proposed framework dynamically determines the power allocation to individual EVs in each time zone using a linear optimization algorithm. This hour-by-hour optimization approach accommodates users by strategically shifting their charging start times. Simulations show that this method has the potential to reduce peak load by 40% compared to uncontrolled charging and reduce energy costs based on hourly fluctuating energy prices. Consequently, this dynamic scheduling solution represents a critical step for the sustainable, safe and economical integration of the EV ecosystem into the energy grid.

Keywords: Scheduling, EV charging, Optimization, Smart Grid

1. INTRODUCTION

The global shift toward sustainable transportation policies has rapidly increased the adoption of electric vehicles (EVs) in recent years, making these technologies a strategic element in achieving carbon neutrality goals. However, the rapid increase in EV penetration not only translates to a quantitative load increase (higher electricity demand) for electricity grids; it also creates a qualitatively new and challenging load profile. Traditional electricity grids and distribution infrastructures have historically been designed for relatively predictable, single-use consumption from centralized generation, and passive loads (such as residential lighting, industrial machinery, etc.). In contrast, EVs are dynamic loads with high power demands, mobility, and uncertain grid connection times. Integrating hundreds, even thousands, of high-capacity batteries into the grid presents "multifaceted technical challenges" that push the design limits of existing infrastructure. Large-scale, unplanned charging processes can disrupt the grid's instantaneous load balance, weakening system reliability.

The primary impacts of uncontrolled charging include increased peak loads, particularly during peak demand periods, overheating and overloading of regional transformers, degraded power quality, and fluctuations in the voltage profile. These impacts not only necessitate grid investments that increase operational costs but also shorten equipment lifespans, negatively impacting system resilience. Therefore, intelligent management of EV charging demand, considering grid capacity, regional load conditions, and energy market indicators, has become essential.

Based on this requirement, this study proposes an innovative and dynamic optimization approach for EV charging scheduling. The proposed model aims to reduce operating costs and grid peak loads within the context of energy tariffs, while simultaneously maximizing user satisfaction by considering hourly energy demand. This framework, built on scheduling principles, strengthens the reliability of grid integration and provides EV users with a more flexible, efficient, and stable charging experience. The following sections provide a detailed overview of the developed framework’s mathematical model, the scenarios used, and the results obtained.

1.1. Literature Review

In this section, studies on optimization methods, user satisfaction and energy management strategies for EV charging stations are examined categorically.

Some studies on EV charging scheduling optimization address the problem of EV charging scheduling, which is a balancing act between efficient use of limited resources and meeting user demands. Dolgui et al. developed deterministic models for scheduling EV charging tasks and addressed the optimization problem with parallel chargers [1]. Detailed mathematical models and algorithms for scheduling regular charging tasks are presented in the study. Multi-objective optimization approaches are widely used to address the complexity of the charge scheduling problem. Wu and Jia investigated the optimization of EV charge scheduling with wind power integration and determined optimal charging policies under stochastic power generation conditions [2]. Boubaker et al. developed a multi-objective optimization framework for EV charge/discharge scheduling in distribution networks using the red deer algorithm [3]. In this study, virtual power plant scheduling was performed considering reliability factors.

Some Studies on Artificial Intelligence and machine learning-based approaches: In recent years, artificial intelligence and machine learning techniques have played an important role in EV charging optimization. An et al. presented a deep reinforcement learning-based approach [4]. In their work, they combined long short-term memory (LSTM) networks with the multi-agent deep deterministic policy gradient (DDPG) algorithm to optimize EV charging/discharging. Xu et al. optimized the integration of regional clean energy resources with EV charging scheduling using machine learning-based demand forecasting [5]. Farhadi et al. developed a data-driven multi-objective optimization framework for charging and discharging dispatch of EV aggregations by considering the correlation of uncertainties [6]. In this study, charging station planning was performed by combining genetic algorithm, recurrent neural networks (RNN), and fuzzy logic methods.

Some studies on smart home energy management systems (HEMS) indicate that the integration of residential EV charging systems with smart HEMS is critical for energy efficiency. Bjørndal et al. examined the indirect effects of smart home charging optimization using real-world data analysis on 438 EVs [7]. The study addressed the co-production of smart mobility systems and the optimization of EV charging in residential energy management systems.

Some studies on renewable energy ıntegration and grid optimization have addressed the integration of renewable energy sources with EV charging systems as an important research area for sustainable energy management. Salam et al. addressed the integration of distributed energy sources into EV charging optimization and developed charging/discharging strategies for grid balancing [8]. Wu and Jia presented optimal planning approaches for wind-integrated EV charging and discharging systems, assuming that wind power can be generated from turbines mounted on high-rise buildings near charging stations in urban areas [2]. Boukhchana et al. performed vehicle-to-grid (V2G) optimization using wireless charging technology and developed real-time scheduling strategies [9]. In this study, optimal planning of charging and discharging processes of EVs was performed using wireless charging infrastructure.

Some studies on multi-user charging station management address the issue of fair resource allocation and user satisfaction at multi-user charging stations as important research topics. Ferhadi et al. studied smart charging infrastructure optimization for connected EVs and developed methods for charging station layout planning, presenting a data-driven multi-objective optimization framework for charging infrastructure [6]. An et al. developed optimal planning methods for EV battery stations by considering battery information collection systems [10]. In this study, real-time traffic and travel distance were taken into account using the particle swarm optimization (PSO) algorithm.

2. MATHEMATICAL MODEL AND SIMULATION

This research aims to optimally distribute energy to consumers within a residential area under limited capacity. The system offers a constraint-based optimization approach by considering users within the same category. In the proposed model, users are classified into a single category and resource allocation strategies specific to that category are applied.

Energy is allocated to users based on their capacity, defined by constraints. This approach allows users' demands to be shifted within a predetermined time window, thus increasing the overall efficiency of the system.

Within the system architecture, energy distribution is optimized and resource allocation is performed based on user demands using linear programming techniques. The proposed solution is discussed within the mathematical framework in Equation (1).

$$x_i(t) \leq D_i(t), \quad \forall i \in N, \forall t \in T \tag{1}$$

Here, $D_i(t)$ represents the total energy demand of user *i* in time period *t*, and $x_i(t)$ represents the amount of energy (in kWh) allocated to that user in the relevant time period. *N*, characterizes the total number of users within the system. *T* represents the time period.

The maximum power capacity that can be allocated to users is limited to maintain system reliability and ensure resource management. In this context, the maximum power that users can receive per hour is set at $L^{\max}$.

$$x_i(t) \le L^{\max}, \quad \forall i \in U, \forall t \in T \tag{2}$$

In Equation (2), the *U* symbol indicates the user class and is subject to resource allocation policies. Equation (3) ensures that the energy consumption of the system at any time does not exceed the maximum power capacity of the system in the relevant time period.

$$\sum_{i \in N} x_i(t) \le P_t^{\max}, \quad \forall t \in T \tag{3}$$

In the optimization process, predicting end-user energy demands is critical. In this context, the implemented optimization strategy is implemented using a linear programming methodology. The primary objective of the system is to maximize the relevant objective function, as stated in the mathematical formulation of Equation (4) presented below.

$$\max \sum_{t=1}^{\tau} \sum_{i=1}^{N} x_i(t) \tag{4}$$

Here, the decision variable $x_i(t)$ represents the amount of energy (in kWh) allocated to user $i \in N$ in the time period $t \in \{1, 2, ..., T\}$. τ indicates the current time step.

2.1. Simulation Study

The scenario considered within the system description aims to optimally distribute the energy needs of 10 EV users to the respective users within the requested timeframe during the 5:00 PM-12:00 PM operating period in a residential area. The system delivers the users' charging requests at the standard charging rate according to the priorities of the objective function. The general parameters of the scenario are listed in Table 1. The changing energy demand profiles of EV users over time periods and the related characteristics are presented in Table 2.

Table 1. System parameter

Parameter	Value	Unit
Total Number of Users	10	pieces
Operation Timeframe	17:00–00:00	hour
System Maximum Hourly Power Capacity	66	kW
User Maximum Power Allocation $\left(P_t^{\max}\right)$	11	kW

Table 2. Users' energy demand

Users	Energy Demand (kWh)	Start Hour	End Hour
User 1	30	17.00	24.00
User 2	40	17.00	24.00
User 3	40	17.00	24.00
User 4	30	17.00	24.00
User 5	35	17.00	24.00
User 6	40	17.00	24.00
User 7	35	17.00	24.00
User 8	40	17.00	24.00
User 9	50	17.00	24.00
User 10	25	17.00	24.00

3. SIMULATION RESULTS

The findings from the simulation study demonstrated that the proposed optimization methodology effectively meets the energy demands of EV users. By applying a rolling horizon-based linear programming technique, the system achieved a significant reduction in grid load during peak hours and successfully allocated energy. Table 3 lists the hourly energy consumed by each user in kWh.

Table 3. Energy distribution table

User	01.12 17:00	01.12 18:00	01.12 19:00	01.12 20:00	01.12 21:00	01.12 22:00	01.12 23:00
User 1	0	0	0	4	11	11	4
User 2	0	0	0	11	11	11	7
User 3	0	0	0	11	11	11	7
User 4	0	0	8	11	11	0	
User 5	11	11	11	2	0	0	
User 6	11	11	11	7	0	0	
User 7	11	11	11	2	0	0	
User 8	11	11	11	7	0	0	
User 9	11	11	11	11	0	0	
User 10	11	11	3	0	0	0	

Additionally, each user is represented by a different color in Figure 1, visualizing their hourly energy intake. This display allows for a comparative analysis of changes in individual consumption profiles over time.

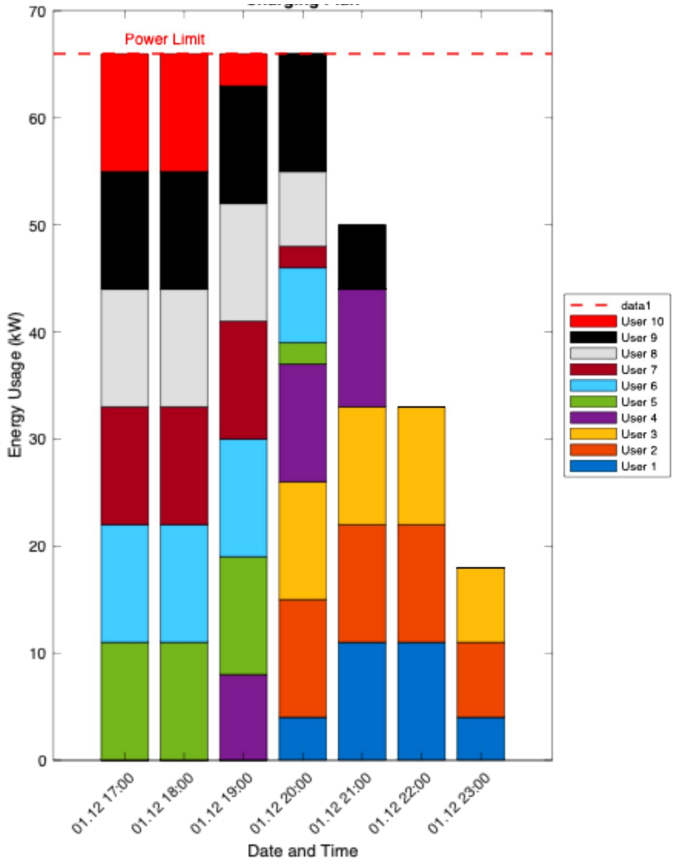

Figure 1. Charging plan

On the other hand, if a standard amount of energy is allocated to all users without any restrictions, prioritization, or user-based differentiation in the energy distribution process, the resulting energy distribution is as shown in Table 4. This table serves as a comparative reference for how energy sharing would be shaped under an ideal and fully egalitarian scenario.

Table 4. Energy distribution table

User	01.12.2025 17:00	18:00	19:00	20:00	21:00	22:00	23:00
User 1	11	11	8	0	0	0	0
User 2	11	11	11	7	0	0	0
User 3	11	11	11	7	0	0	0
User 4	11	11	8	0	0	0	0
User 5	11	11	11	2	0	0	0
User 6	11	11	11	7	0	0	0
User 7	11	11	11	2	0	0	0
User 8	11	11	11	7	0	0	0
User 9	11	11	11	11	6	0	0
User 10	11	11	3	0	0	0	0

Compared to the reference approach presented in Table 4, the energy scheduling model developed within the scope of this study reduces the maximum instantaneous grid load, especially during peak hours, by 40%.

4. CONCLUSION

In this study, operational and structural problems arising in the energy distribution of EV charging stations located in residential areas are investigated using a comprehensive mathematical model. The model is designed to account for the energy demand profiles of different user types, which have different technical requirements in terms of both the amount of energy required and the deferrability of the charging process. The developed structure is based on an optimization mechanism that enables the simultaneous management of these heterogeneous energy demands under a fixed energy capacity.

The primary technical objective of the model is to balance the energy flows within the charging station, including all its operational components, within safe operating limits. In this context, instantaneous power changes, capacity constraints, and time-dependent energy requirements within the system were evaluated together to calculate the optimal energy distribution plan for each time period. The designed model provides a technical control framework that aims to mitigate the risk of overloading the charging station, maintain the thermal and electrical limits of the energy components, and simultaneously meet user energy demands with the highest possible accuracy.

This integrated structure maintains system stability and establishes a fair and applicable energy allocation flow among users. This improves the overall performance of the charging station, minimizes energy delivery delays, and optimizes capacity utilization over time.

Acknowledgments

This study was supported by the scientific research project numbered 25DRP068, funded by Eskisehir Technical University.

References

[1] A. Dolgui, S. Kovalev, and M. Y. Kovalyov, “Scheduling electric vehicle regular charging tasks: A review of deterministic models,” *European Journal of Operational Research*, vol. 325, no. 2, pp. 221–232, 2025.

[2] J. Wu and Q. S. Jia, “On optimal charging scheduling for electric vehicles with wind power generation,” *Fundamental Research*, vol. 4, no. 4, pp. 951–960, 2024.

[3] S. Boubaker, H. Kraiem, N. Ghazouani, S. Kamel, A. Mellit, F. S. Alsubaei, et al., “Multi-objective optimization framework for electric vehicle charging and discharging scheduling in distribution networks using the red deer algorithm,” *Scientific Reports*, vol. 15, no. 1, art. no. 13343, 2025.

[4] D. An, F. Cui, and X. Kang, “Optimal scheduling for charging and discharging of electric vehicles based on deep reinforcement learning,” *Frontiers in Energy Research*, vol. 11, art. no. 1273820, 2023.

[5] P. Xu, X. Wang, and Z. Li, “Impact and optimization of vehicle charging scheduling on regional clean energy power supply network management,” *Energy Informatics*, vol. 8, no. 1, art. no. 13, 2025.

[6] F. Farhadi, S. Wang, R. Palacin, and P. Blythe, “Data-driven multi-objective optimization for electric vehicle charging infrastructure,” *iScience*, vol. 26, no. 10, art. no. 107737, 2023.

[7] E. Bjørndal, M. Bjørndal, E. K. Bøe, J. Dalton, and M. Guajardo, “Smart home charging of electric vehicles using a digital platform,” *Smart Energy*, vol. 12, art. no. 100118, 2023.
[8] S. S. A. Salam, V. Raj, M. I. Petra, A. K. Azad, S. Mathew, and S. M. Sulthan, “Charge scheduling optimization of electric vehicles: A comprehensive review of essentiality, perspectives, techniques, and security,” *IEEE Access*, vol. 12, pp. 121010–121034, 2024.
[9] A. Boukhchana, A. Flah, A. Alkuhayli, R. Ullah, and C. Z. El-Bayeh, “Optimal planning strategy for charging and discharging an electric vehicle connected to the grid through wireless recharger,” *Frontiers in Energy Research*, vol. 12, art. no. 1453711, 2024.
[10] Y. An, Y. Gao, N. Wu, J. Zhu, H. Li, and J. Yang, “Optimal scheduling of electric vehicle charging operations considering real-time traffic condition and travel distance,” *Expert Systems with Applications*, vol. 213, art. no. 118941, 2023.

Design, Prototype Production, and Testing of a Low-Impedance High Short-Circuit Current 18 MVA 33/33 kV Power Transformer

Bugra Akpinar[1]

[1]Power Transformer Design Department, BETA Enerji, Adana, Türkiye
Corresponding author: Bugra Akpinar (e-mail: bugra.akpinar@betaenerji.com)

Abstract

This study focuses on the comprehensive design of an 18 MVA, 33/33 kV power transformer characterized by low impedance and high short-circuit current capability. The main objective of this work has been to develop a transformer concept that is capable of operating reliably under severe short-circuit conditions while maintaining superior electrical, thermal, and mechanical performance characteristics. In this context, it has been aimed to perform detailed electromagnetic and mechanical analyses and to systematically optimize the design parameters to achieve the desired performance targets. During the design process, it has been targeted to achieve the intended low impedance value without compromising efficiency or thermal performance by optimizing the winding geometry, conductor configuration, and magnetic core dimensions. It has been intended that the magnetic core be designed to minimize stray flux and core losses, while the leakage reactance be carefully controlled through appropriate winding placement and interleaving techniques. To enhance mechanical robustness under high short-circuit stresses, it has been aimed to strengthen both the axial and radial mechanical withstand capabilities of the windings, and to dimension and arrange the supporting structures, clamping systems, and spacers to resist the electromagnetic forces expected during short-circuit events. From a thermal perspective, it has been planned to direct the oil circulation paths and cooling ducts in a way that ensures uniform heat distribution and minimizes hot-spot temperatures. The insulation system has been specially considered; it has been aimed to define the dielectric clearances between windings and structural components in accordance with IEC standards to ensure high dielectric reliability. In conclusion, this study has been intended to develop a design methodology that establishes an engineering balance between low impedance requirements and high short-circuit withstand capability. The proposed approach has been targeted to provide a technical basis for future transformer designs, demonstrating how optimized electromagnetic, thermal, and mechanical coordination can contribute to the development of compact, reliable, and high-performance power transformers suitable for modern power systems.

Keywords: Low-impedance transformer, High short-circuit current, Transformer design methodology, Electromagnetic and thermal optimization, Mechanical strength of windings

2nd International Conference on Multidisciplinary Sciences and Technological Developments (ICMUSTED 2025)

December 12-15, 2025

Fire Safety in Electric Vehicles: An Assessment of Battery Risks, Intervention Techniques, and Policy Recommendations

Mehmet Akif Er[1], Omer Kaya[1]

[1]Transportation Department, Engineering and Architecture Faculty, Erzurum Technical University, 25050 Erzurum, Türkiye
Corresponding author: Omer Kaya (e-mail: omer.kaya@erzurum.edu.tr)

Abstract

The rapid global increase in electric vehicle (EV) use introduces new risks to fire safety. The highest fire risk in EVs is observed in lithium-ion batteries, which have a high energy density. This study comprehensively examines the causes of EV fires, risk differences based on battery chemistry, safety criteria in the design of charging units, and fire response processes. Lithium iron phosphate (LFP) batteries are determined to be safer than other lithium-ion chemistries, while nickel cobalt aluminum oxid (NCA) and nickel manganese cobalt oxide (NMC) types, despite their high performance advantages, have a higher risk of thermal runaway. Furthermore, design elements such as the positioning of charging units, ventilation systems, and sprinkler infrastructure in indoor parking lots are found to be decisive in fire safety. It was determined that water-based cooling is the most common approach in responding to EV fires, but long-term monitoring is required due to the ongoing chemical reactions. In this context, the study provides a holistic assessment of the prevention, response, and post-emergency measures for EV fires.

Keywords: EV fires, Battery safety, Charging infrastructure, Fire response strategies

1. INTRODUCTION

The use of electric vehicles (EVs) is becoming increasingly widespread both globally and in Turkey. This increase has brought the risk of fire in EVs to the forefront. Available data indicates that the likelihood of fire in EVs is lower than in internal combustion engine vehicles. For example, a study conducted by the Australian-based EV Fire Safe between 2010 and 2020 found that fires occurred in 0.1% of internal combustion vehicles, compared to only 0.0012% of EVs. This rate suggests that the risk of fire in EVs is approximately 83 times lower [1]. However, while the likelihood of fire is low, when battery-related fires occur in EVs or hybrid vehicles, the severity and difficulty of controlling these fires can reach alarming levels.

The area with the highest risk of fire in EVs is the battery area. Batteries used in these vehicles can be broadly categorized into four main categories: lithium-ion batteries, nickel-metal hydride batteries, lead-acid batteries, and solid-state or flow batteries. Among these types, lithium-ion batteries are the most commonly used battery type in EVs. The primary reasons for this are their high energy density, rapid charging capability, and long cycle life [2]. In EV fires, the thermal energy released from the battery, the release of toxic gases, and the risk of high voltage significantly increase the fire's danger. Therefore, the methods used to respond to EV fires differ significantly from those used in internal combustion vehicle fires. Chemical gases emitted from the battery during a fire pose a serious health risk, and the use of protective equipment is crucial during response.

Another important issue is that EV fires can originate from charging units. A recent fire in a building in Istanbul while a vehicle was charging demonstrates the serious risks posed by the design and infrastructure deficiencies of charging units [3]. To mitigate this risk in indoor parking garages, charging units must be correctly positioned, designed to facilitate easy response in the event of a fire, and appropriate safety distances must be maintained. Furthermore, it is crucial for indoor charging stations to install ventilation and security systems that comply with international standards such as National Fire Protection Association (NFPA) 69 and NFPA 70. EV-related fires that may occur in indoor parking garages can threaten not only the vehicle itself but also other surrounding vehicles. Therefore, adequate distances must be maintained between vehicles, and parking areas must be designed in accordance with fire safety criteria. Additionally, design principles that facilitate rapid and safe response by firefighters should also be considered. However, the Building Fire Regulation published in the Official Gazette dated 19.12.2007 does not address such fire risks comprehensively, as EAs were not yet widespread at that time, and therefore needs to be updated in this respect.

There are significant differences between firefighting responses to EV and internal combustion vehicle fires. When fires occur in EV batteries, the response time is generally longer. There is also a risk of re-ignition after the fire is extinguished. To address this risk, vehicles are typically monitored with thermal cameras and kept under observation for 6–8 hours after the incident. Disabling the high-voltage system during a fire, if possible, is critical for both the safety of firefighters and controlling the fire. Therefore, firefighters responding to EV fires require specialized training.

This study presents research findings on preventive measures to be taken before EV fires break out, response methods to be implemented during the fire, and post-fire safety measures.

Figure 1. Electric vehicle fire

2. FINDINGS

2.1. Types of Batteries Used in Electric Vehicles

User error is one of the most significant factors contributing to fires in EVs. Lithium-ion batteries are the most commonly used battery type in EVs, and fires occurring in these batteries are generally caused by overcharging or overdischarging. In such batteries, a chemical reaction called thermal runaway occurs during a fire, posing a serious health risk due to the release of toxic gases. Another significant factor contributing to EV fires is improper charging devices and stations. The design and location of charging stations should ensure rapid and safe response in the event of a fire. Vehicles can become more dangerous, especially during charging, due to high voltages. Furthermore, modifications to parts without authorized service approval are another user error that increases the risk of fire. While EV manufacturers use a variety of battery models, studies have shown that most companies prefer lithium-ion batteries. Therefore, this study comprehensively covers the most commonly used lithium-ion battery types.

2.1.1. Lithium Iron Phosphate (LFP) Battery

LFP batteries were developed by the Massachusetts Institute of Technology (MIT) in 2003. These batteries are a derivative of conventional lithium-ion technology in terms of chemical composition and utilize lithium ferrophosphate (LFP; $LiFePO_4$) instead of lithium cobaltate [4]. Because their energy density is lower than other lithium-ion types, they are not widely preferred in high-performance EV models. However, their long cycle life and ability to be fully charged offer significant advantages [5]. An uncontrolled increase in the internal temperature of a battery increases the risk of a chain reaction. The thermal runaway temperature in LFP-type batteries is approximately 270 °C [5], making them safer than other lithium-ion battery chemistries. Consequently, the risk of fire is significantly lower with LFP batteries. In some application examples, Tesla prefers Contemporary Amperex Technology Limited (CATL)-supplied LFP batteries in some of its models [6]. Similarly, China-based BYD uses LFP chemistry in its Blade Battery system, which it introduced in 2020. This system has successfully passed rigorous safety tests such as the “nail penetration test” and has demonstrated high resistance to fire [7].

2.1.2. Lithium Nickel Cobalt Aluminum Oxide (NCA) / Nickel Manganese Cobalt Oxide (NMC) Batteries

NCA ($LiNiCoAlO_2$) batteries are notable for their use of high-energy-density cathode materials. They are similar to NMC batteries in terms of specific power and long cycle life. However, they have disadvantages in terms of

safety and cost. The charge capacity of NCA batteries is higher than other battery types, which increases the risk of overheating and thermal instability, creating safety concerns. A study in China examining the thermal effects of cathode materials found the order of thermal stability as lithium cobalt oxide (LCO) > NCA > nickel cobalt manganese (NCM811) >> LFP. Panasonic, Tesla's supplier, produces NCA-type batteries specifically for use in Tesla's high-performance models. NMC batteries are one of the highest-performance types of lithium-ion batteries. The cathode structure contains a combination of nickel, manganese, and cobalt elements [7]. The ratios of these elements determine the battery's energy density, lifespan, and safety features. Therefore, various NMC versions with varying ratios are being developed. A study conducted in the United States examined the aerosol amounts emitted during thermal runaway in lithium-ion batteries and found that NMC batteries emitted more aerosols than other battery types [8]. Research indicates that NMC batteries are widely preferred due to their high performance advantages, but they also present higher risks of fire and thermal runaway.

2.2. Charging Units Used in Electric Vehicles

Unlike internal combustion engine vehicles, EVs run on electricity instead of fuel. These vehicles operate using the energy stored in their batteries after a certain period of charging. This energy is provided by charging units. Today, charging infrastructure is quite diverse, offering various alternatives, including public charging stations, individual charging points under buildings, and integrated solutions in private parking areas. EV battery charging methods can be broadly categorized into two main categories: wired charging systems and wireless (inductive) charging systems.

2.2.1. Wired Charging Method

The wired charging methods used in EVs are basically divided into two main types: Alternating current (AC) and direct current (DC) charging systems. In AC charging, the vehicle converts AC from an external power source (e.g., a wall outlet or wall-mounted station) to DC through its on-board converter (an on-board charger) and charges the battery. This is because EV batteries can only store energy with DC. In contrast, in DC charging systems, the energy conversion occurs directly in the charging unit, and the DC current is delivered directly to the vehicle [9]. These systems, thanks to their high power capacity, offer fast charging and provide quick charging for longer ranges. AC charging systems, typically used in homes, public spaces, and offices, operate with an external cable connection. However, charging times are longer than with DC systems.

Figure 2. Wired charging method

2.2.2. Wireless Charging Method

With technological advancements, wireless charging systems are now used in many areas of daily life. For example, just as we can charge mobile devices in vehicles without using cables, the idea of wirelessly charging EVs is gaining increasing interest. In this context, studies are underway on various concepts, such as vehicles drawing energy from the road surface while in motion or charging without a cable connection while parked. In Norway, in particular, a large-scale investment plan is underway to allow vehicles to dynamically charge their batteries while driving. For this system to be implemented, the road infrastructure must be designed to accommodate static power transfer. Wireless charging stations (docks) used for smartphones or watches transfer energy to the battery via magnetic induction. Similarly, in parked EVs, energy can be transferred via receivers placed under the vehicle or on certain surfaces using systems based on this principle [10]. While wireless charging methods offer advantages such as saving time and reducing the risk of cable-related fires, they still require development in terms of efficiency, cost, and safety.

Figure 3. Wireless charging method

2.2.3. Charging Modes in Electric Vehicles

Mode 1: In this mode, charging is performed using current drawn directly from a household AC outlet. It typically has a single-phase current limit of 16 A and a voltage limit of 250 V, and a three-phase voltage limit of 480 V [11]. An effective grounding system is required for this method. However, due to overheating and electrical safety risks, the use of Mode 1 is prohibited in Europe. Currently, this mode is only used on a limited basis for vehicles with small battery capacities—for example, electric bicycles or e-scooters. Due to these safety concerns, a more protective Mode 2 charging system has been developed.

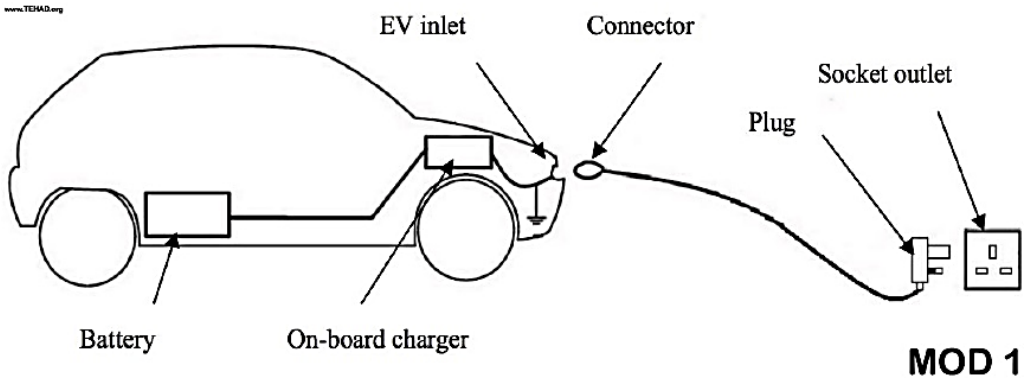

Figure 4. Mode1 type charging method

Mode 2: In this mode, charging is performed using AC current from household outlets, as in Mode 1. However, Mode 2 differs in that it uses a cable with a special protection circuit during charging. This cable cuts off the circuit in cases of leakage current and overheating, reducing the risk of fire and improving user safety. Mode 2 is considered the most widely used charging method today due to its simple installation requirements and high level of safety.

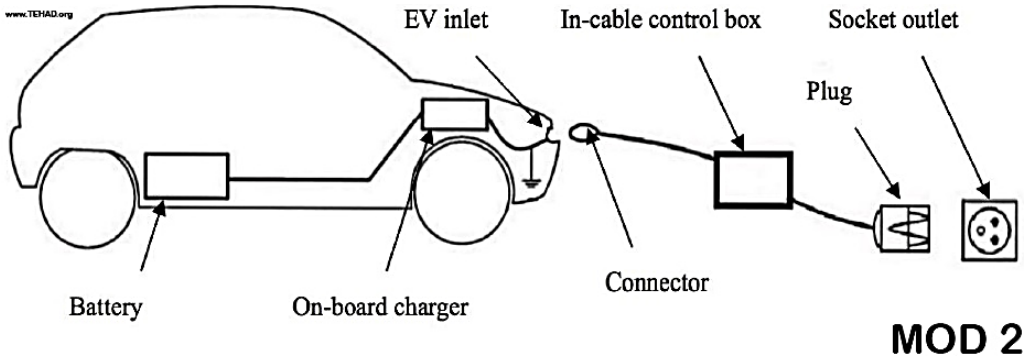

Figure 5. Mode2 type charging method

Mode 3: This mode is typically implemented using wall-mounted charging boxes (wallboxes) at public charging stations or in home parking lots. Charging is done directly via a cable integrated into the charging unit, rather than via an external cable. Mode 3 allows for more controlled energy flow, reducing charging time and improving efficiency. Furthermore, thanks to integrated safety systems, the risk of fire and electrical hazards are significantly reduced. These features make Mode 3 considered one of the most reliable charging methods, both in terms of safety and efficiency.

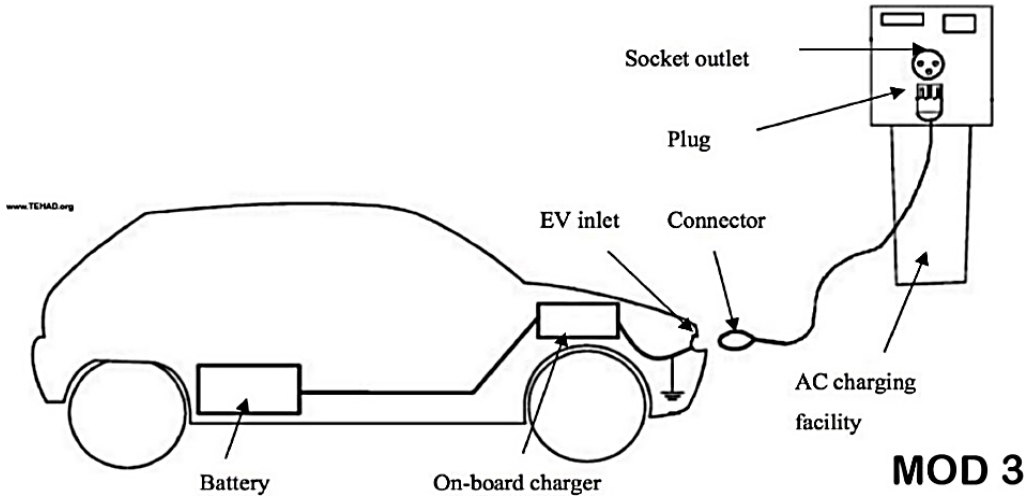

Figure 6. Mode3 type charging method

Mode 4: This charging mode transfers energy directly using DC instead of AC, enabling rapid charging. Thanks to its high current and voltage ratings, vehicles can typically be fully charged in as little as 20–40 minutes, depending on battery capacity. Mode 4 systems incorporate advanced safety protocols, temperature monitoring, and cooling systems to mitigate the risks associated with high power transfer. These measures protect against potential fires, overheating, or electrical faults, thus increasing both user safety and battery life.

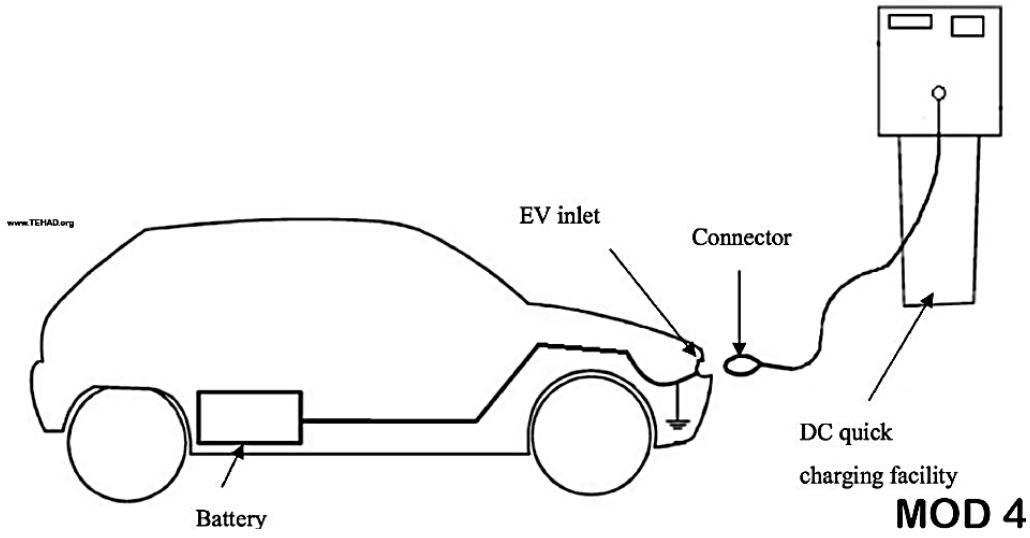

Figure 7. Mode4 charging method

2.2.4. Fire Safety Perspective in Parking Lot Design of Charging Units

Today, EVs are mostly charged in underground parking garages under residential buildings. However, this necessitates careful design due to the risk of fire. The location and design of charging units are crucial, as heating, electrical faults, or battery-related chemical reactions that may occur during charging in parking garages can increase the risk of fire. When designing charging units, priority should be given to facilitating fire response and protecting surrounding vehicles and people against chemical explosions that may originate from batteries. Therefore, locating charging units near parking garage entrances and exits facilitates rapid access for firefighters [12]. Furthermore, the installation of fire alarm systems and the installation of camera systems near charging units are recommended for both early warning and post-fire surveillance. If the parking garage is not a separate section

of the building, structural separations with a fire resistance of at least one hour are required. Furthermore, ventilation systems are also critical. Chemical gases released during EV fires in indoor parking garages can accumulate, creating an explosion risk. Therefore, ventilation systems should be designed and reinforced to prevent such situations. Finally, sprinkler systems play a vital role in first aid in the event of a fire. These systems limit the growth of a fire before firefighters arrive on the scene and, in conjunction with alarm systems, provide early warning, providing a critical advantage in firefighting [13].

2.2.5. Protective Equipment to be Used When Responding to Electric Vehicle Fires

Extinguishing EV fires poses different risks than internal combustion vehicle fires. High-voltage battery systems, in particular, can pose hazards such as electric shock, arcing, and the release of chemical gases. Therefore, it is vital to use appropriate protective equipment during response.

Insulated Gloves: Due to the high voltage risk inherent in EV fires, the use of insulated gloves is mandatory. These gloves typically consist of four layers: an outer fabric, a moisture barrier, a heat barrier, and an inner lining. Insulated gloves must be manufactured to withstand at least 1000 V of electrical current. When touching high-voltage components such as batteries or power systems, only gloves approved to European Norm (EN) 60903 and American Society for Testing and Material (ASTM) D120 standards are essential for safe response.

Figure 8. Insulated glove

Protective Helmet: Helmets used during firefighting must be resistant to heat, impact, and electrical hazards. Protective helmets must protect against factors such as sparks from batteries and high temperatures. The EN 50365 standard defines the characteristics of helmets that provide safety at voltages not exceeding 1000 V AC and 1500 V DC. Therefore, helmets must be checked for compliance with the EN 50365 standard.

Figure 9. Protective helmet

Heat Protective Clothing: The high heat, flames, and electric arcs generated during a fire can cause serious injuries. Therefore, it is important that protective clothing used is both heat-resistant and does not restrict mobility. The

Turkish Standard (TS) EN International Organization for Standardization (ISO) 11612 standard covers the evaluation of protective performance against heat and flame. It is recommended that response equipment comply with this standard.

In addition, the use of additional protective equipment such as face shields, gas masks, and insulated, steel-toed shoes provides additional safety against fire gases, hot particles, and chemicals.

Figure 10. Protective clothing

2.2.6. Electric Vehicle Fire Response Techniques

EV fires are more dangerous and take longer to extinguish than internal combustion vehicle fires. In such fires, it is crucial for bystanders to wait for the arrival of a specialist team before responding. There are serious risks, such as exposure to chemical gases and the fire spreading due to improper intervention.

First aid can be provided for EV fires with a fire blanket. However, this method is only effective for small-scale fires, and its use in large-scale battery fires is reported to be of limited benefit. Crews arriving at the scene must first accurately identify the type of vehicle, as it may not always be readily apparent upon initial inspection.

Before responding, crews must wear appropriate protective equipment to protect against the risk of chemical gas release and battery-related explosions. After ensuring environmental safety, if the vehicle is still running, the crew should shut it down using the power button or ignition key. If possible, it is recommended to access the battery, which is the auxiliary power source, disconnect the connections, and deactivate the battery system cables [14]. The possibility of electrical current in the vehicle should be considered during all these procedures, and the intervention must be carried out with caution. The most commonly used extinguishing method in EV fires is water extinguishing. However, the amount of water used and the cooling time are much longer than in internal combustion vehicle fires. The responding team must also be cautious about the risk of explosion that may arise from reactions between water and battery chemicals.

Following a fire, it is recommended that EVs be monitored for at least 72 hours due to the possibility of recurrence. During this period, the vehicle may be placed in a cooling pool or monitored with thermal cameras to monitor for potential thermal runaways.

In one experiment, an EV fire was initially extinguished with a fire blanket. This method slowed the spread of the fire initially but was not effective in stopping thermal runaway within the battery. Compressed air foam was then used, and the fire was brought under control in approximately 90 seconds. However, it was observed that the chemical reactions within the battery remained active for a long time, requiring a long cooling period [15].

Figure 11. Fire blanket

During an EV fire, or after a small fire has subsided, a device called an emergency plug must be used to control the vehicle's safety (Figure 12). The emergency plug prevents unforeseen vehicle movement in an emergency and instantly and safely disables the battery system. The device allows the system to perceive the vehicle as charging, thus preventing any movement of the vehicle.

Figure 12. Intervention with emergency plug [16]

3. POLICY RECOMMENDATIONS AND IMPLEMENTATION STRATEGIES

The proliferation of electric vehicles necessitates a reassessment of existing fire safety regulations and infrastructure standards. Policy recommendations developed in this context should encompass not only firefighting but also preventative engineering, regulatory updates, infrastructure planning, and increased institutional capacity. Policy and practice recommendations for strengthening EV fire safety are presented below:

i. Legislation and Standard Updates

- Updating the Building Fire Regulation: The 2007 regulation was prepared at a time when EV use was not increasing. The new regulations should include charging infrastructure, ventilation, distance, sprinkler, and material standards specific to EVs.
- Battery Safety Regulation: A dedicated "Battery Safety Regulation" should be established for EV batteries, covering topics such as thermal runaway tests, aerosol emission limits, and recycling safety.
- Compliance with European Standards: International standards such as NFPA 69/70, EN 50365, and TS EN ISO 11612 should be integrated with national legislation.

ii. Charging Infrastructure and Parking Lot Design

- Mandatory Safety Distance: A minimum safety distance of 1.5 meters between vehicles should be mandatory in indoor parking lots.

- Smart Charging Systems: Charging units should monitor temperature, voltage, and current fluctuations in real time and automatically shut down in the event of a fire.
- Ventilation and Sensor Integration: Gas sensors, heat detectors, and automatic smoke exhaust systems should be mandatory in enclosed spaces.
- Fire Response Facilitating Design: Charging points in parking lots should be located near emergency exits and fire department access areas.
- TS 13912 Standard: Provides information on technical infrastructure, inspection and safety adequacy for the installation of electric vehicle charging stations. An example of a parking lot design for EV vehicles is presented in Figure 13.

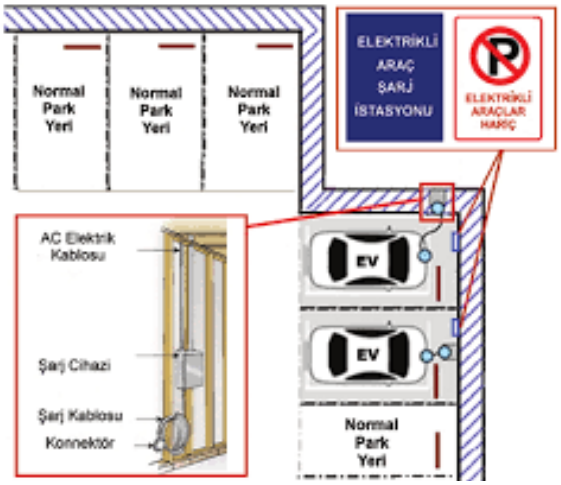

Figure 13. Example of parking lot design for EV vehicles [17]

iii. Training, Inspection, and Institutional Capacity

- Fire Department Training Programs: Specific certification programs on high voltage, chemical gas release, and thermal runaway management should be initiated for teams responding to EV fires.
- User Awareness: Vehicle owners should be informed about charging safety, battery maintenance, and emergency procedures. An EV safety module should be included in driver's license training.
- Periodic Inspections: The electrical infrastructure of charging stations should undergo a fire safety inspection at least once a year.

iv. Research, Data Sharing, and Technological Innovation

- Fire Database: A national database containing all incidents, causes, battery type, response time, and outcome information related to EV fires should be created.
- Artificial Intelligence-Supported Monitoring Systems: AI-based sensor systems and thermal imaging algorithms should be developed to detect thermal runaway and thermal spikes early.
- Academia-Industry Collaboration: Fire safety research and development (R&D) projects should be supported among universities, energy companies, and automotive manufacturers.

v. Insurance and Risk Management Approach

- Risk-Based Insurance Model: Insurance companies should restructure vehicle and parking lot risk analyses based on parameters such as battery type, charging system, and frequency of use.
- Incentive Mechanisms: Tax deductions or insurance premium support should be provided for EVs with safety-certified batteries and charging systems.

4. CONCLUSION

This study systematically examined the characteristics, risk factors, and response processes of electric vehicle fires. The findings indicate that, while EV fires are much less frequent than those in internal combustion vehicles, thermal runaway from batteries makes them more difficult to control. LFP batteries stand out as a safer option due to their chemical stability, while NMC and NCA batteries require more careful monitoring and protection due to their higher energy density. Fire safety in the design of charging units and parking lot layout is critical, especially

in enclosed spaces. Ventilation, sprinkler systems, the use of protective equipment, and trained personnel are essential for effective crisis management in the event of a fire. Furthermore, thermal monitoring for up to 72 hours after extinguishing EV fires is essential to prevent the risk of reignition. Consequently, a multidisciplinary approach to design, legislation, and training is essential for the safe deployment of EV technology. This study provides a scientific basis for the development of fire safety strategies for both manufacturers and fire authorities.

References

[1] E. E. Kandemir. (2024, Aug. 26). *Elektrikli otomobiller ne kadar yangin riski tasiyor?* [Online]. Available: https://insideevs.com.tr/news/731318/elektrikli-otomobiller-yangin-riski/

[2] HedefFilo. (2025, Sep. 20). *Elektrikli araba bataryasi hakkinda bilmek istediginiz tum detaylar* [Online]. Available: https://ev.hedeffilo.com/ev-nedir/bataryalar

[3] Y. Huang, D. Liu, J. Tang, S. Niu, F. M. Bell, and F. Pena-Mora, "Dynamic estimation of the fire service spatial accessibility for EV charging stations: Towards preventing severe fires and explosions," *Process Safety and Environmental Protection*, vol. 195, art. no. 106734, Mar. 2025.

[4] S. Kalluri, M. Yoon, M. Jo, H. K. Liu, S. X. Dou, J. Cho, et al., "Feasibility of Cathode Surface Coating Technology for High-Energy Lithium-ion and Beyond-Lithium-ion Batteries," *Advanced Materials*, vol. 29, no. 48, Dec. 2017.

[5] N. Alias and A. A. Mohamad, "Advances of aqueous rechargeable lithium-ion battery: A review," *Journal of Power Sources*, vol. 274, pp. 237–251, Jan. 2015.

[6] Y. Hu, J. Liang, X. Chen, G. Chen, Y. Peng, S. Tang, et al., "Comparative study of thermodynamic & kinetic parameters measuring techniques in lithium-ion batteries," *Journal of Power Sources*, vol. 606, art. no. 234590, Jun. 2024.

[7] Battery University. (2023, Dec. 8). *BU-205: Types of lithium-ion* [Online]. Available: https://batteryuniversity.com/article/bu-205-types-of-lithium-ion

[8] T. L. Barone, T. H. Dubaniewicz, S. A. Friend, I. A. Zlochower, A. D. Bugarski, and N. S. Rayyan, "Lithium-ion battery explosion aerosols: Morphology and elemental composition," *Aerosol Science and Technology*, vol. 55, no. 10, pp. 1183–1201, Oct. 2021.

[9] Y. Lu, C. Xia, C. Rong, S. Zhao, Y. Liu, M. Chen, et. al., "Optimization design of coupling mechanism for dynamic static hybrid AGV WPT systems," *Electrical Engineering*, vol. 104, no. 6, pp. 4509–4520, Dec. 2022.

[10] F. Karapinar and F. Daldaban, "Elektrikli araclarin sarj yontemleri ve sarj istasyon tipleri," *Erciyes Universitesi Fen Bilimleri Enstitusu Fen Bilimleri Dergisi*, vol. 38, no. 3, 2022.

[11] F. S. D. Durmus and H. Kaymaz, "Elektrikli aras sarj yontemleri," *Akilli Ulasim Sistemleri ve Uygulamalari Dergisi*, vol. 3, no. 2, 2020.

[12] Zurich. (2023, Oct. 12). *Risk topic: Modern vehicle parking and electric vehicle charging* [Online]. Available: https://www.zurich.co.uk/news-and-insight/risk-topic-modern-vehicle-parking-and-electric-vehicle-charging.

[13] M. Peace, "Electric vehicle charging point fire safety considerations," *The Institution of Engineering and Technology*, no. 98, Nov. 2023.

[14] O. Topal, "Turkiye'de elektrikli ve hibrit araclar icin acil mudahale yaklasimlari," *Cevre Sehir ve Iklim Dergisi*, vol. 2, no. 3, 2023.

[15] S. S. Deep, S. Sultana, T.-U. Haque, M. T. Rahman, and S. Saha, "Comment on "Nanoparticles impacts on natural convection nanofluid flow and heat transfer inside a square cavity with fixed a circular obstacle" [Case Studies in Thermal Engineering, 44 (2023) 102829]," *Case Studies in Thermal Engineering*, vol. 73, art. no. 106570, Sep. 2025.

[16] E. Kalelioglu, "Elektrikli Otomobil Kazalarinda Itfaiyecilerin Kullandigi Gizli Silahi "Emergency Plug" Nedir?," *Webtekno*, Nov. 17, 2025. [Online]. Available: https://www.webtekno.com/emergency-plug-acil-durum-fisi-nedir-h207054.html. [Accessed Nov. 18, 2025].

[17] A. Kilic, "Elektrikli araç şarj istasyonlarinin havalandirilmasi," *TUYAK Yangin Muhendisligi Dergisi*, vol. 1, pp. 28–34, 2017.

2nd International Conference on Multidisciplinary Sciences and Technological Developments (ICMUSTED 2025)

December 12-15, 2025

Use of Aggregates Produced from Waste Concrete Samples of Different Strength Classes in Concrete

Melek Demirtas[1], Omer Ozmen[1], Rahman Cankaya[1], Omer Can[1]

[1]Department of Construction, Technical Sciences Vocational School, Canakkale Onsekiz Mart University, Canakkale, Türkiye
Corresponding author: Omer Can (e-mail: omer.can@comu.edu.tr)

Abstract

The rapid growth in the construction sector and urban transformation activities have increased the demand for natural aggregates, which are the main component of concrete. This study investigates the usability of waste concrete samples, resulting from quality control tests in construction laboratories, as recycled concrete aggregate (RCA) as a sustainable waste management strategy. The main objective of the study is to compare the properties of aggregates (low-strength concrete aggregate (LSCA) and high-strength concrete aggregate (HSCA)) obtained from these wastes, separated according to their original strength classes, and the mechanical performance of new concrete produced with these aggregates. Aggregate characterisation revealed that both types of RCA have lower density and higher water absorption rates compared to natural aggregates. LSCA exhibited higher abrasion resistance than HSCA, with a Los Angeles (LA) abrasion loss of 32% compared to 41%. Furthermore, the granulometry of LSCA was found to be more optimal than that of HSCA due to its higher content of fine material during the crushing process. In the concrete produced targeting the C30 class, the average compressive strengths at 28 days were measured as 34.59 MPa for HSCA and 35.63 MPa for LSCA. The results revealed that both waste sources successfully met the targeted C30 strength class and that LSCA performed better than HSCA due to its good granulometric distribution.

Keywords: Recycling, Concrete, Waste concrete, Concrete testing

1. INTRODUCTION

Concrete is the most widely used construction material globally, with aggregates constituting approximately 60-70% of its composition by volume [1]. Increasing population density and accelerated construction activities, particularly due to urban transformation projects, have significantly increased demand. Meeting the demand for aggregates largely from natural resources and quarries leads to environmental degradation, rapid depletion of natural resources, and disruption of the ecological balance [1, 2]. These environmental and economic pressures have pushed the construction industry to seek alternative and sustainable material sources. In this context, recycled concrete aggregate (RCA), obtained from construction and demolition waste, may be an alternative for both the conservation of natural resources and the solution to a serious waste management problem. Studies in the literature show that RCA generally exhibits higher porosity, higher water absorption capacity, and lower density compared to natural aggregates (NA). These characteristics can cause difficulties in the workability of fresh concrete, such as rapid slump loss [3, 4]. However, it has also been reported that the negative effects of RCA can be managed and concrete rigidity increased through methods such as the use of superplasticiser admixtures [5]. Current research suggests that the mechanical performance of concrete produced with RCA can often fall slightly below the target class, and therefore a higher class may need to be targeted in the design [3]. Although research has focused on various sources such as demolition debris from construction sites [2, 6–7] or waste kerbstones [2], there is a clear research gap regarding the evaluation of waste generated during construction material production processes and quality control stages. In accordance with building inspection regulations, building laboratories are required to test fresh concrete samples taken from the field. Thousands of samples broken as a result of these tests create a regular and traceable waste stream.

The main objective of this study is to investigate the usability of waste concrete samples obtained from construction laboratories, whose strength class is known (below C30 and above C30), as aggregate in concrete production. The study divided these wastes into two groups: Low Strength Concrete Aggregate and High Strength Concrete Aggregate. It first determined the physical and mechanical properties of these two aggregate types and then experimentally compared the performance of new C30-targeted concretes produced with these aggregates. This

proposes a circular economy model aimed at both preventing the environmental harm caused by waste and reducing the pressure on quarries.

2. MATERIALS AND METHODS

The experimental studies were conducted at the Construction Materials Laboratories of the Technical Sciences Vocational School at Canakkale Onsekiz Mart University (COMU).

2.1. Materials

The main material of the study, RCA, was obtained from hardened concrete samples that became waste as a result of quality control tests conducted by authorised construction laboratories in the province of Canakkale. These wastes were divided into two main groups according to their original concrete strength classes:

- Low-Strength Concrete Aggregate (LSCA): Aggregates obtained from concrete waste with an original class below C30.
- High-Strength Concrete Aggregate (HSCA): Aggregates obtained from concrete waste with an original class of C30 and above.

Waste samples from both groups were crushed in jaw crushers to produce aggregate fractions with a particle size of 0-16 mm. Portland cement type CEM I 42.5 R was used as the binder in the concrete mixtures. Mains water meeting the requirements of Turkish Standard European Norm (TS EN) 1008 [9] was preferred as the mixing water.

2.2. Method

The experimental programme consisted of two main stages. The first stage involved the physical-mechanical characterisation of LSCA and HSCA, and the second stage involved determining the fresh and hardened properties of the concrete produced with these aggregates.

2.2.1. Aggregate Tests

In order to determine the suitability of both RCA groups for concrete production, the particle size distribution of the aggregates was determined by sieving according to the TS EN 933-1 [10] standard. To determine the aggregate's resistance to impact and abrasion, the Los Angeles (LA) abrasion test was performed in accordance with the TS EN 1097–2 [11] standard. To determine the quality of the fine material and the possible clay content, a methylene blue (MB) test was applied according to the TS EN 933-9 [12] standard. To define the shape characteristics of the aggregate particles, the flatness index was determined based on the TS EN 933-3 [13] standard. Finally, the oven-dry particle density, saturated surface dry (SSD) particle density, and water absorption capacity, which are indicators of the aggregate's density and porosity, were determined in accordance with standards TS EN 1097-6 [14] and TS 706 EN 12620 [15].

2.2.2. Concrete Production and Tests

After completing the aggregate characterisation, two separate series of concrete mixes were designed using LSCA and HSCA. In both series, the C30 concrete class was targeted, referring to TS 802 and TS EN 206 [16] standards. To determine the workability and consistency of the fresh concrete produced, a slump test was performed according to TS EN 12350-2 [17]. Six 150x150x150 mm cube specimens were taken from each series and these specimens were kept in a standard water curing tank for 28 days. Non-destructive tests were first performed on the hardened concrete specimens that had completed the curing period. In this context, a Schmidt hammer test was performed in accordance with TS EN 13791 [18] to determine the surface hardness and approximate compressive strength, and ultrasonic velocity measurements were performed in accordance with TS EN 12504-4 [19] to evaluate the homogeneity of the internal structure of the concrete. Finally, a 28-day compressive strength test was performed on the specimens in a 200-tonne press in accordance with the TS EN 12390–3 [20] standard.

3. RESULTS AND DISCUSSION

3.1. Characterisation of RCA Produced from LSCA and HSCA

The characterisation results of aggregates obtained from LSCA and HSCA revealed both expected and unexpected differences between the two materials. The sieve analysis results are presented in Figure 1 and Figure 2. Examination of the sieve analysis graphs showed that the crushing process produced more fine material (0-4 mm) from LSCA than from HSCA. While the granulometry curve of HSCA exhibited a "lack of fine material," particularly in the fine region, falling below the standard limit curves, the curve of LSCA showed a more continuous and optimal distribution. This indicates that low-strength concrete fractures more easily, resulting in better gradation.

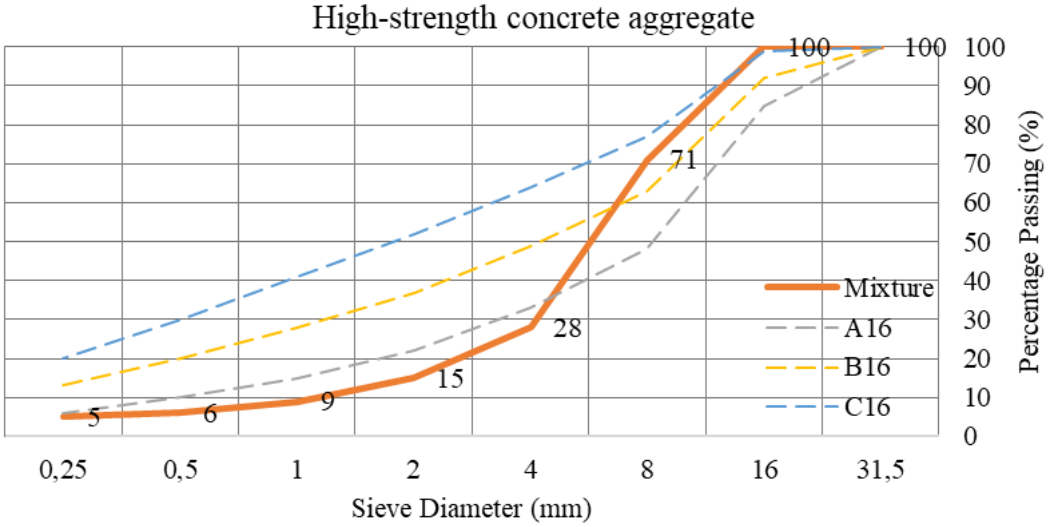

Figure 1. Recycled aggregate sieve analysis results (high-strength)

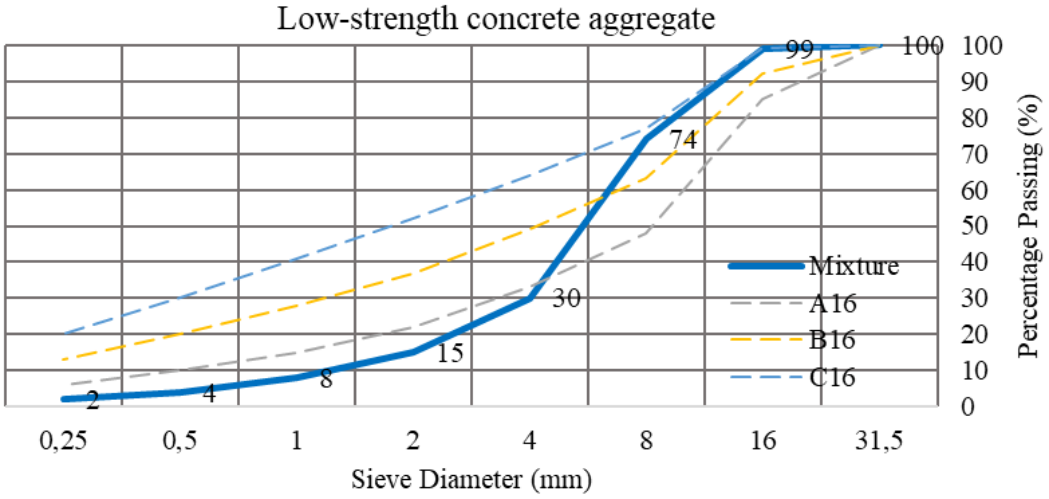

Figure 2. Sieve analysis results of recycled aggregate (low-strength)

When examining the mechanical quality and durability of the aggregates, the LA abrasion test apparatus is shown in Figure 3 and the results are given in Table 1. While HSCA showed a 41% abrasion loss, LSCA exhibited a much better abrasion loss value of 32%. Although both values are below the 50% limit specified by the American Society for Testing and Materials (ASTM) C33 [21] standard for concrete aggregates, the fact that LSCA is mechanically more resistant indicates that the strength of the original concrete is not the only factor determining the abrasion resistance of the aggregate obtained from it. It is likely that during the breakage of low-strength concrete, the weak cement paste separated more easily, revealing cleaner and more resistant original aggregate surfaces. In other quality indicators, both aggregate types yielded excellent results.

MB values were found to be 0.8 g/kg for both groups, indicating no harmful clay content. The MB analysis test results are shown in Figure 4. Flatness indices were measured as 4.05 for HSCA and 3.72 for LSCA, respectively. The test results are presented in Table 2 and Table 3. Both fell into the best category, FI15 class, exhibiting an ideal shape characteristic in terms of cubicity.

Figure 3. LA abrasion test setup

Table 1. LA abrasion test results

Number of Balls	Aggregate Size Range (mm)	HSCA			
		Initial Mass (g)	Final Mass After 500 Cycles (g)	Mass Loss (g)	Loss Percentage (%)
10	10/14	5000	3540	1460	41
LA Category				LA_{50}	
Number of Balls	Aggregate Range (mm)	LSCA			
		Initial Mass (g)	Final Mass After 500 Cycles (g)	Mass Loss (g)	Loss Percentage (%)
10	10/14	5000	3797	1203	32
LA Category				LA_{35}	

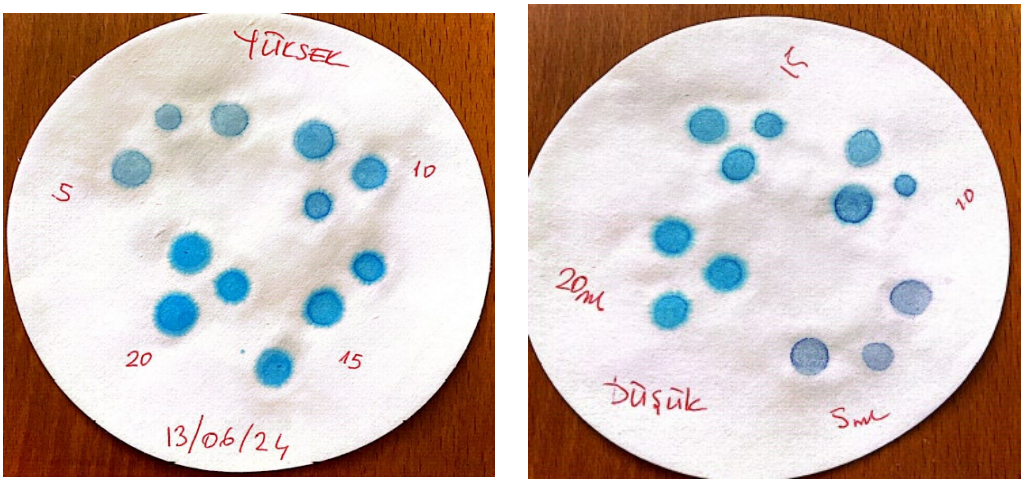

Figure 4. MB analysis experiment

Table 2. HSCA Flatness Index experiment results

Material Information		HSCA		
Mass of the Test Sample Section - g M_0 = 5962		Total Mass of Samples Not Subjected to Treatment - g 35		
Screening with Test Sieves		Screening with Bar Screens		
Particle Size Range (mm)	Particle Size Mass (g)	Sieve Gap Width (mm)	Mass Passing Through the Sieve (g)	$FI_i = (m_i/R_i)\times100$
25 / 31.5	0	16	0	-
20 / 25	0	12.5	0	-
16 / 20	72	10	0	-
12.5 / 16	1598	8	60	-
10 / 12.5	1186	6.3	41	3
8 / 10.	219	5	13	6
6.3 / 8	1496	4	85	6
5 / 6.3	615	3.15	16	3
4 / 5.	741	2.5	25	3
$M_1 = SR_i$ =	5927	$M_2 = Sm_i$ =	240	
$FI = (M_2/M_1)\times100$ =	4.05	Flatness Index Category	FI_{15}	

Table 3. LSCA flatness index test results

Material Information		LSCA		
Mass of the Test Sample Section - g M_0 = 5982		Total Mass of Samples Not Subjected to Treatment - g 46		
Screening with Test Sieves		Screening with Bar Screens		
Particle Size Range (mm)	Particle Size Mass (g)	Sieve Gap Width (mm)	Mass Passing Through the Sieve (g)	$FI_i = (m_i/R_i)\times100$
25 / 31.5	0	16	0	-
20 / 25	0	12.5	0	-
16 / 20	70	10	0	-
12.5 / 16	1600	8	57	-
10 / 12.5	1241	6.3	32	3
8 / 10.	256	5	15	6
6.3 / 8	1691	4	87	5
5 / 6.3	570	3.15	16	3
4 / 5.	508	2.5	14	3
$M_1 = SR_i$ =	5936	$M_2 = Sm_i$ =	221	
$FI = (M_2/M_1)\times100$ =	3.72	Flatness Index Category	FI_{15}	

The density and water absorption test results for LSCA and HSCA are given in Table 4 and Table 5. The test results showed that the density values of recycled aggregates were lower than those of natural aggregates, while their water absorption values were higher. This situation stems from the porous hardened cement paste in the RCA

structure.

Table 4. LSCA density and water absorption test results

LSCA Water Absorption Test Results					LSCA Density Test Results				
Dimension		0/4	4/8.	8/16.	Size		0/4.	4/8	8/16.
Pycnometer + Water + Material Mass (g)	M_2	6916	8133	8198	Measuring Cup Mass (g)	m_1	3188	3188	3188
Pycnometer + Water Mass (g)	M_3	6311	6316	6329	Measuring Cup Volume (l)	v	3	3	3
Material DKY Mass (g)	M_1	1013	3096	3078	Sample + Measuring Cup Mass (g)	m_2	7646	7166	7192
Material Oven-Dried Mass (g)	M_4	934	2968	2978	Loose Bulk Density (kg/dm^3)	ρ_b	1.486	1.326	1.335
Apparent Particle Density (kg/dm^3)	ρ_a	2.84	2.58	2.69	Percentage of Empty Space (%)	n	35	43	46
Oven-Dried Grain Density (kg/dm^3)	ρ_{rd}	2.29	2.32	2.46					
DKY Particle Density (kg/dm^3)	ρ_{ssd}	2.48	2.42	2.55					
Water Absorption (%)	WA24	8.5	4.3	3.4					

Table 5. HSCA density and water absorption test results

HSCA Water Absorption Test Results					HSCA Density Test Results				
Dimension		0/4	4/8.	8/16.	Size		0/4.	4/8	8/16.
Pycnometer + Water + Material Mass (g)	M_2	7288	8137	8161	Measuring Cup Mass (g)	m_1	3188	3188	3188
Pycnometer + Water Mass (g)	M_3	6682	6314	6289	Measuring Cup Volume (l)	v	3	3	3
Material DKY Mass (g)	M_1	1008	3067	3038	Sample + Measuring Cup Mass (g)	m_2	7898	7362	7366
Material Oven-Dried Mass (g)	M_4	944	2950	2973	Loose Bulk Density (kg/dm^3)	ρ_b	1.57	1.391	1.393
Apparent Particle Density (kg/dm^3)	ρ_a	2.79	2.62	2.7	Porosity (%)	n	33	41	45
Oven-Dried Grain Density (kg/dm^3)	ρ_{rd}	2.35	2.37	2.55					
DKY Particle Density (kg/dm^3)	ρ_{ssd}	2.51	2.47	2.61					
Water Absorption (%)	WA24	6.8	4	2.2					

3.2. Fresh and Hardened Concrete Test Results

The fresh concrete properties of C30 target concrete produced with both aggregate types were found to be similar. The slump value of concrete produced with HSCA was measured as 83 mm, while that of concrete produced with LSCA was measured as 85 mm. The slump test setup is shown in Figure 5. These S2 class consistency values showed that, despite LSCA's higher water absorption rate, it did not pose a problem in terms of workability when

adjusted for water according to the saturated dry surface (SDS) condition. Different results were obtained from non-destructive tests performed on hardened concrete specimens. The non-destructive test results are shown in Table 6.

Figure 5. Slump test setup

Table 6. Schmidt hammer test and ultrasonic transit time test results

Sample No.	Schmidt Hammer Readings													Ultrasonic Readings			
	1	2	3	4	5	6	7	8	9	10	Average (R_c)	Strength Estimate (MPa)*	Average Strength Estimate (MPa)	Duration (µs)	Speed - V (km/h)	Strength Estimate (MPa)*	Average Strength Estimate (MPa)
Y1	26	24	25	26	27	26	28	24	29	24	26	30.81	26.56	33	4.2	32.84	33.03
Y2	25	25	24	28	22	29	25	25	24	26	25	27.47		34	4.4	39.69	
Y3	22	27	26	19	29	22	18	23	26	25	24	24.37		35.3	4.2	32.84	
Y4	21	22	26	18	26	24	24	26	20	22	23	21.51		34	4	26.92	
Y5	20	21	29	22	20	20	30	28	24	27	24	24.37		34.6	4.3	36.14	
Y6	28	22	28	22	30	30	26	27	20	22	26	30.81		33.5	4.1	29.77	
D1	22	21	18	21	27	29	23	24	26	27	23	21.51	23.06	33.6	4	26.92	27.10
D2	20	25	24	26	25	20	24	26	19	21	23	21.51		34.2	4.2	32.84	
D3	27	22	23	26	27	25	24	24	24	23	25	27.47		34	3.8	21.84	
D4	19	26	22	27	20	21	22	20	18	22	22	18.89		33.9	3.9	24.28	
D5	23	24	27	26	22	25	25	27	24	21	25	27.47		33.8	4.1	29.77	
D6	19	24	24	24	21	25	27	18	21	19	23	21.51		33.6	4	26.92	

*: Compressive strength estimates were calculated using Rc and V values.

In the estimated strength measurements performed with the Schmidt hammer, HSCA concrete (26.56 MPa) demonstrated higher performance than LSCA concrete (23.06 MPa). Similarly, in the estimated strength analysis performed using the ultrasonic transit velocity, HSCA concrete (33.03 MPa) yielded significantly higher results than LSCA concrete (27.10 MPa). The transmission velocity of HSCA concrete, averaging above 4.2 km/s, indicated a denser and more homogeneous internal structure compared to the velocity of LSCA concrete, which averaged 4.0 km/s. The results of the 28-day compressive strength test are given in Table 7 and the test setup is shown in Figure 6. The compressive strength results revealed a different outcome compared to the non-destructive

test results. Both concrete series achieved the targeted C30 class. The average compressive strength of concrete produced using HSCA was found to be 34.59 MPa, while that of concrete produced using LSCA was 35.63 MPa. LSCA concrete was found to have approximately 3% higher strength than HSCA concrete. This indicates that non-destructive tests (particularly Schmidt) require calibration for concrete containing RCA and may be misleading. The superior performance of LSCA concrete is most likely due to the mechanical quality of the aggregate and, in particular, the better optimised fine material ratio. The improved particle distribution in LSCA fills the fine material voids lacking in HSCA, creating a denser microstructure and a stronger cement paste-aggregate interface. This effect compensates for the potential negative impact of the aggregate's original low strength.

Table 7. Compressive strength test results

Compressive Strength Values (28 days)				
Sample No.	Unit Volume Mass (kg/dm^3)	Fracture Load (kN)	Strength (MPa)	Average Strength (MPa)
Y1	2.27	828.2	36.81	34.59
Y2	2.26	762.8	33.9	
Y3	2.25	773	34.36	
Y4	2.27	755.8	33.59	
Y5	2.23	744.8	33.1	
Y6	2.26	804.5	35.76	
D1	2.27	804.2	35.74	35.63
D2	2.25	781.4	34.73	
D3	2.28	783	34.8	
D4	2.23	798.6	35.49	
D5	2.24	812.8	36.12	
D6	2.26	830.8	36.92	

Y: Concrete produced from HSCA and D: Concrete produced from LSCA

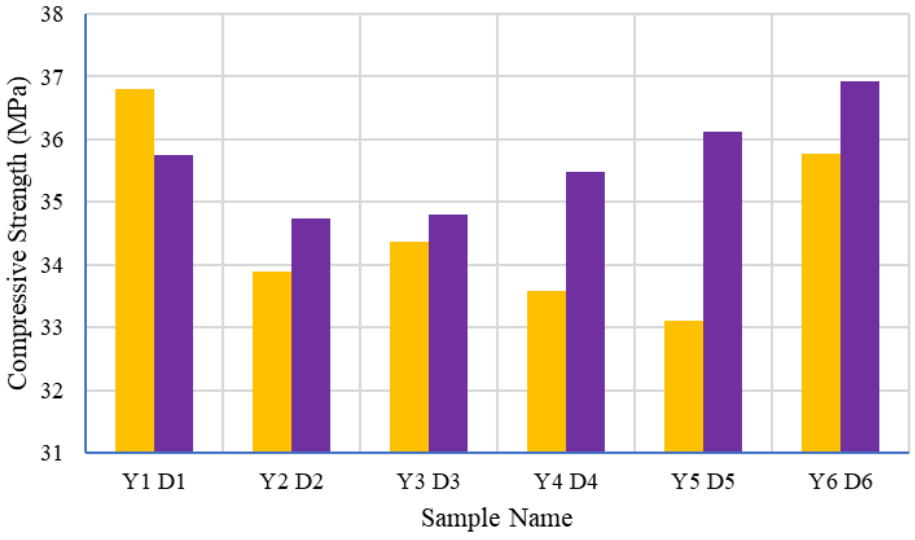

Figure 6. Compressive strength graphs of HSCA and LSCA

4. CONCLUSION

In this study, the properties of recycled aggregates (LSCA and HSCA) obtained from waste concrete sourced from construction laboratories and separated according to low strength class and high strength class were compared, along with the performance of C30 target concrete produced with these aggregates.

- As a result of the sieve analysis, LSCA showed a higher proportion of fine material compared to HSCA. For this reason, the amount of fine aggregate for HSCA was below the Fuller curve.
- The abrasion loss at the end of the abrasion test conducted on LSCA and HSCA aggregates was found to be 41% for HSCA and 32% for LSCA. The ASTM C-33 standard states that the LA percentage should not exceed 50% in concrete production. Accordingly, it was concluded that both types of concrete waste can be used in concrete production.
- The MB test was conducted to determine the quality of the fine material, and the MB values of the HSCA and LSCA materials were found to be 0.8g/kg.
- As a result of the test, the density values of both recycled aggregates were found to be lower than the density values of general natural aggregates, while their water absorption values were found to be higher.
- According to the Schmidt Hammer test results, the average estimated compressive strength was found to be 26.56 MPa for concrete produced from HSCA and 23.06 MPa for concrete produced from LSCA.
- According to the results of the ultrasonic transit time test, the average estimated compressive strength was found to be 33.03 MPa for concrete produced from HSCA and 27.10 MPa for concrete produced from LSCA.
- According to the 28-day compressive strength test results of the cube specimens, the average compressive strength was found to be 34.59 MPa for concrete produced from HSCA and 35.63 MPa for concrete produced from LSCA.

When the results of the study were evaluated collectively, it was observed that the Schmidt Hammer Test results for both groups of specimens were lower than the target concrete strength, while the ultrasonic test results were close to the target strength. The compressive strength results, on the other hand, showed that both groups of specimens achieved the target design strength. The concrete strength produced from LSCA was found to be approximately 1% higher than that from HSCA. This is thought to be due to the fact that the fine material ratio in LSCA is slightly higher than in HSCA. In conclusion, it was found that aggregates obtained from concrete waste with both strengths can be used as aggregates in concrete production.

Acknowledgments

This paper utilizes data from the project entitled “Investigation of the Use of Concrete Wastes/Debris Produced in Different Strength Classes as Recycled Aggregate and the Differences in Mechanical Properties Among Them,” which was supported by the TUBİTAK-2209/A program (2023/2 Term).

References

[1] A. Koken, M. A. Koroglu, and F. Yonar, “The usability of waste concrete as concrete aggregate,” *Selcuk University Technical Sciences Vocational School Technical-Online Journal*, vol. 7, no. 1, pp. 86–97, 2008.

[2] I. Demir, “The use of construction waste in concrete production and its effect on concrete properties,” *Afyon Kocatepe University Journal of Science and Engineering*, vol. 9, no. 2, pp. 105–114, 2009.

[3] G. Durmus, O. Can, and O. Simsek, “Determination of the engineering properties of different classes of concrete produced from recycled aggregates," in *5th International Advanced Technologies Symposium (IATS’09)*, Karabük, Turkey, May 13–15, 2009.

[4] T. C. Hansen and H. Narud, “Strength of recycled concrete made from crushed concrete coarse aggregate,” in *Concrete International: Design and Construction*, 1983, pp. 79–83.

[5] A. Nealen and M. Ruhl, “Consistency aspects in the production of concrete using aggregates from recycled demolition material,” in *Darmstadt Concrete*, 1997.

[6] H. Polat, U. E. Yurtcan, and M. N. Kolak, “Investigation of the usability of waste kerbstones as concrete aggregate,” *Journal of Nature and Science*, vol. 3, no. 2, pp. 37–41, 2014.

[7] M. M. Tufekci, “Investigation of the reusability of recycled aggregates in concrete production,” M.Sc. thesis, Institute of Science, Yıldız Technical University, 2011.

[8] C. Demirel and O. Simsek, “Investigation of the effect of using waste concrete as recycled aggregate in concrete production on compressive strength," in *International Academic Research Congress*, Antalya, Turkey, Oct. 18–21, 2017, pp. 1026–1031.

[9] *Beton - Karma suyu - Numune alma, deneyler ve beton endustrisindeki islemlerden geri kazanilan su dahil, suyun, beton karma suyu olarak uygunlugunun tayini kurallari*, TS EN 1008, Türk Standartları Enstitüsü, 2003.

[10] *Tests for geometric properties of aggregates – Part 1: Determination of gradation – Sieve analysis*, TS EN 933-1, Turkish Standards Institute, Ankara, 2012.

[11] *Tests for mechanical and physical properties of aggregates – Part 2: Methods for determining resistance to fragmentation*, TS EN 1097-2, Turkish Standards Institute, Ankara, 2020.

[12] *Tests for geometric properties of aggregates – Part 9: Determination of fine particles – Methylene blue test*, TS EN 933-9, Turkish Standards Institute, Ankara, 2022.
[13] *Tests for geometric properties of aggregates – Part 3: Flatness index*, TS EN 933-3, Turkish Standards Institute, Ankara, 2012.
[14] *Tests for physical and mechanical properties of aggregates – Part 6: Determination of particle density and water absorption*, TS EN 1097-6, Turkish Standards Institute, Ankara, 2022.
[15] *Concrete aggregates*, TS 706 EN 12620+A1, Turkish Standards Institute, Ankara, 2009.
[16] *Concrete – Properties, performance, production and conformity*, TS EN 206+A2, Turkish Standards Institute, Ankara, 2021.
[17] *Concrete – Fresh concrete tests – Part 2: Slump test*, TS EN 12350-2, Turkish Standards Institute, Ankara, 2019.
[18] *Determination of compressive strength of concrete in structures and precast concrete components in situ*, TS EN 13791, Turkish Standards Institute, Ankara, 2019.
[19] *Concrete tests in structures – Part 4: Determination of ultrasonic pulse wave velocity*, TS EN 12504-4, Turkish Standards Institute, Ankara, 2021.
[20] *Concrete – Tests on hardened concrete – Part 3: Determination of compressive strength of test specimens*, TS EN 12390-3, Turkish Standards Institute, Ankara, 2019.
[21] *Standard specification for concrete aggregates*, ASTM C33-07, ASTM International, West Conshohocken, PA, 2007.

2nd International Conference on Multidisciplinary Sciences and Technological Developments (ICMUSTED 2025)

December 12-15, 2025

Numerical Modelling of Moisture Loss and Oil Uptake in Noodle Strips During Deep-Fat Frying Using Finite Difference and Finite Element Methods

Serpil Pekdogan Goztok[1], Cihat Guner[2], Hakan Basdogan[2], Omer Said Toker[3]

[1]Department of Food Processing Programme, Siirt University, Siirt, Türkiye
[2]Eris R&D Center, Tekirdag, Türkiye
[3]Department of Food Engineering, Yildiz Technical University, Istanbul, Türkiye
Corresponding author: Serpil Pekdogan Goztok (e-mail: serpilpekdogan@gmail.com)

Abstract

This study aimed to experimentally characterize and numerically model moisture loss and oil uptake in noodle strips during deep-fat frying. Noodles of fixed geometry (≈ 10×8×2.5 cm^3) were fried in refined palm oil at 135 °C for up to 240 s, and their moisture and fat contents were determined gravimetrically and by Soxhlet extraction, respectively. The initial moisture and fat contents were ≈ 19.0% and 7.8% (wb). Effective moisture diffusivity (D_w) was determined from Fick's second law for three-dimensional finite slabs, moisture diffusion coefficient D_w = 8.80×10^{-7} m^2/s (R^2 = 0.97). The overall mass transfer coefficient was found to be k_c = 0.0043–0.0054 s^{-1}. Moisture and oil transport were modeled using coupled diffusion equations solved by two numerical models: a finite difference (FD) method implemented in MATLAB and a finite element (FE) method implemented in COMSOL Multiphysics. Oil diffusivity was linked to moisture content through an empirical relationship to capture simultaneous water loss and oil gain. The mass transfer phenomena occurring during deep-fat frying were accurately captured by both the FD and FE models. Both models reasonably reproduced the experimental trends, with rapid moisture depletion and concurrent oil penetration in the early stages, followed by a deceleration associated with crust formation. For moisture loss, the FD model showed better agreement over the entire process (average error −5.50%), whereas the FE model more accurately predicted the final moisture content (final error −2.13%). For oil uptake, the FE model provided the closest fit to experimental data (final error 0.51%; average error −7.17%). Three-dimensional simulations revealed the formation of a low-moisture depletion front and preferential oil accumulation in the crust region. The proposed modelling framework offers a useful tool for optimizing frying conditions, controlling oil uptake, and improving product quality in industrial noodle processing.

Keywords: Deep-fat frying, Noodle, Moisture diffusivity, Oil uptake, Numerical modelling

1. INTRODUCTION

Deep-fat frying is a key thermal processing step widely used in the industrial production of many foods, including potato products, meat products, bakery items, and snacks. During frying, simultaneous heat and mass transfer occur between the product and the hot oil phase, leading to a series of complex physical and chemical processes such as evaporation of internal moisture, development of a porous structure, crust formation, and oil penetration into the product matrix [1–3]. While frying contributes desirable quality attributes such as a crispy crust, characteristic aroma, colour, and pleasant texture, it must be carefully controlled because of its association with high fat content, oxidative degradation products, and the formation of potentially harmful compounds such as acrylamide [3, 4].

Instant noodle products have become one of the most rapidly growing carbohydrate-based foods worldwide due to their ease of preparation, low cost, and long shelf life. In typical industrial processing, noodle dough is mixed, sheeted and cut, then steam-precooked, followed by deep-fat frying in palm oil or its fractions to obtain low-moisture, porous noodle cakes. In commercial applications, palm oil and palm olein/stearin blends are commonly preferred because of their favourable frying stability and oxidative resistance [5–7]. However, the fat content of fried instant noodles often reaches levels of around 20–25%, making the control of oil uptake through formulation and process optimisation an important technological objective [5, 8].

In recent years, fried noodle products have been increasingly examined from nutrition and public health perspectives due to their high fat and sodium contents, acrylamide formation, and oxidative stability issues during

storage [3, 4, 9]. Various strategies have been proposed to reduce oil uptake, including the use of alternative frying oils and oleogel systems, pre-drying or pre-cooking treatments, and incorporation of dietary fibre or hydrophilic/hydrophobic additives into the dough formulation [8, 9]. Although these approaches provide valuable practical information for reducing fat content and improving quality parameters, in many studies the underlying water–oil mass transfer mechanism is not described in terms of fundamental transport parameters such as effective diffusion coefficients and mass transfer coefficients, and remains mainly empirical [2, 9].

In frying and drying studies, moisture loss in foods is most commonly described using diffusion models based on Fick's second law, and the effective moisture diffusivity (D_{eff}) is used as a key parameter characterising internal mass transfer resistance. Reported D_{eff} values for various deep-fat fried foods generally cluster within the range of 10^{-10}–10^{-8} m^2/s, although this range may broaden depending on product structure, temperature, geometry, pretreatments, and the properties of the frying medium [2, 10–13]. Similarly, external mass transfer at the product–oil interface is expressed in terms of convective mass transfer coefficients and empirical rate constants, which play a critical role in process design and optimisation [1, 14]. However, in many studies heat and mass transfer are treated separately, and the actual three-dimensional geometry of the product is simplified, which may lead to less realistic estimates of mass transfer coefficients [14].

Mathematical models developed for deep-fat frying have been successfully applied to describe both heat and mass transfer in various systems such as potato slices, root vegetables, composite products, and bakery items. In these studies, Fick-based differential equations were solved using different mathematical models to predict product centre temperature, moisture content, and oil uptake, and the model results were validated against experimental data [10–12, 15]. Furthermore, studies focusing on the relationship between water loss and oil uptake—especially in potatoes and chicken—have shown that rapid early-stage moisture loss is accompanied by simultaneous oil penetration, whereas at later stages the rate of oil uptake decreases due to crust formation and pore filling [16, 17]. These findings highlight the need to model frying processes not only through empirical final-point measurements, but also by capturing the distributional and time-resolved evolution of diffusion phenomena.

A review of the literature on noodle products shows that most studies focus on the effects of formulation changes—such as frying oil type, oleogel use, emulsifiers, and polysaccharide/thickener additions—on oil uptake, moisture content, colour, and texture [5–8]. While these works provide important practical insights into lowering oil absorption and improving quality, they typically report bulk moisture and fat contents and rarely employ three-dimensional numerical models that describe the spatial and temporal distribution of water and oil in the product during frying via effective diffusion coefficients and mass transfer coefficients. In particular, comprehensive studies applying detailed 3D diffusion-based models to steamed, pre-cooked, thin and porous noodle strips, and systematically comparing FD and FE approaches on the same geometry, are extremely limited.

In this context, the aim of the present study is to investigate, both experimentally and numerically, moisture loss and oil uptake in wheat-based, steam-precooked noodle strips during deep-fat frying in palm oil, and to determine the key mass transfer parameters governing the process. To this end, (i) effective moisture diffusivity and mass transfer coefficients for noodle samples under frying conditions were determined, (ii) a three-dimensional mathematical model was developed to describe water loss and oil uptake based solely on diffusion-driven mass transport, (iii) the model was numerically solved using a finite difference (FD) code developed in MATLAB and a finite element (FE) model implemented in COMSOL Multiphysics, and (iv) the predictions were compared with experimentally measured moisture and oil contents throughout frying to evaluate the performance of the two numerical approaches. In this way, the study seeks to quantitatively describe the characteristic "rapid water loss–limited oil uptake" behaviour of deep-fat fried noodle products within a diffusion-based framework, and to provide a practical tool for the design and optimisation of industrial frying processes.

2. MATERIAL AND METHOD

2.1. Materials and Sample Preparation

Wheat-based, steam-precooked noodle strips produced on an industrial instant noodle line were used in this study. After production under standard factory conditions, samples underwent a standardized pre-frying preparation: steam-precooking was completed on the line, the noodles were then briefly equilibrated at ambient conditions to stabilize surface moisture, and no batter/coating was applied prior to frying. The strip dimensions were kept constant throughout the experiments; noodles were cut to width ≈ 10 cm, length ≈ 8 cm, and thickness ≈ 2.5 cm, and this geometry was transferred unchanged to the numerical models. To define the initial state for numerical modeling, measurements performed immediately before frying (t = 0 s) indicated an initial moisture content of ≈ 19.0% (wb) and an initial fat content of ≈ 7.8% (wb). All experiments were conducted with replicate measurements

at each temperature–time condition, and the resulting data were subsequently used for calibration and validation of the FD and FE models presented in the following sections.

2.2. Frying Procedure

Frying operations were carried out in a thermostat-controlled benchtop fryer using refined palm oil. Palm oil and its fractions (notably palm olein/stearin) are widely adopted in instant-noodle frying and offer thermo-oxidative stability advantages [6, 17–19]. To maintain bath temperature stability, the fryer was pre-equilibrated to the set point, and a high oil-to-product ratio was preserved to minimize temperature sag during processing [20–22]. Experiments were conducted at 135 °C and frying time was set within 0–240 s; during the early stage (0–60 s), sampling frequency was increased to capture crust formation and accelerated mass transfer. Throughout frying, both the oil-bath temperature and the product centre temperature were monitored simultaneously; core temperature was measured with a fine-tip thermocouple inserted into the geometric center of the noodle strip. In deep-fat frying studies, center-probe thermocouple placement is a common practice for core temperature measurement [23–25]. Upon reaching the target time, samples were removed from the bath, briefly drained to remove surface-carried free oil, cooled briefly at ambient conditions, and then subjected to the planned analyses (moisture, fat, etc.). The oil-bath temperature was continuously tracked; when necessary, filtration/renewal was performed, as oil quality indices (e.g., total polar matter (TPM), free fatty acid (FFA), peroxide value (PV)) are critical to product safety and quality in deep-fat frying [21, 24]. Overall, the process entails simultaneous heat and mass transfer accompanied by crust formation phenomena [3, 26].

2.3. Analytical Measurements

Moisture content was determined by the loss-on-drying procedure in a forced-air oven at 105 °C to constant mass, following the principles of Association of Official Analytical Collaboration (AOAC) AOAC 925.10 and the American Association of Cereal Chemists (AACC) 44-15.02 air-oven method; results are reported on a wet basis (% wb) [27–29]. Total fat was quantified by Soxhlet extraction using petroleum ether as solvent, in accordance with the AOAC ether-extract family of methods (e.g., AOAC 920.39 and AOAC 945.16); the equivalence of petroleum ether and hexane for lipid extraction in food matrices is documented in the literature [30–32]. All assays were performed with $n \geq 3$ replicates, and data are expressed as mean ± standard deviation (SD); routine good laboratory practices were applied for sample preparation, instrument calibration, and weighing to ensure analytical precision and repeatability.

2.4. Mathematical Modelling and Numerical Solution

2.4.1. Determination of Effective Moisture Diffusivity

The effective moisture diffusivity (D_w) of noodle strips during frying was determined using Fick's second law of diffusion (Equation (1)):

$$\frac{\partial M}{\partial t} = D_w \frac{\partial^2 M}{\partial x^2} \tag{1}$$

where M is the moisture content (kg water/kg wet product), x is the diffusion distance (m), t is time (s), and D_w is the effective moisture diffusivity (m^2/s).

The initial and boundary conditions were defined as Equation (2):

$$\begin{aligned} t = 0 \quad & -L < x < L \quad M = M_i \\ t > 0 \quad & x = 0 \quad \frac{dM}{dx} = 0 \\ t > 0 \quad & x = L \quad M = M_e \end{aligned} \tag{2}$$

When ambient humidity is constant in the frying process, moisture content is reduced to the fractional moisture ratio (MR), the distance from the center in food is expressed by using dimensionless distance variable ($n = x/L$), and the time is non-dimensional time. Mass Fourier number ($Fo_m = D_w\ t/L^2$) was converted and resolved analytically to achieve Equation (3) for frying of noodle [33].

$$MR = \frac{M_t - M_e}{M_i - M_e} = A_1 \sum_{n=1}^{\infty} \frac{1}{(2n-1)^2} \exp\left[\frac{-(2n-1)^2 \pi^2 D_w t}{A_2}\right] \quad (3)$$

where MR is the fractional MR, M_i is the initial moisture content (kg water/kg dry matter), M_e is the equilibrium moisture content (kg water/kg drymatter), M_t is the moisture content of product at time t (kg water/kg dry matter). L was the half thickness (m) since the frying occurred from both surfaces. For long osmotic dehydration times, only first term of the sum in Equation (4) was used [33].

$$MR = A_1 \exp\left[-\frac{\pi^2 D_w t}{A_2}\right] \quad (4)$$

where A_1 is $\left(8/\pi^2\right)^3$, A_2 is $1/\left(L_1^2 + L_2^2 + L_3^2\right)$ for 3-dimensional finite slab.

$$slope = -\frac{\pi^2 D_w}{A_2} \quad (5)$$

where L_x, L_y, and L_z are half-thicknesses along the x, y, and z directions, respectively. This approach accounts for the 3D geometry of the noodle strips during frying.

Oil uptake during frying was coupled with water loss by relating the effective oil diffusivity (D_o) to the water diffusivity as follows:

$$D_o = D_w \left(1 - \frac{X_i}{X_{inital}}\right)^m \quad (6)$$

where X_i is the moisture content at time i, $X_{initial}$ is the initial moisture content, and m is an empirical constant determined by fitting the model to experimental oil uptake data. This relationship allowed simultaneous prediction of water loss and oil gain during frying.

2.4.2. Mathematical Model

Moisture loss and oil uptake during frying were modeled based solely on diffusion-driven mass transport within the noodle matrix. Porosity changes and shrinkage were neglected, and the noodle samples were assumed to be geometrically fixed, homogeneous, and isotropic. Accordingly, two separate partial differential equations based on Fick's second law were employed for moisture (water) and oil:

$$\frac{\partial C_w}{\partial t} = D_w \frac{\partial^2 C_w}{\partial x^2} \quad (7)$$

$$\frac{\partial C_o}{\partial t} = D_w \frac{\partial^2 C_o}{\partial x^2} \quad (8)$$

Where, C_w and C_o are represent the moisture (water) and oil concentrations of noodle (mol/m^3), respectively, while D_w and D_o is the effective diffusion coefficients (m^2/s). At the beginning of the frying process, the initial moisture and oil distributions were assumed to be uniform:

$$C_w(x, y, z, 0) = C_{w,0} \quad (9)$$

$$C_o(x, y, z, 0) = C_{o,0} \quad (10)$$

During frying, moisture evaporation at the surface and oil penetration into the noodle were described by convective mass transfer boundary conditions. The corresponding surface mass fluxes were expressed as follows:

$$-D_w \left.\frac{\partial C_w}{\partial t}\right|_{surface} = k_w \left(C_{w,surface} - C_{w,e}\right) \quad (11)$$

$$-D_o \left.\frac{\partial C_o}{\partial t}\right|_{surface} = k_o \left(C_{o,surface} - C_{o,e}\right) \quad (12)$$

where k_w and k_o are the mass transfer coefficients for moisture and oil (m/s), and $C_{w,e}$ and $C_{o,e}$ denote the equilibrium concentrations in the frying medium. Experimentally determined mass transfer coefficients were k_w = 0.00043 m/s for water and k_o = 0.00054 m/s for oil.

2.4.3. Numerical Modelling

To investigate the mechanisms of moisture loss and oil uptake during frying, the mass transfer equations were solved in three dimensions. COMSOL Multiphysics (5.2a, USA) and MATLAB (R2019b, MathWorks, USA) were used with academic licenses for numerical modeling. Only diffusion-based moisture and oil transport were considered, while porosity changes, shrinkage, and heat–mass transfer interactions were neglected.

The COMSOL solution consisted of four stages: geometry construction, module selection and parameter definition, mesh generation, and execution of the solution procedure. Mass transfer was solved using the transport of diluted species module based on Fick's second law with a three-dimensional FE approach. Mesh sensitivity analyses indicated that the best convergence was achieved using a mesh structure comprising 660 boundary, 84 edge, and 8 vertex elements.

In the MATLAB environment, the same differential equations were solved using an implicit time-stepping scheme, and the numerical solution was implemented with a FD-based code developed by the researcher. The results obtained from these two numerical approaches (FE and FD) were compared to evaluate the temporal variation of moisture and oil distribution at the noodle center throughout the frying process.

2.5. Statistical Evaluation

The model fit was evaluated by comparing the experimental data obtained during frying with the model predictions. The average deviation over the entire frying period was calculated as the "average error%" (Equation (13)), while the deviation between the model predictions and the targeted experimental data at the end of frying was determined as the "final error%" (Equation (14)).

$$\text{the average error\%} = \sum_{i=1}^{x} \frac{V_{exp_i} - V_{pred_i}}{V_{exp_i}} \times 100 \quad (13)$$

$$\text{the final error\%} = \sum_{i=1}^{x} \frac{V_{exp} - V_{pred}}{V_{exp}} \times 100 \quad (14)$$

where V_{exp} is the experimental data, V_{pred} is the model prediction and i indicates the value at any instant of drying time.

3. RESULTS

3.1. The Effective Diffusion Coefficient

The effective moisture diffusivity of the noodle samples was determined as 8.80×10^{-7} m^2/s, with a coefficient of determination (R^2) of 0.97. Adedenji et al. reported that, for microwave-precooked chicken nuggets subjected to different power levels, frying temperatures and times, the effective moisture diffusivity of breaded and unbreaded samples ranged between 6.39×10^{-10}–15.47×10^{-10} m^2/s and 1.77×10^{-10}–14.0×10^{-10} m^2/s, respectively [31]. Similarly, in a study on the deep-fat frying of potato slices, the effective moisture diffusivity was reported to be 9.1×10^{-9}–1.3×10^{-8} m^2/s, and these values were noted to be consistent with the more compact structure of potato tissue [33]. Demiray et al. determined effective moisture diffusivities of 2.74×10^{-8}, 8.22×10^{-8}, and 1.37×10^{-7} m^2/s for chicken nuggets fried at 160, 170, and 180 °C, respectively [34]. The value of 8.80×10^{-7} m^2/s obtained for the noodle samples in the present study is close to the value reported by Demiray et al. at the highest frying

temperature, whereas water transport occurred much more rapidly than in chicken nuggets and potato slices reported in the literature [16, 18, 20, 34, 35]. It is thought that the gluten–starch matrix of the noodle dough provides a more permeable network structure, with greater porosity formation during frying compared with chicken nuggets or potatoes, and that the smaller sample thickness further accelerates the transport of water from the interior to the surface [35–37].

In this study, the mass transfer coefficient was found to be in the range k_c = 0.0043–0.0054 s^{-1}. These values are comparable to those reported in the literature for the frying of chicken nuggets. Demiray et al. reported mass transfer coefficients for oil uptake in chicken nuggets in the range 0.0082–0.0094 s^{-1}, and indicated that the rate of oil uptake increased with increasing temperature [34]. Consistent with this, the value of the exponent m = 0.25 obtained in the equation used to model oil uptake indicates a pronounced deceleration in the later stages of frying. This behavior is also considered to be in agreement with the underlying physical mechanism, whereby the crust structure densifies and pores become filled with oil as frying progresses, thereby reducing the effective diffusion pathway for oil [18, 37]. Moreover, product type and frying conditions are important parameters determining the rate constants of oil absorption and water loss [16, 18, 20, 31, 33, 35], and, to the best of our knowledge, no data are available in the literature on the rate constants and effective diffusivity values for oil and water diffusion in products such as noodles.

Overall, considering the effective moisture diffusivity and mass transfer coefficient calculated for the noodle samples, it can be stated that the system is characterized by "rapid water loss–limited oil uptake". The differences observed between the D_{eff} and k values reported in the literature for chicken nuggets, potatoes and the noodle samples in the present study can be attributed to factors such as product type, size, frying conditions and the type of frying oil, all of which strongly influence mass transfer coefficients [18, 33].

3.2. Numerical Modelling

In this study, two different numerical methods, namely the FD and FE methods, were employed to mathematically model moisture loss and oil uptake in noodle samples during frying. The experimentally determined changes in moisture and oil content were compared with the predictions of both methods, and the time-dependent evolution of three-dimensional diffusion fields was examined in detail.

The findings showed that, during frying, water and oil transfer occur simultaneously and in a nonlinear manner, whereby the moisture content decreases rapidly while, in parallel, oil penetrates into the product. This behaviour is consistent with the typical mass transfer mechanism reported in the literature for noodles, potatoes and similar porous foods [18, 33].

In Figure 1, the experimental moisture and oil contents at the centre of the noodle sample are presented in comparison with the FD and FE model predictions. The moisture content (Figure 1(a)) exhibited a rapid decrease during the first 180 s of frying due to intense surface evaporation, after which the rate of moisture loss declined and approached an almost constant level. Similar findings have been reported in previous studies [33, 37].

The FD model provided predictions that were more consistent with the experimental data in the early stages of frying with respect to moisture loss. The FE model, on the other hand, yielded a more balanced agreement with the experimental data for moisture diffusion over the entire frying period. In particular, after 180 s, the FE model produced results that were closest to the experimental values. For water transfer, the FD method yielded a final percentage error of −14.58% and an average error of −5.50% over the frying period. For the same parameter, the FE method gave a final percentage error of −2.13% and an average percentage error of 15.13%. While the FE method better predicted the target final moisture content, the FD method provided the best overall agreement between model and experimental data for water transfer throughout the frying process.

The time-dependent changes in oil content also increased in a manner consistent with moisture loss (Figure 1(b)). The reduction in oil uptake towards the end of frying is associated with the progressive development of a more pronounced crust at the product surface as temperature rises. The formation of this crust structure restricts moisture escape and consequently hinders oil transfer into the product [20, 35].

The FD approach adapted more rapidly to the experimental data for oil uptake at the centre during the early stages of frying; however, the agreement between the experimental and model data decreased towards the end of frying. In contrast, in the FE model, the agreement with experimental data improved at the end of the frying period. The model performances were also confirmed by percentage error values. For oil transfer, the FD model yielded a final percentage error of −14.77% and an average percentage error of −0.92%, whereas the FE model provided the

closest fit to the experimental data, with a final percentage error of 0.51% and an average error of −7.17%. These results are consistent with the frying mechanism reported in the literature. Ngadi et al. indicated that a rapid increase in surface temperature occurs during the first 30–90 s of frying, which enhances oil penetration accompanying the rapid removal of moisture [18]. Similarly, the present study demonstrates that the model successfully captures the rapid early-stage moisture loss and the associated oil transfer. Final percentage error analysis for water and oil showed that the FE method predicts end-point values more accurately, whereas the FD approach provides a more consistent representation of behaviour over the entire frying period.

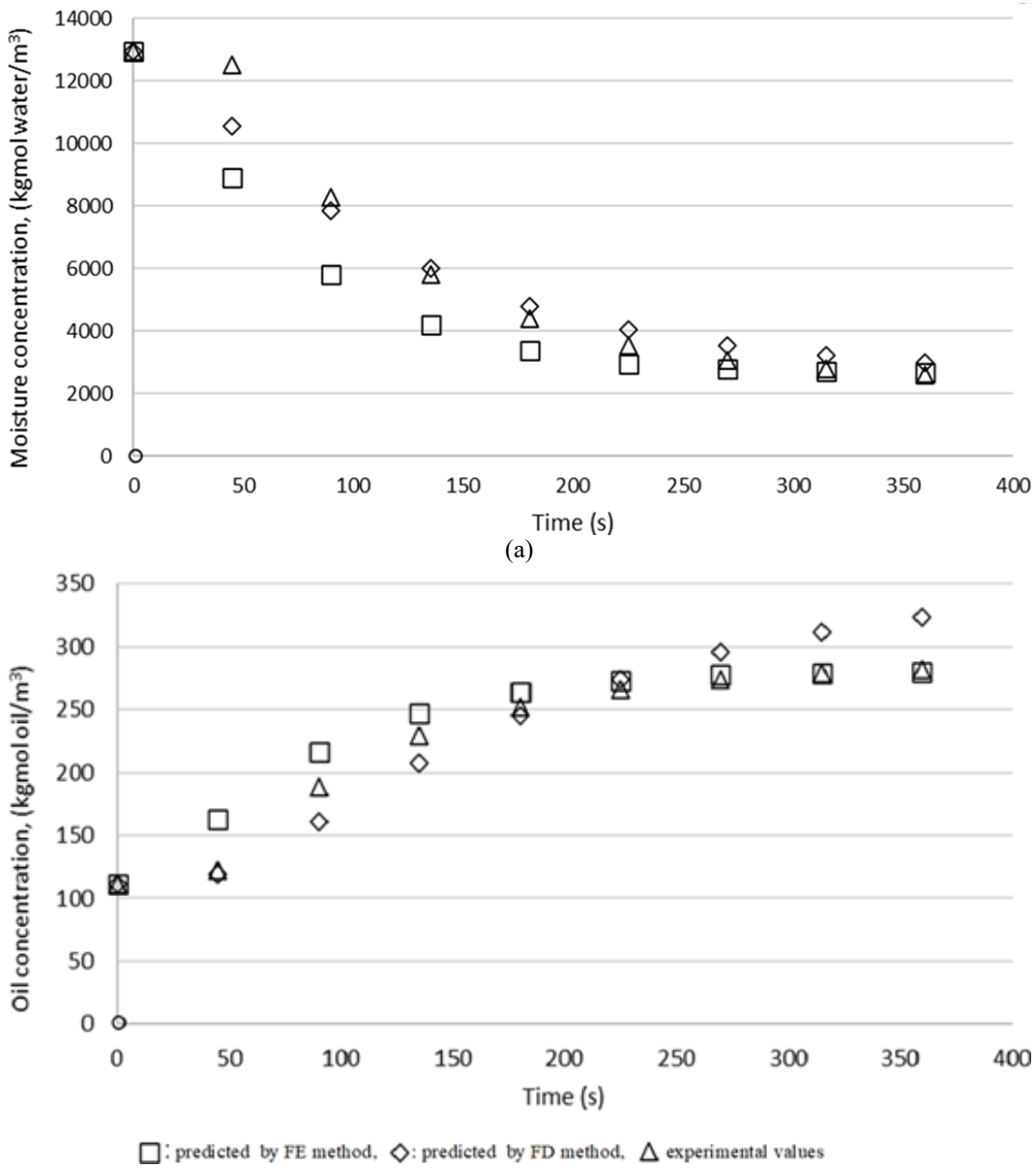

Figure 1. Comparison of experimental and predicted moisture and oil content changes at the centre of noodles during frying: (a) Predicted moisture content and (b) Predicted oil content.

The comparison of FD and FE methods in Figure 2 shows the three-dimensional distributions of moisture and oil in the noodle samples during frying. The representational capability of both methods was evaluated based on the spatial evolution of diffusion. From 90 s onwards, the moisture profiles exhibited a pronounced decrease at the surface, forming a low-moisture "depletion front" progressing towards the centre between 180 and 270 s. This behaviour is explained by crust formation and changes in the pore structure during frying. In the FD model, this front appears sharper and more clearly defined, whereas the FE model better captures the continuity of diffusion, resulting in a more realistic moisture gradient.

A similar time-dependent progression was observed in oil distributions. In particular, the rapid accumulation of oil in the crust region between 180 and 360 s, followed by its migration into the inner regions, was represented with a smoother transition in the FE model.

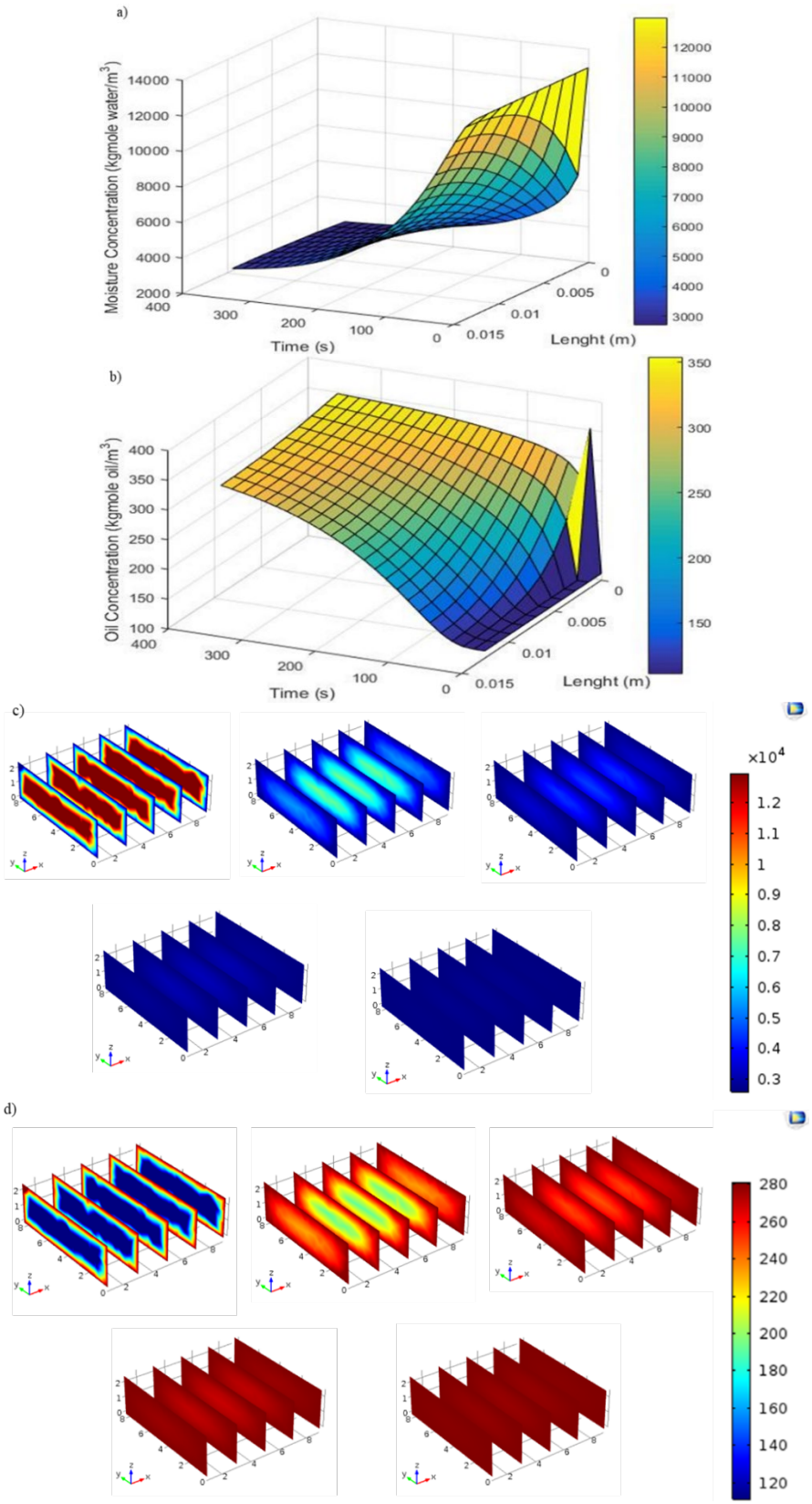

Figure 2. Moisture and oil distributions in noodles during frying: (a) Moisture content predicted by the FD method, (b) oil content predicted by the FD method, (c) moisture concentration (kg mole water/m³) predicted by the FE method, and (d) oil concentration (kg mole oil/m^3) predicted by the FE method.

This modelling approach represents a valuable tool for the optimisation of industrial frying processes, control of oil uptake, reduction of undesired component formation (such as acrylamide), and improvement of process design. The findings obtained are expected to directly contribute to process engineering applications such as determining appropriate frying times in production lines for carbohydrate-rich products like noodles, improving energy efficiency, and standardising final product quality.

4. CONCLUSION

This study demonstrated that a diffusion-based, three-dimensional numerical model (FD and FE) successfully described the coupled phenomena of moisture loss and oil uptake in noodle strips during deep-fat frying. By integrating experimentally obtained transport parameters with FD and FE solutions of Fick's law, the work provides a mechanistic understanding of how moisture and distribute through starch–gluten matrix under frying condition.

The modelling outcomes highlight those noodles exhibit a characteristic "rapid water loss–limited oil uptake" behavior, which is technologically advantageous for developing fried products with lower fat content while maintaining desirable texture. The ability of the models to resolve spatial and temporal gradients in moisture and oil also offers a powerful tool for predicting crust formation, internal moisture distribution, and oil localization within the product.

From an industrial perspective, the proposed approach can support the rational design and optimization of frying processes for carbohydrate-rich products such as noodles. In particular, it can be used to select appropriate frying times and conditions to balance dehydration, oil uptake, and product quality, as well as to evaluate the impact of process modifications (e.g., geometry, formulation, or oil type) without exhaustive trial-and-error experimentation. Furthermore, the framework can be extended to assess strategies aimed at reducing undesirable compounds formed during frying, thereby contributing to healthier product formulations and improved process sustainability.

Acknowledgments

This study was conducted within the framework of a university–industry collaboration between Erisler Gida R&D Center, Siirt University, and Yildiz Technical University. The authors gratefully acknowledge the technical and infrastructural support provided by all partner institutions.

References

[1] A. Safari, R. Salamat, and O.-D. Baik, "A review on heat and mass transfer coefficients during deep-fat frying: Determination methods and influencing factors," *Journal of Food Engineering*, vol. 230, pp. 114–123, 2018. doi: 10.1016/j.jfoodeng.2018.01.022

[2] K. K. Dash, M. Sharma, and A. Tiwari, "Heat and mass transfer modeling and quality changes during deep fat frying: A comprehensive review," *Journal of Food Process Engineering*, vol. 45, no. 4, art. no. e13999, 2022. doi: 10.1111/jfpe.13999

[3] K. Bordin, M. T. Kunitake, K. K. Aracava, and C. S. Trindade, "Changes in food caused by deep fat frying: A review," *Archivos Latinoamericanos de Nutrición*, vol. 63, no. 1, pp. 5–13, 2013.

[4] A. Dangal, R. Tahergorabi, D. R. Acharya, P. Timsani, K. Rai, S. Dahal, et al., "Review on deep-fat fried foods: Physical and chemical attributes, and consequences of high consumption," *European Food Research and Technology*, vol. 250, no. 6, pp. 1537–1550, 2024. doi: 10.1007/s00217-024-04482-3

[5] J. Qi, X. Wang, X. Wang, C. C. Akoh, and Q. Jin, "Effect of oil type and emulsifier on oil absorption of steam-and-fried instant noodles," *Journal of Oleo Science*, vol. 68, no. 6, pp. 559–566, 2019. doi: 10.5650/jos.ess18217

[6] E. Z. H. Ooi, N. A. A. Karim, E.-S. Chan, Y. Wang, T.-K. Tang, S. C. Tong, et al., "Underutilised palm stearin as hard stock for deep-frying medium and its performance for oil uptake in instant noodles," *Journal of the Science of Food and Agriculture*, vol. 104, no. 7, pp. 3958–3970, 2024. doi: 10.1002/jsfa.13278

[7] P. Noonim, B. Rajasekaran, and K. Venkatachalam, "Effect of palm oil–carnauba wax oleogel processed with ultrasonication on the physicochemical properties of salted duck egg white fortified instant noodles," *Gels*, vol. 8, no. 8, art. no. 487, 2022. doi: 10.3390/gels8080487

[8] M. Tanaka, E. Kanai, S. Kitano, H. Takizawa, T. Asakura, S. Tanabe, et al., "Reducing the oil content of fried noodles through forming a rough and coarse gluten network," *Journal of Food Processing and Technology*, vol. 8, pp. 1–5, 2017.

[9] N. Mahmud, J. Islam, W. Oyom, K. Adrah, S. C. Adegoke, and R. Tahergorabi, "A review of different frying oils and oleogels as alternative frying media for fat-uptake reduction in deep-fat fried foods,"

Heliyon, vol. 9, no. 11, art. no. e21500, 2023. doi: 10.1016/j.heliyon.2023.e21500
[10] G. Gholamibozanjani, S. Y. Leong, I. Oey, P. Bremer, P. Silcock, and M. Farid, "Heat and mass transfer modeling to predict temperature distribution during potato frying after pre-treatment with pulsed electric field," *Foods*, vol. 10, no. 8, art. no. 1679, 2021. doi: 10.3390/foods10081679
[11] M. O. Ngadi, K. C. Watts, and L. R. Correia, "Finite element method modelling of moisture transfer in chicken drum during deep-fat frying," *Journal of Food Engineering*, vol. 32, no. 1, pp. 11–20, 1997. doi: 10.1016/S0260-8774(97)00095-2
[12] A. Ahromrit and P. K. Nema, "Heat and mass transfer in deep-frying of pumpkin, sweet potato and taro," *Journal of Food Science and Technology*, vol. 47, no. 6, pp. 632–637, 2010. doi: 10.1007/s13197-010-0100-7
[13] R. G. Math, V. Velu, A. Nagender, and D. G. Rao, "Effect of frying conditions on moisture, fat, and density of papad," *Journal of Food Engineering*, vol. 64, no. 4, pp. 429–434, 2004. doi: 10.1016/j.jfoodeng.2003.11.010
[14] Y. E. Kose, "Kinetic modeling of heat and mass transfer during deep fat frying of churro," *Bilge International Journal of Science and Technology Research*, vol. 6, no. 1, pp. 46–51, 2022. doi: 10.30516/bilgesci.1064191
[15] L. S. Kassama and M. O. Ngadi, "Pore development in chicken meat during deep-fat frying," *LWT – Food Science and Technology*, vol. 37, no. 8, pp. 841–847, 2004. doi: 10.1016/j.lwt.2004.03.010
[16] M. K. Krokida, V. Oreopoulou, and Z. B. Maroulis, "Water loss and oil uptake as a function of frying time," *Journal of Food Engineering*, vol. 44, no. 1, pp. 39–46, 2000. doi: 10.1016/S0260-8774(99)00163-6
[17] H. Mori and T. Kaneda, "Food uses of palm oil in Japan," *Food and Nutrition Bulletin*, vol. 15, no. 2, pp. 1–4, 1994. doi: 10.1177/156482659401500214
[18] M. Ngadi, Y. Li, and S. Oluka, "Quality changes in chicken nuggets fried in oils with different degrees of hydrogenation," *LWT – Food Science and Technology*, vol. 40, no. 10, pp. 1784–1791, 2007.
[19] M. Aniołowska, H. Zahran, and A. Kita, "The effect of pan frying on thermooxidative stability of refined rapeseed oil and professional blend," *Journal of Food Science and Technology*, vol. 53, no. 1, pp. 712–720, 2016. doi: 10.1007/s13197-015-2020-z
[20] A. Ignat, L. Manzocco, N. P. Brunton, M. C. Nicoli, and J. G. Lyng, "The effect of pulsed electric field pretreatments prior to deep-fat frying on quality aspects of potato fries," *Innovative Food Science and Emerging Technologies*, vol. 29, pp. 65–69, 2015. doi: 10.1016/j.ifset.2014.07.003
[21] T. Yilmaz, "Evaluating the quality change of sunflower oil while frying different foods," *Italian Journal of Food Science*, vol. 32, pp. 973–984, 2020.
[22] W. Cheevasathianchaiporn and C. Tangduangdee, "Mathematical modeling of frying oil temperature during deep-fat frying," *Kasetsart Journal (Natural Science)*, vol. 43, pp. 860–869, 2009.
[23] P. Thanatuksorn, K. Kajiwara, and T. Suzuki, "Characterization of deep-fat frying in a wheat flour–water dough sheet: Temperature profiles and transitions," *Journal of the Science of Food and Agriculture*, vol. 87, pp. 2648–2656, 2007.
[24] J. Dehghannya, A. Ghaderi, and B. Ghanbarzadeh, "Three-dimensional modeling of coupled momentum, heat, and mass transfer during potato frying: Effects of oil temperature, type, frying load, and fryer heating cycles," *Current Research in Food Science*, vol. 10, art. no. 101097, 2025. doi: 10.1016/j.crfs.2025.101097
[25] P. Gupta, I. H. Mondal, K. K. Dash, Geetika, T. Suthar, K. Ramzan, et al., "Deep fat frying characteristics of Malpoa: Kinetics, heat, and mass transfer modeling," *Processes*, vol. 12, no. 12, art. no. 2662, 2024. doi: 10.3390/pr12122662
[26] R. P. Singh and S. Debnath, "Heat and mass transfer in foods during deep-fat frying," in *Batters and Breadings in Food Processing*, K. Kulp, Ed.: AACC International, 2013.
[27] AACC International, "Method 44-15.02: Moisture—Air-oven methods," in *Approved Methods of the AACC*, 10th ed. St. Paul, MN: American Association of Cereal Chemists, 2000.
[28] Association of Official Analytical Chemists, "Official method 925.10: Moisture (Loss on drying)," in *Official Methods of Analysis*, Washington, DC: Association of Official Analytical Chemists, 1995.
[29] Association of Official Analytical Chemists, "Official method 920.39: Fat (crude) or ether extract," in *Official Methods of Analysis*, Washington, DC: Association of Official Analytical Chemists, 1995.
[30] Thermo Fisher Scientific, "Rapid determination of fat in meat using accelerated solvent extraction (ASE)," Application Note 334, 2011.
[31] Z. Erbay and F. Icier, "A review of thin layer drying of foods: Theory, modeling, and experimental results," *Critical Reviews in Food Science and Nutrition*, vol. 50, no. 5, pp. 441–464, 2010. doi: 10.1080/10408390802437063
[32] A. A. Adedeji, M. O. Ngadi, and G. S. V. Raghavan, "Kinetics of mass transfer in microwave precooked and deep-fat fried chicken nuggets," *Journal of Food Engineering*, vol. 91, no. 1, pp. 146–153, 2009. doi: 10.1016/j.jfoodeng.2008.08.018
[33] A. N. Gargari, N. Asefi, and L. Roufegarinejad, "Simulation of heat transfer in deep fat frying of foods: An

appropriate method for predicting the temperature distribution in a potato model," *Potato Research*, vol. 65, no. 4, pp. 933–957, 2022.

[34] I. D. Demiray, H. Ergezer, E. Demiray, and O. Sufer, "Deep-fat frying of chicken nuggets: Impacts on mass transfer and some quality indices," *Food Science & Nutrition*, vol. 13, no. 6, art. no. e70451, 2025. doi: 10.1002/fsn3.70451

[35] A. O. Oladejo, H. Ma, W. Qu, C. Zhou, B. Wu, X. Yang, et al., "Effects of ultrasound pretreatments on the kinetics of moisture loss and oil uptake during deep fat frying of sweet potato (Ipomea batatas)," *Innovative Food Science and Emerging Technologies*, vol. 43, pp. 7–17, 2017. doi: 10.1016/j.ifset.2017.07.019

[36] F. Pedreschi, P. Hernández, C. Figueroa, and P. Moyano, "Modeling water loss during frying of potato slices," *International Journal of Food Properties*, vol. 8, no. 2, pp. 289–299, 2005. doi: 10.1081/JFP-200059480

[37] A. M. Ziaiifar, F. Courtois, and G. Trystram, "Porosity development and its effect on oil uptake during frying process," *Journal of Food Process Engineering*, vol. 33, no. 2, pp. 191–212, 2010. doi: 10.1111/j.1745-4530.2008.00267.x

2nd International Conference on Multidisciplinary Sciences and Technological Developments (ICMUSTED 2025)

December 12-15, 2025

Investigation of the Usability of Bayburt Yellow Tuff in Structural Lightweight Concrete Production

Omer Bayrak[1], Emin Erdem[2]

[1]Civil Engineering, Bayburt University, Bayburt, Türkiye
[2]Department of Chemistry, Pamukkale University, Denizli, Türkiye
Corresponding author: Omer Bayrak (e-mail: cermeomer1342@gmail.com)

Abstract

Buildings being less affected by earthquakes depends on reducing the dead load of the building as much as possible and the aggregate used in reinforced concrete elements having the desired properties and being light. Lightweight natural aggregates are generally composed of perlite, pumice, and tuffite, which are formed as a result of volcanism and are exposed to high temperatures. The yellow tuff extracted in the Bayburt region provides significant economic income to the region through decorative stone carving, fountains, and the production of load-bearing wall blocks for masonry structures. In this study, the usability of aggregates obtained from Bayburt yellow tuff (BYT) waste generated in the enterprises in the production of structural lightweight concrete was investigated. For this purpose, BYT wastes obtained from the enterprises were ground in the laboratory to a maximum particle diameter (D_{max}) of 11.2 mm and separated into 9 different sieve classes (0-0.063, 0.063-0.125, 0.125-0.25, 0.25-0.5, 0.5-1, 1-2, 2-4, 4-8, and 8-11.2 mm). Aggregate tests were carried out. A granulometry curve was determined in accordance with D_{max} = 8 mm (Turkish Standards European norm (TS EN) 802). In addition to BYT aggregate, perlite and pumice aggregates commercially used in lightweight concrete production were also used for comparison. Lightweight concrete (LC) mixes were prepared with a cement dosage of 400 kg/m^3 and a water/cement ratio of 0.55. LCs produced with BYT aggregate were compared with lightweight concretes produced with perlite and pumice aggregates at the same cement dosage. It was determined that BYT aggregate cannot be used in LC production due to its lack of pozzolanic properties (2.8 MPa), its unit weight value being higher than the lightweight aggregate standard (2.0 g/cm^3) (2.06 g/cm^3), and its low inherent strength (23.8 MPa). However, it was determined that BYT aggregate mixtures prepared using at least 400 doses of cement, a water/cement ratio of 0.55, and plasticizer chemical additives had an average 28.2 MPa 28-day compressive strength (higher than LC produced with pumice (14.4 MPa) and lower than LC produced with perlite (41.8 MPa)), but could be successfully used as a normal concrete aggregate.

Keywords: Lightweight concrete, Bayburt waste yellow tuff

Use of Bayburt White Tuff as Cement Substitute Material

Omer Bayrak[1], Emin Erdem[2]

[1]Civil Engineering, Bayburt University, Bayburt, Türkiye
[2]Department of Chemistry, Pamukkale University, Denizli, Türkiye
Corresponding author: Omer Bayrak (e-mail: cermeomer1342@gmail.com)

Abstract

Today, approximately 8% of air pollution stems from carbon dioxide emitted into the environment during cement productio. White-colored volcanic tuffs from the Bayburt region, used for interior and exterior cladding of buildings and also for decorative purposes, have an important potential in the production of blended cement due to their pozzolanic properties. In this study, waste Bayburt white tuff (BWT) generated in the enterprises was used both as lightweight aggregate in the production of non-structural lightweight concrete (N-SLC) blocks and as cement replacement material after fine grinding. BWT wastes were ground to a maximum grain diameter (D_{max}) of 11.2 mm and separated into 9 different sieve classes (0-0.063, 0.063-0.125, 0.125-0.25, 0.25-0.5, 0.5-1, 1-2, 2-4, 4-8, 8-11.2 mm) and aggregate tests were carried out. The granulometry curve (TS EN 802) was determined in accordance with D_{max} 8 mm. 0-0.063 micron BBT was substituted into the cement at rates of 0%, 10%, 20%, 30% and 40%. N-SLC mixtures prepared with a binder dosage of 200 kg/m^3 and a water/cement ratio of 0.50 were compacted in 10x10x10cm cube molds by first shaking and then applying a pressure of 12 MPa. Compressive strength tests were performed after the N-SLC blocks were stored in a humid environment for 7 and 28 days. It was determined that the dry densty values of the N-SLC block elements averaged 1.4 g/cm^3, and their 28-day compressive strength values ranged from 5.6 to 7.6 MPa, exceeding the 5 MPa required by the relevant standard. It was determined that the addition of BWT powder, while slightly decreasing in strength, achieved the desired strength. As a result, it was determined that BWT aggregate can be successfully used as an aggregate in N-SLC production, and that BWT powder can be substituted for cement up to 30%.

Keywords: Lightweight concrete, Bayburt waste white tuff

2nd International Conference on Multidisciplinary Sciences and Technological Developments (ICMUSTED 2025)

December 12-15, 2025

Investigation of Parameters Affecting Pedestrian Crossing Speeds: Empirical Findings from Türkiye

Mehmet Burhan Sume[1], Erdem Dogan[1]

[1]Civil Engineering, Kirikkale University, Kirikkale, Türkiye
Corresponding Author: Mehmet Burhan Sume (e-mail: mehmetsume96@gmail.com)

Abstract

Insufficient pedestrian crossing times in intersection signal systems cause pedestrians to make dangerous crossings and reduce road safety. Therefore, accurately determining pedestrian crossing speeds is crucial. This study examined pedestrian crossing speeds and analyzed the factors affecting these speeds. The study examined the crossings of 500 pedestrians using bird's-eye video recordings from eight different intersections in the provinces of Izmir, Kirikkale, and Samsun in Türkiye. In addition to pedestrian speeds, numerous variables, including the intersection's signalization status, geometric characteristics, pedestrian-vehicle intersections, average vehicle speeds, pedestrian group crossings, and pedestrian crossing usage, were analyzed using statistical methods to determine their impact levels. The results obtained in this study can contribute to the current work of researchers and professionals working in this field. The purpose of this study is to help improve pedestrian crossing safety by examining the speeds at which pedestrians cross intersections and the factors affecting these speeds.

Keywords: Pedestrian speed, Intersection analysis, Pedestrian behavior, Statistical analysis, Traffic safety

1. INTRODUCTION

Throughout history, transportation has been a fundamental need in human life. Roads have been symbols of civilization's development, and population and vehicle numbers have steadily increased. Today, pedestrian and vehicle density in many city centers is significantly higher than in the past. This excess has necessitated the development of traffic systems. Intersections play a crucial role in these traffic systems. As critical intersections where multiple roads intersect, they are frequently used by numerous pedestrians and vehicles, often resulting in simultaneous contact. Pedestrians are the most vulnerable road users during these encounters. Inadequate time allowed for pedestrians in intersection designs leads to dangerous crossings, which lead to various accidents at intersections. Many pedestrians are injured or killed each year due to these accidents. According to data from the United States Department of Transportation's National Center for Statistics and Analysis, a total of 7,314 pedestrians were killed and an estimated 68,244 injured in traffic crashes in the United States in 2023. This means one pedestrian died every 72 minutes in the United States in 2023. These pedestrian deaths in the U.S. in 2023 accounted for 18% of all traffic deaths that year [1]. As another example, Poland has the second-worst pedestrian fatality rate in the European Union. Between 2007 and 2012, 9,101 pedestrians died and 71,328 were injured in traffic accidents in Poland. Approximately 30% of pedestrian injury accidents occurred at unsignalized zebra crossings [2]. In Türkiye, according to data from the Ministry of Transport's General Directorate of Highways (KGM), a total of 6,351 people lost their lives in traffic accidents in 2024, 21% of which (1,333 people) were pedestrians. In 2024, 1,884 accidents occurred at pedestrian crossings in Türkiye, resulting in 3,318 injuries and 149 deaths [3]. Based on these data, accurate analysis of pedestrian behavior at intersections is important for the safety of road users and the efficiency of traffic systems.

The primary objective of this study is to contribute to the existing literature by analyzing pedestrian crossing speeds at intersections and the factors affecting these speeds. In this context, the crossings of 500 pedestrians using eight different intersections in the provinces of Kirikkale, Samsun, and Izmir in Türkiye were examined. The data obtained from the examination of intersections of different characteristics were subjected to statistical analysis. The analyses were conducted in the Python environment and summarized in tables. The obtained results are supported by visuals and compared with various sources in the literature. The final section of the study proposes various recommendations, and the study concludes.

1.1. Literature Review

Because pedestrian behavior is variable, average pedestrian speeds can vary across countries and even regions. Some studies indicate that cultural differences significantly influence pedestrian behavior. Interventions to improve road safety should take these cultural factors into account [4]. Another study that clearly demonstrates the variation in pedestrian speeds across countries is conducted by Goh et al. [5]. Goh et al. summarize the average pedestrian speeds across countries in Table 1.

Table 1. Average pedestrian walking speeds in different countries

Country	Average Walking Speed (m/s)
Asia	
Riyadh, Saudi Arabia	1.08
Madras, India	1.20
Hong Kong	1.20
Thailand	1.22
Singapore	1.23
Colombo, Sri Lanka	1.25
Israel	1.31
Malaysia	1.39
Jordan	1.34
USA	
Columbia	1.32
New York	1.35
Pittsburg	1.47
Others	
England	1.31
Calgary, Canada	1.40

According to the data summarized in the table, average pedestrian speeds range from 1.08 to 1.40 m/s. The speed data determined in a follow-up study are as follows: In Malaysia, the average and 15th percentile pedestrian speeds at signalized pedestrian crossings are 1.31 m/s and 1.09 m/s, respectively. At non-signalized pedestrian crossings, the average and 15th percentile pedestrian speeds are 1.39 m/s and 1.15 m/s, respectively. However, the design speed applied at the intersections is 1.22 m/s, and neither intersection can ensure safe pedestrian crossing time [5]. In another study, pedestrian speed data was collected at an unsignalized intersection and then a signaling system was installed at the intersection. After the installation, the average pedestrian speed decreased by 23% compared to the pre-installation speed, from 1.37 m/s to 1.05 m/s. The recommended design speed decreased from 0.73 m/s to 0.52 m/s. Both values are lower than the pedestrian design speed applied at the intersection (1.20 m/s) [6]. Some studies have shown that the crossing speed is higher at unsignalized intersections [7, 8]. In a study conducted at a four-leg signalized intersection in Mumbai, India, the average pedestrian crossing speed was found to be 1.34 m/s, which is different from the design speed (1.20 m/s). Another study determined the 15th percentile speed of pedestrians crossing at crosswalks to be 1.24 m/s. It has been stated that this value may be suitable for the signalized design speed of pedestrian crossings [9]. In a study conducted in Türkiye, the average crossing speed was found to be 1.31 m/s and the 15th percentile crossing speed was found to be 1.07 m/s. In addition, the study stated that the recommended average walking speed in Türkiye is 1.4 m/s given by the Turkish Standards Institute [10]. In Jordan, a design speed of 1.11 m/s was recommended [11]. There is a consensus in studies that the 15th percentile speed should be the design speed. Studies generally indicate that the recommended pedestrian speed is lower than the current design speeds. This indicates that pedestrians do not have enough time to cross. However, there are also studies where the design speed is lower than the recommended speed range. In a study conducted in India, 16 signalized intersections were examined and the 15th percentile crossing speed was between 1.11 and 1.31 m/s. These values exceed the design crossing speed of 0.95 m/s [12].

When these studies in the literature were examined, it was determined that the 15th percentile pedestrian speeds determined were different from the current design speeds. The times allocated for pedestrians to cross at intersection signals do not match the speeds of pedestrians at the local level. This can cause pedestrians to have difficulty crossing the street or make dangerous crossings. Therefore, improvements in intersection designs are necessary.

In studies examining other factors affecting pedestrian speed, the most striking parameter is group crossings. Many studies have found that pedestrians crossing in groups are slower than individual pedestrians [4, 7, 8, 11, 13–19]. It is thought that distraction during group crossings may be a factor in this situation.

Another study found that as pedestrians' crossing distance increases, their crossing speed also increases [20]. This is thought to be due to pedestrians' desire to minimize the time they spend in the intersection. Pedestrians crossing wider crosswalks are found to be faster than those crossing narrower crosswalks. This is likely due to pedestrians' greater ease of movement in wider crosswalks [8, 11, 17]. Drivers' behavior towards pedestrians is generally negative. Some studies have found that drivers tend not to yield to pedestrians [21, 22]. This situation causes safety problems and significant improvements are needed for pedestrian safety [16].

In this study, the investigation of pedestrian speed was conducted using video analysis. A separate study has stated that pedestrian-vehicle interactions and pedestrian behavior can be analyzed through video analysis [23]. In our study, video analysis was conducted using the open-source software Kinovea®. This software determined the speeds of pedestrians and vehicles, and calculated the geometric properties of pedestrian crossings. Some studies have been conducted to evaluate the reliability of Kinovea, and the program is reported to be accessible and easy to use based on the parameters examined, and to be a reliable tool for measuring speed-based training data [24, 25]. Numerous studies exist in the literature examining pedestrian speed. These studies examine various factors, but few studies examine multiple factors simultaneously. This study examines pedestrian speeds and a total of 20 parameters affecting these speeds.

2. MATERIALS AND METHODS

2.1. Data Collection

The data in this study were obtained from a total of eight signalized and unsignalized intersections with varying numbers of branches in the provinces of Izmir, Samsun, and Kirikkale. The general characteristics of the intersections examined are given in Table 2.

Table 2. General characteristics of the examined intersections

Province	Intersection Number of Legs	Intersection Control Type	Number of Inspected Intersections
Kirikkale	Five-Legged	Non-Signalized	1
Samsun	Four- Legged	Non-Signalized	1
Izmir	Four- Legged	Signalized	5
Izmir	Three- Legged	Non-Signalized	1

Izmir is located in western Türkiye, Samsun in northern Türkiye, and Kirikkale in central Türkiye. The cities studied have distinct characteristics. Of the eight intersections studied, five are signalized and three are unsignalized. In terms of the number of intersection legs, six of the eight are four-leg intersections, while three- and five-leg intersections have one each. The vast majority of the intersections studied are four-leg signalized.

The intersections were recorded between 8:30 am and 4:30 pm, in good weather conditions, with fifteen-minute drone recordings. The recorded footage was used to examine various conditions, including pedestrian-vehicle intersections, group crossings, carrying goods or pets, visibility of pedestrian crossings, types of intersection controls, and the dates and times of video recordings for the intersections studied. Intersection features such as the width and length of pedestrian crossings, the geometric characteristics of intersections, and the presence of pedestrian crossing lines and sidewalks were also analyzed. Pedestrian speeds were calculated by measuring the distance and time pedestrians crossed. All data analyzed in the videos was grouped and listed in Table 3.

The analyzed data consists of numerical or categorical variables. Numerical variables include the date and time of the video, the length and width of the crosswalk, the number of vehicles impacting the pedestrian and their average speed, group size, the distance and time the pedestrian crossed, and the pedestrian's speed. Categorical variables are cities (Kirikkale, Izmir, and Samsun), the time of the video (morning, noon, evening), and the geometric characteristics of the intersection (3-leg unsignaled, 4-leg signaled, 4-leg unsignaled, and 5-leg unsignaled). All other groups have two variables, yes or no.

The Google Earth program was used to determine the physical characteristics of the intersections. This program used the distance measurement feature to measure the geometric characteristics of the intersections based on their actual locations. (Figure 1)

Table 3. Analyzed data

Crosswalk and Intersection Features		Pedestrian Behavior	Pedestrian-Vehicle Interactions
City	Geometric Features of the Intersection	Carrying Goods or Dogs	Pedestrian-Vehicle Contact at the Crossing
Video Date	Signalization	Pedestrian Crossing Usage	Number of Cars Impacting the Pedestrian
Video Time	Presence of Crosswalk Lines	Group Size	Number of Motorcycles Impacting the Pedestrian
Length and Width of The Pedestrian Crossing (m)	Existence of Obstacles at the Crossing	Pedestrian's Crossing Distance (m)	Number of Heavy Vehicles Impacting the Pedestrian
Existence of Usable Sidewalks	Visibility of the Road from the Pedestrian's Eyes While Crossing	Pedestrian Speed (m/s)	Average Speed of Vehicles Impacting the Pedestrian (km/h)

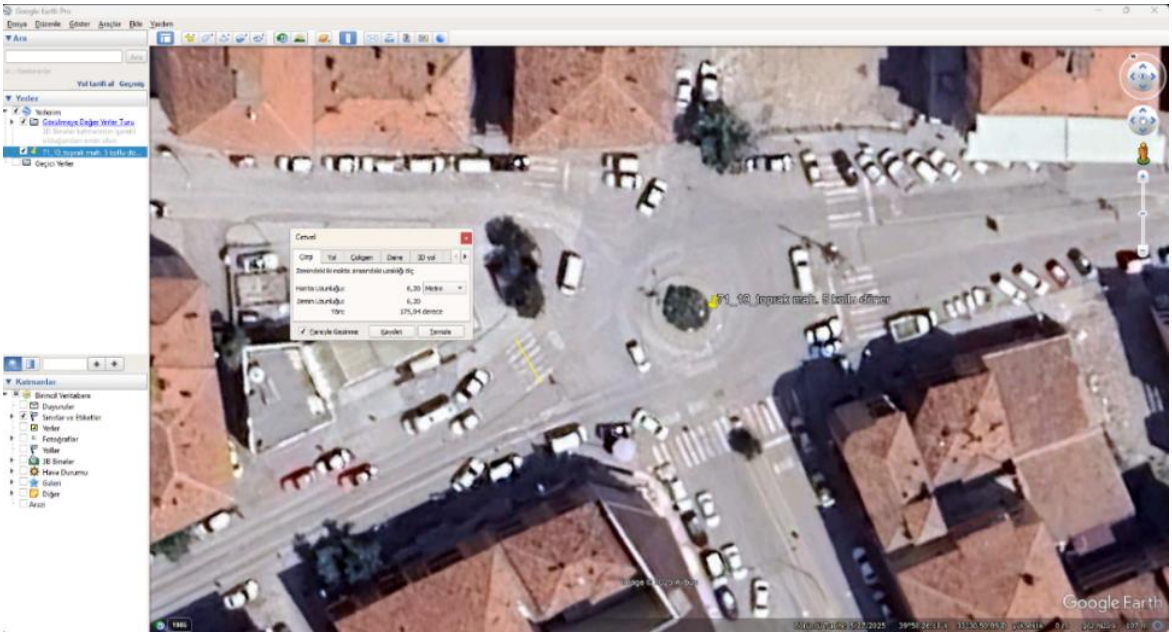

Figure 1. Google Earth example pedestrian crossing distance measurement

The obtained values were transferred to Kinovea, a video analysis program, and the necessary calibrations were performed, and measurements and analyses were continued in this program. The measurement-based data were measured using Kinovea's video measurement tools. Since the length and width of the pedestrian crossing (m), the average speed of vehicles impacting the pedestrian (km/h), and the pedestrian's crossing distance (m) are measurement-based data, they were measured using Kinovea's measurement features (Figure 2). The average speed of vehicles impacting the pedestrian (km/h) was calculated using Kinovea's moving object tracking feature (Figure 3). All other data is not based on metric measurements. It was visually extracted from the videos and converted into data.

A coordinate system (red) was placed on the video screen to better identify the location of pedestrians and crossings. The origin of the coordinate system was chosen as the center of the intersection. Pedestrian speed was calculated using the following formula.

$$v = \frac{\sum_{i=1}^{n} d_i}{\sum_{i=1}^{n} t_i} \quad (1)$$

Here, v is pedestrian speed (m/s), d_i is distance traveled (m), and t_i is elapsed time (s). The entire distance traveled by a total of (n) pedestrians, from the moment they first stepped onto the roadway to cross the roadway until the moment they exited the roadway, was marked with dots at short intervals. The orange dots in Figure 2 represent

the paths followed by pedestrians crossing the roadway (d_i). These dots were then connected to measure the distances each pedestrian crossed. The distances between two points are shown within the orange signs. The times at which pedestrians entered and exited the intersection were recorded, and the total crossing times were calculated t_i. The program's path-following feature calculated the approximate speeds of vehicles at the moment they contacted pedestrians (Figure 3).

Figure 2. Kinovea program sample pedestrian crossing measurement

Figure 3. Kinovea program path tracking feature

Vehicles that impacted pedestrian speed by contacting them were tracked using the program's path tracking feature before reaching the point of contact, and tracking was discontinued shortly after the contact was completed. The program automatically displays the distance and elapsed time the vehicle traveled during the tracking period. Using the data obtained, the vehicle's speed was calculated as in Equation (1). Since the speed data was in m/s, it was converted to km/h.

2.2. Data Analysis

The obtained data were subjected to a two-stage analysis process in the Python environment. In the first stage, descriptive statistical analysis was conducted to reveal the general distribution of the numerical data. This analysis

yielded general statistical values for the numerical variables, such as mean, minimum, maximum, standard deviation, and 15-85 percentiles.

In the second stage, the effects of various factors on pedestrian speed were evaluated using various tests. Statistical analyses are basically divided into two groups: parametric and non-parametric tests. If the data are not normally distributed and consist of small samples, non-parametric tests are applied [26]. To determine which tests to apply to the existing data set, first, tests called normality tests are applied. The Shapiro-Wilk Normality Test was applied to determine whether the data set in this study was normally distributed. Among normality tests, the Shapiro-Wilk test is said to be the most powerful test for all distributions and sample sizes [27].

The Shapiro-Wilk test revealed that the data were not normally distributed, and therefore, non-parametric tests were applied. These tests are the Mann–Whitney and Kruskal–Wallis tests. The Mann-Whitney U test was applied to groups with two variables, and the Kruskal-Wallis H test was applied to groups with three or more variables to examine whether the variables had significant effects on pedestrian speed. For example, the Mann-Whitney U test was used to examine whether there was a significant difference between the speed of pedestrians at signalized intersections and those at unsignalized intersections. However, the Kruskal-Wallis H test was used to test whether there was a significant difference between the median pedestrian speeds for the provinces of Izmir, Kirikkale, and Samsun. When the Kruskal-Wallis test result was significant, pairwise (post-hoc) comparisons were made between the groups with significant differences to determine which two groups had the most significant difference. In these pairwise comparisons, the Bonferroni correction method was applied to correct the risk of obtaining erroneous results [28]. When the P-values obtained from these tests are <0.05, a significant difference is indicated between the groups. By examining all variables in this manner, those that significantly affected pedestrian speed were identified.

3. RESULTS

3.1. Descriptive Analysis

Descriptive analysis was applied to determine the general distribution of numerical groups. The results of the descriptive analysis are presented in Table 4.

Table 4. Descriptive analysis results (numerical groups)

Variable	Mean	Std	Min	Max	Mode	P15	P50 (Median)	P85
Group Size	1.16	0.48	1.00	4.00	1.00	1.00	1.00	1.00
Number of Cars Impacting Pedestrians	0.62	1.29	0.00	12.00	0.00	0.00	0.00	1.00
Number of Heavy Vehicles Impacting Pedestrians	0.04	0.21	0.00	2.00	0.00	0.00	0.00	0.00
Number of Motorcycles Impacting Pedestrians	0.06	0.28	0.00	2.00	0.00	0.00	0.00	0.00
Average Speed of Impacted Vehicles (km/h)	8.81	14.14	0.00	60.00	0.00	0.00	0.00	25.00
Length of the Pedestrian Crossing (m)	9.09	2.77	0.00	19.23	7.00	7.00	9.18	11.27
Width of the Pedestrian Crossing (m)	4.16	1.21	0.00	6.00	3.00	3.00	4.25	5.50
Pedestrian’s Crossing Distance (m)	12.04	7.72	4.30	67.19	7.00	7.33	10.18	15.00
Pedestrian Speed (m/s)	1.35	0.36	0.36	3.93	1.23	1.05	1.32	1.58

Std: Standard deviation, Min: Minimum, Max: Maximum, P15: 15th percentile, P50 (Median): 50th percentile, and P85: 85th percentile

According to the descriptive analysis results, at least 85% of pedestrians cross the street alone. Group crossings are rare. More than 50% of pedestrians do not encounter any vehicles while crossing. In cases where vehicles are encountered, the vehicle speed affecting the pedestrian is sometimes greater than 25 km/h. The average length and width of the crossings used by pedestrians are 9.18 and 4.25 meters, respectively. It is believed that the length and width of the crossings do not pose any problems in terms of usability. However, there are significant differences in the lengths of pedestrian crossings (It is between 7.33 and 15 meters according to the 15-85 percentile). Pedestrian preferences played a role in this. Some pedestrians followed the rules and used the crosswalks, while others took alternative routes, making dangerous and lengthy crossings. The median pedestrian speed was 1.32 m/s, and the 15th percentile speed was 1.05 m/s, which are consistent with literature data.

3.2. Normality Test

Determining whether the data distribution is normal serves as a guide for the remainder of the analysis. The Shapiro-Wilk Normality Test was used in this study. Based on the test results, W=0.853 and p=0.00000 was determined. Because the W-value was not equal to 1 and the p-value was less than 0.05, it was determined that the pedestrian speed data were not normally distributed. Therefore, the analysis continued with non-parametric tests.

3.3. Hypothesis Tests and Results

3.3.1 Hypothesis Testing and Results Based on Categorical Variables

The Kruskal-Wallis test was applied to categorical groups with three or more variables. The test results are given in Table 5.

Table 5. Kruskal-Wallis test results

Variable	H	p	Number of Observations	Significance Status
City (Kirikkale, Izmir, Samsun)	2.281	0.31972	500	p > 0.05 Meaningless
Video Time (Morning, Afternoon, Evening)	3.761	0.15250	500	p > 0.05 Meaningless
Video Date (March 2024, June 2024, March 2025)	2.281	0.31972	500	p > 0.05 Meaningless
Intersection Geometry (3-, 4-, and 5-Leg Intersections)	10.406	0.01541	500	p < 0.05 Significant

Here, the H statistic represents the distance between the ranked means of categorical variables. However, the key indicator of significance is the p-value. A value less than 0.05 indicates that the relevant variable significantly affects pedestrian speed. According to the results in Table 5, no significant difference was found between cities (Kirikkale, Izmir, Samsun) affecting pedestrian speeds. Similarly, no significant difference was observed between pedestrian speeds during morning, afternoon, or evening crossings.

Based on these test results, it was determined that the geometric characteristics of the intersection may have an impact on pedestrian speed. There are four different intersection types. A Post-Hoc pairwise comparison test with Bonferroni correction was applied to measure the relationship between each. The test results are presented in Table 6. The number of observations (n) for each intersection type is given in the definitions section immediately below the table.

Table 6. Post-Hoc test results by intersection geometry (2: Four-legged non-signalized intersection (n = 68), 3: Three-legged non-signalized intersection (n = 15), 4: Four-legged signalized intersection (n = 334), and 5: Five-legged non-signalized intersection (n = 83))

Variable	Median 1	Median 2	U	p_raw	p_adj (Corrected)	Significance Status
(2 vs 3)	1.330	1.180	743.50	0.00581	0.03487	p < 0.05 Significant
(2 vs 4)	1.330	1.335	11367.50	0.98995	1.00000	p > 0.05 Meaningless
(2 vs 5)	1.330	1.290	3178.50	0.18297	1.00000	p > 0.05 Meaningless
(3 vs 4)	1.180	1.335	1425.50	0.00476	0.02854	p < 0.05 Significant
(3 vs 5)	1.180	1.290	426.00	0.05309	0.31851	p > 0.05 Meaningless
(4 vs 5)	1.335	1.290	15483.50	0.09878	0.59270	p > 0.05 Meaningless

Here, Median 1 and Median 2 are the median values of the two different intersection types being compared. The nature of the test involves comparing the medians between two variables. The U value is one of the outputs of this test. As this value decreases, the probability of the difference between the groups being significant increases. The P-raw value is the raw p-value resulting from the test. Because there are more than two groups, the Bonferroni correction is applied to control the false positive rate. The final decision is made based on this p-value. According to the test results, pedestrian speeds at four-leg signalized and four-leg unsignalized intersections are higher than at three-leg unsignalized intersections. The density distribution graphs are shown in Figure 4 and Figure 5.

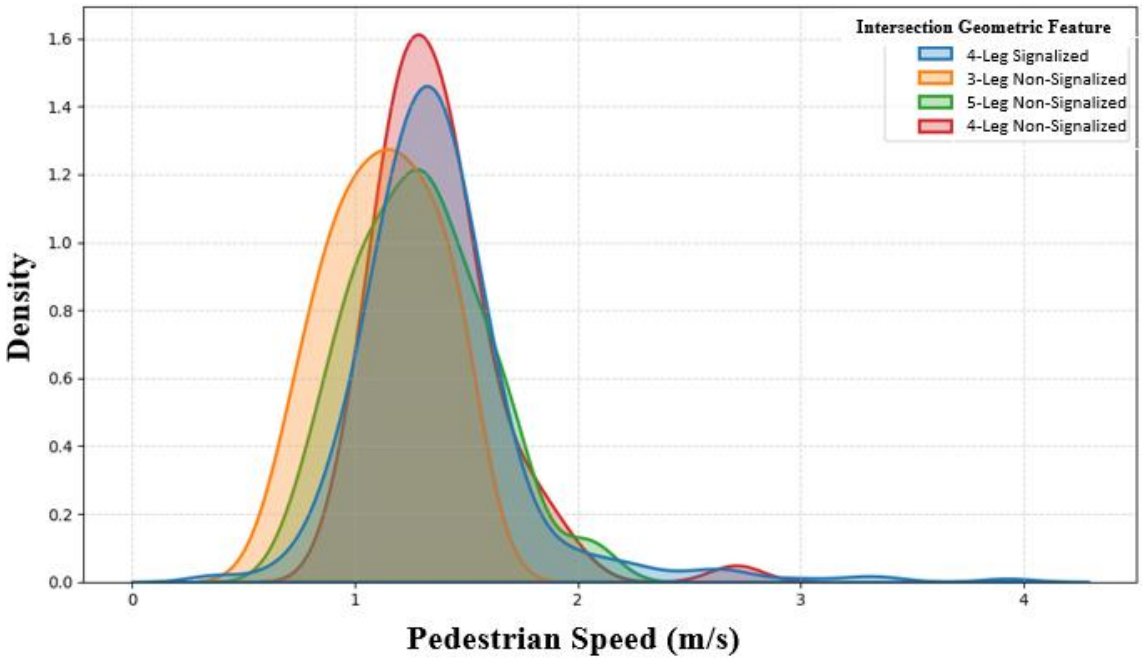

Figure 4. Relationship between geometric features of the intersection and pedestrian speed

Figure 4 shows the values around which pedestrian speeds at each intersection type are concentrated. The peaks of the curves indicate the highest number of pedestrian observations at that speed. Peaks to the right indicate higher average pedestrian speeds. The curve for the unsignalized 3-leg intersection (orange) has a wider spread than the others and is more leftward. Therefore, it is expected to contain lower speeds.

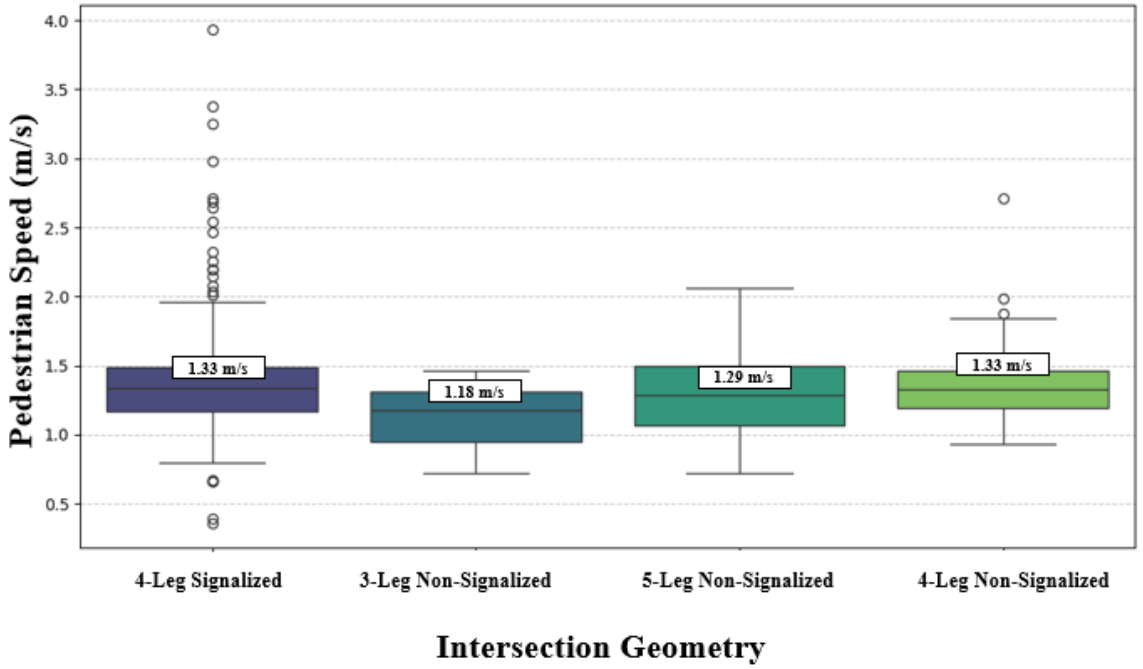

Figure 5. Box plot showing the relationship between geometric features of the intersection and pedestrian speed

Each box represents an intersection type. The lines in the middle of the boxes represent the median values for each intersection type. The intersection with the highest median line (i.e., the highest average pedestrian speed) is the four-leg signalized and unsignalized intersection (1.33 m/s). Furthermore, the four-leg signalized intersection exhibits the greatest variation in pedestrian speed. Speeds here are outliers.

The Mann-Whitney U test was applied to bivariate groups. The results of the test are given in Table 7.

Table 7. Mann-Whitney U test

Variable	Median 1	Median 2	U	p	n1	n2	Significance Status
Signalization	1.290	1.335	25031.50	0.07702	166	334	p > 0.05 Meaningless
Pedestrian Crossing Usage	1.320	1.320	27128.00	0.61865	168	332	p > 0.05 Meaningless
Relationship Between Pedestrian-Vehicle Contact and Pedestrian Speed	1.330	1.290	32120.00	0.01260	327	173	p < 0.05 Significant
Presence of Crosswalk Lines	1.310	1.320	6955.50	0.35005	33	467	p > 0.05 Meaningless
Existence of Obstacles at the Crossing	1.320	1.320	3282.50	0.82072	487	13	p > 0.05 Meaningless
Visibility of the Road from the Pedestrian's Eyes While Crossing	1.310	1.320	1610.50	0.71593	6	494	p > 0.05 Meaningless

In this test applied to groups with two categorical variables, the Median-1 value corresponds to No, and the Median-2 value corresponds to Yes. The U value is the magnitude of the difference between the two variables and is used to calculate the p-value. When p-values are less than 0.05, the difference between the variables is significant. The number of observations for each variable is n1 for No and n2 for Yes. The presence or absence of signalization at the intersection did not significantly affect pedestrian speed, and the p-value is close to the threshold. Whether or not a crosswalk was used did not significantly affect pedestrian speed. However, in situations where there is no pedestrian-vehicle intersection, pedestrian speed is relatively higher than in situations where there is. Pedestrians are thought to be more cautious at these intersections. The distributions of the results are shown in Figure 6 and Figure 7. In situations where pedestrian-vehicle intersections occur, the curve is expected to include lower speeds because its width is wider. Figure 7 shows that the maximum speed is higher in situations where there is no intersection. In cases where there is no intersection, the number of observations and outliers are greater and the median speed is higher.

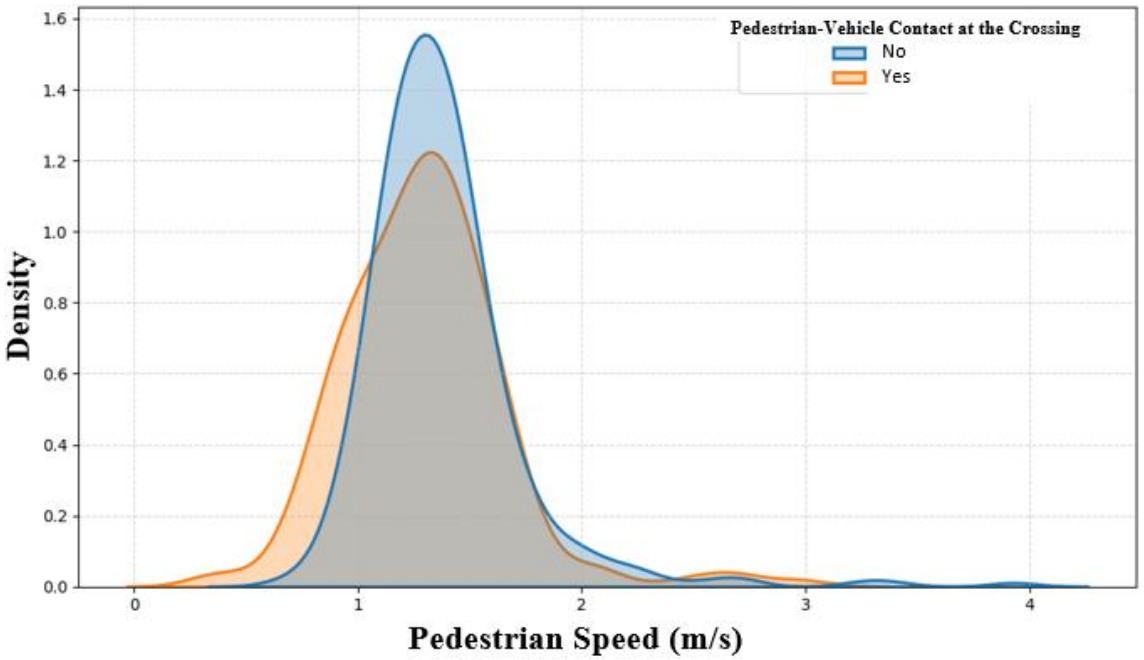

Figure 6. Relationship between pedestrian-vehicle contact and pedestrian speed

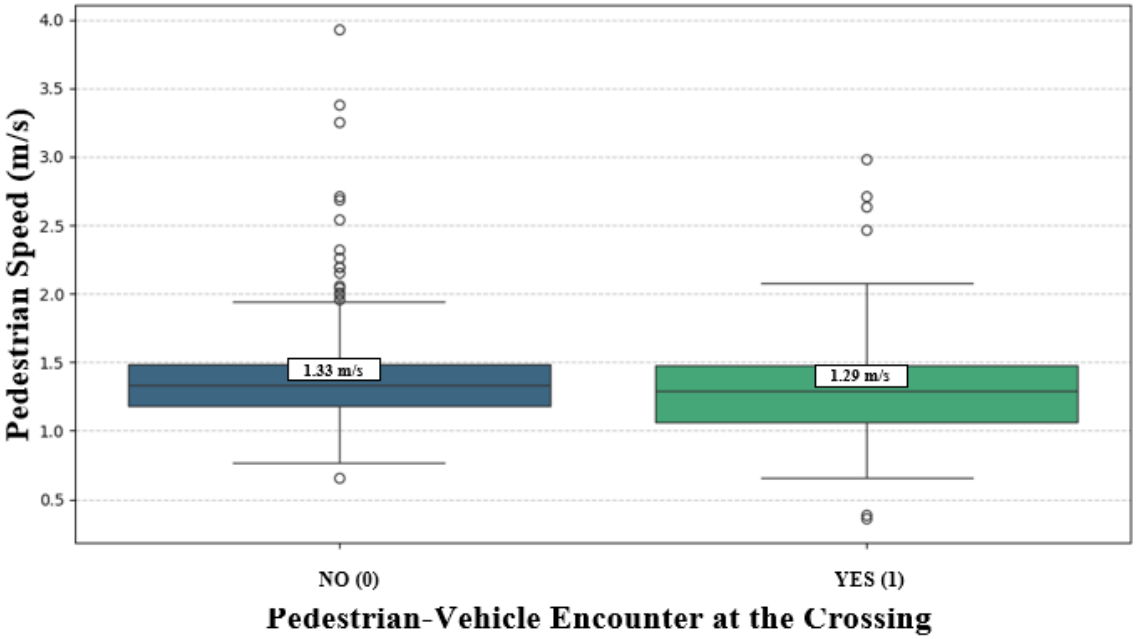

Figure 7. Box plot showing the relationship between pedestrian-vehicle contact and pedestrian speed

3.3.2 Hypothesis Testing and Results Based on Numerical Variables

Correlation analysis was used to determine the direction and strength of the relationship between numerical variables and the dependent variable (pedestrian speed). The Spearman Rank Correlation Coefficient was preferred in this analysis. This preference is because Spearman is a non-parametric technique and does not require the variables to be linearly related. This technique provides more robust and reliable results, especially in cases where the data set is not normally distributed and contains outliers. Another justification for choosing Spearman is the findings in the literature. Various comparative studies have found that rank-based correlation methods, such as Spearman, perform better than linear correlation methods [29]. For these reasons, Spearman correlation analysis was preferred, and the analysis results are shown in Table 8.

Table 8. Spearman correlation analysis results

Independent Variable	Number of Observations	Spearman Rho (ρ)	p-value	Significance
Group Size	500	-0.086	0.05578	$p > 0.05$ Meaningless
Number of Cars Impacting the Pedestrian	155	-0.134	0.00267	$p < 0.05$ Significant
Number of Heavy Vehicles Impacting the Pedestrian	21	-0.047	0.29717	$p > 0.05$ Meaningless
Number of Motorcycles Impacting the Pedestrian	28	-0.088	0.05037	$p > 0.05$ Meaningless
Average Speed of Vehicles Impacting the Pedestrian (km/h)	204	-0.137	0.00207	$p < 0.05$ Significant
Length of The Pedestrian Crossing (m)	500	0.029	0.51589	$p > 0.05$ Meaningless
Width of The Pedestrian Crossing (m)	500	0.058	0.19357	$p > 0.05$ Meaningless
Pedestrian's Crossing Distance (m)	500	0.088	0.04995	$p < 0.05$ Significant

When the analysis results were examined, it was determined that as the number of cars impacting pedestrians and their speeds increased, pedestrian speed decreased. This is thought to be a result of pedestrians' perception of danger. As the pedestrian's crossing length increased, pedestrian speed also increased. This is similar to results in

the literature. The number of motorcycles impacting pedestrians and group size did not reach significance in this analysis, but they are very close to the significance threshold. It may have reached significance in different samples. The other groups in Table 8 were not found significant in this study. The relationships between the groups that were significant in the Spearman Correlation Analysis and pedestrian speeds are shown in Figure 8, Figure 9, and Figure 10.

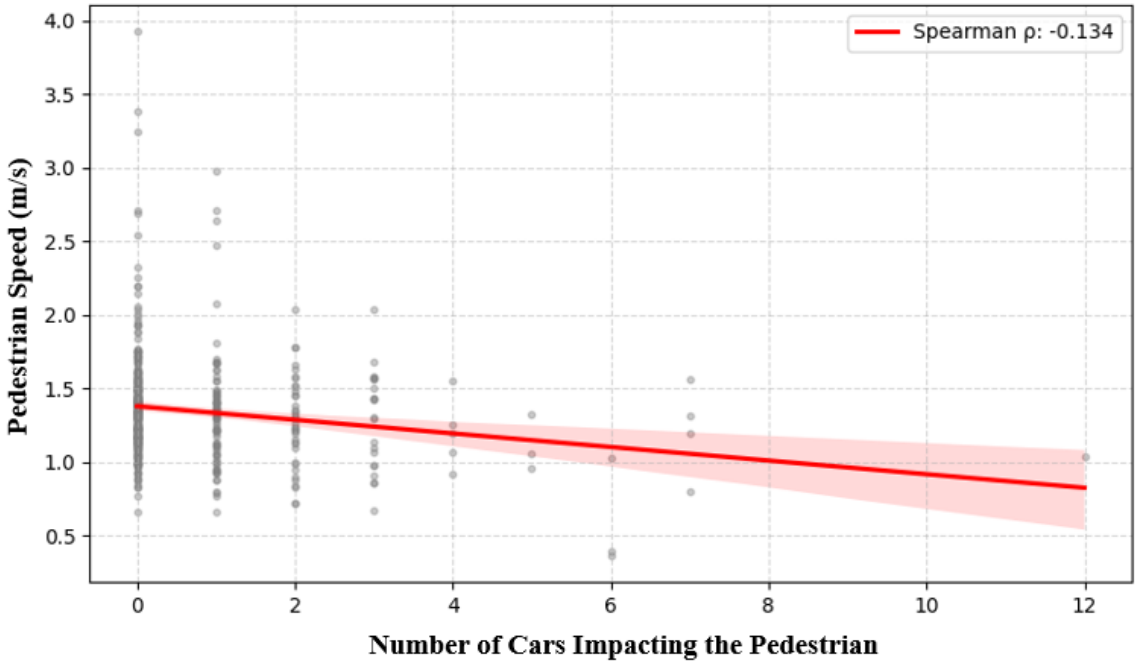

Figure 8. Relationship between the number of cars impacting a pedestrian and pedestrian speed

Spearman's coefficient = -0.134, and the direction of the relationship is negative. This means that the number of cars impacting pedestrians varies between 0 and 12. It was found that pedestrian speed decreases as the number of cars impacting pedestrians increases. According to the correlation, the strength of this relationship is weak because the correlation value is close to 0.00. However, since the p-value = 0.0267 < 0.05, this relationship is statistically significant (meaning the relationship is not coincidental). The gray dots show the distribution of the data, and the number of cars is concentrated in the range of 0-3.

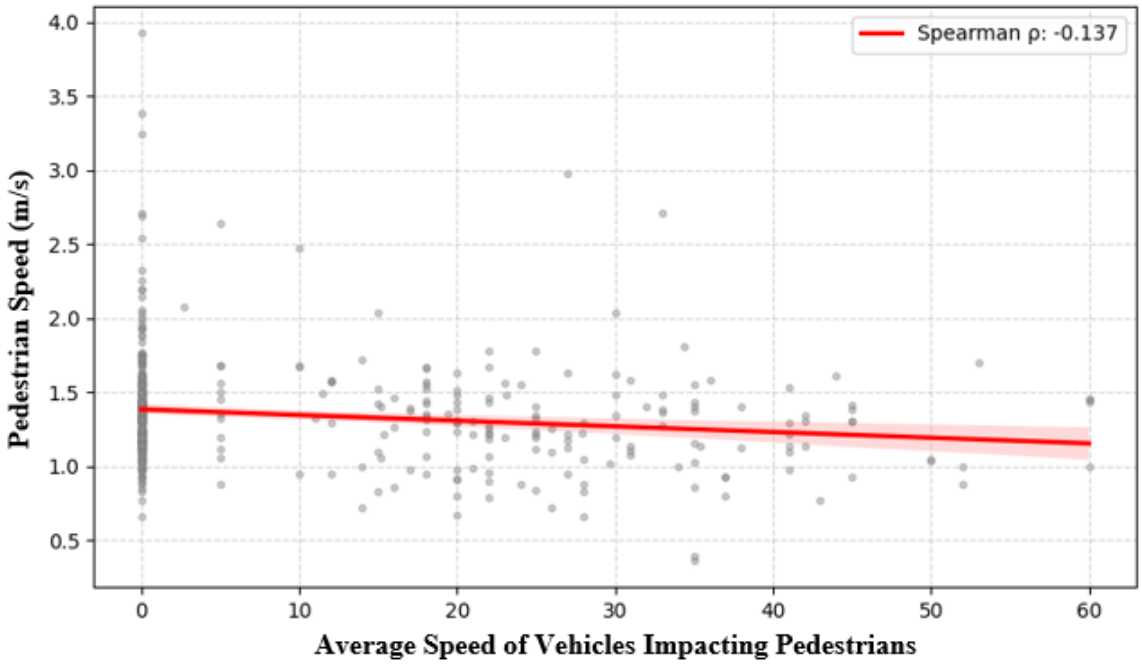

Figure 9. Relationship between average speed of vehicles impacting pedestrians and pedestrian speed

Similarly, the Spearman coefficient was calculated as -0.137, which is negative. In other words, as the speed of cars impacting pedestrians increases, pedestrian speeds decrease. The coefficient indicates that the relationship between the two variables is present but weak. Furthermore, the p-value = 0.00207, indicating that the relationship between the two variables is statistically significant. Gray dots represent the distribution of the data, with car speeds concentrated above 0 km/h (the state where no vehicles impact the pedestrian).

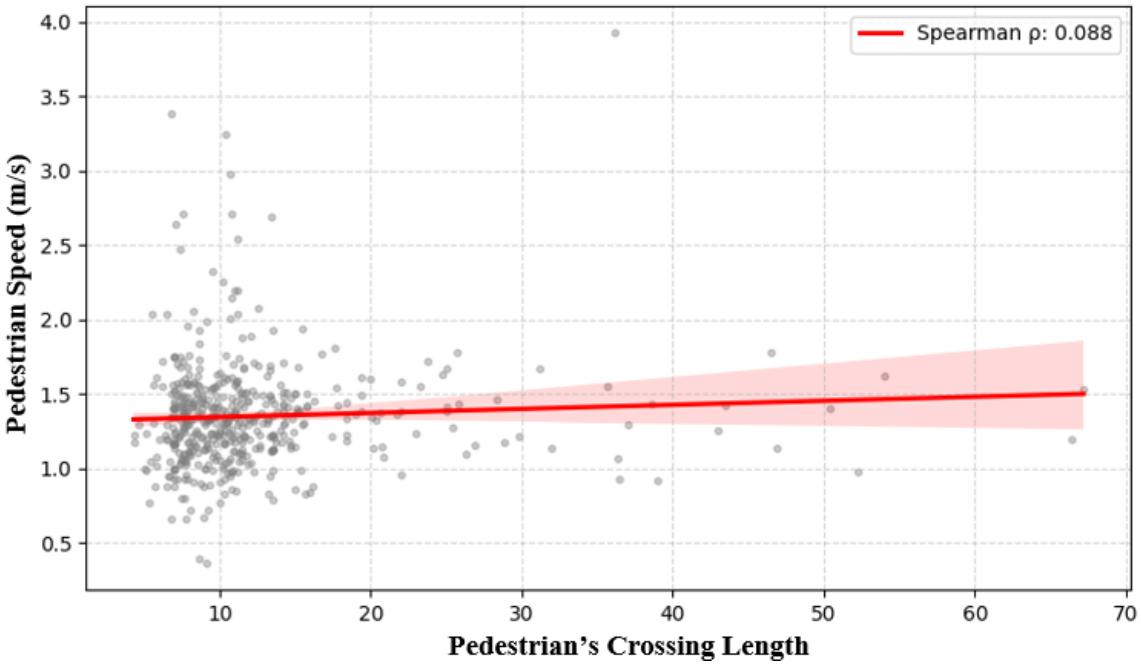

Figure 10. Relationship Between pedestrian's crossing length and pedestrian speed

Spearman's coefficient = 0.888, and the direction of the relationship is positive. In other words, as the distance pedestrians cross increases, pedestrian speeds also increase. The coefficient indicates that the relationship between the two variables is present but weak. Since the p-value = 0.04995 < 0.05, the relationship is at the statistically significant limit. It was observed that the crossing distance data were mostly concentrated between 5 and 15 meters. As a result of all the tests performed, the variables found to significantly affect pedestrian speed are compiled in Table 9.

Table 9. Groups with significant effects on pedestrian speed as a result of data analysis (2: Four-legged non-signalized intersection, 3: Three-legged non-signalized intersection, and 4: Four-legged signalized intersection)

Variable	p-value (< 0.05)
Intersection Geometric Feature (2 vs 3)	0.03487
Intersection Geometric Feature (3 vs 4)	0.02854
Pedestrian-Vehicle Contact at the Crossing	0.01260
Number of Cars Impacting the Pedestrian	0.00267
Average Speed of Vehicles Impacting the Pedestrian (km/h)	0.00207
Pedestrian's Crossing Distance (m)	0.04995

4. CONCLUSION

The study determined the speeds of pedestrians attempting to cross intersections and the factors affecting them within a sample. The results showed that the median pedestrian speed was 1.32 m/s, and the 15th percentile speed was 1.05 m/s. In another study conducted in Türkiye [10] the average crossing speed was 1.31 m/s, and the 15th percentile speed was 1.07 m/s, which are quite similar to the results in this study. Furthermore, the average pedestrian speeds and 15th percentile speeds found in various sources in the literature are consistent with the results. According to the data presented in Table 1, the average pedestrian speed is between 1.08 and 1.47 m/s.

Furthermore, the 15th percentile speeds found in the literature review are generally between 0.73 and 1.31 m/s. The 15th percentile speed value of 1.05 m/s found in this study is within this range. It is recommended that the preferred design speeds at intersections in Türkiye be reconsidered based on these results.

The data obtained within the scope of the study showed that pedestrian crossing speed is affected not only by individual characteristics but also by environmental and physical factors. For example, the average pedestrian speed at four-leg intersections was found to be higher than at three-leg unsignalized intersections. Furthermore, the speeds of pedestrians crossing with vehicles were found to be relatively lower than in situations where there were no intersections. This is thought to be due to pedestrians' perception of safety. Similarly, it was observed that when the number and speed of vehicles impacting pedestrians increased, pedestrian speed generally decreased. This situation may be due to pedestrians' perception of safety, as well as the general driver refusal to yield to pedestrians, as reported in other studies [21, 22]. Pedestrians generally wait for vehicles to pass completely, wanting to remain safe. As pedestrians traveled longer distances within the intersection, their speeds also increased. This finding was similar to the study in the literature [20]. Pedestrians exhibit this behavior to minimize the risk they will be exposed to at the intersection.

In light of these results, it is recommended that a design speed of 1.05 m/s be used as a basis for intersection design and signal duration determination to increase the safe passage of different pedestrian groups (e.g., elderly, disabled, or child pedestrians). At intersections, pedestrians should be allowed to cross in the shortest possible distance. As crossing distances increase, pedestrians engage in dangerous and illegal crossings. Furthermore, preventative measures should be taken to reduce pedestrian contact with vehicles and enable safer crossings. This study examined pedestrian speed and some of the factors that influence it. The most significant difference distinguishing this study from other pedestrian speed studies is that it simultaneously examines many different parameters, both specific and general. This study does not include factors such as pedestrians' personal characteristics, adverse weather conditions, or driver behavior toward pedestrians. Future studies should also examine these factors and analyze larger data sets.

Acknowledgments

The video recordings required for this study were obtained from the video data set collected within the scope of the TUBITAK project number 123M640.

References

[1] National Highway Traffic Safety Administration and U.S. Department of Transportation, *Traffic Safety Facts: 2023 Data - Pedestrians*, Washington, DC, Jun. 2025.

[2] P. Olszewski, P. Szagała, M. Wolański, and A. Zielińska, "Pedestrian fatality risk in accidents at unsignalized zebra crosswalks in Poland," *Accid Anal Prev*, vol. 84, pp. 83–91, Dec. 2015. doi: 10.1016/j.aap.2015.08.008

[3] Trafik Guvenligi Dairesi Baskanligi, Ulasim Etutleri Subesi Mudurlugu, and Karayollari Genel Mudurlugu, *2024 Yili Trafik Kazalarina Ait Ozet Bilgiler [Summary Information on Traffic Accidents in 2024]*, Ankara, Jul. 2025.

[4] L. M. B. Acela, E. Sousa, S. Faria, R. Almeida, and E. F. Freitas, "Pedestrian crossing behavior in social groups: exploring cultural contexts through a comparative study," *Case Stud Transp Policy*, vol. 19, Mar. 2025. doi: 10.1016/j.cstp.2024.101333

[5] B. H. Goh, K. Subramaniam, Y. T. Wai, and A. A. Mohamed, "Pedestrian crossing speed: the case of Malaysia," *International Journal of Civil & Environmental Engineering*, vol. 2, no. 4, pp. 323–332, 2012. doi: 10.7708/ijje.2012.2(4).03

[6] G. Asaithambi, M. O. Kuttan, and S. Chandra, "Pedestrian road crossing behavior under mixed traffic conditions: A comparative study of an intersection before and after implementing control measures," *Transportation in Developing Economies*, vol. 2, no. 2, Oct. 2016. doi: 10.1007/s40890-016-0018-5

[7] N. M. Zafri, A. I. Rony, and N. Adri, "Analysis of pedestrian crossing speed and waiting time at intersections in Dhaka," *Infrastructures (Basel)*, vol. 4, no. 3, pp. 1–20, Jul. 2019. doi: 10.3390/infrastructures4030039

[8] I. Kaparias and I. Tsonev, "Pedestrian behaviour in integrated street designs: A mesoscopic analysis," *Transp Res Part F Traffic Psychol Behav*, vol. 99, pp. 113–126, Nov. 2023. doi: 10.1016/j.trf.2023.10.015

[9] A. Forde and J. Daniel, "Pedestrian walking speed at un-signalized midblock crosswalk and its impact on urban street segment performance," *Journal of Traffic and Transportation Engineering (English Edition)*, vol. 8, no. 1, pp. 57–69, Feb. 2021. doi: 10.1016/j.jtte.2019.03.007

[10] P. Onelcin and Y. Alver, "The crossing speed and safety margin of pedestrians at signalized intersections,"

in *19th EURO Working Group on Transportation Meeting, EWGT2016*, Istanbul, Turkey, 2016, pp. 3–12. doi: 10.1016/j.trpro.2017.03.002
[11] M. S. Tarawneh, "Evaluation of pedestrian speed in Jordan with investigation of some contributing factors," *J Safety Res*, vol. 32, pp. 229–236, 2001.
[12] A. Bansal, T. Goyal, and U. Sharma, "Modelling the pedestrian speed at signalised intersection crosswalks for heterogeneous traffic conditions," *Traffic & Transportation*, vol. 31, pp. 681–692, 2019.
[13] S. Marisamynathan and P. Vedagiri, "Modeling pedestrian delay at signalized intersection crosswalks under mixed traffic condition," in *2nd Conference of Transportation Research Group of India (2nd CTRG)*, Mumbai, Dec. 2013, pp. 708–717. doi: 10.1016/j.sbspro.2013.11.165
[14] S. Marisamynathan and P. Vedagiri, "A new approach to estimate pedestrian delay at signalized intersections," *Transport*, vol. 33, no. 1, pp. 249–259, 2018. doi: 10.3846/16484142.2016.1158208
[15] M. Giannoulaki and Z. Christoforou, "Pedestrian walking speed analysis: A systematic review," *Sustainability (Switzerland)*, vol. 16, no. 11, pp. 1–19, Jun. 2024. doi: 10.3390/su16114813
[16] D. Muley, M. Kharbeche, L. Downey, W. Saleh, and M. Al-Salem, "Road users' behavior at marked crosswalks on channelized right-turn lanes at intersections in the state of Qatar," *Sustainability (Switzerland)*, vol. 11, no. 20, pp. 1–19, Oct. 2019. doi: 10.3390/su11205699
[17] N. M. Asmael and M. Q. Waheed, "Analysis of pedestrian characteristics crossing along roads," *Transport Problems*, vol. 18, no. 4, pp. 189–200, 2023. doi: 10.20858/tp.2023.18.4.15
[18] Y. Poojari, E. Prashanth, D. Divya, and M. Kalyani, "Modelling pedestrian crossing behaviour at a midblock section," *Slovak Journal of Civil Engineering*, vol. 29, no. 3, pp. 15–21, Sep. 2021. doi: 10.2478/sjce-2021-0017
[19] S. Ahmed, S. Hossain, M. E. Shaik, and A. Shakik, "Evaluation of speed characteristics and gap acceptance behavior of pedestrians of Asian countries: A review," *Transp Res Interdiscip Perspect*, vol. 27, art. no. 101199, Jun. 2024. doi: 10.1016/j.trip.2024.101199
[20] D. Muley, W. Alhajyaseen, M. Kharbeche, and M. Al-Salem, "Pedestrians' speed analysis at signalized crosswalks," in *9th International Conference on Ambient Systems, Networks and Technologies (ANT 2018)*, Doha, 2018, pp. 567–574. doi: 10.1016/j.procs.2018.04.102
[21] H. Amado, S. Ferreira, J. P. Tavares, P. Ribeiro, and E. Freitas, "Pedestrian-vehicle interaction at unsignalized crosswalks: a systematic review," *Sustainability (Switzerland)*, vol. 12, no. 7, pp. 1–23, Apr. 2020. doi: 10.3390/su12072805
[22] C. Feliciani, L. Crociani, A. Gorrini, G. Vizzari, S. Bandini, and K. Nishinari, "A simulation model for unsignalized pedestrian crosswalks based on evidence from field observation," *J. Advanced Computational Intelligence and Intelligent Informatics*, vol. 18, no. 1, pp. 1–20, 2014.
[23] P. Olszewski, I. Buttler, W. Czajewski, P. Dąbkowski, C. Kraśkiewicz, P. Szagała, et al., "Pedestrian safety assessment with video analysis," in *6th Transport Research Arena*, Warsaw, Poland, 2016, pp. 2044–2053. doi: 10.1016/j.trpro.2016.05.172
[24] P. Fernández-González, A. Cuesta-Gómez, J. C. Miangolarra-Page, and F. Molina-Rueda, "Reliability and validity of Kinovea to analyze spatiotemporal gait parameters," *Revista Internacional de Medicina y Ciencias de la Actividad Fisica y del Deporte*, vol. 22, no. 87, pp. 565–578, Sep. 2022. doi: 10.15366/rimcafd2022.87.009
[25] J. M. Jiménez-Olmedo, A. Penichet-Tomás, L. Villalón-Gasch, and B. Pueo, "Validity and reliability of smartphone high-speed camera and Kinovea for velocity-based training measurement," *Journal of Human Sport and Exercise*, vol. 16, no. 4, pp. 1–11, 2021. doi: 10.14198/jhse.2021.164.11
[26] G. Norman, "Likert scales, levels of measurement and the 'laws' of statistics," *Advances in Health Sciences Education*, vol. 15, no. 5, pp. 625–632, Dec. 2010. doi: 10.1007/s10459-010-9222-y
[27] N. Mohd Razali and Y. Bee Wah, "Power comparisons of Shapiro-Wilk, Kolmogorov-Smirnov, Lilliefors and Anderson-Darling tests," *Journal of Statistical Modeling and Analytics*, vol. 2, no. 1, pp. 21–33, 2011.
[28] R. A. Armstrong, "When to use the Bonferroni correction," Ophthalmic Physiol Opt., vol. 34, no. 5, pp. 502–508, 2014. doi: 10.1111/opo.12131
[29] S. Ascione, V. Piscopo, and A. Scamardella, "Comparison of linear and rank-correlation for the sea state estimation," in *2024 IEEE International Workshop on Metrology for the Sea, MetroSea 2024 - Proceedings*, 2024, pp. 250–255. doi: 10.1109/MetroSea62823.2024.10765705

Performance Properties of Lightweight Aggregate Hybrid Foam Concretes

Selcuk Memis[1]

[1]Department of Civil Engineering, Kastamonu University, Kastamonu, Türkiye
Corresponding author: Selcuk Memis (e-mail: smemis@kastamonu.edu.tr)

Abstract

Hybrid geopolymers are binder systems in which an alkali-activated binder phase (N-A-S-(H)/C-(N)-A-S-H gels formed by activating Al-Si rich sources such as fly ash, slag, metakaolin with NaOH/Na_2SiO_3 etc.) and portland cement (ordinary portland cement (OPC)) hydration products (especially C-S-H/C-A-S-H) develop together in the same matrix. The aim is to combine the early age strength/setting advantages of cement with the low CO_2, thermal stability, and some durability advantages of geopolymer in a single material. In this study, the fresh and hardened properties of geopolymers, cement–geopolymer hybrids, and cementitious mortars with six different binder compositions produced using pumice aggregate were investigated. The fly ash (FA) and cement (OPC) ratios were systematically varied; sodium hydroxide (NaOH) and sodium metasilicate (Na_2SiO_3) were used for activation. The flow, unit weight, water absorption, thermal conductivity (λ), and 3-7-28 day flexural/compressive strengths were measured. The 28-day compressive strength reached 6.14 MPa in the pure geopolymer series, while the hybrid systems achieved a range of 2.90–5.53 MPa. The lowest water absorption (32%) and relatively low λ value (≈ 295 W/mK) were observed in hybrit group at 2. The results show that density and λ increase with increasing cement ratio in the hybrid systems, while water absorption decreases. The findings suggest that geopolymer and hybrid binders are suitable alternatives for the design of lightweight and fire-resistant structural elements.

Keywords: Sustainability, Pumice, Geopolymer concrete, Hybrid binders, Thermo-mechanical performance

2nd International Conference on Multidisciplinary Sciences and Technological Developments (ICMUSTED 2025)

December 12-15, 2025

The Role of Biodiesel Addition in Reducing Vapor Pressure in Gasoline–Methanol–Ethanol Ternary Blends

Abdulvahap Cakmak[1]

[1]Department of Mechanical Engineering, Faculty of Engineering and Natural Sciences, Samsun University, Ballica Campus, Ondokuzmayis, 55420 Samsun, Türkiye
Corresponding author: Abdulvahap Cakmak (e-mail: abdulvahap.cakmak@samsun.edu.tr)

Abstract

This study examines how adding biodiesel affects the vapour pressure and other physicochemical properties of gasoline–methanol–ethanol ternary fuel blends. Vapour pressure is a key factor influencing volatility, evaporation, engine performance, and emissions, especially in blends with low-boiling-point alcohols such as methanol and ethanol. However, blending methanol and ethanol into hydrocarbon-based gasoline significantly raises the vapour pressure of the mixture due to azeotropic interactions, even though methanol and ethanol individually have lower vapour pressures. To overcome this, biodiesel, a high-boiling, low-volatility renewable fuel, was incorporated into various ternary blend formulations. Biodiesel was added to alcohol-gasoline blends containing total alcohol (methanol and ethanol) at 10%, 20%, and 30%v/v, with biodiesel concentrations of 1%, 3%, and 5%v/v, respectively. The vapour pressure, density, distillation, and sulphur content measurements were taken using standard testing methods. The highest dry vapour pressure equivalent (DVPE) value of 72 kPa was recorded at a 10% v/v alcohol content, 6.04% higher than base gasoline. However, with the addition of 1% v/v biodiesel, the DVPE decreased slightly to 71.5 kPa. Biodiesel was also found to enhance the density and distillation properties of the ternary blends. Crucially, the measured fuel properties largely complied with the European standard for gasoline (EN 228), except for some samples' DVPE and distillation values at E70 and E100. These findings suggest that biodiesel can serve as a volatility stabiliser in alcohol-containing fuel formulations and as a renewable fuel component. The study highlights the limitations of current work and offers recommendations for further research into engine performance, combustion characteristics, and the long-term storage stability of the blends.

Keywords: Alcohol-gasoline blends, Biodiesel, Fuel volatility, Physicochemical properties, Vapor pressure

1. INTRODUCTION

Driven by rapid industrial growth, increasing energy demands, and heightened concern over climate change, research into alternative fuels with lower environmental impact and improved carbon performance has gained significant attention among scientists [1]. In this context, incorporating various alcohols into gasoline blends has attracted growing interest in reducing emissions, decreasing fossil fuel consumption, and enhancing fuel quality. Among these alcohols, methanol and ethanol are the most widely used in engine applications due to their advantageous properties, including renewability, broad availability, compatibility with existing engine technologies, oxygenated structure, and high octane rating.

Methanol and ethanol have long been commercially blended into gasoline in small fractions, varying by country, to extend fuel supplies and improve gasoline quality, particularly its octane rating. However, growing concerns over the limited availability of fossil fuel resources and their associated environmental and health impacts have highlighted the need to gradually reduce fossil fuel consumption and increase the share of renewable fuels in the energy market. There are ongoing projections and policy initiatives, supported by government regulations and incentives, to gradually increase the share of ethanol and methanol in the transportation sector. For example, the United States renewable fuel standard (RFS) mandates blending biofuels, including ethanol, into gasoline, targeting 36 billion gallons of renewable fuel use by 2022 and beyond [2]. Similarly, the European Union's renewable energy directive (RED II) requires member states to achieve at least a 14% share of renewable energy in transportation by 2030, with advanced biofuels playing a significant role [3]. China has also implemented E10 (10% ethanol) mandates in several provinces, with plans for nationwide expansion [4]. These initiatives reflect a global trend toward increasing alcohol fuel usage to reduce dependence on fossil fuels, improve energy security, and lower greenhouse gas emissions.

Methanol and ethanol are oxygenated fuels with a low carbon-to-hydrogen ratio, contributing to cleaner combustion. As a result, ethanol–methanol–gasoline blends tend to reduce emissions of carbon monoxide (CO), hydrocarbons (HCs), particulate matter (PM), and air toxics from gasoline engine vehicles. Additionally, due to their higher octane number, methanol and ethanol provide a convenient and cost-effective way to upgrade low-octane gasoline. However, when alcohols, particularly short-chain alcohols like methanol and ethanol, are blended with gasoline, the resulting mixture exhibits reduced distillation temperatures. It deviates from ideal mixing behavior due to forming a near-azeotropic mixture (non-ideal blending). This effect is especially pronounced at low alcohol concentrations (3-10%, v/v) [5], where the final blend may exhibit a vapor pressure higher than that of pure gasoline or the alcohol alone. Therefore, although methanol and ethanol have relatively low reid vapor pressures (RVP) of about 32 kPa and 13 kPa, respectively, their blended RVP in gasoline (60 kPa) can range from 65 kPa up to as high as 200 kPa, depending on the alcohol content in the blend. When blending to meet an RVP requirement, refineries need to remove some butane from the gasoline to compensate for the RVP increase caused by the alcohol. However, at higher alcohol blending levels, both methanol and ethanol cause only a slight increase in RVP, and the RVP response curve becomes relatively flat.

Vapour pressure refers to the pressure exerted by the vapour of a liquid in equilibrium with its liquid phase in a closed container. It serves as an indicator of a fuel's volatility and is a critical property of automotive gasoline. Higher vapour pressure indicates greater volatility, and vice versa. Excessively high and low vapour pressures can affect engine operation and cold-start performance. High vapour pressure may lead to fuel line blockages, engine stalling, unstable engine operation, and increased evaporative HC emissions. Conversely, a vapour pressure that is too low can cause difficulties during cold starts. Therefore, the EN 228 gasoline specification defines allowable vapour pressures based on the type of gasoline and its ethanol content. According to this standard, the vapour pressure of winter-grade gasoline should range from 60 to 90 kPa, while summer-grade gasoline should fall between 45 and 60 kPa. However, the upper limit for summer vapour pressure increases depending on the ethanol content.

As the use of methanol and ethanol in gasoline blends is expected to rise, it is crucial to lower the vapour pressures of these blends. Several researchers [6–10] have studied this challenge by investigating various strategies, such as incorporating higher alcohols or other oxygenated additives and optimizing blending ratios, to mitigate the increase in vapour pressure while maintaining or improving fuel properties and engine performance. From this context, this study examines the vapour pressures of dual-blends of methanol and ethanol with gasoline by adding biodiesel as biofuel components.

Biodiesel has already been widely used as a biofuel for diesel engines worldwide. Compared to ethanol and methanol, biodiesel is a highly available fuel with better lubricity, a higher boiling point, and a lower vapor pressure. These unique properties make biodiesel especially interesting for research, particularly when mixed with dual alcohol–gasoline blends. Combining these biofuels allows for taking advantage of each, resulting in a single fuel with improved overall qualities. To the best of the authors' knowledge, no previous study has investigated the effect of biodiesel on vapour pressure reduction in methanol–ethanol–gasoline blends, thereby underscoring the novelty of the present research.

2. MATERIAL AND METHOD

To conduct this research, the fuel samples were first prepared, followed by fuel analyses performed following European standard/International Organisation for Standardisation (EN/ISO). The test fuel samples were prepared using commercial 95-octane gasoline obtained from a fuel station, methanol and ethanol (95% purity) supplied by TEKKIM, and biodiesel meeting the EN 14214 specification provided by DP Tarımsal Enerji. To prepare the methanol–ethanol–gasoline–biodiesel blends, high-quality pipettes, beakers, and volumetric burettes with maximum precision were used. First, three dual alcohol–gasoline blends were prepared by adding methanol and ethanol to gasoline at volumetric ratios of 5%, 10%, and 15% v/v each. The resulting mixtures contained total alcohol contents of 10%, 20%, and 30% v/v, designated as A10, A20, and A30, respectively. Subsequently, biodiesel was blended with these dual alcohol–gasoline fuels at volumetric ratios of 1%, 3%, and 5% v/v, producing the quaternary blends labeled A10+B1, A20+B3, and A30+B5, respectively. Furthermore, base summer gasoline was incorporated as a reference for comparative analysis of fuel properties. In this study, the base gasoline may contain up to 3% v/v methanol and 5% v/v ethanol. Ideally, a base gasoline free of ethanol and methanol would have been used; however, such a fuel is currently unavailable on the market. Figure 1 shows the composition of fuel samples. DVPE, density, sulfur content, and distillation temperature were measured using the standard test methods and the equipment listed in Table 1.

Table 1. The equipment used for fuel specification

Property	Equipment	Method	Accuracy
Density	Mettler Toledo DE40	EN ISO 3675	±0.0001 g/cm^3
RVP	Herzog HVP 972	EN 13016	±0.2 kPa
Distillation	Herzog OptiDist^{TM}	EN ISO 3405	±0.1 °C
Sulfur	Analytik Jena Multi EA 3100	EN ISO 20846	±1 ppm

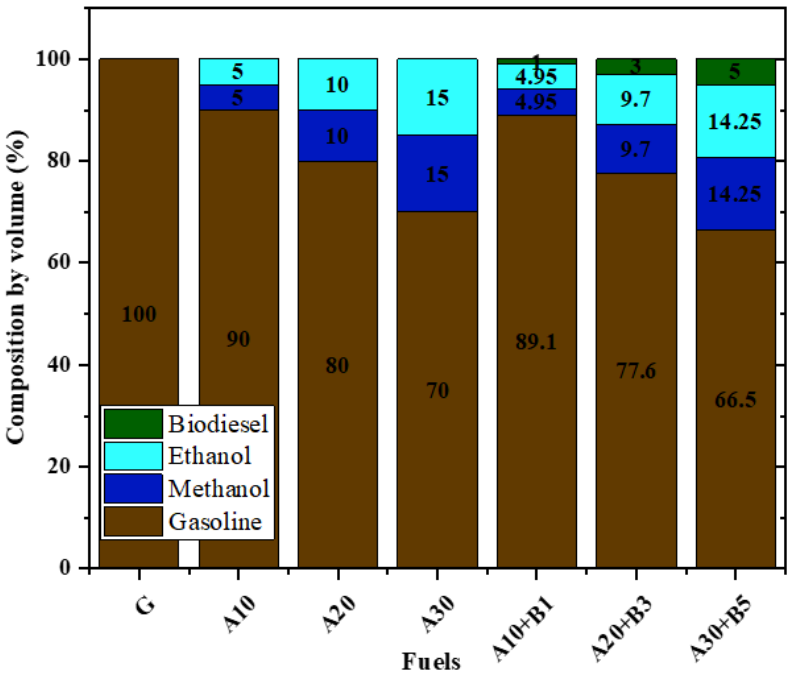

Figure 1. Composition of fuel samples

3. RESULTS

The RVP indicates the front-end volatility of gasoline and is closely related to its butane content. The RVP of gasoline blends can be adjusted by adding or removing normal butane during refining [11]. It is always reported in absolute pressure units such as psi, kPa, or bar. A higher RVP value corresponds to greater fuel volatility. Since the differences between RVP and DVPE are minimal, DVPE is generally considered equivalent to RVP [12]. Figure 2 presents the measured DVPE values of the fuel samples. In this figure, the numerical values are displayed inside each bar, while the relative change compared to the base gasoline is indicated above the bar. Since the ethanol content of summer gasoline is 5% v/v, the allowable increase in vapor pressure is 8 kPa, setting an upper DVPE limit of 68 kPa. The measured DVPE was 67.9 kPa. When the alcohol fraction was increased to 10% v/v, the DVPE rose to 72 kPa, about 6% higher than the base gasoline. This behavior suggests the presence of an azeotropic mixture at such low blending ratios. Further increases in alcohol concentration led to only a slight reduction in DVPE; for example, increasing the alcohol fraction from 20% to 30% v/v decreased DVPE by just 0.5 kPa, although values remained higher than the base gasoline. Adding 1%, 3%, and 5% v/v biodiesel to the A10, A20, and A30 blends decreased the DVPE by only 0.8, 0.7, and 1.7 kPa, respectively. This shows that the azeotropic effect of the hydroxyl group stays strong at low alcohol levels. As a result, biodiesel's vapor pressure-reducing ability is limited in these conditions, implying that a higher biodiesel blending ratio might be necessary to achieve a more substantial reduction. However, the DVPE values of all fuel samples, except for the base gasoline, fall outside the EN 228 specification, which defines an RVP range of 45–68 kPa for summer gasoline.

Fuel density is a crucial factor that affects engine performance, emissions, durability, and the operation of fuel system parts. High-density fuels generally provide more energy per volume, improving fuel economy and power output. However, high or low density can hamper spray atomization and air-fuel mixing, reducing combustion efficiency. Density influences flow rates, injector and pump calibration, and fuel metering accuracy in fuel systems. Deviations from the expected density can lead to improper injection, lowering efficiency, and raising emissions. Fuels must meet standard density ranges to ensure optimal engine performance and reliability. According to the EN 228 specification, gasoline density should be between 720 and 775 kg/m^3 at 15 °C. Figure 3

presents the density measurement results at 15 °C for the prepared fuel samples. Since methanol, ethanol, and biodiesel each have higher densities than gasoline, the ternary (dual alcohol–gasoline) and quaternary (dual alcohol–biodiesel–gasoline) fuel blends exhibited higher density values than neat gasoline. As the proportion of alcohols and biodiesel in the blends increased, the density values rose accordingly, as expected. The highest density, measured at 767.3 kg/m^3, was observed for the A30+B5 fuel sample, representing a 3.2% increase relative to gasoline. Despite these increases, the density values of all fuel samples remained within the acceptable range defined by the EN 228 specification limits.

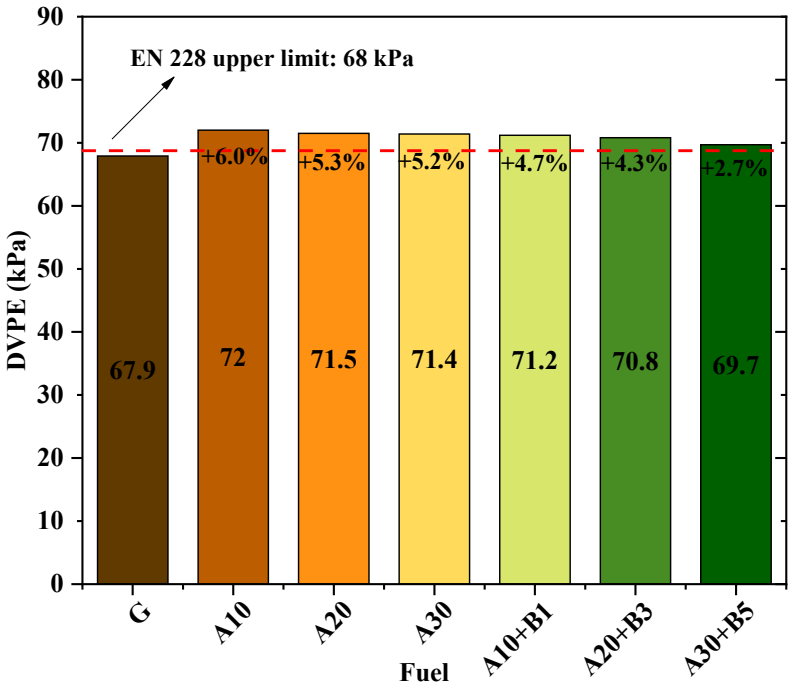

Figure 2. DVPE measurement results

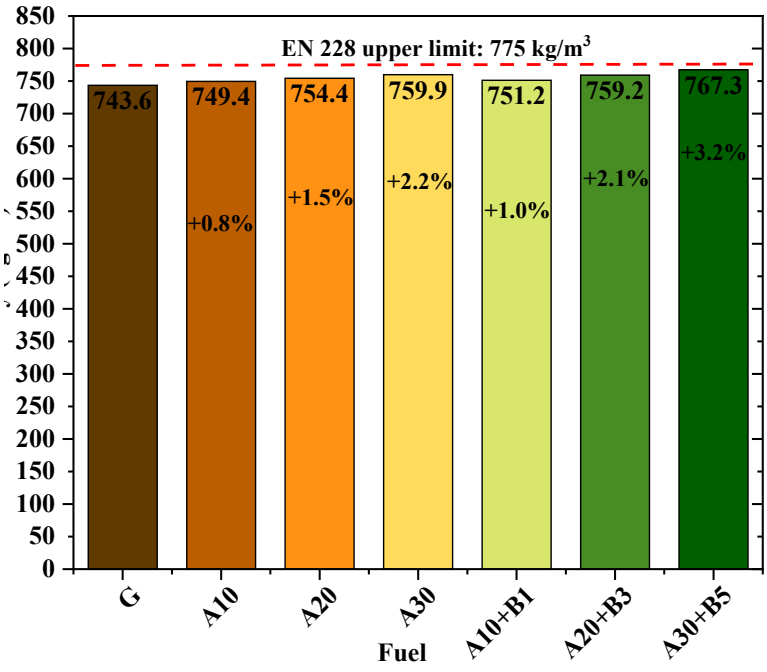

Figure 3. Density measurement results

The lower heating value (LHV) is a critical parameter in fuel selection for internal combustion engines, as it directly influences energy efficiency, combustion characteristics, and fuel handling [13]. Although no specific fuel regulation currently mandates a minimum LHV, it remains a key performance indicator. The LHVs of the fuel samples were estimated using the weighted average method, based on the mass fraction of each component and

their respective LHVs. Figure 4 illustrates the LHV results for the various fuel blends. Since methanol (50 wt% oxygen), ethanol (34.7 wt% oxygen), and biodiesel (11 wt% oxygen) are oxygenated fuels, they inherently possess lower calorific values compared to gasoline. Consequently, both ternary (dual alcohol–gasoline) and quaternary (dual alcohol–biodiesel–gasoline) blends exhibit reduced heating values, which may lead to lower engine power output unless compensated by higher volumetric fuel delivery or improved combustion efficiency. In engine applications, the fuel injection system meters and delivers fuel based on volume rather than mass. Therefore, the heating value of a fuel should be evaluated on a volumetric basis. The energy densities of the tested fuels G, A10, A20, A30, A10+B1, A20+B3, and A30+B5 were calculated as 32.3, 30.9, 29.6, 28.2, 31.0, 29.7, and 28.5 MJ/L, respectively. Compared to gasoline, the volumetric calorific values of these blends were lower by 4.1%, 8.4%, 12.6%, 4.0%, 8.0%, and 11.7%, respectively. Although methanol, ethanol, and biodiesel have significantly lower heating values than gasoline by approximately 54%, 38%, and 14%, respectively, the overall decrease in the fuel blends' volumetric energy content was less severe due to the higher density of these oxygenated components, which helps offset their lower energy content per unit volume.

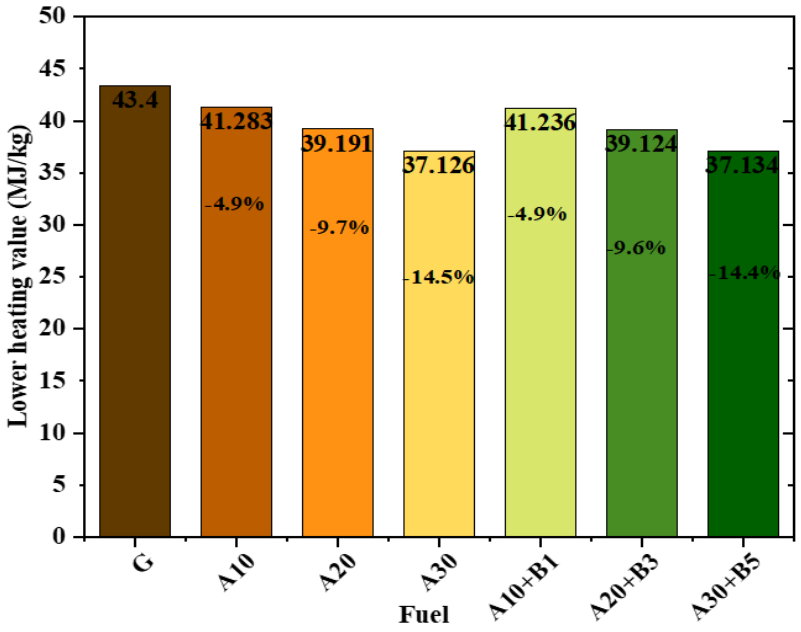

Figure 4. Lower heating values of fuel samples

The sulfur content of the fuel samples was measured as 1.6, 1.4, 1.2, 1.1, 1.3, 1.3, and 1.4 mg/kg for G, A10, A20, A30, A10+B1, A20+B3, and A30+B5, respectively. These values are well below the maximum limit of 10 mg/kg specified in the EN 228 standard, indicating full compliance. The observed reduction in sulfur content with increasing alcohol content is attributed to methanol and ethanol being inherently sulfur-free. Consequently, binary alcohol-gasoline blends and ternary blends with biodiesel exhibit improved sulfur profiles, contributing to cleaner combustion and reduced SOx emissions.

The volatility characteristics of gasoline were further investigated through distillation profiling, which offers more comprehensive information over a wider temperature range than DVPE measurements. Figure 5 shows the distillation curve of fuel samples. Gasoline shows a wide range of distillation curves because it contains various hydrocarbons with different boiling points. Due to the presence of low-boiling-point components such as butanes, pentanes, and light olefins, the temperature at which 5% of the fuel is distilled was 35.7 °C, about 7 °C lower than that of the fuel blends. Between the 10% and 30% distilled fractions, the distillation curves of all fuels were nearly the same, but they diverged in the 40% to 80% distillation range. This divergence results from the low boiling points of methanol and ethanol, which, as pure compounds, boil at constant temperatures. Most of the alcohol content in the blends evaporates within this range. As the remaining alcohol content decreases, the distillation curves converge again beyond the 80% threshold. The decrease in distillation temperature within the 40% to 80% distilled volume range will negatively impact fuel economy and engine performance. Despite its high boiling point of 340–360 °C, the addition of biodiesel did not noticeably alter the distillation temperatures of the ternary blends. This suggests that alcohol is the dominant factor in shaping the distillation curves, thereby reducing the influence of biodiesel at low blending ratios.

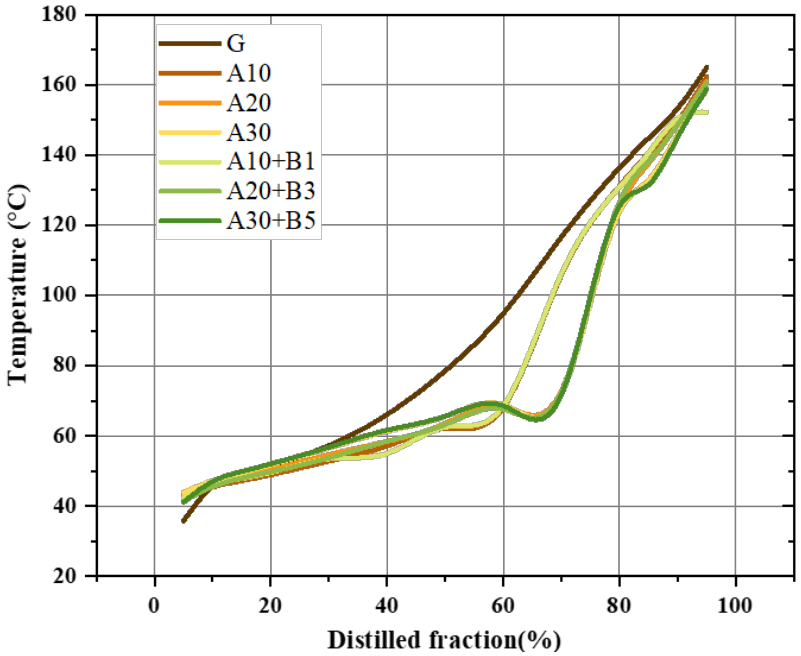

Figure 5. Distillation curve of fuel samples

Table 2 presents the specific distillation data for all fuel samples. In gasoline distillation analysis, specific temperatures are reference points to characterize volatility behavior. These include E70, E100, and E150, representing the percentage of fuel evaporated at 70, 100, and 150 °C, respectively. In addition, IBP and FBP denote the initial and final boiling points, corresponding to the temperatures at which the first and last drops distill. Although the EN 228 regulation does not specify a limit for IBP, it requires the FBP to be equal to or lower than 210 °C. According to Table 2, all fuel samples meet the E150 and FBP limits. However, most ternary and quaternary blends fall outside the E70 and E100 ranges specified by EN 228. This is due to the high volatility of these fuels. While such high volatility can improve cold start, warm-up, and driveability, it may also lead to vapor lock and unstable engine operation. In addition, high volatility can increase fuel consumption and evaporative hydrocarbon emissions [9].

Table 2. Detailed distillation data

	Unit	G	A10	A20	A30	A10+B1	A20+B3	A30+B5	EN 228 Limit
IBP	°C	35.7	32.7	34.4	36.7	36.3	37.7	35.1	-
E70	%v/v	43.4	62.1	64.5	64.3	62.6	65.8	64.8	22-50
E100	%v/v	62.7	68.6	76.3	82.8	68.4	76	82.7	46-71
E150	%v/v	88.2	90.1	90.6	91.8	89.9	90.5	91.9	≥ 75
FBP	℃	190.9	183.9	181	182	190.6	189.4	187.1	≤ 210
Residue	%v/v	1	1	1	1	1	1	1	≤ 2

4. CONCLUSION

The results indicate that all gasoline–methanol–ethanol ternary blends had higher vapour pressure than the standard gasoline. Although adding biodiesel to these blends lowered the vapour pressure, the measured values still surpassed the EN 228 limit. The increase in RVP observed in alcohol–gasoline blends could not be reduced below the EN limit by adding 5% vol. biodiesel, indicating that a higher biodiesel fraction is required. Therefore, its effectiveness in lowering the vapor pressure of lower alcohol–gasoline blends is limited, owing to the strong azeotropic behavior of these mixtures. The other measured fuel characteristics showed slight improvements with biodiesel added to the ternary blends. Although biodiesel has a very low octane number, which could reduce the knocking resistance of the final blend, this adverse effect can be offset by the high octane numbers of methanol and ethanol. Future studies could focus on utilizing higher biodiesel fractions or reformulating methanol–ethanol–gasoline blends with novel additives to achieve better vapor pressure control. If any additive significantly improves, subsequent investigations should include fuel stability assessments, engine performance tests, and fuel–material compatibility evaluations.

Acknowledgments

The author wishes to sincerely thank Fatih Bilgin, Director of the Fuels Analysis Laboratory at Guzel Enerji A.S., for his technical support and assistance with this study.

References

[1] E. Vanzela, W. C. Nadaleti, R. A. Bariccatti, P. A. Cremonez, E. de Rossi, P. B. Filho, et al., "Physicochemical properties of ethanol with the addition of biodiesel for use in Otto cycle internal combustion engines: Results and revision," *Renewable and Sustainable Energy Reviews*, vol. 17, no. 74, pp. 1181–1188, 2017. doi: 10.1016/j.rser.2017.03.053

[2] U.S. Environmental Protection Agency (EPA), "Renewable fuel standard program (RFS2) regulatory impact analysis. Office of transportation and air quality," EPA-420-R-10-006 [Online], Feb. 2010.

[3] EN. (2025, Aug. 06). *European Parliament & Council. Directive - 2018/2001 - EN - EUR-Lex* [Online]. Available: https://eur-lex.europa.eu/eli/dir/2018/2001/oj

[4] H. Hao, Z. Liu, F. Zhao, J. Ren, S. Chang, K. Rong, et al., "Biofuel for vehicle use in China: Current status, future potential and policy implications," *Renewable and Sustainable Energy Reviews*, vol. 82, pp. 645–653, 2018. doi: 10.1016/J.RSER.2017.09.045

[5] V. F. Andersen, J. E. Anderson, T. J. Wallington, S. A. Mueller, and O. J. Nielsen, "Vapor pressures of alcohol-gasoline blends," *Energy and Fuels*, vol. 24, pp. 3647–3654, 2010. doi: 10.1021/ef100254w

[6] L. M. Rodríguez-Antón, F. Gutiérrez-Martín, and C. Martinez-Arevalo, "Experimental determination of some physical properties of gasoline, ethanol and ETBE ternary blends," *Fuel*, vol. 156, pp. 81–86, 2015. doi: 10.1016/j.fuel.2015.04.040

[7] L. M. Rodríguez-Antón, M. Hernández-Campos, and F. Sanz-Pérez, "Experimental determination of some physical properties of gasoline, ethanol and ETBE blends," *Fuel*, vol. 112, pp. 178–184. 2013. doi: 10.1016/j.fuel.2013.04.087

[8] E. Vanzela, W. C. Nadaleti, R. A. Bariccatti, P. A. Cremonez, E. de Rossi, P. B Filho, et al., "Physicochemical properties of ethanol with the addition of biodiesel for use in Otto cycle internal combustion engines: Results and revision," *Renewable and Sustainable Energy Reviews*, Vol. 74, pp. 1181–1188, 2017. doi: 10.1016/j.rser.2017.03.053

[9] N. E. Bulbul and A. Cakmak, "The effectiveness of iso-alcohols in reducing vapor pressure and enhancing fuel properties of ethanol-gasoline mixtures," *International Journal of Automotive Engineering and Technologies*, vol. 14, pp. 1–10, 2025. doi: 10.18245/ijaet.1591917

[10] L. M. Rodríguez-Antón, F. Gutiérrez-Martín, and M. Hernández-Campos, "Physical properties of gasoline-ETBE-isobutanol (in comparison with ethanol) ternary blends and their impact on regulatory compliance," *Energy*, vol. 185, pp. 68–76, 2019. doi: 10.1016/J.ENERGY.2019.07.050

[11] T. M. M. Abdellatief, M. A. Ershov, V. M. Kapustin, M. Ali Abdelkareem, M. Kamil, and A. G. Olabi, "Recent trends for introducing promising fuel components to enhance the anti-knock quality of gasoline: A systematic review," *Fuel*, vol. 291, art. no. 120112, 2021. doi: 10.1016/J.FUEL.2020.120112

[12] F. Leach, R. Stone, and D Richardson, "The influence of fuel properties on particulate number emissions from a direct injection spark ignition engine," *SAE Technical Paper*, 2013. doi: 10.4271/2013-01-1558

[13] N. I. Masuk, K. Mostakim, and S. D. Kanka, "Performance and emission characteristic analysis of a gasoline engine utilizing different types of alternative fuels: A comprehensive review," *Energy and Fuels*, vol. 35, pp. 4644–4469, 2021. doi: 10.1021/acs.energyfuels.0c04112

2nd International Conference on Multidisciplinary Sciences and Technological Developments (ICMUSTED 2025)

December 12-15, 2025

Shunt Reactor (without Tap Changer) Design, Manufacturing, and Testing

Ali Tas[1]

[1]R&D Department, Beta Enerji ve Teknoloji A.S., Adana, Türkiye
Corresponding author: Ali Tas (e-mail: ali.tas@betaenerji.com)

Abstract

This study covers the design, manufacturing, and testing processes of a dual-input FR3 vegetable oil transformer, developed to enhance efficiency, safety, and sustainability of power conversion equipment in solar power plants (SPPs). Unlike conventional single-input transformers, this design allows feeding from two different high-voltage sources, providing operational flexibility and reducing the number of required equipment, thereby lowering operating costs. The transformer is designed according to the International Electrotechnical Commission (IEC) 60076 standards, incorporating low-loss silicon steel cores, high voltage (HV) and low voltage (LV) coil structures with aluminium foil, electrostatic shielding for harmonic suppression, and FR3 vegetable oil offering high dielectric strength, improved thermal performance, and environmental sustainability. Critical manufacturing processes include core stacking, foil and flat conductor winding, insulation design, corrugated tank production, and vacuum oil filling. The prototype underwent routine testing, including direct current (DC) resistance, short-circuit losses and impedance, no-load losses, voltage ratio, and applied/induced voltage tests to validate the design. The dual-input configuration allows use across two different lines or sites, while FR3 oil reduces carbon footprint, enhances fire safety, and extends equipment lifetime, contributing to sustainable energy infrastructure.

Keywords: Dual-input transformer, FR3 vegetable oil, Solar power plant (SPP)

Use of Bayburt Green-Spotted White Tuff in the Production of Structural Lightweight Concrete

Omer Bayrak[1], Emin Erdem[2]

[1]Civil Engineering, Bayburt University, Bayburt, Türkiye
[2]Department of Chemistry, Pamukkale University, Denizli, Türkiye
Corresponding author: Omer Bayrak (e-mail: cermeomer1342@gmail.com)

Abstract

Volcanic tuffs extracted from the Bayburt region, which are white in color with green spots, are used not only for cladding structures but also for load-bearing walls due to their light weight, microporous nature, and ease of processing. Due to their low density (1.8 g/cm^3), tuffs have significant potential as aggregates in lightweight concrete production. Large amounts of waste are generated from green-speckled Bayburt white tuffs (GBWT) with a density lower than 2 g/cm^3 in industrial facilities. This study aimed to produce structural lightweight concrete (SCL) using GBWT aggregates obtained from waste. GBWT waste was ground to a maximum particle size (Dmax) of 11.2 mm and classified into 9 different sieve sizes (0-0.063, 0.063-0. 125, 0.125-0.25, 0.25-0.5, 0.5-1, 1-2, 2-4, 4-8, 8-11.2 mm) and aggregate tests were conducted. A granulometry curve compliant with Dmax 8 mm (Turkish Standards European norm (TS EN) 802) was determined. SCL mixtures prepared with a binder dosage of 450 kg/m³ and a water/cement ratio of 0.50 were poured into 10×10×10 cm^3 cube molds in two layers. The produced SCL samples were cured in lime-saturated water for 7 and 28 days, after which compressive strength tests were performed. As a result, it was determined that the dry unit weight values of the produced SCLs averaged 1.6 g/cm^3 and their 28-day compressive strength values ranged between 17.9 and 20.6 MPa, exceeding the 17.2 MPa value required by American Concrete Institute (ACI) (213R, 2014), and that SCL could be successfully used in production.

Keywords: Lightweight concrete, Bayburt spotted white tuff, Waste

2nd International Conference on Multidisciplinary Sciences and Technological Developments (ICMUSTED 2025)

December 12-15, 2025

Investigation of the Suitability of Waste Concrete Paving Blocks as Aggregate in Concrete

Melisa Kayrak[1], Arda Sahin[1], N. Sebnem Karahan[1], Omer Can[1]

[1]Department of Construction, Technical Sciences Vocational School, Canakkale Onsekiz Mart University, Canakkale, Türkiye
Corresponding author: Omer Can (e-mail: omer.can@comu.edu.tr)

Abstract

Aggregate is a fundamental component in concrete production, constituting approximately 60-70% of the mixture, and increasing construction activities are placing significant pressure on natural aggregate (NA) resources. This study investigates the usability of recycled concrete aggregate (RCA) obtained from concrete paving stones that have become waste as a result of quality control tests, with the aim of sustainable resource management and waste recovery. In this context, waste paving stones were crushed into aggregate, and the physical and mechanical properties of these aggregates, such as granulometry, Los Angeles abrasion resistance, Methylene Blue, flatness index, unit volume weight, and water absorption, were determined according to standards. As a result of aggregate characterisation, it was determined that RCA has a higher water absorption rate (2.6% - 8.2%) and lower density compared to NAs, while the Los Angeles abrasion loss (53%) was slightly above the standard limit value (50%). In the second stage, C30 concrete class was targeted using these aggregates, and the slump value of the fresh concrete produced was measured as 80 mm. As a result of the 28-day compressive strength, Schmidt hardness, and ultrasonic transit time tests performed on the hardened concrete samples, an average compressive strength of 34.17 MPa was obtained, demonstrating that the targeted C30 class performance was successfully achieved. These results demonstrate that concrete paving stone waste can be effectively utilised as aggregate in structural concrete, particularly when certain limitations, such as the Los Angeles abrasion value, are taken into account.

Keywords: Recycled aggregate, Concrete production

1. INTRODUCTION

Concrete, which consists of 60 to 70 per cent aggregate by volume, is the dominant building material in the global construction industry [1]. Demographic growth, urbanisation, and urban renewal programmes accelerating new construction have dramatically increased the demand for this fundamental component of concrete. The mass consumption of natural aggregates (NAs) through quarrying, a traditional method of aggregate supply, leads to ecosystem destruction, environmental degradation, and serious pressure on existing natural resources [1]. As a result of these economic and environmental challenges, the sector has embarked on a search for sustainable alternative materials

In this context, converting construction and demolition waste into recycled concrete aggregate (RCA) offers a solution to waste management problems and holds significant potential in terms of resource conservation. The current literature contains comprehensive studies focusing on the use of demolition waste, particularly from urban regeneration projects, in concrete production as RCA [2, 3]. These studies reveal that the differences exhibited by RCA compared to NA, such as higher porosity, lower density, and increased water absorption rate, can have adverse effects on the rheological properties and workability of fresh concrete.

The fact that academic studies have focused predominantly on demolition rubble has created a research gap regarding the potential of waste generated during construction material manufacturing processes or quality control (QC) tests. Concrete paving stones (of various types and sizes, such as interlocking, rectangular, or rain gutters), widely used in urban infrastructure (squares, roads, etc.), are subjected to standard compliance tests both at production facilities and in inspection laboratories. Numerous paving stones broken during these QC tests are disposed of as waste material [4].

There are findings that the mechanical strength of concrete containing RCA may fall short of the targeted design class, and it has been suggested that this situation should be compensated for by designing according to a higher

strength class [2]. However, it has also been demonstrated that chemical admixture technologies, particularly superplasticisers (SP), can balance the high water demand of RCA and improve the stiffness performance of concrete [5]. In a similar waste recovery study, research using concrete kerbstones removed during road renovation works as aggregate revealed that a 20% replacement with RCA yielded positive results [6]. Another study emphasised the idea that concrete obtained from demolished structures should be treated not as "waste" but as a value-added "by-product" [7].

The primary objective of this research is to analyse in detail the reusability of concrete paving stone waste, a specific waste source broken during factory/laboratory QC, as aggregate in concrete production. In this regard, the physical and mechanical properties of the RCA in question were characterised, and the performance of concrete produced with these aggregates in the target strength class C30, both in its fresh and hardened states, was examined. The fundamental aim of this study is to comprehensively investigate the usability of concrete paving stone waste, resulting from laboratory and factory QC, in concrete production by crushing it back to aggregate size. The study aims to characterise the physical and mechanical properties of this specific type of RCA and to analyse the performance (fresh and hardened concrete properties) of the targeted C30 class concrete using these aggregates. This aims to both recover a waste material that poses an environmental problem and reduce the pressure on quarries.

2. MATERIALS AND METHODS

Experimental studies were conducted at the Construction Materials Laboratory of Canakkale Vocational School, Canakkale Onsekiz Mart University (COMU).

2.1. Material

The main material of the study, RCA, was obtained from concrete paving stones of various sizes and shapes that had become waste as a result of laboratory QC tests (compression, abrasion, etc.). These waste paving stones were crushed in jaw crushers at the quarry to produce aggregate fractions of different sizes and then transported to the laboratory. CEM I 42.5 R type Portland cement was used as the binder in the concrete mixture. Suitable municipal tap water was preferred as the mixing water.

2.2. Method

The study was conducted in two main stages. In the first stage, the characterisation of RCA was carried out, and in the second stage, the mechanical properties of the concrete produced with RCA were determined.

2.2.1. Aggregate Tests

To determine the suitability of the obtained RCA for use in concrete production, a comprehensive aggregate characterisation was first carried out. In this regard, the particle size distribution of the aggregate was determined by sieving according to the Turkish Standard European Norm (TS EN) 933-1 [8] standard. To determine the aggregate's mechanical resistance to impact and abrasion, the Los Angeles abrasion test was performed in accordance with the TS EN 1097–2 [9] standard. The methylene blue (MB) test was applied according to the TS EN 933-9 [10] standard to determine the quality of the fine material and its possible clay content. The flatness index (FI) was determined based on the TS EN 933-3 [11] standard to define the shape characteristics of the aggregate particles. Finally, the oven-dry particle density, saturated surface dry (SSD) particle density, and water absorption capacity, which will determine the porosity of the aggregate and its effect on the water requirement of fresh concrete, were determined in accordance with the TS EN 1097-6 [12] standard.

2.2.2. Concrete Production and Tests

After completing the RCA characterisation, a mix design was developed targeting C30 class concrete, referencing TS 802 and TS EN 206 [13] standards. A slump test was conducted according to TS EN 12350-2 [14] to determine the workability and consistency of the produced fresh concrete. Six cube specimens measuring 150×150×150 mm^3 were taken from the fresh concrete mixture and these specimens were kept in a standard water curing tank for 28 days. Non-destructive tests were first performed on the hardened concrete specimens that had completed the curing period. In this context, a Schmidt hammer test was performed in accordance with TS EN 13791 [15] to determine the surface hardness and approximate compressive strength, and ultrasonic velocity measurements were taken in accordance with TS EN 12504-4 [16] to evaluate the homogeneity of the internal structure of the concrete. Finally,

to determine the final mechanical performance of the specimens, a 28-day compressive strength test was performed on a 200-tonne press in accordance with the TS EN 12390–3 [17] standard.

3. FINDINGS AND DISCUSSION

3.1. RCA Characterisation

A sieve analysis was performed on the RCA samples. Figure 1 shows the sieve analysis test and Figure 2 shows the granulometry curve graph. When examining the granulometry curve presented in Figure 2, it can be seen that less fine material (0-4 mm) was exposed compared to coarse material during the crushing of the paving stones. This situation caused the mixture to remain in the lower region in terms of fine material according to the Fuller curve. To compensate for this deficiency in the concrete mix design, natural fine aggregate supplementation or an appropriate gradation adjustment may be required.

Figure 1. Sieve analysis test

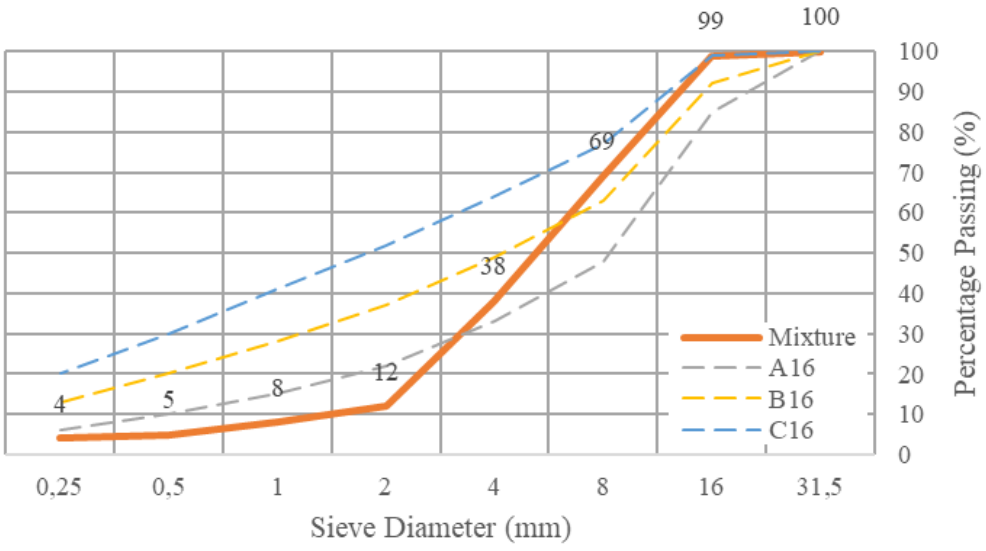

Figure 2. Sieve analysis results of recycled aggregate

The Los Angeles abrasion test was conducted according to TS EN 1097–2 to determine the abrasion resistance of the aggregate. The test results are given in Table 1. The Los Angeles abrasion test apparatus is shown in Figure 3. According to Table 1, the Los Angeles (LA) abrasion loss for the 10/14 mm fraction was measured as 53%. The American Society for Testing and Materials (ASTM) C-33 [18] standard recommends that the LA loss for concrete aggregates should be a maximum of 50%. The obtained value is 3% above this limit. This indicates that RCA has a slightly lower resistance to abrasion compared to NAs. The high LA value stems from the weaker cement paste-

aggregate interface in the RCA structure. This result may limit the material's use in applications where abrasion load is critical, but it can be considered acceptable for standard structural concretes such as C30 class.

Figure 3. Los Angeles abrasion test setup

Table 1. Los Angeles abrasion test results

Ball Count	Aggregate Size Range (mm)	Aggregate (Pavement)			
		Initial Mass (g)	Final Mass After 500 Cycles (g)	Mass Loss (g)	Loss Percentage (%)
10	10/14	5000	3259	1741	53
Los Angeles Category				$LA_{DECLARATION}$	

The shape determination test of the prepared RCA was conducted in accordance with TS EN 933-3. The results obtained are presented in Table 2. As seen in Table 2, the FI was found to be 1.2 and falls into the FI15 category. This indicates that the aggregate has an excellent shape characteristic in terms of cubicity and will not cause problems in terms of interlocking and workability within the concrete.

Table 2. FI test results

Material Information		Paving Stone Waste		
Test Sample Mass (g) $M_0 = 5970$		Total Mass of Samples Excluded from Processing (g) 44		
Screening with Test Sieves		Screening with Bar Screens		
Particle Size Range (mm)	Particle Size Mass (g)	Sieve Gap Width (mm)	Mass Passing Through the Sieve (g)	$FI_i = (m_i/R_i)\times100$
25 / 31.5	0	16	0	-
20 / 25	0	12.5	0	-
16 / 20	53	10	0	-
12.5 / 16	455	8	0	-
10 / 12.5	356	6.3	1	0
8 / 10.	2154	5	24	1
6.3 / 8	1652	4	33	2
5 / 6.3	596	3.15	5	1
4 / 5.	660	2.5	8	1
$M_1 = SR_i =$	5926	$M_2 = Sm_i =$	71	
$FI = (M_2/M_1)\times100 =$	1.2	FI Category	FI_{15}	

The MB value was found to be 0.5 g/kg (Figure 4). This value is well below the risk threshold of 1.5 g/kg, confirming that the aggregate does not contain harmful clay minerals or contamination.

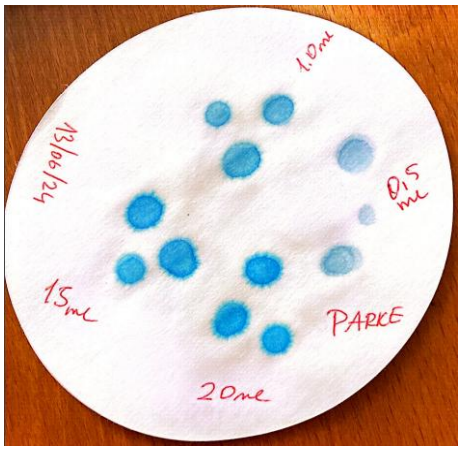

Figure 4. MB analysis test

Particle density and water absorption tests were conducted according to TS EN 1097-6. The results in Table 3 show that the density values of RCA are lower than those of NAs. Conversely, the water absorption rates (2.6% to 8.2%) are significantly higher than those of NAs (0.5% to 2%). This is due to the presence of hardened cement paste from the original concrete in the structure of RCA and the porous nature of this paste. In particular, the high water absorption rate in the fine fraction (8.2%) will directly affect the workability of fresh concrete and the net water/cement ratio, requiring careful consideration of the SSD condition in the mix design.

Table 3. Density and water absorption test results

Water Absorption Test Results					Density Test Results				
Size		0/4	4/8.	8/16.	Size		0/4.	4/8	8/16.
Pycnometer + Water + Material Mass (g)	M_2	7283	8126	8109	Measuring Cup Mass (g)	m_1	3188	3188	3188
Pycnometer + Water Mass (g)	M_3	6676	6289	6260	Measuring Cup Volume (l)	v	3	3	3
Material DKY Mass (g)	M_1	1001	3078	3050	Sample + Measuring Cup Mass (g)	m_2	7692	7283	6925
Material Oven-Dried Mass (g)	M_4	925	2965	2973	Loose Bulk Density (kg/dm^3)	ρ_b	1.501	1.365	1.246
Apparent Particle Density (kg/dm^3)	ρ_a	2.91	2.63	2.65	Porosity (%)	n	36	43	50
Oven-Dried Grain Density (kg/dm^3)	ρ_{rd}	2.35	2.39	2.48					
DKY Particle Density (kg/dm^3)	ρ_{ssd}	2.54	2.48	2.54					
Water Absorption Calculation (%)	WA24	8.2	3.8	2.6					

3.2. Fresh and Hardened Concrete Test Results

The fresh concrete consistency test was conducted using the slump cone method in accordance with TS EN 12350-2. Despite RCA's high water absorption potential, a slump value of 80 mm (S2 consistency class) was obtained in the fresh concrete produced by adjusting the mixing water according to the DKY condition (Figure 5). This value is within the target workability range for a C30 class concrete.

Figure 5. Slump test setup

The ultrasonic transit time and Schmidt hammer test results are given in Table 4, and the test images are shown in Figure 6. According to the results in Table 4, the estimated compressive strength measured with the Schmidt hammer was 28.15 MPa on average. The estimated strength calculated using the ultrasonic transit velocity is 36.77 MPa. The ultrasonic transit velocity being above 4.0 km/s indicates that the internal structure of the concrete is "very good" and homogeneous.

Figure 6. Schmidt hammer test and ultrasonic wave velocity test application

According to Table 5, the average unit volume mass of concrete specimens produced with RCA was found to be 2.27 kg/dm^3. This value is 5-6% lower than the density of normal concrete produced with NAs. This reduction in weight is directly attributable to the low-density structure of RCA.

The compressive strength test was performed on 150x150x150mm cube specimens after 28 days of curing, in accordance with TS EN 12390–3. The compressive strength test results are given in Table 5 and the test graph is shown in Figure 7. The average compressive strength of the sample was determined to be 34.17 MPa. This value is close to the average strength value required for the targeted C30 class and is very close to meeting the minimum requirement (37 MPa) for C30/37 class concrete according to the TS EN 206 standard. Although the LA abrasion value of the aggregate is 3% above the limit, the fact that the compressive strength exceeds the target class C30 strongly supports the use of paving stone waste as aggregate in structural concrete production. The differences between the Schmidt (28.15 MPa) and ultrases (36.77 MPa) estimates and the actual compressive strength (34.17 MPa) indicate that non-destructive methods may require calibration for RCA concrete, but that the Ultrases method provides a closer estimate.

Table 4. Schmidt hammer test and ultrasonic wave velocity test results

Sample No.	Schmidt Hammer Readings													Ultrasonic Readings			
	1	2	3	4	5	6	7	8	9	10	Average (R_c)	Strength Estimate (MPa)*	Average Strength Estimate (MPa)	Duration (µs)	Speed - V (km/h)	Strength Estimate (MPa)*	Average Strength Estimate (MPa)
P1	26	28	23	26	22	20	23	26	20	20	24	24.37	28.15	34.6	4.3	36.14	36.77
P2	24	28	28	24	22	20	22	24	24	20	24	24.37		34.1	4.4	39.69	
P3	24	21	29	28	22	26	27	26	22	30	25	27.47		34.6	4.3	36.14	
P4	29	24	23	28	32	23	23	27	28	24	26	30.81		33.9	4.4	39.69	
P5	27	28	28	23	29	22	24	25	21	22	25	27.47		34.5	4.3	36.14	
P6	28	24	29	27	28	24	28	24	28	26	27	34.42		35.7	4.2	32.84	

*: Compressive strength estimates were calculated using Rc and V values.

Table 5. Compressive strength test results

Compressive Strength Values (28 days)				
Sample No.	Unit Volume Mass (kg/dm^3)	Fracture Load (kN)	Strength (MPa)	Average Strength (MPa)
P1	2.26	780.9	34.71	34.17
P2	2.3	756.7	33.63	
P3	2.23	760.9	33.82	
P4	2.27	791.4	35.17	
P5	2.29	748.1	33.25	
P6	2.25	774.6	34.43	

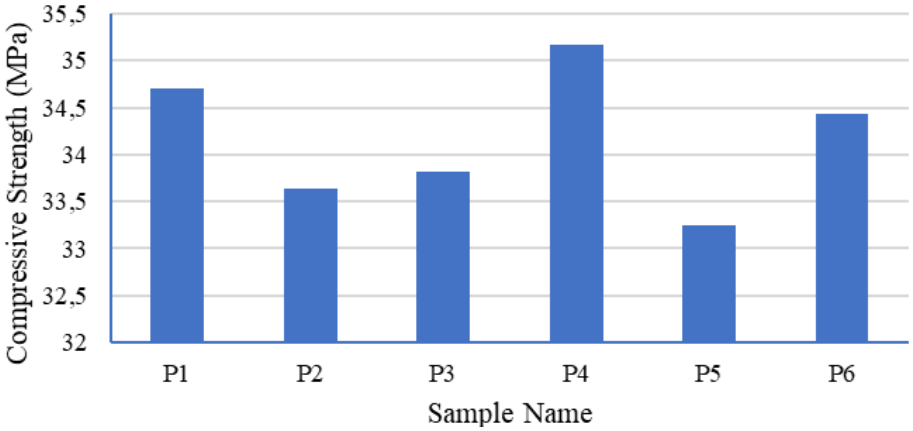

Figure 7. Pressure resistance graph

4. RESULTS

In this study, the usability of recycled aggregates obtained from waste concrete paving stones, which were discarded as a result of QC tests, in concrete production was investigated. Based on the findings, the following conclusions were reached:

- It was determined that RCA produced from waste paving stones has a lower density and significantly higher water absorption rates ranging from 2.6% to 8.2% compared to NAs. This situation necessitates the precise adjustment of the mixing water in concrete design according to the DKY condition.
- The Los Angeles abrasion loss of RCA was measured as 53%. This value is slightly (3%) above the 50% limit specified by the standards. However, the FI (FI15) and MB (0.5 g/kg) results of the aggregate are excellent.

- In the production of the targeted C30 class concrete using RCA, a workability value of 80 mm (S2 consistency) was achieved. After 28 days of curing, the average compressive strength of the samples was measured as 34.17 MPa.
- Although the LA abrasion value was slightly above the limit, the compressive strength of the final concrete successfully met the C30 class target. This proves that aggregates obtained from waste paving stones can be an effective alternative to NAs in standard structural concrete applications (up to C30/37 class) that do not require high abrasion resistance.

This study demonstrates that paving stone waste, which poses an environmental problem, can be converted into a valuable raw material in concrete production, thereby contributing to both waste management and the conservation of natural resources.

Acknowledgments

This paper utilises data from the TUBITAK-2209/A 2023/2 term project entitled “Investigation of the Reusability of Concrete Paving Stone Waste as Aggregate”.

References

[1] A. Koken, M. A. Koroglu, and F. Yonar, “The usability of waste concrete as concrete aggregate,” *Selcuk University Technical Sciences Vocational School Technical-Online Journal*, vol. 7, no. 1, pp. 86–97, 2008.

[2] G. Durmus, O. Can, and O. Simsek, “Determination of the engineering properties of different classes of concrete produced from recycled aggregates," in *5th International Advanced Technologies Symposium (IATS’09)*, Karabük, Turkey, May 13–15, 2009.

[3] T. C. Hansen and H. Narud, “Strength of recycled concrete made from crushed concrete coarse aggregate,” in *Concrete International: Design and Construction*, 1983, pp. 79–83.

[4] B.T. Yuksel, “The use of blast furnace slag in the production of paving stones and kerbs,” in *Earthquake Symposium*, Kocaeli, 2005, pp. 870–880.

[5] A. Nealen and M. Ruhl, “Consistency aspects in the production of concrete using aggregates from recycled demolition material,” in *Darmstadt Concrete*, 1997.

[6] H. Polat, U. E. Yurtcan, and M. N. Kolak, “Investigation of the usability of waste kerbstones as concrete aggregate,” *Journal of Nature and Science*, vol. 3, no. 2, pp. 37–41, 2014.

[7] M. M. Tufekci, “Investigation of the reusability of recycled aggregates in concrete production,” M.Sc. thesis, Institute of Science, Yıldız Technical University, 2011.

[8] *Tests for geometric properties of aggregates – Part 1: Determination of gradation – Sieve analysis*, TS EN 933-1, Turkish Standards Institute, Ankara, 2012.

[9] *Tests for mechanical and physical properties of aggregates – Part 2: Methods for determining resistance to fragmentation*, TS EN 1097-2, Turkish Standards Institute, Ankara, 2020.

[10] *Tests for geometric properties of aggregates – Part 9: Determination of fine particles – Methylene blue test*, TS EN 933-9, Turkish Standards Institute, Ankara, 2022.

[11] *Tests for geometric properties of aggregates – Part 3: Flatness index*, TS EN 933-3, Turkish Standards Institute, Ankara, 2012.

[12] *Tests for physical and mechanical properties of aggregates – Part 6: Determination of particle density and water absorption*, TS EN 1097-6, Turkish Standards Institute, Ankara, 2022.

[13] *Concrete – Properties, performance, production and conformity*, TS EN 206+A2, Turkish Standards Institute, Ankara, 2021.

[14] *Concrete – Fresh concrete tests – Part 2: Slump test*, TS EN 12350-2, Turkish Standards Institute, Ankara, 2019.

[15] *Determination of compressive strength of concrete in structures and precast concrete components in situ*, TS EN 13791, Turkish Standards Institute, Ankara, 2019.

[16] *Concrete tests in structures – Part 4: Determination of ultrasonic pulse wave velocity*, TS EN 12504-4, Turkish Standards Institute, Ankara, 2021.

[17] *Concrete – Tests on hardened concrete – Part 3: Determination of compressive strength of test specimens*, TS EN 12390-3, Turkish Standards Institute, Ankara, 2019.

[18] *Standard specification for concrete aggregates*, ASTM C33-07, ASTM International, West Conshohocken, PA, 2007.

2nd International Conference on Multidisciplinary Sciences and Technological Developments (ICMUSTED 2025)

December 12-15, 2025

Spintronics: The Future of Electronics – A Comprehensive Overview of Dilute Magnetic Semiconductors

Muhammet Arucu[1]

[1]Department of Computer Technologies, Bandirma Onyedi Eylul University, Gonen, 10900 Balikesir, Türkiye
Corresponding author: Muhammet Arucu (e-mail: marucu@bandirma.edu.tr)

Abstract

The unrelenting downscaling of conventional charge-based electronics is rapidly approaching fundamental thermodynamic and physical limits, necessitating a paradigm shift toward alternative state variables. Spin transport electronics (Spintronics)—exploiting the electron's intrinsic spin degree of freedom—emerges as the most promising candidate to overcome these bottlenecks, offering non-volatility, higher processing speeds, and reduced power consumption. This paper presents a comprehensive review of dilute magnetic semiconductors (DMSs), the pivotal material class anticipated to bridge the gap between modern semiconductor logic and magnetic storage. We critically examine the physical mechanisms underlying carrier-mediated ferromagnetism in III-V and II-VI compounds, framed within the theoretical context of the zener model and Ruderman–Kittel–Kasuya–Yosida (RKKY) interactions. Furthermore, the thermodynamic challenges hindering the realization of room-temperature ferromagnetism, including solubility limits and phase separation, are analysed. Finally, we evaluate the transformative potential of DMSs in realizing next-generation devices such as spin field-effect transistors (Spin-FETs) and fault-tolerant quantum computing architectures.

Keywords: Spintronics, Dilute Magnetic Semiconductors, Ferromagnetism, Spin Polarization, Carrier-Mediated Exchange.

1. INTRODUCTION

For more than five decades, improvements in semiconductor technology have relied on aggressive geometric scaling of silicon-based metal-oxide semiconductor field-effect transistors (MOSFETs). As channel lengths shrink below 5 nm and oxide thicknesses reach the atomic limit, power dissipation, quantum tunneling, and short-channel effects have become prohibitive [1]. These limitations have triggered a global search for beyond- complementary metal-oxide semiconductor (CMOS) technologies that circumvent the fundamental barriers of charge-based electronics [2].

Spin transport electronics (Spintronics) offers a transformative approach by exploiting the spin degree of freedom of electrons, enabling non-volatile, high-speed, and energy-efficient devices [3, 4]. Because electron spin orientation—up or down—can encode binary information without continuous power, spintronic systems promise orders of magnitude reductions in standby power consumption. More importantly, spin-based architectures enable the integration of memory and logic within the same device platform, overcoming the von Neumann bottleneck that currently dominates power and area consumption in modern processors [5].

Spintronics offers a fundamental solution to these challenges. While classical electronics utilizes only the charge of the electron (-e), spintronics exploits the electron's intrinsic angular momentum, or “spin” (↑ up or ↓ down). Spin provides a non-volatile state that can retain data without continuous energy consumption. The figure 1 illustrates the quantum mechanical principle of superposition in electron spin states, showing a spin-up electron (red) along a vertical magnetic field, a spin-down electron (blue) in the opposite direction, and their linear superposition resulting in a coherent state with spin oriented perpendicular to the field.

Dilute magnetic semiconductors (DMSs) stand at the intersection of semiconductor physics and magnetism. By doping conventional non-magnetic semiconductors (e.g., GaAs, InAs, ZnO, GaN) with a small fraction of transition-metal ions, one may obtain materials that simultaneously exhibit semiconducting carrier transport and magnetic ordering. This unique combination makes them ideal candidates for spin injection, spin manipulation, and electrically controlled magnetism [6]. This paper provides a fully revised and coherent overview of the physical principles, material systems, fabrication techniques, challenges, and applications associated with DMSs.

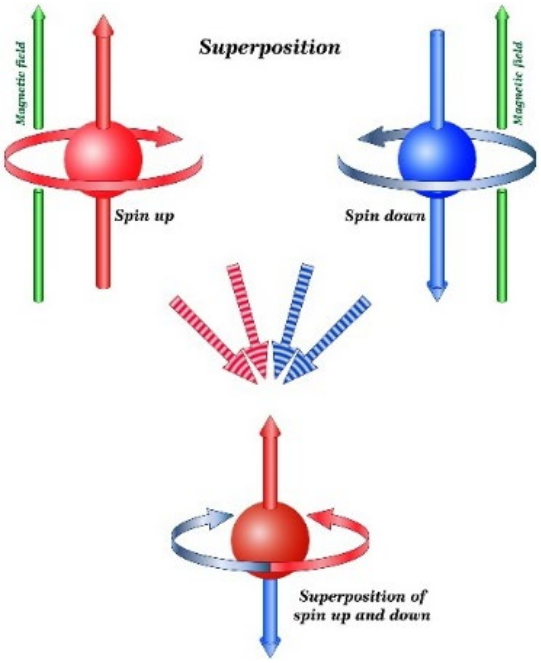

Figure 1. The diagram shows electron spin up, spin down, and their superposition state

2. PHYSICAL FOUNDATIONS OF DMSs

DMSs are fabricated by incorporating a small fraction (typically 1–10%) of paramagnetic transition-metal ions—most commonly Mn, but also Fe, Co, Cr, or V—into the lattice of a conventional non-magnetic semiconductor host (e.g., GaAs, InAs, ZnO, GaN, or Si) [7, 8]. The emergence of collective magnetism in these otherwise dilute systems arises from the indirect exchange interaction between the localized d- or f-electron spins of the magnetic dopants and the delocalized charge carriers (holes or electrons) in the host bands, an interaction that can mediate long-range ferromagnetic, antiferromagnetic, or spin-glass order depending on carrier type, density, and dopant separation (see Table 1 for a comparison of key DMS material systems) [9, 10].

Table 1: Comparison of prominent DMS material systems

Material System	Host	Dopant	Curie Temp (TC)	Current Status and Challenges
III-V Group	GaAs	Mn	~180-200 K	Well-understood model system. Limited by sub-room temperature T_C.
III-V Group	InAs	Mn	~60-90 K	Low T_C, but exhibits high electron mobility.
II-VI Group	ZnSe	Mn	< 50 K	Excellent optical properties; difficult to achieve p-type doping.
Oxides	ZnO	Co, Mn	> 300 K (Debated)	Reports of high T_C, but magnetism origin is controversial (extrinsic phases vs. intrinsic).
Nitrides	GaN	Mn	> 300 K (Theoretical)	High potential for room temperature applications; challenges in phase separation.

2.1. Crystal Structure and Magnetic Doping

In archetypal systems such as (Ga,Mn)As, manganese atoms substitute gallium atoms in the zinc-blende lattice, generating localized magnetic moments (S = 5/2) and introducing holes into the valence band. These holes play a critical role in mediating long-range magnetic coupling among dopants. However, solubility limits and defect formation complicate this process, often requiring non-equilibrium growth conditions such as low-temperature molecular beam epitaxy.

2.2. The Origin of Ferromagnetism / Carrier-Mediated Ferromagnetism

Ferromagnetism in DMS is generally described by Carrier-Mediated Ferromagnetism. Since the magnetic ions are dilute, they are too far apart to interact directly. Consequently, the magnetic interaction is mediated by the free

charge carriers (typically holes) in the system. As holes delocalize and move from one Mn ion to another, they transmit spin information, aligning the Mn spins in a parallel configuration (ferromagnetic order). Theoretically, the observed spin-related phenomena in magnetic materials, particularly in DMSs and certain metallic systems, are often described within the framework of the Zener carrier-mediated ferromagnetism model [11], originally proposed by Clarence Zener, which posits that the alignment of localized magnetic moments arises from the indirect exchange interaction between localized d- or f-shell electrons (typically from transition metal or rare-earth impurities) and the delocalized conduction electrons belonging to the s- and p-bands; this indirect coupling is more rigorously formulated through the Ruderman–Kittel–Kasuya–Yosida (RKKY) interaction [12], a second-order perturbative mechanism in which itinerant carriers become spin-polarized by one localized moment and subsequently transmit this polarization to another distant localized moment via Friedel-like oscillations of the spin density in the conduction electron sea, thereby mediating long-range oscillatory magnetic ordering that can be either ferromagnetic or antiferromagnetic depending on the inter-moment distance and the Fermi wavevector of the host material [13].

3. PROMINENT MATERIAL SYSTEMS AND FABRICATION TECHNIQUES

Different material families exhibit varying degrees of magnetic ordering, dopant solubility, and carrier control. Among these, III–V semiconductors have been the most extensively studied, while oxide- and nitride-based systems offer the potential for room-temperature ferromagnetism but remain subject to debate regarding the intrinsic origin of their magnetic properties.

3.1. III-V Group: GaMnAs and InMnAs

The III–V compound family, particularly (Ga,Mn)As, remains the most thoroughly investigated and theoretically best-understood class of DMSs, serving as the benchmark system for carrier-mediated ferromagnetism in semiconductors. The equilibrium solubility limit of Mn in GaAs is below 0.01%, rendering conventional high-temperature growth inapplicable. Ferromagnetic (Ga,Mn)As is therefore synthesized exclusively by low-temperature molecular beam epitaxy (LT-MBE) at substrate temperatures of 180–300 °C, far below the regime where surface segregation or precipitation of secondary phases (e.g., MnAs) occurs [14]. This non-equilibrium approach enables metastable Mn concentrations up to ~10–12%, well into the metallic regime required for hole-mediated exchange [15].

The DMS crystal structure shown in Figure 2 is a “Zinc-Blende” (Zinc-Sulfide) lattice structure. The blue spheres represent Gallium (Ga) atoms (the main structure), the red spheres represent Arsenic (As) atoms, and the green spheres represent Manganese (Mn) atoms randomly placed in place of the blue spheres (substitutional doping).

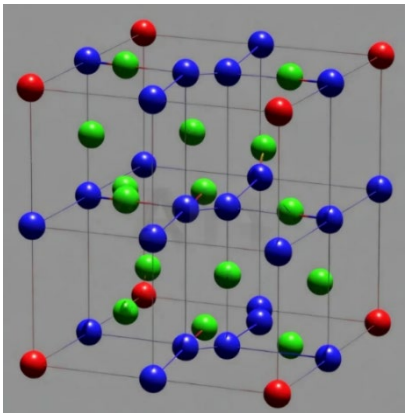

Figure 2: Mn atoms substitute Ga atoms, providing both local magnetic moments and holes to the system

Despite intensive optimization of growth conditions, post-growth annealing, and co-doping strategies, the highest experimentally verified Curie temperature in (Ga,Mn)As thin films and heterostructures remains approximately 200 K. The persistent gap to room-temperature ferromagnetism continues to restrict practical device applications of this material system [16].

3.2. Oxides and Nitrides: ZnO- and GaN-Based DMSs

Following seminal mean-field Zener-model predictions by Dietl and co-workers in 2000, transition-metal-doped wide-bandgap semiconductors such as ZnO ($E_g \approx 3.37$ eV) and GaN ($E_g \approx 3.4$ eV) were proposed as prime

candidates for achieving robust ferromagnetism well above room temperature, owing to their large hole effective masses and strong p–d hybridization [11].

These materials are typically prepared by pulsed laser deposition (PLD), metal-organic chemical vapor deposition (MOCVD), or ion implantation followed by annealing. However, reproducible room-temperature ferromagnetism has proven elusive; reported high-T_C values are frequently attributable to nanoscale secondary phases, clusters, or defect-induced magnetism rather than intrinsic carrier-mediated ordering, rendering the physical origin in most oxide and nitride DMSs highly controversial. While isolated reports claim T_C exceeding 400 K, no consensus exists on intrinsic, defect-free room-temperature ferromagnetism in these systems, and their integration into functional spintronic devices remains limited [8, 17].

Table 2: Comparison of conventional and spintronic technologies

Feature	Conventional Electronics (Charge-Based)	Spintronics (Spin-Based)
Fundamental Particle	Electron (Charge: -e)	Electron (Charge: -e + Spin: ↑↓)
State Variable	Charge quantity	Spin orientation (Up/Down)
Data Volatility	Volatile (Data loss upon power cut)	Non-Volatile (Data retention without power)
Energy Consumption	High (Due to leakage currents)	Low (Quantum state switching)
Switching Speed	Limited by capacitance (RC delay)	Fast (governed by spin relaxation time)
Material Basis	Semiconductors (Si, Ge)	Magnetic Semiconductors, Ferromagnets

4. KEY CHALLENGES IN DMS RESEARCH

The commercialization of DMS technology remains stymied by the persistently low Curie temperature (T_C), which marks the transition from ferromagnetic to paramagnetic order and must exceed 350–400 K (77–127 °C) for reliable operation in ambient environments encountered in consumer electronics, automotive systems, and data centers [3, 4]. Achieving room-temperature or above ferromagnetism in DMSs is essential to prevent thermal randomization of spin alignments, which would otherwise degrade device performance through loss of non-volatility, reduced magnetoresistance ratios, and impaired spin injection efficiency [18].

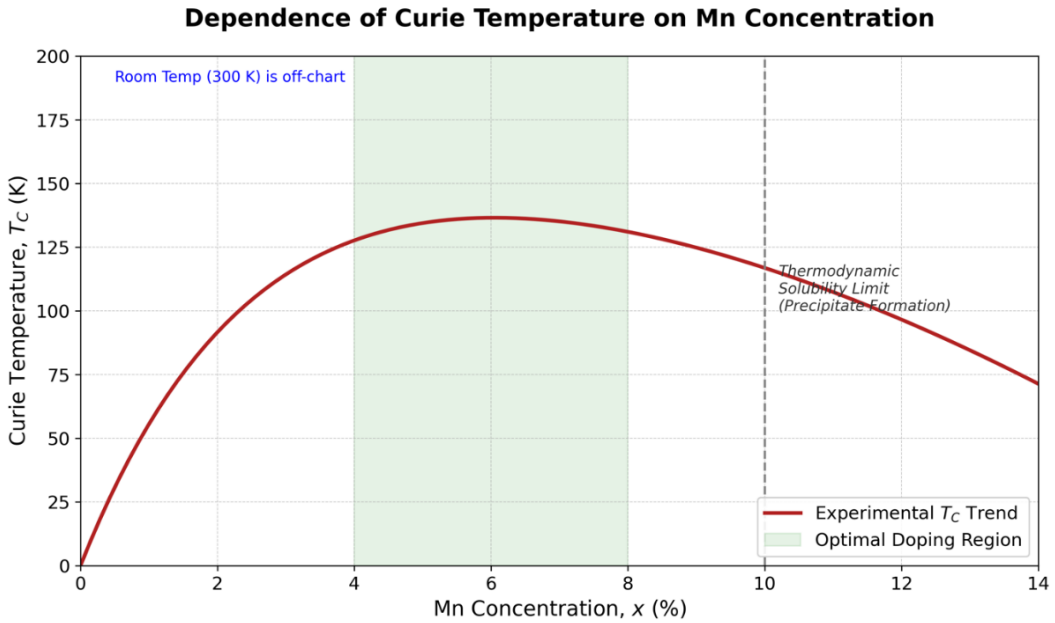

Figure 3. The plot shows that the Curie temperature increases with Mn concentration up to an optimal doping range, but decreases beyond the solubility limit due to secondary phase formation

Figure 3 illustrates the characteristic dependence of the Curie temperature on Mn concentration in DMSs such as (Ga,Mn)As. As the Mn content increases, carrier-mediated ferromagnetism strengthens and T_C rises sharply, reaching a maximum within the optimal doping window. Beyond this region, however, thermodynamic solubility limits are exceeded, leading to the formation of precipitates and compensating defects that suppress long-range magnetic order. The trend underscores the fundamental challenge of achieving room-temperature ferromagnetism through conventional doping strategies. The figure illustrates the experimentally observed dependence of the Curie

temperature on Mn concentration in (Ga,Mn)As, showing an initial increase up to an optimal doping range (4–8%) followed by a decline beyond the thermodynamic solubility limit where secondary phase formation suppresses ferromagnetism.

4.1. Thermodynamic Limits and Solubility

High concentrations of magnetic dopants are desirable for strong ferromagnetism, yet they violate thermodynamic solubility limits. Excess dopants precipitate as secondary magnetic phases (e.g., MnAs) that degrade device performance. Non-equilibrium growth partially mitigates this issue but introduces defect complexities that must be carefully managed. However, thermodynamic constraints impose a solubility ceiling: in prototypical systems like (Ga,Mn)As, Mn concentrations beyond ~8–10% trigger phase instability during growth, manifesting as the nucleation of metallic MnAs precipitates or other secondary phases (e.g., Mn clusters or arsenide) that disrupt lattice coherence, introduce spin-glass-like disorder, and quench carrier-mediated exchange. These limits arise from the mismatch in valence, ionic radius, and formation enthalpy between the dopant (e.g., Mn^{2+}) and host cation (e.g., Ga^{3+}), exacerbated at elevated growth temperatures; non-equilibrium techniques such as LT-MBE partially circumvent this, but fundamental Gibbs free energy barriers preclude arbitrarily high doping without structural degradation, as corroborated by density functional theory (DFT) calculations and in situ reflection high-energy electron diffraction (RHEED) monitoring [19, 20].

4.2. Defect Chemistry and Self-Compensation

A major intrinsic limitation in III–V DMSs, especially in (Ga,Mn)As, arises from the tendency of a fraction of the incorporated Mn atoms to occupy interstitial rather than substitutional sites (Mn_I instead of Mn_Ga). Interstitial Mn acts as a double donor, releasing electrons that compensate (neutralize) the holes generated by substitutional Mn acceptors. This self-compensation strongly reduces the effective hole concentration essential for carrier-mediated ferromagnetism and consequently lowers the Curie temperature significantly. In addition, close Mn_Ga–Mn_I pairs exhibit antiferromagnetic coupling, which further decreases the average magnetic moment contributed by each Mn atom. To mitigate these detrimental effects, controlled low-temperature post-growth annealing is commonly employed; this process allows mobile interstitial Mn to diffuse out toward the surface or to form less harmful complexes, partially restoring the hole density and enhancing T_C. Careful optimization of the annealing conditions is crucial, as excessive thermal treatment can introduce other compensating defects such as arsenic antisite, highlighting the delicate defect-engineering balance required in these metastable materials [21, 22].

Increasing the magnetic doping concentration generally raises T_C; however, beyond a certain threshold, the crystal lattice degrades, leading to the formation of secondary phases (precipitates). Particularly in GaMnAs structures, a fraction of Mn atoms occupies interstitial sites rather than substitutional sites. These interstitial Mn atoms act as double donors, compensating the holes necessary for ferromagnetism and reducing the magnetic moment. Post-growth annealing processes are standardly used to mitigate this issue by diffusing interstitial Mn to the surface.

5. APPLICATIONS AND FUTURE DIRECTIONS

DMSs serve as a foundational materials platform for a wide range of emerging spintronic devices in which electrical control of magnetism, non-volatility, and low switching energies are essential. Their ability to combine magnetic ordering with conventional semiconductor properties opens a pathway toward hybrid charge–spin architectures that surpass the limitations of purely charge-based electronics. Although practical implementations remain at varying levels of technological maturity, DMS systems provide a coherent route to integrating spin functionality into semiconductor environments, enabling innovative device concepts in logic, memory, and quantum information processing.

5.1. Spin Field-Effect Transistors (Spin-FETs)

The Datta–Das Spin-FET remains one of the most widely discussed paradigms in spin-based logic, relying on the controlled precession of spin-polarized carriers during their propagation through a semiconductor channel. Efficient operation of the device requires three key capabilities: the injection of highly spin-polarized carriers, the coherent manipulation of their spin states during transport, and the selective detection of the final spin orientation. DMS materials play a critical role in enabling these functionalities because they can provide ferromagnetic contacts that are lattice-matched to III–V semiconductor heterostructures and capable of generating robust spin polarization. Their carrier-mediated magnetic properties allow spin injection and spin filtering to occur through mechanisms that are inherently compatible with semiconductor band structures.

Within the channel region, the Rashba spin–orbit interaction generates a momentum-dependent effective magnetic field that rotates the injected spins by an angle controlled through the gate voltage. The presence of DMS layers, either as spin injectors or as gate-modulated magnetic components, enhances the tunability of this precession because their magnetic characteristics can be adjusted through doping, strain, or electric fields. At the drain contact, the device converts the accumulated spin phase into an electrical signal by exploiting the magnetization-dependent conductance. Through this mechanism, the Spin-FET circumvents conventional charge-switching limitations and offers a route to ultra–low-power logic devices. Despite the challenges in achieving room-temperature operation with long spin coherence, DMS-based structures continue to provide an attractive materials platform for next-generation spin logic technologies.

5.2. Magnetic Random Access Memory (MRAM)

Magnetic random access memory has emerged as the leading non-volatile memory technology for replacing embedded flash and static random access memory (SRAM), owing to its high endurance, fast switching, and excellent data retention characteristics. Conventional MRAM structures rely on metallic ferromagnets and magnetic tunnel junctions, but DMS materials introduce new opportunities for electrically controlled magnetism within a fully semiconductor-based memory element. Because the magnetic ordering in DMS is mediated by carrier concentration, the magnetization can be modulated not only by conventional spin-transfer or spin–orbit torques but also by electric fields that alter the carrier density. This capability offers a fundamentally different approach to memory switching, enabling voltage-controlled magnetic anisotropy and magnetization reversal with considerably lower energy consumption than current-driven mechanisms.

Moreover, the crystallographic and electronic compatibility of DMS with III–V semiconductor platforms allows MRAM structures to be integrated directly into existing semiconductor processes. This monolithic integration provides a promising pathway toward logic-in-memory architectures that mitigate the latency and power bottlenecks associated with modern processor design. DMS-based magnetic tunnel junctions (MTJs) may also support enhanced functional capabilities such as magneto-optical readout, multilevel storage, and tunable spin polarization. Although significant material challenges remain, particularly regarding Curie temperature and defect engineering, DMS materials constitute a promising avenue for next-generation MRAM technologies that combine high performance, low power, and seamless semiconductor compatibility.

5.3. Quantum Information Processing

Electron spins in semiconductors represent an appealing platform for quantum information processing due to their long coherence times, compatibility with lithographic patterning, and ability to interface with photonic and superconducting systems. DMS materials provide additional advantages by offering tunable magnetic exchange interactions arising from the controlled incorporation of transition-metal dopants. This tunability enables precise engineering of spin splitting, g-factors, and qubit–qubit coupling strengths, which are essential for realizing scalable quantum gate operations. In many DMS systems, strong magneto-optical effects allow spins to be initialized, manipulated, and read out using optical techniques, giving rise to hybrid architectures that combine spin-based qubits with photonic quantum communication channels.

Furthermore, DMS layers can be incorporated into quantum dots, nanowires, and heterostructures, where quantum confinement enhances spin coherence and enables electrically tunable quantum states. Their ability to host both localized magnetic moments and delocalized carriers provides a unique environment for implementing exchange-based two-qubit gates or dipolar coupling networks. The capacity to integrate these functionalities within semiconductor manufacturing frameworks offers a realistic pathway toward constructing large-scale quantum circuits. Although challenges related to magnetic noise, dopant homogeneity, and thermal stability must still be resolved, DMS systems hold considerable promise for hybrid quantum technologies that bridge the gap between condensed matter physics, spintronics, and quantum information science.

6. CONCLUSION

DMS constitute a critical technological bridge, aiming to integrate the non-volatile memory capabilities of magnetism with the logic processing power of semiconductors within a single material system. While prototypical systems like (Ga,Mn)As have successfully validated the fundamental principles of spintronics, the realization of stable, homogeneous ferromagnetism at and above room temperature remains a formidable materials science challenge. Current limitations, primarily driven by thermodynamic solubility and self-compensation mechanisms, necessitate novel approaches in non-equilibrium growth and defect engineering. Future research must increasingly focus on low-dimensional structures, such as nanowires and quantum dots, where spin coherence can be more

effectively preserved. Ultimately, surmounting these physical barriers through advanced nanofabrication and deeper theoretical modelling will be the key to unlocking the full potential of the spintronic revolution.

References

[1] A. Chaudhry and M. J. Kumar, "Controlling short-channel effects in deep-submicron SOI MOSFETs for improved reliability: A review," *IEEE Trans. Device Mater. Rel.*, vol. 4, no. 1, pp. 99–109, Mar. 2004.

[2] V. K. Khanna, "Short-channel effects in MOSFETs," in *Integrated Nanoelectronics: Nanoscale CMOS, Post-CMOS and Allied Nanotechnologies*, New Delhi, India, 2016, pp. 73–93.

[3] S. A. Wolf, D. D. Awschalom, R. A. Buhrman, J. M. Daughton, S. Von Molnár, M. L. Roukes, et al., "Spintronics: A spin-based electronics vision for the future," *Science*, vol. 294, no. 5546, pp. 1488–1495, Nov. 2001.

[4] D. D. Awschalom and M. E. Flatté, "Challenges for semiconductor spintronics," *Nature Phys.*, vol. 3, no. 3, pp. 153–159, Mar. 2007.

[5] Z. Guo, J. Yin, Y. Nai, D. Zhu, K. Shi, and G. Wang, "Spintronics for energy-efficient computing: An overview and outlook," *Proc. IEEE*, vol. 109, no. 8, pp. 1398–1417, Aug. 2021.

[6] Y. Ohno, D. K. Young, B. Beschoten, F. Matsukura, H. Ohno, and D. D. Awschalom, "Electrical spin injection in a ferromagnetic semiconductor heterostructure," *Nature*, vol. 402, no. 6763, pp. 790–792, Dec. 1999.

[7] J. K. Furdyna, "Diluted magnetic semiconductors," *J. Appl. Phys.*, vol. 64, no. 4, pp. R29–R64, Aug. 1988.

[8] T. Dietl, "A ten-year perspective on dilute magnetic semiconductors and oxides," *Nature Mater.*, vol. 9, no. 12, pp. 965–974, Dec. 2010.

[9] T. Dietl and H. Ohno, "Dilute ferromagnetic semiconductors: Physics and spintronic structures," *Rev. Mod. Phys.*, vol. 86, no. 1, pp. 187–251, Mar. 2014.

[10] P. Parida, J. Patra, V. R. Singh, and V. K. Verma, "Dilute magnetic semiconductors and its applications—An overview," in *Proc. Int. Conf. Adv. Nanomater. Appl.*, Singapore, 2024, pp. 181–220.

[11] T. Dietl, H. Ohno, F. Matsukura, J. Cibert, and D. Ferrand, "Zener model description of ferromagnetism in zinc-blende magnetic semiconductors," *Science*, vol. 287, no. 5455, pp. 1019–1022, Feb. 2000.

[12] R. Skomski, J. Zhou, J. Zhang, and D. J. Sellmyer, "Indirect exchange in dilute magnetic semiconductors," *J. Appl. Phys.*, vol. 99, no. 8, art. no. 08D504, Apr. 2006.

[13] B. Lee, T. Jungwirth, and A. H. MacDonald, "Theory of ferromagnetism in diluted magnetic semiconductor quantum wells," *Phys. Rev. B*, vol. 61, no. 23, pp. 15606–15609, Jun. 2000.

[14] A. Shen, F. Matsukura, S.P. Guo, Y. Sugawara, H. Ohno, M. Tani, et al., "Low-temperature molecular beam epitaxial growth of GaAs and (Ga,Mn)As," *J. Cryst. Growth*, vol. 201, pp. 679–683, May 1999.

[15] K. Takamura, F. Matsukura, Y. Ohno, and H. Ohno, "Growth and properties of (Ga,Mn)As films with high Mn concentration," *J. Appl. Phys.,* vol. 89, no. 11, pp. 7024–7026, Jun. 2001.

[16] T. Jungwirth, J. Sinova, J. Mašek, J. Kučera, and A. H. MacDonald, "Theory of ferromagnetic (III,Mn)V semiconductors," *Rev. Mod. Phys.*, vol. 78, no. 3, pp. 809–864, Aug. 2006.

[17] K. Ueda, H. Tabata, and T. Kawai, "Magnetic properties of cobalt-doped TiO_2 rutile thin films grown by PLD," *Appl. Phys. Lett.*, vol. 79, no. 7, pp. 988–990, Aug. 2001.

[18] I. Žutić, J. Fabian, and S. Das Sarma, "Spintronics: Fundamentals and applications," *Rev. Mod. Phys.*, vol. 76, no. 2, pp. 323–410, Apr. 2004.

[19] S. Sanvito, "First-principles materials design for spintronics," *Nature Mater.*, vol. 6, no. 11, pp. 803–811, Nov. 2007.

[20] K. S. Burch, D. B. Shrekenhamer, E. J. Singley, J. Stephens, B. L. Sheu, R. K. Kawakami, et al., "Magneto-optical signatures of MnAs cluster formation in (Ga,Mn)As," *Phys. Rev. Lett.*, vol. 97, no. 8, art. no. 087208, Aug. 2006.

[21] D. Chiba, A. Werpachowska, M. Endo, Y. Nishitani, F. Matsukura, T. Dietl, et al., "Anomalous hall effect in field-effect structures of (Ga,Mn)As," *Phys. Rev. Lett.*, vol. 104, no. 10, art. no. 106601, Mar. 2010.

[22] K. W. Edmonds, P. Bogusławski, K. Y. Wang, R. P. Campion, S. N. Novikov, N. R. S. Farley, et al., "Mn interstitial diffusion in (Ga,Mn)As," *Phys. Rev. Lett.*, vol. 92, no. 3, art. no. 037201, Jan. 2004.

2nd International Conference on Multidisciplinary Sciences and Technological Developments (ICMUSTED 2025)

December 12-15, 2025

Investigation of Photon and Neutron Interaction Probabilities of Some Selected High Entropy Alloys

Bunyamin Alim[1], Erdem Sakar[2]

[1]Department of Electricity and Energy, Technical Sciences Vocational School, Bayburt University, Bayburt, Türkiye
[2]Department of Physics, Faculty of Science, Ataturk University, Erzurum, Türkiye
Corresponding author: Bunyamin Alim (e-mail: balim@bayburt.edu.tr)

Abstract

High-entropy alloys, which are seen as the materials of the future in areas requiring advanced technology such as aviation, energy, defence and medicine, are generally formed by the combination of five or more metal atoms in equimolar ratios. The random arrangement of atoms in the production of high entropy alloys allows, through a synergistic effect, to obtain advanced tribological properties such as high strength and hardness, good wear resistance, excellent corrosion resistance and high fracture toughness in a single alloy. In this context, there are a limited number of studies investigating the usability of these alloys, which have an important place in material science studies, in nuclear security systems. In this presented study, photon-matter interaction parameters of two different high entropy alloys with compositions $Ti_{25}Zr_{35}Nb_{20}Hf_5Ta_{15}$ and $W_{35}Ta_{35}Mo_{10}Nb_{10}V_{10}$ were investigated and the obtained results were compared with the coded $Co_{25}Ni_{25}Fe_{25}Cr_{25}$ alloy, which was previously reported in the literature to have superior photon and neutron absorption capacity. The obtained data show that the two new types of alloys investigated have superior photon absorption cross sections throughout the entire energy range of the high entropy alloy. Their superior photon absorption capacities, combined with their good tribological properties, offer hope that these alloys could be alternative materials for nuclear application.

Keywords: High entropy alloy, Photon, Neutron, Phy-X/PSD

1. INTRODUCTION

Alloys, which have a wide range of uses from biomedical applications to the aerospace industry, are materials formed by combining multiple metals. Alloys, which can be modified according to the specific field of science, medicine, and engineering, are among the most indispensable elements of today's technology. Unlike traditional alloys formed by combining two or three metals, high entropy alloys (HEAs), whose popularity and application areas have been increasing day by day in recent years, are formed by combining five or more metals in equimolar ratios or in proportions ranging from 5% to 35% of each component [1]. The equimolar nature of the alloy's components allows for maximum disorder, with nearly equal contributions from each component. This allows for simple solid solution structures such as body centered cubic (BCC), face centered cubic (FCC), and close-packed hexagonal (HCP) [2, 3]. To achieve improved tribological properties, HEAs can be produced using suitable combinations of all metals in the periodic table. Numerous studies in the literature address the corrosion resistance [4], hardness [5] and wear resistance [6], and excellent high-temperature strength [7] of HEAs.

Alloys used in high-temperature applications such as aerospace and nuclear power plants must possess high thermal stability and enhanced mechanical properties under extreme conditions. The most important material group suitable for this requirement is refractory high-entropy alloys (RHEAs). RHEAs possess high mechanical strength and phase stability due to their slow diffusion and high Gibbs potential at high temperatures [8, 9]. Numerous studies on the strength, ductility, thermal stability, and oxidation resistance of RHEAs are available in the literature. However, there are very limited studies addressing the interaction parameters of both RHEAs and HEAs with ionizing radiation (X-ray, gamma ray, and neutrons).

In this study, the interaction cross-sections of two different high-entropy alloys, as presented by Iroc et al. [10] and Hu et al. [11], with high-energy photons and fast neutrons were investigated. Calculations were performed in the energy range of 15 keV to 15 MeV to represent a wide energy range in determining photon-matter interaction parameters. In addition to this energy range, results were also obtained for some specific photon energies emitted from Am, Ba, and Na radioactive sources. To provide a comparative evaluation of photon shielding capacities, the obtained data were compared with the HEA1-coded CoNiFeCr alloy, which demonstrated high photon absorption

capacity in the study of Sakar et al. 2023 [12]. Furthermore, neutron absorption results were presented comparatively with some concrete types found in the literature.

2. MATERIAL AND METHOD

Photons, which have zero rest mass, are electromagnetic waves that travel at the speed of light in a vacuum. Because they have no electrical charge, they cannot undergo Coulombic interactions with a target material, unlike alpha, beta, or other ionic radiation. The interaction mechanisms between photons and materials are controlled by three fundamental phenomena: photoelectric effect, Compton scattering, and pair production [13]. In addition to the energy of the photons, the atomic composition and density of the target material play an important role in these interactions. The mass attenuation coefficient is a crucial parameter at the core of photon-matter interactions, representing the interaction cross-section between the target material and the incident photon [14, 15]. This parameter can be calculated theoretically for entire material groups, in addition to individual atoms, using online tools such as WinXCOM [16] and Phy-X/PSD [17]. The linear attenuation coefficient, obtained by multiplying the energy-dependent mass attenuation coefficient (MAC) parameter by the density of the target material, expresses the decrease in photon intensity per unit length. This parameter is also used in the calculation of parameters such as half-value layers (HVL), tenth value layers (TVL), and mean free path (MFP). Finally, other parameters such as effective atomic number, effective electron density, and effective conductivity are obtained by using the MAC parameter and the mole percentages of the target material components in appropriate equations. Numerous studies in the literature address these calculations [15, 18, 19].

Photon absorption parameters of the high-entropy alloys investigated in this study were obtained using Phy-X/PSD software in the continuous energy range of 15 keV to 15 MeV. In addition to the continuous energy range, calculations were also made for the radioisotopes Am, Ba, and Na emitted at energies of 0.059 MeV, 0.081 MeV, 0.356 MeV, and 0.511 MeV. These radioisotopes are among the most frequently used radioisotopes in experimental studies. The empirical method proposed by Kaplan [20] and Chilton [21] was used in the calculation of fast neutron absorption cross sections in the final section of the study. The elemental contents and densities of the alloys investigated in the study are given in Table 1.

Table 1. Chemical composition (in mole fraction %) and density of the high entropy alloys

HEA	^{22}Ti	^{23}V	^{24}Cr	^{26}Fe	^{27}Co	^{28}Ni	^{40}Zr	^{41}Nb	^{42}Mo	^{72}Hf	^{73}Ta	^{74}W	Density (g/cm^3)	Ref.
A1	0.250	-	-	-	-	-	0.350	0.200	-	0.050	0.150	-	8.28	[10]
A2	-	0.100	-	-	-	-	-	0.100	0.100	-	0.350	0.350	15.41	[11]
A3	-	-	0.250	0.251	0.251	0.248	-	-	-	-	-	-	7.81	[12]

3. RESULTS

The changes in the MAC values of the high-entropy alloys studied with energy are shown in Figure 1. The energy dependence of the absorption cross sections is clearly seen, with an exponential decrease with increasing energy. The photoelectric effect, which dominates photon-matter interactions at low energies, maintained its dominance up to approximately 0.08 MeV. From 15 keV to this energy level, MAC values exhibited a sharp decrease. From 0.08 keV to 2.5 MeV, the process was controlled by Compton scattering. Indeed, the MAC values of all alloys had minimum values in this region. Above 2.5 MeV, the probability of electron-positron pair formation, i.e., pair production, increased. Because pair production, unlike Compton scattering, is an absorption mechanism, MAC values increase relative to the Compton region. From the graph, it is clear that the A2 alloy has a higher MAC value than the other HEAs at all photon energies. According to the element contents given in Table 1, this alloy contains 35% W and Ta in mole fraction. Both the high atomic numbers and the large amounts of these components cause the A2 alloy to have a much higher MAC value than other alloys. The relative changes in the MAC values of HEAs compared to A3 are shown in the inset of the graph. It is clear that both alloys have very high MAC values compared to A3, except in the Compton region. A column chart of the MAC values calculated at specific gamma-ray energies for Am, Ba, and Na radioisotopes, the most frequently used radioisotopes in experimental radiation studies, is shown in Figure 2. According to this calculation, made at photon energies of 0.059, 0.081, 0.356, and 0.511 MeV, alloy A2 has the highest MAC value. The descending order of MAC values for the alloys in these charts is A2 > A1 > A3.

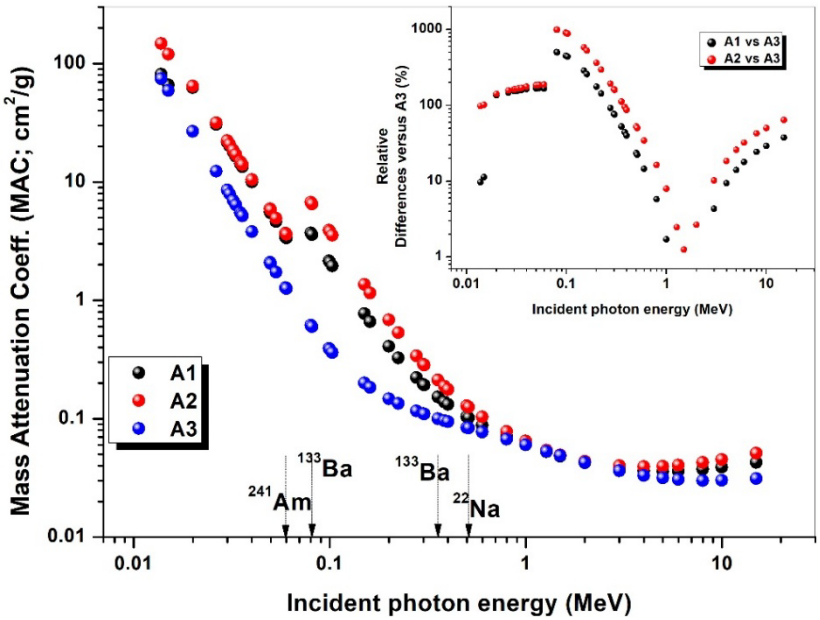

Figure 1. Variation of MAC values of the investigated HEAs

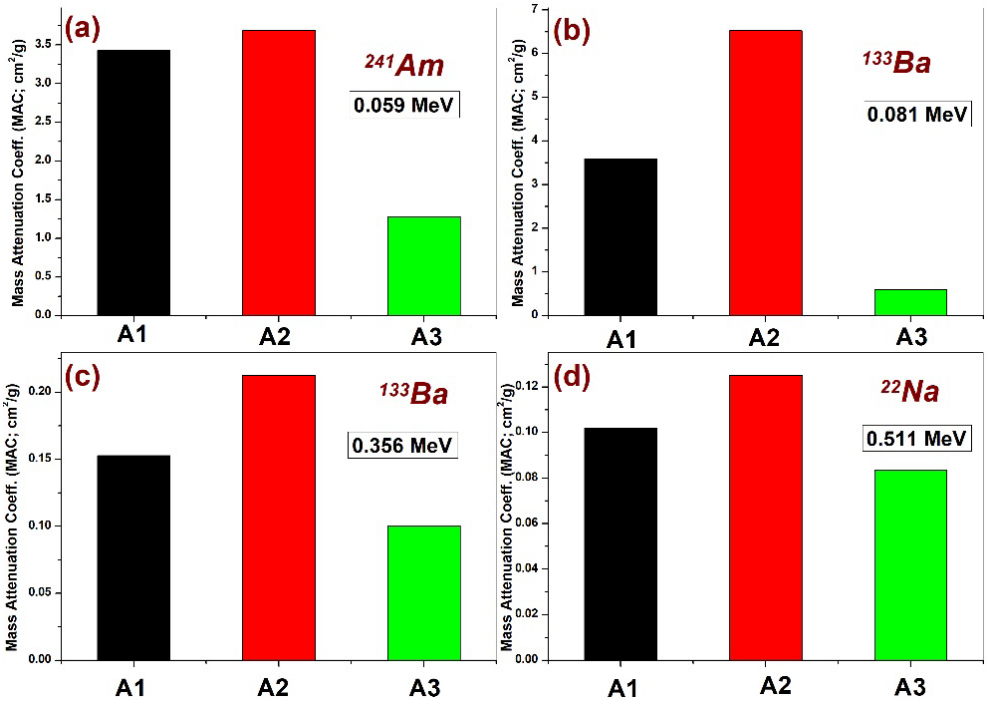

Figure 2. Variation of MAC values of the investigated HEAs at some specific radioisotope energies

The linear attenuation coefficient (LAC) curve shown in Figure 3 is quite similar to the MAC curve. It is clear from this graph that the difference between LAC values is quite pronounced compared to the difference between MAC values at any given energy value. Since the LAC parameter includes material density, the superiority of the A2 alloy, which has both the highest MAC value and the highest density, is evident in the graph. Including the absorption edge energies of the K-layer, the A2 alloy has a significantly higher LAC value than A1 and A3.

The changes in HVL and MFP values obtained from the linear attenuation coefficient are presented in Figure 4, respectively. It is clear in Figure 4(a) that the A3 alloy has the highest HVL, marked in blue, among the HVL changes representing the material thickness that reduces the intensity of photons at any energy value to half value. On the other hand, supporting the MAC and LAC results, the A2 alloy has the lowest HVL values. The maximum HVL value of this alloy is 1.144 cm, while these values are 2.327 and 2.951 cm for alloys A1 and A3, respectively. These results support the fact that alloy A2 has a higher absorption cross section. A similar curve to the HVL is observed for the MFP variations given in Figure 4(b). The increasing MFP values with increasing energy indicate

that the distance between successive successful interactions increases at higher energies. MFP values, which are on the order of $1x10^{-3}$ cm at low energy, increase to 4.257 at 15 MeV photon energy. The graph shows that the sequential successful interaction distances are lower in the A2 alloy compared to the other alloys at all energy values.

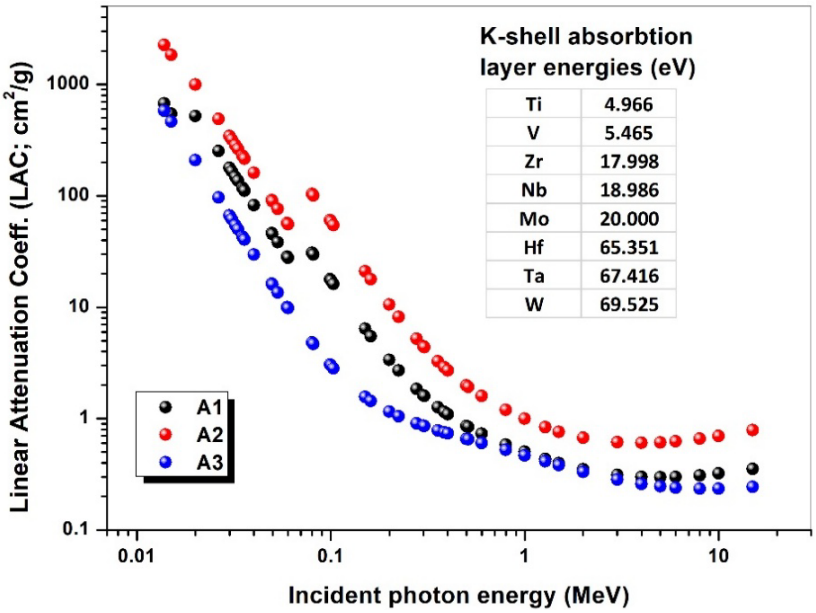

Figure 3. Variation of LAC values of the investigated HEAs

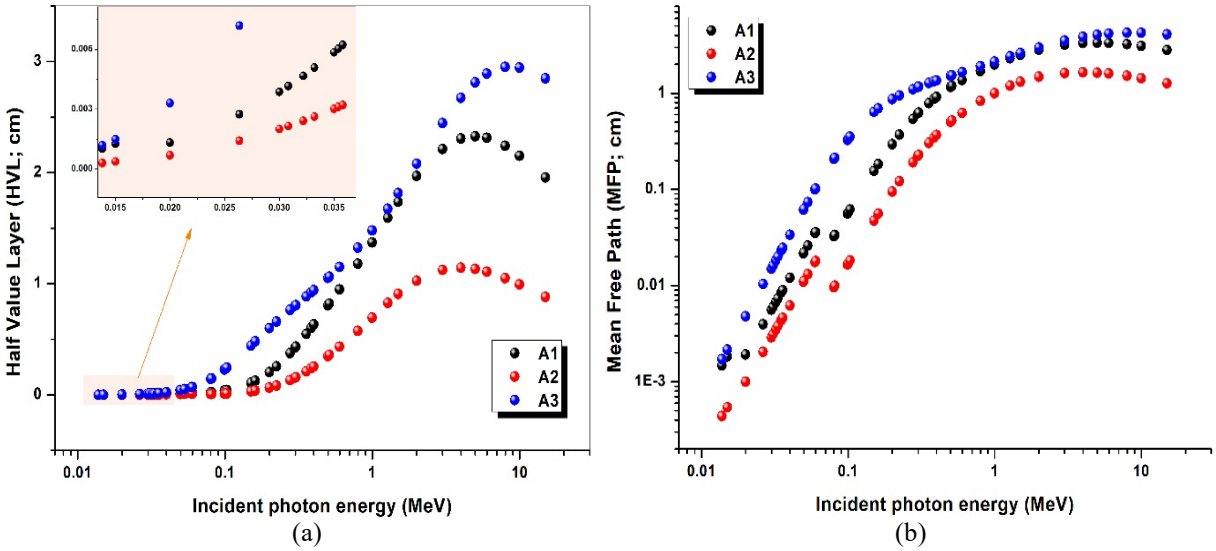

(a) (b)

Figure 4. Variation of (a) HVL and (b) MFP of the investigated HEAs

Another important parameter in photon-matter interactions is the effective atomic number. Z_{eff} is an imaginary virtual number that indicates how materials behave in response to photons in materials composed of multiple components. It is known that materials composed of combinations of elements with high atomic numbers have high photon absorption capacities. Therefore, it can be safely said that materials with high Z_{eff} values also have higher photon absorption capabilities. From the energy-dependent Zeff change curve given in Figure 5, it can be seen that the A2 alloy has the highest effective atomic number at all energy values. Since the A2 alloy consists of atoms with higher atomic numbers than other alloys, the Z_{eff} value varies between 65-70. In contrast, this value for the A1 alloy varies between 45 and 58. In the A3 alloy, which consists of elements with similar atomic numbers, the Z_{eff} change remains at 26 throughout the entire energy range. The atomic numbers of the Fe, Ni, Co and Cr atoms forming this alloy are very close to each other, which is the reason why the energy-dependent Zeff values change very little. The sudden increases and decreases seen on the Zeff curves are due to the K-layer absorption edges of the heavy metals in the alloys.

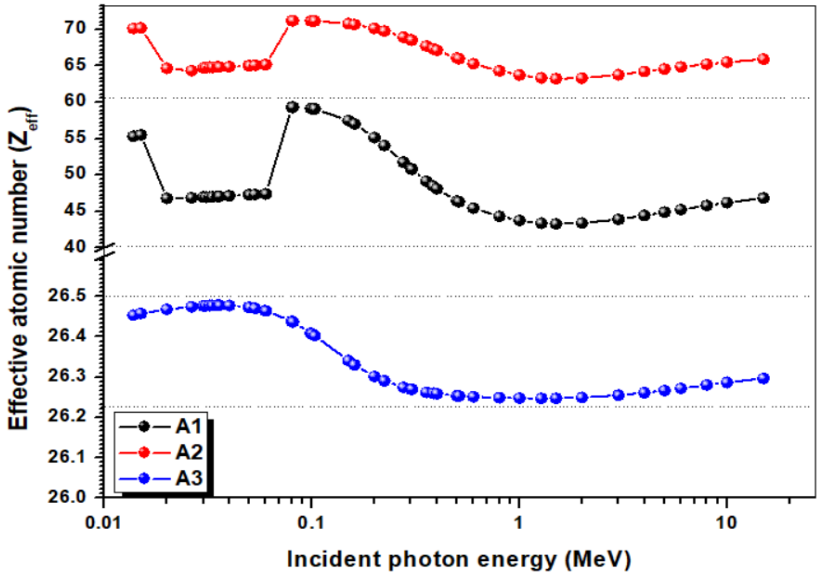

Figure 5. Variation of Z_{eff} values of the investigated HEAs

In this study, in addition to photon-matter interactions, fast neutron absorption cross sections, were also calculated. The obtained data were compared with results for several important concrete types (OC: Ordinary Concrete, SS: Steel Scrap, and SM: Steel Magnetite) previously reported in the literature to have high neutron interaction cross sections. According to the fast neutron removal cross section (FNRCS) values given in Figure 6, the A2 alloy has the highest cross-section at 0.184 cm^{-1}, while the standard concrete has a value of 0.093 cm^{-1}. Although SS and SM concretes have higher FNRCS values than the A1 alloy, the A2 and A3 alloys have better neutron interaction capacity than these concrete types.

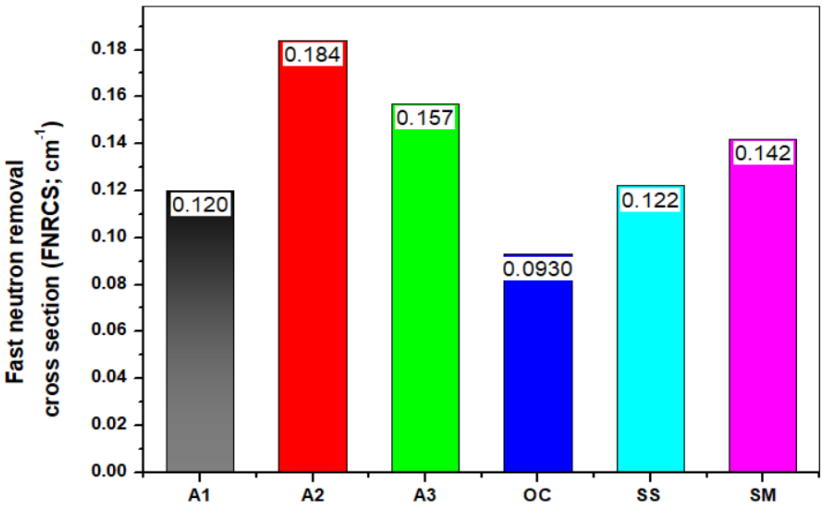

Figure 6. Variation of FNRCSs of the investigated HEAs

4. CONCLUSION

In this study examining the photon and neutron absorption capacities of high-entropy alloys, the photon absorption capacities of two different HEAs with $Ti_{25}Zr_{35}Nb_{20}Hf_5Ta_{15}$ (A1) and $W_{35}Ta_{35}Mo_{10}Nb_{10}V_{10}$ (A2) structures were determined over a wide energy range, as well as at specific gamma-ray energies. To ensure a sound assessment, the obtained results were compared with those of the $Co_{25}Ni_{25}Fe_{25}Cr_{25}$ (A3) alloy, previously studied in the literature as a good photon absorber. Neutron results were also compared with several important concrete types. The findings reveal that the $W_{35}Ta_{35}Mo_{10}Nb_{10}V_{10}$ alloy has the highest photon and neutron absorption capacity. The $Ti_{25}Zr_{35}Nb_{20}Hf_5Ta_{15}$ alloy also has a higher capacity than the $Co_{25}Ni_{25}Fe_{25}Cr_{25}$ alloy. This study provides hope that these two new alloys, previously reported in the literature for their superior tribological properties, may be reliable materials for use in high-dose radiation environments.

References

[1] V. Verma, C. H. Belcher, D. Apelian, and E. J. Lavernia, "Diffusion in high entropy alloy systems – A review," *Progress in Materials Science*, vol. 142, art. no. 101245, Apr. 2024. doi: 10.1016/j.pmatsci.2024.101245

[2] X. D. Xu, S. Guo, T. G. Nieh, C. T. Liu, A. Hirata, and M. W. Chen, "Effects of mixing enthalpy and cooling rate on phase formation of AlxCoCrCuFeNi high-entropy alloys," *Materialia*, vol. 6, art. no. 100292. Jun. 2019. doi: 10.1016/j.mtla.2019.100292

[3] B. S. Murty, J. W. Yeh, S. Ranganathan, and P. P. Bhattacharjee, "High-entropy alloys: basic concepts," in *High-Entropy Alloys*, Elsevier, 2019, pp. 13–30. doi: 10.1016/B978-0-12-816067-1.00002-3

[4] Y. Shi, B. Yang, and P. Liaw, "Corrosion-resistant high-entropy alloys: A review," *Metals*, vol. 7, no. 2, art. no. 43, Feb. 2017. doi: 10.3390/met7020043

[5] J.-K. Xiao, H. Tan, J. Chen, A. Martini, and C. Zhang, "Effect of carbon content on microstructure, hardness and wear resistance of CoCrFeMnNiCx high-entropy alloys," *Journal of Alloys and Compounds*, vol. 847, art. no. 156533, Dec. 2020. doi: 10.1016/j.jallcom.2020.156533

[6] C.-Y. Hsu, T.-S. Sheu, J.-W. Yeh, and S.-K. Chen, "Effect of iron content on wear behavior of AlCoCrFexMo0.5Ni high-entropy alloys," *Wear*, vol. 268, no. 5–6, pp. 653–659, Feb. 2010. doi: 10.1016/j.wear.2009.10.013

[7] H. M. Daoud, A. M. Manzoni, N. Wanderka, and U. Glatzel, "High-temperature tensile strength of Al10Co25Cr8Fe15Ni36Ti6 compositionally complex alloy (high-entropy alloy)," *JOM*, vol. 67, no. 10, pp. 2271–2277, Oct. 2015. doi: 10.1007/s11837-015-1484-7

[8] O. N. Senkov, D. B. Miracle, K. J. Chaput, and J.-P. Couzinie, "Development and exploration of refractory high entropy alloys—A review," *J. Mater. Res.*, vol. 33, no. 19, pp. 3092–3128, Oct. 2018. doi: 10.1557/jmr.2018.153

[9] S. S. Sohn, A. K. da Silva, Y. Ikeda, F. Kormanni W. J. Lu, W. S. Choi, et al., "Ultrastrong Medium-Entropy Single-Phase Alloys Designed via Severe Lattice Distortion," *Advanced Materials*, vol. 31, no. 8, art. no. 1807142, Feb. 2019. doi: 10.1002/adma.201807142

[10] L. K. Iroc, O. U. Tukac, B. B. Tanrisevdi, O. El-Atwani, M. A. Tunes, Y. E. Kalay, et al., "Design of oxygen-doped TiZrHfNbTa refractory high entropy alloys with enhanced strength and ductility," *Materials & Design*, vol. 223, art. no. 111239, Nov. 2022. doi: 10.1016/j.matdes.2022.111239

[11] X. Hu, X. Liu, D. Yan, and Z. Li, "A high-density non-equiatomic WTaMoNbV high-entropy alloy: Alloying behavior, microstructure and mechanical properties," *Journal of Alloys and Compounds*, vol. 894, art. no. 162505, Feb. 2022. doi: 10.1016/j.jallcom.2021.162505

[12] E. Sakar, O. Guler, B. Alim, Y. Say, and B. Dikici, "A comprehensive study on structural properties, photon and particle attenuation competence of CoNiFeCr-Ti/Al high entropy alloys (HEAs)," *Journal of Alloys and Compounds*, vol. 931, art. no. 167561, 2023.

[13] E. Sakar, M. Buyukyildiz, B. Alim, B. C. Sakar, and M. Kurudirek, "Leaded brass alloys for gamma-ray shielding applications," *Radiation Physics and Chemistry*, vol. 159, pp. 64–69, 2019.

[14] A. H. Abdalsalam, E. Sakar, K. M. Kaky, M. H. A. Mhareb, B. C. Sakar, M. I. Sayyed, et al., "Investigation of gamma ray attenuation features of bismuth oxide nano powder reinforced high-density polyethylene matrix composites," *Radiation Physics and Chemistry*, vol. 168, art. no. 108537, 2020.

[15] B. Alim, E. Sakar, A. Baltakesmez, I. Han, M. Sayyed, and L. Demir, "Experimental investigation of radiation shielding performances of some important AISI-coded stainless steels: Part I," *Radiation Physics and Chemistry*, vol. 166, art. no. 108455, 2020.

[16] L. Gerward, N. Guilbert, K. B. Jensen, and H. Levring, "WinXCom—A program for calculating X-ray attenuation coefficients," *Radiation Physics and Chemistry*, vol. 71, no. 3–4, pp. 653–654, Oct. 2004. doi: 10.1016/j.radphyschem.2004.04.040

[17] E. Sakar, O. F. Ozpolat, B. Alim, M. Sayyed, and M. Kurudirek, "Phy-X/PSD: Development of a user friendly online software for calculation of parameters relevant to radiation shielding and dosimetry," *Radiation Physics and Chemistry*, vol. 166, art. no. 108496, 2020.

[18] B. Alim, "A comprehensive study on radiation shielding characteristics of Tin-Silver, Manganin-R, Hastelloy-B, Hastelloy-X and Dilver-P alloys," *Appl. Phys. A*, vol. 126, no. 4, art. no. 262, Apr. 2020. doi: 10.1007/s00339-020-3442-7.

[19] E. Sakar, "Determination of photon-shielding features and build-up factors of nickel–silver alloys," *Radiation Physics and Chemistry*, vol. 172, art. no. 108778, 2020.

[20] M. F. Kaplan, "Concrete radiation shielding," Jan. 1989. [Online]. Available: https://www.osti.gov/biblio/6553025. [Accessed: Dec. 18, 2022].

[21] A. B. Chilton, J. K. Shultis, and R. E. Faw, "Principles of radiation shielding," Jan. 1984. [Online]. Available: https://www.osti.gov/biblio/5954378. [Accessed: Dec. 18, 2022].

2nd International Conference on Multidisciplinary Sciences and Technological Developments (ICMUSTED 2025)

December 12-15, 2025

Structural and Gamma-Ray Absorption Properties of Newly Developed Ni_3Al Based Superalloys

Merve Durdag[1], Bunyamin Alim[2], Erdem Sakar[1]

[1]Faculty of Science, Department of Physics, Ataturk University, Erzurum, Türkiye
[2]Department of Electricity and Energy, Technical Sciences Vocational School, Bayburt University, Bayburt, Türkiye
Corresponding author: Erdem Sakar (e-mail: erdem@atauni.edu.tr)

Abstract

Ni_3Al-based superalloys are advanced engineering materials that provide strength, oxidation, and creep resistance at high temperatures. These alloys are based on the regular L_{12} crystal structure of Ni_3Al and generally contain a γ′ (Ni_3Al) phase precipitated within a γ (Ni) matrix. This microstructure ensures the maintenance of high-temperature strength. Additions of elements such as boron, zirconium, and chromium enhance ductility and oxidation resistance. Ni_3Al-based alloys are widely used in jet engines, gas turbines, and power generation systems. Despite their light weight, they exhibit high mechanical performance. In this presented study, high energy photon absorption capacities of three different superalloys with the structures of $Al_{10}Cr_{15}Nb_1Mo_1W_1Ni_{30}$, $Al_{8.5}Cr_{17}Nb_1Mo_1W_1Ni_{25.5}$, and $Al_{9.5}Cr_{15.5}Nb_1Mo_1W_1Ni_{28.5}$ were investigated in addition to their crystallographic and morphological structures. Step sintering method was used in the production of these alloys, which were selected in the light of literature information. X-ray diffraction (XRD) and scanning electron microscope (SEM) analyses were used to characterize the alloys. Photon absorption capabilities were obtained using a high purity germanium (HPGe) detector and a Ba radioactive source. XRD analyses revealed that all three superalloys are polycrystalline, containing the Cr_2O_3 structure in addition to the classical Ni_3Al phases. SEM images revealed the formation of highly homogeneous, tightly packed pyramidal structures extending from the surface. Photon absorption experiments revealed that the three superalloys produced had better photon interaction cross sections compared to the pure Ni_3Al structure, thus possessing higher photon absorption capacity at all energy levels examined.

Keywords: Ni_3Al, Superalloy, Gama-ray, Phy-X/PSD

1. INTRODUCTION

Turbine blades and rocket engines, which play a crucial role in the aviation industry, are exposed to high temperatures for extended periods. Similarly, reactor cores and fuel elements in nuclear power plants operate under high temperatures and high radiation doses. This equipment, which must generally operate at temperatures exceeding 1000 °C, requires high corrosion resistance and high strength. Superalloys are a group of materials suitable for such applications [1, 2]. Superalloys, obtained by combining up to ten metals in appropriate proportions, are among the most important technological elements in today's world.

Ni-based superalloys are the most frequently preferred alloys for high-temperature applications. Ni can maintain its crystallographic structure at room temperature up to 1400 °C. This characteristic is the primary reason why Ni-based materials are attracting attention. However, simply maintaining its crystalline structure at high temperatures doesn't guarantee that any material can be used in high-temperature applications [3, 4]. Materials for applications in aerospace and nuclear applications, where extreme conditions prevail, must possess many advanced tribological properties. For example, in a polycrystalline material, at high temperatures, crystallographic planes tend to slip, leading to rapid diffusion. However, in such materials, the dislocation velocity, and therefore the diffusion rate, must be minimal. Therefore, Ni-based alloys are doped with metals such as Ti and Al. Current research is focused on Ni_3Al and NiTi-based alloys in addition to Ni-based superalloys. Ni_3Al alloys exhibit more attractive properties than conventional Ni-based alloys due to their high melting point (~1395 °C), low density, abnormal temperature dependence of yield strength, and excellent corrosion resistance [5, 6]. Several studies on the ductility [7], precipitation [8], and thermodynamic stability [9] of Ni_3Al alloys are available in the literature. However, no studies investigating the photon and neutron absorption cross sections of either Ni_3Al alloy or Ni_3Al-based superalloys were found in the literature. On the other hand, there are limited studies in the literature on photon and neutron absorption of Ni-based alloys. Sayyed et al. [10] investigated the photon absorption capacities of MAR-

247, Inconel-625, Inconel-718, Nimocast-75 and WI-52 alloys, and Sriwonga et al. [11] investigated the photon absorption capacities of Inconel 600, 718, and 725 alloys. In this presented study, the structural and radiation absorption capabilities of three different superalloys in the Ni_3Al-Cr-Nb-Mo-W structure ($Al_{10}Cr_{15}Nb_1Mo_1W_1Ni_{30}$, $Al_{8.5}Cr_17Nb_1Mo_1W_1Ni_{25.5}$, and $Al_{9.5}Cr_{15.5}Nb_1Mo_1W_1Ni_{28.5}$) were investigated.

2. MATERIAL AND METHOD

Powder metallurgy was used in the production of the alloys investigated in this study. The powders, placed in a mixing vessel at the mass ratios given in Table 1, were mixed at 50000 rpm for 30 minutes. The samples, formed into 13 mm diameter pellets using a hydraulic press and a die set, were gradually heated from 250 °C to 1200 °C. After holding at 1200 °C for 30 minutes, the pellets were gradually cooled to room temperature to obtain a crystalline superalloy. The crystallographic structures of the produced alloys were analyzed using X-ray diffraction (XRD), and their morphological structures were analyzed using scanning electron microscope (SEM).

Table 1. Weight fraction and densities of the produced superalloys

Superalloy Composition	Short Name	Al	Cr	Nb	Mo	W	Ni	Density (g/cm^3)
$Al_{10}Cr_{15}Nb_1Mo_1W_1Ni_{30}$	SA1	0.085	0.245	0.029	0.030	0.058	0.553	6.827
$Al_{8.5}Cr_{17}Nb_1Mo_1W_1Ni_{25.5}$	SA2	0.077	0.296	0.031	0.032	0.062	0.502	6.838
$Al_{9.5}Cr_{15.5}Nb_1Mo_1W_1Ni_{28.5}$	SA3	0.082	0.259	0.030	0.031	0.059	0.538	6.832

Gamma-ray absorption experiments of the investigated alloys were conducted using a ^{133}Ba radioactive source and a high purity germanium (HPGe) detector (Figure 1(a)). Experimental mass attenuation coefficient (MAC) coefficients were calculated from the obtained gamma-ray absorption spectra using the well-known Beer-Lambert law [12, 13]. Numerous studies in the literature describe the calculation of fundamental photon shielding parameters such as MAC, half-value layers (HVL), and effective atomic number (Z_{eff}). Theoretical gamma-ray absorption calculations were conducted using Phy-X/PSD software [14]. Details regarding the calculation of theoretical MAC, HVL, and Z_{eff} parameters, which allow for both verification of experimental data and evaluation over a wide energy range, can be found in our previous work [15, 16]. In this study, which used a narrow-beam geometry, the spectra, an example of which is given in Figure 1(b), were analyzed with Origin Pro version 8. In the analyses, both blank measurements and measurements with samples were fitted using the Gaussian equation for fields below the photon energies of 53, 81, 160, 223, 276, 302, 356, and 383 keV, which are the characteristic energies of the ^{133}Ba source.

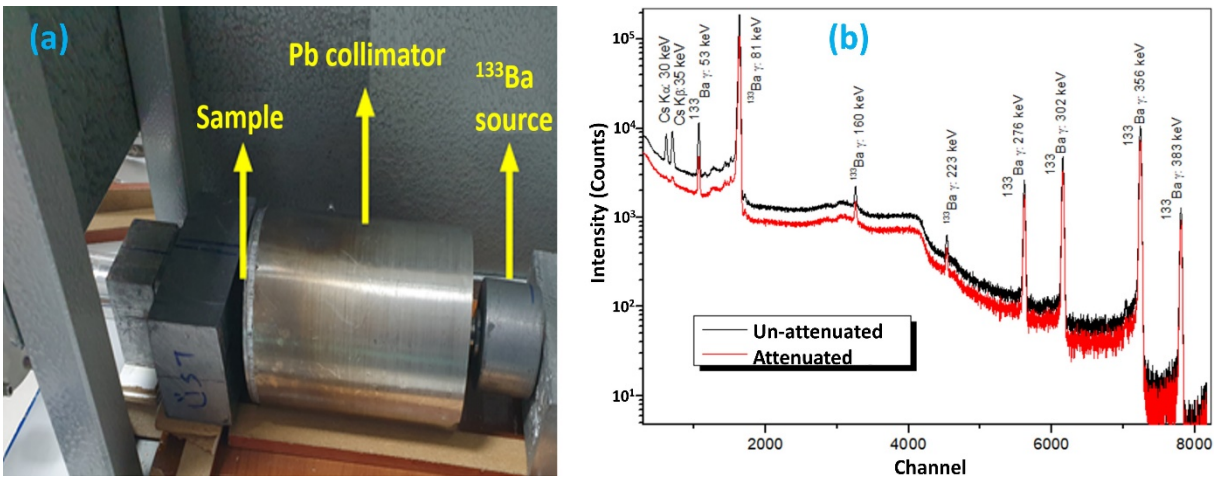

Figure 1. (a) Actual image of the experimental measurement system and (b) an example spectrum taken with ^{133}Ba

3. RESULTS

The spectra obtained from XRD measurements to determine the crystallographic structures of alloys produced using the sintering technique are shown in Figure 2. From these spectra, it can be seen that all superalloys have a polycrystalline structure and exhibit the characteristic peaks of Ni_3Al. Conducting the experimental production process in an oxygen environment also resulted in the formation of some metal oxide compounds in the structure. Indeed, prominent Cr_2O_3 and NiO peaks are present in all spectra. No peaks related to the metals or metal oxides

Nb, Mo, and W, which are present in very small amounts in the superalloys, were observed. The similar profile of the three spectra shown in the figure demonstrates the reproducibility of the production method.

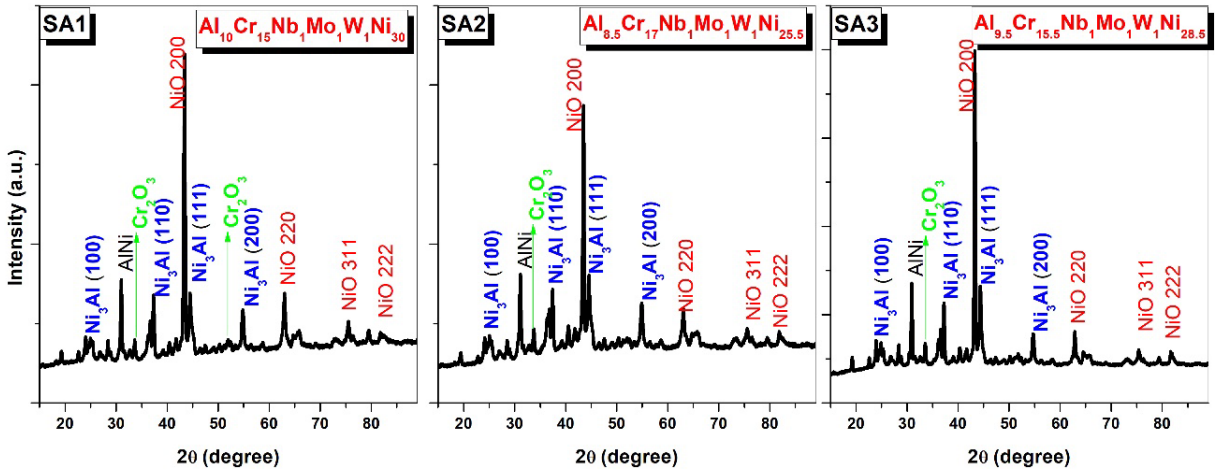

Figure 2. XRD spectrum of the investigated superalloys

SEM images of the produced superalloys, taken at a 1-micron scale, are shown in Figure 3 to determine their surface morphology. It can be seen that the produced alloys have a fairly homogeneous distribution. The absence of any voids and the absence of agglomeration of the alloy in any specific region can be considered evidence that the mixing process during sample production achieved sufficient homogenization. Furthermore, the similar geometric shapes and nearly equal grain regions of the structure support this finding. The SEM images provided support the polycrystalline structure of the produced alloys. The relatively similar elemental contents of the alloys resulted in the emergence of similar structures. This can be considered evidence that the sintering method used in the production of the alloys was systematically applied. Furthermore, the absence of agglomerations on the surface indicates that the doped metals are also present within the crystal structure. In metal doping processes applied at low rates to cubic structures, metal atoms generally tend to settle at the corner points of the cubic structure. This causes the lattice constants a, b, and c, which are equal in the cubic structure, to differ, transforming the structure into a rectangular prism. Furthermore, when the doping level is very low, the structure can bend outward or inward, depending on the atomic radius of the doped metal. In the case of heavy metal doping, the crystals bend outward due to the increased atomic radius. This is essentially the presence of the gamma double prime phase. SEM images of alloys obtained with heavy metal doping of Ni_3Al-based alloys show triangular pyramidal structures extending outward from the surface. This can be considered evidence of the presence of the gamma double prime phase. However, both the base areas and valley depths of the triangular pyramidal structures formed on the surface differ. This difference is thought to be due to the particle sizes of the metal powders used.

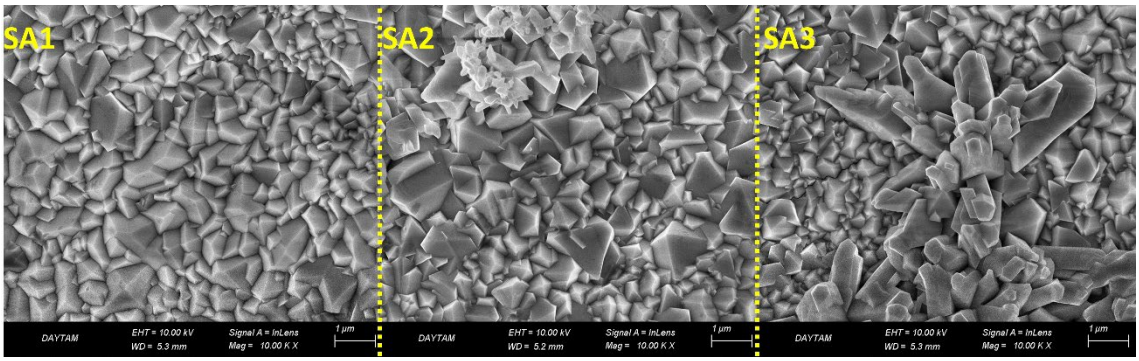

Figure 3. SEM images of the investigated superalloys

The results of gamma-ray absorption experiments conducted to determine the usability of the produced superalloys in radiation-safe environments are presented in Table 2. From this table, it is clear that the experimental and theoretical values are in good agreement. This demonstrates the accuracy of both the alloy production and the experimental measurements (measurement time, test geometry, analysis procedures, etc.). Because the data in Table 2 are in good agreement across eight different energies, results from a wider energy range, where experimental results are not available, can be theoretically examined. This allows for the understanding of interaction cross-sections in both lower and very high energy regions. For this purpose, the MAC, HVL, and Z_{eff}

variations obtained using Phy-X/PSD software are presented in Figures 4 and 5(a,b), respectively. In addition to the newly produced superalloys, all these graphs also include the corresponding values for the Ni_3Al alloy.

Table 2. Experimental and theoretical MAC values of the investigated superalloys (SA1, SA2, and SA3)

Energy (MeV)	SA1			SA2			SA3		
	Theo.	Exp.	Std. Dev.	Theo.	Exp.	Std. Dev.	Theo.	Exp.	Std. Dev.
5.32E-02	2.144	2.038	0.1916	2.145	2.039	0.1917	2.147	2.148	0.2019
8.10E-02	1.074	1.021	0.0960	1.098	1.088	0.1023	1.081	1.038	0.0976
1.61E-01	0.262	0.234	0.0220	0.266	0.246	0.0231	0.263	0.246	0.0231
2.23E-01	0.167	0.151	0.0142	0.169	0.149	0.0140	0.168	0.152	0.0143
2.76E-01	0.135	0.135	0.0127	0.136	0.133	0.0125	0.135	0.136	0.0128
3.03E-01	0.125	0.122	0.0115	0.125	0.121	0.0114	0.125	0.119	0.0112
3.56E-01	0.110	0.108	0.0102	0.110	0.106	0.0100	0.110	0.110	0.0103
3.84E-01	0.105	0.105	0.0099	0.105	0.103	0.0097	0.105	0.100	0.0094

From the MAC change graphs shown in Figure 4, it is clear that all superalloys and the Ni_3Al structure share similar characteristics. In all samples, the MAC values decrease with increasing energy, implying a lower cross-section for high-energy photons. Increasing photon energy reduces their wavelength, thus reducing their interaction cross-sections. This results in higher penetrating power for high-energy photons. The graph also reveals that all three newly produced superalloys exhibit very similar characteristics. This is due to the fact that these three alloys are composed of the same elements and the very similar proportions of these elements within the structure. This is clearly evident in both the main and inset graphs. It can also be seen from the graphs that all alloys exhibit very similar characteristics at the intermediate energy level, the Compton region, where a sudden decrease occurs in the low-energy region where photoelectric interactions dominate. In general, the graph suggests that heavy metal doping into the Ni_3Al structure enhances the photon shielding ability of this compound.

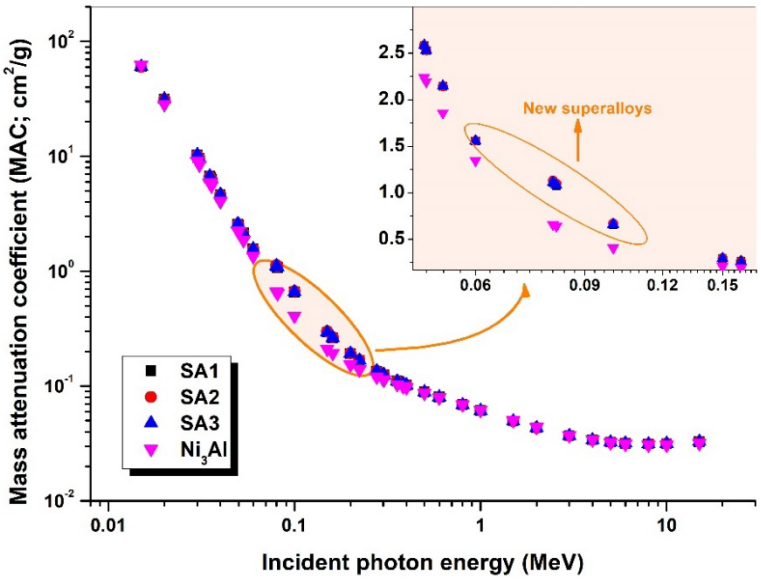

Figure 4. Variation of MAC values of the investigated superalloys and Ni_3Al

The changes in the half-value layer values, which represent the material thickness required to reduce the photon intensity to half-value, over the 15 keV-15 MeV range are presented in Figure 5(a). This value, which increases with increasing photon energy, indicates that photons can be absorbed by thicker materials at higher energies. At lower energies, almost complete absorption of photons results in HVL values very close to zero. In the inset of the graph, the HVL changes over the 4-15 MeV energy range can be seen from the HVL variation in the newly produced superalloys, which halve the photon intensity at shorter distances than Ni_3Al. Indeed, at a photon energy of 10 MeV, the HVL value of Ni_3Al is 3.414 cm, while the average for other superalloys is 3.224 cm. In materials such as alloys, polymers, glass, or concrete, which are composed of multiple elements, an imaginary number representing the entire material with a single number provides considerable ease of interpretation in terms of

radiation. For this purpose, the effective atomic number is the imaginary number that indicates which element the material behaves like in response to the exciting radiation at any given energy value. This parameter is high in materials composed of combinations of elements with high atomic numbers. It is known that materials with a higher abundance of elements with high atomic numbers interact better with gamma rays. The Z_{eff} change graph in Figure 5(b) clearly shows lower values for the Ni_3Al compound than for other superalloys across the entire energy range. This supports the notion that Ni_3Al has lower photon absorption than other superalloys. The Z_{eff} values of the produced superalloys, however, fluctuate significantly depending on the energy. This value, which exhibits a sudden jump in the 60 keV energy region, drops significantly after 60 keV. It is known that all naturally occurring elements have atomic structures that reflect their own characteristics. One of these characteristic quantities is the absorption edge. This quantity, specific to each element's K, L, or M shells, causes maximum absorption of incident photons at the absorption edge energy. The sudden jump seen in the graph is due to the K-layer absorption edge of the heavy metals contained in the produced superalloys.

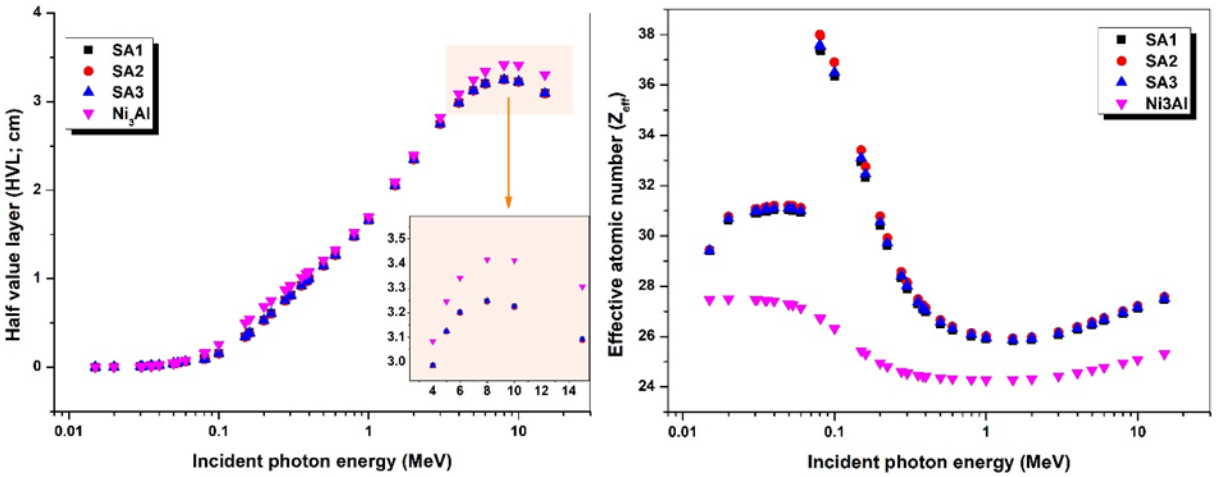

(a) (b)

Figure 5. (a) Variation of HVL values of the investigated superalloys and Ni_3Al and (b) variation of Z_{eff} values of the investigated superalloys and Ni_3Al

4. CONCLUSION

In this study, the structural properties and photon absorption capacities of three different Ni_3Al-based superalloys (SA1, SA2, and SA3) doped with chromium, niobium, molybdenum, and tungsten produced by the step-sintering method were systematically investigated. XRD and SEM analyses revealed that the alloys have a polycrystalline structure with homogeneous distribution and characteristic pyramidal shapes (gamma double-noble phase) on their surfaces. Radiation absorption experiments and theoretical calculations showed that these new superalloys have higher MAC, lower HVL, and higher (Z_{eff} compared to pure Ni_3Al over the entire energy range investigated (53-383 keV). These findings demonstrate that doping with heavy metals such as Cr, Nb, Mo, and W significantly improves Ni_3Al's gamma-ray shielding ability while maintaining its high-temperature performance. Consequently, these studied superalloys stand out as multifunctional material candidates for advanced engineering applications where high temperatures and radiation coexist (such as nuclear reactors and aerospace).

Acknowledgments

This study was supported by Ataturk University Scientific Research Projects Grant No: FAB-2022-11396.

References

[1] P. Jozwik, W. Polkowski, and Z. Bojar, "Applications of Ni3Al based intermetallic alloys—Current stage and potential perceptivities," *Materials*, vol. 8, no. 5, pp. 2537–2568, May 2015. doi: 10.3390/ma8052537

[2] J. W. Martin, Ed., *Concise Encyclopedia of the Structure of Materials*, 1st ed. Amsterdam, Boston: Elsevier, 2007.

[3] J. Pei, Y. Li, C. Li, Z. Wang, Y. Liu, and H. Li, "Microstructure-dependent oxidation behavior of Ni-Al single-crystal alloys," *Journal of Materials Science & Technology*, vol. 52, pp. 162–171, Sep. 2020. doi: 10.1016/j.jmst.2020.04.006

[4] S. V. Raju, B. K. Godwal, A. K. Singh, R. Jeanloz, and S. K. Saxena, "High-pressure strengths of Ni3Al and Ni-Al-Cr," *Journal of Alloys and Compounds*, vol. 741, pp. 642–647, Apr. 2018. doi: 10.1016/j.jallcom .2018.01.142

[5] P. Paufler, J. H. Westbrook, and R. L. Fleischer, Eds., *Intermetallic Compounds – Principles and Practice*, Chichester: John Wiley & Sons, 1995. doi: 10.1002/crat.2170300706

[6] C. Senderowski, "Nanocomposite Fe-Al intermetallic coating obtained by gas detonation spraying of milled self-decomposing powder," *J. Therm. Spray Tech.*, vol. 23, no. 7, pp. 1124–1134, Oct. 2014. doi: 10.1007/s 11666-014-0086-1

[7] K. Aoki and O. Izumi, "Improvement in room temperature ductility of the $L1_2$ type intermetallic compound Ni_3Al by boron addition," *J. Japan Inst. Metals*, vol. 43, no. 12, pp. 1190–1196, 1979. doi: 10.2320/jinstmet 1952.43.12_1190

[8] Y. Wu, C. Li, X. Xia, H. Liang, Q. Qi, and Y. Liu, "Precipitate coarsening and its effects on the hot deformation behavior of the recently developed γ'-strengthened superalloys," *Journal of Materials Science & Technology*, vol. 67, pp. 95–104, Mar. 2021. doi: 10.1016/j.jmst.2020.06.025

[9] B. Xu, H. Yin, X. Jiang, C. Zhang, R. Zhang, Y. Wang, et al., "Computational materials design: Composition optimization to develop novel Ni-based single crystal superalloys," *Computational Materials Science*, vol. 202, art. no. 111021, Feb. 2022. doi: 10.1016/j.commatsci.2021.111021

[10] M. I. Sayyed, F. Q. Mohammed, K. A. Mahmoud, E. Lacomme, K. M. Kaky, M. U. Khandaker, et al., "Evaluation of radiation shielding features of Co and Ni-based superalloys using MCNP-5 code: Potential use in nuclear safety," *Applied Sciences*, vol. 10, no. 21, art. no. 7680, Oct. 2020. doi: 10.3390/app10217680

[11] K. Sriwongsa, J. Sirimongkolchaikul, C. Sukrasorn, T. Bussaparoek, S. Kanunghet, T. Phansuea, et al., "Radiation and fast neutron shielding properties of nickel-based superalloys: Inconel 600, 718 and 725 superalloys," *Integrated Ferroelectrics*, vol. 224, no. 1, pp. 120–133, Mar. 2022. doi: 10.1080/10584587. 2022.2035602

[12] B. Alim, E. Sakar, A. Baltakesmez, I. Han, M. Sayyed, and L. Demir, "Experimental investigation of radiation shielding performances of some important AISI-coded stainless steels: Part I," *Radiation Physics and Chemistry*, vol. 166, art. no. 108455, 2020.

[13] B. Alim, O. F. Ozpolat, E. Sakar, I. Han, I. Arslan, V. P. Singh, et al., "Precipitation-hardening stainless steels: Potential use radiation shielding materials," *Radiation Physics and Chemistry*, vol. 194, art. no. 110009, 2022.

[14] E. Sakar, O. F. Ozpolat, B. Alim, M. Sayyed, and M. Kurudirek, "Phy-X/PSD: development of a user friendly online software for calculation of parameters relevant to radiation shielding and dosimetry," *Radiation Physics and Chemistry*, vol. 166, art. no. 108496, 2020.

[15] E. Sakar, B. Alim, O. F. Ozpolat, B. C. Sakar, A. Baltakesmez, and U. Akbaba, "A surveying of photon and particle radiation interaction characteristics of some perovskite materials," *Radiation Physics and Chemistry*, vol. 189, art. no. 109719, 2021.

[16] E. Sakar, "Determination of photon-shielding features and build-up factors of nickel–silver alloys," *Radiation Physics and Chemistry*, vol. 172, 2020. doi: 10.1016/j.radphyschem.2020.108778

2nd International Conference on Multidisciplinary Sciences and Technological Developments (ICMUSTED 2025)

December 12-15, 2025

Convergence Analysis for Parallel Iteration Methods

Yasin Berkay Can[1], Nazli Kadioglu Karaca[1], Isa Yildirim[1]

[1]Department of Mathematics, Ataturk University, Erzurum, Türkiye
Corresponding author: Yasin Berkay Can (e-mail: canyasinberkay@gmail.com)

Abstract

In this study, we introduce new parallel iterative schemes for approximating fixed points of altering points of Lipschitz mappings defined between two nonempty convex subsets C_1 and C_2 of a normed linear space X. Given two mappings $T_1 : C_1 \to C_2$ and $T_2 : C_2 \to C_1$ and an initial pair (x_1, y_1), we propose a multi-step coupled iteration process generated by the sequences $\{x_n\}$, $\{y_n\}$, $\{z_n\}$, $\{u_n\}$, $\{w_n\}$, and $\{v_n\}$ where each iteration involves successive applications and convex combinations of T_1 and T_2 controlled by a real sequence $\{\alpha_n\} \subset [0,1]$. The general form of the process includes the updates $x_{n+1} = T_2 z_n, y_{n+1} = T_1 u_n, z_n = T_1 T_2 w_n, u_n = T_2 T_1 v_n, w_n = T_1\left[(1-\alpha_n)T_2 y_n + \alpha_n T_2 T_1 y_n\right], v_n = T_2\left[(1-\alpha_n)T_1 x_n + \alpha_n T_1 T_2 y_n\right]$. We prove strong convergence theorems and establish data dependence results that demonstrate the stability and robustness of the proposed iterative process under suitable Lipschitz conditions. Furthermore, to illustrate the practical effectiveness of the method, we apply the proposed iterative schemes to obtain approximate solutions of nonlinear variational inequality problems. The contributions of this study include a novel parallel iteration framework, new convergence and stability analyses, and an application to important classes of optimization and equilibrium problems, enriching the existing literature on fixed point theory and variational inequalities.

Keywords: Altering points, Nonexpansive mappings, Parallel algorithm

2nd International Conference on Multidisciplinary Sciences and Technological Developments (ICMUSTED 2025)

December 12-15, 2025

On Nearness Ideals of Nearness Semigroups

Mehmet Ali Ozturk[1], Ozlem Tekin[1]

[1]Department of Mathematics, Adiyaman University, 02040 Adiyaman, Türkiye
Corresponding author: Ozlem Tekin (e-mail: oumdu@adiyaman.edu.tr)

Abstract

Semigroups are recognized as foundational algebraic structures and continue to draw significant interest across various branches of mathematics and computer science. They serve as essential tools in theoretical computer science, graph theory and optimization. Numerous classes of ideals such as quasi-ideals, interior ideals have been defined and examined within semigroup theory. Although set theory provides the groundwork for many mathematical and engineering investigations, the classical framework does not always capture the uncertainty, incomplete information, and non-absolute situations that arise in real-world problems. To address these limitations, several generalized extensions of set theory have been proposed. Among these, rough set theory offers a mechanism for analyzing objects that cannot be clearly distinguished due to variations in their decision attributes. Near set theory extends the principles of rough sets by employing the observable features of objects to define nearness relations and to classify the universe of discourse accordingly. The development of this theory was inspired by applications in image processing and by studies on how humans perceive similarity among physical objects. Its central component, the probe function, assigns real values to specific characteristics of objects such as pixel intensity in images or behavioral traits in biological entities thereby enabling the comparison of elements located in different perceptual granules. The algebraic development of the near set framework was advanced and researchers introduced the concept of nearness semigroups. Later, ordered (gamma) nearness semigroups are proposed and several of their structural properties are investigated. In the present study, we examine the fundamental characteristics of nearness semigroups and investigate the ideals of semigroups defined on a weak nearness approximation space. This work presents and discusses multiple characterizations of these structures, offering insights into their essential features, underlying relationships, and their role within the wider theory of the nearness semigroups.

Keywords: Semigroups, Weak nearness approximation spaces, Nearness semigroups, Nearness ideals

2nd International Conference on Multidisciplinary Sciences and Technological Developments (ICMUSTED 2025)

December 12-15, 2025

Investigation of Temperature Changes During the Composting of Pomegranate Processing Solid Wastes with the Addition of Bioactivator

Kemal Suluk[1], Fevzi Sevik[2], Barbaros S. Kumbul[3], Kamil Ekinci[4]

[1]Faculty of Engineering and Architecture, Mus Alparslan University, Mus, Türkiye
[2]Vocational School of Health Services, Bingol University, Bingol, Türkiye
[3]Rafet Kayis Faculty of Engineering, Alanya Alaaddin Keykubat University, Antalya, Türkiye
[4]Faculty of Agricultural Sciences and Technologies, Isparta University of Applied Sciences, Isparta, Türkiye
Corresponding author: Fevzi Sevik (e-mail: fsevik@bingol.edu.tr)

Abstract

This study investigated the effect of bioactivators on compost temperature changes to increase the compostability of pomegranate processing waste generated in the fruit juice industry. Eight different mixtures were created within the scope of the study; fifteen aerobic reactors with a volume of 100 L were used to compost pomegranate processing solid wastes (PPSW) with different combinations of animal wastes, with and without bioactivators. The composting process was monitored for 28 days, and temperature changes were recorded using a PLC-based automation system. Findings showed that in mixtures composed entirely of PPSW (M1–M2), due to their acidic character and polyphenolic structure, temperature increase was limited, and the transition to the thermophilic phase was not achieved. In contrast, mixing pomegranate processing solid wastes with animal manures significantly improved the temperature profile; in particular, in mixtures containing poultry manure (M5–M6), temperatures reached 55–60 °C, resulting in a strong and sustained thermophilic phase. This temperature range demonstrates that pathogen removal was achieved in the compost. In mixtures containing both cattle and poultry manure (M7–M8), a more balanced temperature profile was achieved and the duration of the thermophilic phase was prolonged thanks to both manure sources. The addition of bioactivators generally accelerated the temperature increase, enhanced recovery after mixing, and prolonged the thermophilic phase; this effect was particularly evident in mixtures M6 and M8. The results indicated that PPSW alone does not provide sufficient thermophilic activity; the use of nitrogen-rich fertilizer additives and bioactivators is necessary to optimize composting performance. Bioactivator-assisted composting of pomegranate processing solid wastes stands out as an effective waste management strategy that reduces environmental impacts, allows for the production of organic products with high hygienic quality and increased agricultural potential.

Keywords: Bioactivator, Pomegranate processing solid waste, Reactor composting, Temperature change

1. INTRODUCTION

Pomegranate (*Punica granatum L.*), one of the characteristic fruits of the Mediterranean region, is one of the oldest cultivated species, with cultivation dating back to 3000 BC. Today, it is intensively produced in many countries, particularly India, Iran, China, Turkey, and the United States, and is among the most widely consumed fruits globally. In Turkey, the Aegean, Mediterranean, and Southeastern Anatolia regions are particularly central to pomegranate cultivation. While production volumes have varied by region over the years, the general trend is towards continuous increase. Indeed, national pomegranate production, which was approximately 73,000 tons in 2004, has shown significant growth, reaching 703,000 tons by 2020 [1].

Pomegranates stand out not only for their fresh consumption but also as one of the most processed fruits in the juice industry. During the juice production process, pomegranates are processed through the stages of pre-selection, washing and crushing, respectively, and are then converted into the final product, pomegranate juice. However, a significant number of organic by-products (waste) are generated in the processing line. Pomegranate processing solid wastes (PPSW) consists of the stems, leaves, peels, seeds, and rotten fruit removed during the pre-sorting processes of the raw materials arriving at the facilities, as well as the pomegranate pulp resulting from the juice production process [2, 3] and constitutes approximately half (~50%) of the total fruit weight [4]. If these wastes, which have a high organic matter content, are not managed appropriately, environmentally detrimental practices such as being diverted to landfills or dumped in uncontrolled open areas can occur [5]. This poses a serious threat to both environmental health and human health [6].

PPSW, which increases in quantity every year, is a type of waste that cannot be easily biodegraded due to its high lignocellulosic structure and pronounced acidic character. These characteristics of PPSW necessitate its use through environmentally sustainable methods, and composting is considered one of the most suitable disposal strategies in this context [7]**.** Composting is a process that stabilizes organic materials of plant and animal origin through aerobic microbial activity, transforming them into an environmentally friendly product with soil-enhancing properties. In this context, composting of PPSW is considered one of the most viable disposal options in terms of both reducing waste volume and increasing the agricultural use potential of the resulting organic product.

One of the main challenges encountered in the composting of PPSW is its high phenolic compound content and lignocellulosic structure, which slows down the decomposition rate. Therefore, the use of bioactivators, which support microbial populations or enhance enzymatic activity during the composting process, has become an important strategy to increase decomposition efficiency. Depending on the mixing ratio of the waste, the addition of bioactivators offers advantages such as increasing the mineralization rate of organic matter, improving the carbon-nitrogen balance, and enhancing the microbial growth capacity in the initial phase of compost. These components contribute to a more pronounced and healthy development of temperature changes, one of the most critical indicators of the composting process, thus improving both the speed and quality of the process [5, 8].

Temperature is one of the most important indicator parameters in composting, which is an exothermic process [9, 10]. It directly affects organic matter removal and pathogenic bacterial inhibition. Studies on the effect of bioactivators on temperature dynamics in the composting of PPSW are limited, and studies on fruit processing wastes with high lignocellulosic content are particularly lacking in the literature. The aim of this study was to investigate the effect of bioactivators added to waste mixtures on process temperature during the composting of PPSW (pre-screening waste and pomegranate pulp) using a reactor composting system.

2. MATERIAL AND METHOD

2.1. Composting Materials

PPSW used in the study was maintained from Anadolu Etap, operating in the Egirdir/Isparta district, and its moisture content was reduced by partial drying and then shredded. Cattle manure (CM) was provided by Isparta University of Applied Sciences Agricultural Research and Application Center, and poultry manure (PM) was provided by Gurelli chicken farm operating in Isparta province. The bioactivator (BA) material (BZT® Compost Activator) in the study was provided by Design Group Consulting Services Inc. Composting process was carried out in the Compost Laboratory of Isparta University of Applied Sciences. The physical and chemical properties of the materials used in the study are given in Table 1.

Table 1. Physico-chemical values of compost materials used in the study (MC: Moisture content, OM: Organic matter, pH: Potential of hydrogen, EC: Electrical conductivity, TC: Total carbon, TN: Total nitrogen, and C/N: Carbon/nitrogen ratio)

Parameter	PPSW	CM	PM
MC (%)	60.00	70.00	8.10
OM (%)	92.62	80.47	66.93
pH	5.35	8.77	8.43
EC (dS/m)	2.40	6.25	6.03
TC (%)	41.49	45.75	29.38
TN (%)	1.35	1.32	2.26
C/N	30.73	34.66	13.00

2.2. Composting Process

For the composting of PPSW, 8 (eight) mixtures were prepared, and 4 (four) of these mixtures were made with the addition of BAs. The initial MC of all mixtures was adjusted to around 60%. The first and second mixtures (M1 and M2) consisted entirely of PPWS (Table 2). In addition, 2.25% lime was added to the mixture on a wet basis to adjust the pH balance of mixtures M1 and M2. The bioactivator was added to the mixtures using the spring method by dissolving 25 g of activator recommended for 100 kg of dry matter in water. The composting process was carried out in 100 L stainless steel aerobic reactors, as shown in Figure 1 [11, 12]. Temperature changes during composting were also monitored and recorded by the PLC automation system (Figure 2).

The BA used in this study consists of microbial and enzymatic components formulated in a whey-based liquid carrier matrix. The product contains *Bacillus spp*. and *Lactobacillus spp*. species, both vegetative and spore-forming, and various enzymes are incorporated into the formulation to support the biological activity of these microorganisms during the composting process. The bioactivator's composition is based on microbial-enzymatic activity, which aims to increase the rate of hydrolysis and decomposition of organic matter.

Table 2. Compost mixtures (dry matter basis)

Mixture	C/N	MC (%)	PPSW (%)	CM (%)	PM (%)	BA (g/kg)
M1 (R1)	30.73	60.00	100	-	-	-
M2 (R2-R3)			100	-	-	25/100
M3 (R4-R5)	32.28	64.71	60	40	-	-
M4 (R6-R7)			60	40	-	25/100
M5 (R8-R9)	21.38	60.00	60	-	40	-
M6 (R10-R11)			60	-	40	25/100
M7 (R12-R13)	26.16	60.00	60	20	20	-
M8 (R14-R15)			60	20	20	25/100

Figure 1. Reactors used in the composting system

Figure 2. Composting system startup (day 0) programmable logic controller (PLC) screenshot

3. RESULTS

The composting process of PPSW with other wastes continued for 28 days, with and without the addition of bioactivators. During the active composting process, the compost mixtures were mixed on the 5th, 20th, and 28th days.

M1 mixture is a single reactor composting study, consisting entirely of PPSW and does not contain bioactivators (Table 2, Figure 3). A limited temperature increase was observed in the pile at the beginning of the composting process. The temperature remained between 28 and 32°C during the first days, indicating low microbial activity due to the acidic, polyphenolic, and lignocellulosic structure of the pomegranate waste. The sudden temperature drop recorded around day 5 is due to mixing and natural aeration. However, the temperature subsequently rose again and remained relatively stable between 30 and 38°C. However, the mixture failed to transition to the thermophilic phase. This indicated that PPSW cannot provide sufficient substrate to support microbial warming due to its high C/N ratio and low nitrogen content. As temperatures gradually approach ambient temperature towards the end of the process, this indicated a decrease in microbial activity, the depletion of the easily degradable organic fraction, and the transition to the compost maturation phase. These general trends reveal the need to supplement PPSW with bioactivators, nitrogen-rich additives or animal fertilizers when composting alone.

The addition of bioactivator at a rate of 25/100 g kg^{-1} on a dry matter basis to the M2 mixture, consisting of 100% PPSW, significantly improved the temperature dynamics from the beginning of the composting process. The rapid temperature rise to 35–45 °C in the first days in the R2 and R3 reactors is associated with the activator's increased microbial diversity and enzymatic hydrolysis capacity. This trend provided a significant advantage compared to the M1 mixture without activator, which had a relatively weak initial heating. In the middle period of the process, the temperature in the M2 mixture remained in the 35–45 °C range for an extended period, while the M1 mixture showed more limited activity in the 30–38°C range. However, due to the polyphenolic and lignocellulosic structure of PPSW, the M2 mixture also failed to transition to a fully thermophilic phase (>50°C); however, it has a significant advantage over M1 in terms of approaching the thermophilic border region. In general, the addition of activator provided higher microbial activity, more pronounced temperature increase and a more controlled cooling trend in the M2 mixture compared to M1 (Figure 4).

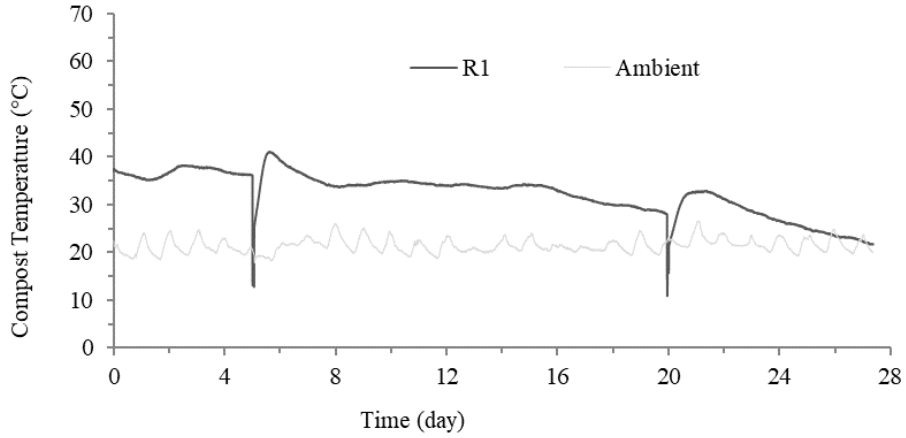

Figure 3. Temperature change of M1 during the composting period

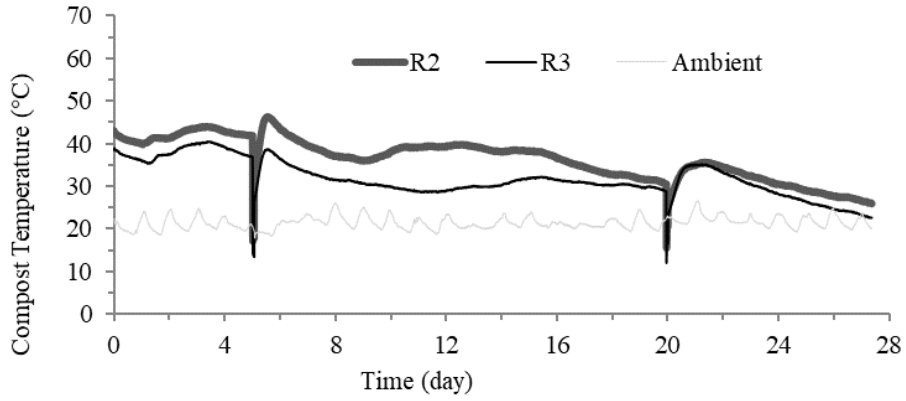

Figure 4. Temperature change of M2 during the composting period

The composting process in the M3 and M4 mixtures, consisting of 60% PPSW and 40% cattle manure, began with a much stronger temperature increase compared to the M1 and M2 mixtures due to the high microbial load provided by the manure. In the M3 mixture without activator, the temperature rose to 45°C and exhibited a short-term thermophilic tendency. However, in the M4 mixture, to which 25/100 g kg^{-1} activator was added, the temperature approached 50 °C, reaching a more pronounced thermophilic phase. Furthermore, the high temperatures were maintained for a longer period. In later stages of the process, the temperature decreased to 30–35°C, and the compost entered the maturation phase. The M4 mixture demonstrated that the activator significantly increased composting performance in terms of both the maximum temperature level and the stable temperature profile (Figure 5 and Figure 6).

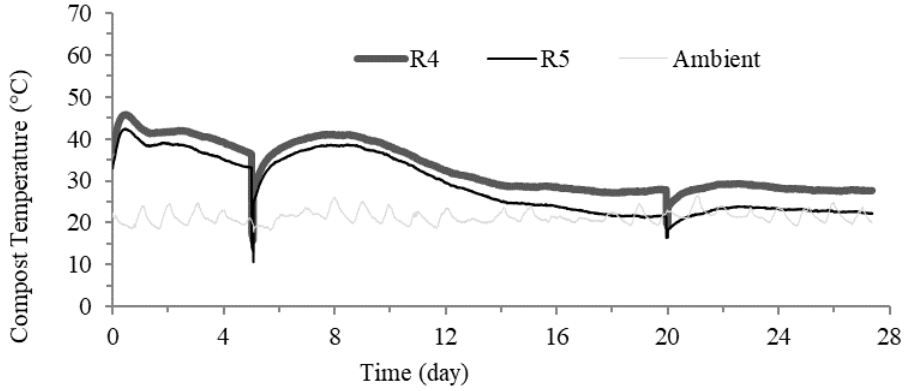

Figure 5. Temperature change of M3 during the composting period

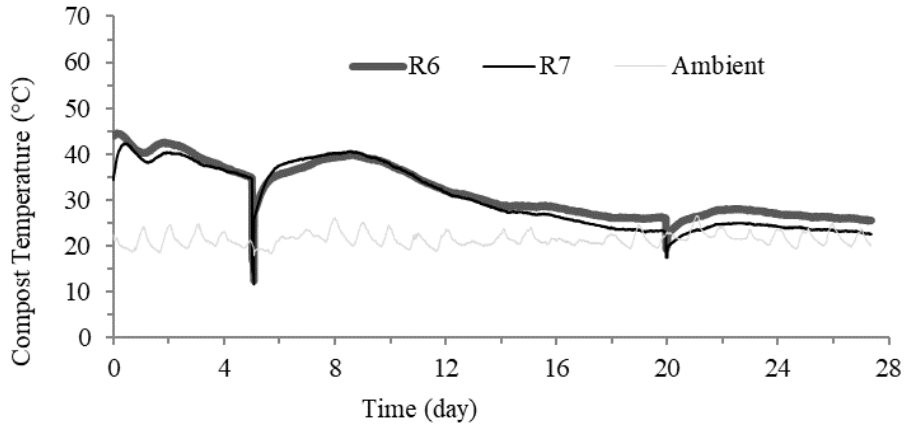

Figure 6. Temperature change of M4 during the composting period

Mixtures- M5 (Figure 7) and M6 (Figure 8), consisting of 60% PPSW and 40% poultry manure, exhibited the strongest temperature increase compared to all other mixtures at the beginning of the composting process, due to the high nitrogen content and dense microbial load of poultry manure. In the M5 mixture without activator addition, the reactors reached 55–60°C, creating a distinct thermophilic phase. This temperature range also indicated significant inhibition of pathogenic microorganisms. In contrast, in the M6 mixture containing 25% activator, both reactors (R10–R11) quickly entered the thermophilic zone and maintained the 50–60°C range for extended periods, exhibiting a more stable and sustainable temperature profile. Pathogen removal was also observed in the M6 compost mixture. Generally speaking, although both mixtures exhibit strong biological activity, the M6 mixture stands out as the most successful formulation in terms of composting performance because it remained in the thermophilic region for a longer time throughout the process, maintains sanitation temperatures above 55°C more stably, and recovers faster after mixing processes.

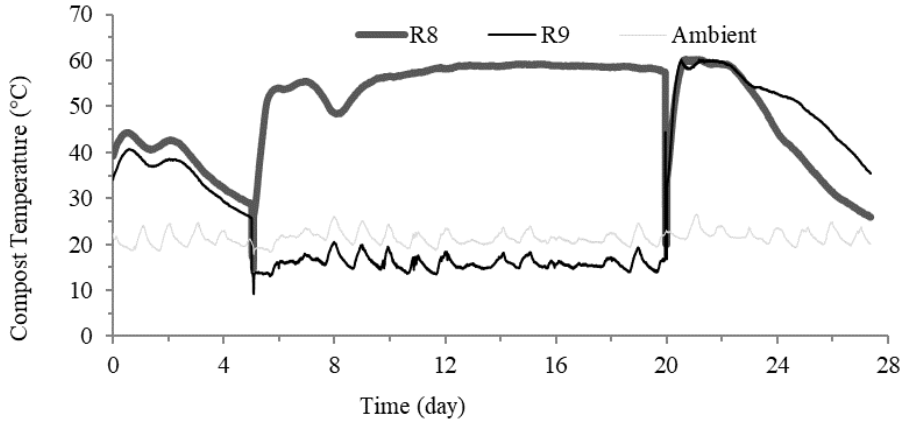

Figure 7. Temperature change of M5 during the composting period

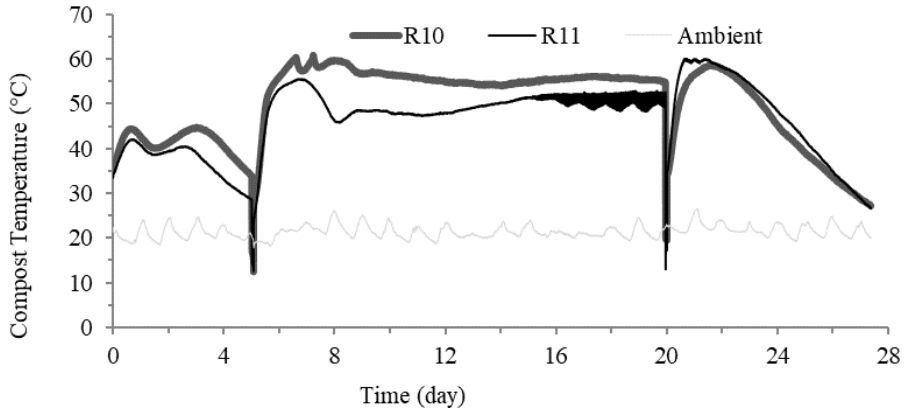

Figure 8. Temperature change of M6 during the composting period

The M7 (Figure 9) and M8 (Figure 10) mixtures, consisting of 60% PPSW, 20% cattle manure, and 20% poultry manure, exhibited a rapid temperature increase at the beginning of composting due to the combined use of both cattle and poultry manure, providing a balanced organic nitrogen profile and a high microbial load. In the M7 mixture without activator, reactors R12 and R13 reached levels of 55–60°C, creating a strong thermophilic phase. This temperature range demonstrated effective inactivation of pathogenic microorganisms. In the M8 mixture, the addition of activator contributed to both a faster initial temperature increase and a longer and more stable preservation of the thermophilic phase in reactors R14 and R15. This indicates that the activator increases the microbial respiration rate, enzymatic hydrolysis, and heat generation capacity. As a general conclusion, although both mixtures provided a successful thermophilic phase and effective pathogen removal thanks to the high temperature profile, the M8 mixture stands out as a superior formulation in terms of composting performance by showing a more balanced, more stable and longer-lasting biological activity throughout the process with the support of the activator.

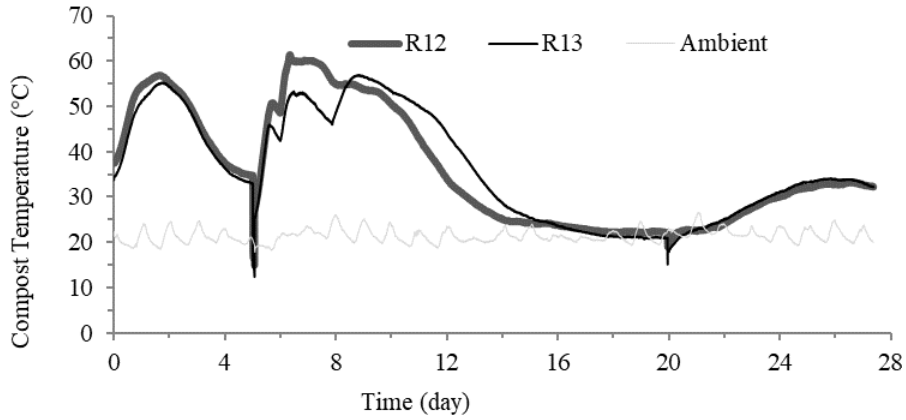

Figure 9. Temperature change of M7 during the composting period

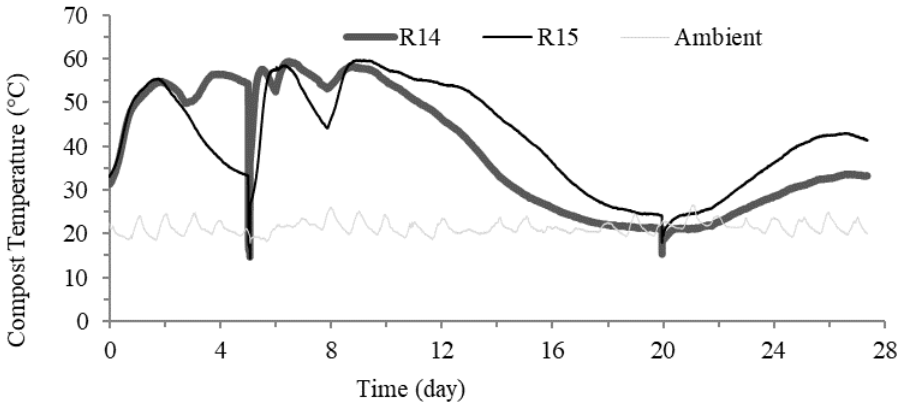

Figure 10. Temperature change of M8 during the composting period

4. CONCLUSION

This study was conducted to determine the composting of pomegranate processing solid wastes, both alone and in combination with various organic additives. The effect of activator addition on the temperature profile was evaluated in detail. The findings indicated that pomegranate waste, due to its high C/N ratio, acidic structure, and polyphenolic content, generated a limited temperature increase during composting alone, and its capacity to transition to the thermophilic phase remained quite weak. This was clearly observed in the M1 and M2 mixtures; although activator addition increased initial microbial activity, the temperature increase was limited to 40–45 °C due to the structural properties of pomegranate waste.

In contrast, when pomegranate processing solid wastes was mixed with animal manures (cattle and poultry manure) at different ratios, the temperature profiles were significantly improved. In particular, in mixtures using poultry manure (M5–M6), temperatures reached 55–60 °C, creating strong and long-lasting thermophilic activity. This temperature range demonstrated that pathogen removal was achieved in the compost, and it was concluded that the poultry manure additive played a critical role in sanitation. In mixtures M7 and M8, where cattle and poultry manure were used together, a balanced temperature profile was achieved thanks to the effects of both fertilizers; the thermophilic phase both initiated more rapidly and lasted longer.

When the overall effect of activator addition to the composting process was evaluated, it was observed that the activator accelerated temperature rise, enhanced stability, accelerated post-mix recovery, and significantly increased the duration of the thermophilic phase compared to mixtures without activator. Mixtures M6 and M8 provided the strongest examples of this effect; in particular, maintaining temperatures above 55°C for extended periods demonstrated that microbial activity, enzymatic hydrolysis, and biological conversion rates were positively supported by the activator.

Overall, while composting pomegranate processing solid wastes alone is not fully feasible, it is clear that it must be supplemented with nitrogen-rich organic waste materials (especially poultry manure) and/or an activator to achieve a strong thermophilic phase and ensure pathogen removal. This study demonstrated that due to the high C/N ratio and difficult-to-decompose lignocellulosic structure of pomegranate waste, composting performance is significantly dependent on ingredient selection and mixing ratios. It has been shown that mixtures supplemented with animal manure and added activators increase both the efficiency and the hygienic quality of the composting process. Therefore, it is concluded that the most suitable approach for the sustainable management of pomegranate processing solid wastes is optimized mixtures using a combination of nitrogen-rich fertilizer and an activator.

References

[1] TUIK. (2024). *Plant production statistics* [Online]. Available: https://data.tuik.gov.tr/Bulten/Index?p=Bitkisel-Uretim-Istatistikleri-2024-53447. [Accessed Oct. 25, 2025].

[2] D. Lampakis, P. Skenderidis, and S. Leontopoulos, "Technologies and extraction methods of polyphenolic compounds derived from pomegranate (Punica granatum) peels. A mini review," *Processes*, vol. 9, no. 2, art. no. 236, 2021.

[3] C. Venkitasamy, L. Zhao, R. Zhang, and Z. Pan, "Pomegranate," in *Integrated Processing Technologies for Food and Agricultural By-Products*, Z. Pan, R. Zhang, and S. Zicari, Eds.: Academic Press, 2019, pp. 181–216

[4] F. Marra, B. Petrovicova, F. Canino, A. Maffia, C. Mallamaci, and A. Muscolo, “Pomegranate wastes are rich in bioactive compounds with potential benefit on human health,” *Molecules*, vol. 27, no. 17, art. no. 5555. doi: 10.3390/molecules27175555

[5] E. Ekinci, C. Soyoz, B. S. Kumbul, R. Yildirim, S. Yazici, and H. Ruzgar, “Composting of pomegranate peels with bioactivator in a rotary drum composting system,” *European Journal of Science and Technology*, vol. 25, pp. 318–324, 2021.

[6] A. El Barnossi, “Agricultural applications of pomegranate peels,” in *Sustainable Applications of Pomegranate Peels*, M. Jeguirim and B. Khiari, Eds.: Academic Press, 2025, pp. 135–149.

[7] F. Sevik, I. Tosun, and K. Ekinci, “Characteristics of pomegranate processing wastes and determination of disposal strategies,” in *IMASCON Uluslararasi Marmara Fen ve Sosyal Bilimler Kongresi*, Kocaeli, Türkiye, 2018, pp. 1769–1774.

[8] M. W. Sadik, H. M. El Shaer, and H. M. Yakot, “Recycling of agriculture and animal farm wastes into compost using compost activator in Saudi Arabia,” *Journal of International Environmental Application and Science*, vol. 5, no. 3, pp. 397–403, 2010.

[9] R. T. Haug, *The Practical Handbook of Compost Engineering*, Boca Raton, FL: Lewis, 1993.

[10] P. F. Strom, “Effect of the temperature on bacterial species diversity in thermophilic solid-waste composting,” *Appl. Environ Microb.*, vol. 50, no. 4, pp. 899–905, 1985.

[11] K. Suluk, I. Tosun, and K. Ekinci, “Co-composting of two-phase olive-mill pomace and poultry manure with tomato harvest stalks,” *Environmental Technology*, vol. 38, no. 8, pp. 923–932, 2017. doi: 10.1080/09593330.2016.1217279

[12] F. Sevik, I. Tosun, and K. Ekinci, “Composting of olive processing wastes and tomato stalks together with sewage sludge or dairy manure,” *International Journal Of Environmental Science And Technology*, vol. 13, pp. 1207–1218, 2016. doi: 10.1007/s13762-016-0946-y

2nd International Conference on Multidisciplinary Sciences and Technological Developments (ICMUSTED 2025)

December 12-15, 2025

Effect of Different Reactor Sizes on Mass and Volume Changes in the Composting Process

Fevzi Sevik[1], Kemal Suluk[2], Barbaros S. Kumbul[3], Kamil Ekinci[4]

[1]Vocational School of Health Services, Bingol University, Bingol, Türkiye
[2]Faculty of Engineering and Architecture, Mus Alparslan University Mus, Türkiye
[3]Rafet Kayis Faculty of Engineering, Alanya Alaaddin Keykubat University, Antalya, Türkiye
[4]Faculty of Agricultural Sciences and Technologies, Isparta University of Applied Sciences, Isparta, Türkiye
Corresponding author: Fevzi Sevik (e-mail: fsevik@bingol.edu.tr)

Abstract

In this study, the effects of different reactor sizes on mass and volume changes during the composting process were investigated. The composting process was carried out at the Compost Laboratory of Isparta University of Applied Sciences, and cattle manure (CM), quail manure (QM), and straw (S) were used as materials. The aim the study was to demonstrate the effect of reactor volume by using the same starting mixture in all reactors. The prepared mixture was composted in 50 L, 100 L, and 200 L reactors in three replicates for 45 days, with mixing applied on days 7, 14, and 28. The carbon/nitrogen (C/N) ratio of the mixture, initially determined to be 17.00, was found to decrease to 15.07 in the 50 L reactor and to 11.90 in the 200 L reactor at the end of the process. It was determined that as the reactor volume increased, organic matter decomposed more effectively, and therefore, the decrease in the C/N ratio increased. It was observed that mass and volume losses occurred throughout the composting process, and these losses varied directly with reactor size. The lowest mass loss occurred in the 50 L reactors with 10%, while the highest mass loss occurred in the 200 L reactors with 33%. Similarly, volume losses ranged from 34% to 48%, with the greatest volume loss occurring in the 200 L reactor. The results indicated that larger reactors provided a more effective composting process and a higher rate of organic matter degradation. This study demonstrated that reactor size is an important parameter affecting composting efficiency.

Keywords: Composting, Mass loss, Reactor, Volume effect, Volume loss

1. INTRODUCTION

The environmentally sustainable management of organic waste has become an increasingly important area with the strengthening of the circular economy approach. Composting is an environmentally friendly recycling method that stabilizes organic materials of plant and animal origin through microbial activity. Throughout the process, parameters such as temperature, moisture content, oxygen level, and organic matter composition determine decomposition kinetics and final product quality [1, 2].

Aeration rate and reactor shape are important factors in maintaining the thermophilic phase in the composting process [3]. The reactor volume used in composting systems directly affects fundamental process dynamics such as heat retention capacity, oxygen transfer, microbial activity level, and the continuity of the thermophilic phase. Changes in reactor size can significantly alter the mineralization rate of organic matter, the rate of temperature increase, and moisture management [4, 5]. This is a critical factor affecting performance indicators, particularly mass loss and volume reduction observed throughout the process.

The effect of reactor size on composting processes is an intricate topic influenced by several factors such as aeration, mixing, and heat management. Research has indicated that scaling up composting systems can lead to significant alterations in thermal dynamics, microbial activity, and substrate degradation efficiency. Larger reactors typically exhibit different heat generation and retention characteristics compared to smaller systems. For example, Jaschke and Schmidt-Baum demonstrated that the spatial correlation between heat production and aerobic digestion was significant in reactor design, especially for pilot-scale systems where heat recovery was critical for composting efficiency [6]. Such differences in thermal management can affect moisture retention and overall metabolic rates of microbial communities, impacting compost quality and maturation times.

This study aims to experimentally demonstrate the effects of different reactor volumes on mass losses, volume reductions, and temperature changes during composting processes. By holistically assessing the decisive role of

reactor size on decomposition kinetics, process efficiency, and stabilization trends [7], this study contributed to both academic and applied literature on scaling and process optimization.

2. MATERIAL AND METHOD

2.1. Composting Materials

cattle manure (CM), quail manure (QM), and straw (S) were used in the composting process. CM, QM, and S materials were obtained from Isparta University of Applied Sciences farms. The composting process was carried out in the Isparta University of Applied Sciences Compost Laboratory. The physical and chemical properties of the materials used in the study are given in Table 1.

Table 1. Physical-chemical analysis results of compost materials to be used in the study

Parameter	CM	QM	S
Moisture Content (MC) (%)	75.00	65.00	4.94
Organic Matter (OM) (%)	79.55	64.42	88.78
Total Carbon (TC) (%)	37.30	36.48	39.94
Total Nitrogen (TN) (%)	1.09	5.21	1.06
Carbon/Nitrogen (C/N) Ratio	34.38	7.00	37.93

2.2. Experimental Design and Composting System

A uniform starting mixture was prepared to investigate the effect of reactor volumes on the composting process. The proportions of CM, QM and S used in the compost mixture are given in Table 2. The initial mixture was composted in 50, 100 and 200 L reactors in three replicates. Information on reactors of three different sizes is given in Table 3. The composting process was carried out for 45 days and was mixed on days 7, 14, and 28.

Table 2. Compost mixture (dry matter basis)

Mixture	CM (%)	QM (%)	S (%)
Composting mixture	70	25	5

Table 3. Mixtures and reactor information

Mixtures	Reactor Volumes, L	Reactor No
M1	50	R1, R2, R3
M2	100	R4, R5, R6
M3	200	R7, R8, R9

The composting process was carried out in 50, 100, and 200 L aerobic reactors and the reactors used in the study are shown in Figure 1.

50 and 100 L volume reactors 200 L volume reactors

Figure 1. Reactors where the composting system is carried out

2.3. Physico-Chemical Analyses

During the composting process, reactor weights and reactor headspace were measured and recorded at the beginning, mixing, and end of the process. Throughout the study, two samples were taken from each material and mixture to determine their physical and chemical properties. Moisture content was determined by drying the samples in an oven at 70 ± 5 °C until constant weight was achieved, and organic matter analysis was determined by incinerating the dry samples at 550 °C for 4 hours [8]. Total carbon (C) and nitrogen (N) values were determined using an elemental analysis device (Vario MACRO CN).

3. RESULTS

In order to determine the effects of reactors of different sizes on the composting process, changes in C/N ratios, mass loss and volume reduction of the mixtures (M1, M2, M3) were examined.

3.1. C/N Changes

The C/N ratio generally indicated the degree of maturity of the compost [2]. In the composting process, a uniform mixture was prepared, and the C/N content of this mixture was initially determined to be 17.00. Mixture M1 was composted in a 50 L reactor, and the C/N ratio was 15.07, while this ratio was 11.90 in mixture M3, where the reactor volume was 200 L. The greatest change occurred in mixture M3 due to organic matter decomposition with increasing reactor volume (Figure 3). As organic matter decomposition progresses, the carbon content of the compost material decreased due to carbon loss, and the nitrogen content increased, resulting in a decrease in the C/N ratio at the end of the process [9].

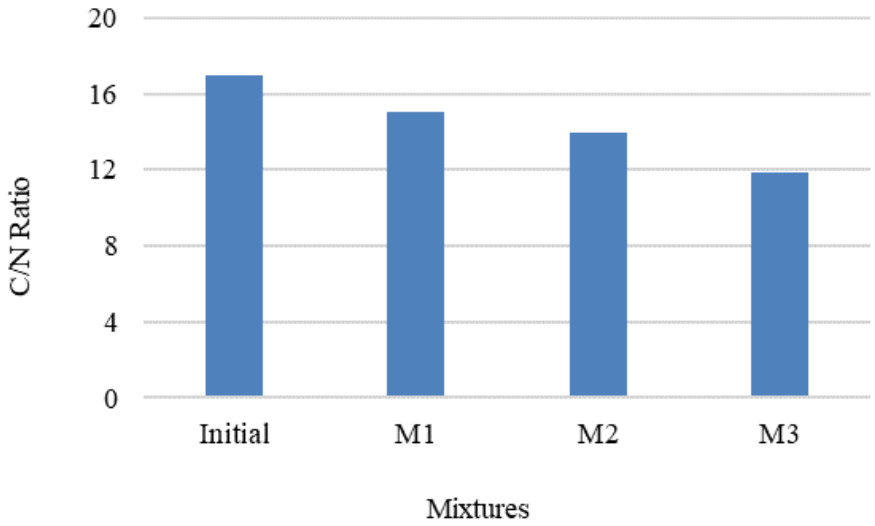

Figure 2. Initial and end of process C/N changes of the mixtures

3.2. Mass changes

During the composting process, the decomposition of organic waste resulted in a decrease in the mass and volume of the material within the reactor. This decrease varied depending on the type of waste in the reactor and the process operating conditions. This change was clearly observed during reactor mixing and at the end of the process.

It was observed that mass losses increased as reactor volumes increased from M1 to M3 within the mixtures (Figures 3–5). Furthermore, the reactor replicates for each mixture showed similar mass losses. The least mass loss occurred at 10% in mixture M1, while the greatest loss occurred at 33% in mixture M3. This suggested that composting and organic matter degradation were more effective in the 200 L reactors than in the 50 and 100 L reactors.

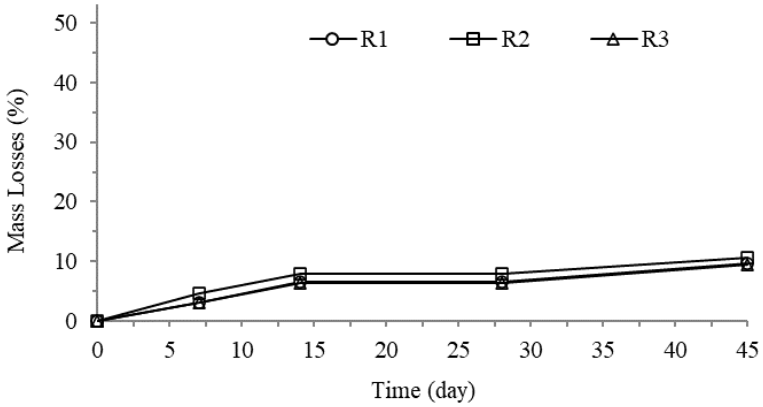

Figure 3. Mass changes of the reactors of the M1 mixture

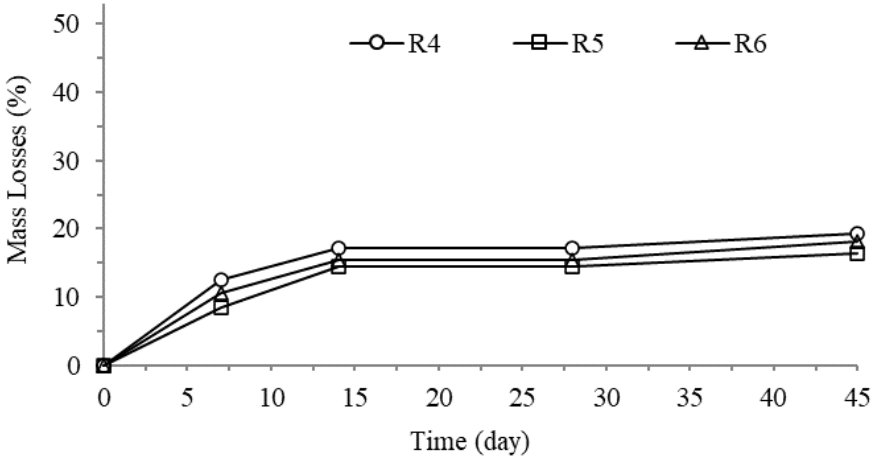

Figure 4. Mass changes of the reactors of the M2 mixture

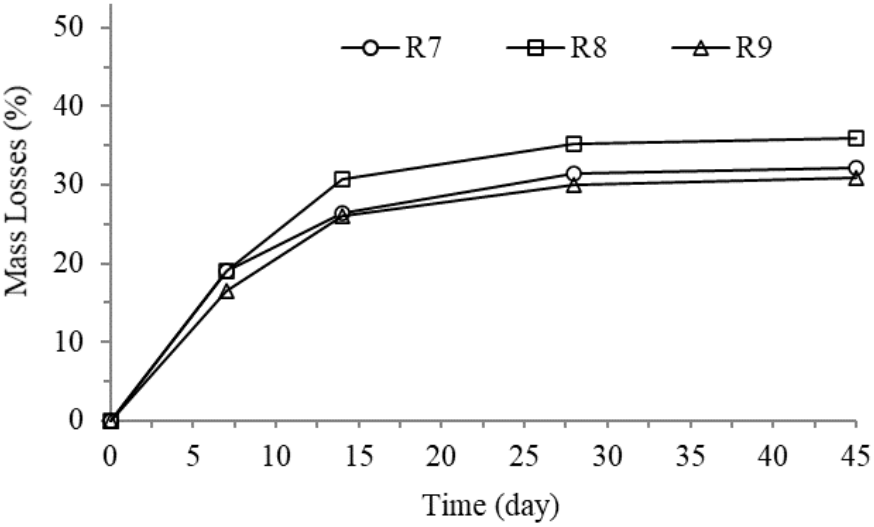

Figure 5. Mass changes of the reactors of the M3 mixture

3.3. Volume changes

During the composting process, volume losses also occured in the compost material along with mass losses. It was observed that volume losses increased with increasing reactor volumes from M1 to M3 within the mixtures (Figures 6–8). Furthermore, the reactor replicates of each mixture showed similar volume losses. The least volume loss occurred at 34% in mixture M1, while the greatest loss occurred at 48% in mixture M3. The changes in volume losses of the mixtures were similar to mass losses [10–12]. Breitenbeck and Schellinger [13] stated that the decrease in compost volume due to the decomposition of organic matter during composting may be due not only

to weight loss but also to the presence of smaller particles resulting from the deterioration of the structure of organic compounds.

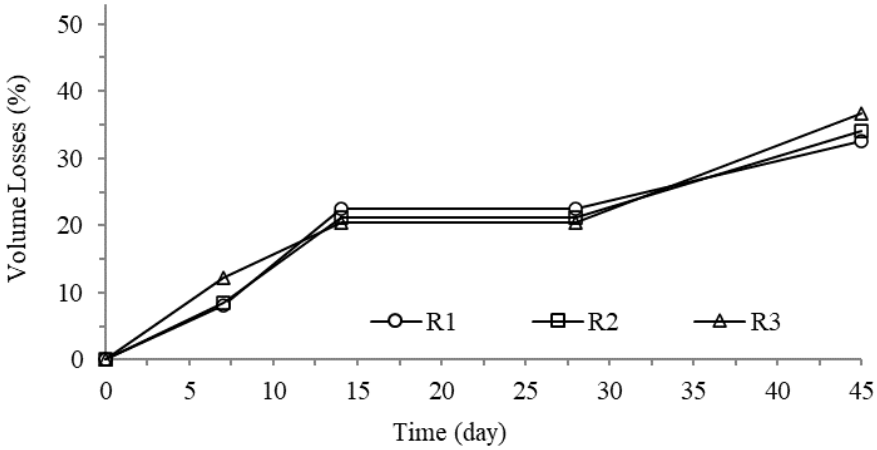

Figure 6. Volume changes of the reactors of the M1 mixture

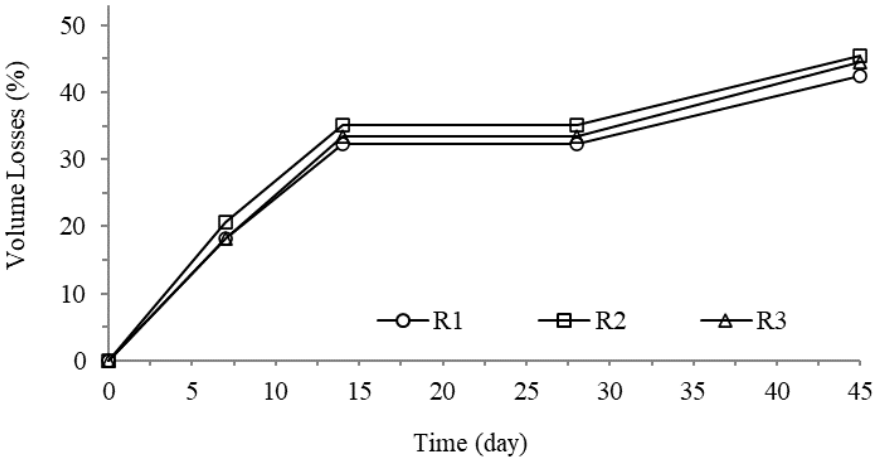

Figure 7. Volume changes of the reactors of the M1 mixture

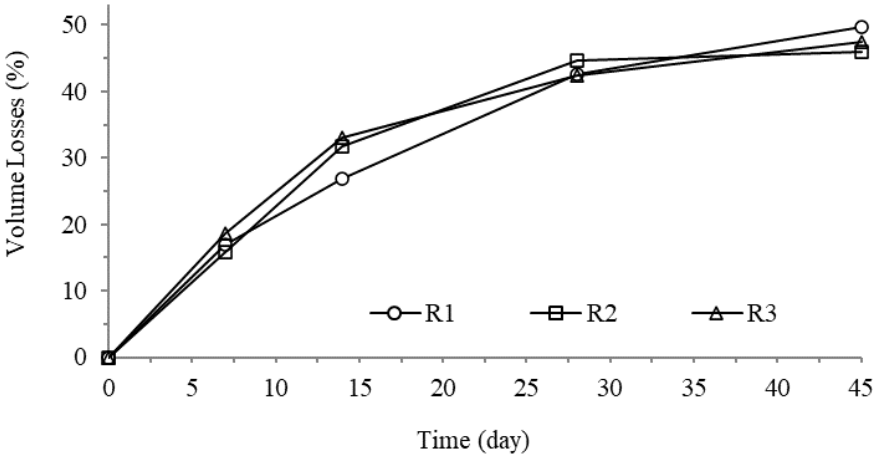

Figure 8. Volume changes of the reactors of the M1 mixture

4. CONCLUSION

In this study, the effects of a uniform starting mixture prepared using CM, QM, and S on composting performance in different reactor volumes (50, 100, and 200 L) were evaluated in detail. The findings clearly demonstrated that reactor size was a critical operational variable directly affecting mass and volume losses. At the end of the process, losses were found to systematically increased with increasing reactor volume, with the highest mass (33%) and

volume (48%) losses occurring in the 200 L reactor. The decrease in the C/N ratio from 17.00 to 15.07 in M1 and 11.90 in M3 supported the notion that organic carbon decomposition was more effective and compost maturity was achieved at a higher level in larger volume systems. Furthermore, the close correlation between repeated measurements across all reactors confirmed that the process was methodologically reliable, controlled, and reproducible. In this context, the study results demonstrated that reactor size was a key design parameter to consider when optimizing composting efficiency. Furthermore, it was recommended that different waste compositions and aeration strategies be incorporated into future studies to further understand process dynamics.

References

[1] R. T. Haug, *The Practical Handbook of Compost Engineering*, CRC Press, 1993.

[2] M. P. Bernal, J. A. Alburquerque, and R. Moral, "Composting of animal manures and chemical criteria for compost maturity assessment," *Bioresource Technology*, vol. 100, no. 22, pp. 5444–5453, 2009.

[3] W. Qasim, B. E. Moon, F. G. Okyere, F. Khan, M. Nafees, and H. T. Kim, "Influence of aeration rate and reactor shape on the composting of poultry manure and sawdust," *Journal of the Air and Waste Management Association*, vol. 69, no. 5, pp. 633–645, 2019.

[4] S. M. Tiquia and N. F. Y. Tam, "Fate of nitrogen during composting of chicken litter," *Environmental Pollution*, vol. 110, no. 3, pp. 535–541, 2000.

[5] A. S. Kalamdhad and A. A. Kazmi, "Effects of turning frequency on compost stability and some chemical characteristics in a rotary drum composter," *Chemosphere*, vol. 74, no. 10, pp. 1327–1334, 2009.

[6] N. Jaschke and T. Schmidt-Baum, "Heat recovery of compost reactors: Field study of operational behaviour, heating power and influence factors," *Ecological Chemistry and Engineering S*, vol. 28, no. 2, pp. 201–217, 2021.

[7] A. Gomez, "The evaluation of compost quality," *TrAC Trends in Analytical Chemistry*, vol. 17, no. 5, pp. 310–314, 1998.

[8] USCC, *Test Methods for the Examination of Composting and Compost (TMECC)*, Houston: Edaphos International, 2002.

[9] D. Raj and R. S. Antil, "Evaluation of maturity and stability parameters of composts prepared from agro-industrial wastes," *Bioresource Technology*, vol. 102, no. 3, p. 2868–2873, 2011.

[10] K. Suluk, I. Tosun, and K. Ekinci, "Co-composting of two-phase olive-mill pomace and poultry manure with tomato harvest stalks," *Environmental Technology*, vol. 38, no. 8, pp. 923–932, 2016.

[11] F. Sevik, I. Tosun, and K. Ekinci, "Composting of olive processing wastes and tomato stalks together with sewage sludge or dairy manure," *Int. J. Environ. Sci. Technol.*, vol. 13, pp. 1207–1218, 2016.

[12] F. Sevik, I. Tosun, and K. Ekinci, "The effect of FAS and C/N ratios on co-composting of sewage sludge, dairy manure and tomato stalks," *Waste Manag.*, vol. 80, pp. 450–456, 2018.

[13] G. A. Breitenbeck and D. Schellinger, "Calculating the reduction in material mass and volume during composting," *Compost Sci. Util.*, vol. 12, pp. 365–371, 2004.

Fungal Intoxications

Nesrin Cakici[1], Meltem Asik[2]

[1]Çanakkale Health Services Vocational School, Canakkale Onsekiz Mart University, Canakkale, Türkiye
[2]Department of Food Safety and Quality, Canakkale Onsekiz Mart University, Canakkale, Türkiye
Corresponding author: Nesrin Cakici (e-mail: ncakici17@gmail.com)

Abstract

This review article was designed to assess current knowledge on mushroom poisonings by reviewing academic studies published between 2015 and 2024. Studies indicate that Amanita phalloides and other Amanita species, particularly those containing amatoxins, are responsible for the majority of deaths due to mushroom poisoning. Studies conducted in various countries indicate that most cases occur as a result of consuming misidentified wild mushrooms, and that poisonings predominantly occur during the summer and autumn months. Cases reported in Türkiye between 2018 and 2023 indicate that mushroom poisoning is a significant public health problem in our country. The increase in the frequency of poisonings, coupled with increased seasonal rainfall, demonstrates the impact of climate change on mushroom ecology and toxicity risk. While early treatment, fluid and electrolyte support, and the use of agents such as silibinin and N-acetylcysteine are crucial, the lack of a specific antidote to amatoxins complicates clinical management. In conclusion, mushroom poisoning is an area of research that is likely to become even more important in the future due to food safety, public health awareness, and climate change. Effective education programs, control mechanisms and national treatment protocols should be developed.

Keywords: Fungal intoxications, Amatoxin, Hepatotoxicity, Food safety, Climate change

1. INTRODUCTION

Mushroom poisoning has become a growing public health problem worldwide due to increased trends in wild collection, climate change, and the inability to identify wild mushrooms. If a person collecting wild mushrooms is not an expert in this field, poisoning and death can occur. Even small amounts of some mushrooms are toxic enough to kill a person. Published scientifically based academic studies demonstrate the global prevalence of mushroom poisoning and, in particular, the role of Amanita species containing amatoxins in serious and fatal cases [1]. Amatoxins inhibit ribonucleic acid (RNA) polymerase II, halting messenger RNA (mRNA) synthesis, and this mechanism leads to progressive hepatocyte apoptosis and necrosis, resulting in the characteristic hepatotoxic picture [2, 3].

Research indicates that *Amanita phalloides*, *Amanita virosa*, and *Amanita verna* are responsible for most fatal hepatotoxic mushroom poisonings worldwide [2, 4]. Epidemiological studies in Turkey, China, Iran, and Europe indicate that the primary cause of poisoning is misidentification of wild mushrooms, and that the number of deaths increases significantly during the summer-autumn periods when fungal blooms increase [1, 5]. Cases reported in Türkiye parallel increased rainfall and climate change, demonstrating that regional poisonings are sensitive to climatic factors [4, 6]. Furthermore, pediatric populations are prone to more severe clinical presentations and complications due to lower body weight and delayed recognition of symptoms [7]. Clinically, amatoxin exposure follows a three-stage course: an initial gastroenteric phase, followed by a short latent period, and then liver and kidney failure [8, 9]. While therapeutic approaches such as silibinin and N-acetylcysteine (NAC) have shown clinical benefits, the current lack of a specific antidote is a significant limitation in patient management [10, 11]. Therefore, strengthening national treatment protocols and raising public awareness are critical to reducing morbidity and mortality from mushroom poisonings. In this context, this review comprehensively evaluates the available evidence regarding the epidemiology, toxicological mechanisms, clinical features, treatment approaches, and public health impacts of mushroom poisonings.

2. MATERIAL AND METHOD

A systematic literature search covering the period 2015–2024 was conducted in PubMed, Web of Science, and Google Scholar databases. Search terms were “mushroom poisoning, mushroom intoxication, amatoxin, Amanita phalloides, hepatotoxic mushroom, and wild mushroom consumption.” Inclusion criteria included (1) human

clinical studies, (2) outbreak reports, (3) studies addressing amatoxin mechanisms in the body, (4) pediatric and adult case series, and (5) review articles published in peer-reviewed journals. Publications published before 2015 (excluding pioneering articles), studies on non-toxic mushroom species, and non-scientific sources were excluded. Data from included studies were compiled to include the reported mushroom species, clinical findings, treatment approaches, and clinical outcomes.

3. FINDINGS

3.1. Epidemiology and Toxicology

Global epidemiological data indicate a seasonal increase from late spring to autumn in most outbreaks reported in China, Turkey, Iran, and Central Europe. This is consistent with the dependence of wild mushroom growth on climatic conditions [5, 12]. The rapid increase in annual case numbers in Türkiye has been reported to be associated with increased humidity, increased precipitation, and ecological changes, supporting the determinant effect of climatic factors on the incidence of poisoning [4, 6]. Furthermore, pediatric cases are at higher risk for severe clinical presentations and complications due to lower body weight and increased susceptibility to toxin load [7]. Etiologically, more than 95% of severe hepatotoxicity cases are associated with amatoxin-producing Amanita species, and species such as Amanita phalloides play a significant role in the global mortality burden [3]. Alpha-amanitin and beta-amanitin produced by these species inhibit RNA polymerase II, halting protein synthesis and leading to irreversible liver damage [2].

3.2. Clinical Findings and Treatment Approaches

Fungi can also cause toxic poisoning through the mycotoxins they produce in foods. Ochratoxins and aflatoxins, in particular, cause damage to the kidneys and liver. According to studies conducted to date, mushroom poisonings have been grouped into nine groups (Table 1) [7].

Table 1. Types of mushroom poisoning

No	Types
1	Phalloides syndrome (Amanita phalloides mushroom)
2	Orellanus syndrome
3	Giromitra syndrome
4	Muscarine syndrome (Amanita muscaria mushroom)
5	Pantherina syndrome (Amanita pantherina mushroom)
6	Psilocybin syndrome
7	Koprinus syndrome
8	Paxillus syndrome
9	Gastrointestinal syndrome

The most prominent symptoms of poisoning are nausea and vomiting, bloody and watery diarrhea, muscle cramps, and abdominal pain. In severe cases, severe symptoms such as liver failure, high fever, and coma may occur, and death occurs 2-4 days after ingestion. The clinical course of amatoxin-containing mushroom poisoning consists of three defined phases. The gastrointestinal phase, which begins 6-12 hours after poisoning, is characterized by severe nausea, vomiting, abdominal pain, and watery diarrhea. This phase can often be confused with foodborne infections, leading to a delay in early diagnosis [8]. The subsequent latent phase, although clinically suggestive of recovery due to symptomatic relief, is actually a critical period during which progressive cellular damage to the liver begins. The third phase, the kidney damage associated with liver failure, develops hepatocellular necrosis due to the toxin's inhibitory effect on RNA polymerase II. The clinical picture worsens with jaundice, coagulopathy, hypoglycemia, hepatic encephalopathy, and renal dysfunction [8, 9].

Mortality during this period can vary significantly depending on the timing of treatments administered and the patient's liver health. When examining treatment approaches, silibinin, which blocks amatoxin entry into the liver, plays a central role in modern clinical treatment and has been reported to improve survival in many studies [10], [11]. NAC, with its antioxidant and hepatoprotective properties, makes a significant contribution, especially as early supportive therapy [13]. In advanced cases, extracorporeal liver support systems are used to support toxin removal and metabolic balance; in cases of sudden and severe liver failure, liver transplantation remains the only

life-saving treatment option [6, 9]. Treatment success depends largely on the timing of clinical presentation and the effective implementation of multidisciplinary treatment approaches.

3.3. Case Examples

Case reports from Turkey and surrounding regions predominantly involve the consumption of Amanita phalloides due to misidentification with edible species. Clinical outcomes vary significantly depending on the length of stay and treatment protocols. Studies show that patients receiving early combination therapy with silibinin and NAC generally have better survival rates than those receiving late admission [4, 13, 14]. However, in cases of late diagnosis, where fulminant liver failure develops, mortality remains high unless liver transplantation is performed [6, 15]. Pediatric cases, in particular, are more susceptible to serious complications and require intensive follow-up [7]. The recurrence of poisonings in similar geographic areas suggests the need for intensified local education efforts.

For example, a 2019 case report from Türkiye documented the successful treatment of a patient with severe mushroom poisoning. The patient experienced gastrointestinal symptoms followed by a rapid increase in liver enzymes (aspartate transaminase (AST) and aka alanine aminotransferase (ALT)). The treatment protocol included silibinin (Legalon SIL) along with fluid therapy. The study emphasized that early initiation of silibinin treatment significantly contributes to normalization of liver function and recovery without the need for liver transplantation [13].

Similarly, a large retrospective analysis published in 2023, encompassing 204 patients, examined the clinical course of cyclopeptide (amatoxin) poisoning. This study confirmed that, although gastrointestinal symptoms are the most common initial finding, the severity of the outcome is entirely related to the degree of liver damage (hepatolysis). Researchers emphasized that the time between mushroom consumption and the start of treatment is the most critical prognostic factor [8].

In terms of pediatric cases, studies highlight that children are more vulnerable to the toxic effects of amatoxins due to their smaller body mass. Clinical observations suggest that pediatric patients require more aggressive supportive care and closer monitoring for encephalopathy compared to adults [7]. Collectively, these real-world examples demonstrate that although Amanita phalloides poisoning has a high lethal potential, timely multidisciplinary interventions using agents such as silibinin can be lifesaving.

3.4. Climate Change and Public Health

The impact of climate change on the increase in reported mushroom poisoning cases has been increasingly emphasized in recent years. Ecological factors such as increased rainfall, soil moisture, and temperature fluctuations favor the proliferation of many wild mushrooms, including the poisonous Amanita species, leading to an increase in poisoning cases, particularly during the summer and autumn months [1, 16]. Ecological modeling studies suggest that the geographic distribution of poisonous mushroom species may expand and their incidence may increase in the future, even in areas previously considered low-risk [12]. From a public health perspective, a significant portion of poisonings is attributed to lack of knowledge and misidentification of wild mushrooms, highlighting the critical importance of public education about poisonous species. There is no universal rule for determining whether a mushroom is poisonous. Commonly held rules for identifying poisonous mushrooms can be misleading. Therefore, there is no specific rule for mushroom poisoning; therefore, unidentified or suspicious mushrooms should not be eaten.

3. RESULTS

The increasing incidence of mushroom poisonings stems from the risks of inadvertent mushroom consumption, failure to recognize poisonous species, and alternative options other than cultivated mushrooms. Amanita phalloides, in particular, can have fatal consequences. Experts say that rapid intervention in this situation can save lives. Findings indicate that amatoxin-containing species such as Amanita phalloides, A. virosa, and A. verna cause severe hepatotoxicity and death in many regions of the world. Data from many regions indicate that consumption of misidentified wild mushrooms remains the most significant risk factor, with most cases occurring during the summer and fall seasons.

Clinically, amatoxin poisoning typically follows a three-stage course; early, nonspecific symptoms lead to delays in diagnosis and a significantly increased risk of death when liver failure develops. While therapeutic agents such as silibinin and NAC offer some clinical benefit, the lack of a specific antidote to amatoxins remains a significant

limitation. In advanced cases, in vitro liver support systems and liver transplantation are lifesaving options, but access to these interventions varies depending on regional and infrastructure conditions. Case studies demonstrate a wide geographic and clinical variability, with pediatric cases being more susceptible to toxicity, even rare species can present a severe course, and early medical intervention being crucial for survival. This highlights the need to promote accurate mushroom diagnosis in the community, raise public health awareness, and strengthen toxicity detection systems.

Taking all the findings together, mushroom poisoning is not only a toxicological problem but also a multifaceted area of study directly related to climate change, food safety, and public health. Therefore, developing comprehensive strategies to reduce future morbidity and mortality, establishing national treatment protocols, strengthening early detection and referral chains, expanding public education, and implementing climate change-adapted prevention policies are of paramount importance.

References

[1] Z. He, S. Wang, P. Tong, and Y. Li, "Wild mushroom poisoning: A multidisciplinary review." *Toxicology*, vol. 498, art. no. 153378, 2024.

[2] T. Kayes, A. R. Ali, and M. Hossain, "Amanita phalloides-associated liver failure: Mechanisms and management." *International Journal of Molecular Sciences*, vol. 25, no. 4, art. no. 2145, 2024.

[3] X. Yin, A. A. Yang, and J. M. Gao, "Mushroom toxins: Chemistry and toxicology." *Journal of Agricultural and Food Chemistry*, vol. 67, no. 21, pp. 5993–6007, 2019.

[4] D. T. Gokce, D. Ari, N. Ata, H. Gokcan, R. Idilman, M. M. Ulgu, et al., "Mushroom intoxication in Türkiye: a nationwide cohort study based on demographic trends, seasonal variations, and the impact of climate change on incidence," *The Turkish Journal of Gastroenterology*, vol. 36, no. 1, art. no. 61, 2025.

[5] H. Li, H. Zhang, Y. Zhang, K. Zhang, J. Zhou, Y. Yin, et al., "Mushroom poisoning outbreaks—China, 2019," *China CDC Weekly*, vol. 2, no. 2, art. no. 19, 2020.

[6] M. Altuntas, O. Balci, and E. Gunes, "Predictors of poor outcome in mushroom poisoning," *Anatolian Journal of Emergency Medicine*, vol. 4, no. 2, pp. 51–57, 2021.

[7] M. Tobias, G. Hall, and M. Patel, "Diagnosis and management of Amanita phalloides toxicity," *Cureus*, vol. 16, no. 5, pp. 1–12, 2024.

[8] J. Lecot, M. Cellier, A. Courtois, D. Vodovar, G. Le Roux, A. Landreau, et al., "Cyclopeptide mushroom poisoning: A retrospective series of 204 patients," *Basic Clin Pharmacol Toxicol.*, vol. 132, no. 6, pp. 533–542, 2023.

[9] E. Kieslichova, S. Frankova, M. Protus, D. Merta, E. Uchytilova, J. Fronek, et al., "Acute liver failure due to Amanita phalloides poisoning: therapeutic approach and outcome," *Transplant Proc.*, vol. 50, no. 1, pp. 192–197, 2018.

[10] G. Lacombe and M. St-Onge, "Silibinin in suspected amatoxin-containing mushroom poisoning," *Emergency Medicine Journal*, vol. 33, no. 1, pp. 76–77, 2016.

[11] M. E. Mullins, "Milk thistle therapy for amatoxin-induced hepatic failure," *Chest*, vol. 148, no. 3, pp. 632–641, 2015.

[12] B. K. Matin, H. Jalili, and L. Falahi, "Economic burden and epidemiology of cyclopeptide mushroom outbreak in Iran," *BMC Health Services Research*, vol. 22, art. no. 1456, 2022.

[13] I. Yildirim, A. Sahin, O. Baran, M. C. Arar, and H. G. Sarikaya, "Successful treatment of mushroom poisoning with Silybin: A case report," *Turkish Journal of Intensive Care*, vol. 17, no. 3, pp. 173–176, 2019.

[14] O. Tatlı and A. A. Altinel, "Mushroom poisoning: An updated review," *Turkish Journal of Emergency Medicine*, vol. 25, no. 1, pp. 10–16, 2025.

[15] F. Celik, S. Ataseven, and M. Aydin, "Outcomes of hepatotoxic mushroom poisoning," *Turkish Journal of Gastroenterology*, vol. 32, no. 7, pp. 601–608, 2021.

[16] A. Patra, K. Singh, and R. Sharma, "Mycetism: A neglected and challenging emergency," *Toxicology*, vol. no. 481, art. no. 153354, 2022.

2nd International Conference on Multidisciplinary Sciences and Technological Developments (ICMUSTED 2025)

December 12-15, 2025

The Trifid Incisive (Nasopalatine) Canal: A Rare Variation of the Maxilla

Burhan Yarar[1], Melike Tasci[1]

[1]Anatomy Department, Medicine Faculty, Ataturk University, Erzurum, Türkiye
Corresponding author: Burhan Yarar (e-mail: drburhan25@gmail.com)

Abstract

The incisive, or nasopalatine, canal is located in the midline of the anterior maxilla, just behind the incisors. The palatal opening of this canal is known as the incisive foramen. The part of the canal that opens into the nasal cavity is called Stenson's foramen, forming two canals on either side of the nasal septum. The nasopalatine nerve and the terminal branch of the nasopalatine artery pass through this canal, which contains fibrous and adipose tissue, as well as minor salivary glands. This study identified a trifid incisive canal in a dry maxilla without age or sex records, which was found in the bone collection of our university's anatomy laboratory. The measurements were taken using a digital calliper. The canal started as a single opening on the palatal side, extending 2.97 mm upwards to create three separate canals, which were divided by a Y-shaped septum. These three separate channels, extending 6.92 mm upward (total channel length 9.89 mm), opened into the nasal cavity as three separate foramina. The foramina were symmetrically positioned on the right and left sides at the anterior, and there was a single foramen on the midline at the posterior. On the nasal opening side of the canal, the nasal crista was observed to have disappeared. The transverse diameter of the palatal opening was measured at 4.45 mm, while the sagittal diameter was measured at 4.76 mm. At the nasal opening, the transverse diameter of the right anterior, left anterior and posterior foramen were 1.03, 1.13, and 1.20 mm; the sagittal diameter of the right anterior, left anterior and posterior foramen were 1.36, 1.59, and 0.95 mm, respectively. Understanding the morphological and morphometric characteristics of this canal is crucial for procedures such as local anaesthesia and dental implant placement in the anterior maxilla.

Keywords: Maxilla, Incisive canal, Trifid canal, Variation

FELVERA: Development of an Web and Mobile Application for Animal Welfare

Numan Tugrul Ertugrul[1], Irem Baysal[1], Semanur Cicek[1], Vildan Sozen[1], Zuhal Aslan Akyol[1]

[1]Department of Computer Technologies, Cide Rifat Ilgaz Vocational School of Higher Education, Kastamonu University, Kastamonu, Türkiye
Corresponding author: Irem Baysal (e-mail: ibaysal250@gmail.com)

Abstract

The main goal of this study is to facilitate the pet adoption process in a digital environment, to be able to regularly monitor animal health, and to create a community among animal lovers. The project was developed using a user-centered design approach. Both the website and mobile application were created using the Flutter framework, and user and animal information was securely managed through the Firebase database. The developed application was evaluated in closed beta tests with a group of 20 users from a sample of pet owners and animal lovers across Turkey. User feedback forms, in-app interaction logs, and system logs were used to collect data. The application is available on the App Store, Google Play, and felvera.com.tr. The tests showed that users were able to effectively use features such as profile management, adoption applications, and health tracking. Thanks to the project, users can both regularly monitor the health status of animals and communicate safely with potential owners. In contrast to the scattered information and lack of reliable sources experienced in traditional adoption methods, this gap is filled by combining adoption, health tracking, lost animal reports, and social interaction functions on a single platform. Furthermore, social awareness is raised through social responsibility campaigns such as “Bring Your Pet Home”. It has been demonstrated that the developed platform offers a comprehensive and user-friendly solution for animal welfare. This enables more realistic solutions to be produced by facilitating comparisons.

Keywords: Animal adoption, Animal welfare, Health monitoring, Social responsibility

2nd International Conference on Multidisciplinary Sciences and Technological Developments (ICMUSTED 2025)

December 12-15, 2025

Smart Platform for Book Swapping, Sales, and Social Interaction

Numan Tugrul Ertugrul[1], Samet Sargin[1], Mehmet Yasa[1], Umut Temel[1], Zuhal Aslan Akyol[1]

[1]Department of Computer Technologies, Cide Rifat Ilgaz Vocational School of Higher Education, Kastamonu University, Kastamonu, Türkiye
Corresponding author: Samet Sargin (e-mail: ssametsargin@gmail.com)

Abstract

The main purpose of the study is to enhance the reading experience of book enthusiasts and increase accessibility. The aim is to develop a social digital platform that facilitates book purchasing and exchange, supports sustainability with personalised recommendations. User-centred design (UCD) principles and Agile methodology were applied together during the application development process. Flutter was chosen to provide cross-platform support for mobile and web versions, and Firebase integration was implemented for data security. Prototype forms and user surveys were used as primary data collection tools to test the application's functionality. In the first phase of the project, the infrastructure and user interface were successfully completed. Feedback from volunteer users revealed that the book exchange system and personalised recommendation engine were particularly popular. Tests showed that the exchange system, recommendation engine, and social interaction areas were functional. Thus, a prototype that met the project objectives was developed and brought to the delivery stage. This application offers an economical solution to rising book prices, supports environmental sustainability, and creates a dynamic reading ecosystem through personalised algorithms and social interaction features.

Keywords: Library application, Book exchange, Personalised recommendations, Sustainability, Social interaction

2nd International Conference on Multidisciplinary Sciences and Technological Developments (ICMUSTED 2025)

December 12-15, 2025

Library Automation System with Automatic Penalty and Email Notification Module

Zuhal Aslan Akyol[1], Numan Tugrul Ertugrul[1], Osman Mert Ergin[1]

[1]Department of Computer Technologies, Cide Rifat Ilgaz Vocational School of Higher Education, Kastamonu University, Kastamonu, Türkiye
Corresponding author: Osman Mert Ergin (e-mail: osmanmert_ergin@outlook.com)

Abstract

This study presents a desktop-based library automation system developed using C# and Microsoft SQL Server to improve operational efficiency in small and medium-sized libraries. The system provides complete create, read, update, and delete (CRUD) functionality for managing books, members, and borrowing records, thereby minimizing manual tracking efforts. Its most innovative component is an integrated module that automatically calculates penalties for overdue books and sends automated email notifications to users. This automation reduces staff workload, minimizes human error, and enhances overall resource management. The system was tested in a controlled prototype environment and demonstrated reliable performance in penalty calculation and email delivery. Future enhancements include the development of web and mobile interfaces, barcode/quick response (QR) code integration, and proactive reminder notifications for upcoming due dates.

Keywords: Library automation, C#, SQL server, CRUD, Penalty calculation, Email notification

2nd International Conference on Multidisciplinary Sciences and Technological Developments (ICMUSTED 2025)

December 12-15, 2025

AI-Based Risk Prediction Model for Airport Ground Operations

Onur Arslan[1]

[1]Faculty of Applied Sciences, Istanbul Okan University, Istanbul, Türkiye
Corresponding author: Onur Arslan (e-mail: onur.arslan@okan.edu.tr)

Abstract

Ground operations constitute one of the most dynamic and risk-intensive components of the civil aviation system. Apron areas are characterized by high traffic density, restricted maneuvering zones, time-sensitive workflows, and simultaneous interactions between aircraft, ground support equipment, and personnel. Although safety management systems (SMSs) provide structured procedures for hazard identification and risk mitigation, safety-related events are still predominantly evaluated after their occurrence, limiting the effectiveness of proactive intervention strategies. Artificial intelligence (AI) technologies offer a significant opportunity to improve anticipatory safety management by analyzing historical and real-time operational data to predict the likelihood of hazardous situations before they materialize. While AI applications have been widely explored in domains such as flight delay prediction, aircraft maintenance optimization, and air traffic flow management, the use of AI for predicting risk in airport ground operations remains relatively underexplored. This study proposes a four-stage conceptual framework for integrating AI-based risk prediction models into airport ground operations: (1) operational data collection and digitalization, (2) preprocessing and identification of critical risk variables, (3) implementation of machine learning–based prediction systems, and (4) integration of predictive outputs into SMS-informed decision-making processes. The model aims to support early identification of high-risk scenarios, reduce apron-related incidents, and enhance situational awareness among operational managers. The originality of this study lies in presenting one of the first systematic conceptual approaches specifically developed for AI-supported ground safety management.

Keywords: Ground operations, Aviation safety, Artificial intelligence, Risk prediction, SMS

1. INTRODUCTION

Ground operations represent a critical phase of the aviation system, encompassing aircraft handling, towing, fueling, baggage operations, catering services, and vehicle movements around the apron. This operational environment is characterized by narrow maneuvering spaces, simultaneous task execution, intensive human–equipment interaction, and strict time constraints, all of which significantly increase the probability of safety incidents.

Apron operations are therefore prone to various types of risks, including ground vehicle collisions, personnel injuries, wingtip strikes, jet blast incidents, and ground support equipment damage. These events may not only disrupt flight operations but also pose serious threats to human life and airport infrastructure reliability [1]. Safety management systems (SMSs) have been implemented globally to mitigate such risks through structured processes including hazard identification, risk assessment, safety assurance, and safety promotion. While SMS provides a systematic framework for risk control, many aviation organizations still rely heavily on reactive safety approaches where hazards become visible only after an undesired event has occurred [2].

In recent years, artificial intelligence (AI) has demonstrated significant potential in aviation-related applications such as predictive maintenance, flight delay forecasting, air traffic flow optimization, and safety performance analysis [3, 4]. However, despite these advances, the application of AI in predicting operational risks specifically within airport ground operations remains limited and underexplored in academic literature.

Given the complexity and dynamic nature of apron environments, there is a critical need for proactive, data-driven tools capable of identifying high-risk situations before incidents occur. AI-based prediction models can analyze large volumes of operational data to detect hidden patterns and generate early warnings for potential hazards, thus enhancing decision-making processes and improving situational awareness [3, 5]. This study addresses this gap by proposing a conceptual AI-based risk prediction model tailored specifically for airport ground operations. The

proposed framework aims to support proactive safety management by forecasting potential risk scenarios and integrating predictive insights directly into SMS decision-making mechanisms.

2. MATERIALS AND METHODS

This study adopts a conceptual modeling approach to develop a structured framework for AI-based risk prediction in airport ground operations. Instead of performing empirical data analysis, the research focuses on integrating theoretical knowledge, existing aviation safety literature, and artificial intelligence methodologies to propose a systematic and adaptable prediction model.

The conceptual framework is constructed through comprehensive review and synthesis of previous studies related to aviation safety management, risk assessment techniques, and AI-supported predictive systems [2, 3]. This approach enables the identification of critical elements required for effective risk prediction and supports the development of a generalized model applicable to different airport environments.
The methodology of the study is based on four sequential stages:

1. Reviewing international safety reports and operational guidelines published by organizations such as International Civil Aviation Organization (ICAO) and International Air Transport Association (IATA) to identify common apron safety risks and operational challenges [5].
2. Examining existing machine-learning and predictive analytics techniques applied in aviation safety studies to determine suitable model structures and predictive capabilities [1, 3].
3. Identifying potential operational risk variables influencing apron safety, including human factors, operational density, environmental conditions, equipment status, and time pressure indicators [4].
4. Structuring a four-stage AI-supported risk prediction model that integrates data-driven analysis with SMS decision-making principles.

The proposed methodology provides a theoretical foundation for future empirical research and allows aviation stakeholders to evaluate potential implementation strategies for AI-based safety prediction systems in apron environments. The conceptual nature of the study enables flexibility for adaptation according to airport size, operational complexity, and technological readiness.

This structured approach ensures that the proposed model aligns with both established SMS principles and contemporary AI techniques, contributing to the advancement of proactive safety management practices in airport ground operations.

3. RESULTS

The proposed AI-based risk prediction model for airport ground operations consists of four sequential and interconnected stages designed to support proactive safety management. This framework enables the systematic transformation of raw operational data into meaningful risk predictions that can be operationally utilized by safety managers and ground supervisors.

3.1. Stage 1: Data Collection and Digitalization

Airport ground operations generate large volumes of heterogeneous data obtained from various internal and external sources. These include vehicle GPS records, aircraft turnaround logs, weather data, equipment usage records, hazard reporting systems, and near-miss documentation. The centralization and digitalization of such data are critical for enabling effective AI-based analysis and real-time risk monitoring [3].

3.2. Stage 2: Data Preprocessing and Variable Identification

In this stage, raw data undergo preprocessing procedures such as data cleaning, normalization, handling missing values, and categorization of hazard types. Additionally, significant operational risk variables are extracted and structured to enhance model accuracy. These variables include human-factor indicators, operational density measures, environmental conditions, equipment status, and temporal performance constraints [4].

Table 1 presents the key operational risk variables considered in the conceptual model and their primary impact areas in airport ground safety management.

Table 1. Key operational risk variables in airport ground operations

Risk Category	Examples of Variables	Impact Area
Human factors	Fatigue, workload, distraction	Operator performance
Operational density	Number of vehicles, aircraft proximity	Collision probability
Environmental factors	Weather, visibility, surface conditions	Situational awareness
Equipment condition	Maintenance status, equipment age	Mechanical reliability
Time pressure	Turnaround duration, schedule delay	Decision accuracy, punctuality

This categorization enables the model to prioritize risk-sensitive zones and identify critical variables influencing incident probability.

In this stage, machine-learning algorithms such as random forest, support vector machines (SVMs), gradient boosting, and neural networks are applied to the processed datasets. These algorithms generate risk indices and probability scores for specific safety threats, including ground vehicle collisions, equipment malfunction, congestion hazards, and human error-induced incidents [1, 3].

The output of the AI module supports the identification of high-risk areas and enables step-by-step risk evaluation for proactive intervention planning.

3.3 Stage 3: AI-Based Risk Prediction Module

In this stage, machine-learning algorithms such as random forest, SVMs, gradient boosting, and neural networks are applied to the processed datasets. These algorithms generate risk indices and probability scores for specific safety threats, including ground vehicle collisions, equipment malfunction, congestion hazards, and human error-induced incidents [1, 3].

The output of the AI module supports the identification of high-risk areas and enables step-by-step risk evaluation for proactive intervention planning.

3.4. Stage 4: Integration into SMS Decision-Making

The predicted risk scores are integrated into existing SMS mechanisms, informing ramp supervisors and safety management teams through real-time dashboards, alerts, and digital reporting systems. This integration allows decision-makers to implement proactive safety strategies such as redistributing personnel, adjusting turnaround schedules, enhancing monitoring protocols, and reinforcing safety barriers in high-risk zones [2]. Figure 1 illustrates the conceptual flow of the proposed AI-based risk prediction model, demonstrating the transformation process from raw data acquisition to integrated safety decision support.

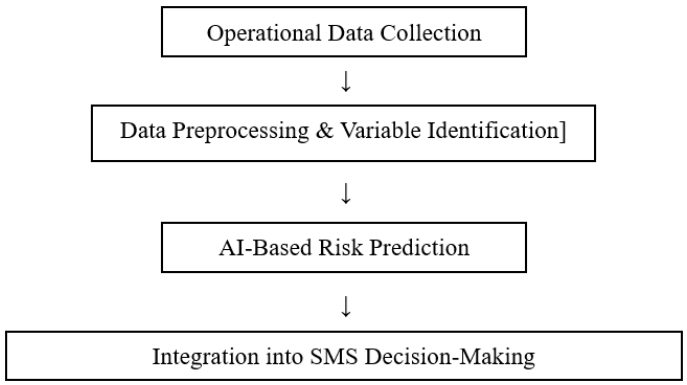

Figure 1. Conceptual flowchart of the AI-based risk prediction model for airport ground operations

The Figure 1 visualizes how predictive outputs are systematically embedded into operational safety processes, enhancing situational awareness and facilitating evidence-based safety decisions.

3.5. Operational Implementation Framework

The proposed model suggests the incorporation of AI modules into existing airport operational control centers.

Supervisors can access real-time risk maps, predictive charts, and historical trend analyses to support decision-making. This implementation framework enhances transparency and accountability.

3.6. Limitations and Future Implications

The primary limitations of the model include dependency on data accuracy, technological infrastructure readiness, and workforce digital literacy. Future research should validate the framework with real operational datasets and assess its performance under varying operational conditions.

4. DISCUSSION

The conceptual AI-based risk prediction model proposed in this study integrates artificial intelligence techniques with SMS principles to strengthen proactive safety strategies in airport ground operations. Unlike traditional reactive safety approaches, which focus on post-incident analysis, the proposed framework emphasizes early risk detection and preventive intervention planning.

The integration of predictive analytics into apron operations offers substantial benefits, including improved hazard visibility, enhanced situational awareness, and optimized decision-making processes. By identifying high-risk conditions in advance, airport operators can take preventive actions such as reallocating resources, redesigning operational workflows, and reinforcing safety protocols in critical zones [3, 5].

Furthermore, the adaptability of the proposed model allows it to be implemented across varying airport sizes and operational complexities. However, its effectiveness is directly influenced by data quality, system interoperability, and organizational readiness to adopt digital safety solutions. Limitations also include reliance on the availability of real-time data and the need for workforce training in AI-supported decision systems [3, 4].

Despite these limitations, the proposed framework represents a significant step toward transforming apron safety from a reactive to a predictive and intelligence-driven approach. Future empirical validation using real operational data will enable further optimization and benchmarking of model performance.

5. CONCLUSION

This study proposes a conceptual AI-based risk prediction model specifically designed for airport ground operations. The four-stage framework systematically integrates data collection, preprocessing, artificial intelligence-based prediction, and SMS decision-making mechanisms to enhance proactive safety management. The proposed model contributes to the existing aviation safety literature by introducing a structured approach for predicting operational risks before they manifest as incidents or accidents. With advancing digitalization and increasing availability of operational data, AI-supported systems provide strong potential for improving safety performance and minimizing operational disruptions in apron environments. Future research should focus on applying the model to real-world airport datasets, evaluating algorithm performance, and refining variable selection to enhance prediction accuracy. The framework may also serve as a foundation for the development of integrated digital safety monitoring platforms in modern airport management systems.

References

[1] J. Wang and H. Xu, “Predictive analytics for ramp safety,” *Safety Science*, vol. 118, pp. 304–312, 2019.

[2] A. J. Stolzer, C. D. Halford, and J. Goglia, *Safety Management Systems in Aviation*, Ashgate Publishing, 2015.

[3] Y. Li and X. Chen, “Machine learning applications in aviation safety analysis,” *Journal of Air Transport Management*, vol. 89, pp. 101–118, 2020.

[4] L. Zhang and Q. Zhao, “Artificial intelligence in airport operations: A review,” *Aerospace Science and Technology*, vol. 108, pp. 106–121, 2021.

[5] S. S. Dawson and C. H. Michler, “Afforestation, restoration and regeneration – Not all trees are created equal,” *Journal of Forestry Research*, vol. 25, no. 1, pp. 3–20, 2014.

2nd International Conference on Multidisciplinary Sciences and Technological Developments (ICMUSTED 2025)

December 12-15, 2025

Solo Travel Research: A Bibliometric Analysis

Yeliz Guler[1]

[1]Tourism Management, Dokuz Eylul University, Izmir, Türkiye
Corresponding author: Yeliz Guler (e-mail: yelizglr@gmail.com)

Abstract

With the increase in demand for experience-oriented tourism and the effect of individualization, solo travel has gained a place in the tourism market. With the effect of growing demand, studies on solo travel are also increasing in the same direction. When the literature is examined, it has seen that there is a remarkable increase in the studies conducted between 1996 and 2025, but there is no comprehensive bibliometric mapping study for solo travel research. This study aims to fill the gap in the literature by presenting a quantitative review of the "solo travel research" literature. The data set of the study was obtained from the Web of Science Core Collection database using the keyword "solo travel" and 110 articles were reached. The research design is bibliometric analysis. Data were analyzed by the VOSviewer program, focusing on annual publication counts, country and institution-specific productivity, authorship, and co-authorship networks. Among the findings, the first study on solo travel was conducted in 1996 and the number of studies published since 2010 has increased, reaching 28 studies per year by 2025. The United States is the country with the highest number of studies (22) and Australia is the country with the highest number of citations (941). Griffith University (Australia) is the most productive university and has the highest number of citations, with 10 studies and 406 citations. The author with the most citations, studies, and highest link strength is Yang Elaine Chiao Ling. The keyword analysis revealed that the most frequently used keywords were "solo travel," "gender," "solo female travel," and "motivation." This study presents the contribution of solo travel research to the literature by year, by country, by university and by author.In this context, the establishment of new inter-institutional collaborations provides resources for the development of new co-authorship networks and future research.

Keywords: Solo travel, Solo travel research, Tourism research

2nd International Conference on Multidisciplinary Sciences and Technological Developments (ICMUSTED 2025)

December 12-15, 2025

Determining Green Transformation Strategies in Businesses Using the SWARA Method

Sadrettin Codur[1], Ahmet Cem Esenlikci[1]

[1]Property Protection and Security, Karadeniz Technical University, Trabzon, Türkiye
Corresponding author: Sadrettin Codur (e-mail: sadrettincodur@ktu.edu.tr)

Abstract

Green economy, which lies at the heart of sustainable development goals, is defined as a low-carbon, resource-efficient economic system that enhances social welfare, highlighting the importance of energy, water, waste management, and biodiversity-based practices. The increasing climate crisis in recent years, fluctuations in fossil fuel prices, carbon regulation mechanisms, and policy frameworks such as the European Union (EU) Green Deal have made it inevitable for businesses to turn to sustainable practices. In this context, organizations need a multidimensional assessment process to identify the most suitable option among various green practices with different environmental and economic impacts. Accordingly, this study utilizes the literature to identify six criteria (green innovation and dynamic capabilities, energy efficiency and resource management, green supply chain and logistics management, legal compliance and corporate governance, social responsibility and stakeholder participation, economic sustainability and operational efficiency) were selected from the literature, and the step-wise weight assessment ratio analysis (SWARA) method, which evaluates the relative importance difference between the criteria based on expert opinions, was preferred as a multi-criteria decision-making method. The results obtained from the analysis showed economic sustainability and operational efficiency as the most important criteria, while social responsibility and stakeholder participation were criteria with relatively lower importance compared to the others.

Keywords: Green economy, Sustainability, Multi-criteria decision-making method, SWARA

1. INTRODUCTION

Increasing environmental issues, climate change, resource scarcity, and societal expectations on a global scale have made it imperative for businesses to adopt sustainability-based strategies. Businesses are evaluated not only on their economic performance but also on their environmental and social impacts. This transformation has reshaped the factors that determine the competitiveness of businesses and made sustainability-focused decision-making processes multidimensional. Therefore, the evaluation of practices developed within the scope of the green economy requires a holistic approach that considers not only environmental impacts but also a broader framework, including innovation capacity, corporate competencies, social responsibility, and economic sustainability. In this context, the six criteria evaluated in this study stand out as factors determining business performance in modern sustainability literature.

Green innovation and dynamic capabilities (K1), one of the key determinants of green transformation, represent businesses' capacity to adapt to environmental changes and their ability to develop innovative sustainability solutions. Teece (2018) states that dynamic capabilities strengthen a company's capacity to produce technological innovations and its strategic adaptability to environmental uncertainties. Green innovation encompasses many areas, such as low-carbon technologies, eco-friendly product designs, and sustainable process improvements, and directly affects companies' long-term competitiveness [1]. Recent studies show that green innovation capacity significantly improves both environmental and financial performance [2].

The second fundamental component of a sustainable business model, energy efficiency and resource management (K2), encompasses the efficient use of natural resources, energy-saving practices, and circular economy principles. Energy efficiency and resource management are fundamental elements in ensuring sustainability within an organization. Businesses can significantly enhance their sustainability efforts by optimizing energy consumption and managing resources effectively. Implementing energy-efficient technologies and renewable energy sources, optimizing resource use, and adopting circular economy principles are critical to reducing environmental impact and achieving sustainability goals [3]. Furthermore, increased efficiency in resource use plays a key role in reducing greenhouse gas emissions and lowering operating costs.

Another key criterion in sustainability-based decision-making is green supply chain and logistics management (K3), which aims to minimize the environmental impact of all processes from raw material procurement to distribution. It is stated that green supply chain practices both reduce the carbon footprint and improve environmental risk management in business processes. Carbon-neutral logistics, environmentally friendly purchasing, the use of recyclable packaging, and sustainable modes of transport are important components of this area. Green logistics is becoming increasingly critical in terms of international competitiveness and is decisive in companies' environmental certification processes [4].

The corporate suitability of sustainability practices, legal compliance and corporate governance (K4) criteria play a significant role in terms of third-party expectations and international regulations. Today, businesses' compliance with environmental regulations and corporate governance standards is seen as an integral part of sustainable strategies. Environmental legislation, carbon reporting requirements, waste management regulations, and international policy frameworks such as the European Union (EU) Green Deal encourage businesses to act more responsibly from an environmental perspective. It is noted that environmental governance practices directly affect corporate reputation, investor confidence, and long-term sustainability performance. Corporate governance requires businesses to implement their environmental policies in a transparent, accountable, and regulation-compliant manner [5].

Another dimension that is increasingly coming to the fore in sustainability efforts is social responsibility and stakeholder engagement (K5). Social impact, employee welfare, local community contribution, and stakeholder communication constitute the social dimension of sustainable development. Parmar et al. (2010) emphasize that stakeholder theory has become an integral part of decision-making processes in current sustainability practices and that businesses' environmental performance is closely monitored by social stakeholders [6]. Recent research shows that social responsibility performance plays a decisive role in businesses' long-term competitiveness and brand value [7].

Finally, the economic sustainability and operational efficiency (K6) criterion, which forms the economic pillar of sustainability approaches, encompasses the objectives of creating cost advantages, optimizing resource use, increasing competitiveness, and ensuring long-term financial stability. Hart and Dowell (2019) demonstrate that environmental sustainability practices do not negatively affect economic performance; on the contrary, they provide long-term efficiency gains [8]. Therefore, economic sustainability is a critical assessment dimension in terms of the applicability of green strategies and the competitive advantage of businesses.

Each of these six criteria represents a different dimension of business sustainability performance and provides a perspective for determining strategic priorities. Therefore, determining the relative importance of the criteria based on expert opinions makes the multi-criteria decision-making (MCDM) process more reliable. The step-wise weight assessment ratio analysis (SWARA) method offers an effective approach to prioritizing green economy applications by enabling step-by-step assessment of the differences in importance between criteria. This study aims to develop a decision support model for sustainability performance assessments by weighting the six criteria using the SWARA method.

2. MATERIAL AND METHOD

The purpose of the SWARA (Step-wise Weight Assessment Ratio Analysis) method is to rank the criteria from the most to the least important. It has been applied in various research contexts across many studies. The following steps describe the SWARA methodological procedure [9–12].

Step 1: s_j represents the scores assigned to the criteria. Decision-makers assign a value of 1.00 to the most important criterion and evaluate the remaining criteria in relation to it. They determine the relative importance of criterion j compared to the preceding criterion $(j-1)$. Scores are assigned in increments of five between 0 and 1.

Step 2: In this stage, the criteria are ordered from the most important to the least important.

Step 3: k_j represents the coefficient values and is calculated as follows:

$$k_j = \begin{cases} 1 & j = 1 \\ s_j + 1 & j > 1 \end{cases} \tag{1}$$

Step 4: The adjusted weights q_j are determined, and q_j is calculated as follows:

$$q_j = \frac{k_{j-1}}{k_j} \tag{2}$$

Step 5: Calculation of the final weights.

$$w_j = \frac{q_i}{\sum_{j=1}^{n} q_j} \tag{3}$$

3. RESULTS

The criteria considered in solving the problem and the expert evaluation table are presented in Table 1 below.

Table 1. Criteria and expert opinions

Criteria	Expert 1	Criteria	Expert 2	Criteria	Expert 3
Green Innovation and Dynamic Capabilities (K1)	–	K4	-	K6	-
Economic Sustainability and Operational Efficiency (K6)	0.10	K2	0.05	K3	0.10
Energy Efficiency and Resource Management (K2)	0.15	K6	0.15	K1	0.20
Green Supply Chain and Logistics (K3)	0.20	K1	0.20	K2	0.25
Legal Compliance and Corporate Governance (K4)	0.25	K3	0.30	K4	0.30
Social Responsibility and Stakeholder Engagement (K5)	0.30	K5	0.40	K5	0.40

Table 2 presents the calculations based on the data obtained from Expert 1. The same procedure was repeated for the other two experts.

Table 2. Criteria and expert evaluations

Criteria	s_j (Relative Importance)	k_j	q_j	w_j (Normalized Weight)
K1	–	1	1	0.2331
K6	0.1	1.1	0.9091	0.2119
K2	0.15	1.15	0.7905	0.1842
K3	0.2	1.2	0.6588	0.1535
K4	0.25	1.25	0.527	0.1228
K5	0.3	1.3	0.4054	0.0945

In Table 3, the average criterion weights were determined based on the score assignments of all experts. The final criterion weights are presented in order of priority.

Table 3. Final criterion weights in order of priority

Rank	Criterion	Expert 1	Expert 2	Expert 3	Average Weight (Arithmetic Mean)
1	K6	0.2119	0.189	0.2456	0.2155
2	K1	0.2331	0.1575	0.1861	0.1922
3	K2	0.1842	0.2174	0.1488	0.1835
4	K3	0.1535	0.1212	0.2233	0.166
5	K4	0.1228	0.2283	0.1145	0.1552
6	K5	0.0945	0.0866	0.0818	0.0876

4. CONCLUSION

This study analyzed the strategic priorities for businesses undergoing green transformation by evaluating six key criteria selected from the literature using the SWARA method. As environmental regulations and global climate crises necessitate a shift towards sustainable business models, determining the relative importance of these strategies becomes crucial for effective resource allocation and decision-making.

The analysis results revealed that economic sustainability and operational efficiency (K6) is the most significant criterion. This finding indicates that for businesses, the transition to a green economy is not merely an environmental obligation but is fundamentally driven by the need to maintain competitiveness, optimize resource usage, and ensure long-term financial stability. It suggests that successful green transformation strategies must be built upon a solid economic foundation that harmonizes profitability with environmental goals.

Green innovation and dynamic capabilities (K1) emerged as the second most important factor. This highlights the critical role of adaptive capacity and technological advancement in responding to environmental uncertainties. Businesses that prioritize low-carbon technologies and sustainable design improvements are better positioned to achieve both environmental and financial performance.

Conversely, social responsibility and stakeholder engagement (K5) was identified as the criterion with the relatively lowest weight. While the social dimension remains an integral part of sustainable development, this result suggests that in the strategic hierarchy of green transformation, experts and decision-makers currently prioritize structural, operational, and economic capabilities over social drivers.

In conclusion, this study provides a decision support model suggesting that managers should primarily focus on investments that enhance operational efficiency and innovation capacity to facilitate a successful green transition. Future research could expand on these findings by applying this model to specific industries or by comparing the results using fuzzy-based MCDM methods to address the uncertainties in expert evaluations.

References

[1] D. J. Teece, “Business models and dynamic capabilities,” *Long Range Planning*, vol. 51, no.1, pp. 40–49, Feb. 2018.

[2] Y. S. Chen, Y. H. Lin, C. Y. Lin, and C. W. Chang, “Enhancing green absorptive capacity, green dynamic capacities and green service innovation to improve firm performance: an analysis of structural equation modeling (SEM),” *Sustainability*, vol. 7, no. 11, pp. 15674–15692, Nov. 2015.

[3] R. S. Pawar and S. Dawkhar, “Strategies for integrating sustainability into business operations,” *International Journal for Multidisciplinary Research*, vol. 5, no. 1, pp. 1–7, Jan. 2023.

[4] H. Buhari, M. S. Basingab, A. Rizvan, M. Sanchez-Chero, C. Pavlatos, and G. Fotis, “Sustainable green supply chain and logistics management using adaptive fuzzy-based particle swarm optimization,” *Sustainable Computing: Informatics and Systems*, vol. 46, art. no. 101119, Mar. 2025.

[5] G. Aras, G. and D. Crother, “Governance and sustainability: an investigation into the relationship between corporate governance and corporate sustainability,” *Management Decision*, vol. 46, no. 3, pp. 433–448, Jan. 2008.

[6] B. L. Parmar, R. E. Freeman, J. E. Harrison, A. J. Wicks, S. Colle, and L. Purnell, “Stakeholder theory: The state of the art,” *Cambridge University Press*, 2010.

[7] M. A. Engin, and Z. Parlak, “Labour standards and corporate social responsibility: The case of Turkish apparel industry,” *Labor History*, vol. 66, no. 2, pp. 243–260, Jun. 2024.

[8] S. L. Hart, and G. Dowell, “A natural-resource-based view of the firm: Fifteen years later,” *Journal of Management*, vol. 45, no. 5, pp. 1469–1495, Sep. 2019.

[9] H. Yurdoglu and N. Kundakci, “SWARA ve WASPAS yontemleri ile sunucu secimi,” *Balikesir Universitesi Sosyal Bilimler Enstitusu Dergisi*, vol. 20, no. 38, pp. 253–270, Dec. 2017.

[10] O. Derse, and E. Yontar, “SWARA-TOPSIS yontemi ile en uygun yenilenebilir enerji kaynaginin belirlenmesi,” *Endustri Muhendisligi*, vol. 31, no. 3, pp. 389–419, Nov. 2020.

[11] T. Sivageerthi, S. Bathrinath, M. Uthayakumar and R. K. A. Bhalaji, “A SWARA method to analyze the risks in coal supply chain management,” *Materials Today: Proceedings*, vol. 50, pp. 935–940, Jun. 2021.

[12] O. Eroglu and C. Gencer, “Classification on SWARA method and an application with SMAA-2,” *Journal* of *Polytechnic Dergisi*, vol. 24, no.4, pp. 1707–1718, Dec. 2021.

2nd International Conference on Multidisciplinary Sciences and Technological Developments (ICMUSTED 2025)

December 12-15, 2025

Psychological Factors Influencing University Students' Trust in AI-Based Learning Assistants

Ezgi Dagtekin[1], Ercan Erkalkan[2]

[1]The MacDuffie School, Massachusetts, USA
[2]Department of Electronics and Automation, Marmara University, Istanbul, Türkiye
Corresponding author: Ercan Erkalkan (e-mail: ercan.erkalkan@marmara.edu.tr)

Abstract

Artificial intelligence (AI)-based learning assistants and chatbots are increasingly integrated into higher education. While these tools are often evaluated in terms of technical performance, their successful and ethical use also depends on psychological factors such as trust, perceived risk, technology anxiety, and students' general attitudes toward AI. This paper adopts a psychology-oriented perspective to examine how university students form trust in AI-based learning assistants. Drawing on recent literature in mental health, human AI interaction, and trust in automation, we propose a conceptual framework that organizes psychological predictors of trust into four groups: cognitive appraisals (perceived competence, reliability, and usefulness), affective reactions (anxiety, fear, comfort), social-relational factors (anthropomorphism, perceived empathy, and autonomy support), and contextual moderators (privacy, transparency, and ethical norms). A narrative review approach is used to synthesize empirical findings on AI tools in education and mental health support, with a specific focus on college and university populations. Based on this synthesis, we derive research questions and hypotheses for future survey and experimental studies with students. The paper highlights that trust in AI is not a purely technical outcome but a psychological process shaped by individual differences and learning environments. Finally, practical implications are discussed for instructors, university administrators, and designers of educational AI systems, including guidelines to foster appropriate reliance rather than blind trust or total rejection.

Keywords: Psychology, AI, Trust in AI, University students, Learning assistants

1. INTRODUCTION

Artificial intelligence (AI)-based systems such as chatbots, recommendation engines, and conversational agents are now widely used in education and mental health support for university students. Recent systematic reviews show that AI-based conversational agents can reduce symptoms of depression, anxiety, and psychological distress when used as supportive tools, especially among young adults and students [1–3]. However, these reviews also emphasize that the effectiveness and safety of such tools depend on how users perceive and relate to AI, not only on algorithmic accuracy [4].
From a psychological perspective, AI systems are not neutral technologies. Students interpret AI tools through existing beliefs, emotions, and social experiences. Concepts such as trust, perceived fairness, technology anxiety, and sense of control play a decisive role in whether students choose to rely on AI recommendations or actively reject them. Inadequate trust may lead to underuse of potentially helpful tools, whereas inappropriate trust can create overreliance and neglect of critical thinking in learning or health-related decisions [5].

Despite the rapid diffusion of AI-based learning assistants for example, AI-powered homework helpers, writing support tools, or course-specific chatbots many studies still emphasize technical performance rather than psychological processes. There is a need for psychology-oriented frameworks that explain how and why students trust or mistrust AI and which psychological factors predict appropriate reliance [1, 6, 7].

The main purpose of this paper is to develop a psychology centered conceptual framework for understanding university students' trust in AI-based learning assistants. The contribution of the paper is threefold. First, it synthesizes empirical findings on AI tools in education and mental health focusing on college and university populations. Second, it identifies key psychological constructs that influence trust and reliance on AI. Third, it proposes research questions and hypotheses that can guide future empirical work in the "Social, Humanities, and Administrative Sciences" domain.

The remainder of the paper is organized as follows. Section 2 presents the material and method, describing the narrative literature review strategy and the psychological constructs considered. Section 3 introduces the proposed framework and summarizes the main themes identified in the literature. Section 4 concludes with implications, limitations, and suggestions for future research.

2. MATERIAL AND METHOD

This study follows a narrative literature review approach rather than a systematic meta-analysis. The aim is not to estimate pooled effect sizes, but to organize and interpret recent psychological evidence regarding trust in AI among students and young adults. Narrative reviews are suitable when the goal is to integrate findings from diverse study designs and to propose conceptual frameworks rather than to test a single, predefined model statistically.

To identify relevant research, major scholarly databases and publishers (such as IEEE Xplore, ScienceDirect, SpringerLink, PubMed, and Frontiers) were consulted using combinations of the following keywords in English: artificial intelligence, chatbot, conversational agent, trust, psychology, university students, mental health, technology acceptance, and human-AI interaction. The focus was on studies and reviews published between 2018 and 2025 that satisfied at least one of the following criteria: (i) The sample consisted primarily of university or college students, or of young adults in an educational context; (ii) the study examined psychological outcomes of AI use (e.g., attitudes, trust, anxiety, well-being, or motivation); or (iii) the study dealt with AI-based conversational agents or learning support tools relevant to students [8, 9].

Recent reviews on AI-driven conversational agents in mental health and digital well-being were used as anchor sources for identifying further empirical work [8, 9]. In addition, reviews on trust in AI and trustworthy AI from a psychological viewpoint were included to understand how trust has been conceptualized and measured [4–6]. As this paper is based on a literature review and does not involve new data collection from human participants, formal ethics committee approval was not required.

2.1. Psychological Constructs Considered

Based on the selected literature, four groups of psychological constructs were considered when organizing the proposed framework. The first group consists of cognitive appraisals, including perceived competence, accuracy, reliability, usefulness, and fairness of AI systems. The second group covers affective reactions such as technology-related anxiety and fear, curiosity, comfort, and perceived emotional safety when interacting with AI. The third group relates to social-relational factors, such as anthropomorphism (seeing AI as humanlike), perceived empathy, interpersonal warmth, and perceived autonomy support in learning. Finally, contextual moderators include privacy concerns, perceived transparency and explainability, norms in the educational environment, and ethical regulations. These constructs are frequently mentioned in psychological research on human-AI trust and are grounded in social-cognitive models of trust and technology acceptance [4, 5].

Table 1. Summary of inclusion and exclusion criteria and study designs used in the narrative review

Criterion Category	Description	Representative Examples of Studies or Typical Applications
Inclusion criteria	Peer-reviewed publications between 2018 and 2025 focusing on university students or young adults and reporting psychological constructs related to AI-based systems	Narrative and empirical studies on trust, attitudes, perceived risk, technology anxiety, motivation, or well-being in relation to AI-based learning assistants
Exclusion criteria	Publications without psychological measures, studies outside higher education, or articles lacking sufficient methodological information	Technical system descriptions without psychological outcomes; studies based on from kindergarten to 12th grade (K–12) samples; reports not published in peer-reviewed venues
Study designs	Experimental interventions, survey-based quantitative studies, and qualitative or mixed-method investigations	Controlled experiments manipulating properties of AI-based assistants; large-scale online surveys in higher-education settings; interview-based or focus-group studies on students' experiences with AI-supported learning

2.2. Inclusion and Exclusion Criteria and Study Designs

The narrative review focuses on peer-reviewed publications released between 2023 and 2025. The selection strategy follows explicit inclusion and exclusion criteria in order to ensure conceptual relevance to university students and AI-based learning assistants.

- Inclusion criteria: Empirical or review article published in a peer-reviewed journal, conference proceedings, or edited volume between 2023 and 2025.
- Inclusion criteria: sample composed primarily of university or college students or young adults in an educational context.
- Inclusion criteria: Focus on psychological constructs related to AI-based systems, such as trust, attitudes, perceived risk, technology anxiety, motivation, or well-being.
- Inclusion criteria: Use of AI-based conversational agents, learning assistants, recommendation tools, or comparable educational AI systems.
- Exclusion criteria: Publications limited to technical performance, algorithm design, or system architecture without psychological measures.
- Exclusion criteria: Studies conducted exclusively with clinical populations, K–12 students, or general consumers outside higher education.
- Exclusion criteria: Articles lacking sufficient methodological information or not available in English.

The final body of evidence covers three main study designs: experimental interventions that expose students to AI-based tools under controlled conditions, survey-based quantitative studies that measure psychological constructs in naturalistic educational settings, and qualitative or mixed-method investigations that explore subjective experiences with AI-supported learning.

3. FINDINGS AND PROPOSED FRAMEWORK

In the context of this narrative review, "results" refer to the main conceptual themes and relationships identified in the literature rather than statistical findings from a single empirical dataset. The proposed framework suggests that trust in AI-based learning assistants among university students emerges from the interaction of cognitive appraisals, affective reactions, social relational factors, and contextual moderators.

Figure 1 organizes the conceptual framework around trust in AI-based learning assistants. The central node represents students' trust and appropriate reliance on AI, surrounded by four clusters of predictors: cognitive appraisals, affective reactions, social-relational factors, and contextual moderators. Directed arrows indicate expected positive or negative associations between each cluster and trust, as well as moderating influences of contextual factors on the links between cognitive, affective, and social-relational variables and trust.

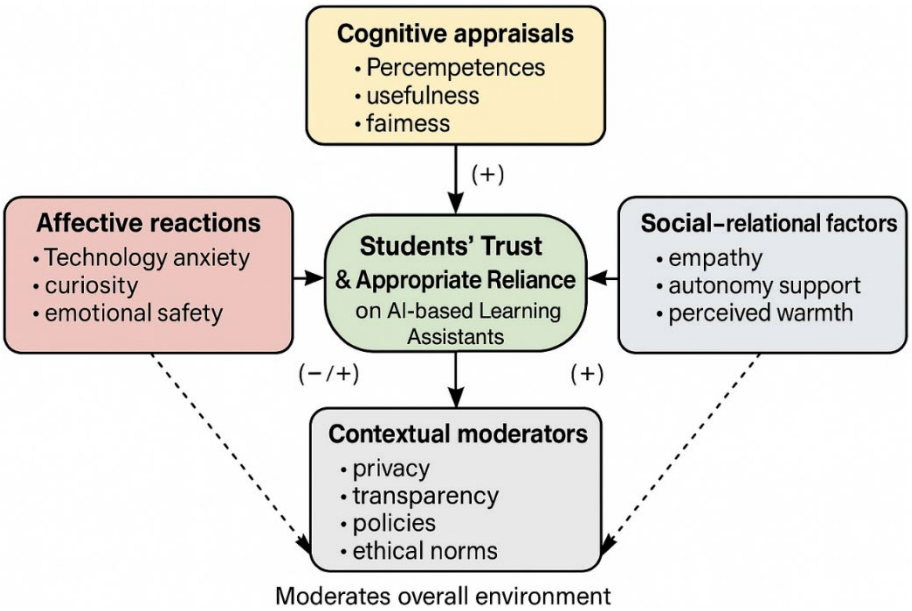

Figure 1. Psychology-oriented framework of university students' trust in AI-based learning assistants

Table 2 provides a concise overview of how key psychological construct clusters have been operationalized across different study designs and summarizes the dominant empirical associations with trust in AI-based learning assistants.

Table 2. Key psychological constructs, typical study designs, and dominant empirical patterns related to trust in AI-based learning assistants

Construct Cluster	Representative Variables	Typical Study Designs	Dominant Empirical Patterns
Cognitive appraisals	Perceived competence, accuracy, usefulness, fairness	Experimental interventions; survey-based quantitative studies	Higher cognitive appraisals associated with increased trust, stronger continuance intention, and higher perceived learning support
Affective reactions	Technology anxiety, fear, curiosity, emotional safety	Survey-based cross-sectional and longitudinal designs; experimental studies	Higher anxiety associated with lower trust and reduced usage; higher emotional safety associated with greater engagement and willingness to experiment with AI tools
Social-relational factors	Anthropomorphism, perceived empathy, autonomy support, interpersonal warmth	Survey-based studies; laboratory experiments; qualitative interviews	Supportive social cues associated with stronger perceived empathy and more appropriate reliance, particularly when autonomy support remains salient
Contextual moderators	Privacy concerns, transparency, institutional policies, ethical norms	Survey-based studies; policy analyses; mixed-method research	Clear policies and transparent communication associated with higher trust and a weaker negative impact of privacy concerns on usage intentions

3.1. Cognitive Appraisals: Perceived Competence, Reliability, and Usefulness

A consistent finding in the literature is that users are more likely to trust and rely on AI tools when they perceive them as competent and reliable. In educational settings, this means that students must believe the AI assistant provides correct, up-to-date, and relevant information. Studies on conversational agents for mental health similarly show that perceived accuracy and helpfulness are strongly associated with continued use [1–3, 9]. Perceived usefulness in supporting learning outcomes such as clearer explanations, improved grades, or time savings also plays a central role. When students experience that an AI assistant helps them clarify complex concepts or structure their study routines, trust tends to increase. Conversely, if AI suggestions frequently conflict with course materials or instructor feedback, students may downgrade the system's reliability and reduce their reliance.

3.2. Affective Reactions: Anxiety, Fear, and Emotional Safety

Beyond rational evaluations, affective reactions strongly shape trust in AI. Psychological research indicates that technology anxiety and fear of making serious mistakes with the help of AI can reduce willingness to engage with AI tools, even when their technical performance is objectively high [7]. For some students, AI-based assistants may reduce anxiety by providing non-judgmental, always-available support. For others, especially those with concerns about surveillance or job displacement, AI can evoke worry, anger, or feelings of dehumanization [1, 2]. In mental health contexts, reviews highlight both the potential of chatbots to alleviate symptoms and the risk that emotionally vulnerable users might receive responses that feel invalidating or unsafe [1–3, 8, 9]. From a psychological standpoint, emotional safety the feeling that one can interact with an AI assistant without being ridiculed, monitored excessively, or harmed is a critical precursor to trust.

3.3. Social-Relational Factors: Anthropomorphism, Empathy, and Autonomy Support

Many students implicitly treat AI systems as social partners, especially when they are designed with humanlike language, names, or avatars. Anthropomorphism can increase perceived empathy and warmth, which may enhance trust and engagement. However, if the system's behaviour does not match these expectations for example, by giving generic or insensitive responses users may feel disappointed or even betrayed [4, 5, 8]. For educational AI assistants, perceived autonomy support helping students make their own decisions instead of prescribing answers

appears to be particularly important. When AI tools explain options, encourage reflection, and respect students' choices, they reinforce a sense of agency and intrinsic motivation, consistent with self-determination theory.

3.4. Contextual Moderators: Privacy, Transparency, and Ethical Norms

Trust in AI is also shaped by the broader context in which students encounter these systems. Transparency about data usage, storage, and model limitations is known to influence perceived trustworthiness [4, 5]. In university settings, students may have additional concerns: whether their interactions with AI-based learning assistants are monitored by instructors or administrators; how AI-generated content is evaluated in terms of academic integrity and plagiarism; and whether the institution provides guidelines or training on responsible AI use. The presence of clear ethical norms and institutional policies may reduce uncertainty and support appropriate reliance that is, using AI when it is helpful but still engaging in critical thinking and seeking human support when needed.

3.5. Proposed Research Questions and Hypotheses

Based on the reviewed literature and the proposed framework, several research questions (RQs) and illustrative hypotheses (Hs) can guide future empirical work with university students:

- RQ1: How do cognitive appraisals such as perceived competence, reliability, and usefulness predict students' trust in AI-based learning assistants?
  H1: Higher perceived competence and usefulness will be positively associated with trust and intended continued use.
- RQ2: What is the role of affective reactions such as technology anxiety, fear, and emotional safety in shaping trust?
  H2: Technology anxiety will be negatively associated with trust, controlling for perceived competence.
- RQ3: How do social relational factors such as anthropomorphism, perceived empathy, and autonomy support—influence appropriate reliance on AI?
  H3: Perceived empathy and autonomy support will predict appropriate reliance, defined as using AI as a supportive tool without fully delegating decisions.
- RQ4: How do contextual moderators such as privacy concerns, perceived transparency, and institutional policies influence the relationship between psychological factors and trust?
  H4: High perceived transparency and strong institutional guidelines will weaken the negative effect of privacy concerns on trust.

Each research question in the proposed set corresponds to a specific group of links in the conceptual framework. RQ1 addresses pathways from cognitive appraisals to trust in AI-based learning assistants. RQ2 focuses on affective reactions, including technology anxiety and emotional safety. RQ3 targets social-relational factors and appropriate reliance. RQ4 examines the moderating influence of contextual factors such as privacy concerns, transparency, and institutional policies on the associations between cognitive, affective, and social-relational variables and trust.

These questions can be investigated through cross-sectional surveys, longitudinal designs, or controlled experiments in which students interact with specific AI-based learning tools in real or simulated course settings.

4. CONCLUSION

This paper has developed a psychology-oriented framework for understanding university students' trust in AI-based learning assistants. Rather than focusing solely on algorithmic performance, the framework emphasizes that trust is a multidimensional psychological process shaped by cognitive appraisals, affective reactions, social relational factors, and contextual moderators. The narrative review of recent research in mental health, human AI interaction, and trust demonstrates that AI tools can support students' learning and well-being, but only when psychological needs such as competence, autonomy, and emotional safety are respected [1–6, 8, 9].

For practitioners, including designers and educators, the framework suggests several practical implications. First, they should provide transparent information about what AI tools can and cannot do. Second, interactions should be designed to support autonomy and critical thinking rather than passive dependence. Third, students' emotional concerns such as anxiety and fear about AI should be openly discussed and addressed. Finally, universities should establish clear institutional policies on privacy, academic integrity, and responsible AI use so that students can rely on AI tools appropriately.

4.1. Implications for Higher Education in Türkiye

Higher-education institutions in Türkiye currently experience rapid diffusion of AI-based tools in both formal and informal learning environments. University students frequently engage with global large language models and locally developed educational platforms without systematic guidance regarding trustworthy and responsible use. The proposed framework highlights several priorities for institutional policy and course design in this context.

First, measurement of psychological constructs such as trust in AI, technology anxiety, and perceived autonomy support requires culturally adapted scales. Existing instruments from the technology acceptance and trust in automation literature can be translated and validated for Turkish university students through standard psychometric procedures, including exploratory and confirmatory factor analysis. Rigorous adaptation will support longitudinal monitoring of students' attitudes and perceived risks.

Second, curriculum design in Türkiye can incorporate explicit discussions of academic integrity, plagiarism, and appropriate reliance on AI-based learning assistants. Clear course-level rules, sample use cases, and reflective assignments can align students' expectations with institutional norms. Courses in fields such as engineering, social sciences, and teacher education can embed short modules on critical evaluation of AI-generated content.

Third, university-level governance can develop transparent policies regarding data protection, logging of student–AI interactions, and support services. Collaboration between information technology units, ethics committees, and counseling centers can ensure that AI-based tools complement rather than replace human support in mental health and academic advising. Context-sensitive policy design in Türkiye will enable university students to benefit from AI-based learning assistants while maintaining psychological safety and trust.

Acknowledgments

The author would like to thank colleagues and students at Marmara University for their feedback on early versions of this work.

References

[1] H. Li, Y.-C. Lee, R. E. Kraut, and D. C. Mohr, "AI-based conversational agents for mental health: Systematic review and meta-analysis," *NPJ Digital Medicine*, vol. 6, arft. No. 236, 2023.

[2] M. Casu, S. Triscari, S. Battiato, L. Guarnera, and P. Caponnetto, "AI chatbots for mental health: A scoping review of effectiveness, feasibility, and applications," *Applied Sciences*, vol. 14, no. 13, art. no. 5889, 2024.

[3] R. Dehbozorgi, S. Zangeneh, E. Khooshab, D. H. Nia, H. R. Hanif, P. Samian, et al., "The application of artificial intelligence in the field of mental health: A review," *BMC Psychiatry*, vol. 25, art. no. 132, 2025.

[4] S. Afroogh, A. Akbari, E. Malone, M. Kargar, and H. Alambeigi, "Trust in AI: Progress, challenges, and future directions," *Humanities and Social Sciences Communications*, vol. 11, art. no. 1568, 2024.

[5] Y. Li, B.Wu, Y. Huang, and S. Luan, "Developing trustworthy artificial intelligence: Insights from research on interpersonal, human-automation, and human–AI trust," *Frontiers in Psychology*, vol. 15, 2024.

[6] A. Kuper, G. C. Lodde, E. Livingstone, D. Schadendorf, and N. Krämer, "Psychological factors influencing appropriate reliance on AI-enabled clinical decision support systems: Experimental web-based study among dermatologists," *Journal of Medical Internet Research*, vol. 4, no. 7, art. no. e58660, 2025.

[7] J. De Freitas, S. Agarwal, B.Schmitt, and N. Haslam, Psychological factors underlying attitudes toward AI tools," *Nature Human Behaviour*, vol. 7, pp. 1845–1854, 2023.

[8] Y. Hua, S. Siddals, Z. Ma, I. Galatzer-Levy, W. Xia, C. Hau, et al., "Charting the evolution of artificial intelligence mental health chatbots from rule-based systems to large language models: A systematic review," *World Psychiatry*, vol. 24, no. 3, pp. 383–394, 2025.

[9] W. Zhong, J. Luo, and H. Zhang, "The therapeutic effectiveness of artificial intelligence-based chatbots in alleviation of depressive and anxiety symptoms in short-course treatments: A systematic review and meta-analysis," *Journal of Affective Disorders*, vol. 356, pp. 459–469, 2024.

2nd International Conference on Multidisciplinary Sciences and Technological Developments (ICMUSTED 2025)

December 12-15, 2025

A Multi-Objective Optimization Approach for Airport Ground Handling and Resource Management Operations

Seckin Unver[1,2], Merve Gozde Sayin[2,3]

[1]Industrial Engineering Department, Marmara University, Istanbul, Türkiye
[2]TAV Technologies, Istanbul, Türkiye
[3]Mathematics Department, Middle East Technical University, Ankara, Türkiye
Corresponding author: Seckin Unver (e-mail: sunver@tav.aero)

Abstract

It is a non-stop decision-making process at airports to handle flights and passengers while coordinating various fixed-location resources such as gates, baggage belts and check-in counters. The proposed resource management system (RMS) introduces a customizable, multi-objective optimization framework driven by user-selected performance indicators that adapt the system to operational priorities to manage this complexity. The RMS integrates two major enhancements: a distance-optimizing model that assigns resources in close physical proximity to reduce various parameters such as passenger walking distances, aircraft towing, and equipment repositioning; and a balancing model that promotes fairness by distributing workloads evenly across gates, counters, and zones to prevent resource fatigue and avoid local congestions. An integer linear programming (ILP) model is developed to apply the weighted scalar multi-objective structure, and the results are obtained by deriving pareto-front solutions. Preliminary test results based on flight and layout data gathered from Izmir Adnan Menderes International Airport (ADB) show measurable gains in operational efficiency, including reductions in terminal crowding, smoother passenger flow between key facilities, and more predictable distribution of resource usage across peak and off-peak periods. Further analysis also indicates that RMS helps decrease operational delays caused by excessive clustering of flights in specific areas and improves staff allocation consistency by minimizing uneven workload patterns. RMS enhances service quality, supports real-time decision-making, and contributes to more resilient and efficient airport operations overall by continuously monitoring utilization, maintaining spatial coherence in assignments, and adapting dynamically to operational demands.

Keywords: Resource management system, Airport ground handling, Multi-objective optimization, Integer linear programming

2nd International Conference on Multidisciplinary Sciences and Technological Developments (ICMUSTED 2025)

December 12-15, 2025

Digitalization in Literature, Ergodic Literature, and Hypertexts: An Example from German

Harun Gocerler[1]

[1]Department of German Language and Literature, Tekirdag Namik Kemal University, Tekirdag, Türkiye
Corresponding author: Harun Gocerler (e-mail: hgocerler@nku.edu.tr)

Abstract

Literature, where the significant consequences of digitalization are evident, is no longer merely a cultural transmission element where literary works are consumed; it has also become part of an interactive process where readers engage with books and authors. The ability to produce writing in a digital environment, the acceptance of hypertext and multimodal writing, live broadcasts where authors and readers meet face-to-face, social media platforms, etc., have inevitably begun to influence the way literature is produced and consumed. Publishers and authors have begun to produce works not in spite of the reader, but by taking the reader's thoughts into account more than ever before. Based on this situation, this study examines the literary structure of German author Susanne Berkenheger's narrative "Zeit für die Bombe," which is considered one of the pioneers of the digital narrative system in Germany, by presenting an ergodic style with hypertext support. The analysis reveals the growing importance of concepts such as changing reading habits among the younger generation, the accessibility of literary works, transformations in the production process, and the role of digital publishing in literature.

Keywords: Ergodic literature, Digital literature, Hypertexts, Digital publishing, New reading habits

2nd International Conference on Multidisciplinary Sciences and Technological Developments (ICMUSTED 2025)

December 12-15, 2025

Andrzej Wajda: A Political Critique of Danton (1983)

Ismail Tasar[1]

[1]Digital Game Design, Faculty of Communication, Mimar Sinan Fine Arts University, Istanbul, Türkiye
Corresponding author: Ismail Tasar (e-mail: aspturkiye@gmail.com)

Abstract

Andrzej Wajda's Danton (1983) brings the last days of Georges Jaques Danton, one of the most iconic characters of the French Revolution, to the audience. Based on Stanislawa Przbyszewska's play, the film is a political allegory that questions the relationship between revolutionary ideals and authoritarian power. This study explores Wajda's production process, his position within the revolutionary cinematic community, and its sociopolitical context in early 1980s Poland, highlighting the significance of Danton's film as both a historical and cultural text. It is also concluded that Danton's film is a fictional work that criticizes both the extreme aspects of revolutionary madness and the increasing authoritarian tendencies in post-communist Poland. The visual style, narrative structure, and character dynamics in the film illustrate the director's complex portrayal of leadership, morality, and the inevitable corruption of power. Danton's film is still an important feature film for understanding the interaction between cinema, politics and memory in the last period of Europe's late century.

Keywords: Andrzej Wajda, Danton, Political Cinema, Polish Cinema

1. INTRODUCTION

The 18th century was a highly turbulent period for France. The French Revolution, which took place towards the end of the century, had significant consequences not only for France but also for Europe and indeed the entire world. Furthermore, with its dramatic upheavals and ideological fervor, the French Revolution has long been a fertile subject for cinema. The 1983 film Danton [1] is an important masterpiece that carries on this tradition. Adapted from Stanislawa Przybyszewska's play The Danton Case (1929) [2], the film serves as both a historical drama and a mirror reflecting the political struggles of 1980s Poland under the influence of the USSR, thereby contributing to the art of cinema.

Andrzej Wajda is a Polish director known for his politically charged films opposing totalitarianism, such as Popiol i Diament (Ashes and Diamonds, 1958) [3], Katyn (2007) [4], and Danton (1983). Wajda's film Danton (1983), which recounts the execution of Georges Jacques Danton, one of the key figures of the French Revolution, is significant in that it symbolically depicts Poland's turbulent post-war period. Wajda approached Danton (1983) as an examination of the communist regime and the winds of change sweeping through Poland in the 1980s. In Wajda's film, the conflict between Danton's populist rhetoric and Robespierre's rigid doctrine emerges as a subtle yet powerful commentary on authoritarian tendencies in Poland.

Within the scope of this article, Andrzej Wajda's directing style and political philosophy, the historical and cinematic representation of the French Revolution, the visual and narrative techniques in the film, and the political environment of 1980s Poland will be analyzed. The film Danton (1983) will be examined using content analysis in terms of the political discourse and social criticism it reflects. The primary sources for this examination consist of books and articles related to the director, the film, and the relevant period. In addition, the film Danton (1983) will be watched repeatedly and examined. The examination will be conducted by reviewing the relevant sources and taking notes on the necessary points.

2. ANDRZEJ WAJDA

Andrzej Wajda was born on March 6, 1926, in Suwalki, Poland, to Jakub and Aniela Wajda [5]. With an uncle who was a defender of farmers' rights and a well-educated family, Wajda went first to the Krakow Academy of Fine Arts after World War II, then to Lodz, where a film school had been established, and finally to Warsaw [5]. During those years, teachers at the Academy of Fine Arts who painted in the French post-impressionist style were influential. But Wajda thought this was not suitable for Poland, that it was at odds with the conditions and realities outside. The destruction of the war could be seen everywhere. Wajda then joined the Polish United Workers' Party.

He enrolled as a student at a film school he saw advertised in a newspaper. Thus, he turned from painting to film. At film school, he learned the technical knowledge he needed. He wanted to describe the political environment and influence and guide the masses through his films [5].

Wajda is known for making propaganda films that reflect the political structure of Eastern Europe in both social and cultural terms, and for being the political director of Eastern European cinema. The political context he created from his perspective is important in showing how significant politics is in his films. The relationship between the audience and the film's message is important to Wajda because he wants to influence and guide people with his films [6]. The dominant ideology of the Marxist view regarding classes and political systems is not sufficient in explaining Wajda's political films. Foucault can serve as a more appropriate tool for understanding Wajda's films. With the help of Foucault's postmodern social theory, interclass relations, power balances, and social structures can be better understood. All the sources that influenced and benefited Wajda enabled him to use his political films as a propaganda tool to influence society [6].

Wajda stated that if he joined a party, he would be forced to follow its policies, and because he believed this would lead to one-sidedness and stifle his artistic creativity, he decided not to join any party (he was a member of the Polish United Workers' Party). He welcomed the lifting of Soviet pressure on Poland after the fall of the Wall with joy. Wajda said he would continue to make films that tell Poles about their history and culture and raise their awareness [7]. Falkowska mentions that Wajda's political cinema is characterized by features such as adherence to historical facts, simplification of moral dilemmas, and a desire to engage with the audience's conscience [8]. These elements are also evident in the film Danton (1983).

Wajda attempted to explore concepts such as the French Revolution, fascism, democracy, representation, and dictatorship through his film Danton. He examined the traces of the French Revolution, which forms the foundation of modern Europe, through concepts such as justice and equality. Filmed during a period approaching the collapse of the USSR, the film reflects the director's view of the Jacobins. It addresses how the revolution devoured its own children as a result of different social interests and tensions. In the film, the masses have always sided with those who speak the loudest. The director, who does not find the leaders democratic, does not trust the people either [9]. Wajda said that of the two eyes given to the director by God, one is for looking through the camera, and the other is for seeing everything around him. He argues that these skills must be developed until the day comes when one can no longer make films. Furthermore, in order to capture art, the director must not be self-centered and must be able to detach himself from the subject of the film [10].

To understand Wajda, it would be appropriate to look at what he said about censorship. The director mentions the existence of two types of censorship. The first is internal censorship imposed by the artist on himself. It stems from the fear of the unknown. The second is external censorship imposed by various institutions in the name of protecting public morality, order, etc. The director says he cannot understand why so few films were made in France about events with such significant social and political impact, such as the Algerian War and May 1968. He suggests that the reason for this situation in France may be internal censorship rather than external censorship, because he believes there is no political censorship in France [10]. The cultural sphere in 1980s Poland faced strict censorship, but directors like Wajda managed to overcome these restrictions by using metaphors based on historical distance. Anna Gruszecka notes that Polish directors have the ability to evade censorship by using historical narratives for political criticism [11].

3. THE FRENCH REVOLUTION

George Rudé states that there were a number of nationalist uprisings in Belgium against Austria and in Poland against Russia; he also mentions a coup carried out by the Geneva Bourgeoisie in the Dutch Republic (Netherlands). However, in none of these cases, as in the French Revolution, did any social group achieve a lasting victory over another social group. None of these initiatives could be democratic or progressive because they failed to extend their political authority to the whole country. Only the French Revolution achieved this [12]. To better understand the causes of the French Revolution, it is useful to look at France during the "ancien régime" period. Looking at the French social structure in the 18th century, we see the palace and the aristocracy at the top, the bourgeoisie and the middle class below them, and the peasants, shopkeepers, and artisans at the bottom. The aristocracy had long been excluded from official institutions and were therefore resentful. The bourgeoisie did not have a share in the government commensurate with their wealth. Peasants were despised and subjected to excessive taxation. This situation in society increased tensions and conflicts, which became even more acute towards the end of the century [12]. Towards the end of the Ancien Régime, the peasants' anger and complaints increased exponentially. After 1778, France supported the American War of Independence. Subsequently, prices fell in many areas and an economic crisis began. Added to all this were the disasters and famines of 1787-1789. Prices rose

excessively. Unemployment also increased due to the free trade agreement signed with England in 1786. Heavy taxes continued unabated. Poverty and hardship were the main factors driving the people to join the revolution. [12].

The Declaration of the Rights of Man and of the Citizen was proclaimed as a founding document on August 26, 1789, to guide the work of the National Assembly. The French Revolution began with the demand for national sovereignty. The highest authority on matters concerning the people was no longer hereditary titles, kings, or churches, but the nation [13]. The 1789 popular revolution is examined in two parts, involving peasants and sans-culottes (wage workers, shopkeepers). Although the political origins of the two were common, they had different causes and consequences. The popular movement began first and ended first. Although the sans-culottes' constant interventions in the streets contributed to the revolution only for a short time, they were quite significant in terms of their impact [12]. The nobility lost their rights in many areas, such as economic, legal, and feudal privileges. Their titles would no longer be inherited, and the nobility ceased to exist. From then on, they would have the status of citizens. Church property was nationalized and sold. Although the Jacobins attempted to divide these lands into small parcels and sell them to peasants, it was the wealthy who benefited most from these sales [12].

Louis XVI was executed by guillotine on January 21, 1793, partly due to the influence of the secret correspondence that was discovered. With the help of the constitution, members of parliament would be directly elected by male voters for the first time. Inflation continued to rise. Riots spread to the streets. Robespierre scorned the people's reaction to price increases, calling them "nonsense." Grocery stores were occupied, and prices were lowered to the level demanded by the rebels [12]. The Jacobins owed their rise to the active participation of the people. They established close ties with the sans-culottes and formed an alliance with them. Thanks to this support from the Jacobins, the poor achieved significant gains in the autumn of 1793. The fall in prices and the right to vote were some of these gains. However, the alliance between the two sides was far from lasting. As a result, the revolutionary government under Robespierre and his friends fell in July 1794 [12].

The first consequence of the French Revolution was to divide European societies into "patriots" and "counter-revolutionaries." The Russian empress and the kings of Spain and Sweden opposed the French Revolution. England, on the other hand, took a positive approach. Most European countries opposed the revolution because they feared the strengthening of democrats and dissidents in their own countries. In countries such as the Ottoman Empire and Russia, the distance from France and the traditional social structures made it difficult for such revolutionary ideas to take root. As one of the legacies of the revolution, the fire of "nationalism" raged across Europe and even the world for centuries [12]. The French Revolution has been addressed in various forms in cinema many times since the beginning of the twentieth century.

4. DANTON (1983)

The screenplay for the film Danton, directed by Andrzej Wajda, was written by Jean-Claude Carrière. The film is adapted from the play The Danton Case (1929) by Stanisława Przybyszewska. The film was produced by Margaret Menegoz, with music by Jean Prodromides and editing by Halina Prugar-Ketling. The main cast includes: Gerard Depardieu as Danton, Wojciech Pszoniak as Robespierre, Patrice Chereau as Camille Desmoulins, and Serge Merlin as Philippeaux [14].

It is the spring of 1794 and the second year of the republic. The film begins at a checkpoint during Danton's entry into Paris. The guillotine seen as Danton's carriage enters the city seems to foreshadow what is to come. The people waiting in line to buy bread with ration cards show their affection for Danton as soon as they see him. Antoine tries to convince Robespierre that Danton is plotting a coup. The exaggerated acting that is effective throughout the film is also evident in this scene. It gives the impression of theatrical acting rather than cinematic acting. At Antoine's insistence, the printing press where Danton's writings are published is destroyed. Antoine again demands that Danton be sent to the guillotine. When Robespierre objects to this demand, he insists that at least Desmoulins be executed, claiming that Desmoulins called on the people to revolt against the Committees. Despite Citizen Amar and Fabre presenting evidence against Danton, Robespierre states that he is against Danton's execution.

Despite Westermann suggesting a coup to Danton, Danton is not enthusiastic about the idea. He underestimates the Committee's power and believes that removing a secret police officer named Heron is sufficient to demonstrate the Committee's strength. Robespierre then arranges a meeting with Danton and asks him to announce his support for the Committee to the public. Believing that Robespierre had distanced himself from the people, Danton refuses this request. That same night, at the request of Robespierre and members of the government, Danton, Lacroix, Philippeaux, and Desmoulins are arrested and sent to the Luxembourg prison. The arrest of Danton, the hero of

August 10, does not please the members of the congress. Robespierre tried to convince the members with a harsh speech from the podium. During the trials, the people showed their affection for Danton. Danton defended himself with the support of the people. Unhappy with the course of the trial, Robespierre met with Judge Fouquier and demanded that the enemies of the republic be eliminated. He threatened him, saying he would be arrested if he did not comply. Danton is silenced and prevented from defending himself. He is then sentenced to death. The executions take place one after another. In accordance with Danton's will, his severed head is removed from the basket it fell into and shown to the public.

Wajda, adopting a symbolic narrative, reflects the chaotic environment within Poland through the French Revolution. The director also wanted to address the rise of conservatism through the film. For conservatism rises in times of great change and turmoil. In this concept, the continuation of the old is desired, and the new is opposed. The committee is helpless because the aristocracy, clergy, and traditions that existed before the revolution are no longer guiding forces. The committee does not know what to do. Power, the source of sanctity, is in the hands of non-sacred individuals. When the poverty of the people is added to this, Wajda's conservative ideals are sufficiently nourished. Wajda proposes conservatism for Poland through symbols [15].

Wajda, who never shies away from showing his dissident side in his films, also displays his dissident stance in the film Danton (1983). The film deals with the bloody climate of terror that followed the French Revolution. Through the character of Danton, Wajda questions the revolution and examines the violence and oppression carried out in the name of protecting it. This film can also be read as a reaction to the Soviet Union's pressure on Eastern Europe, particularly Poland [16]. Wajda uses a narrative that is linear in some respects and cyclical in others. The rise and fall of the French Revolution is examined in three main sections. First, the initial victory of the revolution and Danton's rise as a charismatic leader; second, the growing tension between Danton's populist approach and Robespierre's rigid doctrine; and finally, the tragic end with Danton's arrest, trial, and execution.

Wajda chose a theatrical approach for the visual style of the film, in terms of lighting and composition. The use of theatrical lighting and shadows better reflects the emotional states of the characters. The color palette is dominated by shades of brown and gray, wood tones. This color palette makes the darkness of the French revolutionaries more realistic. In scenes depicting deaths, reminiscent of a festival of terror, high-contrast black-and-white visuals intensify the effect of moral contrast. Wajda's preference for long takes, particularly in courtroom scenes, enhances the audience's sense of the gravity of events. In terms of camera usage, close-ups of characters are favored. This makes it possible to successfully reflect the intense changes in expression in gestures and facial expressions. Through his preferred wide shots, Wajda successfully emphasizes Danton's loneliness. The characters are positioned in front of large backgrounds, a compositional choice suitable for a theatrical staging. Wajda characterizes Danton as a charismatic and populist leader. Danton's speeches are passionate and persuasive. Robespierre, on the other hand, represents ideological purity in the film. The tension in the film arises from the conflict between Danton's pragmatic populism and Robespierre's ideological absolutism. Antoine, Desmoulins, and the revolutionary court stand out as the characters that catalyze the main conflict in the film. Wajda approaches almost every character in a multidimensional way. Avoiding clichés, he films the characters within broader historical processes and in an ethically ambiguous manner. The film uses period marches and music that leans toward melancholic and introspective themes. Gunshots, the cries of crowds, and the sound of the guillotine heighten the emotional impact of important scenes.

Danton questions the nature of the revolution, which is like a double-edged sword. The film shows that the initial promises of the French Revolution, such as liberty and equality, were fulfilled to a certain extent. However, these promises later exposed the revolution to structural conflicts that would destroy it. Danton's rhetoric suggests broad participation, but his subsequent actions emphasize compromise on principles. The film discusses how revolutionary ideals were corrupted as a result of power struggles. Robespierre's ideological purity is presented as both virtue and evil. His rigid doctrine breeds suspicion and violence. Wajda uses Robespierre as a tool to criticize authoritarian tendencies. This use is a veiled criticism of the repressive communist regime in 1980s Poland. The film also emphasizes the role of the people in shaping the outcome of the revolution. While Danton's populist rhetoric captivates the people, it also shows the audience that the people can be manipulated. Scenes reminiscent of a festival of terror show the manipulation that directs the people's emotions toward violence.

5. CONCLUSION

Within the scope of this assignment, Andrzej Wajda's film Danton (1983) has been examined in terms of the political discourse and social criticism it reflects, and within the framework of the sociological criticism method. Andrzej Wajda is an important director of Eastern European cinema, known for his political and propaganda films. Wajda wants to influence people with his films and guide them in the direction he desires. The director has made

such well-known cinema films. Wajda used his film Danton (1983) to symbolically narrate the destruction Poland experienced after the war, through concepts such as the French Revolution, fascism, democracy, representation, and dictatorship. Through his films, we can also read Wajda's critiques of contemporary European societies. Society sides with the powerful, and Wajda criticizes this situation. Wajda's use of historical distance allows him to make political criticism while circumventing censorship.

Many European states opposed the French Revolution to prevent concepts such as nationalism, human rights, and democracy from spreading in their own countries. The wave of nationalism led to the breakup of large empires. For example, as a result of the effects of nationalism, the Ottoman Empire broke up, and states such as Turkey, Greece, and Bulgaria emerged. Wajda's film Danton received a mixed response in Poland in 1983. Tomasz K. Kaczmarek mentions that the film was praised by artists for its artistic value and historical accuracy. However, some critics claimed that the film was too allegorical and ambiguous. Although the authorities did not allow direct criticism, the film is quite clear to those who can read its political subtext. The film has managed to build a cult following among intellectuals and students. Internationally, the film has received positive reviews from critics for its direction, performances, and fidelity to historical facts. The film won the 1983 BAFTA Award for Best Foreign Language Film. Andrzej Wajda won the 1984 London Film Critics' Circle Award for Director of the Year [17].

The Danton film remains a fundamental work in discussions of revolutionary cinema and Polish film history. It is possible to say that the political critiques in the film are still relevant today in terms of democratic values and historical memory in Poland. Andrzej Wajda's Danton is a masterful blend of historical drama, political criticism, and cinematic art. The film successfully narrates the ideological fervor of the French Revolution in parallel with the authoritarian realities of 1980s Poland. The film is also a timeless masterpiece on the fragility of freedom and the corruption of power. Wajda's successful use of visual narrative techniques and his subtle portrayal of the moral complexity of revolutionary leaders reinforce the film's thematic depth. Wajda has succeeded in producing a film that questions the corruption of authority and power through universal themes. Danton is an important work for students of cinema, history, and political theory who wish to understand the interaction between history, cinema, and politics.

References

[1] IMDB. (2025, Sep. 1). *Danton* [Online]. Available: https://www.imdb.com/title/tt0083789/

[2] Culture. (2025, Sep. 2). *Stanislawa Przybyszewska: A brilliant preoccupied with revolution* [Online]. Available: https://culture.pl/en/article/stanislawa-przybyszewska-a-brilliant-playwright-preoccupied-with-revolution

[3] IMDB. (2025, Oct. 2). *Popiół i diament* [Online]. Available: https://www.imdb.com/title/tt0052080/

[4] IMDB. (2025, Oct. 2). *Katyn* [Online]. Available: https://www.imdb.com/title/tt0879843/

[5] Wajda. (2025, Oct. 5). *Kalendarium* [Online]. Available: https://wajda.pl/andrzej-wajda/

[6] J. Falkowska, *The Political Films of Andrzej Wajda: Dialogism in Man of Marble, Man of Iron, and Danton*, Oxford: Berghahn Books, 1996.

[7] B. Hollander, (2025, Sep. 1). *I just can't stand aside* [Online]. Available: http://www.wajda.pl/en/wywiad80.html

[8] J. Falkowska, "Nostalgia and remorse: Films of the eighties," in *Andrzej Wajda: History, Politics & Nostalgia in Polish Cinema*, J. Falkowska, Ed. Berghahn Books, 2008 pp. 182–223.

[9] E. Z. Guler, "Siyaset bilimi egitiminde yeni yontem arayislari: Avrupa uzerine dusunen filmler," *Siyasal: Journal of Political Sciences*, vol. 40, no 2, pp. 167–180, Mar. 2009.

[10] A. Wajda, *Cinema and I*, F. Ant, Trans. Istanbul: Es Yayinlari, 2006.

[11] A. Gruszecka, "Censorship in the People's Republic of Poland (1944-1989)," *Journal of Publishing Culture*, vol. 2, pp. 1–8, 2014.

[12] G. Rudé, *The French Revolution*, A. I. Dalgic, Trans. Istanbul: Iletisim Yayinlari, 2015.

[13] W. Doyle, *The French Revolution*, H. Gur, Trans. Ankara: Dost Kitabevi, 2015.

[14] IMDB. (2025, Oct. 3) *Danton – Full Cast & Crew* [Online]. Available: https://www.imdb.com/title/tt0083789/fullcredits/

[15] S. Sidal, "A nationalist conservative director in post-world war ii polish cinema: Andrzej Wajda," *Journal of Human and Social Sciences*, vol. 4, pp. 45–68, 2015.

[16] W. Doyle, *The French Revolution*, H. Gur, Trans. Ankara: Dost Kitabevi, 2015.

[17] T. K. Kaczmarek, "The Politics of Danton," *Polish Film Quarterly*, vol. 4, no. 1, pp. 23–37, Mar. 1985.

2nd International Conference on Multidisciplinary Sciences and Technological Developments (ICMUSTED 2025)

December 12-15, 2025

Designing Adaptive Conceptual Stories via Artificial Intelligence for Science and Mathematics Learning

Ilhan Polat[1]

[1]Ministry of National Education, Van, Türkiye
Corresponding author: Ilhan Polat (e-mail: ilhan_polatt@hotmail.com)

Abstract

Understanding abstract concepts in science and mathematics education is a critical threshold in students' cognitive development. To overcome this challenge and effectively eliminate deep-rooted misconceptions, an innovative approach is presented that combines the emotional power of narrative learning with the potential of generative artificial intelligence (GenAI). In this context, the primary aim of this study is to examine, within a theoretical framework, the ability of AI-generated conceptual stories to concretize abstract concepts in elementary school Science and Mathematics lessons and to support teachers with an application-oriented guide to maximize this potential. The inherent power of stories to establish emotional connections, combined with AI's ability to generate high-fidelity, personalized content, creates a lasting and meaningful learning foundation, particularly for elementary school students whose abstract thinking skills are still developing. This model aims to position teachers not just as users of technology but as creative and critical partners guiding conceptual learning. The study offers a theoretical conceptual framework and a concrete blueprint for implementation. This framework includes AI program recommendations suitable for teachers, detailed concept teaching principles, and discipline-specific (Science/Math) learning outcome-focused activity tables. The applicability of the model is demonstrated with sample texts, while effective prompt examples provide teachers with an instant content creation guide. Finally, recommendations for parents have been integrated into the model to facilitate the transfer and reinforcement of learning into the home environment. This holistic approach aims to maximize student active participation and conceptual depth.

Keywords: Artificial intelligence-supported storytelling, Conceptual concretization, Elementary science and mathematics education

2nd International Conference on Multidisciplinary Sciences and Technological Developments (ICMUSTED 2025)

December 12-15, 2025

Evaluating the Basic Life Skills Activity Book: Alignment with Life Skills Course Outcomes and the 21st Century Skills Framework

Ilhan Polat[1], Mehmet Akif Ersoz[1]

[1]Ministry of National Education, Van, Türkiye
Corresponding author: Ilhan Polat (e-mail: ilhan_polatt@hotmail.com)

Abstract

The primary school level is of critical importance for individuals to successfully adapt to social life and gain personal autonomy. The basic life skills elementary school activity book has been prepared as part of the "Life Skills Approach" project implemented by the Ministry of National Education within the scope of the Turkey century education model. The alignment of this book with the life skills course learning outcomes and 21st Century Skills is important in terms of ensuring program integrity. In this context, the study aims to analyze the alignment of the basic life skills elementary school activity book with the life skills course teaching program learning outcomes and the 21st century skills framework. Document analysis was used as a qualitative research method in the study. Within the scope of the study, the objectives of the activities in the basic life skills elementary school activity book were compared with the life skills course learning outcomes and the 21st century skills framework. The analysis showed that the vast majority of the activity book's objectives directly supported the learning outcomes of the life skills course. The activities in the book strongly target critical skills in the categories of life and career skills and learning and innovation skills. Another contribution is that it enriches the program with critical 21st-century skills such as entrepreneurship, financial literacy, and applied sustainability awareness through its original objectives. The omission of some 21st century skills, such as media literacy, in the book is thought to reflect a deliberate pedagogical choice that prioritizes the developmental priorities of elementary school students. In conclusion, the basic life skills activity book can be described as a forward-thinking and enriching educational resource that prepares students for both current curriculum goals and the practical life skills required in the 21st century.

Keywords: 21st century skills, Basic life skills, Life skills course curriculum

2nd International Conference on Multidisciplinary Sciences and Technological Developments (ICMUSTED 2025)

December 12-15, 2025

EfficientNet with Data Augmentation for Potato Disease Detection and Sustainable Agriculture

Mansouria Sekkal[1], Badir Benkrelifa Lahouaria[1]

[1]Department of Electronics and Telecommunications, University of Belhadj Bouchaib, Ain Temouchent, Algeria
Corresponding author: Mansouria Sekkal (e-mail: mansouria.sekkal@univ-temouchent.edu.dz)

Abstract

Potato is one of the world's most important crops, yet it remains highly vulnerable to fungal and bacterial diseases that threaten both yield and food security. Conventional diagnostic methods are time-consuming and dependent on expert expertise, limiting their practicality in real agricultural settings. In this study, we propose an advanced deep learning framework for automatic potato leaf disease detection. The model is based on EfficientNetB3, a state-of-the-art convolutional neural network architecture, fine-tuned on an open-source potato leaf dataset. To enhance robustness and prevent overfitting, several data augmentation techniques, including rotation, brightness adjustment, zoom, and flipping, were applied. Additionally, hyperparameter optimization improved the model's generalization, achieving 98.2% accuracy in multi-class classification of potato diseases. This improvement demonstrates the potential of EfficientNet in plant disease detection tasks. Beyond technical contributions, the system can be integrated into a mobile application for farmers, enabling early detection, reducing crop losses, and minimizing pesticide use. This approach not only enhances agricultural productivity but also contributes to sustainable agriculture and environmental protection. The study highlights the interdisciplinary role of artificial intelligence in supporting food security and ecological sustainability.

Keywords: Artificial intelligence, Deep learning, EfficientNet, Potato disease detection, Sustainable agriculture

2nd International Conference on Multidisciplinary Sciences and Technological Developments (ICMUSTED 2025)

December 12-15, 2025

AI-Powered MRI Analysis for Early and Accurate Medical Diagnosis

Mansouria Sekkal[1], Badir Benkrelifa Lahouaria[1]

[1]Department of Electronics and Telecommunications, University of Belhadj Bouchaib, Ain Temouchent, Algeria
Corresponding author: Mansouria Sekkal (e-mail: mansouria.sekkal@univ-temouchent.edu.dz)

Abstract

Magnetic resonance imaging (MRI) plays a crucial role in modern healthcare, but its interpretation remains challenging due to the complexity of images, the variability of pathologies, and the reliance on expert radiologists. In this study, we present an artificial intelligence–based framework for the automated analysis of MRI scans, focusing on the early and accurate detection of diseases in brain and other organ imaging. The proposed approach employs convolutional neural networks (CNNs) enhanced with transfer learning, fine-tuned on publicly available MRI datasets. To improve robustness and reduce overfitting, several data augmentation techniques—including rotation, brightness adjustment, zoom, and flipping—were applied. Additionally, hyperparameter optimization was carried out to refine the learning rate, batch size, number of epochs, and dropout rate. Experimental results demonstrate that the model achieved an accuracy of over 96% in distinguishing between normal and abnormal MRI scans. Designed as a decision-support tool, this system aims to assist radiologists by reducing diagnostic time and minimizing human error. By integrating artificial intelligence into medical imaging**.** This research highlights the potential of deep learning in advancing healthcare technologies.

Keywords: Artificial intelligence (AI), MRI, Deep learning, Transfer learning, Medical diagnostics

2nd International Conference on Multidisciplinary Sciences and Technological Developments (ICMUSTED 2025)

December 12-15, 2025

Alginate/Chitosan-Based Nanostructures as Sustainable Nanopriming Agents for Wheat Seeds

Arruje Hameed[1], Muhammad Mujahid[1], Tahir Farooq[2], Amjad Hameed[3]

[1]Department of Biochemistry, Government College University Faisalabad, Faisalabad, Pakistan
[2]Department of Applied Chemistry, Government College University Faisalabad, Faisalabad, Pakistan
[3]Nuclear Institute for Agriculture and Biology (NIAB), P.O. Box 128, Jhang Road, Faisalabad, Pakistan
Corresponding author: Arruje Hameed (e-mail: arrujeh@yahoo.com)

Abstract

Wheat is a major cereal crop and staple food around the globe. Over the years, its yield is generally encumbered by environmental factors including temperature, water and salinity. Great efforts have been made to reduce the detrimental effects of climate change. Recent studies have shown that nanotechnology may improve agricultural sustainability by encouraging plant growth and development in both stressful and normal conditions. Priming has become an important approach that modulates the morphological, physiological, and biochemical features in seeds, enabling them to resist environmental factors. Alginate/Chitosan nanostructures were prepared as priming agents for wheat seeds. The prepared nanostructures were characterized using scanning electron microscopy (SEM), X-ray diffraction (XRD) and Fourier transform infrared spectroscopy (FTIR). Various biochemical parameters were analysed using nanoprimed seeds to measure the effective role of nanostructures in promoting seed germination. The nanopriming significantly upregulated the antioxidants, hydrolytic enzymes and potent biomolecules in treated seeds. The nanopriming induced a significant increase in enzymatic and non-enzymatic antioxidants and resistance the oxidative damage. The priming treatments also caused a significant reduction in malondialdehyde (MDA). The nanopriming induced changes in physio-biochemical attributes in primed seeds positively influenced the germination, ensuring sustainable wheat growth.

Keywords: Priming, Nanostructures, Wheat, Seed treatment, Biochemistry

A Natural Ally Against Pine Aphids: *Pauesia Silana* as a Key Biocontrol Agent of *Cinara Maghrebica*

Leila Bourouba[1]

[1]Laboratory for the Improvement of Plant Protection Techniques in Mountain Agrosystems: Case of Aures, Agronomy Department, Institute of Veterinary and Agronomy Science, University Batna 1, 05000 Batna, Algeria
Corresponding author: Leila Bourouba (e-mail: leila.bourouba@univ-batna.dz)

Abstract

The Aleppo pine (*Pinus halepensis* Mill.) is a key forest species in the Mediterranean region, providing ecological and socio-economic services under semi-arid conditions. However, its stands are increasingly threatened by infestations of the Maghreb pine aphid (*Cinara maghrebica*), which causes significant damage through phloem sap extraction and honeydew production that favors the growth of sooty molds. This study investigates the role of *Pauesia silana* (Hymenoptera: Braconidae, aphidiinae) as a parasitoid of *Cinara maghrebica* in northeastern Algeria. Systematic sampling of Aleppo pine stands was conducted across urban, peri-urban, and natural habitats from 2019 to 2021. Aphid colonies were collected and reared in the laboratory to assess parasitism rates and to confirm the identity of emerging parasitoids. Results highlight the presence of *Pinus silana* as a specific and effective natural enemy of *Cinara maghrebica*. The parasitoid demonstrated significant regulatory potential, with parasitism rates varying according to habitat type and seasonal conditions. Its activity was particularly pronounced during periods of moderate temperatures, suggesting an important synchrony between aphid population peaks and parasitoid reproduction. These findings provide valuable insights into the ecological interactions shaping Aleppo pine forest health and emphasize the potential of *Pinus silana* as a sustainable biological control agent. Promoting its conservation within integrated pest management strategies could reduce reliance on chemical treatments and support the long-term resilience of Mediterranean pine ecosystems under climate change.

Keywords: Aleppo pine, Biological control, *Cinara maghrebica*, Forest ecosystems, *Pauesia silana*, Parasitoid

Antagonistic Yeasts as Biocontrol Agents Against Phytopathogenic Fungi

Kheira Hiba Benghaffor[1], Hadri Zouheyr[1]

[1]Department of Agricultural Sciences, Ahmed Zabana University, Relizane, Algeria
Corresponding author: Kheira Hiba Benghaffor (e-mail: hibabenghaffor86@gmail.com)

Abstract

Phytopathogenic fungi are responsible for significant agricultural losses worldwide, affecting both the quality and quantity of crops. The widespread use of chemical fungicides has led to the development of resistance and raised environmental and health concerns, prompting the search for sustainable alternatives. Among these options, the use of antagonistic yeasts as biocontrol agents has emerged as a promising solution. This research is based on a comprehensive bibliographic review using scientific databases (PubMed, ScienceDirect, Springer, Google Scholar), selecting articles published between 2010 and 2024. Keywords used included: antagonistic yeasts, biocontrol, phytopathogenic fungi, postharvest, and antifungal mechanisms. Studies evaluating the inhibitory effects of yeasts on plant pathogenic fungi under in vitro, in vivo, or postharvest conditions were included in the selection criteria. The results indicate that various yeast species, such as *Saccharomyces cerevisiae, Aureobasidium pullulans, Wickerhamomyces anomalus, and Metschnikowia pulcherrima*, exhibit significant antifungal activity against pathogens such as *Botrytis cinerea, Fusarium spp., and Penicillium expansum.* The identified mechanisms of action include competition for nutrients and space, production of antifungal metabolites (mycocins, volatile compounds), secretion of hydrolytic enzymes (chitinases, β-glucanases), and induction of host plant resistance. The reviewed studies highlight the concrete potential of yeasts as biocontrol agents, particularly in postharvest applications. However, their effectiveness depends on several factors: yeast species, dosage, formulation, application timing, and environmental conditions. Major challenges remain, such as improving formulations, standardizing treatments, and analyzing interactions with host plants and existing microbiota. In conclusion, antagonistic yeasts offer an eco-friendly alternative to chemical fungicides, with promising prospects for sustainable agriculture. Further research and validation under real-world cultivation conditions are still required to fully integrate these agents into plant protection strategies

Keywords: Antagonistic yeasts, Biocontrol, Phytopathogenic fungi, Postharvest diseases

2nd International Conference on Multidisciplinary Sciences and Technological Developments (ICMUSTED 2025)

December 12-15, 2025

Morphological and Cultural Characterization of *Verticillium Dahliae Kleb.*, the Causal Agent of Verticillium Wilt in Olive (*Olea Europaea L.*)

Saliha Ogab[1], Houria Chaalal[1], Tahar Maza[1], Fatima Zohra Zoudji[2]

[1]Environment and Rural Development, Department of Agronomy, University of Relizane, Algeria
[2]Laboratory of Plant protection, Department of Agronomy, University Abdelhamid Ibn Badis, Mostaganem, Algeria
Corresponding author: Saliha Ogab (e-mail: saliha.ogab@univ-relizane.dz)

Abstract

Verticillium dahliae Kleb., the fungus responsible for verticillium wilt in olive trees, inflicts significant damage on the trees and has spread to many olive-growing regions in Algeria. Two isolates of the pathogen are from Sidi Belabes and three are from Mostaganem, they were identified and characterized morphologically and culturally. They were tested across a range of temperatures and pH levels during their growth on potato dextrose agar (PDA) medium. Variations in temperature and pH levels affected fungal growth and appearance. The isolates of *Verticillium dahliae* showed optimal growth and sporulation at pH 6.5 on temperature of 22 °C. This preliminary work deserves to be continued and should target larger populations of the fungus in order to confirm the results obtained. In the future, the study should focus on the identification of pathotypes and the search for resistant local cultivars, as Algerian cultivars have not yet been characterized.

Keywords: Olive trees, *Verticillium dahliae Kleb*., Isolates, Pathogen

Role of Edible Coating on Post-Harvest Management of Fruits and Vegetables

Tusneem Kausar[1], Ashiq Hussain[1]

[1]Institute of Food Science and Nutrition, University of Sargodha, Sargodha, Pakistan
Corresponding author: Tusneem Kausar (e-mail: tusneem.kausar@uos.edu.pk)

Abstract

Edible coatings play a significant role in the post-harvest management of fruits and vegetables by enhancing their shelf life, quality, and safety. Edible coatings act as a barrier to moisture loss from fruits and vegetables which helps in maintaining the texture, weight, and overall appearance of the produce, especially during storage and transportation. By preventing dehydration, they reduce the chances of wilting and shrivelling. Edible coatings also help to regulate gas exchange, which can slow down the ripening process and extend freshness. Coatings made from materials like alginate or chitosan are semi-permeable, allowing controlled respiration. Some edible coatings contain antimicrobial agents, such as essential oils (e.g., clove, cinnamon) or natural preservatives, which inhibit the growth of bacteria, molds, and yeasts. This helps in reducing spoilage and maintaining the safety and hygiene of the produce. The coatings provide a layer of protection against physical damage, such as bruising and puncturing, during handling, transportation, and storage. This protection helps maintain the quality of the produce and reduces losses. By reducing water loss and oxidation, edible coatings help preserve the nutrients in fruits and vegetables, such as vitamins (especially Vitamin C) and antioxidants, which can degrade during storage. Many edible coatings are derived from natural, biodegradable materials, making them an environmentally friendly option compared to synthetic, non-biodegradable coatings. They contribute to reducing waste, as they are compostable and safe for the environment. Edible coatings help retain the flavor of fruits and vegetables by reducing the loss of volatile compounds that contribute to taste and aroma. This improves the overall sensory quality of the produce. This review will provide the elaborate research knowledge on edible coatings composition, methods of production, regulations, pros and cons.

Keywords: Edible coating, Shelf life, Quality, Safety, Environment friendly

2nd International Conference on Multidisciplinary Sciences and Technological Developments (ICMUSTED 2025)

December 12-15, 2025

Comparison the Values of Reverse Harmonic Index of Two Types Hexagonal Cactus Chain Graphs

Mukaddes Okten Turaci[1]

[1]Department of Mathematics, Pamukkale University, Denizli, Türkiye
Corresponding author: Mukaddes Okten Turaci (e-mail: moktenturaci@pau.edu.tr)

Abstract

Graph theory has found widespread application in fields such as chemistry and biology, where it has become an important area of study in the natural sciences, particularly in mathematical chemistry. Additionally, graph theory has applications in applied mathematics, computer science, and social network analysis. In chemical graph theory, numerous graph parameters have been used to establish relationships between molecular structures and chemical behavior, physical properties, or biological effects. These parameters are generally referred to as topological indices. These indices have been used in quantitative structure-property relationship (QSPR) and quantitative structure-activity relationship (QSAR) analyses. For example, a topological index helps us to predict certain physico-chemical properties like boiling point or enthalpy of vaporization and stability. The Wiener index is the first defined topological index, and it is used to predict the boiling points of alkane compounds. Many topological indices have been defined in the literature, and recently, studies have been conducted on topological indices based on reverse degree. One of these indices is the reverse harmonic index. Let $G = (V(G), E(G))$ be a graph. A cactus graph is connected graph in which no edge lies in more than one cycle. This graph has been used in communication networks and chemistry. Hexagonal systems are considerable importance in theoretical chemistry because they are the natural graph representation of benzenoid hydrocarbon. In this study, the values of the reverse harmonic $RH(G)$ have been computed for the two types hexagonal cactus chains called the para-chain L_n and the ortho-chain O_n. Then, the results obtained have been compared with a graphic. These obtained numerical values can contribute significantly to the modelling and prediction of various physicochemical properties of the para-chain L_n and the ortho-chain O_n graphs.

Keywords: Graph theory, Reverse topological indices, Reverse harmonic index, Hexagonal cactus chains

Chitosan-Modified Silver-Doped Phosphate Glass: Physical, Structural, and Mechanical Improvements

Siti Norfariza Farhana Binti Mohd Razak[1], Nurhafizah Binti Hasim[1], Nur Hidayah Binti Ahmad[1], Norshahirah Binti Mohamad Saidi[1], Mohd Fuad Bin Mohamad[2]

[1]Advanced Optical Materials Research Group, Faculty of Science, Universiti Teknologi Malaysia, Johor, 81310 Skudai, Malaysia
[2]Department of Chemistry, Faculty of Science, Universiti Teknologi Malaysia, Johor, 81310 Skudai, Malaysia
Corresponding author: Nurhafizah Binti Hasim (e-mail: nurhafizah.h@utm.my)

Abstract

Phosphate-based glass is a biodegradable and bioactive material whose properties can be optimized by incorporating metal oxides and bioactive compounds. This study examines the effect of chitosan incorporation on the physical, structural, and mechanical properties of silver-doped phosphate biopolymer glass. Glass samples containing 0.0, 0.8, and 1.0 mol% chitosan, with a fixed 0.5 mol% silver content, were produced via the melt-quenching technique and characterized using Fourier transform infrared spectroscopy (FTIR), ultrasonic testing, and ultraviolet-visible (UV–Vis) spectroscopy. UV–Vis measurements were performed to evaluate the optical behaviour of the glasses, particularly transmittance and absorbance, which reflect changes in transparency. FTIR spectroscopy was used to examine structural features and functional groups, confirming the successful incorporation of silver chloride and chitosan into the glass network. Increasing chitosan content led to higher density and packing density, accompanied by a decrease in molar volume, indicating a more rigid and tightly connected glass structure. Ultrasonic testing was employed to assess mechanical performance, and the resulting acoustic impedance values showed an initial increase with higher chitosan concentrations, suggesting enhanced compactness and structural stiffness of the material. Overall, the incorporation of chitosan improves the structural integrity and mechanical performance of silver-doped phosphate glass while modifying its optical properties. These findings highlight the potential of chitosan-modified phosphate glasses for biomedical and bioactive material applications.

Keywords: Chitosan, Density, UV-Vis, FTIR, Ultrasonic testing

2nd International Conference on Multidisciplinary Sciences and Technological Developments (ICMUSTED 2025)

December 12-15, 2025

Methylammonium Iodide Doped CMC Electrolyte: A Safer and Environmentally Friendly Solution for Sustainable Power Storage

Na'imah Husna Nasaruddin[1], Nur Hidayah Ahmad[1]

[1]Physics Department, Faculty of Science, University Teknologi Malaysia, 81310 Skudai, Johor, Malaysia
Corresponding Author: Nur Hidayah Ahmad (email: nurhidayahahmad@utm.com)

Abstract

With the expending population in the world, the need to satisfy the increasing demand for power storage pushing the renewable energy research to thrive and expanding. Common electrochemical like a battery has gone through many research to get produce much safer and environmentally friendly. Solid biopolymer electrolyte been getting lot of attention due to its biodegradable properties, as well as cost-saving and abundant. Carboxymethyl cellulose (CMC) is a perfect biopolymer to be used for the electrolyte in a battery. The liquid electrolyte used in battery could cause combustion when exposed to the air or leaking due to long period. By doping the CMC with methylammonium iodide (MAI) to enhance the conductivity and the electron transport properties. Propylene carbonate (PC) is used as the plasticizer for the CMC-MAI system as it has high dielectric constant and boiling point. 8wt.% PC was used as it has the highest conductivity making it the perfect concentration to plasticize the solid biopolymer electrolyte for optimum electron transfer. The characterisation of the CMC-MAI-PC will be done by using electrical impedance spectroscopic (EIS) and transference number measurement (TNM). In this review, the progress regarding the half-cell application with CMC-MAI-PC as the electrolyte will be discussed as the ionic inductivity for the CMC-MAI has been optimized to ensure the highest conductivity for the half-cell. The half-cell properties such as the open circuit voltage (OCV), cyclic voltammetry (CV), galvanometric charge-discharge (GCD) and the life cycle will be investigated. The in depth research and understanding of CMC-MAI electrolyte can be improved and developed for the future of sustainable electrochemical power storage in the future.

Keywords: Solid biopolymer electrolyte, Carboxymethyl cellulose, Electrochemical, Half-cell, EIS

A Green Laser Ablation Approach to Ag/*Cinnamon Cassia* Nanohybrid for Sensitive Colorimetric Glucose Sensing Applications

Fitriyatun Naldiyah[1], Wulandari Dwi Lestari[1], Adeka Delvis Tama[1], Muhammad Dimas Adytia Airlangga[1], Nurul Hidayat[1]

[1]Department of Physics, Universitas Negeri Malang, Malang, Indonesia
Corresponding author: Nurul Hidayat (e-mail: nurul.hidayat.fmipa@um.ac.id)

Abstract

Diabetes is a disease that many people suffer from, especially diabetes mellitus which is caused by high blood sugar levels in the body. Glucose ($C_6H_{12}O_6$) is a type of monosaccharide sugar that is the main source of energy for the body, and is a type of sugar that causes diabetes if consumed in excess. Factors that cause diabetes are diet and the types of food consumed. Early monitoring of diabetes is important to control blood sugar levels. One way that can be done is to develop a nanotechnology-based glucose sensor. Nanohybrid materials are a combination of organic and inorganic materials that are combined to improve performance and can be developed as nanotechnology. In this study, silver nanoparticles (AgNPs)/*Cinnamon cassia* synthesized using the neodymium-doped yttrium aluminium garnet (Nd:YAG) laser ablation method with a wavelength of 1064 nm was used as a glucose sensor. The laser ablation synthesis method was chosen because of its advantages of being clean, fast, and without additional chemicals. To determine the improvement of this sensor, a synthesis process was carried out to determine the best energy optimization with several variations, namely, 200 mJ, 250 mJ, 300 mJ, 350 mJ, and 400 mJ. Each energy variation in the AgNPs/*Cinnamon cassia* colloid was mixed with glucose levels (0%, 1%, 2%, 3%, 4%, and 5%). Based on the results of the ultraviolet-visible (UV-Vis) test, at an energy variation of 200 mJ the sensitivity was 0.06749 a.u./%, 250 mJ had a sensitivity of -0.01737 a.u./%, 300 mJ had a sensitivity of 0.01109 a.u./%, 350 mJ had a sensitivity of 0.03949 a.u./%, and 400 mJ had a sensitivity of 0.07309 a.u./%. In this study, 400 mJ energy had the highest sensitivity with near constant linearity. Therefore, the combination of AgNPs/Cinnamon cassia has great potential in increasing the sensitivity of glucose sensors and becoming an innovation in the health sector.

Keywords: Nanohybrid, Cinnamon cassia, AgNPs, Laser ablation, Glucose sensor

2nd International Conference on Multidisciplinary Sciences and Technological Developments (ICMUSTED 2025)

December 12-15, 2025

Composition-Dependent Thermal, Mechanical, and Electrical Responses of CMC–CA–Glycerol Biopolymeric Films

Noorul Ain Binti Kamal Ariffin[1], Nurhafizah Binti Hasim[1]

[1]Advanced Optical Material Research Group, Faculty of Science, University of Technology Malaysia, 81310 Skudai, Johor, Malaysia
Corresponding author: Nurhafizah Binti Hasim (e-mail: nurhafizah.h@utm.my)

Abstract

This study was conducted in the field of sustainable polymer development, focusing on the preparation of biodegradable plastics based on carboxymethyl cellulose (CMC) as a more environmentally responsible alternative to conventional petroleum-based plastics. The main issue addressed is limitations of pure CMC films which are low mechanical strength, brittleness, and high hydrophilicity. It also evaluates how citric acid crosslinking and glycerol plasticization jointly affect these properties. Seven biodegradable plastic samples were fabricated via the solution casting technique, consisting of pure CMC, CMC crosslinked with CA, and five CMC–CA films plasticized with 3%, 6%, 9%, 12%, and 15% glycerol. Thermal behaviour was analyzed using differential scanning calorimetry (DSC) and thermogravimetric analysis (TGA), mechanical properties were measured through tensile testing, surface wettability was evaluated through water contact angle (WCA) measurements, and electrical properties were examined using electrical impedance spectroscopy (EIS). The results demonstrate that citric acid crosslinking enhances the thermal stability and structural integrity of CMC films, while glycerol contributes to improved flexibility but reduces tensile strength at higher concentrations. Increased glycerol content also promotes greater hydrophilicity, and the electrical parameters, namely resistance, conductivity and dielectric response exhibit composition-dependent variations. Overall, the findings confirm that an optimised CMC–CA–glycerol formulation can produce biodegradable plastic films with desirable thermal, mechanical, surface and electrical characteristics, thereby demonstrating strong potential for application in biopolymer-based sustainable material systems.

Keywords: Carboxymethyl cellulose, Citric acid, Glycerol, Differential scanning calorimetry, Thermogravimetric analysis

2nd International Conference on Multidisciplinary Sciences and Technological Developments (ICMUSTED 2025)

December 12-15, 2025

High-Sensitivity Atrazine Sensor Using Aluminum Plasmonics and Molecular Imprinting

Mohamed Esseddik Ouardi[1,2], Kada Abdelhafid Meradi[1,2], Fatima Tayeboun[2,3]

[1]Department of Science and Technology, University of Ain Temouchent, 46000 Ain Temouchent, Algeria
[2]Laboratory of Materials Sciences and Applications, University of Ain Temouchent, 46000 Ain Temouchent, Algeria
[3]University Djillali Liabes, 22000 Sidi-Bel-Abbes, Algeria
Corresponding author: Mohamed Esseddik Ouardi (e-mail: mohamed.ouardi@univ-temouchent.edu.dz)

Abstract

The pervasive use of atrazine, a potent triazine herbicide, has led to its concerning persistence as a contaminant in water resources, where it acts as an endocrine disruptor with significant ecological and public health implications. Regulatory limits for atrazine in drinking water are exceptionally stringent, often set at parts-per-trillion levels, demanding analytical methods that combine ultra-high sensitivity with robust selectivity. While conventional techniques like gas chromatography-mass spectrometry (GC-MS) are reliable, their operational complexity and lack of portability highlight the need for advanced sensing platforms suitable for on-site, rapid monitoring. This paper presents a comprehensive simulation study of a novel, high-performance plasmonic sensor designed for the specific and sensitive detection of atrazine in aqueous environments. Departing from conventional gold and silver-based sensors, the proposed design utilizes a 40 nm aluminum thin film on a quartz substrate, engineered to operate in the far- to deep-ultraviolet (FUV-DUV) spectral range. This strategic use of aluminum plasmonics capitalizes on its ability to generate sharper resonance profiles and lower radiation damping in the UV region compared to noble metals in the visible spectrum. To confer molecular specificity, the aluminum surface is functionalized with a molecularly imprinted polymer (MIP) layer, which creates synthetic, atrazine-selective cavities within its matrix. The sensor's performance was rigorously modeled using the transfer matrix method (TMM). The binding of atrazine molecules into the MIP cavities was simulated via a Langmuir adsorption isotherm, translating the subsequent localized refractive index change into a quantifiable shift in the plasmonic resonance angle. The simulated results demonstrate exceptional performance, with a sensitivity of 130 °/RIU and a remarkably high figure of merit (FOM) of 97 RIU^{-1}. The sensor achieves a theoretical limit of detection (LOD) of 0.8 pM, with a linear response spanning from 1 pM to 10 nM. Crucially, the sensor model predicts outstanding selectivity, showing a response to atrazine that is over 20 times greater than that for structurally similar interferents (simazine and propazine) at 100-fold higher concentrations. This is a direct consequence of the precise molecular imprinting process. Furthermore, the sensor exhibits excellent resilience to matrix effects, with atrazine recovery rates of 98-102% in the presence of humic acid, demonstrating effective resistance to fouling by natural organic matter. This study establishes a compelling theoretical foundation for an aluminum-based MIP-functionalized plasmonic sensor. The predicted metrics–ultra-high sensitivity, picomolar detection limits, and exceptional specificity in complex aqueous matrices–suggest this platform is a highly promising candidate for the next generation of environmental monitoring tools, paving the way for its physical fabrication and real-world application in trace pesticide detection.

Keywords: Surface plasmon resonance, Plasmonics, Pesticide, Sensors

Tailoring the Structural, Electrical, and Magnetic Properties of $Ni_{0.35}Zn_{0.25}Cd_{0.4}Fe_{1.97}Ce_{0.03}O_4$/GNPs Composites

Muhammad Ajaz Un Nabi[1]

[1]Department of Physics, Government College University, Faisalabad, Pakistan
Corresponding author: Muhammad Ajaz Un Nabi (e-mail:majazunnabi@gcuf.edu.pk)

Abstract

This study explores the impact of graphene nanoplatelets (GNPs) incorporation on the magneto-dielectric properties of nickel-zinc-cadmium-cerium ferrite (NZCCF)/GNPs composites. A series of $Ni_{0.35}Zn_{0.25}Cd_{0.4}Fe_{1.97}Ce_{0.03}O_4$/x-GNP (x = 0, 1.25, 2.5, 3.75, and 5 wt%) composites were synthesized using the sol–gel auto-combustion (SGAC) method. X-ray diffraction (XRD) confirmed the formation of a cubic spinel phase in all samples, with enhanced crystallite size upon GNPs addition. Increased d-spacing at lower GNPs concentrations suggested slight lattice expansion. Electrical analysis via current–voltage (I–V) characteristics demonstrated semiconducting behavior, with reduced resistivity upon GNPs incorporation. Dielectric characterization revealed that the 2.5 wt% GNP composite exhibited the lowest real permittivity and highest tangent loss, indicating potential for high-frequency applications. Magnetic measurements showed improved properties for the NZCCF/2.5 wt% GNPs composite, including enhanced saturation magnetization (79.03 emu/g), coercivity (179 Oe), remanence (6.38 emu/g), and squareness ratio (0.08). The combination of optimized dielectric and magnetic properties in the 2.5 wt% GNP composite highlights its promise for energy storage and high-frequency device applications.

Keywords: Ni-Zn-Cd ferrite, Spinel ferrite/GNPs composites, Rare earth substituted ferrites, Magnetic properties, Dielectric properties

2nd International Conference on Multidisciplinary Sciences and Technological Developments (ICMUSTED 2025)

December 12-15, 2025

Cadmium Sulfide Thin Film-based Photodetector: Fabrication and Photoresponse Evaluation

Erman Erdogan[1]

[1]Department of Electronics and Automation, Vocational High School, Bilecik Seyh Edebali University, 11100 Bilecik, Türkiye
Corresponding author: Erman Erdogan (e-mail: erman.erdogan@bilecik.edu.tr)

Abstract

In this work, a CdS/p-Si heterojunction device was created by electrodepositing CdS thin films onto an n-Si substrate. Ohmic and Schottky connections were formed using the thermal evaporation process to build the device. Visible light of varying intensities was used to assess the semiconductor-semiconductor heterojunction photodetector's current-voltage. X-ray diffraction (XRD) and a scanning electron microscope (SEM) were used to investigate the resulting structure. Examining the CdS thin film's XRD analysis reveals distinct XRD peaks. Electrical tests and SEM results corroborate these structural characterisation findings, which are consistent with findings in the literature. A granular texture can be seen in the created CdO thin film's SEM image. Using the Debye-Scherer equation, the crystal size value was determined to be 15.31 nm. Current-voltage (I-V) measurements in both light and dark conditions were used to estimate the device's characteristics. Using visible light sources with energies ranging from 20 mW/cm^2 to 80 mW/cm^2, photodetector parameters were established. In visible light, the constructed heterojunction's highest photodetector parameters were D = 1.93×10^4 (80 mW, V = –1.0 V) Jones and R = 50.1 mA/W (80 mW, V = –1.0 V).

Keywords: Photodetector, Responsivity, Detectivity, CdS, Electrodeposition

2nd International Conference on Multidisciplinary Sciences and Technological Developments (ICMUSTED 2025)

December 12-15, 2025

Experimental Evidence of Thermally Activated Transport at the Mobility Edge in 4H Silicon Carbide Metal-Oxide-Semiconductor Field Effect Transistor

Sabrina Meguellati[1], Mustapha Sarra[1]

[1]ETA Laboratory, Institute of Electronics and Telecommunications, Mohamed El Bashir El Ibrahimi University of Bordj Bou Arreridj, Algeria
Corresponding author: Sabrina Meguellati (e-mail: s.meguellati@univ-bba.dz)

Abstract

We provide experimental evidence of thermally activated transport in n-channel, lateral 4H silicon carbide metal-oxide-semiconductor field effect transistor (4H-SiC MOSFET). The transfer curves are measured at high and low fields in a range of temperatures (300 K to 550 K) and, hence the field effect mobility, show a positive dependence with temperature. The Arrhenius analysis yielded average activation energies around 40 meV, while the inverted channel conductivity shows thermally activated behaviour close to the metallic minimum ($\sigma_{min} = 3.7\times10^{-5}$ S), with non-ideal energy dependence following reverse Meyer-Neldel rule (with energy $E_{MN} = -148$ meV). The associated localized states are attributed to a dominant positive oxide charge and, probably, backed by recent studies on scattering, dipoles at the oxide/semiconductor interface. The studied sample shows an anomaly at 400 K that was explained by traps compensation effects. This study confirms the disorder-related hypothesis of temperature-dependent transport enhancement in 4H-SiC MOSFET despite the low channel mobility.

Keywords: 4H-SiC, Thermal activation, Mobility edge, Conductivity, Meyer-Neldel rule

2nd International Conference on Multidisciplinary Sciences and Technological Developments (ICMUSTED 2025)

December 12-15, 2025

Normalized Differential Conduction Analysis of Temperature-Dependent Gate Conduction in 4H-SiC MOS Capacitor

Sabrina Meguellati[1], Mustapha Sarra[1]

[1]Institute of Electronics and Telecommunications, Mohamed El Bashir El Ibrahimi University of Bordj Bou Arreridj, Algeria
Corresponding author: Sabrina Meguellati (e-mail: s.meguellati@univ-bba.dz)

Abstract

We report on the use of the normalized differential conductance method (NDC) to investigate oxide conduction in a metal–oxide–semiconductor (MOS) capacitor, with thermally grown SiO_2 on 4H-SiC, over a wide range of temperatures (300 K to 570 K). NDC plots of forward current–voltage (I–V) measurements revealed conduction features that are not evident in either the raw I–V curves or standard analysis plots. The inspection of NDC plots at each temperature, in search of possible gate conduction mechanisms, allowed to identify Fowler-Nordheim (FN) and trap-assisted-tunnelling (TAT) throughout the temperature range. The NDC–based FN analysis revealed barrier heights closer to theoretical expectation (2.74 eV at 300K) than standard FN analysis (2.57 eV at 300 K), while both methods yielded temperature coefficients close to the theoretical prediction (NDC: -0.96meV/K, standard FN: –0.98 meV/K vs ideal: –0.7 meV/K). TAT parameters showed an average trap level around 2.8 eV with about 4×10^{14} $cm^{-2}eV^{-1}$ trap density, indicating intrinsic electron trapping in the SiO_2 layer. The NDC method excluded Poole-Frenkel and Schottky emission mechanisms, confirmed by the standard plots' extraction of non-realistic parameters. These results demonstrate that NDC enhances the extraction of physical parameters compared with conventional analysis, establishing it as a rapid and reliable tool for gate oxide reliability assessment in wide-bandgap MOS devices.

Keywords: Gate conduction, 4H-SiC, Normalized differential conductance, Fowler-Nordheim, Trap-assisted-tunnelling

2nd International Conference on Multidisciplinary Sciences and Technological Developments (ICMUSTED 2025)

December 12-15, 2025

Tailoring Phosphate Glass Performance: Structural, Mechanical, and Optical Enhancement via Chitosan Doping

Nurhafizah Hasim[1]

[1]Advanced Optical Materials Research Group, Faculty of Science, Universiti Teknologi Malaysia, Johor, 81310 Skudai, Malaysia
Corresponding author: Nurhafizah Hasim (e-mail: nurhafizah.h@utm.my)

Abstract

Phosphate-based glasses are attractive for functional materials due to their low melting temperature and compositional versatility, yet their application is often constrained by limited mechanical strength and modest optical performance. This work examines how introducing chitosan influences the structural, mechanical and optical properties of zinc–strontium–lithium phosphate glass. Glasses with the composition $(40 - x)P_2O_5 - 30ZnO - 25Li_2O - 5SrO - (x)$ concentrations (0.0–1.0 mol%) were synthesized via melt-quenching. Fourier transform infrared (FTIR) spectroscopy and raman spectroscopy confirmed progressive modifications of the phosphate network as chitosan content increased, indicating enhanced crosslinking and structural rearrangement. Ultrasonic measurements revealed notable improvements in hardness and elastic moduli, demonstrating mechanical reinforcement of the glass matrix. Ultraviolet–visible (UV–Vis) analysis showed increased optical density and reduced transmittance, suggesting improved UV–blocking capability. Overall, chitosan doping provides an effective strategy to tune the multifunctional behaviour of phosphate glasses, highlighting their potential for biomedical devices and protective optical applications.

Keywords: Phosphate glass, Chitosan, FTIR, Ultrasonic testing, UV–Vis

Effect of Incorporating Graphene Oxide Nanoparticles on Ion Mobility in Deep Eutectic Polymer Electrolyte

Siti Norfazleen Farhana Binti Mohd Razak[1], Norshahirah Binti Mohamad Saidi[1]

[1]Advanced Optical Material Research Group, Faculty of Science, Universiti Teknologi Malaysia, Johor, 81310 Skudai, Malaysia

Corresponding author: Norshahirah Binti Mohamad Saidi (e-mail: norshahirah.ms@utm.my)

Abstract

Deep eutectic polymer electrolytes (DES-PEs) have emerged as attractive alternatives to conventional liquid electrolytes due to their enhanced safety, low volatility, and ability to support efficient ion transport. In this study, DES-PE system was prepared using a deep eutectic solvent composed of 1,3-propanediol and ethylene glycol acting as the DES, mixed with polyacrylonitrile (PAN) and lithium perchlorate serving as the host polymer and ion promoter, respectively. Graphene oxide (GO) nanoparticles were added as nanoparticle fillers to enhance the performance of DES-PEs, specifically the ionic conductivity, bulk resistance, and dielectric properties. Electrochemical impedance spectroscopy (EIS) was used as the primary characterization technique to evaluate dielectric properties within the electrolyte system. The presence of the DES reduces polymer crystallinity and increases the amorphous phase, promoting easier movement of Li^+ ions, while GO nanoparticles introduce additional conduction pathways and improve ion mobility. Although the concentration of GO was varied, an optimal GO nanoparticle concentration could achieve high performance of DES-PEs with lower bulk resistance, thereby leading to outstanding ionic conductivity and dielectric properties. Overall, the synergistic interaction between DES and GO nanoparticles highlights their strong potential for improving ion-transport mechanisms in polymer electrolytes and contributing to the development of safer, high-performance materials for next-generation electrochemical energy-storage applications.

Keywords: Deep eutectic solvents, Polyacrylonitrile, GO, EIS

2nd International Conference on Multidisciplinary Sciences and Technological Developments (ICMUSTED 2025)

December 12-15, 2025

Composability of Nanofillers Carboxymethyl Cellulose Doped Ammonium Thiocyanate for Bioplastic Packaging

Hazwani Nadirah Zamri[1], Nur Hidayah Ahmad[1]

[1]Advanced Optical Material Research Group, Faculty of Science, University Teknologi Malaysia, 81310 Skudai, Johor, Malaysia
Corresponding author: Nur Hidayah Ahmad (email: nurhidayahahmad@utm.my)

Abstract

The growing environmental worries about plastics made from oil have sped up the creation of biodegradable packaging materials made from renewable resources. The biodegradability, transparency as well as higher film-forming ability of carboxymethyl cellulose (CMC) make it suitable as a potential biopolymer. Nevertheless, its poor mechanical, thermal durability and high moisture sensitivity limit its practical use. This study intends to optimize the performance of CMC films by integrating ammonium thiocyanate (AT) as an ionic dopant and zinc oxide (ZnO) nanoparticles as reinforcing fillers. Bioplastic films were prepared using the solution casting method where CMC was doped with fixed concentrations of AT and hydrogen peroxide and followed by the incorporation of ZnO at varying loadings (0,2,4,6,8,10 wt%). The resulting CMC–AT–ZnO films were characterized for their physical properties (film thickness, moisture content, water solubility, water vapour permeability, Ultraviolet-visible (UV–Vis) spectroscopy, surface morphology, field emission scanning electron microscope (FESEM) for high-resolution imaging and an energy dispersive X-ray (EDX) (FESEM–EDX) spectroscopy, structural and thermal behaviour Fourier transform infrared spectroscopy (FTIR), X-ray diffraction (XRD) and differential scanning calorimetry / thermogravimetric analysis (DSC/TGA), mechanical strength, biodegradability and microbial activity. The presence of AT improved polymer chain mobility and facilitated ionic interactions while ZnO nanoparticles enhanced mechanical reinforcement, reduced water absorption and increased UV-blocking capability. FTIR and XRD tests demonstrated strong intermolecular contacts and changed crystallinity, whilst DSC/TGA data indicated better thermal stability with increased ZnO content. Mechanical tests showed that ZnO-reinforced films displayed increased tensile strength and biodegradation experiments demonstrated that the films remained ecologically friendly despite the addition of dopants and nanofillers. Microbial tests further demonstrated reduced microbial growth related to the antibacterial impact of ZnO. Overall, the complementary combination of CMC, AT, and ZnO nanoparticles produced bioplastic films with enhanced practical characteristics ideal for sustainable packaging applications. This research provides light on the development of high-performance biodegradable polymers that may replace conventional plastics in a way that is sustainable.

Keywords: Bioplastic, Carboxymethyl cellulose, Ammonium thiocyanate, Zinc oxide nanoparticles, Sustainable packaging

2nd International Conference on Multidisciplinary Sciences and Technological Developments (ICMUSTED 2025)

December 12-15, 2025

Study of the Dynamic of Benthic Diatom Communities in Response to Water Fluctuations Along Specific Rivers in Skikda Province, North East Algeria

Hadjer Kaddeche[1]

[1]Department of Ecology and Environment, University of 20 August 1955, Skikda, Algeria
Corresponding author: Hadjer Kaddeche (e-mail: kaddechehadjer@gmail.com)

Abstract

Benthic diatoms have been widely used to monitor aquatic ecosystems. The current study focused primarily on selected streams in Algeria. The purpose of this study is to analyze the development of diatom flora in response to variations in abiotic parameters across Skikda town's streams. Diatoms sampling was carried out according to the French Standardization Association technique. In addition to diatom sampling, physicochemical analysis of collected water samples were performed through six sampling points. Two of the stations studied have high dissolved oxygen content greater than 8 mg/l and a low nutrient intake. The aforementioned sampling points are populated by diatom indicators of moderate to good water quality including *Nitzschia dissipata*, *Reimeria sinuata* and *Rhoicosphenia abbreviata*. While the taxa *Craticula accomoda* and *Mayamaea permitis* are indicator species of ecosystems loaded with organic matter combined with a strong anthropic impact, which supports their occurrence in stations involving substantial biological oxygen demand. According to the findings, the composition and diversity of benthic diatom communities can provide insights into water components such as organic compounds, water salinity, and water pollutants.

Keywords: Diatom communities, Indicators, Physicochemical analysis, Water components, Streams

2nd International Conference on Multidisciplinary Sciences and Technological Developments (ICMUSTED 2025)

December 12-15, 2025

Discharge Prediction using Artificial Neural Networks: A Case Study for the Enoree River, South Carolina, USA

Betul Mete[1], Sinan Nacar[2], Adem Bayram[1]

[1]Department of Civil Engineering, Karadeniz Technical University, Trabzon, Türkiye
[2]Department of Civil Engineering, Tokat Gaziosmanpasa University, Tokat, Türkiye
Corresponding author: Betul Mete (e-mail: betulmeteofis@gmail.com)

Abstract

This study focuses the predictability of river discharge using artificial neural networks method using hydro-meteorological data. Daily precipitation and air temperature data (1986-2022) from five meteorological stations were processed via the Thiessen polygon method, and the average values were obtained for the Enoree River Basin, South Carolina, USA. To determine the input parameters, correlation analyses were performed between the discharge data provided by a monitoring station in the basin and average precipitation and temperature values, as well as cumulative precipitations. Four models were developed using different input combinations. The performance of the models was evaluated with the root mean square error (RMSE), mean absolute error (MAE), and Nash-Sutcliffe efficiency coefficient (NSEC) statistics. The models including cumulative precipitation as an input parameter had higher NSEC values, ranging from 36.70 to 83.44%, compared to other models. It was concluded that including cumulative precipitation significantly improved model performance. For the best model, which have non-lagged temperature, two-day lagged precipitation, and cumulative precipitation of 15 days, NSEC values range from 0.565 to 0.677. These values are acceptable in the literature. This study highlights the potential of data-driven approaches for discharge predicting, particularly in data-scarce or hydrologically complex regions. Additionally, the study provides a basis for climate change impact assessments in the basin by offering insights into the discharge predictability.

Keywords: Artificial neural networks, Discharge, Enoree River, Modeling, Thiessen polygon method

1. INTRODUCTION

Rivers are one of the most critical resources of accessible freshwater. An essential part of the water used for domestic, agricultural, industrial, and ecological purposes are supplied from rivers [1]. Thus, long-term monitoring of discharge is a key issue of hydrological research [2]. However, the availability of continuous and reliable discharge records remains limited due to financial, logistical, or environmental constraints in many basins [3, 4]. This situation has motivated researchers to predict river discharges using various climatic parameters.

Precipitation and air temperature are significant climatic drivers for river discharge. Precipitation contributes to discharge both directly (runoff) and indirectly (infiltration, percolation, and groundwater recharge). On the other hand, because temperature causes changes in evaporation, it has an indirectly effect on discharges [5]. The nonlinear and complex relationships among precipitation, temperature, and discharge cause challenges for modeling [6]. In recent years, artificial neural networks (ANNs) have widely used for modeling river discharges [7–11].

This study investigates the predictability of river discharge using hydro-meteorological data. Precipitation and air temperature data covering the period from 1986 to 2022 were used in the study. Discharge data were obtained from a monitoring station operated by the United States Geological Survey (USGS), while precipitation and air temperature data were provided from five meteorological stations operated by the National Weather Service for the Enoree River Basin. After the handling of missing values in the time series, ANN models were developed using different combinations of the average precipitation and temperature data obtained using the Thiessen polygon method as input variables to predict discharge. The performance of the models was evaluated using three performance statistics. Beyond model performance evaluation, the results provide a foundation for future studies investigating the potential impacts of climate change on hydrological processes.

2. MATERIAL AND METHOD

2.1. Study Area

The Enoree River Basin, one of the sub-basins of the Broad River Basin, is located within the borders of the South Carolina, USA. The river has 170 km main branch and 1,863 km^2 drainage area [12]. It is covered of 59.6% forest, 26.0% built-up, 10.8% dense short vegetation, and the remaining area consists of cropland, wetland, and open surface waters. In the basin having a subtropical climate, the daily average highest and lowest temperatures are 22 and 11 °C, respectively. The average annual precipitation is approximately 1,200 mm [13]. The discharge data were for the USGS river monitoring station (02160700). Temperature and precipitation data were obtained from five meteorological observation stations namely, Union, Laurens, Spartanburg, Greenville, and Ceasars Head, around the basin operated by National Weather Service. The locations of the stations are illustrated in Figure 1.

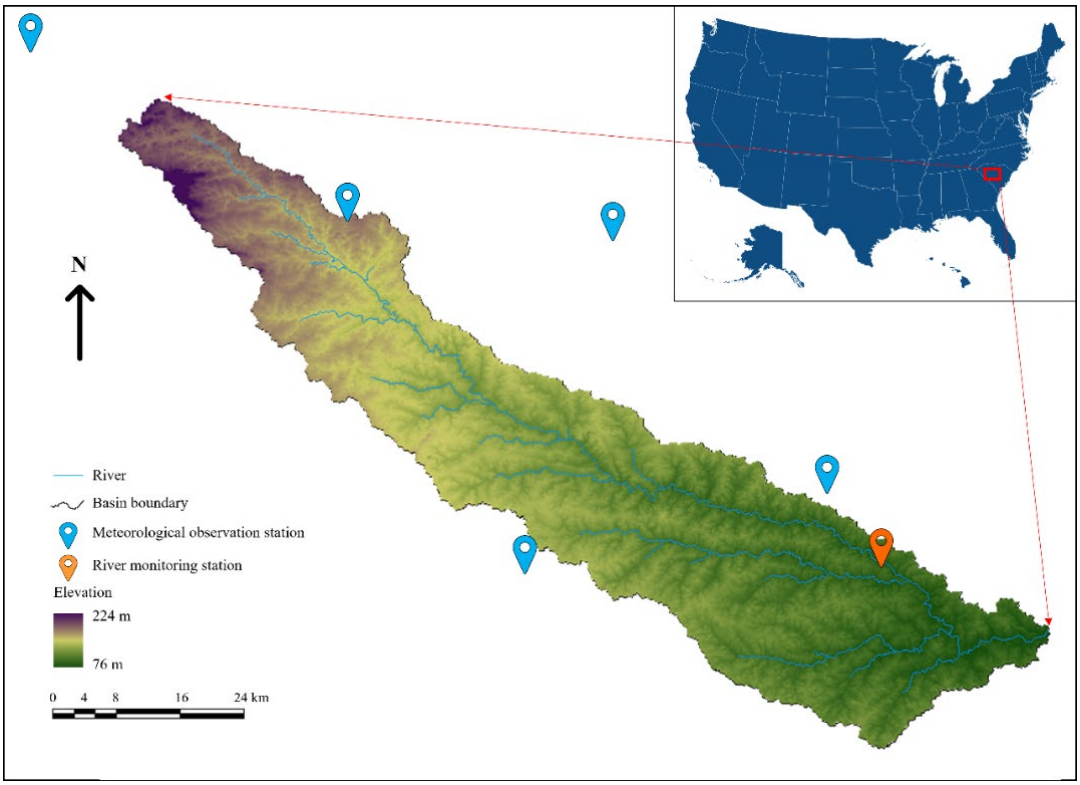

Figure 1. The locations of the stations in the Enoree River Basin, South Carolina, USA

2.2. Thiessen Polygon Method

The Thiessen polygon method is a deterministic spatial weighting technique used to determine the representative area of point-based measurements within a given region [14]. In this method, polygons are constructed around each observation point. Each polygon thus defines the spatial extent over which the corresponding station's measurements are considered valid [15].

This method is widely applied in meteorological and hydrological studies, particularly for estimating areal averages of variables such as precipitation. It is especially useful when observation points are irregularly distributed, and spatial weighting is required. The average area is calculated by weighting each station's value by the area of its corresponding polygon. The method assumes that conditions are homogeneous within each polygon [16]. This study used the Thiessen method to determine the influence areas of the meteorological stations. This process yielded a single value for precipitation and temperature for the basin, considering the influence of the stations on a weighted basis.

2.3. ANNs Method

ANNs are complex systems inspired by the structure of the human brain [17]. Artificial neural cells are connected to each other with different connection geometries. The ANN architecture (Figure 2) has consisted of three or more layers, namely, input layer, hidden layers, and output layer [18]. In a multi-layer network, the number of hidden layers can be more than one [19]. Each layer is composed of neurons that process information through weighted connections. During training, the network adjusts these weights using optimization algorithms to minimize the difference between predicted and actual outputs. Due to the adaptability and ability to learn from data, ANNs are widely used in data-driven studies [20]. The ANNs analyses were performed via MATLAB 2020b software.

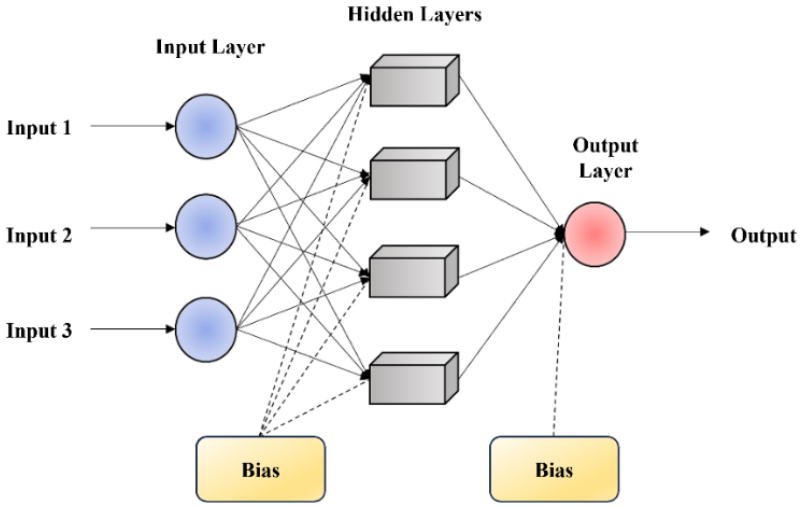

Figure 2. The ANNs architecture

2.4. Construction of the Modeling Data Sets

Preparation of meteorological and hydrological data is a critical step in the development of the discharge prediction models. In this study, firstly, missing values in the precipitation and temperature time series were made up a deficiency using regression analyses. Secondly, Thiessen polygons were generated using ArcMap 10.8 software to determine the spatial influence of each meteorological station for the Enoree River Basin. Using the areas of influence derived from these polygons average precipitation and temperature values were calculated in the basin. The basic statistics of the precipitation and temperature data for each meteorological station and the influence areas of the stations calculated with the help of the Thiessen polygon method are given in Table 1. The drainage area of the USGS station was considered when drawing the polygons.

Table 1. The basic statistics of the precipitation and temperature data and Thiessen polygon area of the meteorological observation stations in the Enoree River Basin (T: Temperature, P: Precipitation, Min: Minimum, Ave: Average, Max: Maximum, Sd: Standard Deviation, C_s and C_k: Skewness and kurtosis coefficients)

Station	Parameter	Min	Ave	Max	Sd	C_s	C_k	Polygon Area (km^2)
Union	T	–10.3	15.6	31.9	8.5	–0.3	–1.0	184.1
	P	0.0	3.6	186.2	10.1	4.9	38.8	
Spartanburg	T	–8.6	16.2	31.9	8.1	–0.3	–1.0	21.2
	P	0.0	3.6	213.4	10.3	5.6	56.6	
Laurens	T	–9.7	16.0	32.2	8.5	–0.3	–1.0	375.0
	P	0.0	3.5	135.9	9.8	4.7	31.2	
Greenville	T	–9.4	16.3	32.8	8.2	–0.3	–0.9	546.1
	P	0.0	3.5	136.1	9.8	4.6	28.6	
Caesars Head	T	–18.1	12.5	27.8	7.8	–0.5	–0.6	19.1
	P	0.0	5.6	213.9	13.9	4.2	27.1	

In order to select input variables, correlation analyses were applied between discharge and lagged versions of precipitation and temperature data. Additionally, the correlations of time series with 5, 10, and 15 days cumulative precipitation (CumP) values with the discharge were also analysed (Table 2). Four different models were established with different combinations of the time series with the highest correlation coefficient (Table 3).

Table 2. Correlation coefficients between possible input parameters and discharge (Bold: The highest value)

	T				P				CumP		
	0	1 day	2 day	3 day	0	1 day	2 day	3 day	5	10	15
Pearson	**–0.217**	–0.203	–0.196	–0.197	0.170	0.503	**0.592**	0.355	**0.640**	0.550	0.502
	0.000	0.000	0.000	0.000	0.000	0.000	**0.000**	0.000	**0.000**	0.000	0.000
Spearman	**–0.434**	–0.430	–0.424	–0.424	0.126	0.278	**0.334**	0.261	0.469	0.530	**0.539**
	0.000	0.000	0.000	0.000	0.000	0.000	**0.000**	0.000	0.000	0.000	**0.000**

Table 3. The input combinations of discharge prediction models

Model	Input variable		
M1	P_{t-2}		
M2	P_{t-2}	T_t	
M3	P_{t-2}	T_t	$CumP_5$
M4	P_{t-2}	T_t	$CumP_{15}$

There were 13,500 daily average data (from January 1986 to December 2022) for each parameter. The data were divided into three sets, training (60.6%), validating (19.7%), and testing (19.7%). The 4th, 5th, 14th, 15th, 24th, and 25th days of each month were allocated for testing, while the 6th, 7th, 16th, 17th, 26th, and 27th days for validating data sets. The rest was included in the training data set. This division was made in such a way that both extreme values remained within the training data set and all three data sets contained representative data for each month. It may be challenging to model extreme values in data sets. Therefore, all data were normalized using Equation (1) to minimize the effects of the size differences of the parameters in the data set on the modeling ability and to increase the model performances.

$$X_n = \frac{X_i - X_{\min}}{X_{\max} - X_{\min}} \cdot 0.8 + 0.1 \tag{1}$$

where, X_n, X_i, X_{min}, and X_{max} stand for the normalized, raw, minimum, and maximum values, respectively.

2.5. Model performance statistics

The performances of the discharge prediction models were compared using the root mean square error (RMSE), mean absolute error (MAE), and Nash-Sutcliffe efficiency coefficient (NSEC) statistics, which were calculated using Equations (2)–(4). Smaller RMSE and MAE values indicate improved model performance [21]. Additionally, the predictive capability of the model becomes stronger as the NSEC value approaches 1 [22].

$$\text{RMSE} = \sqrt{\frac{1}{N}\sum_{i=1}^{N}\left(y_i - yd_i\right)^2} \tag{2}$$

$$\text{MAE} = \frac{1}{N}\sum_{i=1}^{N}\left|\left(y_i - yd_i\right)\right| \tag{3}$$

$$NSEC = 1 - \frac{\sum_{i=1}^{N}\left(y_i - yd_i\right)^2}{\sum_{i=1}^{N}\left(y_i - \bar{y}\right)^2} \tag{4}$$

where N, y_i, yd_i, and $\bar{y}$, stand for data number, monitored and predicted values, and average of monitored values, respectively

3. RESULTS

The prediction abilities of the models were compared with each other based on performance statistics (Table 4). In Table 4, RMSE values range from 11.33 to 14.78, 11.56 to 14.58, and 10.96 to 14.3 m^3/s, respectively, and MAE values vary from 5.83 to 7.80, 6.00 to 8.03, and 5.78 to 7.79 m^3/s, respectively, for the training, validating, and testing data sets. NSEC values change from 0.450 to 0.677, 0.308 to 0.565, and 0.434 to 0.667, respectively, for the same data sets. The lowest RMSE and MAE values, as well as the highest NSEC values were obtained from M4 including P_{t-2}, $T_{t)}$ and $CumP_{15}$ for all data sets. For the best model (M4), the graphical results in the training, validating, and testing data sets are given in Figure 3, where it is seen that the data are distributed around the diagonal line. As the predicted values approach the observed data, the points become more densely clustered along the diagonal, where the relative error is zero.

The coefficient of determination (R^2) value ranges between 0 and 1, with values closer to 1 indicating a stronger agreement between model outputs and monitored data. An R^2 value greater than 0.5 is considered a reasonable value for hydrological purposes in the literature [23]. Therefore, the obtained R^2 values between 0.575 and 0.668 for M4 indicate that the model represents the data at a satisfactory level. Santhi et al. [24] adopted R^2 and NSEC

values greater than 0.6 and 0.5, respectively, as sufficient performance criteria during the calibration for the soil and water assessment tool model. From this perspective, the NSEC values between 0.57 and 0.68 obtained in the current study also indicate that the model exhibits acceptable performance.

Table 4. The performance statistics of the perdiction models concerning the training, validating, and testing data sets (Bold: The best value)

Data Set	Statistic	M1	M2	M3	M4
Training	RMSE (m^3/s)	14.56	14.78	12.00	**11.33**
	MAE(m^3/s)	7.80	7.36	6.24	**5.83**
	NSEC	0.47	0.45	0.64	**0.68**
Validating	RMSE(m^3/s)	14.58	13.75	12.05	**11.56**
	MAE(m^3/s)	8.03	7.40	6.47	**6.00**
	NSEC	0.31	0.38	0.53	**0.57**
Testing	RMSE(m^3/s)	14.3	14.01	11.22	**10.96**
	MAE(m^3/s)	7.79	7.22	6.32	**5.78**
	NSEC	0.43	0.46	0.65	**0.67**

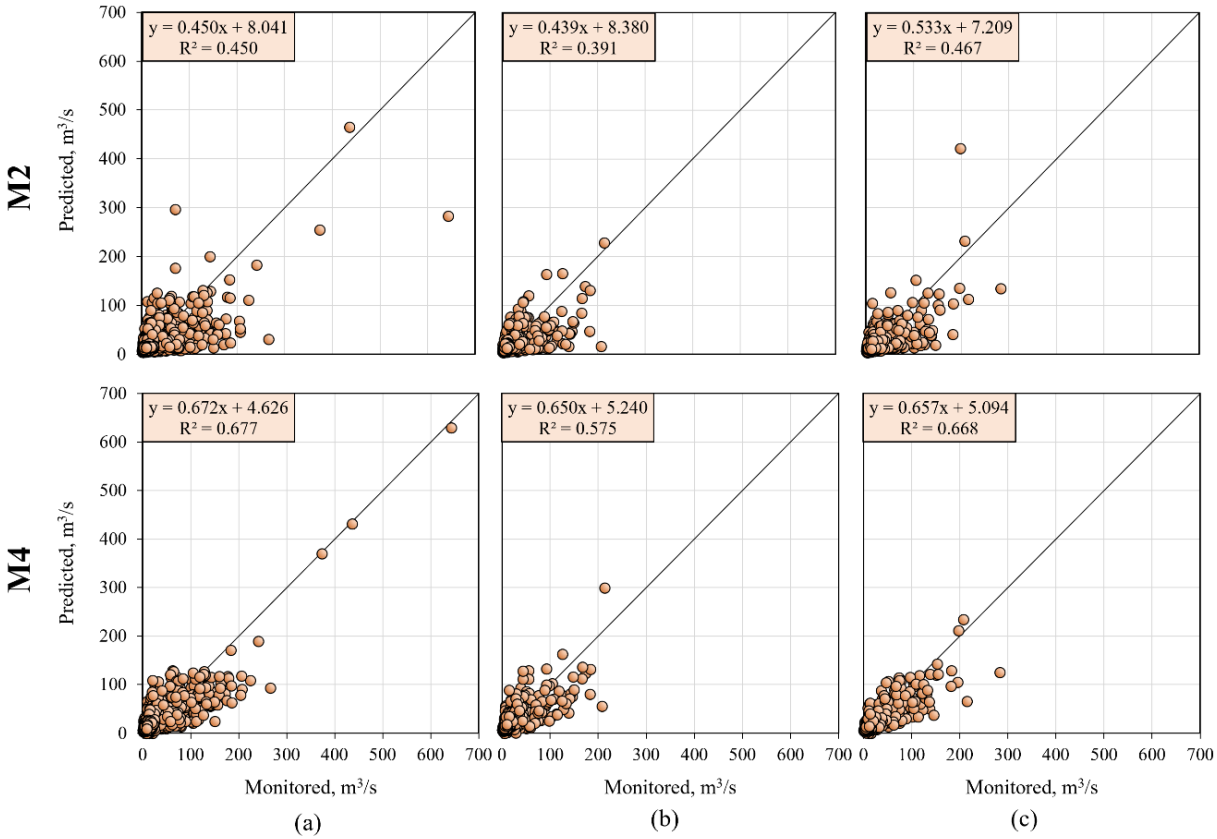

Figure 3. The scatter plots of the discharge monitored versus predicted by M2 and M4 for (a) training, (b) validating, and (c) testing data sets, the Enoree River

4. CONCLUSION

This study investigates the applicability of ANNs for predicting discharge in the Enoree River Basin, South Carolina, USA. Daily precipitation, air temperature, and discharge data from 1986 to 2022 were processed using the Thiessen polygon method to obtain basin-averaged values. To determine input parameters, correlation analyses were conducted between discharge (Q) and lagged (0, 1, 2 and 3 day) average precipitation (P) and air temperature (T) data, as well as cumulative precipitations (CumP) over 5, 10 and 15 day periods. Based on these analyses, four ANN models, namely M1 (P_{t-2}), M2 (P_{t-2} and T_t), M3 (P_{t-2}, T_t, and $CumP_5$), and M4 (P_{t-2}, T_t, and $CumP_{15}$), were developed using different combinations of average and cumulative hydro-meteorological inputs. Model performances were evaluated using different performance metrics. The main conclusions of the study are listed below.

- Correlation analyses indicated that P_{t-2} and $CumP_{15}$ had a stronger relationship with discharge, while T_t had a weaker but notable influence.
- Among four ANNs models with different input combinations, M4 achieved the lowest error metrics and highest predictive efficiency across training, validating, and testing data sets. This indicates that including both short-term lagged precipitation and cumulative precipitation over longer periods improves discharge prediction performance.
- This study highlights the potential of combining readily available meteorological observations with data-driven modeling techniques for river discharge predicting in data-limited regions. The approach presented here can be adapted to other basins to enhance water resources management, flood preparedness, and hydrological planning.
- This study is limited to the use of ANNs with precipitation, air temperature, and their cumulative values as input variables. Different modeling approaches and a broader range of predictors could provide more comprehensive insights into discharge prediction. Future research could explore integrating additional predictors such as soil moisture, evapotranspiration, and remote sensing or machine learning methods.

References

[1] H. Lin, X. Cheng, J. Liu, Q. Shi, T. Li, L. Zheng, X. Hou, and J. Du, "Estimating river discharge across scales with a novel regional gauging method driven by Sentinel satellite data," *Remote Sensing of Environment*, vol. 311, art. no. 114266, Sep. 2024.

[2] A. Wufu, S. Yang, Y. Chen, H. Lou, C. Li, and L. Ma, "Estimation of long-term river discharge and its changes in ungauged watersheds in Pamir Plateau," *Remote Sensing*, vol. 13, no. 20, art. no. 4043, Oct. 2021.

[3] F. Ling, X. Cai, W. Li, F. Xiao, X. Li, and Y. Du, "Monitoring river discharge with remotely sensed imagery using river island area as an indicator," *Journal of Applied Remote Sensing,* vol. 6, no. 1, art. no. 063564, Sep. 2012.

[4] B. Mete, and A. Bayram, "Effects of sediment-storage dams on suspended sediment transport in the Sera Lake Watershed, northeast Turkey," *Environmental Earth Sciences*, vol. 83, no. 8, art. no. 258, Apr. 2024.

[5] S. Zhang, D. Hua, X. Meng, and Y. Zhang, "Climate change and its driving effect on the runoff in the 'Three-River Headwaters' region," *Journal of Geographical Sciences*, vol. 21, no. 6, pp. 963–978, Oct. 2011.

[6] Y. Yan, Z. Yang, and Q. Liu, "Nonlinear trend in streamflow and its response to climate change under complex ecohydrological patterns in the Yellow River Basin, China," *Ecological Modelling*, vol. 252, pp. 220–227, Mar. 2013.

[7] C. B. Uvo, U. Tolle, and R. Berndtsson, "Forecasting discharge in Amazonia using artificial neural networks," *International Journal of Climatology*, vol. 20, no. 12, pp. 1495–1507, Feb. 2000.

[8] S. Nacar, "Estimation of daily streamflow using different artificial intelligence methods-a case study of Haldizen Stream," Master thesis, Dept. Civil. Eng., Aksaray Univ., Aksaray, Türkiye, 2014.

[9] J. Xie, Y. P. Xu, C. Gao, W. Xuan, and Z. Bai, "Total basin discharge from GRACE and water balance method for the Yarlung Tsangpo River basin, Southwestern China," *Journal of Geophysical Research: Atmospheres*, vol. 124, no. 14, pp. 7617–7632, Jul. 2019.

[10] H. Farajpanah, M. Lotfirad, A. Adib, H. Esmaeili-Gisavandani, O. Kisi, M. M. Riyahi, and J. Salehpoor, "Ranking of hybrid wavelet-AI models by TOPSIS method for estimation of daily flow discharge," *Water Supply*, vol. 20, no. 8, pp. 3156–3171, Dec. 2020.

[11] B. N. Ekwueme, "Assessment of machine learning algorithms in modeling river discharge under climate change resilience in a tropical humid basin," *Sustainable Water Resources Management*, vol. 11, no. 4, art. no. 72, Jun. 2025.

[12] C. B. Andersen, G. P. Lewis, M. Hart, and J. Pugh, "The impact of wastewater treatment effluent on the biogeochemistry of the Enoree River, South Carolina, during drought conditions," *Water, Air, & Soil Pollution*, vol. 225, no. 5, art. no. 1955, Apr. 2014.

[13] S. Muthukrishnan, G. P. Lewis, and C. B. Andersen, "Relations among land cover, vegetation index, and nitrate concentrations in streams of the Enoree River Basin, piedmont region of South Carolina, USA," *Developments in Environmental Science*, vol. 5, pp. 515–539, Sep. 2007.

[14] K. E. Brassel and D. Reif, "A procedure to generate Thiessen polygons," *Geographical Analysis*, vol. 11, no. 3, pp. 289–303, Jul. 1979.

[15] R. W. Herschy, T. J. Marsh, R. W. Herschy, and A. H. Schumann, "Thiessen polygon," in *Encyclopedia of Hydrology and Water Resources*, Springer, 1998, pp. 648–649.

[16] T. M. Cengiz, "Determination of regional precipitation in the Meriç-Ergene Basin for the period 1970–2020 using the weighted polygon method," *European Journal of Engineering and Applied Sciences*, vol. 7, no. 2, pp. 103–113, Dec. 2024.
[17] T. Kohonen, "An introduction to neural computing," *Neural Networks*, vol. 1, pp. 3–16, Jan. 1988.
[18] L. F. Scabini and O. M. Bruno, "Structure and performance of fully connected neural networks: emerging complex network properties," *Physica A: Statistical Mechanics and its Applications*, vol. 615, art. no. 128585, Apr. 2023.
[19] M. Zounemat-Kermani, O. Kisi, J. Adamowski, and A. Ramezani-Charmahineh, "Evaluation of data driven models for river suspended sediment concentration modeling," *Journal of Hydrology*, vol. 535, pp. 457–472, Apr. 2016.
[20] Y. J. Wong, Y. Shimizu, A. Kamiya, L. Maneechot, K. P. Bharambe, C. S. Fong, and N. M. Nik Sulaiman, "Application of artificial intelligence methods for monsoonal river classification in Selangor River Basin, Malaysia," *Environmental Monitoring and Assessment*, vol. 193, no. 7, art. no. 438, Jun. 2021.
[21] S. I. Abba, N. T. T. Linh, J. Abdullahi, S. I. A. Ali, Q. B. Pham, R. A. Abdulkadir, R. Costache, V. T. Nam, D. T. Anh, "Hybrid machine learning ensemble techniques for modeling dissolved oxygen concentration," *IEEE Access*, vol. 8, pp. 157218–157237, Aug. 2020.
[22] J. Singh, H. V. Knapp, J. G. Arnold, and M. Demissie, "Hydrological modeling of the Iroquois River Watershed using HSPF and SWAT," *Journal of the American Water Resources Association*, vol. 41, no. 2, pp. 343–360, Jun. 2005.
[23] N. Myo Lin, X. Tian, M. Rutten, E. Abraham, J. M. Maestre, and N. van De Giesen, "Multi-objective model predictive control for real-time operation of a multi-reservoir system," *Water*, vol. 12, no. 7, art. no. 1898, Jul. 2020.
[24] C. Santhi, J. G. Arnold, J. R. Williams, W. A. Dugas, R. Srinivasan, and L. M. Hauck, "Validation of the SWAT model on a large river basin with point and nonpoint sources," *Journal of the American Water Resources Association*, vol. 37, no. 5, pp. 1169–1188, Jun. 2001.

2nd International Conference on Multidisciplinary Sciences and Technological Developments (ICMUSTED 2025)

December 12-15, 2025

Stream Water Quality Assessment in a Dammed Watershed: A Case Study from North East Türkiye

Adem Bayram[1], Betul Mete[1]

[1]Department of Civil Engineering, Karadeniz Technical University, Trabzon, Türkiye
Corresponding author: Betul Mete (e-mail: betulmete@ktu.edu.tr)

Abstract

The aim of this study is to evaluate seasonal and annual water quality in the Harsit Stream Watershed by using the weighted arithmetic water quality index (WA-WQI) and the Canadian Council of Ministers of the Environment water quality index (CCME-WQI). The WQI scores were calculated considering 15 water quality parameters (dissolved oxygen, water temperature, pH, electrical conductivity, suspended sediment, ammonium nitrogen, nitrate nitrogen, total Kjeldahl nitrogen, total nitrogen, ortho-phosphate phosphorus, chemical oxygen demand, aluminum ion, manganese ion, total iron, and total chromium) over a one-year period for two monitoring stations, selected upstream and downstream of the Torul Dam Reservoir, Gumushane, North East Türkiye. Limit values in index calculations were primarily based on the Turkish Surface Water Quality Regulation, complemented by other guidelines where necessary. According to the WA-WQI classification, the upstream water quality changes from very poor to unsuitable for use, whereas poor to very poor for downstream. Moreover, the upstream water quality is marginal, and downstream water quality ranges from marginal to good for the CCME-WQI. The results reveal that the downstream station generally has better water quality than the upstream station. It was concluded that reservoirs have a significant role based on self-purification capacity for improving stream water quality.

Keywords: Harsit Stream, Torul Dam Reservoir, Water Quality Index

1. INTRODUCTION

The demand for fresh water, which is vital for all living things, is increasing day by day. Although nearly three-quarters of the Earth's surface is covered by water, only about 2.5% of which amount is freshwater, making the portion suitable for human consumption extremely limited [1]. Rivers, lakes, and dam reservoirs are available fresh water resources [2]. Water quality is as important as its quantity for ecosystem health, domestic, agricultural, and industrial uses. Both natural processes and anthropogenic activities can affect the water quality of river systems. Dams have been built all over the world to store water and use it when needed [3]. Dams have the potential to affect the water quality of river systems by causing changes in the hydrological regime, sediment transport, and the physical, chemical, and biological characteristics of water [4, 5]. These changes may be positive (improving water storage and supply reliability) or negative (including eutrophication, oxygen depletion, and degradation of aquatic habitats) impacts [6, 7]. Regular monitoring of water quality is of great importance for the protection and sustainable management of river ecosystems. However, its dependence on numerous parameters makes this process complex. Therefore, water quality indices (WQIs) are widely used to express comprehensive data sets into a single and easily interpretable score [8–14].

The Torul Dam, situated on the Harsit Stream within the Eastern Black Sea Basin, Türkiye, was constructed primarily for hydroelectric power generation. On the other hand, the dam also has significant influence on downstream hydrological regimes and ecological processes. Despite the ecological importance of the Harsit Stream Watershed, there has been limited research on its surface water quality, particularly in relation to dam impacts. Existing studies [15–18] have focused mainly on routine monitoring and descriptive analysis of physicochemical parameters, without applying integrative methods such as WQIs. To date, no published study has evaluated the water quality of the Harsit Stream affected by the Torul Dam using index-based approaches that facilitate both temporal and spatial comparisons. This research aims to fill this gap by applying WQIs to assess seasonal and annual water quality upstream and downstream of the Torul Dam Reservoir. Thus, it provides new insights into the implications of dam operations on riverine water quality and contributes to the broader understanding of anthropogenic impacts on freshwater systems.

2. MATERIAL AND METHOD

2.1. Study Area and Water Quality Data

The Harsit Stream, originated from Vauk Mountains in the east border of Gumushane Province, has a143 km length of main branch and 3,280 km^2 drainage area. The stream pouring into the Black Sea in Giresun Province, Türkiye [19]. The watershed is vulnerable to erosion due to its dense short vegetation and steep topography [20]. In addition to natural factors, various anthropogenic activities such as agriculture, mining, industrial discharges, and domestic wastewater inputs, exert significant pressure on water quality of the watershed [21]. The Torul Dam, located in Gumushane province, plays a major role in hydropower generation and water management. Due to hydrological, ecological, and socio-economic importance, the Harsit Stream Watershed is a valuable study area for water quality assessment.

Water quality data belong to two monitoring stations (Fig. 1) were used upstream (40° 33' 56.7" N - 39° 17' 54.6" E) and downstream (40° 38' 41.1" N - 39° 11' 01.4" E) of the Torul Dam Reservoir on the Harsit Stream [22]. The semimonthly data cover the March 2009-February 2010 period and were obtained from a doctoral dissertation Bayram [23]. Dissolved oxygen (DO), water temperature (WT), pH, and electrical conductivity (EC) were measured *in situ*, on the other hand, suspended sediment (SS), ammonium-nitrogen $\left(NH_4^+\text{-}N\right)$, nitrate-nitrogen $\left(NO_3^-\text{-}N\right)$, total Kjeldahl nitrogen (TKN), total nitrogen (TN), ortho-phosphate phosphorus (o-PO_4-P), chemical oxygen demand (COD), aluminum ion (Al^{3+}), manganese ion (Mn^{2+}), total iron (Fe), and total chromium (Cr) analyses were carried out on raw surface water samples collected from the stations.

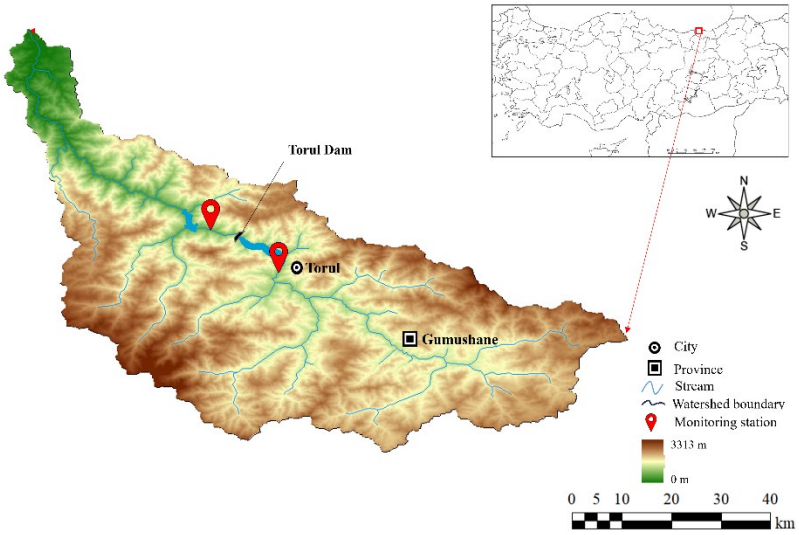

Figure 1. Location of the monitoring stations and Torul Dam Reservoir, Harsit Stream Watershed, North East Türkiye

2.2. Weighted Arithmetic Water Quality Index

The weighted arithmetic water quality index (WA-WQI) was developed by Brown et al. [24]. The method combines multiple water-quality parameters, which may be physical, chemical, or biological, into a single index value. Unit weight (w_i) and quality rating scale (q_i) values were calculated for each parameter to be considered in the index calculation using Equations (1) and (2), in which S_i and V_i represent recommended limit value and monitored value for i^{th} parameter, and V_0 is ideal value of the parameters in pure water [25]. The WA-WQI score is calculated by substituting these values in Equation (3). According to the WA-WQI, the classification of water quality [26] is presented in Table 1.

$$w_i = \frac{\dfrac{1}{\sum\left(\dfrac{1}{s_i}\right)}}{s_i} \tag{1}$$

$$q_i = 100 \times \left(\frac{v_i - v_o}{s_i - v_o}\right) \tag{2}$$

$$WA - WQI = \frac{\sum w_i \times q_i}{\sum w_i} \quad (3)$$

Table 1. Classification of water quality for the weighted arithmetic water quality index [26]

Class	Excellent	Good	Poor	Very poor	Unsuitable for use
Score range	0-25	26-50	51-75	76-100	>100

2.3. The Canadian Council of Ministers of the Environment Water Quality Index

The Canadian Council of Ministers of the Environment water quality index (CCME-WQI) was developed in the late 1990s and introduced in 2001 to provide a standardized framework for summarizing complex water quality data into a single score ranging from 0 to 100 [27]. The method is widely used for monitoring, reporting, and comparing water quality across different regions and time periods. It is based on three factors ie., scope (F_1), frequency (F_2), and amplitude (F_3), calculated using Equations (4)-(6).

$$F_1 = \frac{\text{Number of Failed Parameters}}{\text{Total Number of Parameters}} \times 100 \quad (4)$$

$$F_2 = \frac{\text{Number of Failed Tests}}{\text{Total Number of Tests}} \times 100 \quad (5)$$

$$F_3 = \frac{\sum \text{nse}}{\text{Number of Failed Tests}} \times 100 \quad (6)$$

In Eq. (6) nse is normalized sum of excursions and calculated by Eq. (7).

$$\text{nse} = \frac{\text{Failed Test Value}}{\text{Guideline Value}} - 1 \quad (7)$$

The CCME-WQI score is calculated by substituting these factors in Equation (8). The water quality classification for CCME-WQI is presented in Table 2. Information about the calculation of the index is given in detail by CCME [27], Haldar et al. [28], Kenanoglu [29].

$$CCME - WQI = 100 - \left(\frac{\sqrt{F_1^2 + F_2^2 + F_3^2}}{1.732} \right) \quad (8)$$

Table 2. Classification of water quality for the Canadian Council of Ministers of the Environment water quality index [27]

Class	Excellent	Good	Fair	Marginal	Poor
Score range	95-100	80-94	65-79	45-64	0-44

3. RESULTS AND DISCUSSION

In this study, the water quality of two monitoring stations selected upstream and downstream of the Torul Dam Reservoir in the Harsit Stream Watershed was comprehensively evaluated by considering DO, WT, pH, EC, SS, NH_4^+-N, NO_3^--N, TKN, TN, o-PO_4-P, COD,Al^{3+}, Mn^{2+}, total Fe, and total Cr. The limit values specified in the Turkish Surface Water Quality Regulation [30] was used for the related parameters in the calculations. Because no guideline values are provided in the TSWQR [26] for certain parameter limit values from other regulations and guidelines were used. The limit value is adopted as 25 °C for WT [31], 200 mg/L for SS [32], and 0.05, 0.3, and 0.1 mg/L for Al^{3+}, total Fe, and total Cr [33], respectively. Basic statistics of these parameters for upstream and downstream monitoring stations, along with the limit values with reference to the TSWQR [30], are presented in Table 3.

The water quality scores calculated for each of two stations, using WA-WQI and CCME-WQI, are shown in Figs. 2 and 3, respectively. The seasonal WA-WQI scores varied between 74.51 (summer) and 143.98 (spring) for upstream, and between 61.70 (winter) and 102.24 (spring) for downstream. On an annual basis, the score was 117.53 for upstream and 77.90 for downstream. Downstream station has lower WA-WQI scores indicating higher water quality than upstream station both seasonally and annually (Fig. 2). According to the WA-WQI classification, the stream water quality ranges from very poor to unsuitable for use in the upstream station, while poor to very poor in the downstream station. The seasonal CCME-WQI scores range between 48.86 (spring) and 63.17 (summer) for upstream, and 61.04 (winter) and 102.24 (spring) for downstream. The annual CCME-WQI score was 51.85 for upstream and 61.11 for downstream, where the CCME-WQI scores were better than the upstream station for all periods (Fig. 3). When considering the CCME-WQI classification, water quality is marginal for upstream, while changes between marginal and good for downstream.

Table 3. Basic statistics of the water-quality parameters [23] and the limit values with reference to the TSWQR [30]

Parameter	Unit	Upstream				Downstream				TSWQR [30]		
		min	ave	max	Sd	min	ave	max	Sd	High quality	Slightly polluted	Polluted
DO	mg/L	9.06	10.63	13.00	0.99	6.33	9.23	12.29	1.54	< 8.00	6.00	< 6.00
WT	°C	3.30	10.88	20.90	5.59	5.00	11.45	23.60	5.37	-	-	-
pH	-	7.00	7.84	8.40	0.36	6.83	7.57	8.39	0.48	6.0-9.0	6.0-9.0	6.0-9.0
EC	µS/cm	0.16	0.32	0.53	0.10	0.15	0.27	0.42	0.07	< 400	1000	> 1000
SS	mg/L	8.20	57.89	263.40	57.10	1.60	12.40	58.00	14.60	-	-	-
NH_4-N	mg/L	0.04	0.11	0.21	0.04	0.01	0.05	0.14	0.03	< 0.20	1.00	> 1.00
NO_3-N	mg/L	0.21	0.34	0.55	0.10	0.00	0.30	0.85	0.17	< 3.00	10.00	> 10.00
TKN	mg/L	0.51	0.80	1.21	0.19	0.41	0.71	1.22	0.21	< 0.50	1.50	> 1.50
TN	mg/L	0.83	1.15	1.61	0.19	0.61	1.01	1.67	0.25	< 3.50	11.50	> 11.50
PO_4-P	mg/L	0.08	0.12	0.16	0.02	0.07	0.09	0.11	0.01	< 0.05	0.16	> 0.16
COD	mg/L	2.55	5.75	9.03	1.62	1.00	4.58	8.77	1.77	< 25.00	50.00	> 50.00
Al^{3+}	mg/L	0.00	0.03	0.08	0.02	0.00	0.02	0.09	0.02	-	-	-
Mn^{2+}	mg/L	0.01	0.08	0.26	0.05	0.01	0.06	0.22	0.06	< 0.10	0.50	> 0.50
Total Fe	mg/L	0.23	1.73	8.02	1.72	0.23	0.67	2.81	0.65	-	-	-
Total Cr	mg/L	0.00	0.05	0.23	0.05	0.02	0.03	0.07	0.01	-	-	-

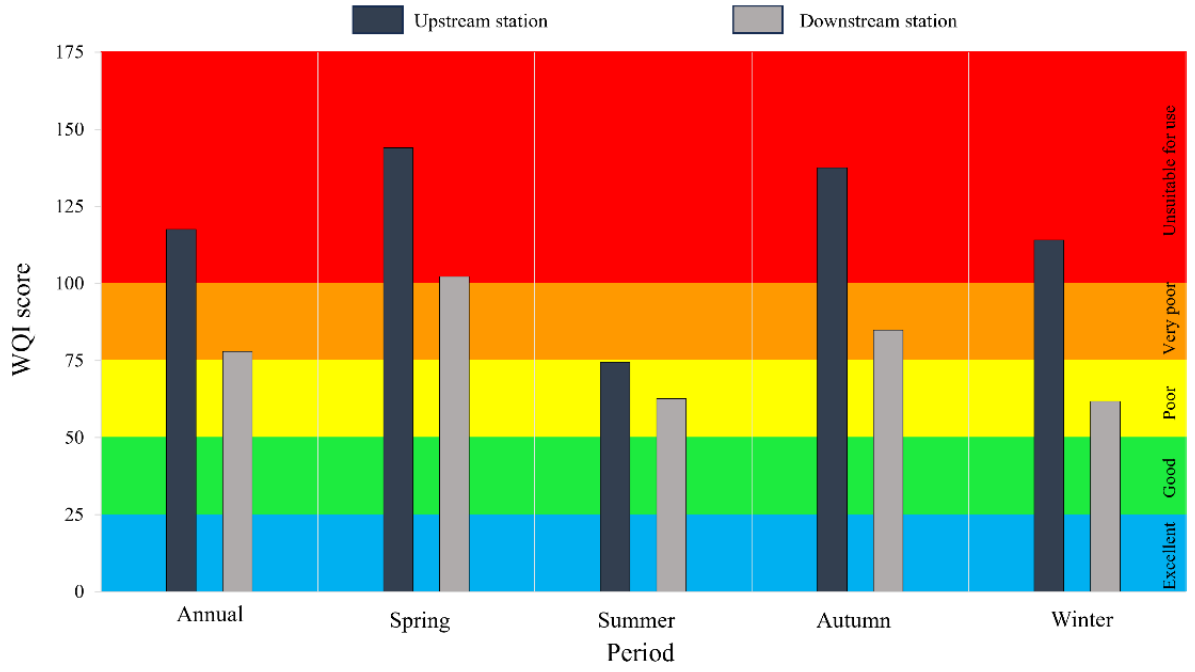

Figure 2. Weighted arithmetic water quality index scores for upstream and downstream of the Torul Dam Reservoir, Harsit Stream, Gumushane, Türkiye

For both indices, WQI scores suggest that downstream water quality is better than upstream. Similarly, Gao et al. [34] found that nutrient and heavy metal concentrations in the Three Gorges Dam Reservoir, China, were generally higher upstream part compared to downstream location. It was stated that this situation was associated with the self-purification of the reservoir. The comparison of WA-WQI and CCME-WQI classifications in this study highlights that the same monitoring station may be evaluated differently depending on the index applied. While WA-WQI classified the upstream water quality from very poor to unsuitable for use, CCME-WQI indicated a marginal status for the same site. Such discrepancies have also been documented in the literature. Chidiac et al. [35] emphasized that the WA-WQI is more sensitive to the parameters with lower permissible limits, which can disproportionately influence the overall score. Similarly, Khatri et al. [36] found that the application of WA-WQI and CCME-WQI to the same groundwater resources in India produced contrasting quality assessments. These results suggest that methodological differences between indices should be carefully considered when interpreting water quality status and comparing results across studies.

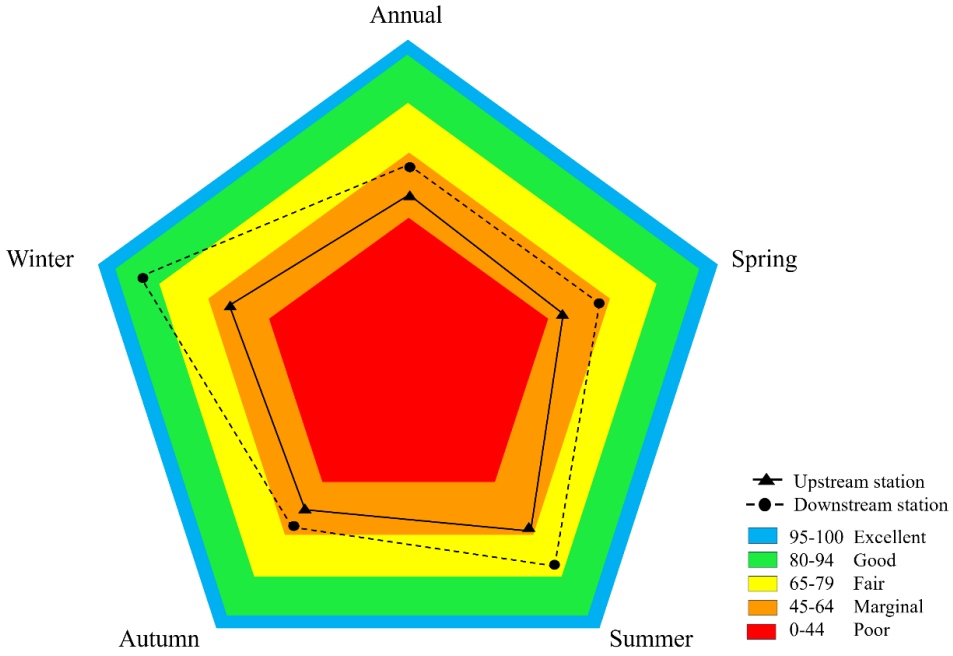

Figure 3. The Canadian Council of Ministers of the Environment water quality index scores for upstream and downstream of the Torul Dam Reservoir, Harsit Stream, Gumushane, Türkiye

4. CONCLUSION

This study evaluated the seasonal and annual water quality of two monitoring stations selected upstream and downstream of the Torul Dam Reservoir on the Harsit Stream, Gumushane, Türkiye. The study considered two indices, namely, the weighted arithmetic water quality index (WA-WQI) and the Canadian Council of Ministers of the Environment water quality index (CCME-WQI). The data cover a one-year period fand include dissolved oxygen, water temperature, pH, electrical conductivity, suspended sediment, ammonium nitrogen, nitrate nitrogen, total Kjeldahl nitrogen, total nitrogen, ortho-phosphate phosphorus, chemical oxygen demand, aluminum, manganese, iron, and chromium. The limit values for these parameters were determined by considering the Turkish Surface Water Quality Regulation [30] and other national and international guidelines. The main conclusions of the study are given below.

- A comparison of the WA-WQI and CCME-WQI revealed notable differences in the classification of water quality. While WA-WQI classified upstream water quality as very poor to unsuitable, CCME-WQI classified the same station as marginal. Similarly, the downstream station was classified as poor to very poor by WA-WQI, and marginal to good by CCME-WQI. These differences highlight the importance of methodological selection when assessing and interpreting water quality status.
- Downstream water quality was superior to upstream. It is thought that this situation is derived from the self-purification capacity of the Torul Dam Reservoir and the regulating effect of the dam on flow and pollutant dynamics.
- It is recommended that the scope of the study can be expanded by using different indices and especially heavy metal data for future studies.

References

[1] S. L. Postel, G. C. Daily, and P. R. Ehrlich, "Human appropriation of renewable fresh water," *Science*, vol. 271, no. 5250, pp. 785–788, 1996.

[2] E. Yeleliere, S. J. Cobbina, and A. B. Duwiejuah, "Review of Ghana's water resources: the quality and management with particular focus on freshwater resources," *Applied Water Science*, vol. 8, no. 3, art. no. 93, Jun. 2018.

[3] R. S. Winton, E. Calamita, and B. Wehrli, "Reviews and syntheses: Dams, water quality and tropical reservoir stratification," *Biogeosciences*, vol. 16, no. 8, pp. 1657–1671, Apr. 2019.

[4] G. Wei, Z. Yang, B. Cui, B. Li, H. Chen, J. Bai, and S. Dong, "Impact of dam construction on water quality and water self-purification capacity of the Lancang River, China," *Water Resources Management*, vol. 23, no. 9, pp. 1763–1780, Nov. 2009.

[5] P. Zhao, X. Tang, J. Tang, and C. Wang, "Assessing water quality of Three Gorges Reservoir, China, over a five-year period from 2006 to 2011," *Water Resources Management*, vol. 27, no. 13, pp. 4545–4558, Aug. 2013.

[6] B. A. Yifru, M. G. Kim, J. W. Lee, I. H. Kim, S. W. Chang, and I. M. Chung, "Water storage in dry riverbeds of arid and semi-arid regions: overview, challenges, and prospects of sand dam technology," *Sustainability*, vol. 13, no. 11, art. no. 5905, May 2021.

[7] A. E. Hanjaniamin, M. S. Tabrizi, and H. Babazadeh, "Dissolved oxygen concentration and eutrophication evaluation in Yamchi Dam Reservoir, Ardabil, Iran," *Applied Water Science*, vol. 13, no. 1, art. no. 9, Nov. 2023.

[8] J. Xia, G. Xu, P. Guo, H. Peng, X. Zhang, Y. Wang, and W. Zhang, "Tempo-spatial analysis of water quality in the Three Gorges Reservoir, China, after its 175-m experimental impoundment," *Water Resources Management*, vol. 32, no. 9, pp. 2937–2954, Mar. 2018.

[9] A. A. Soltani, A. Bermad, H. Boutaghane, A. Oukil, O. Abdalla, M. Hasbaia, R. Olulebsir, S. Zeroural, and A. Lefkir, "An integrated approach for assessing surface water quality: case of Beni Haroun dam (Northeast Algeria)," *Environmental Monitoring and Assessment*, vol. 192, no. 10, art. no. 630, Sep. 2020.

[10] A. Bor and S. Elci, "Impacts of construction of dam on the flow regimes and water quality: a case study from Turkey," *International Journal of Environmental Science and Technology*, vol. 19, no. 5, pp. 4069–4086, Feb. 2022.

[11] K. Kalaitzidou, M. M. Ntona, E. Zavridou, S. Tzeletas, T. Patsialis, A. Kallioras, and N. Kazakis, "Water quality evaluation of groundwater and dam reservoir water: application of the water quality index to study sites in Greece," *Water*, vol. 15, no. 23, art. no. 4170, Dec. 2023.

[12] T. S. Fashagba, M. Bessedik, N. B. ElSayed, C. Abdelbaki, and N. Kumar, "Evaluating the water quality of the Keddara Dam (Algeria) using water quality indices," *Water*, vol. 16, no. 9, art. no. 1291, May 2024.

[13] B. Mete, G. E. Karadeniz, and A. Bayram, "Water quality assessment of the Erfelek Dam Lake in the context of drinking water treatment plant, Sinop Municipality, Northern Türkiye," *The Black Sea Journal of Sciences*, vol. 14, no. 4, pp. 2082–2102, Dec. 2024.

[14] P. Gogoi, B. K. Das, S. K. Koushlesh, C. Johnson, R. Malick, A. Saha, T. Kayal, R. Chakraborty, L. Pradhan, and A. K. Das, "An integrative water quality index and multivariate modeling approach to assess surface water quality, trophic status and nutrient source apportionment in a large tropical reservoir, Hirakud–the longest earthen dam in Asia," *Applied Water Science*, vol. 15, no. 8, art. no. 219, Jul. 2025.

[15] A. Bayram, H. Onsoy, M. Kankal, and M. I. Komurcu, "Spatial and temporal variation of suspended sediment concentration versus turbidity in the stream Harsit Watershed, NE Turkey," *Arabian Journal of Geosciences*, vol. 7, no. 11, pp. 4987–4996, Sep. 2014.

[16] C. Mutlu, B. Eraslan Akkan, and B. Verep, "The heavy metal assessment of Harsit Stream (Giresun, Turkey) using multivariate statistical techniques," *Fresenius Environmental Bulletin*, vol. 27, pp. 9851–9858, 2018.

[17] C. Saydam Eker, "Distinct contamination indices for evaluating potentially toxic element levels in stream sediments: a case study of the Harsit Stream (NE Turkey)," *Arabian Journal of Geosciences*, vol. 13, no. 22, art. no. 1175, Nov. 2020.

[18] A. Bayram and H. Onsoy, "Sand and gravel mining impact on the surface water quality: a case study from the city of Tirebolu (Giresun Province, NE Turkey)," *Environmental Earth Sciences*, vol. 73, no. 5, pp. 1997–2011, Jul. 2015.

[19] A. Bayram, M. Kankal, H. Onsoy, and V. N. Bulut, "The effects of hydraulics structures in the stream Harsit on suspended sediment transport," in *VI. Ulusal Hidroloji Kongresi*, Denizli, 2010, pp. 873–882.

[20] A. Bayram, H. Onsoy, V. N. Bulut, and M. Tufekci, "Effect of Torul and Kurtun dams on suspended sediment concentration in the stream Harsit (Turkey)," in *9th International Congress on Advances in Civil Engineering*, Trabzon, 2010, pp. 1–8.

[21] A. Bayram, H. Onsoy, V. N. Bulut, and G. Akinci, "Influences of urban wastewaters on the stream water

quality: A case study from Gumushane Province, Turkey," *Environmental Monitoring and Assessment*, vol. 185, no. 2, pp. 1285–1303, Apr. 2013.
[22] A. Bayram and H. Onsoy, "Effects of dams on water quality: Torul Dam (the Stream Harsit-Gumushane)," in *5. Ulusal Su Muhendisligi Sempozyumu*, İstanbul, 2011, pp. 957–970.
[23] A. Bayram, "A study on seasonal variation of the stream Harsit water quality and estimation of the suspended sediment concentration using artificial neural networks," Ph.D. thesis, Karadeniz Technical University, Trabzon, Türkiye, 2011.
[24] R. M. Brown, N. I. McClelland, R. A. Deininger, and R. G. Tozer, "A water quality index-do we dare," *Water and Sewage Works*, vol. 117, no. 10, pp. 339–343, 1970.
[25] M. B. Jumber, M. T. Damtie, and D. Tegegne, "Integration of multivariate adaptive regression splines and weighted arithmetic water quality index methods for drinking water quality analysis," *Water Conservation Science and Engineering*, vol. 9, no. 1, art. no. 6, Feb. 2024.
[26] C. Chatterjee and M. Raziuddin, "Determination of water quality index of a degraded river in Asanol industrial area, Raniganj, Burdwan, West Bengal," *Nature, Environment and Pollution Technology*, vol. 1, pp. 181–189, 2002.
[27] CCME, "Canadian water quality guidelines for the protection of aquatic life. CCME water quality index 1.0, Technical report," Canadian Council of Ministers of the Environment [Online], 2001. Available: https://unstats.un.org/unsd/envaccounting/ceea/archive/Water/CCME_Canada.PDF
[28] D. Haldar, S. Halder, P. Das, and G. Halder, "Assessment of water quality of Damodar River in South Bengal region of India by Canadian Council of Ministers of Environment (CCME) water quality index: a case study," *Desalination and Water Treatment*, vol. 57, no. 8, pp. 3489–3502, Feb. 2016.
[29] M. Kenanoglu, "Determination of suspended sediment distribution and water quality parameters in the Borçka Dam Lake Basin," Ph.D. dissertation, Karadeniz Technical University, Trabzon, Türkiye, 2025.
[30] TSWQR, "Turkish surface water quality regulation," The Turkish Official Gazette (no. 31513), Ankara, Türkiye [Online], 2021. Available: https://www.resmigazete.gov.tr/eskiler/2021/06/20210616-1.htm
[31] TSWQR, "Turkish surface water quality regulation," The Turkish Official Gazette (no. 29327), Ankara, Türkiye [Online], 2015. Available: https://www.resmigazete.gov.tr/eskiler/2015/04/20150415-18.htm (in Turkish).
[32] US EPA, "Water quality standards," United States Environmental Protection Agency, [Online], 2003. Available: https://www.epa.gov/sites/default/files/2014-12/documents/akwqs-chapter70.pdf
[33] US EPA, "Water quality standards," United States Environmental Protection Agency, [Online], 2018. Available: https://www.epa.gov/system/files/documents/2022-01/dwtable2018.pdf
[34] Q. Gao, Y. Li, Q. Cheng, M. Yu, B. Hu, Z. Wang, and Z. Yu, "Analysis and assessment of the nutrients, biochemical indexes and heavy metals in the Three Gorges Reservoir, China, from 2008 to 2013," *Water Research*, vol. 92, pp. 262–274, Apr. 2016.
[35] S. Chidiac, P. El Najjar, N. Ouaini, Y. El Rayess, and D. El Azzi, "A comprehensive review of water quality indices (WQIs): history, models, attempts and perspectives," *Reviews in Environmental Science and Bio/Technology*, vol. 22, no. 2, pp. 349–395, Mar. 2023.
[36] N. Khatri, S. Tyagi, D. Rawtani, M. Tharmavaram, and R. D. Kamboj, "Analysis and assessment of ground water quality in Satlasana Taluka, Mehsana district, Gujarat, India through application of water quality indices," *Groundwater for Sustainable Development*, vol. 10, art. no. 100321, Apr. 2020.

2nd International Conference on Multidisciplinary Sciences and Technological Developments (ICMUSTED 2025)

December 12-15, 2025

Influence of Single-Layer Tile Waste Sand on Concrete Properties

Yasmine Mohamed Bouteben[1], Leila Kherraf[2]

[1]Department of Civil Engineering, University of Brothers Mentouri, Constantine, Algeria
[2]Department of Civil Engineering, University of 20 Aout 1955, Skikda, Algeria
Corresponding author: Yasmine Mohamed Bouteben (e-mail: medboutebenyasmine@outlook.fr)

Abstract

With the continued expansion of urbanization, the demand for construction materials particularly sand is steadily increasing. However, the intensive extraction of quarry sand poses significant environmental challenges, such as the degradation and scarcity of natural resources. To address these issues, the integration of tile waste often resulting from low-quality production or broken tiles as a substitute for quarry sand in concrete presents a dual opportunity: it reduces dependence on natural resources while providing a practical solution for recycling waste from the tile industry. The primary objective of this study is to demonstrate the technical feasibility of using tile offcuts as a partial substitute for quarry sand in conventional concrete. The experimental program involves incorporating this tile waste in the form of sand into the concrete mix at varying percentages (0%, 5%, 10%, and 15%) and examining how the properties of the resulting concrete evolve in both the fresh state (density, slump) and the hardened state (compressive strength, tensile strength, water absorption by immersion, and capillary absorption). The results show that incorporating 5% recycled tile sand positively enhances the compressive, flexural, and splitting tensile strength of concrete while also improving water absorption by capillarity.

Keywords: Ttile sand, Concrete, Slump, Compressive strength, Flexural strength

Optimization of Unconfined Compressive Strength in Stabilized Soils Using Taguchi L9 Design

Fadila Benayoun[1], Moufida Moussaoui[2], Souhila Rehab Bekkouche[3]

[1]Urban Techniques Management Institute, University of Larbi Ben Mhidi, Oum El Bouaghi, Algeria
[2]Department of Hydraulics, University Badji Mokhtar Annaba, Algeria
[3]Department of Civil Engineering, University of 20 Aout, Skikda, Algeria
Corresponding author: Fadila Benayoun (e-mail: benayoun.fadila@univ-oeb.dz)

Abstract

This study employs the Taguchi L9 orthogonal array to systematically optimize the unconfined compressive strength (UCS) of stabilized soil by evaluating three key factors: sand content (10%, 20%, and 30%), lime content (2%, 4%, and 6%), and curing duration (7, 14, and 28 days). The analysis of signal-to-noise (S/N) ratios identified curing time as the most influential parameter, followed by sand content and then lime content. The optimal combination for maximizing UCS was determined. The results confirm the efficacy of the Taguchi L9 design as a highly efficient and resource-conservative methodology for the preliminary optimization of soil stabilization mixes, providing a robust framework for cost-effective geotechnical applications where extensive testing is impractical.

Keywords: Soil stabilization, Taguchi method, L9 orthogonal array, Unconfined compressive strength (UCS), Optimization

2nd International Conference on Multidisciplinary Sciences and Technological Developments (ICMUSTED 2025)

December 12-15, 2025

Enhancing Facility Layout Design: An Integrated AHP–NLP Approach

Muhammad Waqas Aslam[1], Zeqiang Zhang[1,2,3]

[1]Technology and Equipment of Rail Transit Operation and Maintenance Key Laboratory of Sichuan Province, School of Mechanical Engineering, Southwest Jiaotong University, Chengdu, 610031 Sichuan, China
[2]State Key Laboratory of Bridge Intelligent and Green Construction, Southwest Jiaotong University, Chengdu, 611756 Sichuan, China
[3]Tangshan Institute, Southwest Jiaotong University, Tangshan, 063000, Hebei, China
Corresponding author: Zeqiang Zhang (e-mail: zhangzq@home.swjtu.edu.cn)

Abstract

Facility layout optimization has traditionally been dominated by quantitative models that often neglect critical, yet subjective, human centric factors. Such negligence may result in inefficient designs, which makes operations less efficient and employees less satisfied. To overcome this limitation our research presents a new hybrid model, the sentiment integrated analytic hierarchy process (SI-AHP), of facility layout design. Our solution is the first to combine the high-level natural language processing (NLP) with the structured decision-making capability of AHP. The proposed framework employs a bidirectional encoder representation for transformers (BERT) based sentiment analysis and topic modelling engine to extract and quantify qualitative insights from unstructured data sources, including employee surveys and safety audit reports. Such latent factors as ergonomic preferences, perceived risk of safety and communication flow are then converted to measurable measures in the AHP framework. This enables rigorous comparison with conventional performance metrics such as material handling costs and process adjacency requirements. The SI-AHP model was tested using a real-life industrial case study. The implementation introduced a layout that not only achieved quantitative goals but showed significant progress in terms of operational efficacy and a high rate of employee satisfaction scores. By integrating subjective human insights with established decision analytic methods, SI-AHP offers a replicable and holistic approach for facility layout design, contributing to the advancement of human centric operations engineering.

Keywords: Facility layout, Natural Language Processing, Sentiment analysis, Topic modelling, BERT-based models

2nd International Conference on Multidisciplinary Sciences and Technological Developments (ICMUSTED 2025)

December 12-15, 2025

Study of Earthquake Ground Motion Duration Recorded in Soft Soils

Issam Aouari[1], Aicha Rouabeh[1], Benahmed Baizid[2], Rachid Bakhti[3]

[1]Department of Civil Engineering, Faculty of Applied Sciences, University of Bouira, 10000 Bouira, Algeria
[2]Laboratory of Development in Mechanics and Materials, University of Djelfa, 17000 Djelfa, Algeria
[3]National School of Public Works Engineering, 16000 Algiers, Algeria
Corresponding author: Issam Aouari (e-mail: i.aouari@univ-bouira.dz)

Abstract

In recent years, increased global seismic activity has underscored the need for accurate estimation of ground motion parameters. The significant duration of strong ground shaking is a crucial indicator in earthquake engineering, directly influencing structural seismic design and the operational reliability of equipment during seismic events. This research investigates the significant duration on soft soil sites, focusing on its dependence on magnitude, distance, and site conditions. While numerous definitions for measuring ground motion duration exist, no single one has been universally accepted, as their relevance depends on the specific engineering application. This study provides a comparative analysis of the prominent definitions found in the literature. A dataset of 600 ground motion records from 300 worldwide stations, with a moment magnitude greater than 4.5 and well-defined soft soil conditions, was assembled from the Pacific Earthquake Engineering Research Center (PEER) strong motion database. The analysis concludes that energy-based definitions of significant duration produce consistent results, showing increased duration in the far-field. In contrast, threshold-based definitions are highly sensitive to distance and show a clear decrease due to attenuation. This finding underscores that the choice of the most appropriate duration definition is inherently tied to the specific engineering context.

Keywords: Strong motion duration, Significant duration, Soft soil, PEER database

2nd International Conference on Multidisciplinary Sciences and Technological Developments (ICMUSTED 2025)

December 12-15, 2025

Approaches to Enhancing Energy Efficiency Through Building Envelope Insulation in Algeria

Sadia Laidi[1], Sidi Mohamed Karim El Hassar[1], Achour Mahrane[2], Rabah Sellami[3], Ilyas Khelifa Kerfah[1]

[1]Built Environment Laboratory, Faculty of Civil Engineering, University of Science and Technology Houari Boumediene (USTHB), El Alia, 16111 Bab Ezzouar, Algiers, Algeria
[2]Solar Equipment Development Unit (UDES), Public Scientific and Technical Establishment – Renewable Energy Development Center, 42415 Tipaza, Algeria
[3]Commission for Renewable Energies and Energy Efficiency (CEREFE), Telemly, Algiers, Algeria
Corresponding author: Sadia Laidi (e-mail: laidisadias@gmail.com)

Abstract

This study analyzes the impact of thermal insulation on the energy consumption of buildings located in semi-arid climate zones. Experimental tests were conducted on the solar house installed at the Solar Equipment Development Unit (UDES) in Bou Ismail during both winter and summer seasons. Air temperatures measured in various zones of the house were compared with numerical simulation results using TRNSYS software, enabling the calibration of a reliable thermal model. This model was then used to simulate the addition of thermal insulation to the exterior walls and roof. For this study, the city of Djelfa was selected as a representative site of the semi-arid climate in central Algeria. The results show that in winter, roof insulation leads to an 18.4% reduction in energy demand—approximately three times the savings achieved by wall insulation (6.78%). In summer, wall insulation has only a marginal effect (1.62%), while roof insulation results in a significant energy saving of 53.42%. These findings confirm the strategic effectiveness of roof insulation in semi-arid regions for enhancing building energy performance, particularly during periods of intense heat. The study highlights the importance of prioritizing roof insulation over wall insulation in similar climatic contexts to achieve substantial energy savings.

Keywords: Building, Energy efficiency, Simulations, TRNSYS, Thermal insulation

2nd International Conference on Multidisciplinary Sciences and Technological Developments (ICMUSTED 2025)

December 12-15, 2025

Utilising Graph Neural Networks for Research Paper Category Prediction and Similarity Search

Bengisu Sahin[1], Sedanur Ozer[1], Emrah Inan[1]

[1]Computer Engineering, Izmir Institute of Technology, Izmir, Türkiye
Corresponding author: Bengisu Sahin (e-mail: bengisusahin@iyte.edu.tr)

Abstract

This study presents a graph-based approach for the analysis and classification of academic articles by utilizing structural and semantic relationships extracted from article metadata. An undirected graph is constructed where nodes represent individual articles and edges denote category-based associations. Node2Vec is employed to perform unsupervised representation learning, capturing latent structural features within the graph. The resulting embeddings are visualized using t-distributed stochastic neighbour embedding (t-SNE) and used for similarity-based article retrieval. Furthermore, graph neural network (GNN) models are applied for node classification to predict the primary engineering discipline of each article. Experimental results indicate that the integration of structural information through graph embeddings significantly improves classification performance and provides valuable insights into inter-article relationships.

Keywords: Article classification, Graph neural networks, Node2Vec, Similarity search

1. INTRODUCTION

In the era of digital information and academic proliferation, the volume of scientific publications in engineering and technology fields is growing at an unprecedented rate. This exponential increase has made it essential to develop intelligent systems that can organize, analyse, and interpret the relationships between scholarly articles. As a response to this need, graph-based data representations and machine learning approaches have gained significant popularity due to their ability to capture the structural and semantic relationships among scientific documents.

In this study, a comprehensive dataset of academic articles was compiled by collecting publicly available content from the Pamukkale University Journal of Engineering Sciences website. With 31 volumes of content published between 1995 and May 2025, this journal, which has been publishing peer-reviewed articles since 1995, covers 12 different engineering specialties. The metadata of each article—including titles, abstracts, and predicted engineering fields—was extracted and used to construct a graph-based representation of the publication network. Each article is modeled as a node, and edges are formed between nodes that share either the same primary or secondary engineering category.

2. RELATED WORK

Graph-based machine learning has gained significant attention with the development of graph neural networks (GNNs), which integrate both structural and attribute-based information via neural message-passing mechanisms [1]. In this paradigm, each node updates its representation by aggregating messages from its k-hop neighbors, similar to the way convolutional kernels operate in convolutional neural networks (CNNs). Graph-based methods have been widely applied to real-world applications such as node classification, link prediction, and recommendation systems. Liu et al. [2] proposed keyword- and popularity-aware frameworks, while Yadav and Gopinathan [3] incorporated author-paper interest alignment. Guo et al. [4] focused on semantic matching between paper titles and abstracts. Metadata filtering [5], API recommendation [6], and survey studies [7–10] further highlight the expanding use of GNNs in information retrieval and recommendation domains.

To improve the quality of node representations, Kipf and Welling [1] introduced graph convolutional networks (GCNs), leveraging normalized adjacency matrices to enable efficient semi-supervised classification. Hamilton et al. [11] proposed GraphSAGE, an inductive framework using neighborhood sampling and aggregation functions. Veličković et al. [12] introduced graph attention networks (GATs), applying attention mechanisms to assign importance weights to neighbors. However, deep GNNs often suffer from the oversmoothing problem, where

repeated neighborhood aggregation leads to indistinguishable node embeddings [13]. Xu et al. [14] showed the theoretical limitations of standard message-passing GNNs, while Klicpera et al. [15] proposed approximate personalized propagation of neural predictions (APPNP), a model that separates feature transformation from propagation using personalized PageRank, thus mitigating oversmoothing. Early efforts often relied on datasets such as the Cora citation network [16], where academic papers are represented as nodes and citations as edges. Each node contains a bag-of-words feature vector and a class label. Embedding-based techniques like node2vec [17] used biased random walks for feature learning, although lacking inductive capabilities.

To support large-scale, standardized evaluation, Hu et al. [18] introduced the open graph benchmark (OGB), including datasets such as ogbn-arxiv. Clement et al. [19] developed a pipeline for extracting co-citation networks from arXiv PDFs. External sources such as Wikipedia [20], paragraph vectors [21], and semantic segmentation [22] have also been explored to enrich graph-based learning. Despite these advances, many studies focus on English-language corpora. Structured datasets in low-resource languages such as Turkish remain scarce. Our study addresses this by constructing a novel citation graph from Turkish engineering publications. Each node represents an article with metadata such as keywords and abstract embeddings. To avoid oversmoothing and preserve feature expressiveness, we adopt APPNP for the classification task. Moreover, to improve accessibility and usability, we developed a Gradio-based web interface allowing users to input raw abstracts in Turkish, receive topic classification predictions, and explore similar articles in the dataset. We further apply the t-SNE algorithm [23] to visualize the semantic structure of the embedding space. In addition, we consider the structural complexity of graphs based on entropy measures [24], which contrasts with our focus on lightweight and interpretable node classification tailored to a domain-specific corpus.

3. MATERIAL AND METHOD

3.1. Dataset Generations

To construct a structured and labeled dataset suitable for graph-based classification and retrieval tasks, we developed a two-stage data preparation pipeline as denoted in Figure 1 (Algorithm 1). In the initial phase, article metadata was collected from publicly accessible pages of the Pamukkale University Journal of Engineering Sciences via a specialized data retrieval tool implemented with Python's Selenium and BeautifulSoup libraries. This scraper navigated through all available journal issues published between 1995 and 2025, dynamically retrieved individual article pages, and extracted the title, abstract, author list, and keywords in both Turkish and English. The collected data was saved in a nested JSON format, uniquely indexed by a composite article ID derived from the article's URL.

Algorithm 1 Article Metadata Collection

```
Initialize the data gathering process using Selenium and BeautifulSoup libraries
Navigate to journal archive page on DergiPark
Scroll and collect all issue URLs
for each issue URL do
    Extract article links from the issue page
end for
for each article URL do
    Access article page
    Extract metadata: title, abstract, authors, keywords (in both Turkish and English)
    Extract references from meta tags
    Save article metadata into a structured JSON object
end for
```

Figure 1. Algorithm 1: Article metadata collection

In the second stage, we applied semantic labeling to assign engineering field categories to each article based on its English keywords as illustrated in Figure 2 (Algorithm 2). This was accomplished using a zero-shot classification model (facebook/bart-large-mnli) from the Hugging Face Transformers library. Since the original dataset lacked ground truth labels, this method allowed us to perform classification without task-specific training. To evaluate the effectiveness of category prediction, a classification experiment was conducted using a 7-label taxonomy

covering major engineering disciplines: Computer, civil, mechanical, electrical, chemical, food, and textile engineering. For each article, the classifier predicted the top two most relevant categories, which were stored as predicted_engineering_field_1 and predicted_engineering_field_2. To optimize performance on large datasets, the classification step was parallelized using Python's ThreadPoolExecutor.

Algorithm 2 Keyword-Based Category Labeling

```
Load collected JSON data into a DataFrame
for each article's English keywords do
    if keywords are non-empty then
        Use zero-shot classifier (facebook/bart-large-mnli) to predict top 2 engineering categories
    else
        Assign "Unknown" as label
    end if
end for
Store labeled data into CSV for further use in graph construction
```

Figure 2. Algorithm 2: Keyword-based category labeling

This labeled dataset was saved in CSV format and served as foundational input for the subsequent graph construction and GNN classification stages.

3.2. Node2Vec

Node2Vec [17] is a semi-supervised algorithm designed for learning low-dimensional vector representations (node embeddings) of nodes in a graph. The algorithm optimizes a graph-based objective function using stochastic gradient descent (SGD), aiming to preserve the neighborhood structure of nodes in the embedding space. These node embeddings serve as compact numerical representations that capture both local and global structural features of the graph.

To generate training samples for embedding learning, Node2Vec employs a second-order biased random walk strategy. This allows for flexible and scalable exploration of node neighborhoods.

3.2.1. Random Walk

In a random walk, a node (e.g., v) transitions to another node (e.g., x) by considering the edge between them $(v,x) \in E$. The decision is made using the following rule:

$$\alpha_{pq}(t,x) = \begin{cases} \frac{1}{p}, & \text{if } d_{tx} = 0 (\text{return}) \\ 1, & \text{if } d_{tx} = 1 (\text{neighbor}) \\ \frac{1}{q}, & \text{if } d_{tx} = 2 (\text{distant node}) \end{cases}$$

This α value is multiplied by the unnormalized transition probability weight π_{vx} to determine the likelihood of transitioning to node x in the next step [17].

Return Parameter (p) Controls the Likelihood of Revisiting the Previous Node in the Walk:

- A low value (e.g., p = 0.25) increases the probability of returning to the previous node, encouraging local exploration.
- A high value (e.g., p = 2) decreases the chance of revisiting, promoting outward exploration.

In-Out Parameter (q) Influences the Breadth of the Walk:

- q > 1: DFS-like behavior — more likely to explore further nodes.
- q < 1: BFS-like behavior — more likely to remain near the current node.
- q = 1: Unbiased behavior — balanced between local and global traversal.

In our implementation, we set $p = q = 1$, which corresponds to an unbiased walk. This means the walker has equal probability of returning, staying near, or moving further from the current position. As a result, the random walks balance between BFS and DFS behaviors, enabling the model to capture diverse aspects of node similarity and structure in the learned embeddings.

3.2.2. Node2Vec Parameters

The following hyperparameters were used during the embedding generation:

- Embedding Dimension: 64
- Walk Length: 30
- Number of Walks Per Node: 200
- Window Size: 10
- Minimum Count: 1
- Batch Size: 4
- $p = 1$, $q = 1$ (Unbiased walk)

3.2.3. Embedding Visualization with t-SNE

To qualitatively assess the separation of node embeddings, we applied t-SNE to reduce the 64-dimensional embeddings to 2D. Each node was then plotted and colored based on its label. The visualizations allow us to observe cluster structures and category separation in the embedding space.

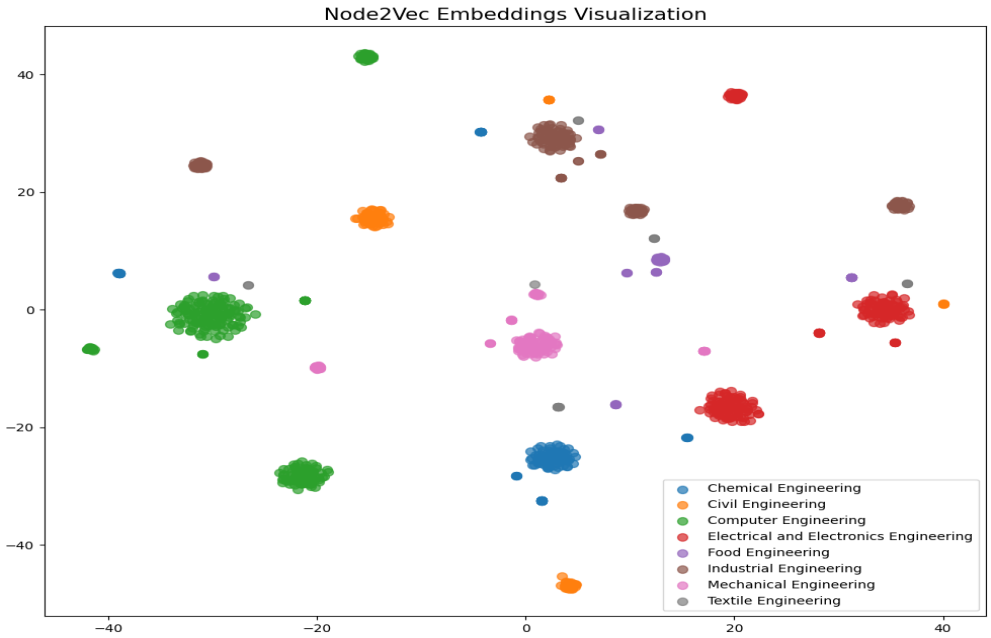

Figure 3. t-SNE visualization of Node2Vec embeddings with 7 labels

As shown in Figure 3, the learned Node2Vec embeddings exhibit meaningful cluster structures in settings. In the 7-label visualization demonstrates subtle and overlapping class boundaries, especially for semantically similar categories. These results suggest that the Node2Vec embeddings capture latent structural patterns that align with category information, with clearer separability when fewer classes are involved.

3.2.4. Similarity Search

To demonstrate the semantic consistency of the learned embeddings, we performed a similarity search based on Node2Vec vectors. A random node (representing a paper) was selected from the graph, and the top-5 most similar nodes were retrieved using cosine similarity via the *most_similar*() function.

Each result includes the paper's identifier, category, and title, along with a similarity score. This experiment illustrates how the Node2Vec embeddings capture structural and semantic similarities between academic articles, enabling applications such as recommendation and clustering.

As an example, the model was queried with *"Population-based local search algorithms for cross-domain search"*. The five most similar articles based on Node2Vec embeddings are listed in Table 1.

Table 1. The query article (article 10) is shown in the first row. Top 5 most similar articles are listed below based on Node2Vec embeddings

Article ID	Tittle	Similarity
10	*Population-based local search algorithms for cross-domain search*	Query
588	Detection and analysis of driver fatigue stages with electroencephalographic signals	0.95
473	Extruder line selection with fuzzy CRITIC and fuzzy MAIRCA for a cable company	0.95
33	System of automatic scientific article summarization in Turkish	0.95
426	Fitzhugh-Nagumo neuron model and hardware verification	0.95
377	Seismic isolation parameters optimization via crow search	0.95

All the retrieved articles belong to the same category (computer engineering), indicating that the learned embeddings effectively capture domain-specific similarity.

3.3. Node Classification

Node classification (NC) aims to infer class labels of unlabeled nodes in a graph using a subset of labeled nodes. In this study, we formulate NC as a supervised learning task on a graph of academic articles, where nodes represent papers and labels denote engineering subfields (e.g., computer, chemical engineering). Node2Vec embeddings are employed to encode structural node features. The graph is constructed and processed using the PyTorch Geometric framework. Labeled nodes are split into training, validation, and test sets via stratified sampling. Three GNN models—GCN, GAT, and APPNP—are trained under identical settings with early stopping. Class imbalance is addressed through weighted cross-entropy loss. Model performance is compared using consistent graph and feature inputs and evaluated via test set metrics and learning curves.

3.3.1. GCN

GCN is a spectral-based graph neural network architecture that performs convolution operations directly on graph-structured data~\cite{b1}. It aggregates information from neighboring nodes by applying a shared linear transformation followed by a non-linear activation function. In our implementation, a 3-layer GCN model is used, where each layer updates node representations by combining features from local neighborhoods. Batch normalization and dropout are applied between layers to improve generalization and prevent overfitting. The model is trained using a weighted cross-entropy loss to handle class imbalance.

3.3.2. GAT

For the node classification task, we utilized the GAT [12], which introduces attention-based aggregation to assign varying importance to neighboring nodes. This allows the model to focus on more informative local structures during feature propagation.

In our implementation on the academic article graph, node features obtained from metadata were processed using a two-layer GAT architecture. The first layer employed 8 parallel attention heads with ReLU activation and dropout, while the second layer used a single head to generate final class logits. Training was performed using cross-entropy loss on labeled nodes, and the entire model was built with PyTorch Geometric.

By enabling adaptive weighting of neighbors, GAT provided more expressive node representations compared to uniform aggregation methods like GCN.

3.3.3. APPNP

For the node classification task, we employed the APPNP [15], which addresses the over-smoothing issue in deep GCNs by decoupling feature transformation and information propagation. In our implementation on the academic article graph, node features derived from article metadata were first processed through a two-layer multi-layer perceptron (MLP), followed by batch normalization, ReLU activation, and dropout regularization. The transformed features were then propagated using APPNP's personalized PageRank-based iterative scheme,

allowing effective information aggregation from semantically related articles. The model was implemented using PyTorch Geometric and achieved better performance compared to baseline models such as MLP and GCN.

4. USER SCENARIO

To facilitate user interaction with the system and make the functionality of the classification and similarity components more accessible, an interactive web-based user interface was developed using the Gradio library in Python. The interface is organized into three main tabs:

- Find Similar Papers: Users can input a paper's title or abstract to retrieve the top five most similar articles in the dataset.
- Predict Category: This section allows users to obtain the predicted engineering subfield of a given article based on its textual content. Additionally, a bar chart displays the confidence scores for all relevant categories.
- Model Performance: It displays a summary of performance metrics for each GNN model used in the node classification task, along with the model identified as the best performing.

This modular interface allows for a streamlined and intuitive exploration of both the dataset and the models' predictions, supporting both quantitative evaluation and qualitative user analysis.

5. RESULTS

To assess model performance, we employed standard classification metrics: Accuracy, precision, recall, and F1-score. We evaluated three GNN models—GCN, GAT, and APPNP—on the node classification task. Table 2 summarizes their overall performance. APPNP achieved perfect scores across all metrics, indicating its effectiveness in capturing class boundaries. GCN followed closely with strong and balanced results. GAT, while showing relatively high precision, suffered from lower recall, suggesting more conservative predictions. Overall, APPNP emerged as the best-performing model.

Table 2. Node classification performance of different GNN models

Model	Accuracy	Precision	Recall	F1-Score	Accuracy
GCN	0.973	0.850	0.863	0.855	0.977
GAT	0.806	0.804	0.701	0.731	0.923
APPNP	1.000	1.000	1.000	1.000	1.000

6. CONCLUSION

This study introduces a GNN-based approach for classifying Turkish academic papers by constructing a custom graph where nodes represent articles and features are derived using Node2Vec. Unlike benchmark datasets, our domain-specific corpus enables topic-focused classification within the engineering field. We compared three GNN models: GCN, GAT and APPNP, under consistent settings, and observed promising classification performance. Additionally, we developed an interactive Gradio interface for real-time category prediction and paper similarity search, making the system accessible for academic use. Future work includes expanding the dataset to other fields, exploring contrastive learning, and integrating additional graph-based tasks such as link prediction.

References

[1] T. N. Kipf and M. Welling, "Semi-supervised classification with graph convolutional networks," *arXiv*, 2017. doi: 10.48550/arXiv.1609.02907

[2] H. Liu, H. Kou, C. Yan, and L. Qi, "Keywords-driven and popularity-aware paper recommendation based on undirected paper citation graph," *Complexity*, vol. 2020, art. no. 2085638, 2020. doi: 10.1155/2020/2085638.

[3] C. Wu, F. Wu, M. An, Y. Huang, and X. Xie, "Neural news recommendation with topic-aware news representation," in *Proc. 57th Annu. Meeting Assoc. Comput. Linguistics (ACL)*, Florence, Italy, Jul. 2019, pp. 1154–1159.

[4] G. Guo, B. Chen, X. Zhang, Z. Liu, Z. Dong, and X. He, "Leveraging title-abstract attentive semantics for paper recommendation," in *Proc. AAAI*, New York, USA, 2020, pp. 67–74.

[5] K. Haruna, M. A. Ismail, A. Qazi, H. A. A. Kakudi, M. Hassan, S. Abdullahi Muaz, et al. "Research paper recommender system based on public contextual metadata," *Scientometrics*, vol. 125, no. 1, pp. 101–114,

Oct. 2020. doi: 10.1007/s11192-020-03642-y
[6] Y. Chen, C. Gao, X. Ren, Y. Peng, X. Xia, and M. R. Lyu, "API usage recommendation via multi-view heterogeneous graph representation learning," *IEEE Trans. Softw. Eng.*, vol. 49, no. 5, pp. 3289–3304, 2023. doi:10.1109/TSE.2023.3252259
[7] C. Gao, Y. Zheng, N. Li, Y. Li, Y. Qin, J. Piao, et al., "A survey of graph neural networks for recommender systems: Challenges, methods, and directions," *ACM Trans. Recomm. Syst.*, vol. 1, no. 1, art. no. 3, pp. 1–51, Mar. 2023. doi: 10.1145/3568022
[8] X. Wang, X. He, M. Wang, F. Feng, and T.-S. Chua, "A survey on knowledge graph-based recommender systems," *ACM Trans. Intell. Syst. Technol.*, vol. 10, no. 2, art. no. 1, pp. 1–37, Jan. 2019. doi: 10.1145/3235029.
[9] W. Huang, T. Zhang, Y. Rong, and J. Huang, "Graph learning: A survey," *IEEE Trans. Artif. Intell.*, vol. 2, no. 2, pp. 109–127, Apr. 2021. doi: 10.1109/TAI.2021.3076021
[10] L. Wu, Y. Chen, K. Shen, X. Guo, H. Gao, S. Li, et al., "Graph neural networks for natural language processing: A survey," *arXiv*, 2021. doi: 10.48550/arXiv.2106.06090
[11] W. L. Hamilton, R. Ying, and J. Leskovec, "Inductive representation learning on large graphs," in *Proc. 31st Int. Conf. Neural Inf. Process. Syst. (NeurIPS)*, Long Beach, CA, USA, 2017, pp. 1025–1035.
[12] P. Veličković, G. Cucurull, A. Casanova, A. Romero, P. Liò, and Y. Bengio, "Graph attention networks," *arXiv*, 2017. doi: 10.48550/arXiv.1710.10903
[13] Q. Li, Z. Han, and X. Wu, "Deeper insights into graph convolutional networks for semi-supervised learning," in *Proc. AAAI Conf. Artif. Intell.*, vol. 32, no. 1, pp. 3538–3545, 2018.
[14] K. Xu, W. Hu, J. Leskovec, and S. Jegelka, "How powerful are graph neural networks?," *arXiv*, 2018. doi: 10.48550/arXiv.1810.00826
[15] J. Klicpera, A. Bojchevski, and S. Gunnemann, "Predict then propagate: Graph neural networks meet personalized PageRank," in *Proc. Int. Conf. Learn. Represent. (ICLR)*, New Orleans, LA, USA, 2019.
[16] P. Sen, G. Namata, M. Bilgic, and L. Getoor, "Collective classification in network data," *AI Magazine*, vol. 29, no. 3, pp. 93–106, 2008.
[17] A. Grover and J. Leskovec, "node2vec: Scalable feature learning for networks," in *Proc. ACM SIGKDD Int. Conf. Knowl. Discov. Data Min. (KDD)*, San Francisco, CA, USA, 2016, pp. 855–864. doi: 10.1145/2939672.2939754
[18] W. Hu, M. Fey, M. Zitnik, Y. Dong, H. Ren, B. Liu, M. Catasta, and J. Leskovec, "Open graph benchmark: Datasets for machine learning on graphs," in *Proc. NeurIPS*, vol. 33, pp. 22118–22133, 2020.
[19] C. B. Clement, M. Bierbaum, K. P. O'Keeffe, and A. A. Alemi, "On the use of arXiv as a dataset," *arXiv*, 2019. doi: 10.48550/arXiv.1905.00075
[20] M. Łopuszyński and Ł. Bolikowski, "Tagging scientific publications using Wikipedia and natural language processing tools," in *Theory and Practice of Digital Libraries – TPDL 2013 Selected Workshops (CCIS)*, Ł. Bolikowski, V. Casarosa, P. Goodale, N. Houssos, P. Manghi, and J. Schirrwagen, Eds. Cham: Springer, 2014, vol. 416, pp. 25–36. doi: 10.1007/978-3-319-08425-1_3
[21] A. M. Dai, C. Olah, and Q. V. Le, "Document embedding with paragraph vectors," *arXiv*, 2015. doi: 10.48550/arXiv.1507.07998
[22] A. A. Alemi and P. Ginsparg, "Text segmentation based on semantic word embeddings," *arXiv*, 2015. doi: 10.48550/arXiv.1503.05543
[23] L. van der Maaten and G. Hinton, "Visualizing data using t-SNE," *Journal of Machine Learning Research*, vol. 9, no. 86, pp. 2579–2605, 2008.
[24] A. Wijesinghe, Q. Wang, and S. Gould, "A regularized Wasserstein framework for graph kernels," in *2021 IEEE International Conference on Data Mining (ICDM)*, pp. 739-748, 2021.

2nd International Conference on Multidisciplinary Sciences and Technological Developments (ICMUSTED 2025)

December 12-15, 2025

Leveraging Large Language Models for Event Detection in Water Resources Literature

Bengisu Sahin[1], Ozge Yaren Turkseven[2], Emrah Inan[1]

[1]Department of Computer Engineering, Izmir Institute of Technology, Izmir, Türkiye
[2]Department of International Water Resources, Izmir Institute of Technology, Izmir, Türkiye
Corresponding author: Bengisu Sahin (e-mail: bengisusahin@iyte.edu.tr)

Abstract

Event extraction is a critical task in information extraction that focuses on identifying event-related information within texts. Although event extraction has been researched for decades, it remains a highly challenging task. To carry out event extraction, a system must comprehend the text's semantics and ambiguity, while also organising the extracted information into structured formats. To address these challenges, we utilise open-source large language models for event extraction within a specific domain, ensuring greater flexibility. In this study, we present a new dataset designed for extracting events related to water resources. Experimental results reveal that the "gemma3:4b" model outperforms the others, which is why we choose to continue using it for few-shot settings. As we integrate samples from 0 to 5, the F1 score improves to 44.22. This encourages us to incorporate more samples into the prompt design, and with 20 samples, the model achieves the highest F1 score of 68.77.

Keywords: Event extraction, Generative models, Groundwater, Water resources, Large language model

1. INTRODUCTION

Event extraction is a critical task in information extraction within natural language processing (NLP). An event is an activity that takes place at a specific time and location, or it can be viewed as a change in state. A typical event extraction task involves two key subtasks: event detection, which focuses on identifying events within the text, and event classification, which categorises them into appropriate classes [1]. For event detection, it involves identifying the participants in the event through argument extraction and defining their attributes via argument role labelling. In essence, event extraction structures unstructured text by answering what, who, when, where, why, and how questions of an event, particularly in news texts.

In the present study, event extraction is primarily approached as a classification problem, with the goal of identifying and categorising each event argument [2]. Previous research has demonstrated that traditional classification-based approaches to event extraction are data-hungry and suffer from data scarcity problems [3]. Despite significant progress, classification-based methods demand a large amount of training data to achieve optimal performance [4]. Furthermore, these methods typically struggle to handle new event types that have not been encountered during the training phase [5]. Recently, generative language models have become widely adopted across several NLP subfields, including event extraction. These generative approaches often differ from traditional methods of identifying and categorising events and their arguments, bringing both new opportunities and challenges, particularly in relation to training and evaluation [6].

To tackle challenges related to domain adaptation and the need for extensive training datasets, we leverage open-source large language models for event extraction within a specific domain, offering greater flexibility. In this study, we introduce a new dataset tailored for extracting events related to water resources. Experimental results reveal that the "gemma3:4b" model outperforms the others, which is why we choose to continue using it for few-shot settings. As we integrate samples from 0 to 5, the F1 score improves to 44.22. This encourages us to incorporate more samples into the prompt design, and with 20 samples, the model achieves the highest F1 score of 68.77.

The paper is structured as follows: Section 2 reviews the relevant literature and examines current methodologies. Section 3 outlines the approach for extracting events within the domain of water resources. Section 4 presents the experimental results of various open-domain models applied to the generated dataset. Finally, Section 5 concludes the study and suggests potential directions for future research.

2. RELATED WORK

In the early stages of event extraction, most methods rely on feature engineering for statistical classifiers. The features are typically derived from constituent parsers, dependency parsers, and contextual information. These models make use of statistical techniques such as nearest neighbour, maximum-entropy classifiers, and conditional random fields [7]. Sha et al. [8] proposed enhancing the bidirectional recurrent neural network (RNN) with dependency bridges, which transmit syntactic information when modelling words in a sentence. They demonstrate that using both hierarchical tree structures and sequential structures in the RNN simultaneously leads to improved performance compared to the traditional sequential structure.

Liu et al. [5] investigate an approach to event extraction by explicitly treating it as a machine reading comprehension (MRC) problem. They show that this approach can improve performance by effectively utilising both the model and data within the MRC framework. Furthermore, they propose an unsupervised question generation method that connects MRC with event extraction. Their method generates questions that are both relevant to the topic and dependent on the context, thereby better guiding an MRC model in question-answering tasks.

Ren et al. [9] focus exclusively on document-level event argument extraction using retrieval-augmented generation (RAG). Specifically, they first retrieve the top-k potentially relevant documents from the training corpus. The relevance of a document is assessed using a T5-encoder-based Siamese network, which compares the input text and event schema. The retrieved documents are then provided as additional input to the model, alongside the input document and schema information. Wang et al. [10] present InstructUIE as a unified information extraction framework for multiple IE tasks, aligned with UIE. Specifically, all IE tasks are redefined as natural language generation tasks, guided by expert-designed instructions that outline the required output format. InstructUIE facilitates joint training across multiple IE tasks using a collection of 32 datasets, creating a unified and semantically consistent label set. This approach enables cross-task knowledge sharing and benefits from an expanded pool of training data.

Hsu et al. [11] formulate joint modelling for event extraction as a text generation task using pretrained generative language models. Leveraging these models, they employ an attention-based autoregressive decoder to generate event mentions, entity mentions, along with their labels and relationships. The task dependencies are encoded through the attention mechanism of the transformer-based decoder, enabling the model to learn the relationships between tasks and task instances in a flexible manner.

In recent years, there have been two primary methods for utilizing large language models in event extraction. The first approach relies on prompting-based methods, where the model is treated as a black box and given task instructions in zero- or few-shot settings. These methods have the advantage of requiring no additional training, although their effectiveness can vary depending on the task and domain. The second approach of research emphasizes instruction-tuning of large language models, which directly adapt models to information extraction tasks through supervised fine-tuning on task-specific instructions. [12] investigated the integration of annotation guidelines with textual descriptions of event types and roles into instruction-tuned LLMs. They suggested five ways to automatically generate these annotation guidelines and evaluated how well they worked on the ACE05 and RichERE datasets [13, 14]. The results demonstrated that the use of structured guidelines leads to improved performance in low-resource settings and facilitates generalization across different annotation schemas.

Domain-specific studies are crucial because general-purpose event extraction methods often face to capture the nuances of specialized contexts. These challenges in event extraction have been addressed by examining how models perform when encountering specialized language patterns and discourse. BRAD, a dataset based on nineteenth-century African American newspapers, was introduced in [15] and revealed significant performance gaps when models encountered domain-specific language and historical writing styles. Their experiments with BERT-based models highlighted the urgent need for domain adaptation, especially to handle evolving language and specialized terminology.

In this study, we contribute to domain specific event extraction research by introducing a novel dataset focused on water resource related events. Instead of relying on additional fine-tuning as in instruction-tuning approaches, we adopt a few-shot prompting setting, which allows the use of open-source large language models without task-specific retraining. By evaluating models on a specialized dataset, we demonstrate that domain-specific data can substantially enhance performance in few-shot settings, helping to bridge the gap between general-purpose event extraction methods and the requirements of domain-oriented applications.

3. PROPOSED METHOD

3.1. Dataset Preparation

We utilise a sample study [16] to generate an event detection dataset tailored to water resources literature as a domain-specific task. Turkseven et al. [16] focus on how climate change presents a major threat to island ecosystems, highlighting the importance of sustainable groundwater management. They suggest that nature-based solutions, such as rainwater harvesting, provide innovative strategies to alleviate water scarcity and ensure the long-term sustainability of water resources.

Table 1. Excerpts of the generated dataset for water resources

Type	Sample
Sentence	Climate change is one of the most crucial threats affecting ecosystems and water resources.
Tokens	"Climate", "change", "is", "one", "of", "the", "most", "crucial", "threats", "affecting", "ecosystems", "and", "water", "resources"
BIO	"B-EVENT", "I-EVENT", "O", "O", "O", "O", "O", "O", "B-EVENT", "I-EVENT", "O", "O", "B-EVENT", "I-EVENT"
Sentence	Understanding the unique status of the islands and the complex relationship between water resources and climate change is of great importance for the creation and development of sustainable policies in these areas.
Tokens	"Understanding", "the", "unique", "status", "of", "the", "islands", "and", "the", "complex", "relationship", "between", "water", "resources", "and", "climate", "change", "is", "of", "great", "importance", "for", "the", "creation", "and", "development", "of", "sustainable", "policies", "in", "these", "areas", "."
BIO	"O", "O", "O", "O", "O", "O", "O", "O", "O", "O", "O", "O", "B-EVENT", "I-EVENT", "O", "B-EVENT", "I-EVENT", "O", "O", "O", "O", "O", "O", "O", "O", "O", "O", "O", "O", "O", "O", "O", "O", "O", "O"

Table 1 presents examples from the generated dataset, including the sentence, token list, and BIO format. The BIO format denotes the token position, where "B-" marks the beginning of an event, "I-" represents the continuation of an event token, and "O" indicates tokens that are not part of an event [17]. In this context, we adapt the generated dataset for use with the transformer-based named entity recognition (T-NER) library [18], which supports the exploration of cross-domain generalisation.

3.2. Event Detection Method

To detect events, we utilise the Ollama library [19], a tool designed to streamline the deployment and operation of Large Language Models (LLMs) for a range of language tasks. Ollama provides a solution that improves the utility of LLMs, making them more adaptable to employ in different contexts, especially on local machines, as open-source models.

From the Ollama library, we utilise Gemma 3 [20], a multimodal extension to the Gemma series of lightweight open models, ranging from 1 to 27 billion parameters. This updated version introduces vision capabilities, expanded language support, and longer context handling—up to 128K tokens. Additionally, the model's architecture has been adjusted to minimise the excessive growth of KV-cache memory when dealing with long contexts. Another model is Llama 3 [21], a series of language models developed to support multilingual tasks, including coding, reasoning, and tool usage. The largest model in the series is a dense Transformer with 405 billion parameters and a context window of up to 128K tokens. Llama 3 has been publicly released, featuring both pre-trained and post-trained versions of the 405B parameter language model. We also make use of Phi-4 [22], a 14-billion parameter language model designed with a training methodology focused on data quality. In contrast to most language models that mainly depend on organic data sources such as web content or code for pre-training, Phi-4 deliberately incorporates synthetic data throughout its training.

4. EVALUATION

In this work, we employ the seqeval [23] as the experimental framework and evaluation metrics. This is a Python-based framework used for sequence labelling assessment. To evaluate the performance of the generative models,

we utilise precision, recall, and F1 score metrics. Figure 1 illustrates the prompt design templates for both the dataset preparation and event detection tasks (below). The first prompt uses definitions and guidelines to identify events in the literature. For the event extraction and detection task, we adapt the prompt design from the PromptNER study [24] with the following:

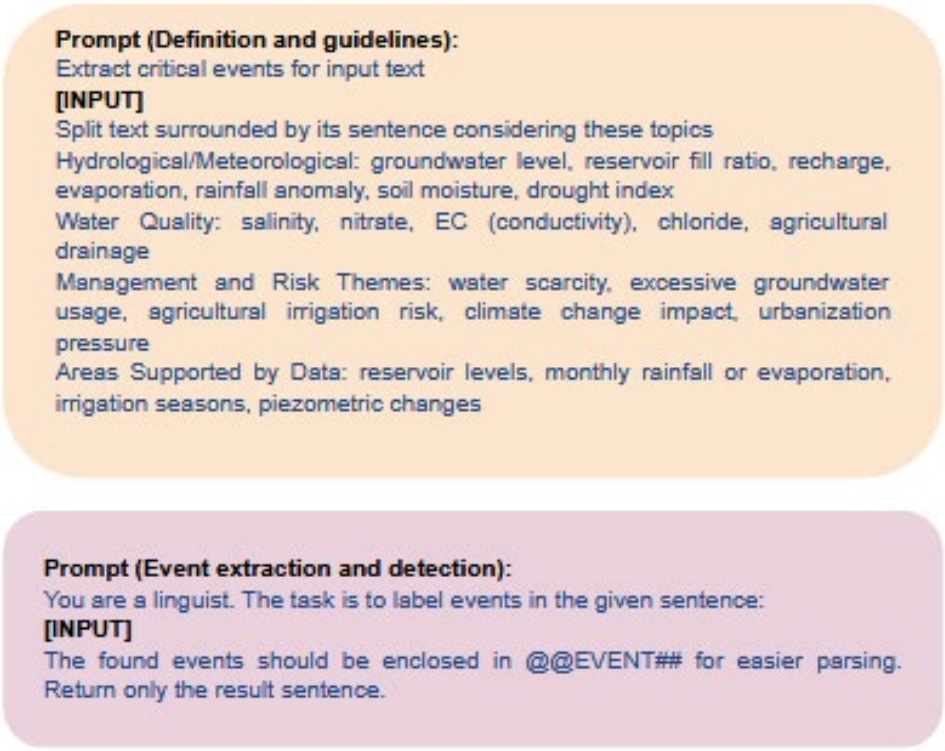

Figure 1. Templates for prompt design used in dataset preparation and event detection

Table 2 presents a comparison of the models from Ollama, where we utilise the "llama3.2" model with 1 billion parameters [25], the "phi3" model with 3.8 billion parameters [26], and the "gemma3" model with 4 billion parameters [27]. Given that these models have relatively small parameter sizes, they tend to yield poor results. Additionally, since these are zero-shot models, no sample is integrated into the chat history of the prompt design. Among these, the "gemma3:4b" model outperforms the others, which is why we choose to continue using it for few-shot settings.

Table 2. Comparison of zero-shot models on the water resources dataset

Model	P	R	F1
llama3.2:1b	21.26	24.34	22.70
phi3:3.8b	19.27	24.34	21.51
gemma3:4b	37.37	24.34	29.48

Table 3 presents the performance of the "gemma3:4b" model with varying sample sizes. The zero-shot setting, with no samples, results in the lowest F1 score of 29.48. As we integrate samples from 0 to 5, the F1 score improves to 44.22. This encourages us to incorporate more samples into the prompt design, and with 20 samples, the model achieves the highest F1 score of 68.77.

Table 3. Comparison of few-shot performance of the gemma3:4b model on the water resources dataset

Model	Samples	P	R	F1
gemma3:4b	0	37.37	24.34	29.48
	5	45.77	42.76	44.22
	10	65.93	58.55	62.02
	20	73.68	64.47	68.77

5. CONCLUSION AND FUTURE WORK

In this study, we leverage open-source large language models for event extraction within a specific domain, offering enhanced flexibility. To assess the performance of these models, we introduce a new dataset tailored for extracting events related to water resources. In the zero-shot setting, where no samples are provided, the "gemma3:4b" model achieves the lowest F1 score of 29.48. As we incorporate samples ranging from 0 to 5, the F1 score improves to 44.22. This motivates us to add more samples to the prompt design, and with 20 samples, the model reaches the highest F1 score of 68.77.

One limitation of this study is the use of large language models with relatively low parameter sizes, due to resource constraints. Another limitation is the relatively small size of the prepared dataset. As a future direction, we plan to parse additional water resources papers to expand the dataset. Additionally, we aim to adapt the large language model approach to automate the extraction of supply chain information [28], as achieving comprehensive supply chain visibility is essential for effective risk management.

References

[1] V. D. Lai, "Event extraction: A survey," *arXiv Preprint*, 2022. doi: 10.48550/arXiv.2210.03419

[2] T. H. Nguyen, K. Cho, and R. Grishman, "Joint event extraction via recurrent neural networks," in *Proc. 2016 Conf. North Amer. Chapter Assoc. Comput. Linguistics: Hum. Lang. Technol.*, San Diego, CA, USA, 2016, pp. 300–309.

[3] J. Liu, Y. Chen, K. Liu, W. Bi, and X. Liu, "Event extraction as machine reading comprehension," in *Proc. 2020 Conf. Empirical Methods in Natural Language Processing (EMNLP)*, Nov. 2020, pp. 1641–1651.

[4] J. Liu, Y. Chen, K. Liu, and J. Zhao, "Event detection via gated multilingual attention mechanism," in *AAAI Conf. Artif. Intell.*, 2018.

[5] J. Liu, Y. Chen, K. Liu, W. Bi, and X. Liu, "Event extraction as machine reading comprehension," in *Proc. 2020 Conf. Empir. Methods Nat. Lang. Process. (EMNLP)*, Nov. 2020, pp. 1641–1651.

[6] É. Simon, H. Olsen, H. You, S. Touileb, L. Øvrelid, and E. Velldal, "Generative approaches to event extraction: Survey and outlook," in *Proc. Workshop Future Event Detection (FuturED)*, Nov. 2024, pp. 73–86.

[7] A. Majumder and A. Ekbal, "Event extraction from biomedical text using CRF and genetic algorithm," in *Proc. 2015 3rd Int. Conf. Comput., Commun., Control Inform. Technol. (C3IT)*, 2015, pp. 1–7.

[8] L. Sha, F. Qian, B. Chang, and Z. Sui, "Jointly extracting event triggers and arguments by dependency-bridge RNN and tensor-based argument interaction," in *Proc. 32nd AAAI Conf. Artif. Intell.*, 2018.

[9] Y. Ren, Y. Cao, P. Guo, F. Fang, W. Ma, and Z. Lin, "Retrieve-and-sample: Document-level event argument extraction via hybrid retrieval augmentation," in *Proc. 61st Annu. Meeting Assoc. Comput. Linguistics (Vol. 1: Long Papers)*, Toronto, Canada, 2023, pp. 293–306.

[10] X. Wang, W. Zhou, C. Zu, H. Xia, T. Chen, Y. Zhang, et al., "InstructUIE: Multi-task instruction tuning for unified information extraction," *arXiv Preprint*, 2023. doi: 10.48550/arXiv.2304.08085

[11] I.-H. Hsu, K.-H. Huang, E. Boschee, S. Miller, P. Natarajan, K.-W. Chang, and N. Peng, "DEGREE: A data-efficient generation-based event extraction model," in *Proc. 2022 Conf. North Amer. Chapter Assoc. Comput. Linguistics: Hum. Lang. Technol.*, Seattle, WA, USA, 2022, pp. 1890–1908.

[12] S. Srivastava, S. Pati, and Z. Yao, "Instruction-tuning LLMs for event extraction with annotation guidelines," *arXiv Preprint*, 2025. doi: 10.48550/arXiv.2502.16377

[13] G. R. Doddington, A. Mitchell, M. Przybocki, L. Ramshaw, S. Strassel, and R. Weischedel, "The automatic content extraction (ACE) program – tasks, data, and evaluation," in *Proc. 4th Int. Conf. Lang. Resour. Eval. (LREC)*, Lisbon, Portugal, May 2004.

[14] Z. Song, A. Bies, S. Strassel, T. Riese, J. Mott, J. Ellis, J. Wright, S. Kulick, N. Ryant, and X. Ma, "From light to rich ERE: annotation of entities, relations, and events," in *Proc. 3rd Workshop on EVENTS: Definition, Detection, Coreference, and Representation*, Denver, CO, USA, 2015, pp. 89–98. doi: 10.3115/v1/W15-0812

[15] V. Lai, M. Van Nguyen, H. Kaufman, and T. H. Nguyen, "Event extraction from historical texts: a new dataset for black rebellions," in *Findings of the Association for Computational Linguistics: ACL-IJCNLP 2021*, Stroudsburg, PA, USA: Association for Computational Linguistics, 2021, pp. 2390–2400. doi: 10.18653/v1/2021.findings-acl.211

[16] O. Y. Turkseven, O. Gunduz, and A. Baba, "Innovative Solutions on Water Management for Islands Under Climate Change," in *Int. Conf. Water Problems Mediterranean Countries*, Cham, Switzerland, Dec. 2023, pp. 33–40.

[17] J. C. S. Alvarado, K. Verspoor, and T. Baldwin, "Domain adaptation of named entity recognition to support credit risk assessment," *Proc. Australasian Lang. Technol. Assoc. Workshop*, Dec. 2015, pp. 84–90.

[18] A. Ushio, and J. Camacho-Collados. “T-NER: An all-round python library for transformer-based named entity recognition,” in *Proceedings of the 16th Conference of the European Chapter of the Association for Computational Linguistics: System Demonstrations*, Apr. 2021, pp. 53–62.
[19] F. S. Marcondes, A. Gala, R. Magalhães, F. Perez de Britto, D. Durães, and P. Novais, “Using ollama,” in *Natural Language Analytics with Generative Large-Language Models: A Practical Approach with Ollama and Open-Source LLMs*, Cham, Switzerland, 2025, pp. 23–35.
[20] G. Team, A. Kamath, J. Ferret, S. Pathak, N. Vieillard, R. Merhej, et. al., “Gemma 3 technical report,” *arXiv Preprint*, 2025. doi: 10.48550/arXiv.2503.19786
[21] A. Grattafiori, A. Dubey, A. Jauhri, A. Pandey, A. Kadian, A. Al-Dahle, et al., “The Llama 3 herd of models,” *arXiv Preprint*, 2024. doi: 10.48550/arXiv.2407.21783
[22] M. Abdin, J. Aneja, H. Behl, S. Bubeck, R. Eldan, S. Gunasekar, et al., “Phi-4 technical report,” *arXiv Preprint*, 2024. doi: 10.48550/arXiv.2412.08905
[23] Seqeval. (2025, Aug. 24). *Python framework for sequence labelling evaluation* [Online]. Available: https://github.com/chakki-works/seqeval
[24] D. Ashok, and Z. C. Lipton, “PromptNER: Prompting for named entity recognition,” *arXiv Preprint*, 2023. doi: 10.48550/arXiv.2305.15444
[25] Llama3.2. (2025, Aug. 24). *Llama3.2 model with 1 billion parameters* [Online]. Available: https://ollama.com/library/llama3.2
[26] Phi3. (2025, Aug. 24). *Phi3 model with 3.8 billion parameters* [Online]. Available: https://ollama.com/library/phi3
[27] Gemma3. (2025, Aug. 24). *Gemma3 model with 1 billion parameters* [Online]. Available: https://ollama.com/library/gemma3
[28] S. AlMahri, L. Xu, and A. Brintrup, “Enhancing supply chain visibility with knowledge graphs and large language models,” *arXiv Preprint*, 2024. doi: 10.48550/arXiv.2408.07705

Degradation Behavior of PET Polymers: Mechanical and FTIR Insights

Ivana Salopek Čubrić[1], Goran Čubrić[2]

[1]Department of Textile Design and Management, University of Zagreb Faculty of Textile Technology, Zagreb, Croatia
[2]Department of Clothing Technology, University of Zagreb Faculty of Textile Technology, Zagreb, Croatia
Corresponding author: Ivana Salopek Čubrić (ivana.salopek@ttf.unizg.hr)

Abstract

The degradation of polymers due to ageing is being recently intensively studied mainly due to the growing concern about the accumulation of plastics and microplastics. The studies indicated the change of certain properties even after a short period of exposure. In this research, polymer materials made of polyethylene terephthalate (PET) were exposed to natural ageing with exposure to the sun, and exposure to shade during summer months. The mean air temperature was 30 °C and relative air humidity 50%. The non-exposed polymers and exposed polymers (sun and shade) were tested for thickness, breaking force, breaking elongation, and liquid absorption capability. The results of aged polymers are brought into the context of the results of non-exposed polymers. As such, they indicated an increase in thickness after both ageing. It was seen that exposure to the sun positively affected the increase of the breaking force of materials, while the elongation of polymers decreased. As far as the polymers exposed to shade are concerned, both the breaking force and elongation decrease in all the cases. The Fourier transform infrared spectroscopy (FTIR) analysis showed that investigated polymer materials show a characteristic infrared absorption band of the carbonyl group and all other absorption bands are completely correlated with standard infrared spectra of polyester. The results indicated that non-aged polymer material could not be distinguished from the polymer materials exposed to natural ageing, indicating there were no chemical changes during the ageing process.

Keywords: Polymer, Material, Degradation, Exposure, FTIR

2nd International Conference on Multidisciplinary Sciences and Technological Developments (ICMUSTED 2025)

December 12-15, 2025

Structural Performance of Hybrid Composite Patch Repairs in Double Lap Configurations with Unidirectional and Woven Fiber Reinforcements

Faycal Mili[1,2], Walid Halloufi[1], Sarah Guenifa[1]

[1]Department of Mechanical Engineering, University of Frères Mentouri, Constantine, Algeria
[2]Mechanics Laboratory, University of Frères Mentouri, Constantine, Algeria
Corresponding author: Faycal Mili (e-mail: mili.faycal@gmail.com)

Abstract

Composite patching is a well-established technique for restoring or enhancing the structural integrity of damaged components. This study focuses on the characterization and optimization of hybrid composite patch repairs applied in double lap configurations. The reinforcement patches are designed using unidirectional or woven fiber architectures, either individually or in hybrid combinations, to assess their influence on load transfer, stress distribution, and damage resistance. Emphasis is placed on comparing the structural performance of different reinforcement strategies in terms of strength, stiffness, and durability. The reinforcement consists of composite patches made from epoxy resin and E-glass, carbon, or Kevlar fibers, designed to strengthen weakened glass/epoxy plates subjected to uniaxial tensile loading. These composite patches are configured using a single ply oriented at 0° or 90°, cross-ply stacking sequences (0°/90°), or angle-ply sequences (+θ/-θ). The principal objective of this research is to demonstrate the effectiveness of composite patch bonding as a repair technique for restoring and enhancing the mechanical performance of damaged structures. Therefore, an optimization approach was undertaken based on the Tsai-Hill failure criterion, aiming to identify the optimal material type and stacking sequence for the composite patch that offers the best reinforcement for the E-glass/epoxy structure. Results obtained highlight the importance of incorporating angle-ply patches compared to those with cross-ply reinforcement. Moreover, the consideration of woven fabrics improves the strength of cross-ply patches. However, the best performance is generally achieved when the plies are arranged in alternating +θ/-θ orientations. These findings underscore a significant improvement in the performance of the hybrid material when patch reinforcements match the material of the structure. Moreover, failure strength of the material declines with unidirectional patches but reaches its maximum when woven fabrics are oriented along warp and weft directions. Consequently, these results demonstrate the role of optimized composite patches in advancing structural repair strategies.

Keywords: Composite, Bonding, Patch, Failure, Optimization

2nd International Conference on Multidisciplinary Sciences and Technological Developments (ICMUSTED 2025)

December 12-15, 2025

Solar-Powered Pneumatic Water Pump: A Sustainable Solution for Water Supply in Off-Grid Areas

Shoukat Mugheri[1], Touqeer Aslam[1], Mazhar Ali[2], Muhammad Kaleem[3], Umair Mehmood[4], Ayaz Ali[4], Ammar Asghar[4]

[1]School of Mechanical Engineering, Southwest Jiaotong University, Chengdu, China
[2]Precision System Training Center, Gwadar, Pakistan
[3]Institute of Refrigeration and Cryogenics, Zhejiang University, Hangzhou, China
[4]Mechanical Department, Pakistan Institute of Engineering and Technology, Multan, Pakistan
Corresponding author: Shoukat Mugheri (e-mail: engrshoukat99@gmail.com)

Abstract

The storage and pumping of water is typically achieved using electrically operated hydraulic pumps. However, the issue with these water pumping systems is their reliance on electricity, which is often unavailable in rural areas facing frequent load shedding. Consequently, electric-powered water pumps are not suitable for such regions. This research presents a reciprocating water pump with a capacity of 48 Liter per minute (LPM), which transforms a manually operated pneumatic pump into an automatically operated solar-powered pneumatic pump. The study encompasses the design and fabrication of this pneumatic reciprocating water pump, alongside an evaluation of its performance within a solar-powered automatic operating system. Various tests were conducted on this prototype across different head values ranging from 10 to 24 ft, with 3 ft intervals, while maintaining a constant pressure of 2 bar. The resulting flow-rates were recorded as 48, 44, 42, 39, 35, and 31 LPM at the outlet. It was observed that as the head increased, the discharge volume decreased. Additionally, when a constant head of 24 ft was maintained, varying the pressure from 2 to 4.5 bar in increments of 0.5 bar resulted in flow rates of 31, 35, 39, 42, 44, and 48 LPM. Energy for the unit is supplied via solar panels; five solar panel modules with a power rating of 150 W are necessary if a battery is included, while four modules suffice if the battery is excluded from the system. This model is suitable for both domestic and commercial consumers.

Keywords: Rural power crisis, Solar energy, Reciprocating water pump, Volumetric flow, Sustainable water management

1. INTRODUCTION

Most of the developing countries are facing energy crisis due to dependence on conventional energy resources. Using fossil fuels have environmental as well as an economic consequences [1]. Pneumatics uses compressed air for machinery; integrated with solar photovoltaics (PV), pumps deliver sustainable automation, efficiency, and renewable energy for diverse applications [2]. In the field of automation from conventional woodworks, machinery stores and space robots, pneumatics technique are too much important in air characteristics, which have made this ideal medium for use in latest production and manufacturing organizations. [3]. Recent field studies highlight methods to supervise and test PV-driven pumping directly from the array, improving diagnostics without auxiliary power, and confirming sensitivity to irradiance, temperature, and component efficiencies [4]. Parallel research explores integrating compressed-air concepts with solar irrigation to enhance autonomy and resilience, suggesting pathways for pneumatic actuation where electricity is intermittent [5]. The project's aim is to install pneumatic water pumping system; a pneumatic system consists of radian plunger and a pump for the pumping of water. A pneumatic piston solenoid valve is used to reciprocate the piston. Two cylinders, one for the pneumatic and one for the hydraulic operation, are used in this venture [6]. The timing unit also provides water supply for the treatment of pumping [7]. The pneumatic device energy analysis is carried out in the framework of simulation.

Previous research has shown that methods for the energy behavior research of pneumatic drive systems have been compared and practiced [8]. The present model is based on an analysis of methods for evaluating energy efficiency. Energy analysis considers all energy losses and the impact of temperature on the useful pneumatic energy available [9]. A five-valve, two-port solenoid valve converts electrical energy into reciprocating motion, reducing human effort and enabling faster, efficient operations [10]. Real-world reliability studies corroborate that irradiance, module temperature, and balance-of-system efficiency dominate delivered flow and uptime, underscoring the value of robust monitoring for rural deployments [11]. Newer sizing frameworks (2025) further formalize trade-

offs among throughput, autonomy, and lifecycle cost for irrigation, offering templates that can be adapted to domestic/commercial contexts [12]. Recent work applies soft-computing and data-driven approaches to optimize PV array size, pump selection, and operating strategies under variable weather and water-lift demands; these approaches consistently improve match between energy supply and hydraulic load [13]. Emerging integrated architectures explore solar-driven systems that combine compressed air with other storage (e.g., pumped hydro or batteries) to stabilize output for water services; these concepts frame design choices in rural contexts where load-levelling and night operation are desirable [14].

This study presents the design, fabrication, and performance evaluation of a pneumatic reciprocating water pump, initially operated manually and subsequently adapted to an automated configuration powered by solar PV energy. The system's operational characteristics were analyzed in terms of flow-head and flow-pressure relationships under varying practical conditions. Particular focus was directed toward PV sizing with and without battery storage to optimize energy utilization. Experimental results demonstrate that solar-powered pneumatic pumping reduces dependency on conventional energy sources, improves efficiency, and provides a cost-effective, sustainable solution for rural domestic and small-scale commercial applications, where grid electricity access is limited or unavailable.

2. DESIGN SYSTEM OF PNEUMATIC RECIPROCATING WATER PUMP

The pneumatic system integrates multiple components to achieve efficient and precise operation, as shown in Fig. 1. A two-stage reciprocating air compressor is used to increase air pressure by reducing its volume, offering 10-15% higher efficiency and greater pressure compared to rotary compressors.

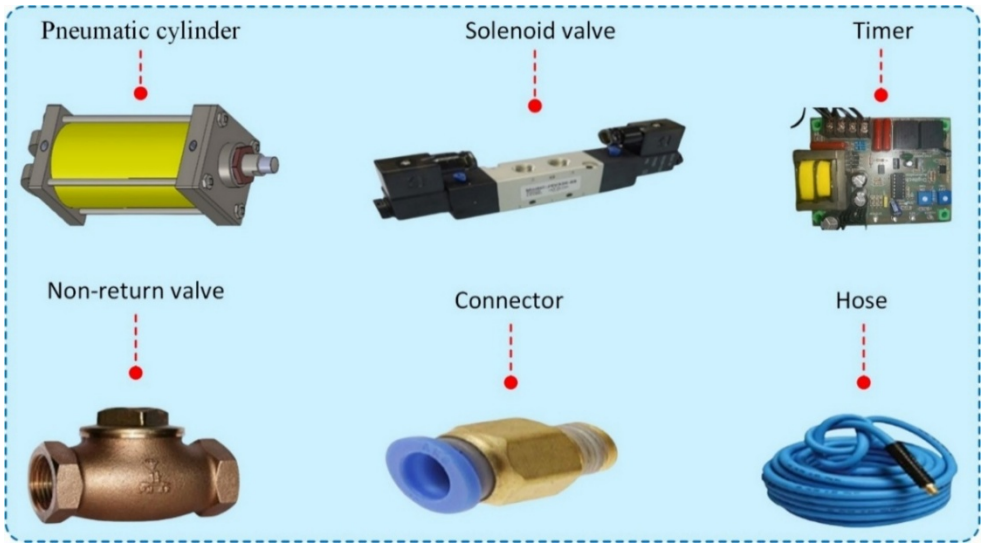

Figure 1. Significant components of the system

The compressed air is regulated through a four-way (5/2) solenoid valve, which converts electrical energy into linear motion and controls double-acting pneumatic cylinders via its five ports—one inlet, two outlets, and two exhausts. A retentive timer in the timing control unit governs the forward and reverse strokes of the cylinders within specified time intervals, ensuring accurate cycle control. The system employs two double-acting pneumatic cylinders, each with a 160 mm stroke length and 25 mm piston rod diameter, one of which is also adapted for suction and discharge of water. Polyurethane hoses are used to deliver compressed air, capable of withstanding pressures up to 10×10^5 Pa, making them reliable under high-pressure conditions. Non-return valves ensure unidirectional fluid flow, preventing backflow and maintaining system efficiency. Connectors, including hose connectors with adopt hose nipples and cap nuts, along with reducers, are employed to secure joints and maintain leak-proof connections throughout the system. By combining these components—compressor, solenoid valve, timer, pneumatic cylinders, hoses, non-return valves, and connectors—the system effectively converts compressed air into controlled mechanical motion. This integration not only enhances reliability and precision but also ensures optimized performance for practical pneumatic applications.

2.1. Components Description

The air is compressed in an air compressor, from the compressor plant the flow media is passed towards the solenoid valve that is connected to the Timing control unit which controls the number of strokes in the cylinder

with definite time, the piston is reciprocated with the help of a pneumatic cylinder, in forward stroke it discharge the water at outlet and in reverse stroke it sucks the water and cycle is continue, the flow rate of water can be increase at the output with optimizing the number of strokes of the piston in the cylinder through timing control unit, as illustrated in Fig. 2.

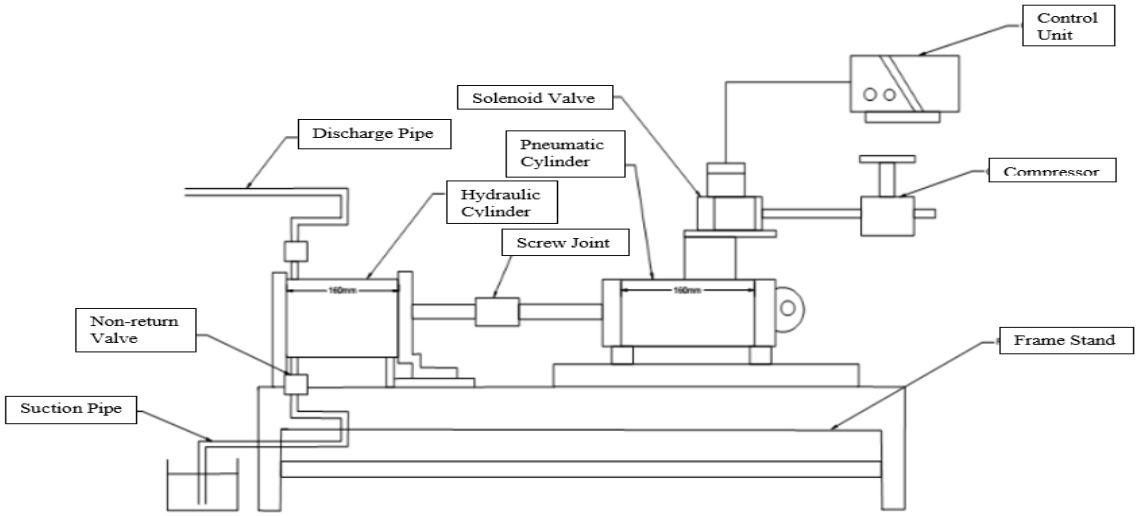

Figure 2. Schematic diagram of pneumatic reciprocating water pump

2.2. Design Modeling

This design modeling includes to identify the different parameters regarding Pneumatic Reciprocating Water Pump. Both pressure and head parameters were evaluated within the ranges of 2-4.5 bar and 10-24 ft, respectively, along with the corresponding force requirements for the forward and backward strokes of the pneumatic reciprocating pump, which varied from 1005 N to 957 N. The specifications of the model cylinders are given in Tab. 1.

Table 1. Specifications of the cylinders

No	Specifications	Pneumatic Cylinder	Hydraulic Cylinder
1	Diameter	8 cm	5.6 cm
2	Pressure	20 N/cm^2	1.92-2.0 N/cm^2
3	Stroke length	16 cm	16 cm
4	Piston rod diameter	2.5 cm	2.5 cm
5	Forward stroke force	1005.8 N	1005.8 N
6	Return stroke force	957.9 N	957.9 N

2.3. Parameters for Finding the Supply of Electricity Using Solar Energy System for Air Compressor

A solar system comprising five panels of 150 W delivers a combined peak capacity of 0.75 kW under standard test conditions, as exhibited in Fig. 3. In locations with 5-6 peak sun hours, such as South Asia, this system can theoretically produce 3.75-4.5 kWh of electricity daily. However, efficiency losses from inverters, temperature, dust, and wiring reduce actual output to about 3.0-3.5 kWh/day, as presented in Fig. 4.

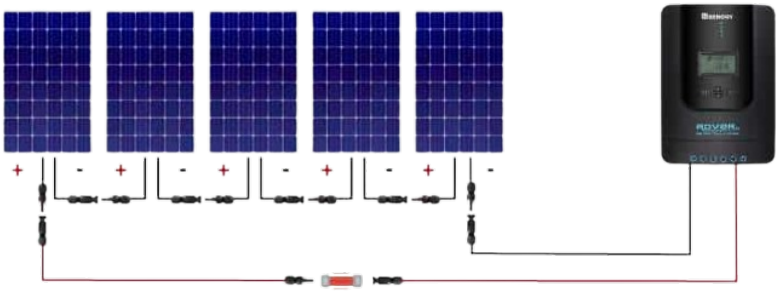

Figure 3. Solar panels wire connections in series

This energy output is sufficient to power small household loads such as fans, lighting, and pumps. Consequently, such systems provide a cost-effective, renewable energy solution, particularly valuable for rural communities in developing regions experiencing persistent energy shortages. Hydraulic power exhibits an increase with rising head height. At a head of 10 ft, the hydraulic power is 24 W, which increases to 57 W at 24 ft. This trend demonstrates that greater power is necessary to elevate water to higher levels, consistent with the underlying principles of pumping system mechanics. The input power at both 60% and 40% loads also increases with the head, as shown in Figs. 4(a) and 4(b). For example, at 10 ft, the input power at 60% load is 40 W, and at 40% load, it's 60 W. As the head increases, the difference between the input power at 60% and 40% load grows, with the 60% load requiring higher input power due to increased operational demand. At the highest head (24 ft), the input power at 60% load is 96 W, while at 40% load, it is 144 W. Run-time is determined by the total energy available (3.0 kWh or 3.5 kWh) and the input power required. As the head increases, the system consumes more power, thus reducing the runtime, as exhibited in Figs. 4(c) ve 4(d). For example, at 10 ft, the run-time at 3.0 kWh ranges from 75 to 50 hours, while at 24 ft, the run-time ranges from 31 to 21 hours. Similarly, for 3.5 kWh, the run-time is slightly longer but follows the same decreasing pattern with increasing head. At 10 ft, it's between 88 and 59 hours, while at 24 ft, it's between 37 and 24 hours. The observations clearly illustrates how system performance changes with increasing head. As head increases, more hydraulic and input power is required, which reduces the available run-time per given energy capacity. This data is essential for evaluating the efficiency and operational feasibility of the pump under varying conditions.

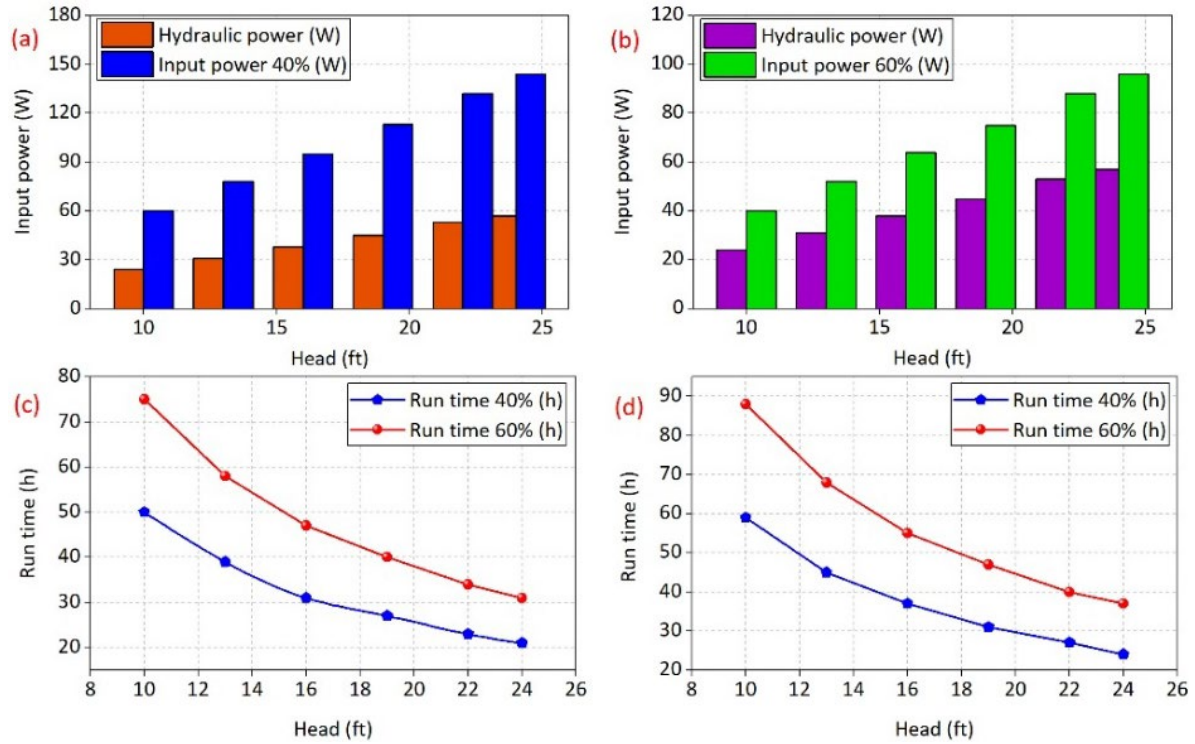

Figure 4. Effect of head on power requirement and run-time performance

2.4. Mathematical Modelling

Power required for compressor and pump is calculated by:

$$P = \frac{W \times N_w}{60}. \tag{1}$$

Low pressure cylinder work done by two stage reciprocating air compressor with inter cooler is calculated by:

$$W_1 = \left(\frac{n}{n-1}\right) \times p_1 v_1 \times \left[\left(\frac{p_2}{p_1}\right)^{\frac{n-1}{n}} - 1\right]. \tag{2}$$

High pressure cylinder work done is calculated by:

$$W_2 = \left(\frac{n}{n-1}\right) \times p_2 v_2 \times \left[\left(\frac{p_3}{p_2}\right)^{\frac{n-1}{n}} - 1\right]. \tag{3}$$

The work done can be calculated by the compressor with low and high pressure cylinder [15]. The velocity of moving fluid is found by:

$$V = \frac{200L}{3\pi d^3}. \tag{4}$$

Force for forward and also return stroke of double acting cylinder is calculated by:

$$F = \frac{\pi}{4} \times \left(D^2 - d^2\right) \times P. \tag{5}$$

Discharge of water at outlet is found by

$$Q = A \times V. \tag{6}$$

Pressure for forward and backward strokes:

$$P = \frac{F}{A}. \tag{7}$$

Head calculated by the equation of the curve [16]

$$H = H_{\max}\left[1 - \frac{Q}{Q_{\max}}\right]^2. \tag{8}$$

3. EXPERIMENTAL SETUP

The The significant components of pneumatic Reciprocating Water Pump are compressor, solenoid valve, timing control unit and pneumatic cylinder, as shown in Fig. 5. The pneumatic reciprocating water pump operates by utilizing compressed air generated from the compressor, which serves as the primary energy source for the system. This compressed air is directed through a solenoid valve that regulates its flow, alternating the supply to different sides of the pneumatic cylinder. A timing control unit governs the actuation of the solenoid valve, ensuring proper sequencing and continuous reciprocating motion. The pneumatic cylinder then converts the controlled air pressure into linear reciprocating movement, which drives the pump mechanism. Through this process, water is drawn in during the suction stroke and discharged during the compression stroke, enabling a continuous pumping cycle.

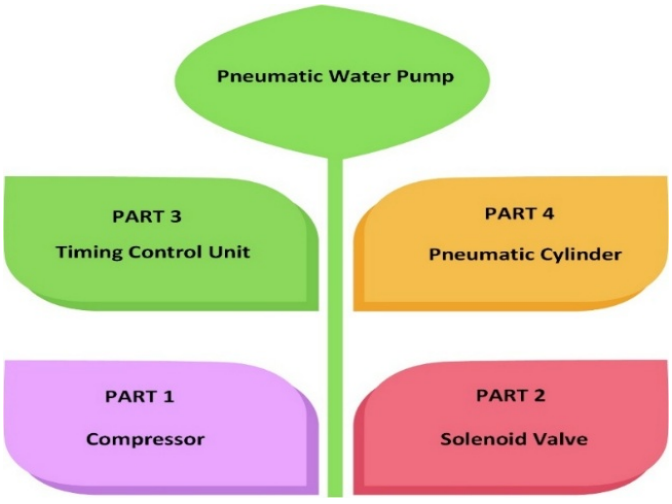

Figure 5. Major parts of pneumatic reciprocating water pump

3.1. Fabrication of Model

The pneumatic reciprocating water pump model was fabricated to experimentally evaluate its performance under varying head conditions and pressures, as seen in Fig. 6. The fabricated pneumatic reciprocating water pump model effectively illustrates how pneumatic systems can be applied for controlled fluid pumping. In this setup, an air compressor delivers pressurized air, which is directed through a solenoid valve to operate the double-acting pneumatic cylinders.

The solenoid valve, governed by a timer, ensures alternate forward and reverse strokes of the cylinders within a fixed cycle, making the pumping action continuous and reliable. The suction pipe draws water into the system, while the non-return valve maintains unidirectional flow, preventing backflow and enhancing efficiency. A gate valve is included to provide manual regulation of water flow, and the pressure gauge measures operating pressure, ensuring safe and stable functioning. This model demonstrates how compressed air can be efficiently converted into mechanical motion for fluid pumping, offering a sustainable and adaptable design for practical applications in irrigation, fluid transfer, and other industrial processes.

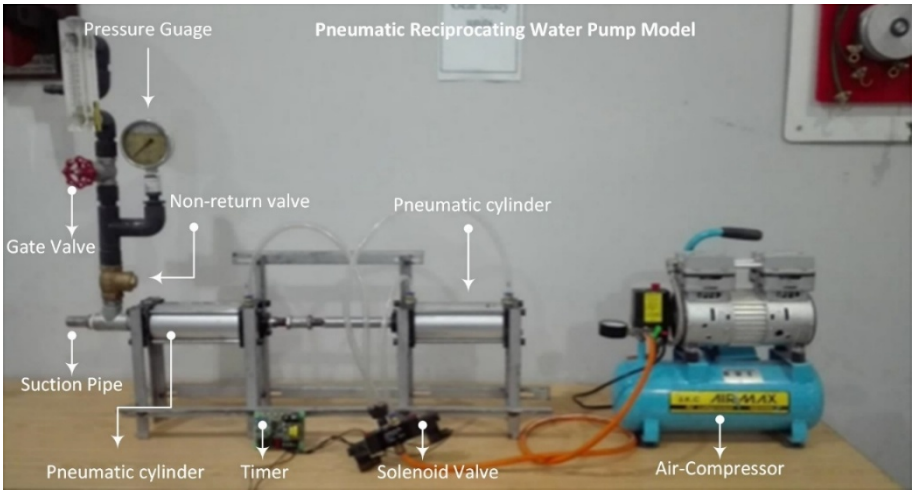

Figure 6. Fabricated model of pneumatic reciprocating water pump for investigation

4. RESULTS AND DISCUSSION

4.1. Effect of Head on Flow Rate

The flow rate of water is strongly influenced by the operating head, as presented in the following analysis. At constant pressure of 2 bar, an increase in head results in a corresponding decrease in flow rate due to the additional energy required to lift the water column. Experimental observations indicate that at a head of 10-24 ft with a difference of 3, the system delivers the outputs of 48, 44, 42, 39, 35, and 31 LPM, which closely aligns with the theoretical outcomes of 51.8, 47.6, 43.7, 42.1, 37.4, and 33.8 LPM. However, when the head is increased, the flow rate decreases significantly in both theoretical and experimental results. The graphical analysis demonstrates close agreement between experimental and theoretical trends, thereby validating the model, while the divergence observed at higher heads illustrates the importance of hydraulic and frictional losses in practical system design. The relationship between head and flow rate at constant pressure is shown in Fig. 7.

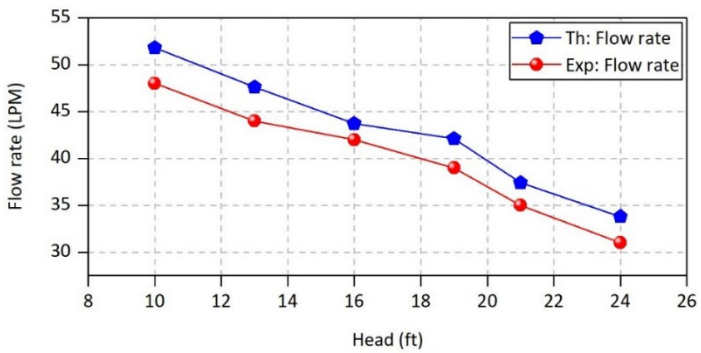

Figure 7. Performance graph of flow rate of water at outlet (head vs flow rate)

4.2. Effect of Pressure on Flow Rate

The discharge of water is affected by pressure. With the increment of pressure as 0.5 bar, flow rate of water rises at the outlet considering head as a constant 24 ft. The model is examined at 2.5-5.0 bar of pressure we achieved flow rate of 31, 35, 39, 42, 44, and 48LPM experimentally and also 33.8, 37.4, 42.1, 43.7, 47.6, and 51.8 LPM theoretically. Theoretical values of flow rate are higher, because we have not considered head loss, frictional loss and others mechanical losses. This indicates the necessity of incorporating loss factors for accurate performance prediction in real applications. Furthermore, such considerations will help in designing more reliable and efficient pump systems under varying operating conditions. The results of pressure and flow rate with constant head as seen in Fig. 8.

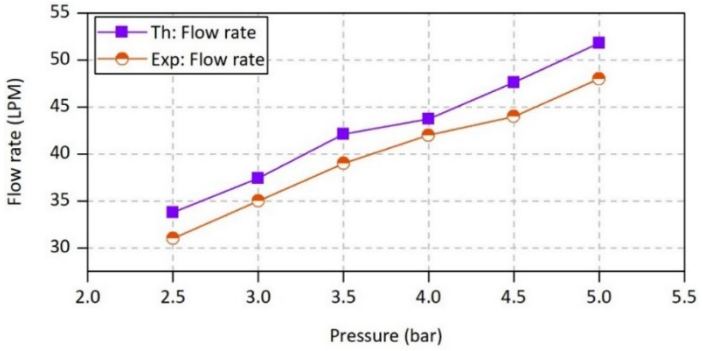

Figure 8. Performance graph of flow rate at outlet (pressure vs. flow rate)

5. CONCLUSIONS

It is concluded that, this system is very useful in the area where there is no electricity or load sheading issue. By using compressed air we can able to suck the water by this system. By increasing the pressure can able to raise the head of water. In this system the discharge of water increases with increase in pressure keeping the head constant. According to requirement we can increase the flow rate by decreasing head keeping the pressure constant. Only things take care in this system is about the leakages. Results will be changed according to the dimensions of the cylinders used in this project.

References

[1] P. M. Falcone, "Sustainable energy policies in developing countries: A review of challenges and opportunities," *Multidisciplinary Digital Publishing Institute*, vol. 16, no. 18, art. no. 6682, Sep. 2023.

[2] A. A. M. Faudzi, K. Bin Osman, M. F. Rahmat, N. D. Mustafa, M. A. Azman, and K. Suzumori, "Controller design for simulation control of intelligent pneumatic actuators (IPA) system," *Procedia Engineering*, vol. 41, pp. 593–599, Oct. 2012.

[3] E. Rakova and J. Weber, "Process simulation of energy behaviour of pneumatic drives," *Procedia Engineering*, vol. 106, pp. 149–157, Sep. 2015.

[4] A. Sahuquet, S. Meunier, J. A. Cherni, A. Charpentier, T. Vezin, A. Darga, G. Zuffinetti, P. K. Kitanidis, and L. Quéval, "Photovoltaic pumping tests: A novel supervision method for photovoltaic water pumping systems," *Heliyon*, vol. 10, no. 21, art. no. e39718, Nov. 2024.

[5] J. Zha, M. Ge, Z. Tang, J. Lei, H. Zhao, and Y. Zhang, "The incorporation of solar energy and compressed air into the energy supply system enhances the environmentally friendly and efficient operation of drip irrigation systems," *Agricultural Water Management*, vol. 302, art. no. 109019, Sep. 2024.

[6] M. K. G. Hussain, T. J. Babu, and D. A. Hussain, "Fabrication of pneumatic water pumping system," *International Research Journal of Engineering and Technology*, vol. 3, no. 7, pp. 2032–2041, Jul. 2016.

[7] Ž. Šitum, T. Žilić, and M. Essert, "High speed solenoid valves in pneumatic servo applications," in *2007 Mediterranean Conference on Control & Automation*, Athens, Greece, 2007.

[8] S. Lemofouet and A. Rufer, "A hybrid energy storage system based on compressed air and super capacitors with maximum efficiency point tracking (MEPT)," *IEEE Transactions on Industrial Electronics*, vol. 53, no. 4, pp. 1105–1115, Jun. 2006.

[9] W. Wang and Z. Gao, "A comparison study of advanced state observer design techniques," in *Proceedings of the 2003 American Control Conference*, Denver, CO, USA, 2003, pp. 4754–4759.

[10] H. R. Lee, J. H. Ahn, and H. Y. Kim, "Design of a solenoid actuator for a cylinder valve in a fuel cell vehicle," *Applied Sciences*, vol. 6, no. 10, art. no. 3390 Oct. 2016.

[11] N. M. Ahmed, A. M. Hassan, M. A. Kassem, A. M. Hegazi, and Y. F. Elsaadawi, "Reliability and performance evaluation of a solar PV-powered underground water pumping system," *Sci. Rep.*, vol. 13, art. no. 14174, Dec. 2023.
[12] M. Kumar, P. Arora, N. Srivastava, J. Padma, R. Singh, and A. C. Bhosale, "Optimal sizing of solar photovoltaic water pumping systems by synergizing irrigation patterns and static heads: A comprehensive study in the Indian context," *Sustainable Energy Technologies and Assessments*, vol. 77, art. no. 104341, May 2025.
[13] I. Saady, B. Majout, M. S. Adouairi, M. Karim, B. Bossoufi, M. M. Almalki, and T. A.H. Alghamdi, "Soft computing approaches for photovoltaic water pumping systems: A review," *Cleaner Engineering and Technology*, vol. 22, art. no. 100800, Oct. 2024.
[14] A. F. Kilicaslan and I. Dincer, "Design and performance assessment of an integrated energy system with compressed air and pumped hydro storage," *J. Energy Storage*, vol. 116, art. no. 116039, Apr. 2025.
[15] I. A. Nwakpang, B. T. Lebele-Alawa, and B. Nkoi, "Performance assessment of a two-stage reciprocating air compressor," *European Journal of Engineering Research and Science*, vol. 4, no. 4, pp. 74–82, Apr. 2019.
[16] E. Salomons, U. Shamir, and M. Housh, "Optimization methodology for estimating pump curves using SCADA data," *Water*, vol. 13, no. 5, Mar. 2021.

2nd International Conference on Multidisciplinary Sciences and Technological Developments (ICMUSTED 2025)

December 12-15, 2025

Optimizing the Effect of Cow Dung on Swelling Soil

Marwa Feligha[1], Souhila Rehab Bekkouche[1], Fadila Benayoun[2], Fatima Zohra Benamara[3]

[1]Department of Civil Engineering, University 20 August 1955, Skikda, Algeria
[2]Urban Technology Management Institute, University of Larbi Ben M'hidi, Oum El Bouaghi, Algeria
[3]Department of Civil Engineering and Hydraulics, University 8 May 1945, Guelma, Algeria
Corresponding author: Marwa Feligha (e-mail: m.feligha@univ-skikda.dz)

Abstract

In a context where the high cost of materials needed to improve and stabilize swelling soils represents a major challenge, it is essential to explore more accessible alternatives, particularly through the use of recycled waste, while favoring a more environmentally friendly approach. The main objective is to determine their potential as sustainable solutions for stabilizing swelling soils. This work is part of this approach and highlights the influence of recycled materials on the properties of swelling soils, thereby reducing costs while improving their geotechnical characteristics. An experimental study focuses on improving a reconstituted soil composed of 75% kaolinite and 25% bentonite using biopolymers, namely cow manure. Physical and mechanical characterization tests on the reconstituted soil before and after treatment were carried out in the laboratory to evaluate the effectiveness of the cow manure treatment at different percentages of 2%, 4%, 6%, and 8% relative to the dry mass of the soil. The results obtained confirm the effectiveness of the chosen additive in relation to the plasticity index, decreased significantly with increasing percentage of cow manure, dropping from 87% for the reconstituted soil to 45% for a mixture with 8% cow manure. In addition, the treated soil showed lower sensitivity to water during compaction, as evidenced by the increasingly flat pressure curves in the compaction test. The maximum unconfined compressive strength of the tested swelling soil increased with the addition of cow manure. We also observed a decrease in the swelling index from 19.93% to 9.38% with increasing percentages of cow manure. Hence, the addition of cow manure had a positive effect on the swelling potential. the use of cow manure offers an effective solution for stabilizing expansive soils.

Keywords: Swelling clay, Cow manure, Tests, Geotechnical parameters

2nd International Conference on Multidisciplinary Sciences and Technological Developments (ICMUSTED 2025)

December 12-15, 2025

Structural Properties of Ni-Doped ZnO Thin Films Investigated by XRD, AFM, and Profilometry

Maya Hanane Rezoug[1,2], Chewki Zegadi[1], Abdelkader Nouri[2], Nasr-Eddine Hamdadou[1], M'hamed Guezzoul[3]

[1]Laboratory of Micro and Nanophysics, National Polytechnic School of Oran,Oran, Algeria
[2]Laboratory for the Development of Renewable Energies and Their Applications in Saharan Areas, Faculty of Exact Sciences, TAHRI Mohammed University, Bechar, Algeria
[3]Laboratory of Materials, National Polytechnic School of Oran Maurice Audin (ENPO-MA), Oran, Algeria
Corresponding author: Maya Hanane Rezoug (e-mail: mayahanane22@gmail.com)

Abstract

ZnO thin films, both pure and Ni-doped, were deposited on glass substrates with and without SnO_2 interlayers using the sol–gel spin coating technique, and their structural and morphological properties were systematically investigated. X-ray diffraction (XRD) confirmed the hexagonal wurtzite polycrystalline structure for most samples, while the undoped ZG-20 film exhibited an amorphous character. The absence of secondary Ni-related phases indicates the successful substitution of Ni^{2+} into the ZnO lattice. Ni incorporation caused peak shifts toward higher 2θ values, evidencing lattice contraction, whereas the SnO_2 interlayer promoted partial lattice relaxation. Structural analysis revealed that Ni doping reduced crystallite size while increasing dislocation density and microstrain, consistent with strain-induced lattice distortion. Atomic force microscopy (AFM) showed significant modifications in surface morphology, where Ni doping produced finer and more homogeneously distributed grains, suppressing the cauliflower-like structures observed in pure ZnO. The SnO_2 interlayer facilitated grain coalescence, leading to smoother surfaces. Film thickness, determined by profilometry, varied between 294 nm (ZG-20) and over 680 nm (NZSG-20), confirming the influence of both Ni content and interfacial layers on film growth. These findings highlight the strong correlation between doping, interfacial engineering, and the structural properties of ZnO thin films, providing valuable insights for tailoring their performance in advanced electronic and optoelectronic applications.

Keywords: ZnO thin films, Ni doping, XRD, AFM, Profilometry

2nd International Conference on Multidisciplinary Sciences and Technological Developments (ICMUSTED 2025)

December 12-15, 2025

Immobilized Microalgae for Sustainable Soilless Agriculture in the Green Transition

Burcu Simsek Uygun[1], Gizem Demirel[1]

[1]Environmental Engineering, Eskisehir Technical University, Eskisehir, Türkiye
Corresponding author: Gizem Demirel (e-mail: gizemdemirel@ogr.eskisehir.edu.tr)

Abstract

Agricultural intensification has brought significant environmental pressures, particularly through the excessive use of chemical fertilizers that lead to nutrient pollution, soil degradation and contamination of water resources with nitrogen-, phosphorus-, and agrochemical-based compounds. High fertilizer inputs increase nitrate leaching, contribute to eutrophication in aquatic ecosystems and accelerate greenhouse gas emissions associated with synthetic fertilizer production. These impacts highlight the urgent need for sustainable nutrient management strategies in modern agriculture. In recent years, microalgae-based biostimulants have gained attention as environmentally friendly alternatives due to their ability to enhance plant growth, improve nutrient-use efficiency and contribute to circular bioeconomy practices. Microalgae such as *Chlorella vulgaris* naturally produce bioactive compounds (e.g., phytohormones, amino acids, polysaccharides) that support root development, stress tolerance and overall plant vitality while avoiding the pollution problems associated with synthetic fertilizers. In this study, the growth response of strawberry (*Fragaria* × *ananassa* Duch.) to immobilized *Chlorella vulgaris* applications was investigated under controlled solid-based soilless cultivation conditions. Sodium–alginate encapsulated immobilized microalgaes were prepared at five concentrations (control, 10%, 20%, 30%, and 40%) to evaluate dose-dependent effects on plant growth. A second experimental set was designed in which the same algal doses previously used for the treatment (removal) of the azo dye maxilon red were applied, enabling comparison between clean and dye-treated algal preparations. Plant height, leaf number, leaf area and visual vigor were monitored throughout the cultivation period. The results indicated that immobilized *C. vulgaris* improved strawberry growth, particularly at the 10% dose, which provided the most consistent and balanced enhancement in leaf formation and overall plant vitality compared to the control group. Conversely, dye-exposed algal treatments exhibited markedly reduced performance, including earlier tissue weakening, lower leaf numbers and suppressed growth. These findings suggest impaired microalgal metabolic activity and reduced biostimulant potential when algae are exposed to environmental contaminants. Overall, the study highlights both the potential of immobilized *C. vulgaris* as a sustainable plant-supporting agent in soilless agriculture and the sensitivity of microalgae-based systems to pollutant stress.

Keywords: *Chlorella vulgaris*, Immobilized microalgae, Soilless strawberry agriculture, Biofertilizer, Sustainable agriculture

1. INTRODUCTION

Water is essential for domestic, agricultural, and industrial activities, yet its quality is increasingly threatened by excessive fertilizer use, industrial effluents, and uncontrolled domestic wastewater discharge. Excess nitrogen (N), phosphorus (P), and synthetic dyes released into aquatic environments cause eutrophication, ecosystem degradation, long-term oxygen depletion, and potential human health risks through contaminated drinking water. Fertilizer-derived nutrients from intensive agricultural practices intensify nutrient pollution, increase nitrate leaching into groundwater, and accelerate algal bloom formation in surface waters, leading to a general decline in water quality. Conventional treatment technologies for nutrient and dye removal are often energy-intensive, costly, and may generate secondary pollution, emphasizing the need for more sustainable alternatives [1].

Microalgae have gained attention as versatile biological tools in both wastewater treatment and sustainable agriculture. Species such as *Chlorella vulgaris* can remove nutrients (N, P), sequester carbon dioxide (CO_2) and produce biomass rich in proteins, pigments and bioactive compounds [2]. Numerous studies demonstrate that *Chlorella vulgaris* efficiently removes ammonium and phosphate from wastewater while producing biomass suitable for fertilizer or bioproduct applications [3, 4]. Microalgal extracts and suspensions have also been used as biostimulants, enhancing root growth, chlorophyll content and stress tolerance in various crops [5, 6].

Beyond free-cell cultures, immobilizing microalgae in polymeric matrices (e.g., calcium alginate) has been proposed to improve operational stability, facilitate biomass recovery and enable repeated reuse [7]. Immobilized *Chlorella vulgaris* maintains metabolic activity over extended periods and can enhance nutrient removal efficiencies compared to suspended cultures [7, 8]. The immobilization matrix provides a protective microenvironment and allows higher cell retention in treatment systems.

Soilless cultivation systems, particularly cocopeat-based substrates, are increasingly important for sustainable food production due to their efficient water and nutrient control and reduced pesticide requirements [9]. Integrating microalgae-based biostimulants into soilless cultivation offers a promising approach for reducing chemical fertilizer inputs while supporting closed-loop nutrient cycling.

In this study, immobilized *Chlorella vulgaris* was evaluated as a biofertilizer component in a cocopeat-based soilless system for strawberry cultivation. Two types of immobilized algaes were tested: (i) microalgae-only immobilized and (ii) immobilized microalgae previously used for the treatment of the azo dye maxilon red, representing a pollutant-affected biomass. Four algal doses (10%, 20%, 30%, and 40%) and a control group (0%) were applied. Plant growth parameters were monitored to assess dose–response behavior and compare dye-contaminated versus uncontaminated microalgae.

A conceptual dose–response model (Equation (1)) was used as an interpretive framework:

$$R = R_{ctrl} + \frac{R_{max} \cdot D}{K_D + D} \quad (1)$$

The general dose–response behaviour of plant growth in relation to immobilized microalgae application can be conceptually described by a saturation-type model, expressed in Equation (1). In this model, R represents the plant growth response (e.g., leaf number or shoot length), R_{ctrl} denotes the response of the control group (0% algae), D is the applied immobilized algae dose (% v/v), R_{max} is the maximum additional growth achievable due to the biostimulant effect, and K_D is the half-saturation constant indicating the dose at which half of R_{max} is obtained [5].

Although full kinetic modelling was not performed in the present study, the experimentally observed growth patterns aligned closely with this conceptual framework. Low-dose applications—particularly 10%—generated the strongest increases in leaf formation and overall vigor, whereas higher doses (30–40%) showed diminishing returns and approached a biological saturation point. In dye-exposed treatments, deviations from this pattern were more pronounced, likely due to reduced microalgal metabolic activity and impaired biostimulant performance, consistent with previous reports on dye-induced stress in microalgae [6, 7].

Preliminary observations further indicated that strawberries treated with non-dyed immobilized microalgae—especially at the 10% dose—maintained better visual quality and exhibited delayed onset of leaf weakening, whereas dye-exposed immobilized microalgaes were associated with faster tissue deterioration, reduced leaf expansion and overall weaker growth. These findings suggest that immobilized microalgae may act either as a growth-enhancing nutrient source or a stress factor depending on prior exposure to pollutants. The primary aim of this study was to identify the most effective immobilized-algae dose and compare the agronomic performance of dye-contaminated and uncontaminated microalgaes.

2. MATERIAL AND METHOD

In this study, two types of immobilized microalgae were used:

- Immobilized algaes containing only *Chlorella vulgaris* and
- Immobilized microalgae previously used for the treatment of the azo dye maxilon red, representing a pollutant-affected biomass.

This dual setup enabled comparison between clean and dye-affected algal formulations across four application doses (10%, 20%, 30%, and 40%), together with an untreated control (0%) [1, 2].

All experiments were carried out under controlled laboratory conditions. Each strawberry seedling was planted in transparent cultivation chambers filled with a standardized substrate prepared as an 80% cocopeat–20% perlite volumetric mixture. This mixture provided sufficient aeration and moisture retention, while the transparency of

the containers enabled qualitative visual observation of root appearance, similar to previously reported transparent rhizosphere systems [3].

A schematic representation of the experimental layout is shown in Figure 1.

Figure 1. Schematic layout of the cocopeat-based strawberry cultivation system

Immobilization was carried out by mixing concentrated algal suspension with 2% sodium alginate and adding the mixture dropwise into a $CaCl_2$ hardening bath to form hydrogel beads, following standard microalgal encapsulation [4, 5]. An example of the prepared immobilized microalgaes is provided in Figure 2.

In the dye-containing wastewater treatment procedure reported by Kesikbas [10], immobilized *Chlorella vulgaris* with an initial fluorescence intensity of approximately 190,000–200,000 RFU was employed to treat wastewater containing maxilon red at an initial concentration of about 8–10 mg/L. Under continuous aeration and violet light, these immobilized cultures achieved nearly 80% color removal ($C/C_0 \approx 0.2$) after roughly 170 hours of operation with a batch reactor. In the present study, immobilized microalgaes that had undergone such dye treatment were subsequently used as “dye-loaded” immobilized biomass in the strawberry pots, representing microalgae that had already interacted with an azo dye under realistic treatment conditions.

Figure 2. Alginate-based immobilized *Chlorella vulgaris*

Immobilized microalgaes were applied directly into the root zone, and application doses were defined based on bead mass relative to substrate volume. Weekly reapplication ensured continuous microalgal presence. Throughout the experimental period, environmental conditions (temperature, humidity and light) were kept stable and no external fertilizers were supplied, allowing isolated evaluation of microalgal effects.

During the cultivation period, the dye-loaded immobilized microalgaes exhibited noticeably faster fading, softening and partial structural collapse than the non-dyed immobilized microalgaes. This behavior was consistent with dye-induced destabilization of alginate hydrogels reported in earlier studies [6, 8], and was recorded weekly through photographic documentation.

Plant development was monitored weekly by measuring:

- Number of leaves,
- Individual average leaf dimensions (length × width), and
- Overall plant vigor (colour uniformity and structural posture).

Qualitative observations of root appearance (color, branching tendency and lateral spread) were also recorded, based on the visibility provided by the transparent containers, following established non-destructive phenotyping practices [9].

At the end of the cultivation period, treatment effects were evaluated descriptively rather than through inferential statistical tests. Growth responses were compared across all dose groups based on measured parameters and visual quality assessments, following semi-quantitative evaluation approaches commonly applied in small-scale plant physiology studies [11]. Among all treatments, the 10% non-dyed algae dose consistently produced the most favourable outcomes in leaf number, leaf area and plant vitality, confirming dose–response patterns previously reported for microalgal biostimulants [1, 12]. In contrast, dye-containing immobilized microalgaes resulted in weaker growth, reduced leaf formation and earlier tissue decline, indicating decreased biostimulant performance due to dye-induced stress effects [6, 7].

3. RESULTS

The effects of immobilized *Chlorella vulgaris* on strawberry (*Fragaria × ananassa* Duch.) growth were evaluated by comparing plant height, leaf number, leaf dimensions and overall vitality across five dose groups (control, 10%, 20%, 30%, and 40%). The second experimental series, in which immobilized algae were exposed to the azo dye maxilon red, enabled a direct comparison between "clean algae" and "dye-affected algae" under identical cultivation conditions.

During the cultivation period, strawberries treated with non-dyed immobilized microalgae exhibited visibly healthier morphology. Plants in the 10% and 20% groups produced a higher number of leaves and larger leaf surfaces, showing stronger turgidity and more uniform canopy structure than the control group. Among all doses, the 10% non-dyed algae application provided the most consistent improvement, while higher doses (30% and 40%) did not provide proportional increases and instead approached a biological saturation point. This trend aligns with the dose–response behavior described conceptually in Eq. (1), indicating that low-to-moderate microalgae doses yield optimal biostimulant effects, whereas higher doses may create minor physiological competition or localized oxygen fluctuations.

Figure 3 presents the temporal change in leaf number for non-dyed algal applications, while Figure 4 shows the corresponding trend for plants treated with maxilon red-containing immobilized microalgaes, with both figures presenting time on the x-axis and leaf number on the y-axis.

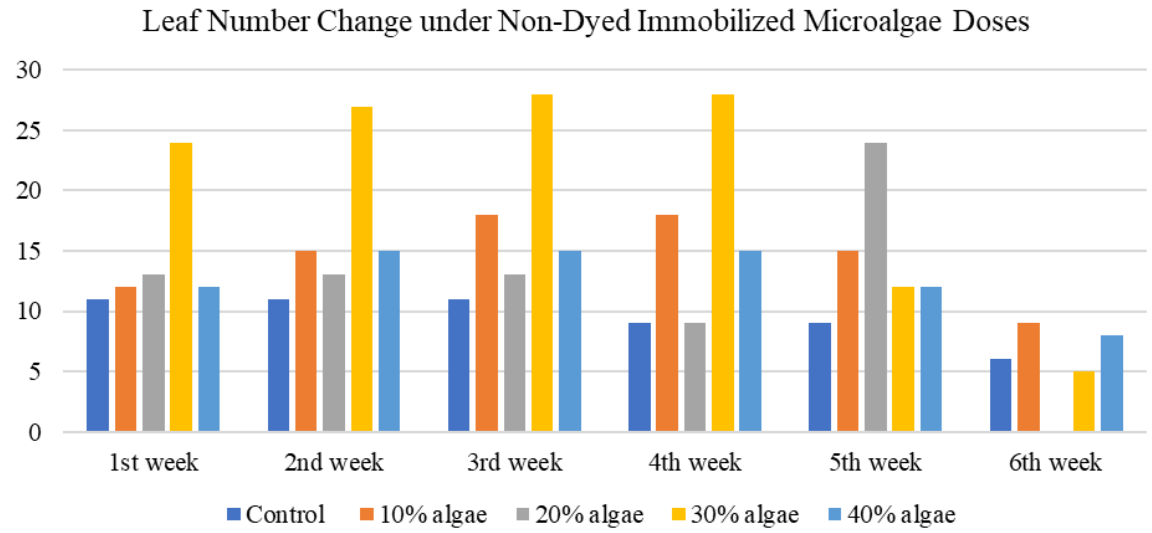

Figure 3. Leaf number development of strawberry plants grown in cocopeat under non-dyed immobilized *Chlorella vulgaris* treatments at different doses (control, 10%, 20%, 30%, and 40%)

In the dye-contaminated series, the growth pattern differed markedly. Leaf formation was initially similar in weeks 1–2, but after week 3 plants in all dye-exposed treatments showed rapid decline and weakening. By the end of week 4, all plants in these treatments had completely wilted, preventing further measurements.

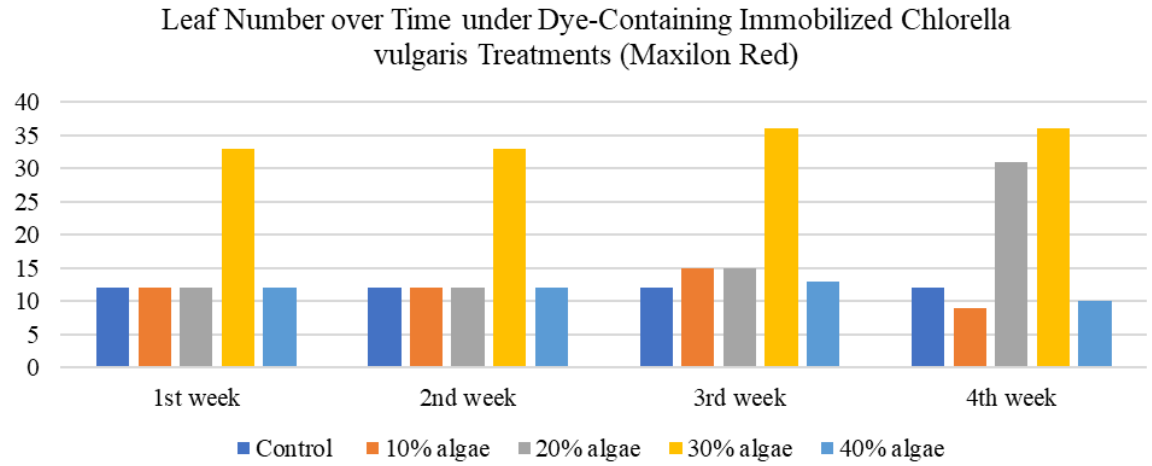

Figure 4. Leaf number development of strawberry plants treated with maxilon red–contaminated immobilized *Chlorella vulgaris* at different doses (control, 10%, 20%, 30%, and 40%)

Leaf area measurements further supported the leaf number trends. Plants treated with 10% and 20% non-dyed algae developed noticeably wider leaf blades, whereas dye-exposed treatments consistently showed reduced leaf area, particularly after the fourth week. This reduction suggests diminished photosynthetic surface formation under dye-affected conditions.

Throughout the experiment, dye-containing immobilized microalgaes underwent faster softening, discoloration and partial structural degradation. These physical changes indicate increased oxidative stress on the immobilized algae, likely weakening metabolic activity and reducing the production of plant-beneficial compounds such as phytohormones, amino acids and polysaccharides. As a result, strawberry plants grown with dye-exposed immobilized microalgaes produced fewer leaves, smaller leaf areas, shorter shoots and displayed earlier loss of vitality compared to the non-dyed treatments.

Figure 5 illustrates the temporal progression of mean leaf area for non-dyed algae treatments, whereas Figure 6 shows the corresponding decline in leaf area for dye-treated plants, with both figures presenting time on the x-axis and leaf area on the y-axis.

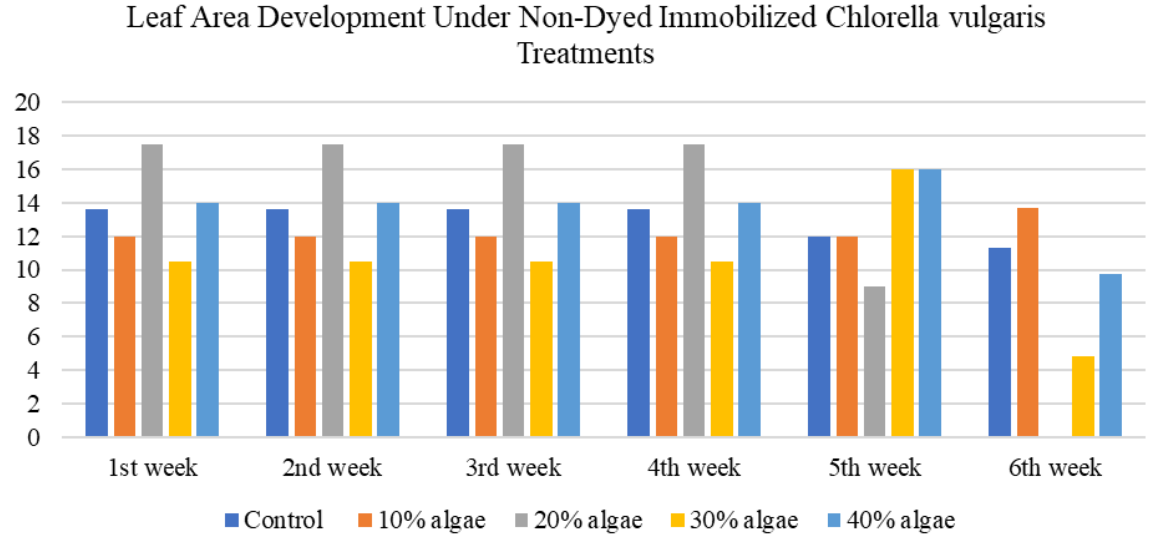

Figure 5. Temporal change in mean leaf area of strawberry plants grown in cocopeat under non-dyed immobilized *Chlorella vulgaris* doses (control, 10%, 20%, 30%, and 40%)

In the dye-contaminated group, leaf area values remained consistently low across all applied doses, indicating a marked inhibition of vegetative growth. By week 4, all plants exhibited severe wilting, extensive tissue deterioration, and loss of structural integrity, ultimately leading to complete plant collapse. As a result of this rapid decline, no reliable growth data could be collected for weeks 5–6, precluding further analysis of longer-term effects. These observations highlight the profound negative impact of pollutant exposure on microalgae-mediated growth promotion and underscore the sensitivity of strawberry plants to residual contaminants in the immobilized biomass.

In addition to leaf number, leaf area measurements showed clear dose-dependent differences. The 10% and 20% non-dyed algae treatments produced the largest leaf areas throughout the cultivation period, indicating improved photosynthetic surface development. In contrast, the 30% and 40% doses did not provide additional benefit and showed signs of reaching a biological saturation threshold. For the dye-containing immobilized microalgaes, leaf area values were consistently lower across all doses, and in later weeks the leaves exhibited faster shrinkage and discoloration. This reduction aligns with the observed impairment of microalgal metabolism in the dye-exposed immobilized microalgaes, which likely reduced the production of biostimulant compounds.

Overall, the combined evaluation of leaf number, leaf area and general plant vigor indicates that the 10% non-dyed immobilized microalgae treatment produced the most favorable growth response. Preliminary tendencies suggest that differences between the 10% non-dyed treatment and the control group would likely be meaningful, while all dye-containing treatments consistently performed worse than their non-dyed counterparts at the same dose. These findings reinforce that microalgal health and prior exposure history are critical determinants of biostimulant efficiency.

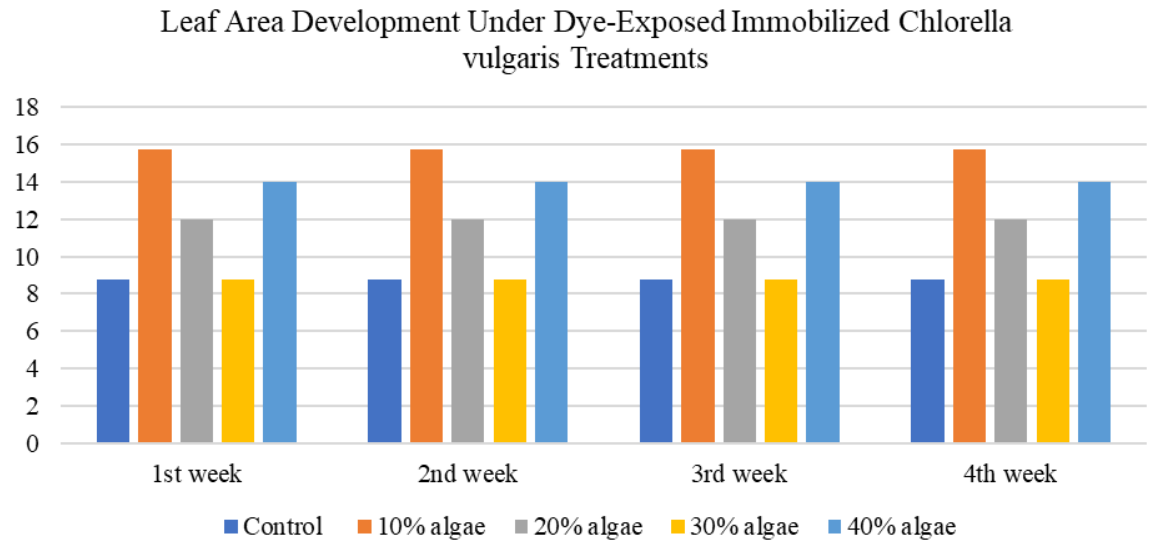

Figure 6. Temporal change in mean leaf area of strawberry plants treated with maxilon red–contaminated immobilized *Chlorella vulgaris* at different doses (control, 10%, 20%, 30%, and 40%)

4. CONCLUSION

This study provides compelling evidence that immobilized *Chlorella vulgaris* holds significant potential as a sustainable, low-cost biological input for solid-based soilless strawberry cultivation. Experimental results indicate that, when applied at optimal low doses, microalgae can substantially enhance plant growth by supplying bioactive compounds, improving nutrient availability, and promoting overall physiological vigor. Notably, the 10% immobilized-algae dose emerged as the most effective, corroborating the principle that "more is not always better" in nutrient or biostimulant application and aligning with previous reports on nitrogen sensitivity and dose-dependent responses in strawberry.

Comparative analysis with dye-exposed microalgal beads underscores a critical consideration for microalgae-based agricultural applications: the environmental history and quality of biomass directly affect its efficacy. The diminished performance observed in pollutant-exposed treatments demonstrates that environmental contaminants can impair microalgal metabolic activity and reduce their plant-growth–promoting capacity. This finding highlights the importance of maintaining uncontaminated biomass sources and suggests that prior pollutant exposure should be carefully managed to preserve biostimulant functionality.

Overall, the study highlights two major implications for sustainable soilless cultivation:

- Low-dose immobilized *Chlorella vulgaris* can serve as a highly effective and eco-friendly biostimulant for strawberry production.
- The integrity and prior exposure history of microalgal biomass are crucial factors in ensuring consistent and reliable agronomic performance.

These insights establish a solid foundation for future research, including optimization of immobilization strategies, long-term yield and quality assessments, understanding pollutant–microalgae interactions, and scaling up microalgal biostimulants for broader agricultural applications. Collectively, the findings advance the prospect of integrating microalgae into sustainable crop production systems while minimizing reliance on chemical fertilizers and mitigating environmental impact.

Acknowledgments

The authors would like to thank Eskisehir Technical University, Department of Environmental Engineering, for providing laboratory facilities and technical support during the experimental work.

References

[1] M. Abdelfattah, A. A. Taher, and A. M. Hassan, "Environmental impacts of nutrient pollution and eutrophication: Sources, effects and control strategies," *Environmental Monitoring and Assessment*, vol. 195, no. 6, pp. 1–15, 2023.

[2] A. Rawat, T. R. Kumar, S. Mutanda, and F. Bux, "Biodiesel from microalgae: A critical evaluation from laboratory to large scale production," *Applied Energy*, vol. 103, pp. 444–467, 2013.

[3] K. Gutwiński and G. Cema, "The growth rate of *Chlorella vulgaris* in municipal wastewater," *Desalination and Water Treatment*, vol. 57, no. 3, pp. 1204–1210, 2016.

[4] S. Acikel and I. K. Korkmaz, "Determination of kinetic coefficients for ammonia and phosphate removal by *Chlorella vulgaris*," *Journal of Environmental Science and Health, Part A*, vol. 55, no. 9, pp. 1150–1158, 2020.

[5] J. Monod, "The growth of bacterial cultures," *Annual Review of Microbiology*, vol. 3, no. 1, pp. 371–394, 1949.

[6] R. M. Droop, "Vitamin B12 and marine ecology. IV. The kinetics of uptake, growth and inhibition in *Monochrysis lutheri*," *Journal of the Marine Biological Association of the United Kingdom*, vol. 48, no. 3, pp. 689–733, 1968.

[7] H. W. Smith and P. F. Handley, "Mathematical modeling of microalgae growth kinetics for nutrient removal optimization," *Water Research*, vol. 210, art. no. 118015, 2022.

[8] A. N. Michels and J. W. Davis, "Comparative evaluation of monod and droop models for microalgae cultivation," *Biochemical Engineering Journal*, vol. 185, art. no. 108626, 2022.

[9] J. A. Bagnall, R. J. King, and S. R. Ashby, "Digital phenotyping in controlled plant growth environments," *Plant Methods*, vol. 17, pp. 1–12, 2021.

[10] M. Kesikbas, "Immobilize *Chlorella vulgaris* alg kulturu ile atik sulardaki boyar madde gideriminin incelenmesi ve alglerin optimum kosullarinin belirlenmesi," M.S. thesis, Dept. Environmental Engineering, Eskisehir Technical University, Türkiye, 2025.

[11] G. W. Snedecor and W. G. Cochran, *Statistical Methods*, 8th ed. Ames, Iowa: Iowa State University Press, 1989.

[12] M. Ronga, C. Biazzi, A. Parati, A. Carminati, and M. T. M. Barbanti, "Microalgae-based biostimulants and their effects on plant physiology," *Agronomy*, vol. 13, no. 2, pp. 1–15, 2023.

2nd International Conference on Multidisciplinary Sciences and Technological Developments (ICMUSTED 2025)

December 12-15, 2025

Implementation of Open Science Framework for Materials Engineering

Elisabeth Viviana Lucero Baldevenites[1], Jose Rogelio Fung Corro[2], Yorlenis Martínez[3]

[1]Department of Mechanical Engineering, University of Las Palmas de Gran Canaria, Las Palmas, Spain
[2]Faculty of Computer Science, International Polytechnic University, Panama, Panama
[3]Faculty of Computer Science, University of the Isthmus, Panama, Panama
Corresponding author: Elisabeth Viviana Lucero Baldevenites (e-mail: viviana.lucero@ulpgc.es)

Abstract

This study seeks to promote collaboration, transparency, and reproducibility in scientific research by analyzing the use of the Open Science Framework (OSF) as a support tool for students and engineers within higher education. Recognizing the increasing relevance of open platforms in contemporary scientific practice, the research explores how OSF contributes to organizing, preserving, and disseminating research data during the academic research cycle. A retrospective cross-sectional observational analytical study was conducted among students and engineers engaged in research activities at the Polytechnic University of Panama between October 2024 and October 2025, based on predefined inclusion criteria associated with their participation in scientific projects. Data were collected through structured surveys evaluating the frequency and purpose of OSF use, as well as the perceived advantages of this platform compared to other research-support tools. Descriptive statistical analyses were performed, including measures of central tendency, standard deviation, and frequency distributions. Results show that approximately 80% of participants rely primarily on OSF to manage and document their research processes, while the remaining 20% depend on alternative databases or digital tools. The findings suggest that the systematic use of OSF contributes to improved data management practices, enhanced project transparency, and more consistent documentation of research procedures. Furthermore, participants reported that OSF facilitates collaboration and long-term preservation of materials, supporting reproducibility and open-access principles. Overall, the study highlights OSF as a valuable and accessible platform capable of strengthening research competencies and preparing future engineers to excel in an academic and professional environment increasingly defined by open science, digital integration, and collaborative knowledge production.

Keywords: Open Science Framework (OSF), Materials engineering, Open platform, Research data management, Reproducibility, Transparency

2nd International Conference on Multidisciplinary Sciences and Technological Developments (ICMUSTED 2025)

December 12-15, 2025

Separation of Toluene – Cyclohexane Mixture Using Intensified Extraction Process by Imidazolium-Based Ionic Liquids

Mohammed Djamel Eddine Allali[1], Hassiba Benyounes[1], Nesrine Amiri[2]

[1]Process Engineering, University of Sciences and Technology of Oran Mohamed Boudiaf, Oran, Algeria
[2]Process Engineering, University of M'Hamed Bougara Boumerdes, Boumerdes, Algeria
Corresponding author: Mohammed Djamel Eddine Allali (e-mail: allali.meddjamel@gmail.com)

Abstract

The separation of cyclohexane from toluene is challenging due to their close boiling points and azeotrope formation. Liquid-liquid extraction is widely used for low-concentration toluene because of its high selectivity and low energy consumption. Recently, imidazolium-based ionic liquids (ILs) have emerged as environmentally friendly alternatives to conventional solvents such as sulfolane, offering high selectivity, low volatility, and reduced toxicity. This work aims to design an extraction process for the azeotropic mixture toluene–cyclohexane using imidazolium-based ILs as an alternative to sulfolane. The liquid–liquid equilibrium (LLE) of the ternary systems toluene + cyclohexane + solvents was modeled using the non-random two-liquid (NRTL) thermodynamic model. Binary interaction parameters were regressed at 303.15 K and 1 atm, showing good agreement with experimental data. The results indicate that ILs provide higher selectivity and distribution coefficients, enhancing extraction efficiency. Aspen Plus simulations in a 12-stage extraction column were performed with different solvent-to-feed ratios. Cyclohexane, the major challenge, achieved 99.75 % purity and 86.5 % recovery with butylmethylimidazolium (BMIM)-$MeSO_4$, compared to 99.52 % purity and 70.8 % recovery with sulfolane. These results demonstrate that BMIM-$MeSO_4$ offers a better balance between cyclohexane purity and recovery, highlighting the potential of ionic liquids for efficient and selective separation of toluene–cyclohexane mixtures.

Keywords: Liquid-liquid extraction, Ionic liquid, Thermodynamic model, Azeotropic mixture

Study of the Effectiveness of Steel Shavings as a Foaming Agent for the Production of Foams Glass

Fayrouz Benhaoua[1], Djalila Aoufi[2], Nacira Stiti[1], Mehdia Toubane[1], Djedjiga Bousalah[1,3]

[1]Research Unit Materials, Processes and Environment, Faculty of Engineering, University M'Hamed Bougara of Boumerdes, 35000 Boumerdes, Algeria
[2]Corrosion, Protection and Durability of Materials Division, Research Center in Industrial Technologies-Echahid Mohammed Abassi, Cheraga, Algeria
[3]Center in Physical and Chemical Analysis, 42004 Bou-Ismail, Algeria
Corresponding author: Fayrouz Benhaoua (e-mail: f.benhaoua@univ-boumerdes.dz)

Abstract

The manufacturing of glass foams is considered, on the one hand, one of the most effective methods for the valorization of all types of glass waste (soda-lime, borosilicate, or cathode ray tube, etc.). On the other hand, it is considered among the methods for the containment of other types of waste besides glass, such as solid waste, tires, mineral wool, fly ash, etc. The mixing of different wastes with an effective foaming agent allows the formation of a more or less porous structure. In the present work, we have developed glass foams based on soda-lime glass waste and steel shavings as a foaming agent. We added 5 to 20% of steel shavings to the cullet powder. The variants are pressed at a force of 100 kN in the form of 4 cm diameter pellets, and each variant undergoes the same thermal regime (sintering at 800 °C). The obtained glass foams are characterized by a remarkable porosity (75%) and lightness (density of 0.88), confirmed by physical tests of porosity and bulk density, as well as by scanning electron microscopy (SEM). These results are very encouraging regarding the use of steel shavings as a foaming agent.

Keywords: Glass waste, Steel shavings, Foam glass, Valorization, Recycling

2nd International Conference on Multidisciplinary Sciences and Technological Developments (ICMUSTED 2025)

December 12-15, 2025

Electromagnetic Frequency and Time Reaction in Electromechanical Systems Under Low Energy Mechanical Faults

Azeddine Ratni[1], Ali Damou[1], Djamel Benazzouz[1], Mohamed Tsebia[2]

[1]Solid Mechanics and Systems Laboratory, University of Boumerdes, Boumerdes, Algeria
[2]Signals and Systems Laboratory, University of Boumerdes, Boumerdes, Algeria
Corresponding author: Azeddine Ratni (e-mail: a.ratni@univ-boumerdes.dz)

Abstract

This study investigates the frequency and time domain response of the electromagnetic torque to bearing faults in a motor speed reducer system. The aim is to characterize how inner race defects affect torque behaviour, enabling the detection and identification of fault signatures. The dynamic model of the system was used to analyse torque signals in both time and frequency domains. In the time domain, the electromagnetic torque signal energy increased from 0.455 N·m in the healthy state to 0.576 N·m with the inner race defect. In the frequency domain, no significant peaks were observed in the healthy system, whereas the introduction of the defect generated a series of characteristic peaks in the torque spectrum. The dominant peak corresponds to the inner race fault frequency of 156 Hz, clearly identifying the defect. These results demonstrate that the electromagnetic torque is highly sensitive to mechanical degradation, providing a more distinctive indicator than conventional measures such as electric current, and offering a practical framework for early detection and assessment of bearing faults in electromechanical systems.

Keywords: Mechanical faults diagnosis, Low-energy mechanical faults, Signal processing, Torque oscillations, Bearing faults

2nd International Conference on Multidisciplinary Sciences and Technological Developments (ICMUSTED 2025)

December 12-15, 2025

Microstructural and Electrochemical Assessment of Co–Cr Dental Alloys in Ringer Solution

Alberto Daniel Rico-Cano[1], Adriana Saceleanu[2], Anca Fratila[2], Julia Claudia Mirza-Rosca[1,3]

[1]Department of Mechanical Engineering, University of Las Palmas de Gran Canaria, Las Palmas de Gran Canaria, Spain
[2]Medicine Faculty, "Lucian Blaga" University of Sibiu, Sibiu, Romania
[3]Materials Engineering and Welding Department, Transilvania University of Brasov, Brasov, Romania
Corresponding author: Julia Claudia Mirza-Rosca (e-mail: julia.mirza@ulpgc.es)

Abstract

Metallic biomaterials must exhibit reliable chemical stability and mechanical integrity to be considered safe for clinical use, particularly in dental and orthopedic applications. Among these materials, cobalt–chromium (Co–Cr) alloys remain a preferred choice due to their resistance to wear, their mechanical strength, and the generally favorable biological response they induce. In this study, two commercial Co–Cr dental alloys—Vitallium 2000 Plus and Vera PDI—were examined to compare their microstructural features and corrosion behavior in Ringer solution. Optical and electron microscopy revealed characteristic dendritic structures in both materials. Vitallium 2000 Plus showed a greater presence of carbides and σ-phase particles embedded within the α-matrix, whereas Vera PDI contained only scattered carbide precipitates. Open-circuit potential measurements demonstrated that both alloys passivate rapidly after immersion, stabilizing toward more noble potentials as exposure time increases. Electrochemical impedance spectroscopy confirmed this trend: the spectra displayed capacitive behavior with two distinguishable time constants, associated with passive-film formation and charge-transfer processes. Fitting the data to an equivalent electrical circuit showed a gradual rise in the resistance of both the compact oxide layer and the passive film, indicating increasing protection as immersion progressed. After one week, the polarization resistance approached values on the order of 10^6 Ω·cm^2, which is typical of materials known for excellent corrosion resistance, such as titanium alloys. Vitallium 2000 Plus displayed slightly higher resistance to corrosion, a result consistent with its higher chromium content and the formation of a more stable Cr_2O_3-rich passive layer. Nonetheless, both alloys produced protective oxides composed mainly of Cr_2O_3 and CoO, which became thicker and more homogeneous over time. The results obtained confirm that the two dental Co–Cr alloys develop robust and long-lasting passive layers in Ringer solution, making them suitable for extended biomedical service.

Keywords: Co–Cr alloys, Dental biomaterials, Corrosion resistance, EIS, Passive films

Electrospinning of Polyacrylonitrile-Nanocellulose Composites Reinforced with Carbon Materials for Advanced Fiber Performance

Mohd Ali Mat Nong[1], Juraina Md Yusof[1], Suzila Sabil[2], Mohd Hafizuddin Ab Ghani[1], Che Azurahanim Che Abdullah[4]

[1]Functional Nanotechnology Devices Laboratory (FNDL), Institute of Nanoscience and Nanotechnology Universiti Putra Malaysia, Serdang, Selangor, Malaysia
[2]Kolej Komuniti Jelebu, Jalan Seperi, Kampung Chempedak, 71600 Kuala Klawang, Negeri Sembilan, Malaysia
[3]Nanomaterials Processing and Technology Laboratory (NPTL), Institute of Nanoscience and Nanotechnology Universiti Putra Malaysia, Serdang, Selangor, Malaysia
[4]Department of Physics, Faculty of Science, Universiti Putra Malaysia, Serdang, Selangor, Malaysia
Corresponding author: Mohd Ali Mat Nong (e-mail: mohd_alee@upm.edu.my)

Abstract

Nanocellulose is an abundant and sustainable material with significant potential for a wide range of future applications. Its unique structural, mechanical, and chemical properties make it suitable for use in electronics, medical devices, and water filtration systems. The incorporation of nanocellulose with carbon-based fillers enables the development of smart composite materials that exhibit enhanced electrical conductivity and mechanical flexibility. This study focuses on the fabrication of electrospun nanofibers using a polyacrylonitrile (PAN)–nanocellulose composite reinforced with carbon-based fillers. Cellulose nanofibers (CNF) were first dispersed in 10 mL of dimethylformamide (DMF), followed by mixing with carbon fillers and subsequent sonication for 4 hours to ensure uniform dispersion. The prepared solution was then loaded into a syringe pump and electrospun at an applied voltage of 10 kV, with a flow rate of 0.8 mL/h. The distance from the syringe needle to the collector was 20 cm. The resulting nanofiber mats were carefully removed from aluminum foil placed on the collector and characterized using a universal testing machine to evaluate their mechanical performance. The findings indicate that nanofibers fabricated from the PAN-nanocellulose–carbon black composite improved flexibility meanwhile nanofibers produced from PAN-nanocellulose-graphite improved stiffness. These improvements highlight the potential of PAN-nanocellulose–carbon fillers in advancing high-performance nanofiber materials.

Keywords: Nanocellulose, Electrospinning, Carbon-based fillers, PAN nanofibers, Mechanical properties

2nd International Conference on Multidisciplinary Sciences and Technological Developments (ICMUSTED 2025)

December 12-15, 2025

Hybrid Voltage Regulation Strategy Combining AVR and Microgrid Coordination for Enhanced Power System Stability

Fazia Ahcene[1,2], Hamid Bentarzi[1,3], Mohammed Tsebia[1,4], Djamila Talah[1,2]

[1]Signals and Systems Laboratory, University of Boumerdes, Boumerdes, Algeria
[2]Faculty of Technology, University Mouloud Mammeri of Tizi-Ouzou, Tizi-Ouzou, Algeria
[3]Institute of Electrical and Electronics Engineering, University of Boumerdes, Boumerdes, Algeria
[4]Faculty of Technology, University of Boumerdes, Boumerdes, Algeria
Corresponding author: Fazia Ahcene (e-mail: fazia.ahcene@ummto.dz)

Abstract

In modern power systems, the synchronous machine is essential for maintaining voltage stability through automatic voltage regulation (AVR). However, when the electrical demand exceeds the generator's production capacity, the AVR system may reach its saturation limit, making proper voltage regulation unable to be maintained. This loss of control can lead to instability or even the shutdown of the generating unit as a protective safety measure. On the other hand, the increasing integration of microgrids based on renewable energy sources is essential for supporting modern distributed energy systems. These microgrids provide local generation and flexibility, which helps stabilize the main grid during critical operating conditions. This study proposes a hybrid control approach that combines the conventional AVR function with a coordination algorithm that manages microgrid integration during voltage saturation periods. The AVR design includes a self-excitation mechanism that decreases reliance on batteries and improves overall energy efficiency. The main objective of this research is to maintain voltage stability and ensure the continuous operation of the synchronous generator under fluctuating loads or generation conditions. We developed and simulated the proposed control strategy using MATLAB/Simulink to analyze the interaction between the AVR and microgrid units. Several scenarios were tested to evaluate the influence of microgrid integration on the voltage stability of the power network. The simulation results demonstrate that properly coordinating microgrid integration can effectively reduce voltage deviations and improve the AVR system's dynamic performance. These results highlight the significant role of microgrids in supporting conventional power systems, improving reliability, and maintaining voltage regulation under demanding conditions. These findings confirm that the interaction between AVR control and microgrids contributes to a more resilient and adaptive energy infrastructure.

Keywords: Synchronous machine, Automatic voltage regulation (AVR), Power system, Microgrids, Renewable energy

2nd International Conference on Multidisciplinary Sciences and Technological Developments (ICMUSTED 2025)

December 12-15, 2025

Next-Generation Deep Learning Architectures for Satellite Image Classification: Integrating Capsule Networks with CNNs and Transformers

Boucif Beddad[1], Samiha Mezrar[2], Postaire Jack-Gerard[3]

[1]Djillali Liabes University of Sidi-Bel-Abbes, Algeria
[2]Higher School of Computer Science 08 May 1945 of Sidi-Bel-Abbes, Algeria
[3]University of Lille, Lille, France
Corresponding author: Boucif Beddad (e-mail: boucif.beddad@univ-sba.dz)

Abstract

Satellite image classification has become a key tool in the remote sensing domain. It has an impact on different areas like environmental monitoring, urban planning, and disaster response. Convolutional neural networks (CNNs), recurrent neural networks (RNNs), and transformer-based models have led to big steps forward in analyzing high-resolution satellite images. Still, they face ongoing issues such as loss of spatial information, high computing needs, and poor performance across different geographies. Capsule networks (CapsNets), with their vector-based setup and dynamic routing, offer a promising option. They keep spatial hierarchies intact and work better under affine transformations. This paper suggests a mixed deep learning approach. It combines the strong points of CNNs, transformers, and CapsNets to tackle the shortcomings of current systems in satellite image classification. We show a side-by-side study on standard datasets like EuroSAT and BigEarthNet to improve the image classification. We look at performance measures, ability to scale, and ease of understanding. Besides reviewing cutting-edge designs, we explore new trends. These include mixing different types of data, learning without supervision, and artificial intelligence that explains itself. We also discuss how CapsNets can add to these new ideas. We point out future paths to build satellite image classification systems that are more efficient, understandable, and work in real-time. These systems should be ready for actual use in the field.

Keywords: Satellite image classification, Capsule networks, Convolutional neural networks, Transformers, Deep learning, Remote sensing, Dynamic routing, Self-supervised learning

2nd International Conference on Multidisciplinary Sciences and Technological Developments (ICMUSTED 2025)

December 12-15, 2025

Harvesting Waste Kinetic Energy from Vehicle Suspensions for Enhanced Mileage and Power Generation

Touqeer Aslam[1], Shoukat Ali Mugheri[1], Ali Azam[1], Manthar Ali[1], Abbas Raza[2]

[1]School of Mechanical Engineering, Southwest Jiaotong University, Chengdu, China
[2]School of Mechanical Engineering, Southeast University, 211102 Nanjing, China
Corresponding author: Touqeer Aslam (e-mail: touqeeraslam.uet@gmail.com)

Abstract

The rapid growth of the automotive sector has increased global fuel consumption and environmental challenges. A significant portion of fuel energy, nearly 84–90%, is dissipated through suspension vibrations, braking, rolling resistance, and tire–road friction, with only 10–16% utilized for propulsion. Among these losses, vehicle suspension systems contribute substantially through energy dissipation in shock absorbers. This study introduces a novel vehicular mechanical energy harvester (VMEH) that converts suspension vibrations into electrical energy using a rack–pinion transmission integrated with one-way bearings and a DC generator. The bidirectional motion of the suspension is transformed into unidirectional rotational motion, enabling continuous energy generation. The system was modeled in SolidWorks 2022 and simulated under sinusoidal vibrations of 30 mm amplitude, 2000 N applied force, and frequencies of 1–4 Hz. Results demonstrated that at 4 Hz and an external resistive moment of 50 Nm, the harvester achieved a maximum output power of 550 W with a peak efficiency of 70%. The proposed VMEH system offers a practical approach for recovering wasted vehicular kinetic energy to enhance fuel economy and provide onboard renewable power for automotive applications.

Keywords: Energy harvesting, Shock absorber, Renewable energy, Mechanical-to-electrical conversion, Vehicle suspension

1. INTRODUCTION

Automobiles are the major source of global transportation and provide a convenient means of transportation to their users. Despite their benefits, they play a significant role in environmental and energy issues. A large portion of vehicles energy is dissipated due to the suspension system, braking system, rolling resistance and surface friction between road and tire and only 10–16% of fuel energy is utilized for useful purposes [1–5]. However, the potential/kinetic energy of moving vehicle is used as an alternative to generate power [6–8].

Liu et al. [9] designed, modelled and simulated a shock absorber with dual overrunning clutches was designed, modeled, and simulated for large vehicles. Tested at 15–50 mm amplitudes and 1–2.5 Hz frequencies, it achieved 44.73 W peak and 22.34 W mean power at 69.19% efficiency. Chen et al. [2] designed a cylinder–piston roadway harvester was designed with 3 cm stroke, 600 rpm speed, and 26,509 J input work. It produced 10,877 J output at 41.03% efficiency under a 34 kg piston load. Chongfeng et al. [10] developed a half-vehicle suspension model was developed for energy harvesting, tested at 0.01–0.05 m amplitude and 2 Hz frequency. The system produced 57.84 W at 13 km/h and 1289 W at 39 km/h. Weiwu et al. [11] designed a shock absorber was modeled and simulated to harvest energy from vehicle oscillations. Using a one-way bearing in the transmission module, vertical vibrations were converted into unidirectional generator shaft rotation. Tests with 10 mm amplitude at 1–2.5 Hz yielded maximum input and output powers of 0.203 W and 0.082 W, respectively.

This work presents a novel rack–pinion-based shock absorber harvester equipped with one-way bearings for efficient conversion of bidirectional suspension motion into unidirectional generator rotation. The system's performance is evaluated through dynamic modeling and simulation using SolidWorks, highlighting its potential for high-power vehicular applications.

2. DESIGN OF VEHICULAR MECHANICAL ENERGY HARVESTER

2.1. Vehicular Mechanical Energy Harvester (VMEH)

The proposed VMEH is presented in Fig. 1. It consists of four modules mainly vibration input module, mechanical transmission, power generation and power storage. The vibration input module (energy input) captures the potential and kinetic energy from moving vehicles over the road bumps and humps using down-and-up pulse motion of the car suspension system. Transmission module converts the bidirectional linear motion of rack into unidirectional rotational motion of the flywheel shaft. The continuous engagement and disengagement of one-way bearings allow both down-and-up pulse motion to obtain unidirectional rotational motion of the flywheel shaft and yields more power output than the traditional designs.

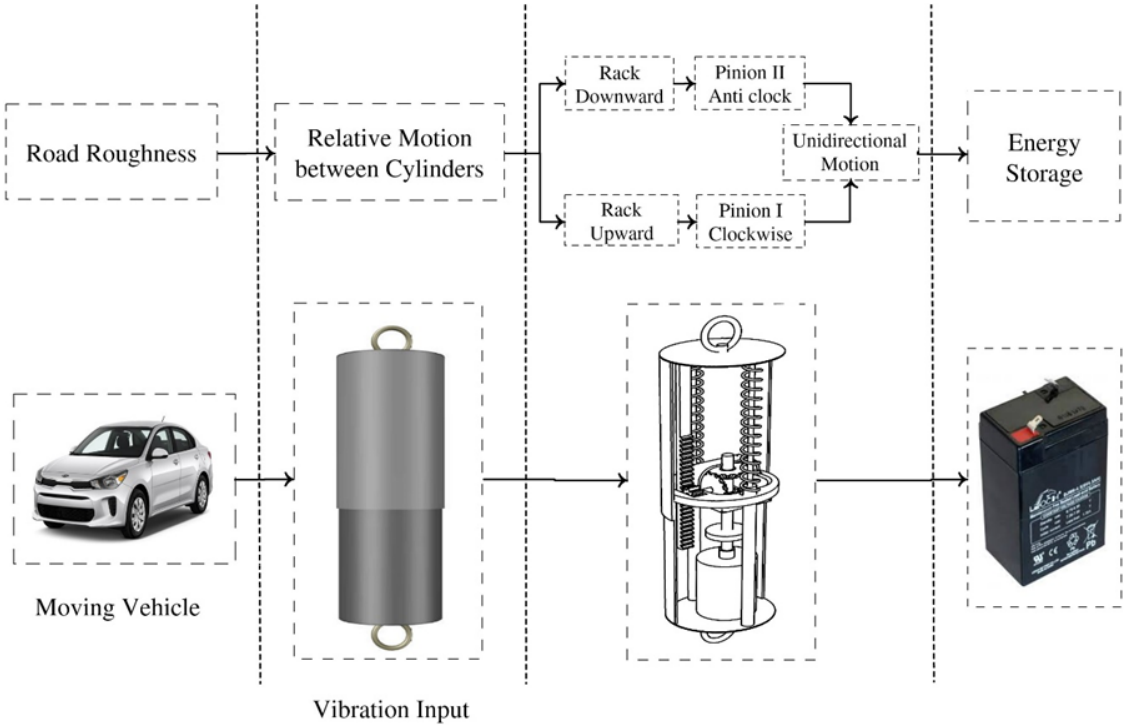

Figure 1. Flow diagram of vehicular mechanical energy harvesting system

During the power generation module, mechanical energy in the form of rotational motion of the flywheel shaft is utilized to rotate the shaft of the DC generator. This system generates DC voltage and battery is used to store DC voltage. The stored power is used for the energy requirements of a vehicle after rectification.

2.2 Computer Aided Design (CAD) modelling of VMEH

The Fig. 2(a) directs the 3D model of mechanical energy harvester fitted inside the casing of the suspension system. The components of the transmission mechanism are fitted in frame through supporting bars. A single-sided rack is meshed with a pinion and the pinion rotates in clockwise and anticlockwise directions due to the outward and inward movements of the rack inside the suspension cylinder. The two way rotations of the pinion are transferred to the one-way bearing and gear shaft. Both one-way bearings are mounted in between the vertical axes bevel gears and their shafts in such a way that bevel gears are integrated with the one-way bearings. A flywheel is mounted on the generator shaft to regulate the motion. VMEH consists of mass of the vehicle acting on the suspension system, springs and an internal damping force of the system so it can be modelled as a mass-spring-damper system.

Fig. 2(b) shows the schematic of VMEH, the single-sided rack is fitted with the upper end of the suspension system and the linear bidirectional motion of the suspension is altered to the unidirectional rotational motion of flywheel shaft with the help of two one-way bearings. The engagement and disengagement of the one-way bearing continue the flywheel shaft in one direction. When a moving vehicle undergoes the vibrations over a rough road, the suspension along with the rack move vertically under the action of applied force F_v due to the weight of the vehicle and the pinion which is meshed with the rack produces angular rotation θp due to the linear movement X_r of rack. The pinion attached to rack rotate in clockwise and anticlockwise directions due to the upward and downward movements of the rack inside the suspension cylinder. The one-way bearings are positioned in between the bevel gears and the shaft in such a way that only unidirectional motion is obtained at flywheel shaft to drive a generator. The power produced from the generator can be stored or be used instantaneously. The upward or outward motion of rack is caused by springs force and second one-way bearing is engaged (upward movement) to drive flywheel shaft and the first one-way bearing is disengaged at the same instant. In this way, continuous engagement and

disengagement of one-way bearings result unidirectional rotational motion and drive the flywheel shaft. The red and blue arrows in Fig. 2(b) indicate the transmitting route of motion from bidirectional linear motion to unidirectional rotational motion.

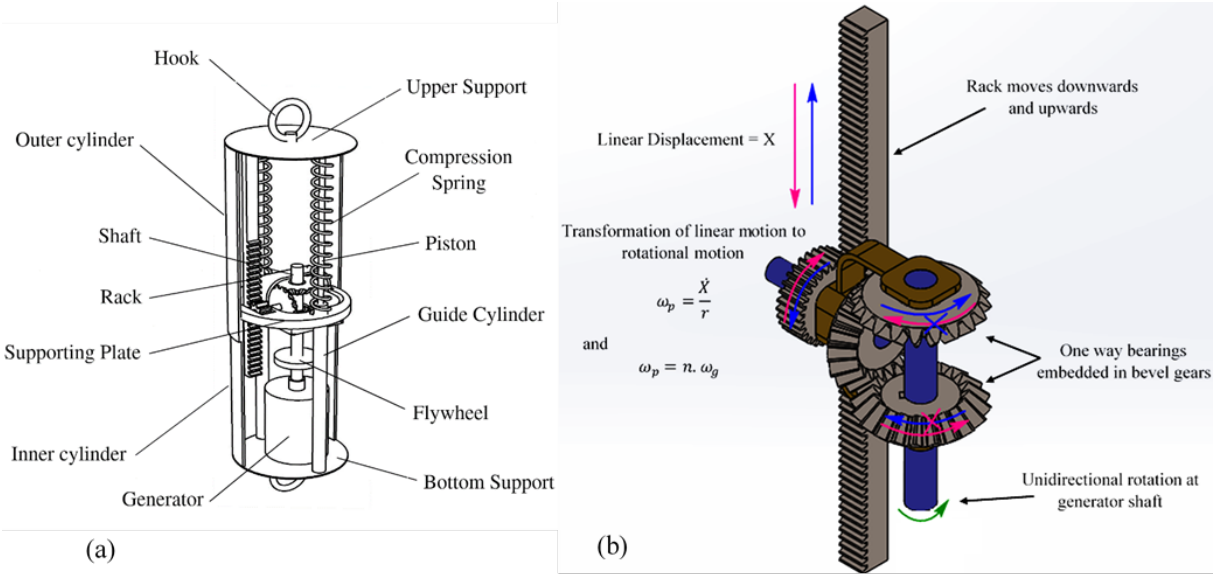

Figure 2. (a) Mechanism of mechanical energy harvester and (b) unidirectional rotation from bi-directional motion

2.3 Mathematical modelling of VMEH

The vehicle applied force F acts at angle θ and rack of the shock absorber moves along vertical. The relationship for the force delivered to the shock absorber by roughness of road is shown in Fig. 3(b) is given as:

$$F_a = F\cos\theta \tag{1}$$

Where F is the resultant force on shock absorber due to impulse, F_a is the vertical component of force F acting on the rack, θ is the angle which force F makes with vertical. The applied force F_a varies with θ as shown in Fig. 3(b).

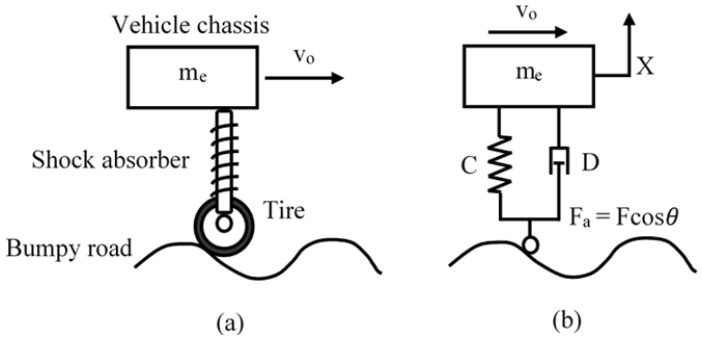

Figure 3. (a) Contact between the tires and speed bump (b) modeling of shock absorber

The applied force F_a gradually increases during initial contact (Fig. 3(a)). The relation between velocity of the vehicle and θ is given as:

$$p\sin\theta = v_o t \tag{2}$$

Where v_0 is velocity of the vehicle and p is the radius of the rough surface of road profile producing impulse. The equation for θ can be written as:

$$\theta(t) = \frac{\tan^{-1}(v_0 t)}{p} \tag{3}$$

The operation of the vehicular mechanical energy harvester VMEH consists of mass acting on the shock absorber, springs and an internal damping force of the system and it is modeled as mass-spring damper system. The helical compression springs are placed in parallel to help the shock absorber to regain its original position under the absence of load. The single degrees-of-freedom (DOF) forced vibrational system with damper can be expressed by using langrangian equation as:

$$\frac{d}{dt}\left(\frac{\partial T}{\partial \dot{x}}\right)+\left(\frac{\partial D}{\partial \dot{x}}\right)-\left(\frac{\partial C}{\partial x}\right)=F_a \tag{4}$$

The effect of spring was ignore during simulation study. According to the definition of shock absorber the forced damped equation can be written as:

$$F=\left[m_e\ddot{X}+D\dot{X}\right] \tag{5}$$

Where X, $\dot{X}$, $\ddot{X}$ are the displacement, velocity and acceleration of rack, T is the torque on the pinion shaft, D is the damping coefficient of the system, and F is the applied vertical force which is a function of cosine.

The equivalent damping D consists of two types of damping;

- Mechanical damping D_m which is caused by the frictional losses in mechanical components i.e. rack, pinions, gears, shafts and flywheel.
- Electrical damping D_e which is caused by internal resistance of the system and electrical load acting on the generator.

Since structural or mechanical damping D_m is produced by the dynamics and misalignment of the moving parts. The total damping is evaluated as:

$$D=D_m+D_e \tag{6}$$

The electrical damping D_e can be evaluated as:

$$D_e=\frac{k_t k_v n^2}{(R_e+R_i)r^2} \tag{7}$$

Where R_e and R_i are the external and internal resistances of generator and k_t and k_v are the torque and voltage constants of the generator.

3. SYSTEM SIMULATION

The simulation study of VMEH was conducted using dynamic modelling software Solidworks (2022) and motion analyses were performed. Each strike of the tire (compression stroke) was considered as a sinusoidal applied force of magnitude 2000N and the maximum amplitude of 30 mm. The CAD model was built in Solidworks and simulated at and various frequencies of 1, 2, 3 and 4 Hz. For simulation, a linear motor was selected to the rack of VMEH compression and extension equivalently and details are in the Table 1.

Table 1. Parameters for simulation of VMEH

Stroke of Tire	Applied Force (N)	Amplitude (mm)	Frequency (Hz)
Sinusoidal form	2000	30	1, 2, 3, 4

In a simulation study, a linear motor is used to drive the rack of shock absorber downward and upward equivalently. The effect of force on shock absorber was selected equal in the downward and upward motion of the rack. The VMEH has an advantage of harvesting large-scale impulse vibrational energy in a short time and constantly producing power over a longer time span by continuous rotation of generator due to engagement and disengagement of one-way bearings. A resistive torque was applied to create the loading effect on gearing mechanism of the mechanical energy harvesting mechanism. This resistive torque acts as an external load on the system.

4. RESULTS AND DISCUSSION

Fig. 4 shows the time-displacement curves for suspension system at different frequencies and applied force. The linear displacement of the shock absorber is constant having a magnitude of 30 mm under different vibrational frequencies. When the test car passes over a rough road (sinusoidal displacement) mechanical energy harvester, the shock absorber reaches the bottom and stays there. However, the generator shaft can still rotate freely with the disengagement of one-way bearing because of rotating inertia which keeps generating the power until the rotational speed of the shaft dies out. In the simulation study, the effect of force on shock absorber is needed to be equal in the downward and upward movement of the rack. The working mechanism of MEH has the advantage of converting large-scale impulse vibration energy in a short time and continuously producing power in longer duration by continuous rotation of generator using engagement and disengagement of one-way bearings.

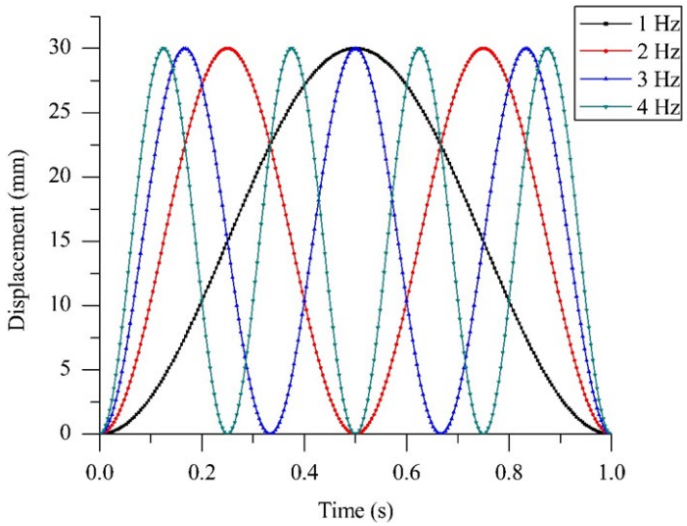

Figure 4. Input displacement of the rack at a vibrational amplitude of 30 mm

The input linear velocity of rack under different frequencies is shown in Fig. 5. Input linear speed of the rack is distributed along Y-axis and time is plotted along X-axis. Rack speed is plotted over a range of frequencies including 1, 2, 3 and 4 Hz. The motion of shock absorber profile is directly simulated as the linear motion of rack. It can be observed that due to an increase in vibrational frequency, the linear speed of rack also increases. Which is due to the fact that higher frequencies are obtained at higher velocities of the car so the speed of rack is dependent on the speed of the test car. The peak linear velocity of the rack was 380 mm/s at 4 Hz. At 1 Hz frequency, the linear speed of rack is 120 mm/s. The power input to the system is directly related to input linear speed of the rack and hence to the vibrational frequency of the system. As the frequency increases, input linear speed of rack also increases which inputs a higher fraction of power input to the system. At constant force, the power input is dependent on input linear speed of rack and hence the velocity of the moving car over a jerky road.

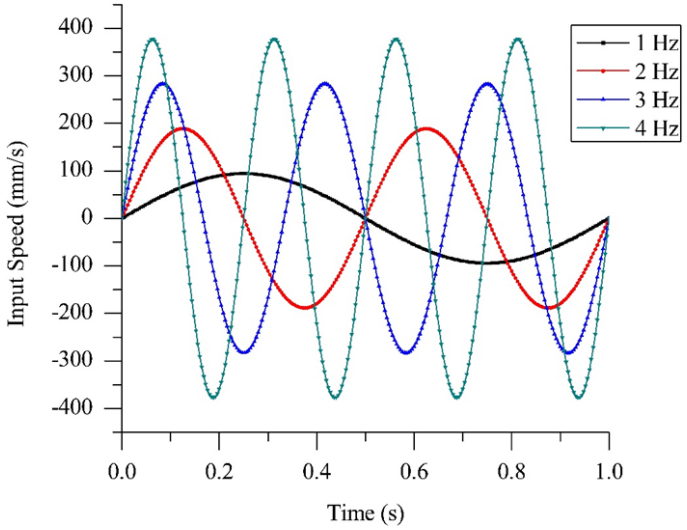

Figure 5. Input oscillation speed vs time at a vibrational amplitude of 30 mm

The input linear velocity of rack under different frequencies is shown in Fig. 5. Input linear speed of the rack is distributed along Y-axis and time is plotted along X-axis. Rack speed is plotted over a range of frequencies including 1, 2, 3, and 4 Hz. The motion of shock absorber profile is directly simulated as the linear motion of rack. It can be observed that due to an increase in vibrational frequency, the linear speed of rack also increases. Which is due to the fact that higher frequencies are obtained at higher velocities of the car so the speed of rack is dependent on the speed of the test car. The peak linear velocity of the rack was 380 mm/s at 4 Hz. At 1 Hz frequency, the linear speed of rack is 120 mm/s. The power input to the system is directly related to input linear speed of the rack and hence to the vibrational frequency of the system. As the frequency increases, input linear speed of rack also increases which inputs a higher fraction of power input to the system as depicted by Eq. 8. At constant force, the power input is dependent on input linear speed of rack and hence the velocity of the moving car over a jerky road.

Fig. 6 shows the distribution of sinusoidal force with respect to time at various frequencies including 1, 2, 2, 3 and 4 Hz. Force acting on the rack is distributed along Y-axis and time is plotted along X-axis. The input force of the rack is constant having magnitude of 2000N at maximum displacement of 30 mm under different vibrational frequencies. The trend of force is sinusoidal as it is the function of cosine. The peak and average values of the applied force remain constant with varying frequencies. Fig. 6 also shows that peak input power to the system is obtained at the points where force has a peak value of 2000N. The negative sign of the forces is showing the reversal of direction and force is changing its magnitude in both directions; upward and downward motion of the rack. In the simulation study, both upward and downward motion of the rack is caused by an applied force of 2000N which reverses its direction periodically. In actual scenario, the force applied by test car will be delivered to the system during downward motion of the bump only, while the upward movement of the rack is obtained using potential energy stored in the springs of the system.

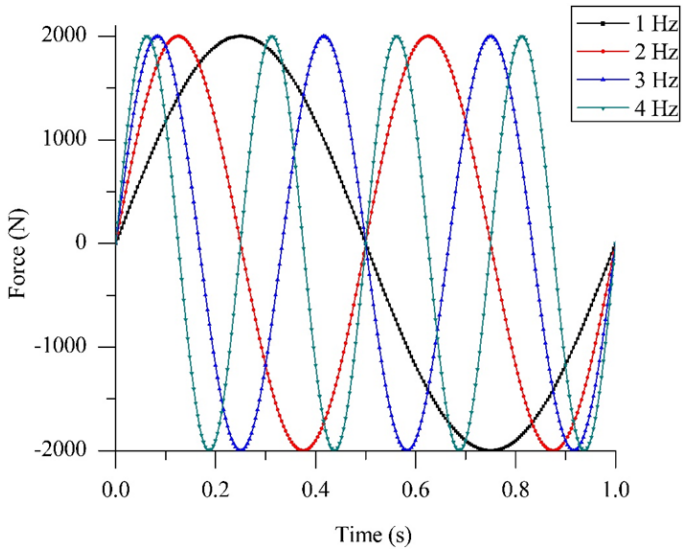

Figure 6. Simulated input force vs time at a vibrational amplitude of 30 mm

Fig. 7 shows the force-velocity loop of the mechanical energy harvester under different vibrational frequencies and applied force. Force is plotted along Y-axis and speed of rack is distributed along X-axis. Force-speed loop starts from zero points of applied force and input velocity. The area of the loop gives a measure of the mechanical power input to the mechanical velocity gives a direct measure of power, therefore, the area enclosed by the force-velocity loop is a direct measure of power input to the mechanical energy harvester VMEH. At small frequencies, the force-velocity loop is converging into a single line which shows that at lower input velocities to the system the power input to the system is very small. To get a high advantage from the system, VMEH should be operated at high frequencies.

Fig. 8 shows the maximum input power to the VMEH is 750W at 4 Hz frequency and 380 mm/s input velocity of the rack. The input to the mechanical energy harvester increases with increasing frequency because the speed and the kinetic energy of the rack also increase at a higher frequency. At high frequencies, the linear velocity of the rack increases, due to which high power is delivered to the system. The power input to the system is directly related to input linear speed of the bump and hence to the vibrational frequency of the system. As the frequency increases, input linear speed of rack also increases which causes a higher fraction of power input to the system as depicted by Eq. (8).

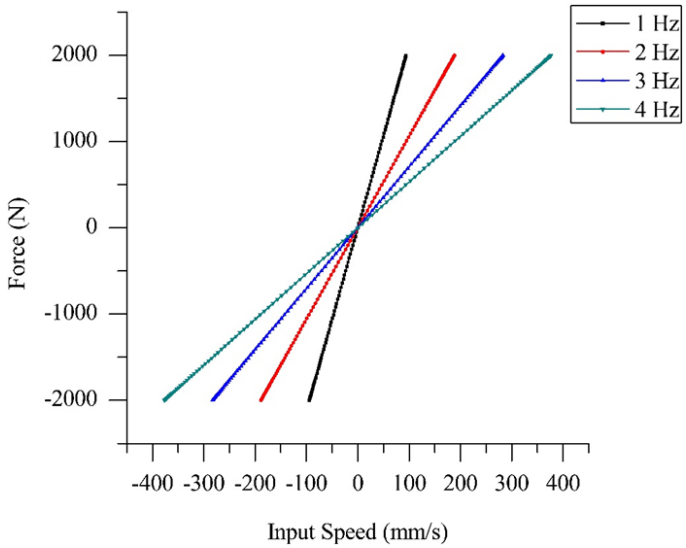

Figure 7. Simulated input speed vs time at a vibrational amplitude of 30 mm

At constant force, the power input is dependent on input linear speed of the shock absorber and hence the velocity of the moving car over the jerky road. Fig. 8 shows an increasing trend of the power input with increasing frequencies but at higher frequencies, the peak value of power input is for a very short duration of time. At lower frequencies, power input remains at its peak value for a greater instant of time as compared to higher frequencies. In other words, as the vibrational frequency of the system increases, the power input curves are becoming steeper.

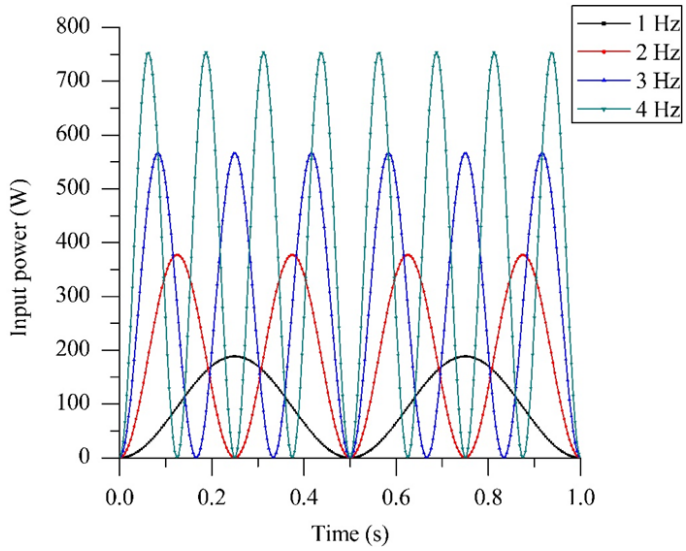

Figure 8. Simulated input power at a vibrational amplitude of 60 mm

Fig. 9 shows the trends of the power output of MEH with varying external loads on the system. It can be observed that the output power is indirectly proportional to the external load. Therefore, higher the external load, lesser will be the output power and hence, efficiency of VMEH. The effects of external load on output power generation of VMEH is studied through simulation. For the simulation of output power, various resistive moments in term of external loads were selected in ranges from 50 to 110 Nm with an interval of 60 Nm at a frequency of 4 Hz. The maximum value of output power obtained is 550 W at an external load of 50 Nm and frequency of 4 Hz. It can be seen from Fig. 10 that output power decreases as the load increases on the system. As the external load increases on the output shaft, the power-time curve experiences a delay due to the effect of the mass inertia of the system. The system gets bulky at higher values of external loads and takes more time to regain its mean position. It can be seen from graph that lower the external load greater will be output power and efficiency. Internal loads including frictional losses and mass inertia of the system should be small to increase the power output and mechanical efficiency of the system.

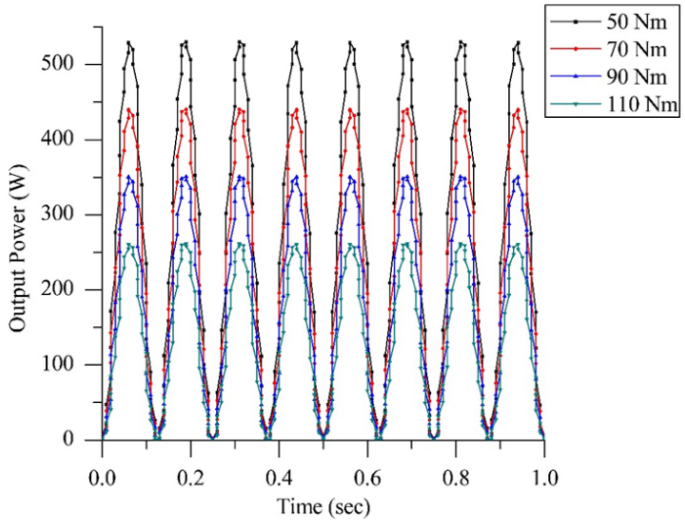

Figure 9. Simulated output power under 4.5 Hz vibrational frequency and vibrational amplitude of 60 mm

5. CONCLUSION

A new energy harvesting system is introduced which is renewable and harvests a large amount of waste energy from vehicles running on the road. The mechanical energy harvesting system (MEH) was modelled and simulated. The maximum displacement of the rack is 30 mm under different vibrational frequencies of 1, 2, 3 and 4 Hz. The mechanical energy harvesting system was modelled and simulated using Solidworks (2022) motion analyses were performed. MEH system can produce sufficient electricity for a large number of vehicles running over the road with a shock absorber energy harvester.

- The input force applied to the rack, which is a function of cosine, is sinusoidal in nature having a peak value of 2000N.
- The maximum displacement of the rack is 30 mm under different vibrational frequencies of 1, 2,3 and 4 Hz. As the vibrational frequency of the system increases, the linear speed of rack also increases. The power input to the system is directly related to the linear speed of the bump and hence to the vibrational frequency of the system. As vibrational frequency of the system increases, the power input curve becomes steeper and possesses its peak value for a shorter duration of time as compared to the scenario at lower frequencies. Maximum power input to the MEH system in each strike is 750 W at 4.5 Hz frequency.
- The area enclosed by the force-displacement loop gives the mechanical work input to the mechanical energy harvester. Whereas the area under the force-input velocity loop gives a measure of the mechanical power input to the mechanical energy harvester. The maximum value of output power obtained is 420 W at an external load of 50 Nm and frequency of 4 Hz. As the external load increases on the output shaft, the system gets bulky and experiences a delay due to increased mass inertia and takes more time to regain its mean position.
- From the simulation results, the mechanical efficiencies of the MEH system obtained were 70 % to 35% at 50 Nm and 110 Nm respectively under the same vibrational frequency of 4 Hz. The mechanical efficiency of the system decreases linearly as the load increases. The internal loads of the system should be small for better efficiency. To get maximum power output, the mass inertia of the system and generator should be small.

References

[1] L. Zuo, B. Scully, J. Shestani, and Y. Zhou, “Design and characterization of an electromagnetic energy harvester for vehicle suspensions,” *Smart Mater. Struct.*, vol. 19, art. no. 045003, Apr. 2010.

[2] C.-C. Ting, D.-Y. Tsai, and C.-C. Hsiao, “Developing a mechanical roadway system for waste energy capture of vehicles and electric generation,” *Appl. Energy*, vol. 92, pp. 1–8, Apr. 2012.

[3] R. Colvile, E. Hutchinson, J. Mindell, and R. Warren, “The transport sector as a source of air pollution,” *Atmos. Environ.*, vol. 35, no. 9, pp. 1537–1565, Mar. 2001.

[4] Z. Li, L. Zuo, G. Luhrs, L. Lin, and Y.-X. Qin, “Design, modeling, and road tests of electromagnetic energy-harvesting shock absorbers,” in *Proc. ASME Dyn. Syst. Control Conf.*, Oct. 2012, pp. 675–684.

[5] M. A. Abdelkareem, L. Xu, X. Guo, M. K. A. Ali, A. Elagouz, M. A. Hassan, *et al.*, “Energy harvesting sensitivity analysis and assessment of the potential power and full car dynamics for different road modes,” *Mech. Syst. Signal Process.*, vol. 110, pp. 307–332, Oct. 2018.

[6] B. Lafarge, S. Grondel, C. Delebarre, and E. Cattan, “A validated simulation of energy harvesting with

piezoelectric cantilever beams on a vehicle suspension using Bond Graph approach," *Mechatronics*, vol. 53, pp. 202–214, Jul. 2018.
[7] L. Xie, J. Li, X. Li, L. Huang, and S. Cai, "Damping-tunable energy-harvesting vehicle damper with multiple controlled generators: Design, modeling and experiments," *Mech. Syst. Signal Process.*, vol. 99, pp. 859–872, Jan. 2018.
[8] S. Singh and N. V. Satpute, "Design and analysis of energy-harvesting shock absorber with electromagnetic and fluid damping," *J. Mech. Sci. Technol.*, vol. 29, no. 4, pp. 1591–1605, Apr. 2015.
[9] Y. Liu, W. Chen, Z. Zhang, and G. Hua, "Energy-regenerative shock absorber for transportation vehicles based on dual overrunning clutches: Design, modeling, and simulation," *Transp. Res. Rec.*, vol. 2573, no. 1, pp. 126–136, 2016.
[10] C. Wei and H. Taghavifar, "A novel approach to energy harvesting from vehicle suspension system: Half-vehicle model," *Energy*, vol. 134, pp. 279–288, Sep. 2017.
[11] W. W. Chen and Z. T. Zhang, "Energy harvesting shock absorbers for vehicles: Design, modeling and simulation," *Appl. Mech. Mater.*, vol. 541–542, pp. 1169–1174, May 2014.

2nd International Conference on Multidisciplinary Sciences and Technological Developments (ICMUSTED 2025)

December 12-15, 2025

Development of an Algorithm for Determining the Characteristics of the Ejection System

Oleksandr Panevnyk[1]

[1]Department of Oil and Gas Machines and Equipment, Ivano-Frankivsk National Technical University of Oil and Gas, Ivano-Frankivsk, Ukraine
Corresponding author: Oleksandr Panevnyk (o.v.panevnik@gmail.com)

Abstract

An algorithm has been developed to determine the characteristics of the ejection system under the condition of cavitation in the mixing chamber of a jet pump in the case of swirling of flows by inclined guide elements placed in its flow part. The limiting operational characteristics of downhole jet pumps have been determined and the influence of the angle of inclination of the elements placed in the flow part of the jet pump on the cavitation characteristics of the ejection system has been investigated. Based on the Bernoulli equation, an analytical dependence has been obtained to determine the influence of design and operating parameters on the minimum pressure at the inlet to the mixing chamber of the jet pump. The obtained relationship is presented in the form of calculation algorithms that determine the conditions for pre-cavitation operation of the ejection system: the maximum permissible flow rate of the working flow and the minimum permissible depth of placement of the jet pump in the well. The relative rotational motion of the mixed flows is taken into account using the coefficient of uneven distribution of longitudinal velocities caused by the swirling of the flow by the inclined guide elements placed in the flow part of the jet pump. The conducted studies have established the inverse effect of the angle of inclination of the guide elements placed in the flow part of the jet pump on the maximum permissible flow rate of the working flow and the directly proportional effect of this parameter on the minimum permissible depth of placement of the ejection system in the well. The scientific novelty of the conducted research lies in establishing the patterns of changes in the operational parameters of the well ejection system under conditions of relative rotational motion of mixed flows.

Keywords: Jet pump, Ejection system, Injected flow, Cavitation, Flow swirl

2nd International Conference on Multidisciplinary Sciences and Technological Developments (ICMUSTED 2025)

December 12-15, 2025

Virtual Students in Programming Fundamentals: Comparing Large Language Models with Vocational Computer Programming Students in Classical Exams

Selma Bulut[1], Adem Korkmaz[2]

[1]Department of Computer Technologies, Kirklareli University, Kirklareli, Türkiye
[2]Department of Computer Technologies, Bandirma Onyedi Eylul University, Bandirma, Türkiye
Corresponding author: Adem Korkmaz (e-mail: ademkorkmaz@bandirma.edu.tr)

Abstract

This study examines how large language models (LLMs) perform as "virtual students" in real examinations within the context of vocational higher education. The research was conducted in the programming fundamentals course of an associate degree computer programming program, and the evaluation is based on constructed-response (open-ended) midterm and final examinations. The exam questions cover C#-based topics such as algorithm design, bit-level operations, numerical properties (e.g., tau and perfect numbers), arrays, and matrix operations. In the study, the midterm, final, and weighted overall achievement scores (bn) of 69 students enrolled in the course were obtained from official grade records and used in anonymized, aggregated form. The same midterm and final questions were presented to four widely used LLMs in the literature (Gemini, ChatGPT, DeepSeek, Claude). The responses produced by each model were graded by the course instructor using the same 0–100 scoring scale and weighting scheme (midterm 40%, final 60%) used for students. According to the results, the overall achievement scores were 82 for Gemini and DeepSeek, and 86 for ChatGPT and Claude; these correspond to BB and BA, respectively, on the institutional letter grading scale. In contrast, when all students are considered, the class mean overall achievement score is 55.99, and 68.98 when only students with a score greater than zero are included. The findings indicate that, in this context, the examined LLMs perform significantly better than the average student and fall within the upper achievement band of the class. In conclusion, the study demonstrates that contemporary LLMs can successfully solve a substantial portion of an introductory programming curriculum when assessed through traditional written examinations and points to the need to reconsider assessment design in programming education and to the pedagogically responsible integration of generative artificial intelligence (AI).

Keywords: Large language models, Generative AI, Programming education, Assessment, Vocational higher education

1. INTRODUCTION

In recent years, generative artificial intelligence (generative AI) and large language models (LLMs) have become key technologies transforming both teaching processes and assessment practices in higher education. LLM-based chatbots are rapidly being integrated into students' learning environments through functionalities such as text generation, code writing, summarization, and personalized feedback; this simultaneously introduces new opportunities and risks for instructional design, academic integrity, and fairness in assessment [1]. Recent studies have shown that the vast majority of university students regularly use generative AI tools in their study and assignment preparation processes, with particularly intensive use in assessment-related activities [2].

The performance of LLMs on exams has emerged as a rapidly expanding research area. OpenAI's GPT-4 model has achieved results comparable to or exceeding human performance in high-level professional examinations such as the bar exam, medicine, and law, thereby reinforcing the discourse of "human-level performance" as an evaluative benchmark for Generative AI [3].

A similar trend is observed in empirical studies that administer real university examinations from different disciplines to LLMs. It has been shown that ChatGPT can achieve performance comparable to that of the average student on a written computer science exam [4] and that, in three different undergraduate course exams in logistics and warehousing, it outperformed students in some sessions while lagging behind the average student in others [5].

In the Turkish context, a study comparing the performance of GPT-4o, Gemini, and Copilot on the questions of the Higher Education Institutions Examination – Basic Proficiency Test (YKS/TYT in Turkish) demonstrated that these models can match or even exceed student averages in many subtests, even in a selective and high-stakes university entrance examination [6]. These findings underscore the importance of systematically comparing LLMs, conceptualized as "virtual students," with real examination data.

Computer programming education is one of the domains in which LLMs are most intensively discussed. A study showing that ChatGPT-3.5 and GPT-4 achieved 94–96% accuracy on introductory Python programming tasks revealed that LLMs are highly competent in automatically solving fundamental programming problems [7].

Investigating the impact of LLM use on student learning outcomes in programming education, Jošt and colleagues reported that increased use of ChatGPT and Copilot in a software development course was negatively correlated with final grades, particularly for tasks requiring higher-order cognitive skills such as code generation and debugging; they warn that overreliance on LLMs may weaken students' independent problem-solving abilities [8].

Although the technical capabilities of LLMs in programming education have been demonstrated by their high accuracy rates on basic coding tasks, there remain essential questions concerning the reliability, optimization, and contextual appropriateness of the solutions they generate. For example, it has been reported that code snippets produced by LLMs may contain security vulnerabilities, inefficient algorithms, or abstractions that are not well-suited to specific problem domains [9]. Moreover, these models tend to reproduce popular solutions present in their training data and therefore may be limited when confronted with problems that require original and creative algorithmic thinking [10]. These findings suggest that LLMs have pedagogical value not as mere "code generators" but when used in an integrated manner with human oversight and critical thinking.

On the other hand, studies emphasizing that ChatGPT provides strong support to instructors in programming courses for developing materials, generating example code, and designing assessments highlight the pedagogical potential of these tools [11–13].

Systematic reviews and mini-reviews that address the role of LLMs in programming education holistically indicate that most existing studies either focus on short programming tasks or are limited to describing how students use LLMs in their everyday learning [10, 14].

By contrast, there is a minimal number of studies examining how LLMs solve traditional exams administered in real course contexts, particularly midterm and final examinations that include open-ended algorithm questions and code-writing tasks in specific languages, such as C#, and how this performance is positioned relative to the official grading system and letter grade distributions. A substantial portion of existing work focuses on multiple-choice or short-answer exams [4, 5] or reports LLM performance solely in terms of the percentage of correct answers; detailed comparisons based on course-level achievement grades, letter-grade intervals, and class distributions are often not provided.

At the same time, the rapid proliferation of generative AI has triggered serious debates in higher education regarding academic integrity and assessment design. It is emphasized that Generative AI tools have the potential to both enrich the learning experience and facilitate unethical behaviors such as cheating and plagiarism, and that institutions therefore need to reconsider their modes of assessment [1, 2].

The widespread accessibility of LLMs also necessitates a thorough re-examination of assessment methods in programming education. The fact that LLMs can easily solve traditional written exams and homework assignments casts doubt on the validity of assessing students' individual competencies. In response, researchers have proposed LLM-resilient assessment strategies. These strategies include open-ended projects, oral defenses (viva voce), peer assessment, context-embedded and multi-step problems, and assessment methods that track the learning process [11, 12]. A common feature of these approaches is that they aim to measure higher-order cognitive skills such as problem comprehension, design decisions, logical flow of code, and debugging processes, rather than merely the final output.

Studies examining the use of ChatGPT as an automatic grading tool in programming courses have shown that the model can assign grades that are highly correlated with those of instructors. However, it may sometimes grade more strictly and still requires human oversight [15].

Taken together, these findings show that LLMs are becoming increasingly visible in programming education, both as "student" and "evaluator." In the existing literature, however, the performance of LLMs is most commonly

reported in terms of isolated code snippets or multiple-choice tests, and their position within the holistic assessment ecosystem of a real course (midterm, final, letter grade distribution) has not been sufficiently explored [4, 5]. Furthermore, studies examining LLM performance in practice-oriented contexts, such as vocational higher education, where curricula often center on a specific programming language (e.g., C#), are relatively rare. This study aims to fill this gap by conceptualizing LLMs as "virtual students" and directly comparing their performance with real student grades and institutional letter grade scales.

This study seeks to contribute to the literature above in the context of a programming fundamentals course offered in a Computer Programming program at a Vocational School of Higher Education in Türkiye. Within the scope of the course, students' actual grades in traditional midterm and final exams are compared with the performance of four different LLMs (Gemini, ChatGPT, DeepSeek, and Claude) on the same examination questions. The models are treated as if they were individual "virtual students" enrolled in the course; for each model, midterm, final, and weighted overall achievement scores are calculated and mapped to the course's official grading scale and letter grade distributions. Within this framework, the study focuses on the following research questions:

- In the traditional midterm and final examinations of the programming fundamentals course, how are the overall achievement scores of the selected LLMs positioned relative to the average student performance?
- Based on the official letter grade intervals of the course (FF–AA), at what level do the different LLMs fall within the class achievement distribution?

By addressing these questions, the study aims to quantitatively assess LLM performance on classical programming examinations within the context of vocational computer programming education and to provide evidence-based implications for future assessment designs.

2. MATERIAL AND METHOD

2.1. Research Design

This study was designed as a descriptive-comparative research study. The aim is to compare students' actual examination performance with that of different LLMs on the same exam questions in the traditional midterm and final examinations administered as part of the programming fundamentals course offered in a Vocational School Computer Programming program. The study does not involve any experimental intervention; instead, it is based on a secondary analysis of existing exam results and on comparing these results with the outputs produced by the LLMs.

2.2. Study Group and Dataset

The student data for this research were obtained from the official examination records of 69 students enrolled in the programming fundamentals course in the relevant academic year. For each student, the dataset includes:

- Midterm exam grade,
- End-of-term (final) exam grade,

Overall achievement grade (bn), calculated according to the formula defined in the course information system.
The overall achievement grade was calculated using the standard weights employed in the course assessment system as follows:

$$\mathrm{bn} = 0.40 \times \mathrm{midterm} + 0.60 \times \mathrm{final} \tag{1}$$

Students who did not take any of the exams or whose grade was zero were retained in the dataset to reflect the distribution accurately; however, additional descriptive analyses can be conducted when necessary by applying the condition "bn > 0". Individual exam papers, response texts, or any personal information of students were not included in the analysis; only numerical grade data associated with student ıdentity document (ID) numbers were used.

The course assessment system converts the overall achievement grade, which ranges between 0 and 100, into the following letter grade intervals:

- 0–39.99: FF
- 45–49.99: DD

- 50–59.99: DC
- 60–69.99: CC
- 70–77.99: CB
- 78–84.99: BB
- 85–91.99: BA
- 92–100: AA

This scale was used both to summarize the achievement distribution of the student group and to qualitatively position the performance of the LLMs (for example, “the model performs at the BA level”).

2.3. Structure of the Examinations

The data used in this study consist of traditional (open-ended) midterm and final examinations prepared for the programming fundamentals course:

- The midterm exam comprises questions such as translating mathematical expressions and formulas into a programming language (C#), performing bit-level operations in the binary number system, and designing flowcharts.
- The final exam consists entirely of C# programming questions, including four constructed-response items on topics such as tau numbers, calculating averages using arrays, creating a new array, transferring the digits of a number into an array, and computing the sum of the diagonals of a matrix.

The exam questions were graded on a 0–100 scale according to an official scoring rubric prepared by the course instructor, and the resulting scores were entered into the institutional automation system.

2.4. Large Language Models Used

In this study, four different LLMs that are widely used in practice were examined:

- Gemini
- ChatGPT
- DeepSeek
- Claude

Each model was exposed to the same midterm and final exam questions using the most recent versions available at the time of the study. In this way, each model produced a complete midterm paper and a complete final paper as if it were a single “virtual student” taking the course.

2.5. LLM Implementation Procedure

The midterm and final exam questions were presented to the models in their original Turkish wording from the exams, in accordance with the following principles:

1. For each exam, the models were first given a general instruction such as: “This is an exam for a programming fundamentals course; provide your answers in C#, with as much detail as a student would be expected to write in an exam, but without unnecessary elaboration.”
2. Each question was shared with the respective model only once, and the first response generated by the model was accepted for analysis. No subsequent corrections, feedback, or regeneration of answers were requested.
3. Depending on the type of question, the models were asked to provide an algorithm, C# code, and, when necessary, an explanation or a flowchart.
4. The midterm and final answers generated by each model were graded by the course instructor on a 0–100 scale using the same scoring approach applied in the real exams, resulting in a midterm grade and a final grade for each model.

During the evaluation process, the responses of each model were treated as a single exam paper; a total score was determined for each exam, and these scores were rendered comparable to the students’ grades within the course grading system.

2.6. Calculation of LLM Achievement Scores

For each LLM, the overall achievement grade was calculated using the same formula applied to the students:

$$\text{bn}_{\text{LLM}} = 0.40 \times \text{midterm}_{\text{LLM}} + 0.60 \times \text{final}_{\text{LLM}} \quad (2)$$

Based on the scores obtained in this study:

- For Gemini and DeepSeek, midterm = 55 and final = 100,
- For ChatGPT and Claude, midterm = 65 and final = 100

were assigned. Using the above formula, the overall achievement grade was calculated as bn = 82 (within the BB interval) for Gemini and DeepSeek, and bn = 86 (within the BA interval) for ChatGPT and Claude. These values were interpreted in comparison with both the students' overall mean achievement and the letter grade distribution.

2.7. Qualitative Observations

In addition to numerical scores, the solution strategies and output formats of the LLMs were also observed qualitatively. In this context, the researcher kept descriptive notes for each model on characteristics such as:

- The length and level of detail of the code produced,
- The way in which the algorithmic steps were explained,
- Whether example inputs and outputs were provided,
- Whether a flowchart was drawn or only described textually.

These qualitative observations were used in the Results section when discussing the nature and quality of the model outputs.

2.8. Ethical Considerations

The student data used in this study consist of official exam grades routinely collected during the course. Individual exam papers, identity information, and personal data were not included in the analysis; the data were used solely as anonymized aggregate statistics (mean grades and letter grade distributions). Since the study did not involve any intervention or additional procedure for the students, it does not constitute an experimental human-subjects study. It was conducted as a secondary, anonymous analysis of existing educational data in accordance with the university's relevant regulations.

3. RESULTS

The examination records of all 69 students enrolled in the programming fundamentals course were analyzed. For the 56 students with a midterm grade, the mean midterm score was 52.32, and for the 48 students with a final exam grade, the mean final score was 93.44. As shown in Table 1, the mean overall achievement grade (bn) for all students (n = 69) is 55.99. When only students with a bn value greater than 0 (n = 56) are considered, the mean overall achievement increases to 68.98. This indicates that a substantial proportion of enrolled students either did not take the exams at all or completely failed the course, and that among those who did sit the exams, overall performance hovers around the threshold of a CC grade.

Table 2. Achievement statistics for the student group

Student Subgroup	Number of Students (n)	Mean bn	Standard Deviation	Corresponding Letter Grade	Position in the Achievement Distribution
All students	69	55.99	36.50	DC	Class average
Students who took the exam (bn > 0)	56	68.98	23.45	CC	Average of successful students
Students who took the midterm	56	(Midterm mean: 52.32)	28.74	–	–
Students who took the final	48	(Final mean: 93.44)	16.12	–	–

When the overall achievement grades are examined according to the course letter grading scale, it is observed that 23 students (33.3%) received FF, seven students (10.1%) received CC, seven students (10.1%) received CB, 15

students (21.7%) received BB, 14 students (20.3%) received BA, and three students (4.3%) completed the course with an AA grade. No students received a grade in the DD or DC range. Accordingly, approximately one-third of the class fails the course, whereas another one-third group (BA–AA) demonstrates a relatively high level of achievement.

For the LLMs' exam performance, the same midterm and final exam questions were administered to four large language models. The evaluation results obtained from this procedure are presented in Table 2.

Table 2. Examination performance of the LLMs

Model	Midterm Grade	Midterm Grade	Midterm Grade	Midterm Grade
Gemini	55	100	82	BB
ChatGPT	65	100	86	BA
DeepSeek	55	100	82	BB
Claude	65	100	86	BA

These values indicate that, in the programming fundamentals course, the LLMs achieve at least a BB level of performance and most frequently perform at the BA level. In particular, the overall achievement scores of ChatGPT and Claude fall within the BA range on the course grading scale and correspond to a level of success reached by only 14 human students. The overall achievement score of 82 for Gemini and DeepSeek falls within the BB range. It is comparable to the performance of the 15 students in the class's upper-achieving group.

When the LLM results are compared with the student averages, it is observed that all models perform substantially better than the average student. While the students' mean overall achievement score is 55.99, Gemini and DeepSeek's 82-point performances are approximately 26 points (46.5%) higher than the average student's, and ChatGPT and Claude's 86-point performances are about 30 points (53.6%) higher. Even when only students with a bn value greater than zero are considered (mean 68.98), Gemini and DeepSeek remain 13 points (18.9%) above this average, and ChatGPT and Claude 17 points (24.7%) above it.

At the letter grade level, while the class average lies around the DC–CC boundary, all LLMs perform within the BB–BA band. These results show that, within the scope of the programming fundamentals course, the LLMs examined in this study answer the traditional midterm and final exam questions significantly more successfully than the average student, and that their performance is on par with, or in some cases exceeds, that of the students in the upper achievement group of the class.

4. CONCLUSION

This study compared the performance of four different large language models (Gemini, ChatGPT, DeepSeek, and Claude) with real student grades in a programming fundamentals course offered in a Vocational School Computer Programming program, using traditional midterm and final examinations. The results showed that all LLMs examined performed substantially better than the average student in the course context. While the mean overall achievement score of the students was bn ≈ 55.99 (68.98 for those with bn > 0), the scores were bn = 82 (BB) for Gemini and DeepSeek and bn = 86 (BA) for ChatGPT and Claude. These values indicate that the LLMs perform within the BB–BA range on the grading scale, that is, at the same level as the students in the class's upper achievement group, and in some cases even above them. Considering that approximately one-third of the class fails the course with an FF grade and that the average student is positioned in the DC–CC band, it can be argued that the LLMs portray a good to outstanding "virtual student" profile in the given programming exam.

The findings are essential because they demonstrate that LLMs can achieve high performance not only on multiple-choice or short-answer tests but also on traditional midterm and final examinations that include open-ended algorithm questions and C# coding tasks. Given that the midterm and final questions covered fundamental programming topics such as bit-level operations, flowchart design, array and matrix operations, and numerical properties (tau numbers, perfect numbers, etc.), it is evident that generative AI tools can automatically solve a substantial portion of an introductory programming curriculum. On the one hand, this underscores the potential of LLMs as powerful learning and practice tools that can support students; on the other hand, it points to the need to redesign traditional written examinations to improve academic integrity and assessment reliability. Structuring questions to place greater emphasis on dimensions such as originality, contextual reasoning, justification, and code design appears critical for enhancing the discriminative power of assessment tools in the age of LLMs.

These findings should also be interpreted in light of the study's limitations. First, the research was conducted within a single course, in a single program, at a single university, and over a single semester; therefore, the generalizability of the results is limited. Second, on the student side, only total midterm, final, and overall achievement grades were used; item-level scores and detailed error-type analyses could not be performed. The performance of the LLMs was likewise scored based solely on the first response produced by each model and evaluated by a single rater; different prompt strategies, multiple attempts, or inter-rater reliability were not examined in this study. Furthermore, only four LLMs were included; other commercial or open-source models were excluded from the analysis. These constraints should be taken into account when interpreting the results.

Several concrete directions for future research may be proposed. First, by conducting detailed item-level scoring, the performance of both students and LLMs can be compared by topic and skill, thereby clarifying in which areas human students are superior and in which areas LLMs are superior. LLM performance profiles can be expanded through similar analyses for different programming languages (Python, Java, etc.) and different course levels (data structures, algorithms, object-oriented programming). In light of these findings, it is essential to develop concrete pedagogical strategies for transforming traditional written examinations in programming education. Assessment formats that are LLM-resilient and focus on measuring higher-order cognitive skills come to the fore. In this regard, open-ended and long-term project-based assessments provide opportunities for students to demonstrate their analysis, design, and integration skills [11]. Oral defenses or structured interviews can enhance the validity of the evaluation by directly probing students' reasoning behind their coding decisions and algorithmic thinking processes [12]. Complex, multi-component, real-world, context-specific problems require originality and contextual fit, areas in which LLMs may struggle to generalize. Moreover, process-oriented assessment methods (e.g., development logs, version control commit histories, planning documents) and approaches such as peer review place the learning trajectory itself, rather than only the final product, at the center [12]. These alternative forms of assessment should aim not only to preserve the reliability and discriminative power of measurement in programming education but also to foster 21st-century skills such as critical thinking and collaboration.

In addition, experimental designs could be developed in which LLMs are positioned not only as virtual test-takers but also as guides, explainers, or providers of automated feedback in real teaching processes; such designs could examine variables such as academic achievement, motivation, self-efficacy, and ethical awareness in combination. Finally, higher education institutions' assessment policies and academic integrity guidelines can be updated in light of empirical findings of this kind, and institutional frameworks can be developed to ensure that generative AI tools are integrated into programming education in a responsible, transparent, and pedagogically grounded manner.

References

[1] X. Weng, P. Whitelock-Wainwright, and S. T. Buck, "Generative artificial intelligence in higher education: Research status and trends," *Australasian Journal of Educational Technology*, vol. 40, no. 1, pp. 1–21, 2024.

[2] K. Bittle and O. El-Gayar, "Generative AI and academic integrity in higher education: A systematic review and research agenda," *Information*, vol. 16, no. 4, art. no. 296, 2025.

[3] OpenAI, "GPT-4 technical report," 2023.

[4] S. Bordt and U. von Luxburg, "ChatGPT participates in a computer science exam," *arXiv Preprint*, 2023. doi: 10.48550/arXiv.2303.09461

[5] S. Franke, "Can ChatGPT solve undergraduate exams from warehousing studies? An investigation," *Computers*, vol. 14, no. 2, art. no. 52, 2025.

[6] S. Bulut, "Performance of generative artificial intelligence models (GPT-4o, Gemini, Copilot) in YKS/TYT exam: A comparative study," *Bilisim Teknolojileri Dergisi*, vol. 18, no. 4, pp. 283–296, 2025.

[7] N. Kiesler and D. Schiffner, "Large language models in introductory programming education: ChatGPT's performance and implications for assessments," *arXiv Preprint*, 2023. doi: 10.48550/arXiv.2308.08572

[8] G. Jošt, V. Taneski, and S. Karakatič, "The impact of large language models on programming education and student learning outcomes," *Applied Sciences*, vol. 14, no. 10, art. no. 4115, 2024.

[9] S. L. Bang, A. Bhattacharyya, K. D. V. Prasad, and S. M. Khaitan, "Security vulnerabilities in ChatGPT-Generated code: A preliminary study," in *Proc. IEEE/ACM 1st Int. Workshop on AI Trustworthiness (AITrust)*, 2023, pp. 1–8. doi: 10.1109/AITrust59154.2023.00009

[10] B. A. Becker, P. Denny, J. Finnie-Ansley, A. Luxton-Reilly, J. Prather, and E. A. Santos, "Programming is hard - or at least it used to be: Educational opportunities and challenges of AI code generation," in *Proc. 54th ACM Tech. Symp. Comput. Sci. Educ. (SIGCSE)*, 2023, pp. 500–506. doi: 10.1145/3545945.3569759

[11] J. Prather, B. A. Becker, M. Craig, P. Denny, D. Loksa, and B. N. Reeves, "It's time to get personal: A Call for personalized assessment in CS1," in *Proc. 2023 ACM Conf. Int. Comput. Educ. Res. (ICER)*, 2023, pp.

329–330. doi: 10.1145/3568813.3600139
[12] E. Kiesewetter, M. Wolfle, and U. Schroeder, “Rethinking assessment in the era of generative AI: towards process-oriented evaluation in programming courses,” in *Proc. IEEE Global Eng. Educ. Conf. (EDUCON)*, 2024, pp. 1–10. doi: 10.1109/EDUCON60312.2024.10578734
[13] R. Bringula, “ChatGPT in a programming course: Benefits and limitations,” *Frontiers in Education*, vol. 9, art. no. 1248705, 2024.
[14] M. Zhu, L. Xu, and B. Ericson, “A systematic review of research on large language models for computer programming education,” *arXiv Preprint*, 2023. doi: 10.48550/arXiv.2506.21818
[15] M. Jukiewicz, “The future of grading programming assignments in education: The role of ChatGPT in automating the assessment and feedback process,” *Computers & Education: Artificial Intelligence*, vol. 6, art. no. 100191, 2024.

2nd International Conference on Multidisciplinary Sciences and Technological Developments (ICMUSTED 2025)

December 12-15, 2025

AI-Based Anomaly Detection in Agricultural Farms Using Drone Data and Deep Learning

Berrimi Fella[1]

[1]Department of Computer Science, Ferhat Abbas University-Setif 1, Setif, Algeria
Corresponding author: Berrimi Fella (e-mail: berrimifella@gmail.com)

Abstract

This work focuses on the detection of anomalies in agricultural farms using artificial intelligence (AI) techniques applied to computer vision and deep learning. The data were collected by drones that capture high-resolution images of olive farms, providing large-scale and real-time monitoring. In our contribution, we developed a you only look once (YOLO)-based model to detect olive trees and classify them into two categories: healthy trees and trees with anomalies such as disease symptoms and structural irregularities. Furthermore, the system was extended to detect harmful animals, including rats and other intruders that threaten the olive trees. Experiments were carried out on an olive tree dataset specifically prepared for this study, and the model achieved promising results with an F1-score of 0.94 and a precision of 0.95. Compared with traditional manual inspection, our AI-based approach demonstrates higher reliability and efficiency, offering a practical solution for smart agriculture. This integration of drones and YOLO-based deep learning models enhances productivity and sustainability by enabling early detection of anomalies, reducing crop losses, and ensuring better resource management.

Keywords: YOLO, Deep learning, Smart agriculture, Anomaly detection

2nd International Conference on Multidisciplinary Sciences and Technological Developments (ICMUSTED 2025)

December 12-15, 2025

Bone Fracture Classification Analysis Base Machine Learning Algorithms

Ei Phyu Sin Win[1]

[1]Computere Engineering and Information Technology Department, Mandalay Technological University, Mandalay, Myanmar
Corresponding author: Ei Phyu Sin Win (e-mail: panthakhin9001@gmail.com)

Abstract

Accurate classification of bone fractures is essential for diagnosis, treatment planning, and patient rehabilitation. Manual evaluation of medical images can be slow and prone to error. Recent advancements in machine learning have enabled the development of automated systems capable of reliably analyzing radiographic images. In this study, supervised learning methods, including convolutional neural networks, support vector machines, and random forests, were used to categorize fractures across various anatomical regions. Image preprocessing, such as normalization, noise reduction, and feature extraction, was performed to improve data quality and model performance. Labeled X-ray and computed tomography (CT) scan datasets were employed for training and validation. Model performance was assessed using multiple metrics: training accuracy 99.85%, precision 99%, recall 1, and F1-score 99%. Results showed that deep convolutional neural networks with optimized hyperparameters outperformed traditional machine learning models in both accuracy and generalization. Hybrid approaches combining handcrafted features with deep representations were effective when computational resources were limited. The study emphasized the importance of high-quality datasets, balanced class distributions, and interpretable models for clinical applications. Future improvements may include integration with hospital information systems, explainable artificial intelligence (AI), and real-time decision support tools to enhance collaboration between medical professionals and automated diagnostic systems. When proper validation and ethical guidelines are followed, machine learning can accelerate fracture classification, minimize diagnostic delays, and improve patient outcomes. Testing on 100 previously unseen images yielded an accuracy of 99.8%. All experiments were conducted using Python IDLE Shell 3.12.8.

Keywords: Bone fracture classification, Artificial intelligence, Radiographic image analysis, Deep learning, Clinical decision support

2nd International Conference on Multidisciplinary Sciences and Technological Developments (ICMUSTED 2025)

December 12-15, 2025

Large Language Model–Assisted Hardware Design: Insights from the Ascon-128 Implementation

Latif Akcay[1]

[1]Department of Computer Engineering, Erzurum Technical University, Erzurum, Türkiye
Corresponding author: Latif Akcay (e-mail: latif.akcay@erzurum.edu.tr)

Abstract

Large language models (LLMs) have emerged as important tools in software and hardware design in recent years. In this study, widely used LLMs are compared on the hardware design of the Authenticated Encryption with Associated Data (Ascon-AEAD128), a current and standard authenticated encryption method. The efficacy of LLMs is investigated by evaluating various parameters, including hardware description code generation, test case development, synthesis script creation, and the proper allocation of ports to the field-programmable gate array (FPGA) structure. The functionality of the generated designs is demonstrated through FPGA resource utilization, maximum clock frequency, performance, and efficiency metrics. Furthermore, the degree of convergence between previously manually developed designs and artificial intelligence (AI)-generated designs is examined, along with current shortcomings and potential improvements. Experimental results clearly demonstrate that LLMs can significantly increase the efficiency of hardware design and implementation. However, the findings clearly indicate that AI methods still have certain limitations in cryptographic hardware development. This study provides valuable insights into future AI-assisted electronic design automation processes and serves as a guide for the development of similar hardware models.

Keywords: LLM-aided hardware design, AI-assisted hardware, AEAD, Lightweight cryptography, FPGA

1. INTRODUCTION

Large language models (LLMs), with the introduction of the revolutionary transformer architecture, have gained significant capabilities in areas such as context recognition, reasoning, structure generation, and domain adaptation [1]. This development has also sparked the idea of models automatically performing tasks previously performed manually by experts in fields such as software engineering, code generation, system design, and implementation. Indeed, numerous studies have been conducted in recent years demonstrating that such processes can be accelerated with the support of artificial intelligence (AI) [2–4]. In the last few years, there has been increasing interest in applying this useful tool, LLMs, to hardware design workflows. Previous models that lacked synthesizability, misunderstood context, and confused software and hardware design concepts have been replaced by models that avoid these simple errors and produce more systematic and domain-aware code. These advanced models, which not only generate code with hardware description languages (HDLs) but also can write scripts that automatically use synthesis and simulation tools, appear poised to significantly speed up these processes, which require considerable effort and time for engineers. On the other hand, the fact that they still cannot perform all these tasks with very high accuracy and the risk of error raises some questions, especially in applications where security is very important, such as cryptography.

Lightweight authenticated encryption algorithms play a critical role in ensuring data security in resource-constrained embedded systems and platforms such as the Internet of Things (IoT), where energy consumption, silicon area, and latency are critical. The Ascon family was recently officially recognized by the National Institute of Standards and Technology (NIST) in the SP 800-232 specification as a result of work conducted within the Lightweight Cryptography standardization process [5]. The family includes the Authenticated Encryption with Associated Data (Ascon-AEAD128) algorithm, the hash method (Ascon-Hash), and the extendable output functions (Ascon-XOF128 and Ascon-CXOF128). Their permutation-based structures, round-based state transformations, and bitwise operations provide a meaningful benchmark for testing and comparing the automatic HDL code generation capabilities of modern LLMs.

In this study, three state-of-the-art LLMs are evaluated from various perspectives, each being directed to generate synthesizable Ascon-AEAD128 hardware using identical prompts. Each model was asked to generate register transfer level (RTL) implementation, a verification testbench, and design constraints for a specific field-

programmable gate array (FPGA), and tests were run using the generated outputs. Despite the absence of any published studies on this subject, there are several studies that highlight potential security issues associated with generating cryptographic hardware using LLMs [6, 7]. Furthermore, many survey studies have been conducted comparing hardware code generation using LLMs, identifying existing shortcomings and challenges, and addressing future actions [8–10].

The remainder of this paper is organised as follows: Section II describes the preferred prompt strategy and hardware design considerations in the study, as well as providing a summary of the Ascon family. Section III presents the synthesis and simulation results, offering a comparative evaluation of the three LLMs. Section VI concludes the paper by highlighting directions for future work on LLM-assisted hardware design and implementation.

2. BACKGROUND AND DESIGN METHOD

In this section, a brief summary of Ascon-AEAD128 and the applied design methodology is provided.

2.1. Ascon-AEAD128

Ascon-AEAD128 is an efficient encryption method designed for data security and confidentiality in resource-constrained embedded systems. Built on the Sponge architecture, the algorithm uses a 320-bit internal state, which is divided into five 64-bit words and then transformed (permuted) on them. The encryption process consists of three main stages: initialization, associated data processing, plaintext processing, and authentication tag computation. In the first stage, the state is initialized using the key and nonce. In the second stage, the state is updated with associated data. Then, in the third stage, the encryption process is performed by injecting message blocks. Finally, the encryption and authentication process is completed by generating a 128-bit authentication tag. Ascon-AEAD128 offers a highly efficient infrastructure for both software and hardware applications, offering low chip area, low power consumption, high performance, and resistance to side-channel analysis. Figure 1 shows the computation stages for both encryption and decryption operations.

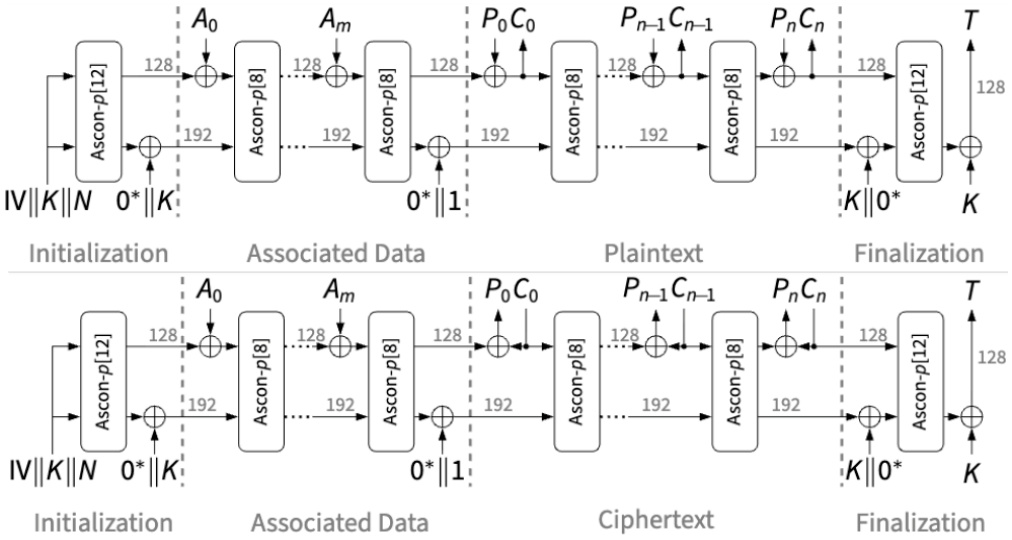

Figure 1. Ascon-AEAD128 authenticated encryption (top) and decryption (bottom) [5]

2.1. Prompting Strategy

In this study, the state-of-the-art LLMs ChatGPT 5.1 [11], Gemini 3 Pro [12], and Claude Sonnet 4.5 [13] were guided by a unified prompt strategy to perform the same task. Figure 2 shows the identical prompt entered all three LLMs. After generating the RTL and test codes, a common prompt, as shown in Figure 3, was used to create input-output constraints for the Xilinx AC701 Evaluation Platform [14] in accordance with a top-level wrapper module.

The main reason behind our prompting strategy is to compare LLMs under consistent input conditions. This allows for a fair assessment of the models' capabilities, such as code correctness and integrity, architectural preferences, and reasoning. Following HDL generation, simple behavioural simulations were run to verify that the encryption hardware generated before synthesis performed correctly at this level. Figure 4 presents an illustrative example of the waveform. This ensures that performance differences are not affected by runtime logic errors but rather stem

from the design capabilities of each model. The two-stage prompting methodology, first design and then generate constraints, allows to separately evaluate each LLM's inherent hardware design capabilities and platform-specific script generation capabilities, minimizing potential prompt-related errors.

Implement the lightweight cryptography standard Ascon-AEAD128 using Verilog as hardware. Create separate implementations for encryption and decryption. Also, prepare testbench code for both designs. Consider the following specifications:

DETAILED SPECIFICATIONS:
1. **Parameters:**
- Key: 128-bit
- Nonce: 128-bit
- Associated Data: 128-bit
- Data Block: 64-bit
- Tag: 128-bit
- State: 320-bit

2. **Permutation Parameters:**
- p^a: 12 rounds (initialization and finalization)
- p^b: 6 rounds (data processing)

3. **Mathematical Operations:**
- S-box layer: 5-bit S-box (for x0, x1, x2, x3, x4)
- Diffusion layer: Column mixing
- Round constants: 12 different round constants

4. **Interface Signals:**

input clk, reset_n, start, encrypt_decrypt;

input [127:0] key, nonce, assoc_data;

input [63:0] data_in;

output reg [63:0] data_out;

output reg [127:0] tag;

output reg ready, valid;

5. **FSM States:**

IDLE, INIT, PROCESS_AD, ENCRYPT (DECRYPT),

FINALIZE, DONE

6. **Desired Format:**

First, define the module interface, then create the FSM, then write the permutation functions. Detail each step with comments.

7. **Requirements for the Verilog Output:**

- A fully synthesizable design (not applicable for testbenches)

- FSM-based controller

- Ready/valid handshake protocol

- 1 round of computation per clock cycle

- Testbench-friendly signals

Also implement/check the following:

--Explain each code section line by line

--First the interface, then the FSM, then the logic

--Is there a potential race condition in this code?

Figure 2. Unified prompt for the three LLMs for Ascon-AEAD128 hardware implementation

I want to synthesize your Ascon-AEAD128 design using Vivado for FPGA. The Xilinx AC701 Evaluation Platform will be used as the development board. To do this, first write a top-level wrapper module. Then create a corresponding xdc file. Check the wrapper and xdc codes you generated and correct any mismatched pins.

Figure 3. Common prompt for input-output (I/O) specifications

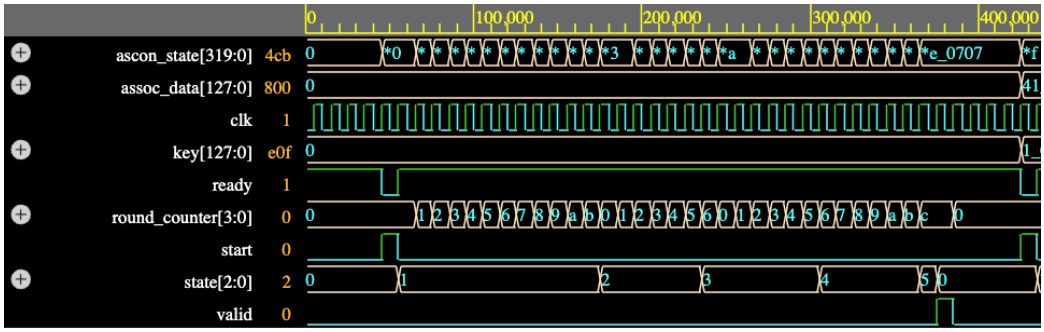

Figure 4. A fragment of simulation waveform from the Ascon-AEAD128 core generated by Claude 4.5 Sonnet

3. SYTHESIS AND EVALUATION RESULTS

In this section, the synthesis results for the LLM-generated Ascon-AEAD128 cores are presented. In addition, the hardware design capabilities and shortcomings of the evaluated models are discussed based on the findings obtained from this study.

3.1. Synthesis Results

Xilinx Vivado Integrated Design Environment (IDE) [15] was used to synthesize the Ascon-AEAD cores generated by the evaluated LLMs. Table 1 shows the FPGA resource utilization achieved by running the tool with the default strategy, the maximum clock frequency at which designs can be synthesized, and the total number of cycles (NoC) required to complete an encryption operation. As can be easily noticed, Cluade 4.5's design operates at a much lower frequency than other models. This is due to the deep combinational logic in the permutation function. The design was developed to perform round constant XOR (64-bit), S-box layer (320-bit parallel S-box, very complex), linear diffusion layer (320-bit rotation + XOR), and state write-back operations in a single cycle. As expected, this extended the critical path and caused a slight decrease in NoC performance. Furthermore, the dramatically high lookup table (LUT) count is due to the use of nested function calls within the permutation function. When Vivado cannot inline these nested functions, it creates separate combinational logic for each function call. On the other hand, Gemini 3 Pro and ChatGPT 5.1 used a similar design approach. The difference in the number of flip-flops (FFs) is due to the hard-coded test data used by Gemini 3 Pro in the top-level wrapper module.

Table 1. Synthesis and performance results of Ascon-AEAD128 implementations on FPGA

LLM	LUTs	FFs	Frequency	NoC
ChatGPT 5.1	946	673	200 MHz	45
Gemini 3 Pro	1187	1181	200 MHz	52
Claude Sonnet 4.5	2864	520	50 MHz	32

3.2. Evaluation of HDL and Constraint Generation by LLMs

Table 2 presents an exhaustive and comparative evaluation of the three LLMs in terms of HDL code quality, functional correctness, synthesis readiness, and constraint generation capability. Furthermore, additional criteria were defined regarding the ability of models to analyse and correct their errors. This evaluation format provides a direct measurement of design reliability and efficiency of each model for automated cryptographic hardware design. Based on the analysis and experience gained from various stages of the study, it is possible to claim that the Claude Sonnet 4.5 model stands out as the most useful design aid among those compared, although it is not the best in every criterion. However, the design approach, which caused the model to consume more hardware resources compared to other models, also resulted in a decrease in clock frequency. Fortunately, the model is also effective at detecting and correcting these errors through feedback.

Table 2. Benchmarking HDL generation and design constraint reliability across LLMs

Evaluation Criteria	ChatGPT 5.1	Gemini 3 Pro	Claude Sonnet 4.5
Code Synthesizability	High	High	High
Functional Correctness	High	High	High
Completeness of Implementation	High	High	High
Readability / Maintainability	High	High	High
Language Standard Compliance	Moderate	Moderate	High
Correctness of Constraints	Low	High	Moderate
Completeness of XDC File	High	High	High
Resource Utilization Efficiency	High	High	Low
Timing Closure Success	High	High	Low
Implicit Enhancement Capability	Low	Moderate	High
Test Case diversity and quality	Low	Moderate	High
Design Reasoning Depth	High	High	High
Self-Correction Ability	Moderate	High	High

4. CONCLUSION

LLMs have been increasingly used in a wide range of applications in recent years. In this context, LLM-aided hardware design has recently become a hot research area. This is shaping the future of electronic design automation (EDA). This study presents a comparative evaluation of three widely used LLMs using a cryptographic hardware design task to demonstrate their readiness for this new era. The same tasks were assigned to the compared models with a common prompting strategy. After that, simulation and synthesis operations were performed for an FPGA platform with the produced outputs. The results were evaluated both in terms of FPGA implementation and in terms of the success of the models in the design, verification, and debugging processes. Despite some serious shortcomings, LLMs are quite promising in terms of providing significant efficiency gains in hardware design.

Acknowledgments

This study involved the comparison of three LLMs (Claude 4.5 Sonnet, ChatGPT 5.1, and Gemini 3 Pro) for HDL code generation. The LLMs were used as research subjects for comparative analysis, not as co-authors or content generators for this manuscript.

References

[1] Y. Mo, H. Qin, Y. Dong, Z. Zhu, and Z. Li, "Large language model (LLM) AI text generation detection based on transformer deep learning algorithm," *arXiv*, 2024. doi: 10.48550/ARXIV.2405.06652

[2] S. Bistarelli, M. Fiore, I. Mercanti, and M. Mongiello, "Usage of large language model for code generation tasks: A review," *SN Comput. Sci.*, vol. 6, no. 6, Jul. 2025. doi: 10.1007/s42979-025-04241-5

[3] Y. Dong, X. Jiang, J. Qian, T. Wang, K. Zhang, Z. Jin, et al., "A survey on code generation with LLM-based agents," *arXiv*, 2025. doi: 10.48550/ARXIV.2508.00083

[4] M.-F. Wong, S. Guo, C.-N. Hang, S.-W. Ho, and C.-W. Tan, "Natural language generation and understanding of big code for AI-assisted programming: A review," *Entropy*, vol. 25, no. 6, art. no. 888, Jun. 2023. doi: 10.3390/e25060888

[5] M. S. Turan, "Ascon-based lightweight cryptography standards for constrained devices: Authenticated encryption, hash, and extendable output functions," *NIST*, Jan. 2025. doi: 10.6028/nist.sp.800-232

[6] Z. Ibnat, P. Calzada, D. Saha, H. Al-Shaikh, S. K. Saha, J. Zhou, et al., "Trusting the machine: How secure is LLM-generated RTL code?," in *2025 ACM/IEEE 7th Symposium on Machine Learning for CAD (MLCAD)*, Santa Cruz, CA, USA, 2025, pp. 1–8. doi: 10.1109/MLCAD65511.2025.11189213

[7] R. Afsharmazayejani, M. M. Shahmiri, P. Link, H. Pearce and B. Tan, "Toward Hardware Security Benchmarking of LLMs," in *2024 IEEE LLM Aided Design Workshop (LAD)*, San Jose, CA, USA, 2024, pp. 1–7. doi: 10.1109/LAD62341.2024.10691745

[8] M. Abdollahi, S. F. Yeganli, M. (Amir) Baharloo, and A. Baniasadi, "Hardware design and verification with large language models: A scoping review, challenges, and open issues," *Electronics,* vol. 14, no. 1, art. no. 120, Dec. 2024. doi: 10.3390/electronics14010120

[9] H. Huang, Z. Lin, Z. Wang, X. Chen, K. Ding, and J. Zhao, "Towards LLM-powered verilog RTL assistant: Self-verification and self-correction," *arXiv*, 2024. doi: 10.48550/ARXIV.2406.00115

[10] G. Yang, W. Zheng, X. Chen, D. Liang, P. Hu, Y. Yang, et al., "Large language model for verilog code generation: Literature review and the road ahead," *MDPI AG,* 2025. doi: 10.20944/preprints202511.0656.v2

[11] ChatGPT 5.1, OpenAI, "Response to prompts on LLM-assisted Ascon-128 hardware design," [Online]. Available: https://chat.openai.com/. [Accessed Nov., 2025].

[12] Gemini 3 Pro, Google, "Generated Verilog/RTL for Ascon-128 encryption core and testbench," [Online]. Available: https://gemini.google.com/. [Accessed Nov., 2025].

[13] Claude Sonnet 4.5, Anthropic, "LLM-based hardware implementation assistance for cryptographic design," [Online]. Available: https://claude.ai/. [Accessed Nov., 2025].

[14] Xilinx, "AC701 evaluation board for the Artix-7 FPGA – User guide UG952," v1.3 [Online], 2015. Available: https://www.xilinx.com/support/documentation/boards_and_kits/artix-7/ac701_ug/v1_0/ug952-ac701-a7-eval-bd.pdf

[15] Xilinx, "Vivado design suite," White Paper WP416, Rev. 1.1, [Online], Jun. 22, 2012. Available: https://docs.amd.com/v/u/en-US/wp416-Vivado-Design-Suite

2nd International Conference on Multidisciplinary Sciences and Technological Developments (ICMUSTED 2025)

December 12-15, 2025

Indoor Particulate Matter Levels in the Department of Environmental Engineering at Eskisehir Technical University, Türkiye

Melike Cengel[1], Ozlem Ozden Uzmez[1]

[1]Environmental Engineering, Eskisehir Technical University, Eskisehir, Türkiye
Corresponding author: Ozlem Ozden Uzmez (e-mail: oozden@eskisehir.edu.tr)

Abstract

Universities are defined as centres of knowledge and innovation, where young generations engage in educational and research activities. Consequently, indoor air quality (IAQ) within university campuses is of great importance for the health and well-being of students, academics, and other staff. Good IAQ can enhance learning capacity and academic performance, whereas poor IAQ can lead to respiratory illnesses, allergies, and reduced concentration. Detailed air quality studies in universities are essential to mitigate potential risks and provide a healthy learning environment. In this study, IAQ was assessed in selected locations within the Environmental Engineering Department at the Iki Eylul Campus of Eskisehir Technical University by simultaneously measuring particulate matter (PM) pollutants (PM_{10} and $PM_{2.5}$) using a DustTrakII online monitoring device. Measurements were carried out at the most frequently occupied locations by students and staff during peak weekdays and lecture hours. The results revealed that laboratories and offices had the highest IAQ, while high-traffic areas—including corridors and cafeterias—showed increased PM levels. Restrooms and classrooms exhibited a moderate air quality profile. However, PM_{10} concentrations were found to be consistently higher than $PM_{2.5}$ concentrations at all locations. An assessment of the indoor-to-outdoor (I/O) ratio showed that I/O values exceeded 1 at all sampling locations, suggesting that indoor sources were the primary contributors to PM concentrations. These results highlight the importance of identifying and controlling internal pollutant sources to ensure healthier IAQ within university settings.

Keywords: Air pollution, Indoor air quality, University campus, Particulate matter

1. INTRODUCTION

With the increase in population, human activities have been growing, leading to a negative impact on air quality. Indoor air quality (IAQ) refers to the quality of the air that is inhaled in enclosed spaces and has a significant effect on human health. Since people spend approximately 90% of their time indoors, the importance of IAQ is becoming increasingly critical.

Indoor air pollution can stem from various sources such as activities within indoor spaces, materials used, and pollutants infiltrating from the outside. These pollutants include dust, smoke, chemical vapours, biological contaminants, and gases such as radon. Prolonged exposure to indoor air pollution can lead to health problems such as allergies, asthma, and sick building syndrome.

Universities are considered centres of knowledge and innovation, where young generations continue their educational and research activities. Therefore, IAQ at the university campuses is great significance for the health of students, academics, and other staff members. Good IAQ can enhance learning capacity and academic performance, while poor IAQ may lead to respiratory diseases, allergies, and issues such as lack of concentration. Detailed air quality studies conducted in universities are essential to mitigate potential risks and ensure a healthy learning environment.

Particulate matter (PM) is defined as a mixture of chemically and physically diverse substances that exist as discrete particles (either liquid droplets or solid matter) across a wide range of sizes. These particles originate from a variety of anthropogenic stationary and mobile sources, as well as natural sources such as wildfires. When outdoor air enters indoor environments through windows and doors, it also brings in PM. A fine fraction of this mixture is known as $PM_{2.5}$. Fine particles are primarily generated through combustion processes such as those from power plants, gasoline and diesel engines, wood burning, and many industrial activities as well as from atmospheric reactions involving gaseous pollutants. Fine PM can penetrate deeply into the lungs, reaching the alveolar sacs where oxygen exchange with the bloodstream occurs [1]. PM_{10} refers to particles with an

aerodynamic diameter of 10 micrometres (μm) or smaller, representing inhalable particles small enough to penetrate deeply into the respiratory tract [1].

In 2022, Bhat et al. aimed to investigate indoor and outdoor air quality at the campus of Eskisehir Technical University in Eskisehir, Türkiye during the COVID-19 pandemic [2]. The study included measurements of various gaseous pollutants (SO_2, NO_2, O_3), fine PM ($PM_{2.5}$), total bacteria, and total fungi. The study employed passive sampling to measure gaseous pollutants, used DustTrak aerosol monitors to determine $PM_{2.5}$ concentrations, and quantified total bacterial and fungal levels using passive sampling methods. Measurements were conducted in various indoor and outdoor locations across the campus. The findings indicated that, in most indoor environments, the indoor/outdoor (I/O) ratios for PM were greater than 1. An improvement in IAQ at the university campus was observed during the pandemic. This study sought to quantitatively evaluate the pandemic's effect on air quality and lays the groundwork for future follow-up investigations.

In 2023, Onat et al. conducted an evaluation of IAQ and thermal comfort conditions in the Environmental Engineering Laboratories at Istanbul University–Cerrahpasa [3]. The objective of the study was to determine PM_4 and CO_2 concentrations in the university laboratories and to examine their effects on IAQ. The research involved PM_4 sampling and monitoring of CO_2 and thermal comfort parameters (relative humidity, temperature, air velocity, and lighting) in five different laboratories. PM_4 samples were collected on quartz filters, and the concentrations of heavy metals were determined using Graphite Furnace Atomic Absorption Spectrometry. The results showed that the 8-hour average PM_4 levels ranged between 57.0 and 186.3 $\mu g/m^3$. The highest mean concentration was detected in Lab C, where pyrolysis and solid waste incineration processes took place. CO_2 levels varied from 484 to 666 ppm, and increased to as high as 2000 ppm in Lab B during active laboratory sessions. It was also determined that lighting levels in all laboratories were not in compliance with standards and that ventilation rates were inadequate. The study recommends opening windows or doors to prevent CO_2 build-up in the laboratories and suggests improving the existing lighting systems. Additionally, the use of fume hood exhaust fan systems was proposed to enhance both ventilation rates and particulate filtration.

In the study of Xie et al. carried out in 2022 [4], they conducted a study to evaluate indoor $PM_{2.5}$ exposure and the associated potential inhalation dose during the winter season at a university campus in Beijing. The primary objective of the study was to determine the contribution of outdoor air pollution to indoor $PM_{2.5}$ levels and to university students' personal exposure. The study involved collecting $PM_{2.5}$ samples from six indoor settings—classroom, student office, laboratory, cafeteria, dormitory, and other indoor areas—alongside samples from two outdoor locations. Students' daily personal exposure and potential inhalation dose were measured on both hazy and clear days. The findings revealed that daily personal exposure (124.8 ± 72.3 $\mu g/m^3$) and potential inhalation dose (2.74 ± 1.53 mg) were significantly higher on hazy days compared to clear days (57.5 ± 31.9 $\mu g/m^3$ and 1.26 ± 0.59 mg, respectively). A positive correlation was observed between indoor and outdoor $PM_{2.5}$ concentrations, and it was determined that outdoor sources accounted for 68–95% of the total indoor $PM_{2.5}$ levels.

The outdoor PM levels at Eskisehir Technical University's Iki Eylul Campus are influenced by its rural location, distant from the city centre, as well as by daily aircraft operations at the university-owned airfield and heavy vehicular traffic. As a result, the transfer of PM from outdoor air to indoor environments via natural ventilation is possible. Students, faculty, and staff who breathe indoor air are consequently exposed to PM. Therefore, assessing indoor PM levels is of particular importance.

A review of the literature indicates that relatively few studies have specifically examined indoor PM concentrations in university settings. Furthermore, studies that simultaneously measure PM at multiple indoor locations are particularly scarce, underscoring the importance of this research. Incorporating the findings of this study into the international literature is also essential for enhancing the visibility and recognition of national research efforts.

This study aims to assess indoor air pollution exposure in the Department of Environmental Engineering at Eskisehir Technical University's Iki Eylul Campus in Eskisehir, Türkiye by measuring PM concentrations in the areas most frequently occupied by students and academic staff.

$PM_{2.5}$ and PM_{10} concentrations were measured simultaneously at six selected sites within the department: a classroom, corridor, restroom, cafeteria, laboratory, and office. Indoor and outdoor PM levels were measured simultaneously using DustTrak real-time monitoring devices. The devices were activated during periods of low activity, operated continuously throughout peak hours, and deactivated once activity subsided. During the measurements, variations in PM levels resulting from occupancy and movement were monitored to identify potential sources. The study also aimed to evaluate the impact of outdoor PM concentrations on IAQ.

2. MATERIAL AND METHOD

2.1. Study Area and Measurement Points

Eskisehir Technical University's Iki Eylul Campus is located at the coordinates 39.814693° latitude and 30.533587° longitude. It is situated in the Gazipasa within the Tepebasi district of Eskisehir in Türkiye. The campus lies to the north of the city, at an elevation of 787 meters above sea level. The campus is 6.4 kilometres away from the city centre. Covering a total area of 4.530.000 square meters, the campus includes 273.330 square meters of green space. While there are few residential areas surrounding the campus, the closest settlement is Muttalip, located 8.7 kilometres away.

Iki Eylul Campus hosts four faculties: Faculty of Engineering, Faculty of Architecture and Design, Faculty of Aviation and Space Sciences, and Faculty of Sports Sciences. Additionally, it houses two institutes: Graduate School of Education and Institute of Earth and Space Sciences. The campus also includes one indoor sports hall, a stadium, School of Foreign Languages, and the university-owned Hasan Polatkan Airport. Figure 1 shows the layout of the Environmental Engineering Department.

Figure 1. Environmental Engineering Department of the Eskisehir Technical University Engineering Faculty

The Department of Environmental Engineering is located within the Faculty of Engineering, positioned between the Departments of Mechanical Engineering and Civil Engineering. There are shared passage corridors and a cafeteria connecting these departments. The Department of Environmental Engineering serves a total of 430 students, 23 academic staff members, and 2 technical personnel. It contains 7 classrooms and 12 laboratories. As mentioned before, $PM_{2.5}$ and PM_{10} concentrations were measured simultaneously at six selected points in the department: classroom, corridor, restroom, cafeteria, laboratory, and office.

2.2. Measurement Program

The measurements were conducted during weekday class hours, when student and academic staff presence was at its peak. Data were collected in the cafeteria, office, corridor, restroom, classroom, and laboratory on days with the busiest class schedules. The instruments were operated fifteen minutes before peak occupancy began and turned off fifteen minutes after occupancy declined, allowing for the observation of pollutant concentration variations over a minimum measurement period of one hour. The measurement durations and locations are presented in Table 1.

Table 1. Measurement Durations and Locations

Measurement Point No	Measurement Point	Measurement Duration (hr:min)
1	Classroom	01:05
2	Cafeteria	02:13
3	Corridor	01:13
4	Laboratory	02:32
5	Office	01:37
6	Restroom	01:15
7	Outdoor	01:38

2.3. DustTrakII Monitoring Devices

The DustTrakII Aerosol Monitor used for PM measurements is an online dust monitoring device capable of simultaneously measuring both mass and size fractions. It is suitable for indoor and outdoor applications, industrial and occupational hygiene assessments, preliminary screening, remote monitoring, and research studies.

Within the Department of Environmental Engineering at Eskişehir Technical University, two DustTrakII Aerosol Monitor 8530 units are available. In this study, simultaneous measurements of indoor $PM_{2.5}$ and PM_{10} levels were conducted using these two devices.

The calibration of the DustTrakII Aerosol Monitors were performed by the manufacturer. To ensure the calibration accuracy of the devices, they were operated simultaneously for 30 minutes using the same inlet before the measurement campaign began, and their results were cross-checked ($R^2 = 0.95$). A zero calibration was conducted before each measurement.

3. RESULTS

3.1. $PM_{2.5}$ Measurement Results

The maximum, minimum, and average values of $PM_{2.5}$ concentrations at all measurement locations are presented in Table 2.

Table 2. The maximum, minimum, and average values of $PM_{2.5}$ concentrations

Measurement Point	Average (µg/m^3)	Maximum (µg/m^3)	Minimum (µg/m^3)	Measurement Duration (Min)
Classroom	23.00 ± 1.33	25.00	21.00	65
Cafeteria	107.00 ± 25.31	187.00	63.00	133
Corridor	104.00 ± 6.44	122.00	95.00	73
Laboratory	60.00 ± 9.14	105.00	50.00	152
Office	44.00 ± 6.63	63.00	36.00	97
Restroom	98.00 ± 1.70	102.00	95.00	75
Outdoor	20.00 ± 8.72	47.00	10.00	98

In Figure 2, average indoor and outdoor $PM_{2.5}$ concentrations are given. According to the measurement results, the average concentrations, in descending order, are as follows: cafeteria > corridor > restroom > laboratory > office > classroom > outdoor environment.

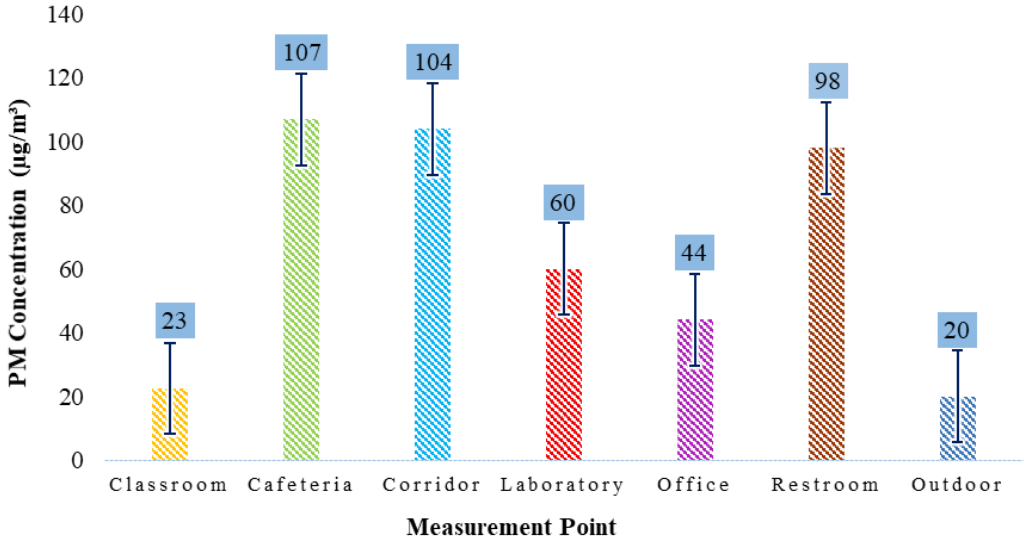

Figure 2. Average values of $PM_{2.5}$ concentrations

i. Classroom: In the classroom environment, $PM_{2.5}$ measurements revealed an average concentration of 23.00 ± 1.33 µg/m^3, ranging from 21.00 to 25.00 µg/m^3. The initially high $PM_{2.5}$ levels were linked to increased human activity immediately after the previous class, as student movement caused resuspension of settled dust. Once students were seated and movement subsided, $PM_{2.5}$ concentrations stabilized, showing minimal fluctuations and highlighting the significant impact of occupant behaviour on indoor particulate levels. Other potential contributors to $PM_{2.5}$ in the classroom include infiltration of smoke and emissions from heating systems during winter, ongoing human activity, and electronic device operation [5].

ii. Cafeteria: $PM_{2.5}$ measurements in the small cafeteria shared by the Environmental, Mechanical, and Civil Engineering Departments showed concentrations between 63.00 and 187.00 µg/m^3, with an average value of 107.00 ± 25.31 µg/m^3. $PM_{2.5}$ concentrations peaked around 11:00 a.m., corresponding to high student movement at the end of classes, and were lowest just before 11:00 a.m. during minimal activity. These results underscore the significant and immediate impact of human presence and activity on indoor PM concentrations. Beyond particle resuspension caused by movement, food preparation—especially high-temperature cooking methods such as frying and grilling—represents a major source of $PM_{2.5}$ emissions, primarily due to the combustion of oils and other organic materials [6].

iii. Corridor: $PM_{2.5}$ concentrations in the shared corridor between the Environmental and Civil Engineering Departments, heavily trafficked by students from both programs, ranged from 95.00 to 122.00 µg/m^3, with an average of 104.00 ± 6.44 µg/m^3. Peak levels were recorded around 11:00 a.m., coinciding with the end of classes or scheduled breaks, reflecting increased particulate resuspension due to human movement. In addition to occupant activity, cleaning practices also affected $PM_{2.5}$ levels, as improper methods contributed to the re-entrainment of settled dust, further elevating particulate concentrations.

iv. Laboratory: $PM_{2.5}$ concentrations in the Environmental Chemistry Laboratory, where students conduct experiments on water quality parameters such as alkalinity, acidity, and hardness, ranged from 50.00 to 105.00 µg/m^3, with an average value of 60.00 ± 9.14 µg/m^3. Observations indicate that student presence and laboratory activities had minimal impact on particulate levels, whereas peak $PM_{2.5}$ concentrations were associated with post-occupancy cleaning procedures. Principal contributors to PM in laboratory settings include vapours released during chemical reactions—particularly those involving combustion—solvent evaporation, aerosol usage, and mechanical wear from laboratory equipment operation [7].

v. Office: Indoor $PM_{2.5}$ concentrations were monitored in an office over the course of a full day during which it was occupied by a single academic staff member. Recorded levels ranged from 36.00 to 63.00 µg/m^3, with an average concentration of 44.00 ± 6.63 µg/m^3. The highest $PM_{2.5}$ levels were observed at the beginning of the monitoring period, likely associated with occupant activity and the use of electronic devices, whereas the lowest concentrations coincided with periods of vacancy. These findings underscore the influence of human presence on indoor PM levels. Additional potential sources of $PM_{2.5}$ in the office environment include emissions from electronic equipment such as printers and photocopiers.

vi. Restroom: $PM_{2.5}$ concentrations in the restroom were measured in the girls' restroom, identified as the most frequently used facility within the department, during a day with high classroom occupancy. Observed $PM_{2.5}$ levels ranged from 95.00 to 102.00 µg/m^3, with an average value of 98.00 ± 1.70 µg/m^3. The lowest concentrations were recorded during periods of inactivity, while peak levels coincided with the end of classes, reflecting increased restroom usage. Elevated $PM_{2.5}$ in this environment can be attributed to multiple factors, including human movement, flushing of toilets, operation of hand dryers, use of cleaning agents, and application of aerosols such as perfumes and deodorants.

vi. Outdoor: To examine the effect of outdoor air quality on IAQ, outdoor pollutant measurements were conducted simultaneously with the indoor measurements. The recorded concentrations ranged between 10.00 to 47.00 µg/m^3, with an average of 20.00 ± 8.72 µg/m^3. The primary sources of outdoor $PM_{2.5}$ were identified as vehicle emissions from the main roads on and around the campus. Since the measurements were conducted during the winter season, emissions from heating activities, including smoke and vapours, may have also contributed to particulate levels. Overall, outdoor $PM_{2.5}$ concentrations were considerably lower than those observed indoors, likely due to the campus's rural setting and the absence of conditions favourable to PM formation, such as warm, dry, or humid air typical of other seasons.

3.2. PM_{10} Measurement Results

The maximum, minimum, and average values of PM_{10} concentrations at all measurement locations are presented in Table 3.

Table 3. The maximum, minimum, and average values of PM_{10} concentrations

Measurement Point	Average (µg/m^3)	Maximum (µg/m^3)	Minimum (µg/m^3)	Measurement Duration (Min)
Classroom	34.00 ± 4.80	28.00	45.00	65
Cafeteria	115.00 ± 26.98	238.00	71.00	133
Corridor	121.00 ± 7.85	146.00	110.00	73
Laboratory	70.00 ± 5.91	104.00	62.00	152
Office	56.00 ± 7.30	75.00	46.00	97
Restroom	114.00 ± 3.57	120.00	107.00	75
Outdoor	30.00 ± 9.25	61.00	20.00	98

According to the measurement results, the average PM_{10} concentrations, in descending order, are as follows: corridor> cafeteria>restroom>laboratory>office>classroom>outdoor environment. In Figure 3, average indoor and outdoor PM_{10} concentrations are given.

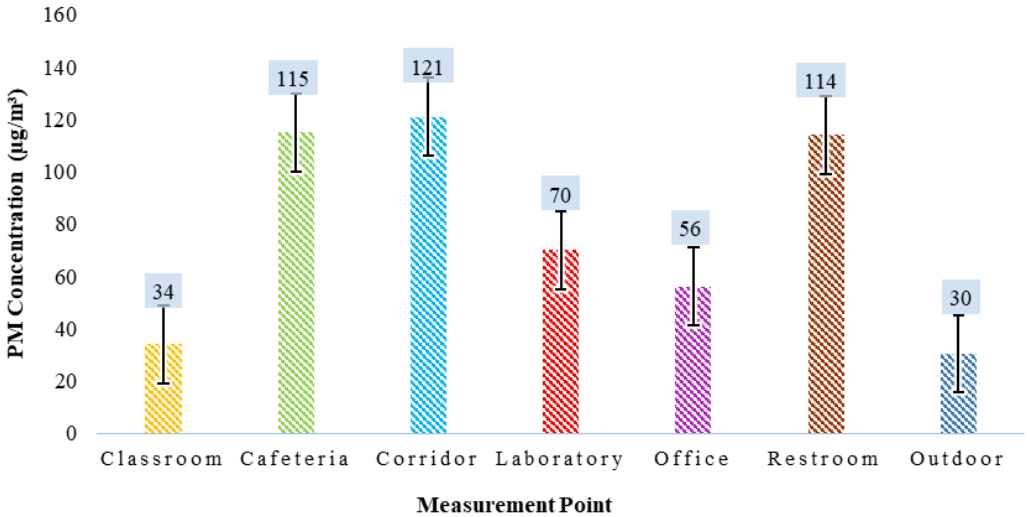

Figure 3. Average values of PM_{10} concentrations

i. Classroom: Classroom PM_{10} measurements revealed an average concentration of 34.00 ± 4.80 μg/m^3, with a minimum of 28.00 μg/m^3 and a maximum of 45.00 μg/m^3. The lowest PM_{10} concentrations were observed at the beginning of the measurement period. Increases during the class were primarily attributed to chalk dust released by the instructor. The highest concentrations coincided with student movement during breaks and the opening of doors, which facilitated the resuspension of settled dust. Major contributors to PM_{10} in the classroom include chalk dust, dust accumulated on surfaces, and resuspension driven by human activity. Limited ventilation can further exacerbate these effects, promoting particulate accumulation and reducing overall IAQ [8].

ii. Cafeteria: PM_{10} concentrations in the cafeteria ranged from 71.00 to 238.00 μg/m^3, with an average value of 115.00 ± 26.98 μg/m^3. Levels were highest during periods of elevated student presence, peaking around 11:00 a.m., corresponding to the end of classes or breaks when occupant movement was most intense. In addition to human activity, PM_{10} emissions were affected by high-temperature cooking appliances, including toasters and tea kettles, as well as frying and grilling processes that generate PM from the combustion of oils and other organic materials. Extended door openings during product deliveries and the cafeteria's proximity to an outdoor smoking area further contributed to elevated PM_{10} levels through dust resuspension and infiltration of tobacco smoke.

iii. Corridor: PM_{10} concentrations in the corridor ranged from 110.00 to 146.00 μg/m^3, with an average value of 121.00 ± 7.85 μg/m^3. Temporal analysis indicated that peak levels occurred around 11:00 a.m., coinciding with the end of classes or scheduled breaks when student movement was at its highest. The primary sources of PM_{10} in the corridor were dust resuspended from the floor due to human activity and PM introduced from outdoors via shoes. In heavily trafficked areas, these factors significantly contribute to elevated indoor PM_{10} concentrations [9].

iv. Laboratory: PM_{10} concentrations in the laboratory ranged from 62.00 to 104.00 μg/m^3, with an average value of 70.00 ± 5.91 μg/m^3. Data analysis suggests that routine laboratory experiments and student presence exerted minimal influence on PM_{10} levels. However, the highest concentrations were observed during post-occupancy cleaning activities, likely due to the resuspension of dust from surfaces and the use of cleaning agents. Additional contributors to PM_{10} in the laboratory environment include wear and friction from operating laboratory equipment, which can generate larger airborne particles [7].

v. Office: PM_{10} concentrations in the office ranged from 46.00 to 75.00 μg/m^3, with an average value of 56.00 ± 7.30 μg/m^3. The highest concentration was observed at the beginning of the measurement period, likely associated with occupant movement and the operation of electronic devices, whereas the lowest concentration occurred during periods of vacancy, highlighting the significant impact of human activity on indoor PM_{10} levels. Primary sources of PM_{10} in the office environment include emissions from electronic equipment such as printers and photocopiers, resuspension of dust from furniture, and the use of cleaning agents [8].

vi. Restroom: PM_{10} concentrations measured in the restroom ranged from 107.00 to 120.00 μg/m^3, with a mean value of 114.00 ± 3.57 μg/m^3. Data analysis indicates that PM_{10} levels were positively correlated with human occupancy, increasing during periods of restroom use and declining when the space was unoccupied. Maximum concentrations were recorded toward the end of class periods, corresponding to heightened restroom activity. Key sources contributing to PM_{10} in this environment include routine cleaning procedures, occupant movement, the application of dust-containing cosmetic products, hair grooming, and the generation of particulates from toilet paper and paper towel usage.

vi. Outdoor: Outdoor PM_{10} concentrations ranged from 20.00 to 61.00 μg/m^3, with a mean value of 30.00 ± 9.25 μg/m^3. Major contributors to outdoor PM_{10} levels included vehicular emissions, industrial activities, dust and PM originating from construction sites, and the combustion of fossil fuels. Overall, outdoor PM_{10} concentrations were markedly lower than those recorded indoors, likely due to increased ventilation and the absence of sustained human activity in outdoor areas. Furthermore, meteorological conditions, including dry and calm winter weather and precipitation on the preceding day—which facilitated the removal of suspended particles from the atmosphere—contributed to the relatively low outdoor PM_{10} levels.

3.3. I/O Ratio

The I/O ratio is a key metric used to evaluate the relationship between indoor and outdoor PM concentrations, providing insight into how outdoor air quality influences indoor environments. An I/O ratio exceeding 1 indicates that particulate levels are higher indoors, while a ratio below 1 suggests that the indoor space is relatively shielded from outdoor particulates. This ratio can be affected by factors such as particle size, the structure and distribution of building cracks, and the rate of air exchange between indoor and outdoor spaces [10].

$$\frac{I}{O} = \frac{C_{in}}{C_{out}} \quad (1)$$

In Equation (1), C_{in} and C_{out} represent the average indoor and outdoor PM concentrations, respectively. Table 4 shows I/O ratios calculated for all measurement points.

Table 4. I/O Ratios for all measurement points

Measurement Point	PM_{10}	$PM_{2.5}$
Classroom	1.1	1.1
Cafeteria	3.8	5.4
Corridor	4.0	5.2
Laboratory	2.3	3.0
Office	1.8	2.2
Restroom	3.8	4.9

As shown in Table 4, the I/O ratios for PM_{10} were highest in the corridor, followed by the cafeteria and restroom (which were equal), then the laboratory, office, and finally the classroom. With the exception of the classroom, all PM_{10} I/O ratios exceeded 1, indicating that indoor activities were the primary sources of PM. The classroom ratio, being close to 1, suggests that indoor and outdoor contributions were approximately equal. The identical I/O ratios for the cafeteria and restroom reflect similar average concentrations, despite differences in their specific pollution sources. For $PM_{2.5}$, I/O ratios decreased in the order of cafeteria, corridor, restroom, laboratory, office, and classroom. Again, all measurement points except the classroom showed I/O ratios above 1, indicating that indoor sources predominantly influenced $PM_{2.5}$ concentrations. The classroom ratio of around 1 highlight that both indoor and outdoor sources contributed similarly to $PM_{2.5}$ levels.

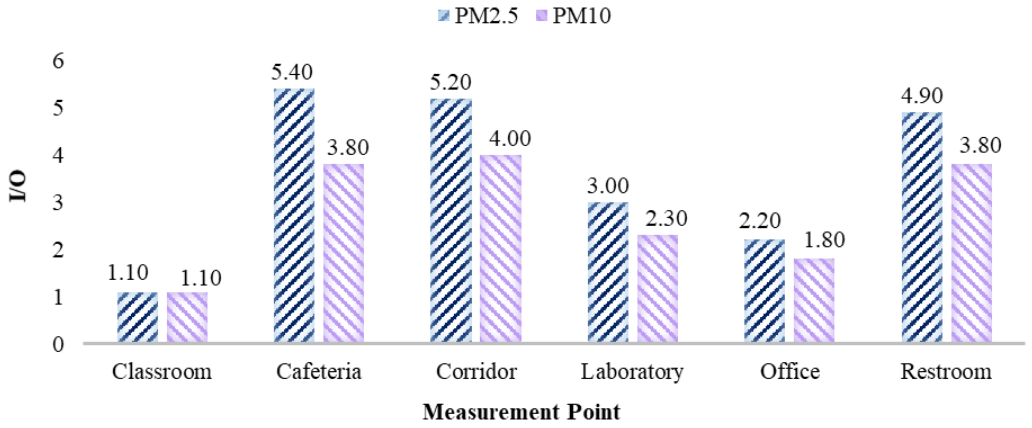

Figure 4. Comparison of $PM_{2.5}$ and PM_{10} I/O ratios across all measurement points

The novelty of this study lies in its simultaneous measurement of $PM_{2.5}$ and PM_{10} concentrations across multiple indoor points. Overall, average concentrations of the two particle sizes were similar, although PM_{10} levels were consistently slightly higher at all sites. This is likely related to the school's rural setting, where accumulated floor dust is predominantly composed of coarse PM_{10} particles. Analysis of I/O ratios for both particle sizes (Figure 4) shows values exceeding 1 at all points, highlighting the significant contribution of indoor sources. While PM_{10} concentrations were higher on average, the elevated I/O ratios observed for $PM_{2.5}$ indicate that indoor activities contribute more substantially to fine PM, primarily due to differences in particle airborne residence times.

3.4. Comparison of $PM_{2.5}$ and PM_{10} Measurement Results

The highest PM_{10} and $PM_{2.5}$ levels were generally observed in areas with high human activity, such as corridor and the cafeteria. In particular, the corridor exhibited fluctuating peaks, highlighting the influence of foot traffic, while the cafeteria showed sharp spikes in PM, likely linked to cooking activities and infiltration of cigarette smoke. More controlled environments, such as laboratory and office, displayed lower and more stable PM levels. In the office, PM concentrations tended to decrease throughout the day, likely due to reduced human activity and/or

effective ventilation. Conversely, in areas such as restroom, cafeteria, and corridor, particulate levels either increased or fluctuated during the day. In the classroom, PM levels showed a gradual upward trend, reflecting increasing activity over time. Across all measurement points, PM_{10} concentrations were higher than $PM_{2.5}$ levels, while $PM_{2.5}$ levels generally exhibited a more stable profile. The smaller size of $PM_{2.5}$ allows it to remain suspended in air longer, whereas PM_{10} levels are more sensitive to human activity and environmental changes.

In the corridor (Figure 5), PM concentrations exceeded those measured in classrooms. PM_{10} levels peaked around 11:00 a.m., coinciding with periods of high activity, while $PM_{2.5}$ remained relatively stable, with elevated concentrations primarily associated with dense foot traffic.

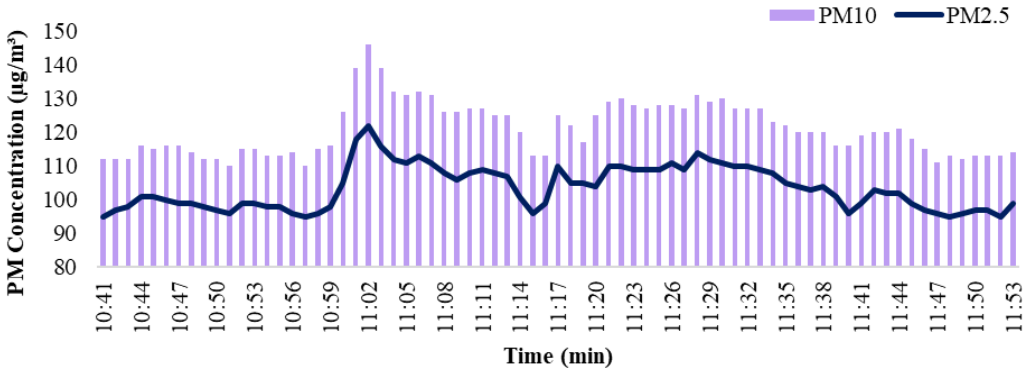

Figure 5. Temporal variation of $PM_{2.5}$ and PM_{10} concentrations in the corridor

Time-dependent measurements in the classroom (Figure 6) showed that PM_{10} concentrations consistently exceeded those of $PM_{2.5}$ and gradually increased throughout the day. A noticeable increase after 2:00 p.m. likely corresponded to increased human activity, increased event intensity, or limited ventilation. Overall, PM levels in the classroom exhibited a controlled upward trend.

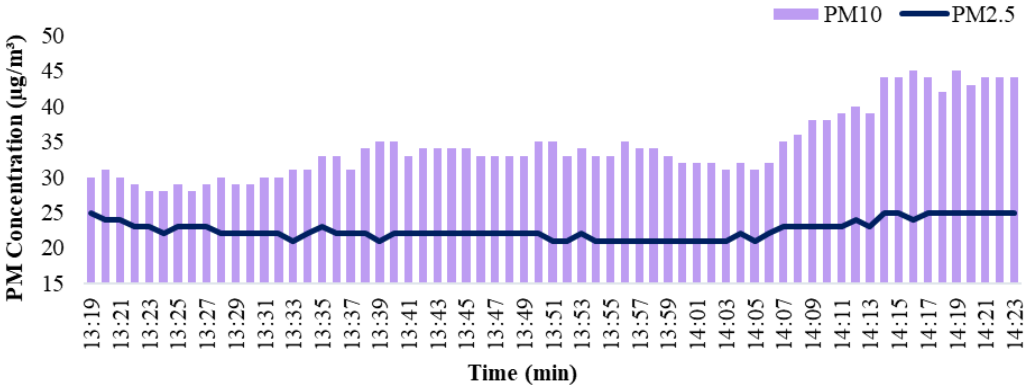

Figure 6. Temporal variation of $PM_{2.5}$ and PM_{10} concentrations in the classroom

In the cafeteria (Figure 7), PM_{10} levels were generally above $PM_{2.5}$, with sudden spikes observed, particularly at 11:00 a.m., corresponding to periods of intense human activity, cooking, and infiltration of smoke. This indicates intermittent deterioration of IAQ in the cafeteria.

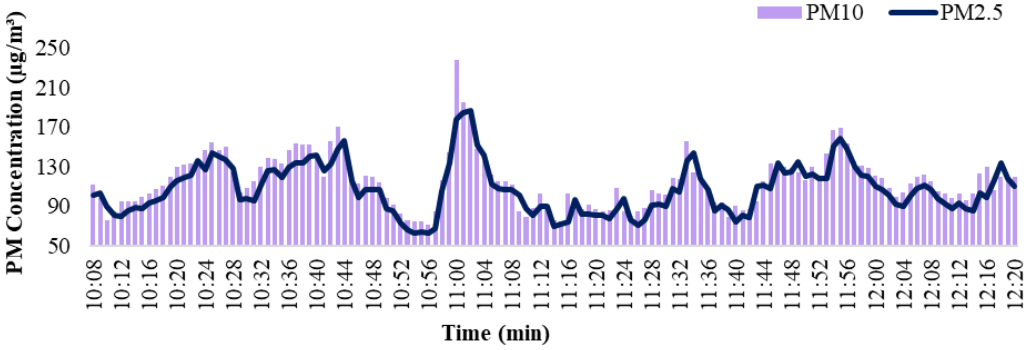

Figure 7. Temporal variation of $PM_{2.5}$ and PM_{10} concentrations in the cafeteria

Laboratory measurements (Figure 8) showed more stable PM_{10} and $PM_{2.5}$ levels, with a gradual increase from the morning and a peak around 11:30 a.m. However, the rise was moderate and followed by a noticeable decrease, reflecting controlled particulate sources or effective ventilation.

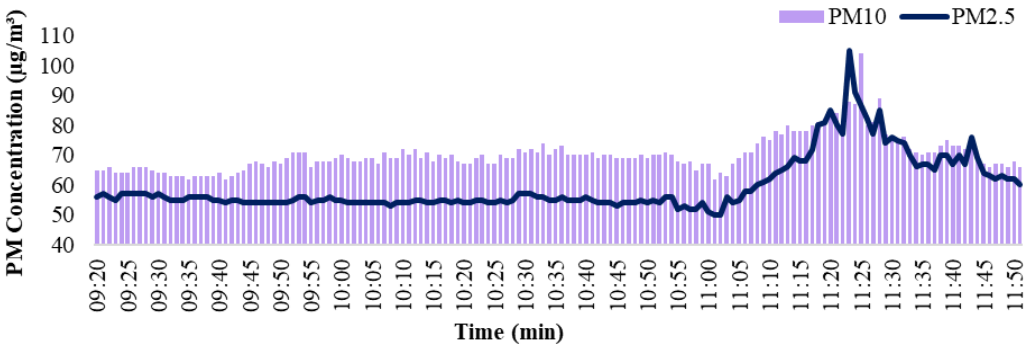

Figure 8. Temporal variation of $PM_{2.5}$ and PM_{10} concentrations in the laboratory

In the office (Figure 9), PM_{10} started at a higher level but gradually decreased over the day, whereas $PM_{2.5}$ remained relatively stable at lower concentrations. The decreasing trend is associated with reduced activity, resulting in improved air quality by the end of the day.

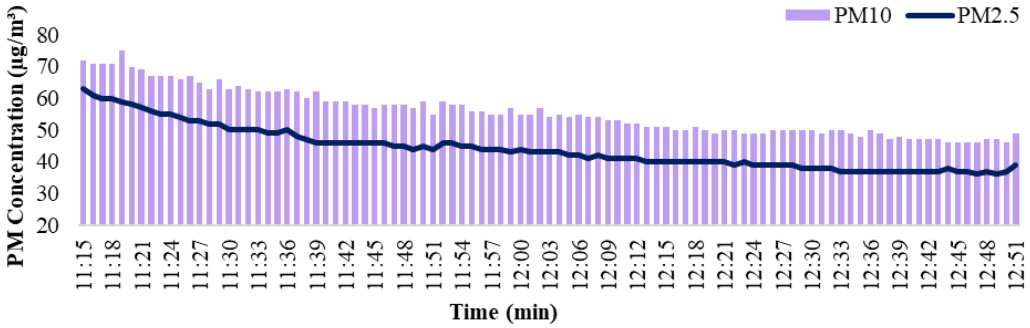

Figure 9. Temporal variation of $PM_{2.5}$ and PM_{10} concentrations in the office

Restroom PM_{10} and $PM_{2.5}$ levels (Figure 10) were higher and more variable. These patterns are attributed to increasing human density from morning to noon and insufficient ventilation in the restroom.

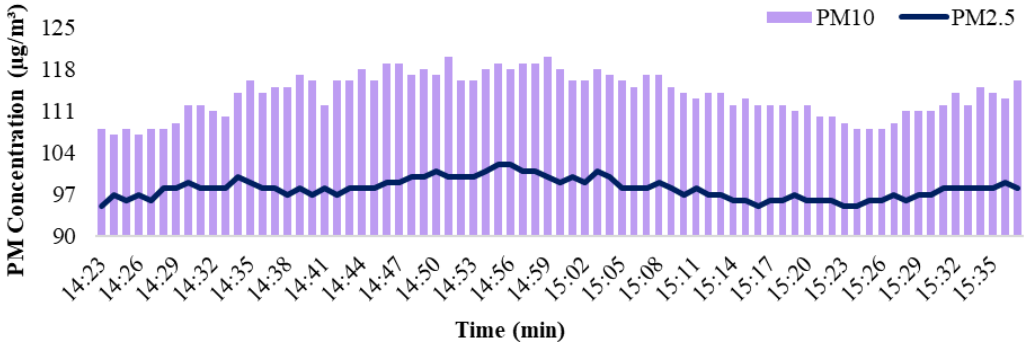

Figure 10. Temporal variation of $PM_{2.5}$ and PM_{10} concentrations in the restroom

These findings indicate that indoor PM levels are heavily influenced by human activity, ventilation performance, and specific indoor sources. Coarse PM_{10} particles respond more readily to immediate disturbances, whereas fine $PM_{2.5}$ particles exhibit greater temporal stability.

4. CONCLUSION

In the study, concurrent indoor PM measurements were carried out at the Department of Environmental Engineering, Iki Eylul Campus, Eskisehir Technical University, Eskisehir, Türkiye. Among the measurement points, laboratory and office exhibited the best air quality, while areas with high human activity, such as corridor and the cafeteria recorded elevated PM levels. Classroom and restroom displayed intermediate air quality profiles.

These findings suggest that improving ventilation in corridors and cafeterias, along with managing human traffic, could help reduce exposure to PM. In restroom, regular cleaning and frequent ventilation should be implemented. For classrooms, ventilation can be intensified during breaks to prevent the accumulation of PM toward the end of the day. In controlled environments like laboratories and offices, maintaining current air quality levels alongside regular monitoring is essential.

Overall, the average PM concentrations obtained in this study exceed those reported in much of the existing literature, highlighting the need for interventions to improve IAQ. Poor air quality is associated with a range of adverse health outcomes, including respiratory and cardiovascular diseases, allergies, asthma, and bronchitis, and may contribute to long-term health complications [11]. Elevated PM levels have also been linked to reduced concentration and cognitive performance [12]. To reduce these risks and maintain a healthy indoor environment, several strategies are recommended. Providing sufficient and continuous ventilation helps dilute and remove indoor pollutants. Cleaning practices should be designed to minimize particle generation and resuspension. Managing class schedules to control student density can further limit particulate accumulation. Implementing these measures is anticipated to not only lower health risks but also improve academic performance and overall quality of life.

Acknowledgments

This study was carried out with the support of the Eskisehir Technical University Scientific Research Project No. 25ADP206 and the TUBITAK 2209-A Project No. 1919B012454380.

References

[1] U.S. Environmental Protection Agency, “Criteria air pollutants,” in America’s Children and the Environment, 2015. [Online]. Available: www.epa.gov/sites/default/files/2015-05/documents/environments-contaminants-criteria-air-pollutants.pdf

[2] M. Bhat, F. Eraslan, A. Awad, S. Malkoc, O. Uzmez, T. Dogeroglu, and E. Gaga, “Investigation of indoor and outdoor air quality in a university campus during COVID-19 lockdown period,” *Building and Environment*, vol. 219, art. no. 109176, 2022.

[3] B. Onat, G. Yasar, B. Uzun, C. Ayvaz, and U. Alver Sahin, “Indoor environmental quality in the university laboratories,” *Pamukkale University Journal of Engineering Sciences*, vol. 29, no. 6, pp. 642–649, 2023.

[4] Q. Xie, Y. Dai, X. Zhu, F. Hui, X. Fu, and Q. Zhang, “High contribution from outdoor air to personal exposure and potential inhaled dose of $PM_{2.5}$ for indoor-active university students,” *Environmental Research*, vol. 215, art. no. 114225, 2022.

[5] B. Ozkan and A. Tereci, “Indoor air quality assessment in the university library during the Covid-19 pandemic,” *Grid Architecture, Planning and Design Journal*, vol. 5, no. 1, pp. 72–96, 2022.

[6] E. Isik and S. Cibuk, “Indoor air quality measurements and analysis in cafeterias and canteens – Tunceli University case,” *Dicle University Journal of Engineering*, vol. 6, no. 1, pp. 39–50, 2015.

[7] G. Yasar, “Investigation of indoor environmental quality in university research laboratories”, M.S. thesis, Institute of Science, Istanbul University, Istanbul, 2018.

[8] A. Sozen and E. Isik, “Indoor air quality measurements and analysis in offices and classrooms: Tunceli University case study,” *Muhendis ve Makina*, vol. 57, no. 677, pp. 53–67, 2016.

[9] Z. Karadeniz, *Indoor Air Quality and Ventilation in Residential Buildings*, Ankara: TMMOB Chamber of Mechanical Engineers, 2024.

[10] C. Chen and B. Zhao, “Review of relationship between indoor and outdoor particles: I/O ratio, infiltration factor and penetration factor,” *Atmospheric Environment*, vol. 45, no. 2, pp. 275–288, 2011.

[11] World Health Organization, *WHO Global Air Quality Guidelines*, 2021. [Online]. Available: https://iris.who.int/bitstream/handle/10665/345329/9789240034228-eng.pdf?sequence=1&isAllowed=y

[12] U.S. Environmental Protection Agency, *Indoor Air Quality Standards and Recommendations*, 2022.

2nd International Conference on Multidisciplinary Sciences and Technological Developments (ICMUSTED 2025)

December 12-15, 2025

Seismic Earth Pressures on Retaining Walls: A Comprehensive Review of Analytical, Numerical, and Experimental Approaches

Ayman Gharbi[1], Fadoua Elkhannoussi[1], Bouraida Elyamouni[1], Abdellatif Khamlichi[1]

[1]National School of Applied Sciences at Tetouan, Abdelmalek Essaadi University, Tetouan, Morocco
Corresponding author: Ayman Gharbi (e-mail: ayman.gharbi@etu.uae.ac.ma)

Abstract

This paper presents a comprehensive review of seismic active thrust acting on cantilever retaining walls by comparing analytical, numerical, and experimental approaches. Starting from classical theories such as Mononobe-Okabe, the review explores pseudo-dynamic enhancements and advanced numerical modeling using the finite element method. Particular attention is paid to key parameters such as soil cohesion, wall flexibility, and failure surface geometry, which significantly affect seismic pressure distribution. Experimental results from centrifuge and shake table tests are also discussed, providing valuable insights and validation for analytical predictions. A comparative application to a practical case study highlights the discrepancies among methods and assesses their conservatism and accuracy. The study concludes with a discussion of current limitations and future directions, emphasizing the need for integrated modeling approaches to achieve realistic seismic design of retaining structures.

Keywords: Seismic earth pressures, Retaining wall, Finite element approach, Pseudo-static approach, Pseudo-dynamic approach

2nd International Conference on Multidisciplinary Sciences and Technological Developments (ICMUSTED 2025)

December 12-15, 2025

Numerical Evaluation of Seismic Performance in Earth Dams: The Case of Fontaine Gazelles Dam, Biskra, Algeria

Alaoua Bouaicha[1], Aissam Gaagai[1], Mosbah Ben Said[1], Ali Hachemi[1]

[1]Scientific and Technical Research Center on Arid Regions, Mohamed Khider University, 07000 Biskra, Algeria
Corresponding author: Alaoua Bouaicha (e-mail: alaoua.bouaicha@univ-biskra.dz)

Abstract

In arid regions where seismic hazards intersect with climate-induced stresses, ensuring the safety and long-term performance of earth dams is of critical importance. Fontaine Gazelles Dam, located in the arid zone of Biskra, Algeria, represents a key hydraulic structure whose stability must be carefully assessed under dynamic loading conditions. This study employs the finite element method (FEM) to investigate the seismic response of the dam, a numerical approach well suited for capturing the complex geotechnical behavior of embankment structures. Through detailed simulations, the research examines deformation patterns, stress redistribution, and potential failure mechanisms under various seismic loading scenarios. Special attention is given to the influence of climate change, particularly its impact on soil moisture variation, material degradation, and overall structural resilience in arid environments. The results highlight both the strengths and vulnerabilities of the dam when subjected to seismic excitation. Critical zones requiring monitoring or reinforcement are identified, providing essential guidance for optimizing maintenance strategies and enhancing the dam's safety. This work offers valuable insights into the seismic performance of earth dams in arid and semi-arid climates and contributes to developing adaptive design and management approaches in regions facing the combined challenges of seismicity and climate change.

Keywords: Bearing capacity, Skirted foundation, Finite element limit analysis (FELA), Pseudo-static approach, Embedment depth

2nd International Conference on Multidisciplinary Sciences and Technological Developments (ICMUSTED 2025)

December 12-15, 2025

Influence of Carbonation on Reinforced Concrete Structures in Southern Algeria

Ben Ammar Ben Khadda[1]

[1]Civil and Hydraulic Engineering Department, Biskra University, Algeria
Corresponding author: Ben Ammar Ben Khadda (e-mail: b.benammar@univ-biskra.dz)

Abstract

The objective of this work is to study the influence of carbonation of concrete by the penetration of carbon dioxide, on the quality and properties of elements of reinforced concrete structures. Studies have shown that carbonation of concrete is the major cause of corrosion of reinforcements in concrete and consequently the degradation of structures, especially in marine environments. The aim of this research was to verify the quality of the reinforced concrete of a degraded and highly carbonated building compared to a healthy building. To this end, several in-situ tests were carried out to assess the quality of the reinforced concrete elements of the two buildings studied. Building 1 is a healthy building located in a dry environment and a non-CO_2-concentrated environment, while building 2 is an industrial building (concentrated environment) located in a location close to the sea. The results showed that the concrete of building 2 is highly carbonated to a depth of approximately 4 cm relative to the exterior surface of the tested elements. However, the carbonation depth does not exceed 2 cm for the elements examined in building 1.

Keywords: Reinforced concrete, Carbonation, Environment, Carbonation depth, Degradation

2nd International Conference on Multidisciplinary Sciences and Technological Developments (ICMUSTED 2025)

December 12-15, 2025

Numerical Study to the Enhancement of Pressure Distribution within the Alveolus of an Aerostaic Bearing

Faiza Ghezali[1]

[1]Mechanical Engineering, Sidi Bel Abbes University, Djilali Liabes, Algeria
Corresponding author: Faiza Ghezali(e-mail: ghezali.f18@gmail.com)

Abstract

The proposed study is based on the study of the pressure profile within a square cell of an air-bearing pad. The current shape of the alveolus cavity is characterized by the presence of a peak in the feedline of the lubricating air supply. In contrast, the new design aims to standardize the pressure distribution within the alveolus cavity by creating eight holes distributed around the injection area and at the ends of the cavity. The simulations were conducted using three-dimensional (3D)-Reynolds averaged Navier-Stokes equations (RANS) analysis and the shear stress transport (SST)-kω model. The finite volume method, integrated within the ANSYS-CFX software, was utilized. Several parameters were examined, including: pressure fields, film thickness, load capacity and stiffness, turbulence intensity. The results obtained indicate a significant improvement in the distribution of pressure, particularly for thin lubricant film thicknesses, while maintaining good rigidity of the lubricant film. Also the Rayleigh effect is less pronounced at the boundary of the alveolus of the bearings for all the film thicknesses studied. Furthermore, it's noted that the intensity of turbulence in the perforated alveolus recorded higher values within the cavity, which ensures the redistribution of pressure in the cavity and maintains it more uniformly compared to the ordinary case without holes.

Keywords: Alveolus, SST-kω, Pressure field, Rayleigh effect

2nd International Conference on Multidisciplinary Sciences and Technological Developments (ICMUSTED 2025)

December 12-15, 2025

A Comparative Finite Element Analysis of Static Coil Geometries for Electromagnetic Eddy Current Separation

Amir Merahi[1], Kaouther Boutarfa[1], Adel Benabboun[2], Meriem Boumehed[1]

[1]Development Smart Grid Laboratory, High School of Electrical and Energetic Engineering of Oran, Algeria
[2]Mostafa Stambouli University, Mascara, Algeria
Corresponding author: Amir Merahi (e-mail: merahi_amir@esgee-oran.dz)

Abstract

This study presents a comparative analysis of the electromagnetic performance of various static coil configurations used in eddy current separators for the recovery of non-ferrous metals. The investigated system consists of a magnetic circuit made of soft steel with a relative permeability of 5000, arranged in a square geometry of 120 mm width. The circuit is surrounded by two cylindrical copper coils, each containing 20 turns (solenoids) with a cross-sectional area of 600 mm^2. These coils are powered by an alternating current of approximately 15 A, generating a strong magnetic field around the ferromagnetic core, which acts as a magnetic flux channel through a 20 mm air gap. A finite element analysis was conducted using COMSOL Multiphysics to evaluate four distinct electromagnetic configurations with core geometries inspired by the forms of the letters U, C, and E. The investigation included U shaped cores arranged in both two coil and four coil setups, a C shaped core utilizing two coils, and an E shaped core design. The cores with U and E shaped geometries represent two classic electromagnet designs that directly influence the magnetic flux distribution and the resulting attraction force. The core with a U shaped geometry, consisting of two parallel limbs connected by a base, is simple to design and generates a strong magnetic force, though with a less uniform flux distribution. Conversely, the core with an E shaped geometry, made up of three limbs joined to a common base, allows the magnetic flux to divide more evenly among the limbs, providing a more balanced attraction force and higher magnetic efficiency, although with a more complex structure. The core with a C shaped geometry, composed of a single open magnetic path shaped like the letter C, offers intermediate performance, with easier coil placement and moderate field uniformity. Simulation results reveal distinct electromagnetic characteristics for each coil configuration. The four coil U shaped topology produces an induced current of 0.1 A, while the two coil U shaped configuration yields 0.08 A. The C shaped geometry generates 0.4 A, showing a notable enhancement in performance. Most significantly, the E shaped geometry demonstrates exceptional results with an induced current reaching 1.2 A, confirming its superior capability for magnetic flux concentration and metallic particle separation efficiency. The magnetic field analysis reveals remarkable homogeneity in multi coil configurations, with less than 15% variation across the active separation zone. The two coil design offers an optimal compromise between efficiency and implementation simplicity, whereas the four coil structure provides broader magnetic coverage. These results establish a solid foundation for optimizing industrial electromagnetic separators, highlighting the potential of the core with an E shaped geometry for the efficient treatment of metallic particles of similar dimensions.

Keywords: Eddy current separation, Finite element method, Static coil design, Magnetic field distribution, Non-ferrous metal recycling

2nd International Conference on Multidisciplinary Sciences and Technological Developments (ICMUSTED 2025)

December 12-15, 2025

Contribution to the Recovery of Paint Sludge in Wastewater Treatment

Aicha Metali[1], Mounir Ziati[1,2], Ikram Rebiai[2], Khedidja Bachi[2]

[1]Laboratory of Soft Technologies, Physicochemical, Valorization of Biological Materials and Biodiversity, Department of Chemistry, Faculty of Sciences, M'hamedBougara University, 35000 Boumerdes, Algeria
[2]Laboratory of Applied Chemistry and Materials, Department of Chemistry, Faculty of Sciences, M'hamed Bougara University, 35000 Boumerdes, Algeria
Corresponding author: Aicha Metali (e-mail: a.metali@univ-boumerdes.dz)

Abstract

Wastewater treatment is an essential step in environmental protection. Various techniques are used for this purpose, with adsorption being one of the most widespread, using different materials. In our study, we tested sludge from the paint industry as an adsorbent to reduce the pollutant load of oil industry wastewater. The dried and calcined paint sludge at 500 °C was activated in the presence of nitric acid 10%. After washing the activated sludge with deionized water and drying in an oven, four different masses (0.5, 1.0, 1.5, and 2.0 g) were mixed with a fixed volume of wastewater for 2 hours. Organic matter content, expressed as chemical oxygen demand (COD) and total organic carbon (TOC), as well as turbidity and suspended solids, were then analyzed. The results revealed a removal of 60 to 61% of COD, 50 to 53% of TOC, 97 to 95% of suspended solids, and 93 to 97% of turbidity after 120 minutes of contact time and in the presence of 1.5 g of calcined and uncalcined sludge, respectively. These results indicate that this waste could be recycled as adsorbents for other industrial effluent.

Keywords: Paint sludge, Adsorption, Wastewater, Environment, Valorisation

2nd International Conference on Multidisciplinary Sciences and Technological Developments (ICMUSTED 2025)

December 12-15, 2025

Microservice Transformation for Infrastructure Modernization of Payment and Electronic Money Institutions

Ahmet Ulker[1], Cansu Barisici[1], Eren Capraz[1], Ilker Ogutcu[1], Mehmet Bulent Muslu[1], Zafer Golgeli[1], Ceren Ulus[2], M. Fatih Akay[3]

[1]Dept. of Technology, PayTR, Izmir, Türkiye
[2]Dept. of Research and Development, EFA Innovation Consulting and Technology, Adana, Türkiye
[3]Dept. of Computer Engineering, Cukurova University, Adana, Türkiye
Corresponding author: M. Fatih Akay (e-mail: mfakay@cu.edu.tr)

Abstract

With today's evolving technology, online payment systems allow for faster financial transactions. This has increased the need for continuous integration and continuous delivery in electronic payment institutions. However, monolithic architectures are still in use today, where all business processes are implemented through a single structure, making updates and enhancements quite time-consuming. Reducing the complexity of this monolithic architecture is particularly important to meet the growth and increasing demands in the financial sector. In this context, transforming the existing monolithic structure into a more flexible and sustainable one is a key strategic action. This study aimed to transform the PayTR infrastructure, established in a traditional monolithic structure, into a microservices architecture. For this purpose, applications, domains, infrastructure, and shared libraries have been used. Endpoint rules have been also defined. The system included a business front end (BFF) layer, a dedicated application programming interface (API) layer, and a dedicated service layer. The resulting new architecture offers significant advantages in terms of speed and security.

Keywords: Payment and electronic money, Microservice architecture, Architecture transformation

1. INTRODUCTION

Today, technology is rapidly evolving due to many factors. Furthermore, online payment solutions have gained significant importance by speeding up transactions. PayTR is a key player in this field, providing merchants with a reliable payment infrastructure to support e-commerce operations. However, PayTR's current system architecture is built on a monolithic structure.

In monolithic architectures, many processes, such as server operations and database management, are interconnected within a single structure. This creates various challenges. This dependency on modules minimizes system flexibility, which delays the rapid adoption of updates and newly developed features. Processes become more complex, increasing maintenance costs. When a system needs to be scaled, the entire system must be scaled within the monolithic architecture, leading to inefficient resource usage. Furthermore, when a company experiences a personnel turnover, it takes considerable time for the new staff to understand and adapt to the workings of a large monolithic system. This creates a complex flow of information, making it difficult for the new team to learn. Microservices transformation is an innovative approach that reduces the problems caused by traditional monolithic-based systems and transforms them into a more flexible programming interface (API). This microservices architecture treats each business function separately as an independent service. This transformation allows developers to work in parallel and efficiently, allowing new features to be integrated into the system more quickly. Furthermore, continuous ıntegration (CI) and continuous delivery (CD) processes are also managed efficiently. In light of all this, microservices architecture transformation is an important strategic necessity, particularly for the financial sector, enabling it to more efficiently meet the increasing demands of today's evolving technology and enabling faster work execution.

This study aimed to reduce the complexity of existing monolithic structures and transform them into a more flexible version to more effectively meet the growth and increasing demands in the financial sector. To this end, the system infrastructure established in the monolithic structure has been transformed and a microservices architecture has been developed.

This study is organized as follows: Section 2 includes relevant literature. Details of the system are presented in Section 3. Results of the study are given in Section 4. Section 5 concludes the paper.

2. LITERATURE REVIEW

[1] aimed to evaluate existing modeling languages and proposed a lightweight, high-level, and platform-independent modeling language. The proposed language integrated many features previously discussed in the literature in a holistic manner. This proposed language has been general enough to describe a wide class of interactive microservices architectures. First, the syntax has been defined using meta-object facility. The core concepts have been explained informally. An alternative hypergraph-based mechanism has been presented to formally express the language's semantics. An architectural style has been proposed using a hierarchical hypergraph type that can represent information about software architectures in an intuitive and compact manner. Finally, the applicability of the proposed language has been demonstrated through an experimental tool that can transform the generated models into different container orchestration systems. The language has been evaluated against the identified features in the context of the TeaStore reference application.

[2] examined the impact of microservices on the financial sector. They evaluated the microservices adopted to meet the sector's rapid growth and increasing transaction volumes. They also examined the benefits provided by different services, such as scalability, fault isolation, and time to market. They also evaluated how large financial institutions use microservices for various operations, such as payment processing, account management, and fraud detection. Examples of the benefits these financial institutions have achieved are provided.

[3] examined the need to transition from monolithic architecture to microservices. They explored how microservices are defined and the challenges that may be encountered during the transition to microservices. An industrial empirical approach has been used. An evidence-based decision-making approach has been adopted for the transformation of monolithic architectures. Strategies for reengineering monolithic architectures and a prioritized classification of challenges that may arise during the transition to microservices have been presented. Additionally, a model has been developed to ensure the appropriate selection of strategies for implementing microservices.

[4] presented an analysis of the transition from monolithic to microservices architecture. The key factors that led to this transformation have been analyzed. The advantages and disadvantages of this transformation have been also evaluated. Literature reviews, empirical case studies, and interviews with professionals have been used. Finally, the incentives that led to the microservices transition have been evaluated.

[5] aimed to analyze the transition from monolithic to microservices architecture. The structure of monolithic and service-oriented architectures has been evaluated. The advantages and disadvantages of these architectures have been analyzed comprehensively. A microservices platform and its basic architecture have been examined.

[6] compared monolithic and microservices architectures on a reference web application. The application, with four different versions, has been developed using Java and C#.NET. Experiments have been conducted in three different deployment environments: local, Azure Spring Cloud, and Azure App Service. Experimental results showed that the monolithic architecture outperformed its microservices-based counterpart on a single machine. Java has been observed to utilize powerful machines more efficiently than .NET for services with higher computational intensity than normal, while this effect diminished when running on machines with limited capacity for services with lower computational intensity than normal. Furthermore, vertical scaling on Azure has been observed to be more cost-effective than horizontal scaling, scaling above a certain number of instances degrades performance, and using Java or C# .NET did not significantly impact scalability performance.

[7] aimed to understand the need and techniques for migrating monolithic applications to microservice architecture. Proposed algorithms for the migration process have been examined, and their advantages and disadvantages have been analyzed. A generalized pipeline, incorporating an auxiliary technological architecture that would enable the transition to microservice-based systems to ensure flexibility and scalability, has been proposed.

[8] aimed to compare the decompositions generated for two monolithic systems with the candidate microservice when data collection techniques have been applied using static and dynamic analysis. The decompositions have been created using a combination of similarity metrics, and an evaluation has been performed according to a complexity metric to answer the question, "Which monolithic data collection, static or dynamic analysis, produces better decompositions?" As a result, it has been observed that static and dynamic analysis techniques exhibited similar results.

[9] proposed two strategies for structured logging of request-response messages, including the entire message body, in a distributed software system based on a microservices architecture. A case study has been conducted, and a prototype has been implemented for each strategy. It has been deployed on an existing Microservices Architecture-based banking system managed by a commercial bank in a Kubernetes cluster. It has been aimed to measure the average request throughput and average response times and in this context, load tests have been carried out for the banking system.

[10] proposed a decision-support framework that companies can use when migrating to microservices and analyzed the features and metrics companies need before restructuring their monolithic systems. They interviewed professionals and conducted a survey to develop an evaluation framework based on grounded theory. The result is a set of insights companies can use when deciding to migrate to microservices

[11] focused on microservice definition and proposed an approach within this framework. The definition consists of analyzing the relationships between source code elements, the relationships with persistent data processed in this code, and the architect's knowledge of the system. The study also defined a function that enables the measurement of microservice quality based on its service delivery capability and its interdependence with other microservices in the resulting architecture. Architectural recommendations have been used to guide the definition process. Experimental results indicate that the performance of microservices obtained using the proposed approach is positive.

[12] analyzed academic studies describing monolithic and microservice architectures. Furthermore, the performance of an application running in a monolithic architecture and the relationship between different variables have been compared with one of the microservices. A web application based on a monolithic architecture running on a virtual server with Kernel-based Virtual Machine has been evaluated. It has been also observed that the same web application, based on microservice architecture but running in containers, has been also based on the microservice architecture. Stress tests have been conducted for both cases with similar features and the same hardware resources. A nonparametric regression mathematical model has been implemented for validation to explain the dependency relationship between performance variables. The results provide a quantitative technical assessment in terms of precision and reliability, applicable to similar problems.

3. DETAILS OF THE SYSTEM

The system has been developed using application, domain, infrastructure, and shared libraries. Endpoint rules have been defined. The system consists of a business front end (BFF) layer, a private API layer, and a private service layer. The system architecture is shown in Figure 1.

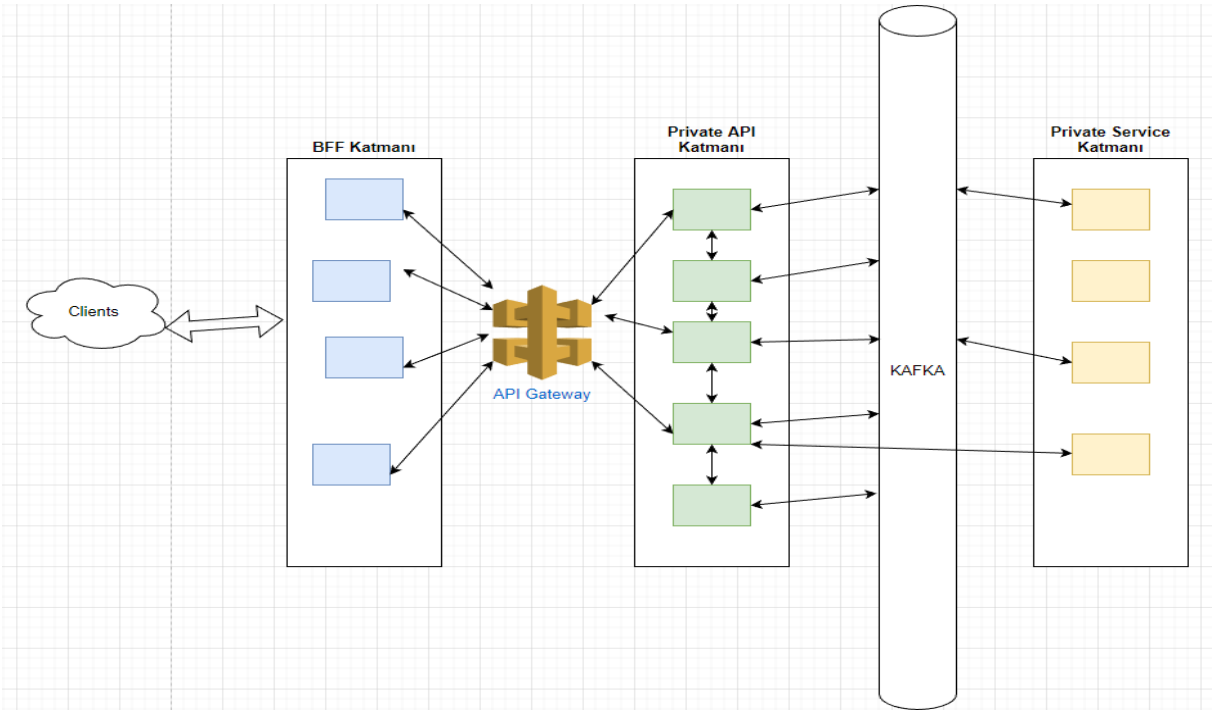

Figure 1. The system architecture

3.1. Business for Frontend

These consist of Public APIs or APIs located in the Demilitarized Zone (DMZ) area. These APIs are developed in accordance with OpenAPI standards. It's available to the customer. Developments are made based on the product/business. Numbers vary depending on customer needs and the products the company offers. Authentication and authorization checks are performed. While they can be delivered directly to customers as product APIs, the interfaces, developed publicly or privately within the company, serve as backends for mobile applications.

3.2. Private API Layer

These are microservices developed entirely privately on the company's internal network, where microservices reside. For operations requiring synchronous communication, they communicate with each other, generally over Google Remote Procedure Call (gRPC), and with the BFF layer. BFF also includes the technological infrastructure to provide some endpoints as representational state transfer (REST)APIs, depending on its needs. For operations requiring asynchronous communication (especially those where accuracy is more critical than speed or where technical decisions are made), they communicate via Kafka. They are the smallest possible units of a business context, and their number varies depending on technical analysis decisions. Microservice contexts are configured to eliminate the need for distributed transactions whenever possible.

3.3. Private Service Layer

Integration is provided between internal company applications and external applications. It is invoked only from the private API layer. This layer enables communication between internal company applications not included in the microservices architecture and external applications required in projects.

3.4. API Gateway

The API Gateway is the structure that forwards requests from BFF or microservices to the relevant RestAPI or gRPC services based on prefixes. For end users, the APISix API Gateway is used. NGINX (ingress) is used within PayTR. This allows the two traffic types to be managed separately. The API gateway architecture is shown in Figure 2.

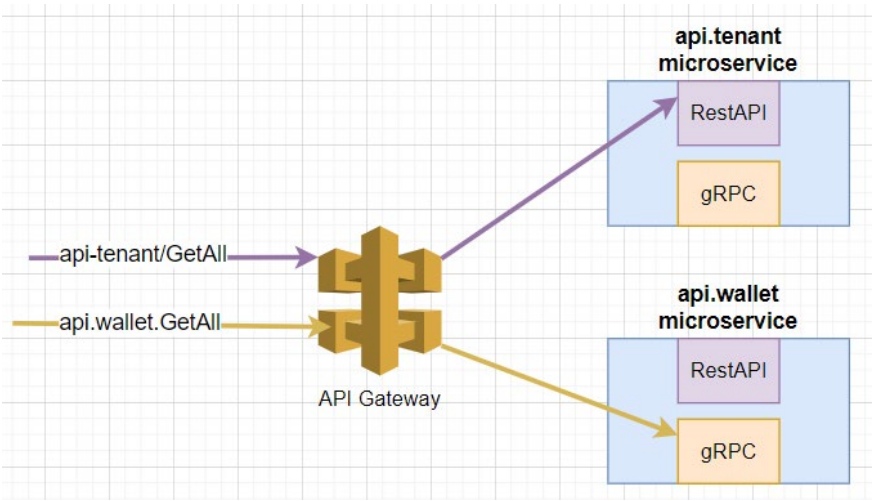

Figure 2. The API gateway architecture

3.5. PayTR Frame

This is the software infrastructure for .NET applications developed within PayTR. Interdependencies between packages are kept to a minimum as much as possible; packages are developed with an emphasis on standardization, without restricting developer capabilities. Each developed package is pushed to the local nexus as a NuGet, allowing developers to download packages from the local nexus server. Versioning is also performed. This allows for back-and-forth between versions, preventing runtime impacts on applications with older package versions during new updates.

3.5.1. PayTR.Frame.AuditMongoDb

Developed to store AuditLogs generated by database update and delete operations. It writes to MongoDB to store the previous version of a changed row in the database table. It is used with the PayTR.Frame.UnitOfWork package.

3.5.2. PayTR.Frame.CoreDomain

This is the domain where central methods used in projects are stored to prevent code duplication. Base classes such as BaseEntity are also located under this package.

3.5.3 PayTR.Frame.Dapper

This package includes the Dapper micro-ORM tool, which replaces EntityFramework for all select operations performed on the database, and provides developers with a QueryRepository. It executes written SQL queries. It facilitates the optimization of select queries and increases performance.

3.5.4. PayTR.Frame.Encrypt

This method contains methods used to encrypt and decrypt records to be kept in the database. It can be run automatically when committing database records or updates, or it can be used manually.

3.5.5. PayTR.Frame.EventBus

This method is used for easy integration into queue structures. It is responsible for recording each record sent to the queue system and then sending it to the queue system. Currently used only with Kafka, it is designed for easy integration with other queue systems.

3.5.6. PayTR.Frame.FluentValidation

This method is designed to ensure the accuracy of incoming and outgoing data from microservices. It includes the open-source FluentValidation package.

3.5.7. PayTR.Frame.GlobalException

This method is used to handle potential errors received within the application. Its primary purpose is to record error details in the log system and to provide more meaningful error messages without providing the user with error details.

3.5.8 PayTR.Frame.Grpc

Designed for microservices using gRPC. It includes gRPC packages developed by Microsoft and Google for .NET. gRPC Interceptor operations are also developed under this package.

3.5.9. PayTR.Frame.IoC and PayTR.Frame.QuartzNet

Used to commonize the use of Autofac in injection operations across projects. PayTR.Frame.QuartzNet contains the Quartz.Net library and configuration used for scheduled tasks.

3.5.10. PayTR.Frame.MediatR

This is one of the libraries used for the Command Query Responsibility Segregation (CQRS) pattern. It is used to transmit commands from a single center to the relevant handler. This is the library for the Mediator Pattern, written by Jimmy Bogard. It also facilitates the transition from gRPC and RestAPI in the API layer of projects.

3.5.11. PayTR.Frame.Redis and PayTR.Frame.Results

Developed for easy integration with Redis for cache operations. It includes repositories that facilitate reading and writing from Redis. Developed for syndicating response messages returned by RestAPIs.

3.5.12. PayTR.Frame.Serilog

Developed to send all request-response parameters received within the application, or any information the developer wishes to be logged, to a central logging system via RabbitMQ. It utilizes the open-source Serilog library.

3.5.13. PayTR.Frame.UnitOfWork

This is a customized version of the open-source library developed for the UnitOfWork pattern under the Microsoft umbrella, specifically for PayTR. It is used for database create, update, and delete operations.

3.5.14. PayTR.{MicroserviceName}.Shared

Contains the code blocks that microservices must share with other microservices. It is not required for every project to have a shared package. It is only published as a package with the project name when necessary.

3.5.15. PayTR.Frame.RateLimiting

Enables the application of request limits (rate limits) on APIs and services. It aims to prevent system abuse and performance issues by controlling the maximum number of requests that can be made in specific time intervals. Limits can be set based on ınternet protocol (IP), user, or token.

3.5.16. PayTR.Frame.Vault

Developed for the secure storage and management of confidential information (connection string, API key, password, etc.). It enhances configuration security by integrating with HashiCorp Vault or similar secure storage systems.

3.6. Centralized Authentication - Authorization Structure

A new version of the library, formerly known as Identity Server, is used, specifically customized for PayTR projects. Client Credentials and ResourceOwner Flows (username, password) are used. The resource owner passwords credentials flow is shown with Figure 3.

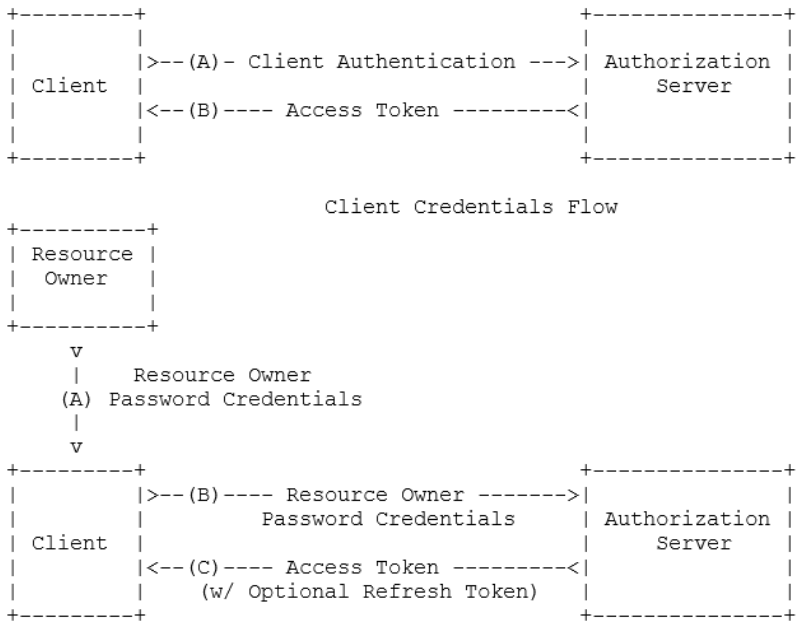

Figure 3. The resource owner passwords credentials flow

3.7. Centralized Application Log Structure

Logs are written to RabbitMQ using the Serilog library and then transferred to Logstash and Elasticsearch for visualization via Kibana. All microservices and BFF logs are stored and displayed in this structure. Centralized application log structure is presented in Figure 4.

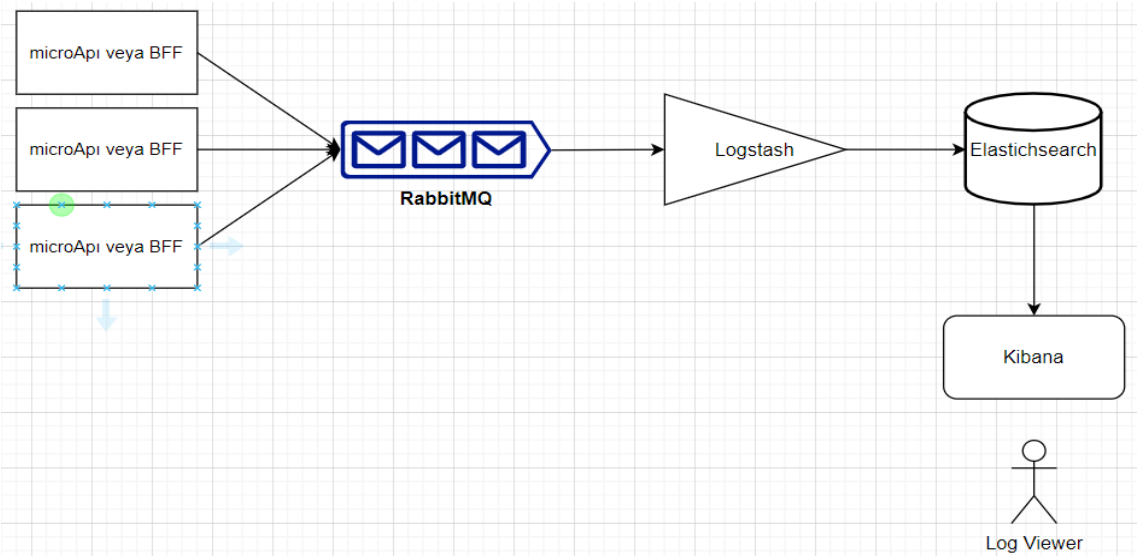

Figure 4. Centralized application log structure

4. RESULTS AND DISCUSSION

- The support rate for effective reconciliation services across multiple banks has reached 80% across applications.
- A minimum of 98% of externally accessible (customer) services has been aligned with the structure.
- 85% of shared services across all company products have been aligned.
- Problem tracking and troubleshooting processes have been streamlined, and operational efficiency has been increased by 50%.
- Customers using one product can integrate other products with 20% fewer steps.
- Communication has been faster and more secure with gRPC and Hyper-Text Transfer Protocol 2.0 (HTTP/2) protocols, and data exchange between services has become more efficient. Event-Driven Architecture has ensured data integrity, and system performance has been improved in high-traffic situations.
- Sharing log systems and cache structures has been facilitated system monitoring, and separate versioning and scaling of microstructures has reduced service disruptions to near zero.
- A faster, more secure, and more flexible system has been achieved, and the product range has also been expanded.

5. CONCLUSION

A monolithic architecture is a traditional software architecture where components operate as a single whole within a single structure. In a monolithic architecture, there are dependencies between processes such as the database, server, user interfaces, and business logic. These dependencies make development processes quite time-consuming. Therefore, to more effectively meet the growth and increasing demands, especially in the financial sector, monolithic architectures need to be transformed into more flexible structures. Microservices transformation, which creates a more flexible structure by dividing a monolithic architecture into independent, smaller services, is gaining significant importance today. In this study, the PayTR infrastructure, established as a monolithic structure, has been transformed into a microservices architecture. gRPC and HTTP/2 protocols have been used to ensure fast and secure communication in the system. A common system log structure has been created to monitor the system. This maked monitoring and troubleshooting processes simpler. Kubernetes has been used to provide maximum protection and minimize costs for server management. This significant transformation has accelerated the technological transformation in the financial sector, increasing competitiveness and reducing costs.

References

[1] J. Esparza-Peidro, F. D. Muñoz-Escoí, and J. M. Bernabéu-Aubán, “Modeling microservice architectures,” *Journal of Systems and Software*, vol. 213, art. no. 112041, Jul. 2024.

[2] V. R. Nomula, “Optimizing financial systems with microservices architecture,” *International Journal of Computer Engineering and Technology (IJCET)*, vol. 15, no. 5, Oct. 2024.

[3] M. Hamza, “Transforming monolithic systems to a microservices architecture,” *ACM SIGSOFT Software Engineering Notes*, vol. 48, no. 1, pp. 67–69, Jan. 2023.
[4] S. Mooghala, “A comprehensive study of the transition from monolithic to micro services-based software architectures,” *Journal of Technology and Systems*, vol. 5, no. 2, pp. 27–40, Nov. 2023.
[5] D. Saxena and B. Bhowmik, “Paradigm shift from monolithic to microservices,” in *2023 IEEE International Conference on Recent Advances in Systems Science and Engineering (RASSE)*, Nov. 2023, pp. 1–7.
[6] G. Blinowski, A. Ojdowska, and A. Przybyłek, “Monolithic vs. microservice architecture: A performance and scalability evaluation,” *IEEE Access*, vol. 10, pp. 20357–20374, Feb. 2022.
[7] R. Mishra, N. Jaiswal, R. Prakash, and P. N. Barwal, “Transition from monolithic to microservices architecture: Need and proposed pipeline,” in *2022 International Conference on Futuristic Technologies (INCOFT)*, Apr. 2022, pp. 1–6.
[8] B. Andrade, S. Santos, and A. R. Silva, “From monolith to microservices: Static and dynamic analysis comparison,” *arXiv Preprint*, Apr. 2022. doi: 10.48550/arXiv.2204.11844
[9] F. Basciftci and F. Aydemir, “Strategies for request-response logging in microservices architecture,” in *2022 IEEE 20th Jubilee International Symposium on Intelligent Systems and Informatics (SISY)*, Feb. 2022, pp. 195–200.
[10] F. Auer, V. Lenarduzzi, M. Felderer, and D. Taibi, “From monolithic systems to microservices: An assessment framework,” *Information and Software Technology*, vol. 137, art. no. 106600, Sep. 2021.
[11] A. Selmadji, A. D. Seriai, H. L. Bouziane, R. O. Mahamane, P. Zaragoza, amd C. Dony, “From monolithic architecture style to microservice one based on a semi-automatic approach,” in *2020 IEEE International Conference on Software Architecture (ICSA)*, May. 2020, pp. 157–168.
[12] F. Tapia, M. Á. Mora, W. Fuertes, H. Aules, E. Flores, and T. Toulkeridis, “From monolithic systems to microservices: A comparative study of performance,” *Applied Sciences*, vol. 10, no. 17, art. no. 5797, Aug. 2020.

2nd International Conference on Multidisciplinary Sciences and Technological Developments (ICMUSTED 2025)

December 12-15, 2025

Experimental Investigation of Concrete by Using Marble Waste as Replacement of Fine Aggregate

Hassaan Amjad[1], Faisal Ahmed[1], Allah Noor[1]

[1]Civil Engineering Department, Swedish College of Engineering and Technology, Rahimyar Khan, Pakistan
Corresponding author: Hassaan Amjad (e-mail: hassaanamjad17@gmail.com)

Abstract

This study investigates the use of marble waste powder as a partial replacement for fine aggregate in concrete, addressing environmental challenges in Pakistan's construction sector and promoting sustainable building practices. Concrete mixtures with marble powder replacement levels of 0–30% were prepared and tested. A total of 126 specimens were examined for workability, compressive strength, split tensile strength, and durability. Marble powder was sourced from processing facilities in Punjab, ensuring regional relevance. Fresh concrete properties were evaluated using slump tests, while hardened performance was assessed through compressive strength at 7, 14, and 28 days, split tensile strength, rapid chloride penetration test (RCPT), and water penetration depth. Results revealed that marble powder significantly influenced concrete behavior. The optimal performance was achieved at 10% replacement, where compressive strength increased by 5%, reaching 32.8 MPa at 28 days compared to 31.2 MPa for the control. Split tensile strength also peaked at 2.7 MPa at this level. Workability tests showed a consistent decline in slump values with higher marble content due to the fineness and increased surface area of marble particles, which raised water demand. Despite this, durability assessments indicated that moderate replacement improved resistance to chloride penetration and reduced water ingress. The findings confirm that marble powder can serve as a sustainable fine aggregate replacement up to 10–15%, providing both environmental benefits and improved concrete performance. This contributes to waste utilization, reduced environmental burden, and advancement of eco-friendly construction technologies. The research recommends updating local construction standards to formally incorporate marble powder as a supplementary material, especially in regions with abundant marble processing waste.

Keywords: Marble waste powder, Fine-aggregate replacement, Compressive strength, Durability, Workability

2nd International Conference on Multidisciplinary Sciences and Technological Developments (ICMUSTED 2025)

December 12-15, 2025

Investigating the Properties Ultra High-Performance Concrete Using Silica Fume and Ground Granulated Blast Furnace Slag

Hassaan Amjad[1], Waseem Asghar[1], Dawood Jan[1]

[1]Civil Engineering Department, Swedish College of Engineering and Technology, Rahimyar Khan, Pakistan
Corresponding author: Hassaan Amjad (e-mail: hassaanamjad17@gmail.com)

Abstract

This study evaluates the development of high-strength concrete using silica fume (SF) and ground granulated blast furnace slag (GGBFS) as partial cement replacements. Three mixes Mix A (20% SF, 20% GGBFS), Mix B (22.5% SF, 22.5% GGBFS), and Mix C (25% SF, 25% GGBFS) were prepared with total replacement levels of 40%, 45%, and 50%, respectively. All materials were characterized per American Society for Testing and Materials (ASTM) standards, confirming the ultra-fine nature of SF (98.5% passing 0.075 mm sieve) and the pozzolanic suitability of GGBFS (93.7% passing 0.075 mm sieve). Compressive strength tests at 7, 14, and 28 days showed that Mix A achieved the highest 28-day strength (131.30 MPa) and superior early-age performance (52.24 MPa at 7 days). Mix B and Mix C recorded 126.17 MPa and 123.01 MPa at 28 days, respectively. A strong inverse correlation ($r = -0.991$) between replacement level and strength was observed, indicating that excessive cement replacement beyond 40% may compromise strength development. Although all mixes exceeded 100 MPa and qualify as high-strength concrete, none reached the 150 MPa threshold for ultra-high-performance concrete (UHPC) classification, with Mix A falling short by 18.7 MPa. The findings establish Mix A's formulation as the optimal balance of cementitious and supplementary materials and provide a foundation for further optimization such as reducing total replacement to 30-35%, incorporating steel fibers, and employing heat curing to achieve true UHPC performance.

Keywords: Silica fume, Ground granulated blast furnace slag, High-strength concrete, Compressive strength, Cement replacement level

2nd International Conference on Multidisciplinary Sciences and Technological Developments (ICMUSTED 2025)

December 12-15, 2025

Production of Bioethanol Using Lower-Quality Algerian Sugar Dates Box-Behnken

Kaouther Zeghida[1], Sarra Guilane[1], Leila Benmansour[1]

[1]Department of Process Engineering, University of Badji Mokhtar, Annaba, Algeria
Corresponding author: Kaouther Zeghida (e-mail: kaouther.zeghida@univ-annaba.dz)

Abstract

The need for renewable biofuels to replace fossil fuels has increased due to the pressing global transition to sustainable energy. Because of its clean combustion, renewability, and compatibility with current fuel infrastructures, bioethanol stands out among the other options. This study explores the use of fermentation-based bioconversion to produce bioethanol from sugar dates, an underutilized agricultural waste that is high in fermentable sugars. To assess and simulate the impacts of three crucial variables substrate concentration, fermentation temperature, and yeast dosage the process was optimized using response surface methodology (RSM) combined with a Box-Behnken design. To evaluate the primary impacts and interactions of these variables on ethanol yield, fifteen experimental runs were carried out. A maximum ethanol output of 50.0 g/L was achieved under ideal conditions, which included a yeast dose of 1.5 g/100 mL, a fermentation temperature of 72 °C, and a substrate concentration of 3 g/100 mL. A very accurate second-order polynomial model was created to forecast ethanol production, providing important information for process control and optimization. Its applicability for energy applications was confirmed when the generated bioethanol was subjected to physical and chemical analysis and found to meet fuel-grade standards. Reliable quadratic model estimation was made possible by the Box-Behnken design, which also reduced the number of experiments needed. Because it avoids extreme values due to its spherical distribution, it can be used in complex bioconversion systems. This study demonstrates how well RSM and statistical modeling work to maximize the production of bioethanol from inexpensive, sugar-rich biomass. The findings show that sugar dates have the potential to be a sustainable feedstock and that RSM can increase process sustainability, scalability, and efficiency. These discoveries support the larger endeavor to create cleaner, renewable energy sources using cutting-edge biotechnological techniques.

Keywords: Bioethanol, Sugar-dates, Fermentation, Response surface methodology, Process optimization

2nd International Conference on Multidisciplinary Sciences and Technological Developments (ICMUSTED 2025)

December 12-15, 2025

Artificial Intelligence Control of Active and Reactive Power for a Three-Level NPC Inverter Connected to Grid Utility

Ghrissi Tahri[1], Fatima Tahri[2], Ali Tahri[3]

[1]Institute of Applied Sciences and Techniques. University Oran 1, Ahmed Ben Bella, Oran, Algeria
[2]Smart Grid Development Laboratory, Higher School of Electrical and Energetic Engineering, Oran, Algeria
[3]Oran Electrical Engineering Laboratory, Department of Electrotechnics, Faculty of Electrical Engineering University of Sciences and Technology Mohamed Boudiaf of Oran, Algeria
Corresponding author: Ghrissi Tahri (e-mail: g84tahri@gmail.com)

Abstract

This paper examines a three-phase, three-level neutral point clamped (NPC) inverter supplied with a direct current (DC) voltage source. It is connected to the grid utility through a passive inductor-capacitor (LCL) filter. The proposed artificial intelligence control strategy aims to transmit the highest-level active power to the public power grid with a unity power factor and high power quality. The fuzzy logic control (FLC) strategy design is based on calculating the instantaneous active and reactive power from the measured grid voltages and currents; thus, the active and reactive currents are decoupled with a conventional proportional integral (PI) controller that uses a conventional sinusoidal pulse width modulation (PWM) to control the amplitude and phase of fundamental components of the inverter output voltages. A simulation analysis using the Matlab Simulink SimPowerSystem toolbox reveals that. The FLC controller tracks active power references with a fast response time of 0.38 ms and rising time of 0.259 ms. It is also significant that the reactive power regulated by the FLC controller follows the zeroed reference with a faster transient response. Furthermore, the load grid current and voltage waveforms were obtained by switching the local load from inductive to capacitive mode at 0.15 seconds. The grid current and voltage are always in phase, and the power factor improves, reaching unity. This control technique allows the NPC inverter grid-connected system to transmit active power while compensating for reactive power and the control system provides dynamic resilience against rapid changes in reactive power and good active power tracking.

Keywords: Neutral Point Clamped, Inductor capacitor inductor filter, Fuzzy logic control, Proportional integral, Pulse width modulation

2nd International Conference on Multidisciplinary Sciences and Technological Developments (ICMUSTED 2025)

December 12-15, 2025

Mechanical Properties of Concrete Reinforced with Steel Fiber

Noshad Ali[1], Waqar Ali[1], Muhammad Hessib[1]

[1]Civil Engineering Department, Swedish College of Engineering and Technology, Rahimyar Khan, Pakistan
Corresponding author: Noshad Ali (e-mail: noshadrizvi1990@gmail.com)

Abstract

Different varieties of fibers are used with cement mortar/concrete which include metallic, polymeric, mineral and vegetable fibers. The aim of this study is to investigate the mechanical properties of concrete reinforced with nail and paper pin. Paper pin of 1 inch length, 0.70 mm diameter and 1.22 mm diameter of head while nail of 1 inch length, 1.23 mm diameter and 3.36mm diameter of head were used. Fibers were added from 0.5% to 2.5% with an increment of 0.5% (0.5%, 1%, 1.5%, 2%, and 2.5%) by weight of cement. Workability, compressive and tensile strength of control concrete and of all modified mixes with addition of nail and paper pin fiber are studies. Workability and compressive strength of all modified mixes with addition of nail fiber is decreased as compared tocontrolmix. Tensile strength of modified mixes with addition of nail fiber is increased as compared to control mix from (0.5% to 1%). On further addition of nail fiber from 1.5% to2.5% tensile strength decreased. With the addition of nail fiber at1% maximum tensile strength 4.48 N/mm^2 i.e., 15.16% more than the compared to control mix was observed. Tensile strength of all modified mixes with addition of paper pin fiber is increase as compared to control mix from (0.5% to 1.5%). On further addition of paper pin fiber from 1.5% the tensile strength decreases. At 1.5% addition of paper pin fiber maximum tensile strength 5.11 N/mm^2 i.e., 31.36% more than that of control mix was observed.

Keywords: Fiber-reinforced concrete, Nail fibers, Paper-pin fibers, Tensile strength, Workability

Influx of Different Growth Geometries on Titanium Thin Film for Medical Applications

Matteo Bertapelle[1], Joel Borges[2], Julia Claudia Mirza Rosca[1,3], Filipe Vaz[2,3]

[1]Mechanical Engineering Department, University of Las Palmas de Gran Canaria, Las Palmas de Gran Canaria, Spain
[2]Laboratory of Physics for Materials and Emergent Technologies (LaPMET), University of Minho, Braga, Portugal
[3]Materials Engineering and Welding Department, Transylvania University of Brasov, Brasov, Romania
Corresponding author: Filipe Vaz (e-mail: fvaz@fisica.uminho.pt)

Abstract

The present study focuses on the differences in behaviour and corrosion properties between three titanium thin films produced with different growth geometries. Two of the thin films were prepared with the same angle of deposition (60º), but different growth geometries (inclined and zig-zag), while the third (the reference sample) was prepared by the conventional geometry (normal incidence, 0º). Multiple analysis was conducted on these samples to reach a better understand the influence of the growth geometry on the corrosion response of the films. Characterization support analysis carried by scanning electron Microscopy (SEM) was used to investigate parameters such as thickness and morphological features, while atomic force microscopy (AFM) was used for surface roughness characterization. X-ray diffraction (XRD) was used to characterize the crystallinity state of the thin films. Regarding corrosion tests in simulated physiological fluid, a mix of alternating and continuous current techniques was used. The obtained results showed that varying the deposition geometry, a significant change on the material corrosion resistance is observed. The results show that there is an improvement in corrosion resistance in both the zigzag and inclined prepared samples, when compared to the conventional geometry grown sample. The sample prepared in the zigzag geometry reveals the highest corrosion resistance in simulated body fluid. These findings reinforce the conclusion that complex surface architectures enable the design of surfaces with distinct properties, specifically optimized for targeted medical applications, where surface features play a decisive role.

Keywords: Thin films, corrosion, Glancing angle deposition, Titanium, Inclination

2nd International Conference on Multidisciplinary Sciences and Technological Developments (ICMUSTED 2025)

December 12-15, 2025

Universal Design of Apparel Labels for People with Visual Impairment

Ilkay Ozsev Yuksek[1], Busra Ozdemir[1], Izel Kabaagac[1], Pelin Altay[1], Sukriye Yuksel Filiz[1], Nevin Cigdem Gursoy[1]

[1]Department of Textile Engineering, Faculty of Textile Technologies and Design, Istanbul Technical University, Gumussuyu, 34437 Istanbul, Türkiye
Corresponding author: Ilkay Ozsev Yuksek (e-mail: ilkay.yuksek@itu.edu.tr)

Abstract

Every individual has different characteristics. These differences may result from the mental and physical characteristics of individuals. Sometimes, these characteristics are called as disabled because the person cannot be able to do some of his/her basic needs. One of these obstacles is that the individual has low or no visual function. A visually impaired person tries to realize visual function by sensing organs. They might have a problem of distinguishing their clothes. In this project, both braille and quick response (QR) code systems were combined on the same label to support independent use by visually impaired people and to provide a richer set of garment information. The design aimed to provide easy access to information about the textile garments and ensure that the individual do not need the help of others.

Keywords: Visual impairment, Labels, Braille, QR code, Embossing

1. INTRODUCTION

There are different degrees of vision loss, up to total blindness. Consequently, several terms are used to describe blindness and visual impairment. Visually impaired people may be unable to distinguish their environment or read newspapers and books even when using corrective lenses; this loss of access to visual information severely affects daily life and independence [1]. There are many practical labelling and marking strategies and commercial products developed specifically for blind or low-vision people [2–5]. For example, some individuals use safety pins or buttons sewn into labels in a coded way to distinguish similar garments by color or style, and some keep written or braille lists that match suits, shirts and ties using braille numbers or letters attached to each piece of clothing [2, 5, 6]. braille clothing identifiers typically consist of study, washable metal or plastic tags carrying short braille inscriptions, often printed or molded in black on a light background. These tags can be sewn into the garment or attached using small holes or fastening systems, and each tag usually contains only two or three braille characters so that users do not need to master the full braille alphabet to interpret the code [3–6]. Various textile label concepts have been developed in Turkey and worldwide. Some solutions integrate braille clothing labels directly into garments or accessories, while others rely primarily on electronic identification technologies, such as Quick response (QR) codes, near field communication (NFC) tags or barcodes linked to mobile applications and voice interfaces [4, 5, 7–9].

The aim of this project was to design textile labels that make the lives of visually impaired people easier, within the framework of universal design. For this purpose, basic problems and needs were identified through interviews with blind, low-vision and legally blind individuals in specific age groups and with their relatives. Based on these interviews, the target group was defined as visually impaired individuals who wish to dress independently and manage their wardrobes without assistance. The project covered three different product groups—blouse, T-shirt and denim pants—and textile label concepts were developed and applied to each of these garments. The labels were sewn onto the blouse, T-shirt and denim pants, and each label combined embossed tactile symbols with a QR code providing extended information about the product, such as care instructions, color and pattern.

2. MATERIALS and METHODS

2.1. Sample Production

According to the interviews with visually impaired people and their relatives, the main requirements they highlighted were: distinguishing color and patterns, accessing care instructions, and being able to shop and manage clothing independently. A high-durability plastic embossing method was preferred in this project for representing

the braille alphabet. Both washing instructions and color information were encoded using embossed braille characters, while pattern information was given through additional plastic embossing motifs. In addition, a QR code was added in place of the conventional barcode on the inner label, since QR codes occupy less space and can contain more information, including links to audio descriptions and accessible digital content, than linear barcodes [7–9]. The standard inner label was re-designed as a multi-page label including information in several languages.

2.2. Designed Models

Different label designs were developed in accordance with the request of the visually impaired people. Three different inner textile labels and outer label designs were prepared for blouse, t-shirt, and denim pants. Twill 2x2 weave, twill 3x1 weave, sateen weave types were selected as woven ground fabrics and ultra violet (UV) ink were used for symbol embossing. The twill 2/2 fabric was selected as denim fabric. The developed label designs for denim pants, boy's t-shirt and girl's blouse are shown in Figure 1.

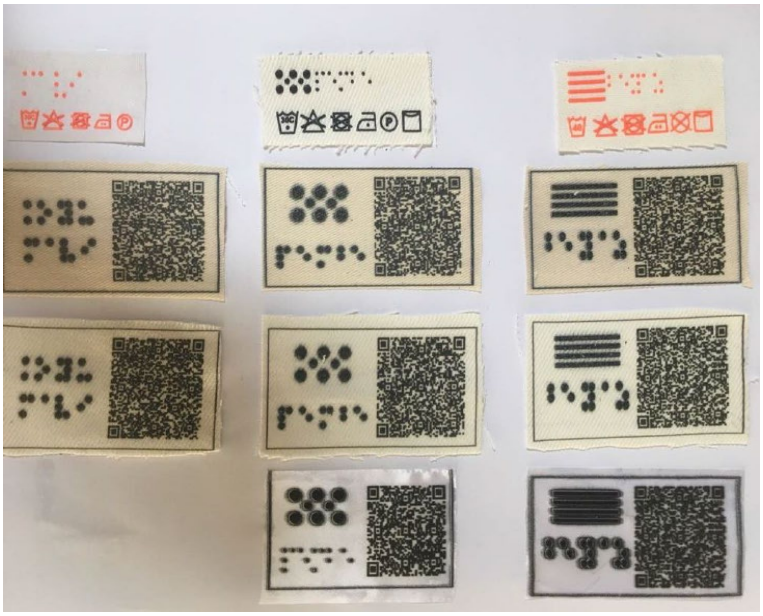

Figure 1. The developed label designs

2.2. Methods of Analysis

The prepared labels were tested with regards to color fastness to crocking (according to International Organization for Standardization (ISO) 105-X12) [10], water (according to ISO 105-E01) [11], home laundering (according to ISO 105-C08) [12] and dry cleaning (according to ISO 105-D01) [13]. For fastness tests, all samples are evaluated according to the American Association of Textile Chemists and Colorists (AATCC) gray scale.

3. RESULTS AND DISCUSSION

The color fastness to rubbing properties of labels are shown in Table 1. According to the color fastness to rubbing evaluation, the label produced with twill 2/2 denim fabric had the best performance against dry and wet rubbing. In sateen fabric, uneven dispersion of UV ink was observed.

Table 1. Color fastness to rubbing results of labels

	Twill 2/2	Twill 3/1	Sateen
Color Fastness to Rubbing (Dry)	3/4	3/4	2
Color Fastness to Rubbing (Wet)	4	3	4

The twill 2/2 denim fabric also has the best performance according to the color fastness to water, home laundering and dry-cleaning analysis which are shown in Tables 2-4 respectively. The labels with twill 3/1 fabric had better performance to color fastness to water; however, sateen labels were better according to the color fastness to

laundering test results. The labels produced with twill 3/1 and sateen fabrics had same results to the test of color fastness to dry cleaning.

Table 2. Color fastness to water results of labels

	Twill 2/2	Twill 3/1	Sateen
Color Change	4/5	4	4/5
Staining	4/5	3	3

Table 3. Color fastness to laundering results of labels

	Twill 2/2	Twill 3/1	Sateen
Color Change	4/5	4	4/5
Staining	4/5	4	4

Table 4. Color fastness to dry cleaning results of labels

	Twill 2/2	Twill 3/1	Sateen
Color Change	4	3/4	3/4
Staining	4/5	3/4	3/4

4. CONCLUSION

This study aimed to develop suitable label designs for visually impaired people in order to make their life easier. Three types of labels were developed suitable for application in denim pants, boy's t-shirt and girl's blouse. Labels included information about the products. The information was supplied by QR code, braille letters, pattern symbols and the symbols of the care instructions. The study can be improved with the future studies as: analysis of mechanical properties of labels, use of silicon-based materials, recyclable embossing material selection and implementation of smooth and rough fabrics to the labels.

References

[1] World Health Organization, "Blindness and visual impairment." [Online]. Available: https://www.who.int/news-room/fact-sheets/detail/blindness-and-visual-impairment. [Accessed Nov. 21, 2025].

[2] VisionAware, "Labeling and marking: a guide for low vision and blindness," APH ConnectCenter, Louisville, KY, USA. [Online]. Available: https://visionaware.org. [Accessed Nov. 21, 2025].

[3] VisionAware – APH ConnectCenter, "Labeling and marking: a guide for low vision and blindness," American Printing House for the Blind, Louisville, KY, USA, 2025. [Online]. Available: https://aphconnectcenter.org/visionaware/new-to-vision-loss/labeling-and-marking/. [Accessed Nov. 21, 2025].

[4] M. Ozsan and F. Hasret, "Gorme engelli bireylerin gunluk yasamini kolaylastirmak adina bir onerme: Braille alfabeli giysiler," *Muhendislik Bilimleri ve Tasarim Dergisi*, vol. 5, pp. 89–94, 2017.

[5] R. M. Alali, "A case study of visually impaired individuals' preferences of the availability of Braille clothing labels in shopping and selection of apparel," M.S. thesis, Dept. Family and Consumer Sciences, Ball State Univ., Muncie, IN, USA, 2017.

[6] R. Alsabhi, "Tactile and sensory fashion garments for the visually impaired: challenges and opportunities," *International Journal of Fashion Design, Technology and Education*, vol. 18, no. 1, pp. 1–9, 2025.

[7] S. J. V. Gatis Filho, J. de A. Macedo, M. M. Saraiva, J. E. A. Souza, F. B. Breyer, and J. Kelner, "My best shirt with the right pants: improving the outfits of visually impaired people with QR codes and NFC tags," in *Design, User Experience, and Usability: Designing Interactions*, A. Marcus and W. Wang, Eds. Cham, Switzerland: Springer, 2018, pp. 543–556.

[8] M. A. Badawy, "Using near field communication technology with voice recognition to help visually impaired people in clothes' selection," *International Design Journal*, vol. 14, no. 6, pp. 41–53, 2024.

[9] I. Ciesielska-Wrobel, "URI textiles professor studying braille clothing tags to help those with visual impairment," University of Rhode Island, Kingston, RI, USA, Jan. 17, 2025. [Online]. Available: https://www.uri.edu. [Accessed Nov. 21, 2025].

[10] International Organization for Standardization, “Textiles — Tests for colour fastness — Part X12: Colour fastness to rubbing,” ISO Standard 105-X12, Geneva, Switzerland, 2016.
[11] International Organization for Standardization, “Textiles — Tests for colour fastness — Part E01: Colour fastness to water,” ISO 105-E01:2013, Geneva, Switzerland, 2013.
[12] International Organization for Standardization, “Textiles — Tests for colour fastness — Part E04: Colour fastness to perspiration,” ISO 105-E04:2013, Geneva, Switzerland, 2013
[13] International Organization for Standardization, “Textiles — Tests for colour fastness — Part D01: Colour fastness to drycleaning using perchloroethylene solvent,” ISO 105-D01:2010, Geneva, Switzerland, 2010.

2nd International Conference on Multidisciplinary Sciences and Technological Developments (ICMUSTED 2025)

December 12-15, 2025

Systematic Study of Design and Operating Parameters in Forced Circulation Solar Water Heaters

Ahmed Remlaoui[1], Driss Nehari[1]

[1]Applied Hydrology and Environment Laboratory, University of Ain Temouchent-Belhadj Bouchaib, 46000 Ain-Temouchent, Algeria
Corresponding author: Ahmed Remlaoui (e-mail: ahmed.remlaoui@univ-temouchent.edu.dz)

Abstract

Forced circulation solar water heaters (FCSWHs) are among the most efficient technologies for utilizing solar energy to supply domestic hot water with high reliability. This study presents a systematic parametric analysis of FCSWH performance using the transient systems (TRNSYS) simulation program. Seven key parameters were investigated: collector area, glycol fraction ratio, storage tank volume, tank height, heat exchanger surface area, fluid flow rate, and pump power consumption. Simulation results reveal that the collector area and heat exchanger surface area exert the greatest influence on thermal efficiency and energy gain. Increasing the storage tank volume enhances daily energy availability but may decrease instantaneous efficiency due to higher heat losses, while tank height is critical for maintaining stratification. The glycol fraction ratio significantly affects heat transfer and antifreeze protection, especially under varying climatic conditions. Flow rate optimization is shown to be essential: low flow rates improve stratification and outlet temperature, whereas higher flow rates increase solar energy capture but raise auxiliary pumping energy demand. Overall, the TRNSYS-based analysis demonstrates that careful optimization of design and operating parameters can improve system efficiency by 10–25%, depending on climatic and operational conditions. The findings emphasize the need for an integrated design approach to balance thermal efficiency, energy performance, and auxiliary power consumption in FCSWH systems.

Keywords: TRNSYS simulation, Forced circulation solar water heater, Parametric study, Thermal efficiency, System performance

2nd International Conference on Multidisciplinary Sciences and Technological Developments (ICMUSTED 2025)

December 12-15, 2025

Comparative Study of the Corrosion Resistance of Magnesium and Zinc in Simulated Body Fluid

Cristina Jimenez-Marcos[1], Francisco Miguel Sanchez-Sosa[1], Julia Claudia Mirza-Rosca[1,2], Ionelia Voiculescu[3], Victor Geanta[3]

[1]Mechanical Engineering Department, Las Palmas de Gran Canaria University, Las Palmas de Gran Canaria, Spain
[2]Materials Engineering and Welding Department, Transilvania University of Brasov, Brasov, Romania
[3]Quality Engineering and Industrial Technology Department, National University of Science and Technology Politehnica Bucharest, Bucharest, Romania
Corresponding author: Ionelia Voiculescu (e-mail: ioneliav@yahoo.co.uk)

Abstract

The use of metal plates currently available to fix bone fractures requires a second surgery to remove the plate, increasing the risk of infection, complicating recovery and increasing the cost of medical care. Stainless steel and cobalt-chromium (Co-Cr) alloys cause problems of compatibility with bone tissue, such as inflammation, corrosion and the release of metal ions that affect bone health and regeneration. In response to these problems, resorbable materials have been developed, with magnesium (Mg) standing out for its biocompatibility, mechanical properties and controlled degradation rate, which makes it suitable for temporary fixation devices and avoids the need for a second surgery. However, research continues on the addition of zinc (Zn) to magnesium alloys, as it can improve mechanical properties and control corrosion rates. Based on microstructural analysis, electrochemical and microhardness tests on three Mg and Zn alloys (Mg1.4Zn, Mg5.3Zn, and Mg7.8Zn), which were manufactured by levitation induction melting, it was determined that the samples have an α-Mg matrix with intermetallic phase precipitation in the microstructure of the samples. Furthermore, it has been demonstrated that corrosion resistance is enhanced by decreasing the Zn content, while Vickers hardness values are elevated by increasing Zn percentages. These findings suggest that, by carefully adjusting the zinc concentration in Mg alloys, it is possible to optimize the balance between corrosion rate and mechanical integrity, which is crucial for the development of resorbable implants that promote bone healing without the drawbacks associated with permanent metal implants.

Keywords: Mg-Zn alloys, Levitation induction melting, Microstructure, Corrosion, Microhardness

2nd International Conference on Multidisciplinary Sciences and Technological Developments (ICMUSTED 2025)

December 12-15, 2025

Numerical Investigation of the Behavior of Strip Footings under Eccentric Loading in Non-Homogeneous Clay Soils

Nassima Zatar[1], Alaoua Bouaicha[2]

[1]Civil Engineering Department, Faculty of Technology, University Mostafa Benboulaid, 05078 Batna, Algeria
[2]Scientific and Technical Research Center on Arid Regions, Mohamed Khider University, 07000 Biskra, Algeria
Corresponding author: Nassima Zatar (e-mail: n.zatar@univ-batna2.dz)

Abstract

The behavior of strip footings embedded in non-homogeneous clay soils presents a significant challenge in geotechnical engineering due to the complex soil–structure interactions and the variability of loading conditions. Spatial variations in cohesion and undrained shear strength strongly affect the ultimate bearing capacity, the failure mechanisms, and the overall stability of shallow foundations. This study employs advanced numerical modeling using OptumG2 software to investigate the seismic and static performance of strip footings subjected to eccentric loading conditions. The main objective is to evaluate the combined influence of three key parameters: the degree of soil heterogeneity (k), the embedment ratio (D/B), and the load eccentricity ratio (e/B) on both the bearing capacity and the configuration of failure envelopes. The numerical results reveal that increasing soil heterogeneity and embedment ratio enhances the load-bearing performance and overall stability, while higher eccentricity tends to reduce the effective bearing capacity and alter the shape of the failure surfaces. The generated failure envelopes provide valuable insight into the interaction between vertical, horizontal, and moment loading components, clearly illustrating the safety domains and ultimate limit states. This research contributes to a deeper understanding of the mechanical response of shallow foundations on non-homogeneous clays and provides practical guidance for optimizing the design of strip footings in spatially variable soil profiles. The findings have direct implications for the safe and economical design of geotechnical systems in natural environments where stratification and strength gradients are significant.

Keywords: Non-homogeneous clay, Eccentric loading, Numerical analysis, Failure envelope, Embedment ratio

2nd International Conference on Multidisciplinary Sciences and Technological Developments (ICMUSTED 2025)

December 12-15, 2025

Oxidation Behaviors of Nickel-Based Superalloys at 1050 °C

Saida Bouyegh[1], Samira Tlili[1]

[1]Research Center in Industrial Technologies, Cheraga, Algiers, Algeria
Corresponding author: Saida Bouyegh (e-mail: s.bouyegh@crti.dz)

Abstract

The purpose of this study was to examine the oxidation behavior of the IN738LC Ni-based superalloy by subjecting specimens taken from the blade root to isothermal oxidations at 1050 °C for different durations (24h, 48h, and 72h). The isothermal oxidation kinetics, physical properties of the alloy (substrate) and the oxide scale were also accomplished. The microstructure of oxides and substrate after oxidation tests were examined by scanning electron microscopy (SEM) equipped with energy dispersive spectroscopy (EDS). Also, the composition and phase changes were predicted by X-ray diffraction (XRD). The results revealed that the IN738 LC Ni-based superalloys' oxidation kinetics followed a parabolic rate curve, suggesting that ion diffusion is in charge of the oxidation process. The oxidation process can occur when specific elements are used to create protective scales; the temperature affects how quickly these elements are consumed. The surface developed scales made up of different oxide phases. The phases of oxidation products have slightly varied compositions; at 1050 °C, the primary components are Cr_2O_3, Al_2O_3, and TiO_2, together with spinels of NiO and $NiCr_2O_4$. The highest protection against additional oxidation was offered by the Cr_2O_3 oxide dense band, while the internal oxide Al_2O_3 was discontinuous. The formation of oxide layers on the surface reveals that the elements (Cr, Ti, Al, and Ni) have trends toward the substrat's diffusion toward the upper part of the scale during hot oxydation, but at varying amounts, which vary exposure durations.

Keywords: Turbine blade, Inconel 738LC, Oxidation kinetics, Microstructure, Oxide layers

Recent Progress on Nanomaterial Application for Improving Water-Based Drilling Fluid

Siti Zulaika Razali[1], Norizah Abdul Rahman[2], Mohd Hafizuddin Ab Ghani[1], Siti Hajar Othman[3], Tan Sin Tee[2], Robiah Yunus[3], Umer Rashid[4]

[1]Institute of Nanoscience and Nanotechnology, Universiti Putra Malaysia, Serdang, Malaysia
[2]Faculty of Science, Universiti Putra Malaysia, Serdang, Malaysia
[3]Faculty of Engineering, Universiti Putra Malaysia, Serdang, Malaysia
[4]Faculty of Applied Sciences, UCSI University, Kuala Lumpur, Malaysia
Corresponding author: Siti Zulaika Razali (e-mail: zulaika@upm.edu.my)

Abstract

Water-based drilling fluids (WBM) are extensively used in the oil and gas industry due to their cost-effectiveness, environmental friendliness, and sustainability. However, shale hydration and wellbore instability remain significant challenges, leading to reduced drilling efficiency, increased non-productive time, and higher operational risks. Recent advances in nanotechnology have introduced functional nanomaterials including metal oxides, silica-based nanoparticles, carbon-based materials, and polymer-nanocomposites as effective shale inhibitors to enhance WBM performance. This review presents recent works on the application of nanomaterials in WBM, focusing on their effects on shale swelling, rheology and filtration control. The mechanisms by which nanoparticles interact with shale, including pore plugging, surface hydrophobization, and hydration inhibition, are discussed. Finally, emerging trends such as hybrid nanomaterials, functionalized composites, and green/bio-based nanoparticles are highlighted, demonstrating their potential to develop next-generation, high-performance, and environmentally sustainable WBM.

Keywords: Shale inhibitor, Nanoparticles, Water-based mud

2nd International Conference on Multidisciplinary Sciences and Technological Developments (ICMUSTED 2025)

December 12-15, 2025

Valorization of Coal Bottom Ash in Sustainable Lightweight Self-Compacting Concrete

Ibtissam Boulahya[1], Abedlkadir Makkani[1]

[1]Civil Engineering Department, Tahri Mohamed University, Bechar, Algeria
Corresponding author: Ibtissam Boulahya (e-mail: ibtissam_boulahya@yahoo.fr)

Abstract

This study investigates the use of coal bottom ash (CBA), obtained from a decommissioned power plant, in lightweight self-compacting concrete (LWSCC). Four mixes were prepared: one control and three mixtures in which natural coarse aggregate was fully replaced by CBA, while Portland cement was partially substituted with CBA powder (10%, 20%, and 30%). Fresh properties were evaluated through slump flow, L-box, and segregation resistance tests, while dry density, compressive strength, and ultrasonic pulse velocity (UPV) were used to assess hardened performance. Results showed that replacing coarse aggregate with CBA improved workability, whereas increasing CBA powder reduced it, though all mixes satisfied the French Association of Civil Engineering (AFGC) standards. Only slight reductions in density and strength were observed, remaining within structural lightweight concrete limits. UPV confirmed good durability. Overall, CBA is a suitable replacement for natural aggregate, and using 10% CBA powder as cement substitute appears to be an effective and sustainable option for producing LWSCC.

Keywords: Coal bottom ash, Lightweight self-compacting concrete, Workability, Mechanical performance, Sustainability

2nd International Conference on Multidisciplinary Sciences and Technological Developments (ICMUSTED 2025)

December 12-15, 2025

Teaching Strategies, Methods, and Techniques Used by Science Teachers

Ulas Kubat[1]

[1]Department of Curriculum and Instruction, University of Minnesota, St. Paul, USA
Corresponding author: Ulas Kubat (e-mail: ulaskubat@)yahoo.com)

Abstract

The purpose of this study is to identify the strategies, methods, and techniques used by science teachers. The specific strategies, methods, and techniques that science teachers employ to achieve the learning objectives of a subject are of paramount importance. The strategies, methods, and techniques used by teachers are crucial for enabling students to comprehend the subject matter and construct knowledge mentally. There is a wide variety of methods, strategies, and techniques that a teacher can use in the classroom. For teachers to create an effective teaching-learning process, they must have a thorough understanding of which strategy, method, or technique to use in specific situations. Each teaching method and technique has aspects where it is effective and others where it has limitations. Science teachers should be able to select the appropriate method based on the instructional objective and be willing to make adjustments based on student feedback when necessary. In line with this purpose, data were collected using a semi-structured interview form administered to 32 science teachers. The analysis of these interviews revealed that the most frequently used teaching strategy was a combination of discovery and expository methods. in terms of teaching methods, the discussion method was found to be the most commonly employed.

Keywords: Science education, Teaching strategies, Methods and techniques, Science teacher

2nd International Conference on Multidisciplinary Sciences and Technological Developments (ICMUSTED 2025)

December 12-15, 2025

The Impact of Out-Door Learning Environments on the Attainment of Objectives in the Teaching-Learning Process

Ulas Kubat[1], Matthew Price[2]

[1]Department of Curriculum and Instruction, University of Minnesota, St. Paul, USA
[2]Special Education, The University of Alabama at Birmingham, Birmingham, USA
Corresponding author: Ulas Kubat (e-mail: ulaskubat@)yahoo.com)

Abstract

The aim of this study is to demonstrate the impact of out-door learning environments on the attainment of learning outcomes in the teaching-learning process. Considering that education is often confined to school buildings and classrooms, this situation can lead to a decline in student interest over time, the complete alienation of students who fall behind the desired academic success, and the rapid forgetting of learned knowledge or the retention of only a small portion. Out-door learning environments offer teachers a wider range of methods and techniques to achieve targeted learning objectives. These environments not only contribute to the development of students' science skills but also enhance their desire to research and explore, leading to positive changes in student achievement. Out-door learning environments facilitate students' attainment of targeted learning objectives and provide them with experiential learning opportunities. When effectively utilized in science education, these environments help improve students' observation, data collection, and application of learned knowledge in daily life. For this purpose, data was collected through semi-structured interview forms with 20 pre-service science teachers. According to the data obtained, out-door school learning environments contributes to the achievement of learning objectives. They help students achieve more lasting objectives by increasing their interest in the subject. It has been revealed that out-door learning environments contribute to abstract knowledge and positively contribute to academic achievement.

Keyword: Out-door learning, Objectives, Science education, Science teacher

2nd International Conference on Multidisciplinary Sciences and Technological Developments (ICMUSTED 2025)

December 12-15, 2025

Use of Artificial Intelligence by Nursing Students: What Impact on Research Integrity?

Imane Bettane[1], Mohammed-Yassine Takzima[2], Amine Mohamed[1], Asma Sbai[1], Latifa Adarmouch[1]

[1]Bioscience and Health Research Laboratory, Community Medicine and Public Health Department, Faculty of Medicine, Cadi Ayyad University, Marrakech, Morocco
[2]Laboratory of Water Sciences, Microbial Biotechnologies, and Natural Resources Sustainability, Unit of Microbial Biotechnologies, Agrosciences, and Environment, Faculty of Sciences-Semlalia, Cadi Ayyad University, Marrakech, Morocco
Corresponding author: Imane Bettane (e-mail: imane.bettane@gmail.com)

Abstract

The rapid integration of artificial intelligence (AI) in higher education is reshaping pedagogical practices and research processes. In nursing sciences, students increasingly rely on generative AI tools for literature retrieval, data analysis, and academic writing. While these technologies provide clear benefits, such as accelerated access to information, improved writing quality, and enhanced digital skills, they also raise concerns regarding academic integrity, plagiarism, source reliability, and ethical compliance. This narrative review critically examines the literature published over the past decade, drawing on academic articles, policy documents, and educational reports. Emerging evidence highlights both opportunities and risks: AI fosters efficiency and innovation but, if used without proper regulation, may undermine critical thinking, generate biased or unverifiable content, and threaten scientific integrity. The findings underscore the urgent need for clear pedagogical and ethical guidelines to govern AI use among nursing students, ensuring a balance between technological innovation, scientific rigor, and academic integrity.

Keywords: Artificial intelligence, Narrative review, Nursing education, Students, Research integrity, Academic ethics

Valorization of Waste Rosehip Seeds – A Green and Novel Procedure

Abdulkadir Keskin[1,2], Betul Akhoroz[3,4], Gulin Amasya[3], Zerrin Sezgin Bayindir[3], Zekiye Goksel[5], Seda Kayahan[5], Yasin Ozdemir[5], Serpil Takac[1], Ayse Ezgi Unlu[1]

[1]Department of Chemical Engineering, Faculty of Engineering, Ankara University, Ankara, Türkiye
[2]Graduate School of Natural and Applied Sciences, Ankara University, 06110 Ankara, Türkiye
[3]Department of Pharmaceutical Technology, Faculty of Pharmacy, Ankara University, 06560 Ankara, Türkiye
[4]Graduate School of Health Sciences, Ankara University, 06110 Ankara, Türkiye
[5]Food Technology Department, Ataturk Horticulture Central Research Institute, Yalova, Türkiye
Corresponding author: Ayse Ezgi Unlu (e-mail: aeunlu@eng.ankara.edu.tr)

Abstract

Rosehip seeds, a waste of rosehip processing, are of significant interest due to their unique composition and potential applications in various industries. These seeds are rich in essential fatty acids, particularly omega-3 and omega-6, as well as a variety of bioactive compounds such as antioxidants, vitamins, and phytochemicals [1]. The high lipid content of rosehip seeds makes them an important source of natural oils, which are increasingly utilized in the cosmetic and pharmaceutical industries for their skin-nourishing, anti-inflammatory, and antioxidant properties [2]. Moreover, rosehip seed oil has been extensively studied for its potential therapeutic effects. This study presents the extraction and purification of lipid from the industrial waste, encapsulation of the extract into nanostructured lipid carriers (NLC) and formulate them as emulgel based nanocosmeceutical product. With this aim, different hydrophobic deep eutectic solvents were screened for the ultrasound assisted extraction of lipids from rosehip seed waste. The highest lipid yield was obtained using menthol-propanol (1:1). Extraction procedure was optimized using experimental design. The optimized extract was purified and a high-pressure homogenizer utilizing the hot homogenization technique was used for the preparation of NLCs containing rosehip seed oil. NLC formulations containing the optimized extract at different concentrations were prepared. The selected formulation was combined with Carbopol gel to prepare the final optimized extract-loaded NLC-enriched emulgel. These NLCs were developed as a novel delivery system for cosmetic/cosmeceutic purposes. This study represents the first time valorization of waste rosehip seeds with hydrophobic deep eutectic solvents and demonstrates the potential of the extract to be transformed into a high value-added cosmetic product through advanced technologies.

Keywords: Rosehip waste, Deep eutectic solvents, Nanostructured lipid carriers, Cosmetic formulation

Acknowledgments

This study is supported by TUBITAK (The Scientific and Technological Research Council of Turkey) - TAGEM (General Directorate of Agricultural Research and Policies) 1005 - Joint Call for Agricultural Research Projects (Project no: 123O471).

References

[1] A. R. Borsa, F. Ranga, M. Fogarasi, A. Borsa, D. C. Vodnar, and C. A. Semeniuc, “Valorisation of rosehip waste into a food ingredient–Focus on its colour, carotenoid content, and techno-functional properties,” *Applied Food Research*, vol. 5, no. 1, art. no. 100999, 2025.

[2] M. Stryjecka, A. Kiełtyka-Dadasiewicz, and M. Michalak, “Physico-chemical characteristics of Rosa canina L. seeds and determining their potential use,” *Applied Sciences*, vol. 15, no. 1, art. no. 168, 2024.

2nd International Conference on Multidisciplinary Sciences and Technological Developments (ICMUSTED 2025)

December 12-15, 2025

Exploring the Determinants of Green Innovation Adoption Among SMEs in Albania

Anxhela Bakiasi[1], Oljam Dervishi[2], Merzai Bakiasi[3]

[1]Department of Management, Faculty of Economy, University of Tirana, Tirana, Albania
[2]Department of Research and Innovation, Reinforce Sustainability (RESU), Tirana, Albania
[3]University of Hohenheim, Stuttgart, Germany
Corresponding author: Anxhela Bakiasi (e-mail: bakiasianxhela1@gmail.com)

Abstract

Green innovation is becoming an important priority for small and medium-sized enterprises (SMEs), especially as businesses face growing pressure to operate more sustainably. In Albania, this issue is gaining attention as the country moves closer to the European Union and adopts policies that are part of the Green Agenda for the Western Balkans. Despite this, little research has been carried out on how Albanian SMEs approach green innovation and what factors encourage or prevent them from adopting such practices. This paper explores the main determinants that shape the adoption of green innovation in the Albanian SME sector. The analysis is based on secondary sources, including national statistics, policy documents, and international reports from institutions such as the World Bank, Organisation for Economic Co-operation and Development (OECD), and Institute of Statistics of Albania (INSTAT). The focus is on understanding both the barriers and the opportunities that SMEs face. Internal challenges such as limited financial resources, lack of access to modern green technologies, and low managerial capacity often slow down adoption. On the other hand, external drivers, including European Union (EU) related regulations, donor programs, and the rising demand for sustainable products-create incentives for businesses to invest in greener solutions. The findings suggest that although many Albanian SMEs recognize the importance of sustainability, the level of adoption remains relatively low. Still, the country's natural potential in renewable energy, agriculture, and sustainable tourism, combined with international financial support, provides a strong base for progress. The paper concludes that clearer policy frameworks, targeted financial incentives, and capacity-building programs would significantly improve the environment for SMEs to engage in green innovation. Highlighting these factors is intended to contribute to ongoing debates among policymakers, business leaders, and researchers about the role of SMEs in Albania's green transition.

Keywords: Green innovation, SMEs, Albania, Sustainability, Adoption factors, Policy support

1. INTRODUCTION

In recent decades, the concept of green innovation has become a central theme in academic research and policy discussions worldwide [1]. Defined broadly as the development and adoption of environmentally friendly products, services, and processes, green innovation has been increasingly recognized as a key driver of sustainable growth and competitiveness [2, 3]. For small and medium-sized enterprises (SMEs), which form the backbone of most economies, adopting green practices is no longer only a matter of corporate social responsibility but also a strategic response to market, regulatory, and financial pressures [4, 5].

The relevance of this topic is particularly strong in developing and transition economies, such as Albania, where SMEs dominate the business landscape and play a vital role in employment and economic growth [6]. Albania's progress toward European Union (EU) integration has further highlighted the need for sustainable business practices, as the country gradually aligns with EU environmental standards and implements policies under the Green Agenda for the Western Balkans [7, 8]. These dynamics make the Albanian context particularly interesting for examining the determinants of green innovation.

Existing literature suggests that multiple internal and external factors shape the adoption of green innovation [8]. Internally, financial resources, managerial attitudes, and firm capabilities are crucial in determining whether enterprises adopt environmentally friendly technologies [9, 10]. Externally, regulatory frameworks, donor programs, and consumer awareness play an equally strong role [11, 12]. However, SMEs in Albania often face barriers such as limited access to finance, insufficient institutional support, and low technological capability, which restrict their ability to adopt sustainable practices effectively [13–15].

This paper aims to explore these determinants within the Albanian SME sector, focusing on how internal capacities and external pressures interact to shape business behavior [16]. By combining economic and policy perspectives, it contributes to the broader debate on how SMEs in developing economies can accelerate their transition toward sustainability [17].

2. MATERIAL AND METHOD

The study employs a qualitative desk research approach, focusing on secondary data sources to explore the determinants of green innovation adoption among SMEs in Albania. Data were collected from institutional reports, policy documents, statistical databases, and international publications. The aim is to identify internal and external factors that influence SME adoption of green practices and to quantify adoption levels where data are available.

2.1. Data Sources

Data were primarily collected from the following sources:

- Institute of Statistics of Albania (INSTAT): Business Register 2022 – provides sectoral distribution of SMEs in Albania [17].
- World Bank Enterprise Surveys: information on business practices and innovation adoption.
- United Nations Development Programme (UNDP) Albania Reports: Insights into sustainability and green economy initiatives [18, 19].
- Organisation for Economic Co-operation and Development (OECD) and European Commission: policy frameworks for SMEs and green growth [20].

2.2. Analysis Approach

A descriptive statistical approach was used to summarize available data. Frequencies, percentages, and simple cross-tabulations were calculated to illustrate patterns of green innovation adoption across sectors. Graphical visualizations were included to highlight adoption levels.

Table 1. Adoption of green practices by SMEs in Albania (2022)

Sector	Number of SMEs	SMEs Adopting Green Practices (%)
Manufacturing	4,200	18
Tourism & Hospitality	2,500	12
Agriculture & Food	3,100	15
Services & Information Technology (IT)	2,800	20
Construction	2,000	10

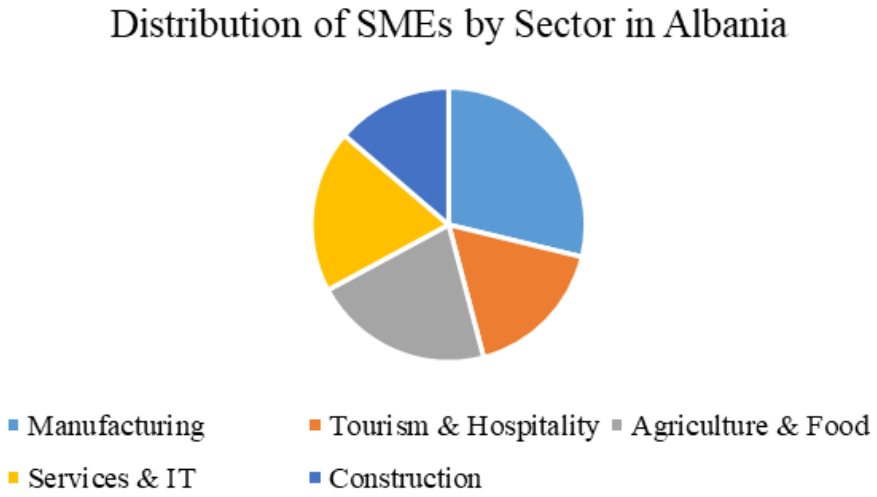

Figure 1. Distribution of SMEs by sector in Albania

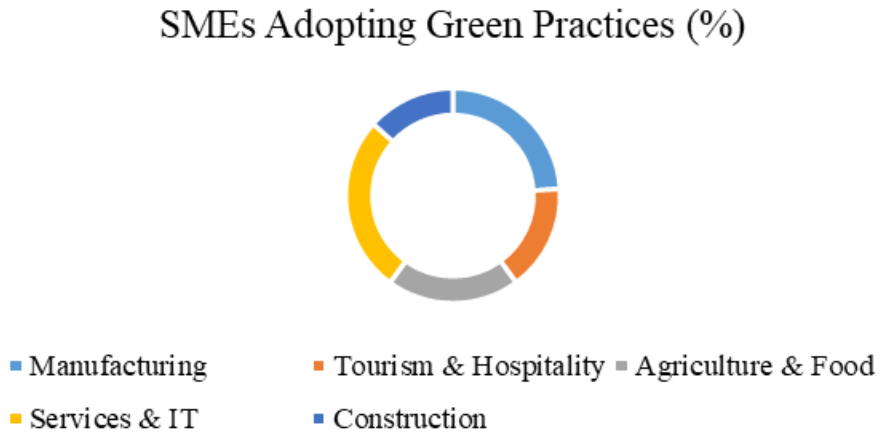

Figure 2. Share of SMEs adopting green practices in Albania

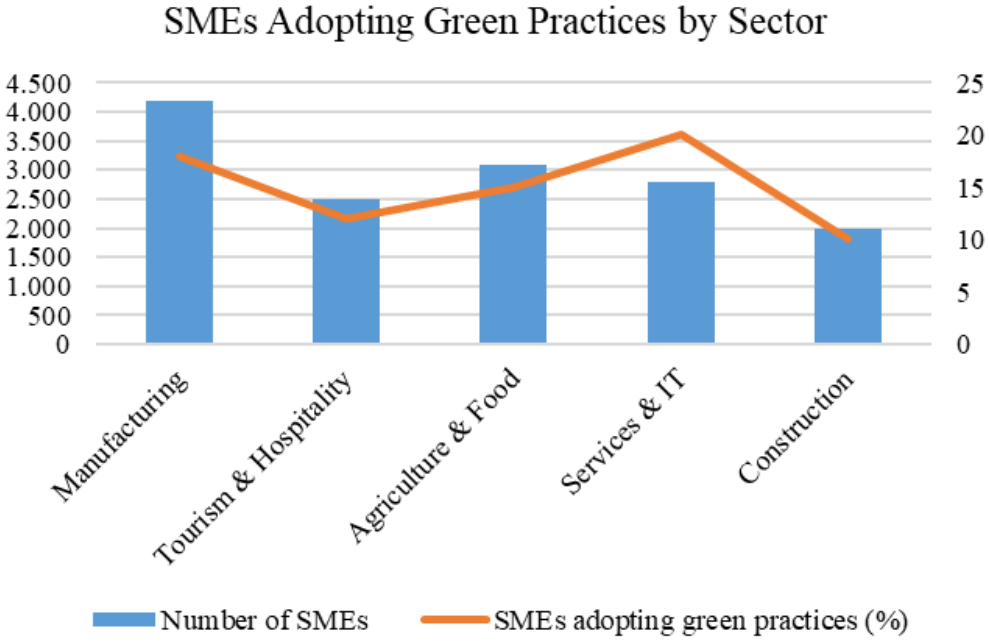

Figure 3. SMEs adopting green practices by sector

3. RESULTS

The analysis of secondary data reveals that the level of green innovation adoption among SMEs in Albania remains relatively modest. As illustrated in Table 1, only a limited share of SMEs across sectors have implemented sustainable practices, with the highest rates observed in the Services & IT sector (20%) and the Manufacturing sector (18%).

These findings suggest that sectors with stronger technological capacity and export orientation tend to integrate environmental innovation more rapidly. From an economic perspective, the results indicate that green innovation is still perceived by many SMEs as a cost rather than an investment opportunity. Limited access to finance, small market size, and high upfront costs of green technologies discourage many firms from adopting environmentally friendly practices. However, evidence from international studies shows that once adopted, such practices can enhance resource efficiency, reduce operational costs, and improve brand competitiveness in both domestic and foreign markets.

This is particularly relevant for Albanian SMEs aiming to access the EU single market, where environmental standards are increasingly stringent. On the policy and institutional side, the analysis shows that external drivers are becoming more influential. The European Union's Green Agenda for the Western Balkans, the National Strategy for Development and Integration, and donor-supported initiatives by UNDP and German Agency for International Cooperation (GIZ) have begun to create a more favorable environment for sustainability.

Nevertheless, gaps in implementation, limited coordination between institutions, and insufficient awareness among entrepreneurs continue to hinder broader diffusion.

Cross-sectoral comparison further highlights that tourism, agriculture, and construction lag behind in green adoption due to their fragmented structure and low technological intensity. These sectors would benefit significantly from targeted capacity-building and financial incentives.

On the other hand, firms operating in Information and Communication Technology (ICT) and manufacturing sectors are better positioned to capitalize on green opportunities, particularly through digitalization and cleaner production technologies.

Overall, the results point to a dual challenge for Albanian SMEs: enhancing their internal capabilities-financial, managerial, and technological, while responding to growing external pressures from markets and regulations. The interplay of these factors determines not only the pace of green transition but also the long-term competitiveness of the SME sector in the context of EU integration.

4. CONCLUSION

This paper has explored the determinants influencing the adoption of green innovation among SMEs in Albania by integrating both economic and policy dimensions. Findings indicate that while awareness of sustainability is growing, the actual implementation of green practices remains at an early stage. Financial constraints, limited technical know-how, and low market demand are major internal barriers, whereas regulatory alignment with the EU and donor programs serve as external motivators.

To accelerate green innovation, policy measures should focus on creating accessible financial instruments such as green credit lines and tax incentives, improving knowledge transfer through training programs, and strengthening collaboration between government agencies, academia, and the private sector. Institutional clarity and a more predictable regulatory environment will be key to building business confidence.

Future research should examine micro-level data on SME innovation behavior, explore sector-specific dynamics, and assess the impact of digital transformation on green competitiveness. Such insights would help policymakers design more targeted interventions to ensure that Albanian SMEs play an active role in the country's sustainable economic transition.

Acknowledgments

We would like to express our sincere gratitude to SMEs across various sectors in Albania for their invaluable contributions to this study. Although this research primarily relied on secondary data, the insights and information provided by business owners and managers through reports and publications were crucial in understanding the determinants of green innovation adoption. We also extend our thanks to the institutions and organizations, such as INSTAT, UNDP Albania, and the World Bank, for making relevant data publicly available. Finally, we acknowledge the guidance and support of our academic advisors and mentors, whose expertise, constructive feedback, and encouragement have been instrumental in completing this research successfully.

References

[1] K. Rennings, "Redefining innovation — eco-innovation research and the contribution from ecological economics," *Ecological Economics*, vol. 32, no. 2, pp. 319–332, 2000.
[2] A. Lutfi, "What factors influence SMEs to adopt green innovations?," *Sustainability*, vol. 15, no. 13, art. no. 10645, 2023.
[3] M. E. Porter and C. van der Linde, "Toward a new conception of the environment-competitiveness relationship," *Journal of Economic Perspectives*, vol. 9, no. 4, pp. 97–118, 1995.
[4] J. Horbach, C. Rammer, and K. Rennings, "Determinants of eco-innovations by type of environmental impact — The role of regulatory push/pull, technology push and market pull," *Ecological Economics*, vol. 78, pp. 112–122, 2012.
[5] G. Biggi, A. Mina, and F. Tamagni, "There are different shades of green: Heterogeneous environmental innovations and their effects on firm performance," *arXiv*, 2023. doi: 10.48550/arXiv.2310.08353
[6] European Commission, "Albania 2023 report," Brussels, 2023.
[7] Regional Cooperation Council, *Green Agenda for the Western Balkans*, RCC, Sarajevo, 2021.

[8] P. Demirel and E. Kesidou, “Stimulating different types of eco-innovation in the UK: Government policies and firm motivations,” *Ecological Economics*, vol. 70, no. 8, pp. 1546–1557, 2011.
[9] OECD, *SME Policy Index: Western Balkans and Turkey 2021*, OECD Publishing, 2021.
[10] World Bank, *Enterprise Surveys: Albania Country Profile*, Washington, USA, 2019.
[11] E. Icka, “Environmental sustainability practices of Albanian microenterprises,” *Midwest Social Sciences Journal*, vol. 8, no. 2, pp. 45–59, 2021.
[12] I. Tomorri and R. Keco, “Challenges and factors affecting the sustainable development of SMEs in Albania,” *Conferencii*, vol. 7, no. 1, pp. 1–10, 2023.
[13] G. Rexhepi, H. Abazi-Alili, S. Abduli, S. Ibraimi, and R. Zuferi, “Green entrepreneurship and firm performance: The case of Albania,” *Sustainable Development*, vol. 31, no. 4, pp. 123–135, 2023.
[14] OECD, *Digital and Green SMEs: Enhancing Innovation and Sustainability*, OECD Publishing, 2025.
[15] European Bank for Reconstruction and Development (EBRD), “EBRD launches €377 million programme to help Western Balkans ‘Go Digital’,” *Reuters*, 2025.
[16] N. A. Setyawan, H. Utami, B. S. Nugroho, M. Ayuwardani, and Suharmanto, “Analysis of the driving factors of implementing green supply chain management in SMEs in the city of Semarang,” *arXiv*, 2022. doi: 10.48550/arXiv.2212.12891
[17] INSTAT, *Business Register 2022*, Institute of Statistics, Albania, 2023.
[18] UNDP Albania, *Sustainable Development and Green Economy in Albania*, Tirana, 2022.
[19] M. Wasiq, “Factors influencing green innovation adoption and its impact on sustainable performance,” *Sustainability*, vol. 15, no. 3, p. 2447, 2023.
[20] OECD, *Eco-Innovation in Industry: Enabling Green Growth*, OECD Publishing, 2009.

2nd International Conference on Multidisciplinary Sciences and Technological Developments (ICMUSTED 2025)

December 12-15, 2025

A Comparative Analysis of Drought Indices Using Remote Sensing and Geospatial Data Processing

Amar Benlakhdar[1], Abdelmoutia Telli[2], Nourelhouda Dekhili[3]

[1]Civil Engineering and Hydraulic Department, Biskra University, Biskra, Algeria
[2]computer Sciences Department, Biskra University, Biskra, Algeria
[3]Mechanical Engineering Department, Biskra University, Biskra, Algeria
Corresponding author: Amar Benlakhdar (e-mail: amar.benlakhdar@univ-biskra.dz)

Abstract

Drought is a prolonged period of below-average moisture that affects water supply and human activities. Traditional drought monitoring relies on meteorological data, which may not fully capture drought impacts. Remote sensing technology offers a solution by providing a broad view and frequent data collection, enabling better monitoring of surface water. Various remote sensing drought indices utilize satellite data to assess drought conditions. The normalized difference vegetation index (NDVI) measures vegetation health and density by analyzing how plants reflect light. The vegetation condition index (VCI) indicates the relative health of vegetation by comparing current vegetation status to past conditions. These indices help water managers identify changes in water availability and support effective drought management. The analysis of different indices reveals varying strengths and weaknesses, making it essential to select the appropriate index based on specific conditions. Future advancements in technology and data collection will enhance our ability to monitor and respond to drought effectively.

Keywords: Drought monitoring, Remote sensing, Vegetation index, Surface water

1. INTRODUCTION

Drought represents an extended period of drier than average moisture conditions that can impact water supply, produce loss, and impair human activities. Traditional approaches to drought monitoring often use indices based on meteorological data, which show limited ability to reflect drought impact by themselves. Because of this, different types of remote sensing data and derived indices have been used to complement the traditional drought monitoring framework. Satellite remote sensing can aid in drought assessment with a synoptic view and frequent coverage, making it possible to monitor large areas over time. In particular, the continuous availability of remotely sensed data collected from a variety of sensors mounted on various orbiting platforms has made it possible to obtain information on surface water behavior in new ways that provide quick overviews and extended adaptability [1].

It is important to monitor and evaluate surface water because of the value of this resource for human consumption and agriculture, and in many cases, drought has led to water scarcity. Comprehensive drought monitoring can benefit water managers by discovering possible long-term changes in water availability and can assist resource managers in supporting drought management and recovery efforts. Drought-driven environmental changes have major effects on ecosystems, agriculture, and food productivity; for agriculture, especially for rainfed culture, the impact of drought can be substantial. In combination with ground-based measures, remote sensing-based drought monitoring has the potential for application in the monitoring of surface water resources [2, 3].

The rest of this paper is organized as follows: Section 2 provides an overview of remote sensing drought indices. Section 3 presents some applications of remote sensing drought indices in surface water monitoring. Section 4 introduces a comparative analysis of main remote sensing drought indices, and Section 5 concludes the paper.

2. OVERVIEW OF REMOTE SENSING DROUGHT INDICES

Remote sensing drought indices have evolved as an effective method for surface water monitoring, as image data in different satellite spectral bands can reveal a lot of information. Depending on the purpose, remote sensing

drought indices are categorized as meteorological, agricultural, or hydrological drought indices. A number of remote sensing indices based on spectral data from remote sensing platforms are being used to monitor drought. These remote sensing drought indices basically account for drought's impact on one or more elements of the hydrological cycle: deficit in precipitation, changes in soil moisture and vegetation canopy, and changes in surface water availability, including changes in streamflow and river/lake water storage [1, 4].

Vegetation-based drought indices are primarily vegetation-related indices that are more correlated with meteorological drought or soil moisture content and streamflow. Drought indices without thematic meaning provide spatial and temporal drought assessments, although many pilots and field measurements are required for assessment. Currently, the most common agricultural drought assessment index used in environmental monitoring using remote sensing the vegetation condition index (VCI). Moreover, VCI derived from near-infrared and thermal bands has been more effective than the other concatenated indices. The VCI mainly uses satellite observations in the normalized difference vegetation index (NDVI) time series. Comparison of rainfall and VCI data shows good correlation. VCI gives very good results in the determination of NDVI and standardized precipitation index (SPI). VCI is used on a global scale in the determination of drought. However, in the (VCI), the change of the biome from the 1 km^2 spatial data to the 4 km^2 spatial data reduced the precision. In addition, when used over forested areas, the assessment cannot be made properly, and it is not observed in the drying-up stages. Generally, the VCI requires environmental data corresponding to the NDVI value, and it is a dimensionless index that provides information within the reality of environmental conditions [5–7]. In environmental science, various indices are used to assess vegetation health and precipitation patterns [8].

2.1. NDVI

NDVI is an index that quantifies vegetation health and density by measuring the difference between near-infrared light reflected and red light absorbed by plants, with values ranging from -1 to 1; higher values indicate healthier, denser vegetation. It is calculated using the Equation (1) where near-infrared reflectance (NIR) represents the reflectance of near-infrared light, which is light just beyond the visible spectrum. Red reflectance (RED) represents the reflectance of red light in the visible spectrum. Both are used to assess vegetation and surface characteristics in remote sensing.

$$\mathrm{NDIV} = \frac{\mathrm{NIR} - \mathrm{RED}}{\mathrm{NIR} + \mathrm{RED}} \tag{1}$$

2.2. VCI

VCI is an index derived from NDVI that measures the relative health or condition of vegetation over time by comparing current NDVI values to historical minimum and maximum values, helping to identify vegetation stress or drought conditions. It measures vegetation health using the Equation (2) where NDVI max and NDVI min refer to the maximum and minimum values of the NDVI within a specific area or time period, indicating the highest and lowest levels of vegetation greenness or health observed. This index helps indicate how the current vegetation condition compares to historical data.

$$\mathrm{VCI} = \frac{\mathrm{NDVI} - \mathrm{NDVI}_{\min}}{\mathrm{NDVI}_{\max} - \mathrm{NDVI}_{\min}} \times 100 \tag{2}$$

2.3. SPI

SPI is a simple drought indicator that measures how much precipitation deviates from the long-term average over a specific period, helping to identify dry or wet conditions. It standardizes precipitation data to allow comparison across different regions and timescales. It is utilized to evaluate precipitation levels. It is defined by the Equation (3) where P is the observed precipitation, μ is the mean precipitation, and σ is the standard deviation of precipitation. Together, these indices provide valuable insights into environmental conditions, helping scientists and researchers monitor changes in ecosystems and weather patterns:

$$\mathrm{SPI} = \frac{\mathrm{P} - \mu}{\sigma} \tag{3}$$

Table 1. Comparative of drought indices [8]

Index	Application	Advantages	Limitations
NDVI	Vegetation health monitoring	Simple, widely used	Affected by soil background and atmosphere
VCI	Drought severity	Applicable globally	Limited precision in forested areas
SPI	Rainfall deficit	Meteorological drought	Requires historical precipitation data

3. APPLICATION OF REMOTE SENSING DROUGHT INDICES IN SURFACE WATER MONITORING

In the literature, the drought monitoring and assessment versions based on remote sensing signals have been developed and implemented in a few case studies in different geographic regions. In Mexico, a semi-distributed approach was proposed that estimates the spatial pattern of groundwater change in separate modeling units based on correlations in the past. The American Academic and High School Institute (AHSI) was used for the drought periods to identify where changes in surface water availability as a result of drought occurred relative to the preceding years. In Iraq, the impact on the degraded reserve storage resources in three northern water reserves generated by the drought was evaluated through the AHSI [9].

Moreover, an attempt was made to use multiple drought indices as a means of water resource assessment in the Zhoujiang River Basin, south of China. The outcome of this study resulted in a moderate drought period associated with changes in drought occurrence and increasing intensity. Luca Lake in Eastern Tyva has also been significantly impacted by meteorological drought; yields of connected wetlands have been found to decrease with respect to the previous year. Additionally, depending on the results from the two indices, it is argued that the combined use of drought indices can provide complementary information for monitoring drought situations [10].

The elaboration of practical applications of remote sensing drought indices has entered into the operational management processes to address the pressures of water scarcity. The (AHSI) index was applied to the Tarim River of Xinjiang for the study period according to satellite radar altimeter observations. The results of this study revealed that the hydrological state of the Tarim River can be continuously modified and lands can be refilled with water, and the management strategy for this river can be more favorable. Transient lakes were identified from a project, and based on lakes' fluctuation detection, a significant percentage of studied lakes were reported to fluctuate between the specified periods. Finally, substantial limitations in rainfall reduction were proved by applying the Regional Climatic Drought Index at a specific level, as well as analyzing the risk and share of potential tipping points between the regional socio-ecological systems and the stabilized lake level [11, 12].

4. COMPARATIVE ANALYSIS OF KEY REMOTE SENSING DROUGHT INDICES

With recent advances in earth observation technology, a variety of remote sensing drought indices have been developed for surface and soil moisture monitoring. Different indices may have various strengths with respect to technical, regional, or meteorological considerations. For instance, one index might better capture vegetation status, thus having better responsiveness to drought conditions, while another might have an improved accuracy level. Therefore, it is valuable to evaluate different remote sensing drought indices to better understand where each index performs strongly and what they can reflect. Consequently, we conducted a comparative analysis and evaluated five representative remote sensing drought indices by using the Zinga Catchment as a study area in Tanzania at three different climatic regions, thus incorporating various climate conditions [13].

With recent The evaluation of remote sensing drought indices considered their stability, symmetry, and responsiveness to extreme weather events. Further, indices for monitoring surface water could be evaluated by considering:

- How accurately the indices reflect the monitoring object,
- The reliability of the index over time,
- The robustness of the index in different climatic conditions. The possible methods for evaluating remote sensing drought indices are using statistical analysis or focusing on field study.

To understand how indices will perform in practice, these are studied in different regions to understand how they will respond to different vegetation conditions. In our current study, the five indices are compared and a detailed

comparative analysis is carried out in order to understand how detection results will change depending on the selected index. While simple drought indices provide a snapshot of drought conditions, they can lead to very different drought forecasts. Based on this comparison, the context-specific application could be used to determine which drought index constitutes the best basis for decision-making. Moreover, it could be combined with hydrological simulation [14–16].

Results from a comparative analysis of several drought indices show similarities based on a statistical clustering approach. Even in drought-prone regions, the index performance can vary; within a single area, indices vary with insufficient levels of accuracy. Moreover, we find significant differences in the ability of different drought indices, which are mostly explained by local climate patterns. Remote sensing technology has been widely used to monitor soil moisture and assess surface water changes. With its broad spatial coverage and regular and near real-time reporting capability, remote sensing technology has the potential to contribute information for drought monitoring on a regional and global scale. In addition, numerous studies have been performed to develop drought indices based on remote sensing data to understand cropping conditions or assess vegetation growth [17].

5. CONCLUSION AND FUTURE DIRECTIONS

This paper highlights the significant advancements made in monitoring hydrological droughts and surface water through remote sensing methods. These techniques offer timely assessments in data-poor regions, crucial for decision-makers and drought management institutions. The integration of remote sensing data with technical developments in hydrology can enhance field experiments and model calibrations. The deployment of additional satellites and drones, combined with machine learning, can improve the accuracy of drought indices. Future research should focus on participatory design, engaging stakeholders to better address drought monitoring needs, particularly in agricultural contexts. Open data sharing between stakeholders and researchers is essential for effective drought early-warning systems. The negative impacts of water scarcity necessitate innovative tools and methods to address societal issues related to drought. Collaboration among scientists, policymakers, and practitioners is vital to optimizing the use of remote sensing in managing drought conditions. Researchers are encouraged to pursue innovative, data-rich objectives to further advance this field.

References

[1] W. Jiao, L. Wang, and M. F. McCabe, “Multi-sensor remote sensing for drought characterization: current status, opportunities and a roadmap for the future,” *Remote Sens. Environ.*, vol. 256, art. no. 112313, 2021. doi: 10.1016/j.rse.2021.112313

[2] T. D. Bhaga, T. Dube, M. D. Shekede, and C. Shoko, “Impacts of climate variability and drought on surface water resources in Sub-Saharan Africa using remote sensing: A review,” *Remote Sens.*, vol. 12, no. 24, art. no. 4184, 2020. doi: 10.3390/rs12244184

[3] M. B. Mukhawana, T. Kanyerere, and D. Kahler, “Review of in-Situ and remote sensing-based indices and their Applicability for integrated drought monitoring in South Africa,” *Water*, vol. 15, no. 2, art. no. 240, 2023. doi: 10.3390/w15020240

[4] A. Farahmand, J. T. Reageri and N. Madani, “Drought cascade in the terrestrial water cycle: Evidence from remote sensing,” *Geophys. Res. Lett.*, 2021. doi: 10.1029/2021GL093482

[5] M. I. Faridatul and B. Ahmed, “Assessing agricultural vulnerability to drought in a heterogeneous environment: A remote sensing-based approach,” *Remote Sens.*, vol. 12, no. 20, art. no. 3363, 2020. doi: 10.3390/rs12203363

[6] S. B. Wassie, D. A. Mengistu, and A. B. Birlie, “Agricultural drought assessment and monitoring using MODIS-based multiple indices: The case of North Wollo, Ethiopia,” *Monitor. Assess.*, vol. 194, art. no. 787, 2022. doi: 10.1007/s10661-022-10455-4

[7] M. Karimi, K. Shahedi, T. Raziei, and M. Miryaghoubzadeh, “Meteorological and agricultural drought monitoring in southwest of Iran using a remote sensing-based combined drought index,” *Stoch. Environ. Res. Risk Assess.*, vol. 36, pp. 3707–3724, 2022. doi: 10.1007/s00477-022-02220-3

[8] A. K. Mishra and V. P. Singh, “A review of drought concepts,” *J. Hydrol.*, vol. 391, no. 1–2, pp. 202–216, 2010. doi: 10.1016/j.jhydrol.2010.07.012

[9] R. Zhang, C. Y. Shi, P. Sun et al., “Multisource data-based integrated drought monitoring index: Model development and application,” *J. Hydrol.*, vol. 615, art. no. 128644, 2022. doi: 10.1016/j.jhydrol.2022.128644

[10] D. Shah and V. Mishra, “Integrated drought index (IDI) for drought monitoring and assessment in India,” *Water Resour. Res.*, 2020. doi: 10.1029/2019WR026284

[11] S. Jia and Y. Yang, “Spatiotemporal characteristics and driving factors of land-cover change in the Heilongjiang (Amur) River Basin,” *Remote Sens.*, vol. 15, no. 15, art. no. 3730, 2023. doi: 10.3390/rs15153730
[12] L. Wang, B. Zhang, Q. Shen, Y. Yao, S. Zhang, H. Wei, et al., “Estimation of soil salt and ion contents based on hyperspectral remote sensing data: A case study of Baidunzi Basin, China,” *Water*, vol. 13, no. 4, art. no. 559, 2021. doi: 10.3390/w13040559
[13] Z. Zhang, W. Xu, Z. Shi, and Q. Qin, “Establishment of a comprehensive drought monitoring index based on multisource remote sensing data and agricultural drought monitoring,” *IEEE J. Sel. Top. Appl. Earth Obs. Remote Sens.*, vol. 14, pp. 2113–2126, 2021. doi: 10.1109/JSTARS.2021.3052194
[14] M. G. Uddin, S. Nash, and A. I. Olbert, “A review of water quality index models and their use for assessing surface water quality,” *Ecol. Indic.*, vol. 122, art. no. 107218, 2021. doi: 10.1016/j.ecolind.2020.107218
[15] S. Elsayed, H. Hussein, F. S. Moghanm, and K. M. Khedher, “Application of irrigation water quality indices and multivariate statistical techniques for surface water quality assessments in the Northern Nile Delta, Egypt,” *Water*, vol. 12, no. 12, art. no. 3300, 2020. doi: 10.3390/w12123300
[16] M. Gad, A. H. Saleh, H. Hussein, M. Farouk, and S. Elsayed, “Appraisal of surface water quality of Nile River using water quality indices, spectral signature and multivariate modeling,” *Water*, vol. 14, no. 7, art. no. 1131, 2022. doi: 10.3390/w14071131
[17] H. Adab, R. Morbidelli, C. Saltalippi, and M. Moradian, “Machine learning to estimate surface soil moisture from remote sensing data,” *Water*, vol. 12, no. 11, art. no. 3223, 2020. doi: 10.3390/w12113223

2nd International Conference on Multidisciplinary Sciences and Technological Developments (ICMUSTED 2025)

December 12-15, 2025

Environmentally Friendly Synthesis, Structural Characterization, Computational Analysis, and Biological Assessment of Benzodiazepine Derivatives

Samir Hmaimou[1], Marouane Ait Lahcen[1], Wiam Lahrich[1], Mohamed Adardour[1], Mohamed Maatallah[1], Abdesselam Baouid[1]

[1]Molecular Chemistry Laboratory, Department of Chemistry, Semlalia Faculty of Sciences, Cadi Ayyad University, 40001 Marrakech, Morocco
Corresponding author: Samir Hmaimou (e-mail: samir.hmaimo@gmail.com)

Abstract

Heterocyclic compounds, particularly benzodiazepine derivatives, have emerged as promising scaffolds for multitarget drug development due to their structural versatility and diverse biological activities. In this study, a series of benzodiazepine derivatives, including HM55 and HM65, were synthesized via condensation and substitution reactions, characterized using Nuclear Magnetic Resonance spectroscopy, and Electrospray Ionization Mass Spectrometry analysis. The cytotoxic potential of HM55 and HM65 was evaluated across multiple cell lines. HM55 exhibited strong activity, particularly in immortalized murine (mouse) microglial cell line (BV-2) microglial cells (88%, effective concentration (EC50) = 26 µM) and diffuse intrinsic pontine glioma (DIPG36 glioma cells) (90%, EC50 = 91 µM), while HM65 showed moderate cytotoxicity in the same lines (58%, EC50 = 33 µM; 86%, EC50 > 100 µM, respectively). In colorectal adenocarcinoma (Caco-2 colon cancer cells), HM55 and HM65 reached 62% (EC50 = 71 µM) and 48% (EC50 = 85 µM) inhibition, respectively, with no hepatotoxicity observed. Regarding α-glucosidase inhibition, HM65 displayed a maximum inhibition of 64% with an half maximal inhibitory concentration (IC50) of 94 µM, outperforming HM55 (22%, IC50 not determined). Antioxidant activity assessed via 2,2-diphenyl-1-picrylhydrazyl (DPPH) assay showed HM65 with 59% radical scavenging (EC50 = 31 µM) and HM55 with 36% (EC50 = 48 µM). Overall, HM55 demonstrated higher cytotoxicity, whereas HM65 exhibited stronger antioxidant and α-glucosidase inhibitory properties, highlighting their complementary pharmacological profiles. In silico studies corroborated the experimental findings, while absorption, distribution, metabolism, excretion, and toxicity (ADMET) profiling provided valuable insights into the pharmacokinetic properties and inhibitory potential of the newly synthesized compounds. Together, these results underscore their complementary pharmacokinetic and binding characteristics, supporting their potential as candidates for optimization as future multitarget inhibitors.

Keywords: Benzodiazepine derivatives, Green synthesis, Biological evaluation, In silico analysis

2nd International Conference on Multidisciplinary Sciences and Technological Developments (ICMUSTED 2025)

December 12-15, 2025

Enhancing Diesel Desulfurization via Oxidation over Modified USY Zeolite Catalyst

Louiza Aichaoui[1], Soraya Aidene[1], Boudjema Hamada[1]

[1]Department of Chemical and Pharmaceutical Process Engineering, University M'hamed Bougara Boumerdes, Boumerdes, Algeria
Corresponding author: Louiza Aichaoui (e-mail: l.aichaoui@univ-boumerdes.dz)

Abstract

The reduction of sulfur content in fossil fuels, particularly diesel, is an environmental priority due to the harmful effects of sulfur oxides (SO_x) on human health, air quality, and industrial equipment. Classical desulfurization processes, such as hydrodesulfurization (HDS), require severe operating conditions (high temperatures and pressures), which motivates the development of gentler and more selective alternative methods, such as oxidative desulfurization (ODS). In this context, this work aims to develop an acid solid catalyst based on ultra-stable Y (USY) zeolite (CBV 500), modified by impregnation with sulfuric acid. The zeolite was first activated by a thermal treatment (dehydration at 150–200 °C followed by calcination at 500 °C), before being functionalized by acid impregnation, followed by a second calcination to stabilize the introduced sulfonic groups (SO_3H). The granulometric characterization of the material revealed a good homogeneity in particle size (median diameter of 9.584 µm), enabling an increase in the available active catalytic surface. The reaction was conducted on a diesel sample under moderate conditions (80 °C, 1 atm, and 4 h) using hydrogen peroxide as oxidative agent and showed a significant improvement in desulfurization efficiency in the presence of modified catalysts (up to 19.82% in certain fractions), compared to a very low efficiency without a catalyst (10.60%). These results pave the way for the optimization of simple, stable and economical catalytic materials for cleaner desulfurization processes compatible with modern industrial requirements.

Keywords: Diesel, Environment, Sulfonic groups, Oxidative desulfurization, Zeolite

Volatile Composition and Antioxidant activity of Blue Safflower Oil

Yasmine Ouali[1], Nacera Dahmani-Hamzaoui[2], Zahia Ghouila[3]

[1]Chemistry Department, University of Sciences and Technology Houari Boumediene, Algiers, Algeria
[2]Chemistry Department, National High School of Marine Sciences and Coastal, Algiers, Algeria
[3]Scientific and Technical Research Center in Physicochemical Analysis, Algiers, Algeria
Corresponding author: Yasmine Ouali (e-mail: oualiyassamine9@gmail.com)

Abstract

Essential oils are a rich natural source of bioactive compounds with various pharmacological properties. In this study, we evaluated the chemical composition and Antioxidant activity of essential oil extracted from *Carthamus Caeruleus* L. roots by conventional hydrodistillation. The essential oil was analyzed by gas chromatography–mass spectrometry, identifying twenty-seven volatile compounds, representing 94.76 ± 2,532% of the total composition. The oil showed a predominance of α-linolenic acid methyl ester (77.40 ± 1,766%) as the only fatty acid methyl ester, marking the first identification of this chemotype, followed by sesquiterpenes and oxygenated sesquiterpenes as major classes. Antioxidant activity was evaluated using two complementary methods: the 2,2-diphenyl-1-picrylhydrazyl radical scavenging assay, and hydroxyl radical scavenging activity. The results revealed respective Inhibitory Concentration 50% values of 403.67 ± 3.77 µg/mL and 162.93 ± 0.58 µg/mL. Overall, these results confirm the potential of this essential oil as a candidate for natural therapeutic applications, due to its richness in bioactive compounds and its antioxidant effect.

Keywords: *Carthamus caeruleus* L., Essential oil, Chemotype, Chromatography, Antioxidant activity

2nd International Conference on Multidisciplinary Sciences and Technological Developments (ICMUSTED 2025)

December 12-15, 2025

Formulation and Characterization of an Ointment Based on Hot Pepper Vegetable Oil

Saida Touzouirt[1,2], Selma Kadja[1], Sylia Badja[1]

[1]Department Process Engineering, University of Boumerdes, Boumerdes, Algeria
[2]Natural Resources Laboratory, Mouloud Mammeri University, Tizi-Ouzou, Algeria
Corresponding author: Saida Touzouirt (e-mail: s.touzouirt@univ-boumerdes.dz)

Abstract

Algeria has a rich reserve of plant-based remedies and traditional know-how that form part of its traditional medicine practices for human use. The objective of this study is to formulate a natural anti-inflammatory ointment based on the vegetable oil extracted from the seeds of hot pepper (*Capsicum annuum*) from the Batna region (Algeria). Phytochemical screening revealed that hot pepper seeds are rich in flavonoids, alkaloids, saponins, quinones, and terpenes. The oil was extracted from the hot pepper seeds using the cold-pressing method in order to preserve its bioactive compounds. This method yielded 8.75% oil. The obtained oil was characterized using various physicochemical and spectroscopic (Fourier transform infrared spectroscopy) methods. An ointment formulation based on the vegetable oil of hot pepper seeds was developed. The rheological study indicates a shear-thinning behavior, ensuring the ointment's stability and good application properties. This ointment demonstrated very good microbiological activity against *Escherichia coli*, *Staphylococcus aureus*, and *Pseudomonas aeruginosa*. The anti-inflammatory study of this ointment revealed a good effect compared to the reference product, Betasone, with edema reduction rates of 28.33% and 26.49% respectively.

Keywords: Hot pepper, Vegetable oil, Capsaicin, Microbiology, Anti-inflammation

2nd International Conference on Multidisciplinary Sciences and Technological Developments (ICMUSTED 2025)

December 12-15, 2025

Nanoencapsulation of Eucalyptus Oil for *Aedes Aegypti* Repellents

Laura Astorga[1,2], Gisela Romero[1], Marina Turrado[1,2], Emiliano Nicodemo[1], Jorge Montanari[1,2,3]

[1]Laboratory of Nanosystems for Biotechnological Applications, National University of Hurlingham, 1688 Buenos Aires, Argentina
[2]Scientific Research Commission of the Province of Buenos Aires, 1900 La Plata, Argentina
[3]National Council for Scientific and Technical Research, Buenos Aires, Argentina
Corresponding author: Laura Astorga (e-mail: laurapatriciaastorga@gmail.com)

Abstract

This study proposes the development of innovative insect repellent formulations that offer longer duration and are safer for humans and the environment. This is achieved by encapsulating natural products in nanotechnological vehicles based on biodegradable materials. The primary goal is to obtain and physicochemical characterize eucalyptus essential oil (EO) for its use in nanostructured lipid carrier (NLC) formulations. This encapsulation is expected to retard EO evaporation, significantly extending the duration of its repellent action against the dengue vector. The essential oil was obtained from the leaves of the plant species using a Figmay steam-distillation unit. The nanocarriers were synthesized by creating an emulsion using a solid lipid, the natural essential oil as the liquid lipid, and a surfactant. The emulsification process was carried out with the Ultra-turrax® T18 at 15,000 rpm. Initial physicochemical characterizations of the essential oil showed a yield of 0.56% and a density of 0.91 g/mL. UV-Vis analysis displayed a maximum absorbance peak at 250 nm, in contrast to the 200 nm reported for the commercial product. Fourier-transform infrared spectroscopy (FTIR) detected a medium absorption peak at 966.67 cm^{-1} assigned to the C-O-C stretching vibration, confirming the presence of 1,8-Cineole as the main active component. The average particle sizes were between 100-250 nm. Upon completion of the physicochemical characterization, the toxicity and repellency capacity of the formulations will be determined.

Keywords: Dengue, Nanoparticles, Repellents

2nd International Conference on Multidisciplinary Sciences and Technological Developments (ICMUSTED 2025)

December 12-15, 2025

Antimicrobial Evaluation and Phytochemical Analysis of *Asphodelus Microcarpus* Extract

Azziza Chabane Chaouch[1], Farid Benkaci-Ali[1], Samira Tata[2]

[1]Laboratory of Functional Organics Analysis, Faculty of Chemistry, University of Sciences and Technologies Houari Boumedienne (USTHB), Algiers, Algeria
[2]Laboratory of Biology of the Microbial Systems, Department of Biology, National Superior School El Bachir El Ibrahimi, Kouba-Algiers, Algeria
Corresponding author: Azziza Chabane Chaouch (e-mail: aziza602009@hotmail.com)

Abstract

Algeria is recognized for its rich biodiversity, encompassing a diverse range of aromatic and medicinal plants, including *Asphodelus microcaprus*, a key species in traditional medicine. This plant is used in various forms; tea, powder, or ointment for treating fevers, indigestion, constipation, and skin lesions, while its fresh roots macerated in oil are used to address ear infections. Consequently, this study aims to enhance the value of *Asphodel*us *microcarpus* by studying its phytochemical profile and evaluating the antimicrobial activity of its bulb extract obtained by maceration with ethanol. The polyphenols and flavonoids were determined spectrophotometrically. The antimicrobial activity was evaluated using the diffusion disc method against 4 bacteria, one yeast and two fungi. The phytochemical study revealed that the ethanolic extract of *Asphodel*us *microcarpus* is rich in polyphenols and flavonoids with a content of 110.69 mg GAE/g and 48.24 mg QE/g respectively. Additionally, *Asphodel*us *microcarpus* extract showed a significant antibacterial activity especially against *Listeria monocytogenes* and *Bacillus subtilis.* This high polyphenol and flavonoids content and significant antimicrobial potential explain the pharmacological properties of Asphodel and provide a scientific basis for the use of this plant in Algerian folk medicine.

Keywords: *Asphodelus microcarpus*, Polyphenols, Antibacterial activity, Flavonoids

2nd International Conference on Multidisciplinary Sciences and Technological Developments (ICMUSTED 2025)

December 12-15, 2025

Coagulation-Flocculation of Humic Substances: Effectiveness of Aluminum Sulfate and the Role of Sulfate and Phosphate Salts

Lynda Hecini[1,2], Fedia Bekiri[1], Naima Bacha[1,2], Wahida Kherifi[1]

[1]Scientific and Technical Research Center in Arid Area, 1682 Biskra, Algeria
[2]Laboratory of Subsurface and Surface Hydraulics, Faculty of Science and Technology, University of Biskra, 07000, Algeria
Corresponding author: Lynda Hecini (e-mail: lindahecini@gmail.com)

Abstract

The surface waters and polluted waters are characterized by high concentrations of organic matter, mainly humic substances responsible for water discoloration and unpleasant odors. These substances form colloids with very small diameters (ranging from 1 nm to 1 µm), making natural sedimentation in water extremely slow or even impossible. Therefore, to achieve effective sedimentation, chemical coagulants—typically trivalent metal salts such as Al^{3+} or Fe^{3+}—are added to the water to destabilize these particles and form settle able precipitates. This process is known as coagulation-flocculation. It is a classical treatment method widely employed in drinking water production plants as well as in the primary treatment of wastewater, primarily targeting the removal of the colloidal fraction. The present study aimed to monitor the removal of humic substances during flocculation tests using aluminum sulfate. Jar-test experiments were first conducted on synthetic humic substance solutions prepared in distilled water to investigate the influence of reaction parameters such as coagulant dose, initial compound concentration, and solution pH. Subsequently, experiments were performed using distilled water enriched with sulfate and phosphate ions introduced in various forms ($CaSO_4$, $MgSO_4$, Na_2SO_4, NaH_2PO_4, KH_2PO_4). The maximum removal efficiency of humic substances was observed within an acidic pH range between 4 and 5. Coagulation occurred according to a stoichiometric dosage, with a mass ratio of 2 mg of aluminum sulfate required for the removal of 1 mg of sodium humate at unadjusted pH. The elimination of this compound in distilled water proceeded through competing mechanisms—electrostatic charge neutralization, ion-exchange reactions, and physical adsorption—where complexation reactions between soluble species and organic matter predominated at the optimum pH conditions of the study.

Keywords: Coagulation-flocculation, Sodium humat, Aluminum sulfate, Mechanisms, Sulfate and phosphate salts

Citric Acid-Crosslinked CMC Bioplastics: Tuning Flexibility, Strength, and Biodegradation for Sustainable Food Packaging

Nur Alya Maisarah Binti Mohamad[1], Nurhafizah Binti Hasim[1]

[1]Advanced Optical Material Research Group, Faculty of Science, University Teknologi Malaysia, 81310 Skudai, Johor, Malaysia
Corresponding author: Nurhafizah Binti Hasim (e-mail: nurhafizah.h@utm.my)

Abstract

Environmental concerns over plastic waste have increased the demand for biodegradable materials in food packaging. Carboxymethyl cellulose (CMC) is a promising biopolymer but its performance is limited by weak water resistance and moderate mechanical strength. Citric acid (CA) and glycerol (Gly) can improve these limitations through crosslinking and plasticization. However, studies combining all three components and evaluating their physical, structural, biodegradation, and microbial characteristics remain limited. This study aims to develop and characterize biodegradable plastics (BDPs) based on CMC crosslinked with CA and plasticized with glycerol at concentrations of 3%, 6%, 9%, 12%, and 15% using the solution casting method. Physical properties including thickness, moisture content, water solubility, water vapour permeability, water absorption capacity, ash content and ultraviolet-visible (UV–Vis) behaviour are measured to determine film uniformity, water interaction and overall stability. Structural characteristics are examined using X-ray diffraction (XRD) and Fourier transform infrared spectroscopy (FTIR) with Gaussian peak analysis to assess crystallinity changes and functional-group interactions. Environmental performance is evaluated through soil-burial biodegradation and microbial testing to observe decomposition patterns and microbial activity. The study examines how different glycerol concentrations influences the strength, flexibility, moisture behaviour and structural stability of CMC–CA–Gly films. Physical analyses describe changes in water sensitivity and film compactness while FTIR and XRD provide insight into chemical bonding and the extent of crosslink formation. Biodegradation and microbial tests show the film's ability to decompose in soil and the level of microbial activity throughout the breakdown process. These combined observations clarify how formulation adjustments support the development of biodegradable plastic films. Overall, this work supports the development of a more balanced and practical CMC-CA-Gly formulation that may serve as an environmentally friendly alternative for food packaging applications.

Keywords: Carboxymethyl cellulose, Citric acid, Glycerol, UV-Vis, XRD

2nd International Conference on Multidisciplinary Sciences and Technological Developments (ICMUSTED 2025)

December 12-15, 2025

On the Thermodynamic Stability of Some Metal Complexes within the Framework of a Density Functional Theory Approach Investigation

Boulanouar Messaoudi[1,2], Baian Alkassas[3]

[1]Higher School in Applied Sciences of Tlemcen, Bel Horizon, 13000 Tlemcen, Algeria
[2]Toxicomed Laboratory, University of Abou Bekr Belkaid, 13000 Tlemcen, Algeria
[3]Department of Chemistry, University of Djillali Liabbes–Sidi Bel Abbes, Algeria
Corresponding author: Boulanouar Messaoudi (e-mail: messaoudiboulanouar@gmail.com)

Abstract

Metal complexes consist of the union of a metal (it can be a transition metal) with a ligand which can be organic or inorganic. This gives and affords this kind of compounds several important characteristics used in various domains. For instance, stoichiometric and catalytic transition-metal reactions have attracted great interest for their many applications in industrial and synthetic processes. They are critical in many thermodynamically feasible processes because they accelerate the reactions by opening a lower activation energy pathway. In spectroscopy, many overviews and reviews have been done using like ultraviolet–visible spectroscopic and resonance Raman investigation of the lowest energy dipole-allowed absorption band of many different complexes. On the other hand, for antitumor activity, a wide variety of metal complexes such as platinum (II) have been investigated. In this sense, it has been found that only neutral complexes exhibit activity while charged species are inactive and relatively nontoxic. However, stereochemistry is a major factor where *trans* isomers are inactive in comparison with active *cis* complexes. It is known that the stability of complexes may be affected by many factors such as coordination number, stereochemistry, entropy. In this study, a theoretical ab initio and thermodynamic based analysis of the stability of some metal complexes is probed using density functional theory (DFT) approach.

Keywords: Complex, Metal, Thermodynamics, Stability, DFT

2nd International Conference on Multidisciplinary Sciences and Technological Developments (ICMUSTED 2025)

December 12-15, 2025

Inverse Partial Least Squares Regression for the Prediction and Optimization of Carboxyl Group Content in Graphene Oxide

Soraya Aidene[1], Abdelsattar Osama Elemam Abdelhalim[2]

[1]Department of Chemical and Pharmaceutical Process Engineering, University M'hamed Bougara, Boumerdes, Algeria

[2]Environmental Research Department, National Centre for Social and Criminological Research (NCSCR), Giza, Egypt

Corresponding author: Soraya Aidene (e-mail: s.aidene@univ-boumerdes.dz)

Abstract

Enhancing the reactivity of graphene oxide through surface functionalization optimization is crucial, particularly by raising the concentration of carboxyl groups (COOH). This research employs Partial Least Squares (PLS) regression to assess the correlation between the percentage of COOH and various experimental parameters, such as oxygen content (%), particle size (nm), and interlayer distances (nm). The model demonstrates significant predictive accuracy, indicating that the primary experimental factors have a substantial impact on surface functionalization. To move from analysis to optimization, an inverse PLS approach is adopted. In this framework, COOH% is utilized as the input, and the optimal experimental conditions are predicted as outputs. By establishing a target COOH% of 50%, the model indicates conditions such as an oxygen content of 90%, a particle size of 773.11 nm, and an interlayer distance of 1.41 nm, which are expected to maximize functionalization efficiency. This inverse modeling approach illustrates that chemometric techniques can offer not only insights into experimental patterns but also direct recommendations for experimental design. The suggested method exhibits significant potential for optimizing the surface chemistry of graphene oxide and can be adapted for the design of nanomaterials with customized properties for catalytic, environmental, and energy-related applications.

Keywords: Chemometrics, Partial Least Squares (PLS), Inverse PLS, Graphene oxide, Carboxyl groups (COOH%)

Biofunctionalized Gold Nanocomposites from *Spatholobus Litoralis* for High-Sensitivity Refractive Index Sensing

Firdausi Nuzulah[1], Sumini Sumini[1], Titin Syufairoh[1], Shelgiana Hayu Krisnanda[1], Nurul Hidayat[1]

[1]Department of Physics, Universitas Negeri Malang, Malang, Indonesia
Corresponding author: Nurul Hidayat (e-mail: nurul.hidayat.fmipa@um.ac.id)

Abstract

Monitoring changes in optical refractive index has important implications in the chemical, biomedical, and environmental fields because any variation in the refractive index value can indicate the presence of molecular interactions, biomolecular adsorption, or changes in solution composition. This study aims to develop a colorimetric-based refractive index sensor using gold nanohybrids (AuNPs) and *Spatholobus litoralis* extract synthesized through the neodymium-doped yttrium aluminium garnet (Nd:YAG) laser ablation method. The laser ablation method was chosen because it is able to produce high-purity gold nanoparticles, uniform in size, and free from additional chemicals, making it environmentally friendly. Meanwhile, *Spatholobus litoralis*, rich in flavonoids and phenolic compounds, functions as a reducing agent and natural stabilizer in the green synthesis process. The research stages included the synthesis of AuNPs in ionized air, and the synthesis of *Spatholobus litoralis* at various rotational speeds of 60, 70, 80, 90, and 100 rpm. As well as characterization using ultraviolet-visible (UV-Vis) spectroscopy to observe the local surface plasmon resonance (LSPR) phenomenon, and also scanning electron microscopy (SEM) to see the morphology and surface structure of AuNPs@*Spatholobus litoralis*. The sensitivity of the sensor to changes in the refractive index is evaluated through analysis of the maximum wavelength shift (λ_{max}), at various concentrations of ethylene glycol solution. And the resulting refractive index concentration is 1.333 for 0% concentration, 1.342 for 10% concentration, 1.349 for 20% concentration, 1.362 for 30% concentration, 1.372 for 40% concentration, and 1.379 for 50% concentration. The research is expected to produce a sensitive, selective, fast-responsive, and stable optical sensor with potential for broad applications in air quality monitoring, biomolecule detection, and disease diagnosis. This research will also encourage innovation based on local natural resources and contribute to the development of science, technology, and a sustainable environment.

Keywords: Refractive index, Colorimetry, Spatholobus litoralis, Gold nanoparticles, Nd:YAG laser ablation

2nd International Conference on Multidisciplinary Sciences and Technological Developments (ICMUSTED 2025)

December 12-15, 2025

Mercury Sensing in Fish via Gold-Based SPR and Chitosan Composite Functionalization

Kada Abdelhafid Meradi[1,2], Mohamed Esseddik Ouardi[1,2], Fatima Tayeboun[2,3]

[1]Department of Science and Technology, University of Ain Temouchent, 46000 Ain Temouchent, Algeria
[2]Laboratory of Materials Sciences and Applications, University of Ain Temouchent, 46000 Ain Temouchent, Algeria
[3]University Djillali Liabes, 22000 Sidi-Bel-Abbes, Algeria
Corresponding author: Kada Abdelhafid Meradi (e-mail: abdelhafid.meradi@univ-temouchent.edu.dz)

Abstract

Mercury ion (Hg^{2+}) contamination in seafood represents a significant global public health concern due to its potent neurotoxic effects and capacity for bioaccumulation in the food chain. While conventional analytical techniques offer high sensitivity, they are often hampered by requirements for sophisticated instrumentation, skilled operation, and complex sample preparation, limiting their use for rapid, on-site monitoring. This paper presents a comprehensive simulation study on the development of a highly sensitive and selective surface plasmon resonance (SPR) biosensor tailored for the detection of trace Hg^{2+} in complex fish tissue matrices. The proposed sensor leverages the well-established Kretschmann configuration with a 50 nm gold thin film, functionalized with two distinct biopolymer coatings: a cross-linked chitosan (CHI) layer and a nanoporous polypyrrole-chitosan (PPy-CHI) composite. These coatings serve to selectively capture and preconcentrate mercury ions at the sensor surface. The core of this work involves a detailed theoretical modeling of the sensor's performance. Using a combination of the Langmuir adsorption isotherm to simulate Hg^{2+} binding and finite-difference time-domain (FDTD) methods to calculate the resultant SPR angle shift, the sensor's response was rigorously characterized. Simulation results demonstrate that the PPy-CHI composite functionalization yields superior performance, exhibiting a high sensitivity of 125.5 mDeg/(µg/L) and an exceptionally low theoretical limit of detection (LOD) of 4.2 ng/L, with a linear response range from 0.05 to 5.0 µg/L. The cross-linked chitosan sensor, while less sensitive, also proved viable with an LOD of 18.5 ng/L. Crucially, the sensor model predicted excellent selectivity for Hg^{2+}, showing a minimal response to a 100-fold excess of common interferent ions (Cu^{2+}, Pb^{2+}, Cd^{2+}, Zn^{2+}), attributed to the strong chelation affinity of chitosan's amine groups for mercury. Furthermore, the sensor exhibited remarkable resilience in a simulated fish tissue matrix, with Hg^{2+} recovery rates between 96% and 101%, indicating strong resistance to non-specific protein fouling. This study successfully establishes a compelling theoretical foundation for the efficacy of a PPy-CHI composite-functionalized SPR sensor for mercury monitoring. The predicted performance metrics–encompassing ultra-high sensitivity, exceptional selectivity, and robustness in a complex food matrix–suggest that this sensor platform holds significant promise for advancing food safety control and warrants subsequent experimental fabrication and validation.

Keywords: Transfer matrix method, Mercury, Food quality, SPR sensor

Enhancing the Thermal Stability of Deep Eutectic Polymer Electrolytes Through Nanoparticle Incorporation

Hazimah Binti Hazman[1], Norshahirah Binti Mohamad Saidi[1]

[1]Advanced Optical Material Research Group, Faculty of Science, Universiti Teknologi Malaysia, Skudai, 81310 Johor, Malaysia

Corresponding author: Norshahirah Binti Mohamad Saidi (e-mail: norshahirah.ms@utm.my)

Abstract

Thermal stability is an important requirement for polymer electrolytes in supercapacitors because the material must remain safe and stable when heat is produced during high current charging and discharging. If the electrolyte cannot handle heat, it may soften, decompose, or lose its ability to transport ions, which affects performance and safety. To address this, deep eutectic polymer electrolytes (DES-PEs) are used because eutectic mixtures have strong internal interactions and low volatility, making them naturally more stable at higher temperatures. In this study, the DES-PEs were prepared using a deep eutectic solvent made from 1,3-propanediol and ethylene glycol, combined with polyacrylonitrile (PAN) as the main polymer and lithium perchlorate as the ion-promoting salt. Graphene oxide (GO) nanoparticles were added as fillers to help strengthen the material and further improve both thermal stability and ion movement in the electrolyte. Thermal stability, which is the main focus of this work, was studied using thermogravimetric analysis (TGA). Electrochemical impedance spectroscopy (EIS) was used to evaluate ionic conductivity, bulk resistance, and dielectric response. With a suitable amount of GO nanoparticles, the DES-PEs are expected to show better heat resistance and improved ion transport. Overall, this work highlights that eutectic-based polymer electrolytes reinforced with nanoparticles can offer safer and more stable materials for future energy storage devices.

Keywords: Thermal stability, Deep eutectic polymer electrolytes, Graphene oxide nanoparticle, Electrochemical performance

2nd International Conference on Multidisciplinary Sciences and Technological Developments (ICMUSTED 2025)

December 12-15, 2025

Comparative Green Synthesis of Zinc Nanoparticles via Pulsed Laser Ablation in Different Liquid Mediums

Nur Nadirah Binti Mohd Nor[1], Fairuz Diyana Binti Ismail[1], Maisarah Binti Duralim[1]

[1]Department of Physics, Faculty of Science, Universiti Teknologi Malaysia (UTM), 81310 Johor Bahru, Johor, Malaysia
Corresponding author: Fairuz Diyana Binti Ismail (e-mail: fairuzdiyana@utm.my)

Abstract

This study investigates the green synthesis of zinc nanoparticles (ZnNPs) using pulsed laser ablation in liquid (PLAL) across four different solvent environments such as deionized water, boiled pandan extract, unboiled pandan extract, and coconut oil. A high-purity zinc ingot round bar (99.5%) served as the solid target, while optimized PLAL settings were applied to ensure high-purity nanoparticle production. A Q-switched neodymium-doped yttrium aluminium garnet (Nd:YAG) laser was used with a wavelength of 532 nm, a pulse repetition rate of 4 Hz, and a pulse energy of 250 mJ, enabling efficient ablation and nanoparticle formation without chemical precursors, surfactants, or stabilizers. The selected solvents provided contrasting polarity, viscosity, and phytochemical content, allowing systematic evaluation of their influence on nanoparticle characteristics. Ultraviolet and visible (UV–Vis) spectroscopy revealed that deionized water produced small, uniform, and well-dispersed nanoparticles with sharp plasmon resonance peaks, indicating strong colloidal stability. In contrast, coconut oil generated broader absorption peaks linked to larger particle sizes and stronger aggregation due to its low polarity and higher viscosity. Boiled and unboiled pandan extracts contributed natural phytochemicals that acted as mild stabilizing agents, with thermal treatment altering the concentration of these compounds and affecting nanoparticle dispersion and optical behavior. The results highlight the critical role of solvent properties in determining ZnNP morphology, optical response, and stability during PLAL synthesis. Overall, this work demonstrates the capability of PLAL as a clean, sustainable technique for producing high-purity nanomaterials while incorporating plant-based solvents to support green nanotechnology. Further characterization using scanning electron microscope (SEM), X-ray diffraction (XRD), Fourier transform infrared spectroscopy (FTIR), and UV–Vis is proposed to deepen understanding of the structural, morphological, and surface chemistry variations arising from different solvent environments and their influence on ZnNP formation mechanisms.

Keywords: Pulsed laser ablation in liquid (PLAL), Zinc nanoparticles (ZnNPs), Solvent effects, Green synthesis

2nd International Conference on Multidisciplinary Sciences and Technological Developments (ICMUSTED 2025)

December 12-15, 2025

Study of Electrical Conductivity in Deep Eutectic Solvent Based on Hydrogen Bond Donor and Hydrogen Bond Acceptor Combinations

Farhan Shazwan Shah Shahbani[1], Norshahirah Mohamad Saidi[1], Nurhafizah Hasim[1], Nur Hidayah Ahmad[1], Muhammad Amirul Aizat Mohd Abdah[2]

[1]Department of Physics. Faculty Science, Universiti Teknologi Malaysia, Johor Bahru, Malaysia
[2]Department of Chemistry. Faculty Science, Universiti Teknologi Malaysia, Johor Bahru, Malaysia
Corresponding author: Farhan Shazwan Shah (email: farhanshazwanshah@graduate.utm.my)

Abstract

Deep eutectic solvents (DESs) have been widely adopted worldwide as alternative solvents for electrolyte preparation in various electrochemical devices due to their distinctive advantages over conventional organic and inorganic solvents. These advantages include excellent chemical and thermal stability, high solubility, elevated viscosity, and favorable thermodynamic characteristics, making DES attractive for energy storage applications. Typically, a DES is formed from two primary components: a hydrogen bond donor (HBD) and a hydrogen bond acceptor (HBA), whose strong hydrogen-bonding interactions lead to a significant reduction in melting point and enhanced physicochemical properties. In this study, 1,3-propanediol (PDO) was selected as the HBD, while ethylene glycol (EG) was employed as the HBA. Different PDO:EG ratios were systematically investigated to evaluate their electrochemical performance. The results revealed that the DES with a PDO:EG ratio of 1:3 exhibited the most favorable properties, achieving an optimum bulk resistance of 75.81 Ω and an ionic conductivity of 1.77×10^{-3} S/cm. These findings indicate that the optimized DES composition possesses strong potential for use as an effective solvent system in the development of polymer electrolytes for advanced electrochemical applications.

Keyword: Deep eutectic solvent, Supercapacitor, Conductivity, Hydrogen bond donor, Hydrogen bond acceptor

2nd International Conference on Multidisciplinary Sciences and Technological Developments (ICMUSTED 2025)

December 12-15, 2025

Grid-Connected Photovoltaic System with a Three-Level NPC Inverter for Power Quality Enhancement

Fatima Tahri[1,3], Ghrissi Tahri[2,3], Ali Tahri[3]

[1]Smart Grid Development Laboratory, Higher School of Electrical and Energetic Engineering Oran, Algeria
[2]Institute of Applied Sciences and Techniques, University Oran 1, Ahmed Ben Bella, Oran, Algeria
[3]Laboratory of Electrical Engineering Oran, Department of Electrotechnics, Faculty of Electrical Engineering, University of Sciences and Technology of Oran Mohamed Boudiaf, Oran, Algeria
Corresponding author: Fatima Tahri (fatimatahri.dz@gmail.com)

Abstract

The main work in this paper is based on the study and analysis of artificial intelligence based on fuzzy logic control (FLC) law synthesis of the active and reactive powers for a grid-connected photovoltaic (PV) system. The photovoltaic system is connected to the grid utility through a three-phase, three-level neutral point clamped (NPC) inverter and inductor-capacitor-inductor (LCL) filter. Measuring the instantaneous active and reactive power from the voltage and current grid is the basis for establishing the two control techniques, traditional proportional-integral (PI) control and FLC. As a result, the control techniques improve and ensure the dynamic performance and stability of a photovoltaic system against abrupt variations in solar irradiation intensity by accurately tracking the active power. According to the results of the Matlab-Simulink simulation, the FLC approach outperforms the traditional PI control in terms of high dynamic performance while requiring less time for convergence and overshoot.

Keywords: Fuzzy logic control, Photovoltaic system, Neutral point clamped inverter, Inductor-capacitor-inductor filter, Proportional-integral

2nd International Conference on Multidisciplinary Sciences and Technological Developments (ICMUSTED 2025)

December 12-15, 2025

Dynamic Energy Management of Smart Microgrids Considering Renewable Variability

Mohammed Tsebia[1,2], Hamid Bentarzi[1,3], Fazia Ahcene[1,4], Djamila Talah[1,4], Azeddine Ratni[5]

[1]Signals and Systems Laboratory, University of Boumerdes, Boumerdes, Algeria
[2]Faculty of Technology, University of Boumerdes, Boumerdes, Algeria
[3]Institute of Electrical and Electronics Engineering, University of Boumerdes, Boumerdes, Algeria
[4]University Mouloud Mammeri of Tizi-ouzou, Faculty of Technology, Tizi-ouzou, Algeria
[5]Solid Mechanics and Systems Laboratory, University of Boumerdes, Boumerdes, Algeria
Corresponding author: Mohammed Tsebia (e-mail: m.tsebia@univ-boumerdes.dz)

Abstract

The growing reliance on renewable energy has significantly increased the importance of microgrids as a promising solution to integrate distributed resources, enhance energy efficiency, and improve system resilience. Smart microgrids are particularly effective in enabling flexible operation through advanced monitoring and control. However, the intermittency and uncertainty of renewable generation introduce serious challenges for energy management, including frequent imbalances between supply and demand, voltage and frequency fluctuations, and difficulties in maintaining optimal dispatch of distributed energy resources (DERs). Addressing these issues requires energy management strategies that are both dynamic and adaptive to the variability of renewables. This research presents a dynamic energy management framework designed for smart microgrids operating under conditions of renewable variability. The proposed system incorporates real-time monitoring and optimization techniques to coordinate distributed generation, storage systems, and controllable loads. By dynamically updating generation and demand schedules according to the observed fluctuations in solar and wind resources, the framework ensures continuous balance, reduces reliance on backup generation, and improves the efficiency of energy utilization. Simulation studies conducted on a multi-microgrid test system validate the effectiveness of the proposed approach. Results show that the dynamic framework reduces frequency deviation, minimizes energy imbalance, and achieves more cost-efficient operation compared with static management strategies. Furthermore, the adaptive scheduling mechanism allows faster response to sudden renewable output changes, improving both reliability and power quality. The findings demonstrate that dynamic energy management represents a key step toward more resilient and smarter microgrids capable of operating reliably under high renewable penetration. Future work will focus on integrating predictive machine learning models to further improve forecast accuracy to extend the framework to large-scale smart grid applications.

Keywords: Smart microgrids, Energy management, Renewable variability, Distributed generation, Energy optimization

2nd International Conference on Multidisciplinary Sciences and Technological Developments (ICMUSTED 2025)

December 12-15, 2025

Inexpensive, Thin, and Dual-Band Metamaterial Absorber with Inner-Nested Split Ring Resonators

Yunus Kaya[1], Ugur Cem Hasar[2], Mehmet Ertugrul[3]

[1]Department of Electronics and Automation, Bayburt University, 69010 Bayburt, Türkiye
[2]Department of Electrical and Electronics Engineering, Gaziantep University, 27310 Gaziantep, Türkiye
[3]Department of Metallurgy and Materials Engineering, Karadeniz Technical University, 61080 Trabzon, Türkiye
Corresponding author: Yunus Kaya (e-mail: ykaya@bayburt.edu.tr)

Abstract

In this study, a thin, inexpensive, and dual-band metamaterial (MM) absorber operating in the microwave Ku- and K-bands (12–18 GHz and 18–27 GHz) is presented. The suggested MM-based absorber consists of a inner-nested slit ring resonator structure on a grounded FR-4 dielectric substrate. The geometric dimensions of the suggested MM absorber unit cell have been optimized to exhibit nearly 100% absorption at two frequency points in the microwave Ku- and K-bands. In addition, the effect of FR-4 dielectric substrate thickness on absorption was also investigated and as a result of the simulations, it was concluded that the absorption rate value was maintained with the change of substrate thickness (between 0.8–1.2 mm). The suggested MM-based absorber, with its thin and compact structure, low manufacturing cost, and high absorption rate, is a potentially groundbreaking design for microwave applications.

Keywords: Metamaterial absorber, Dual-band, Thin, Inexpensive

1. INTRODUCTION

Metamaterials (MMs), which do not exist in nature and are obtained artificially, have unusual electromagnetic (EM) properties such as negative magnetic permeability (μ), negative dielectric constant (ε) and, as a result of these properties, negative refractive index (n) [1]. MMs, whose first experimental studies were carried out in the 2000s, have become the focus of more research and researchers' attention in recent years thanks to their unusual EM properties at the subwavelength scale [2]. Recently, MMs have been used in exotic application areas such as antennas, sensors, super lenses, EM cloaking, EM energy harvesting, EM filters, lens imaging, and absorbers [1–3].

MM-based absorber structures have generally been suggested as slit ring resonators (SRR) [4, 5]. These suggested MM-based absorbers have found a wide place in the literature due to their thin structures, absorption rates close to 100%, simple designs, and manufacturing advantages [6, 7].

In this study, a dual-band MM absorber, which exhibits almost 100% absorption ratio in microwave Ku- and K-bands (12–18 GHz and 18–27 GHz), consisting of a inner-nested SRR structure and designed on a 1 mm thick FR-4 dielectric substrate, which is widely used and inexpensively available in the market, is suggested. The suggested MM absorber provides an absorption rate of 99.85% at the 16.305 GHz frequency point in the microwave Ku-band and 99.93% at the 24.45 GHz frequency point in the microwave K-band, according to the simulation results.

2. MM ABSORBER DESIGN AND ABSORPTION COEFFICIENT

The suggested MM absorber is designed to be manufactured using double-sided copper FR-4 board material, which is commonly used in the market for printed circuit board (PCB) in real-world applications. The FR-4 dielectric substrate is 1 mm thick (d) and the copper is 0.035 mm thick (t). Additionally, while FR-4 has a partial permittivity of 4.3 and a loss tangent of 0.025, copper has an electrical conductivity of 5.8×10^7 S/m. In the design, the back side of the square shaped FR-4 with a side of 12 mm (L_1) is completely grounded with a copper surface, while the front surface is formed with a metasurface with inner-nested SRR (a square ring with four sides split inside a circular ring with four sides split) made of copper. The other dimensions of the suggested

MM absorber, whose three-dimensional (3D) and front views are shown in Figures 1(a) and 1(b), respectively, are as follows: R_1 = 5.4 mm, R_2 = 4.8 mm, L_2 = 6.6 mm, L_3 = 5 mm, and g = 0.6 mm.

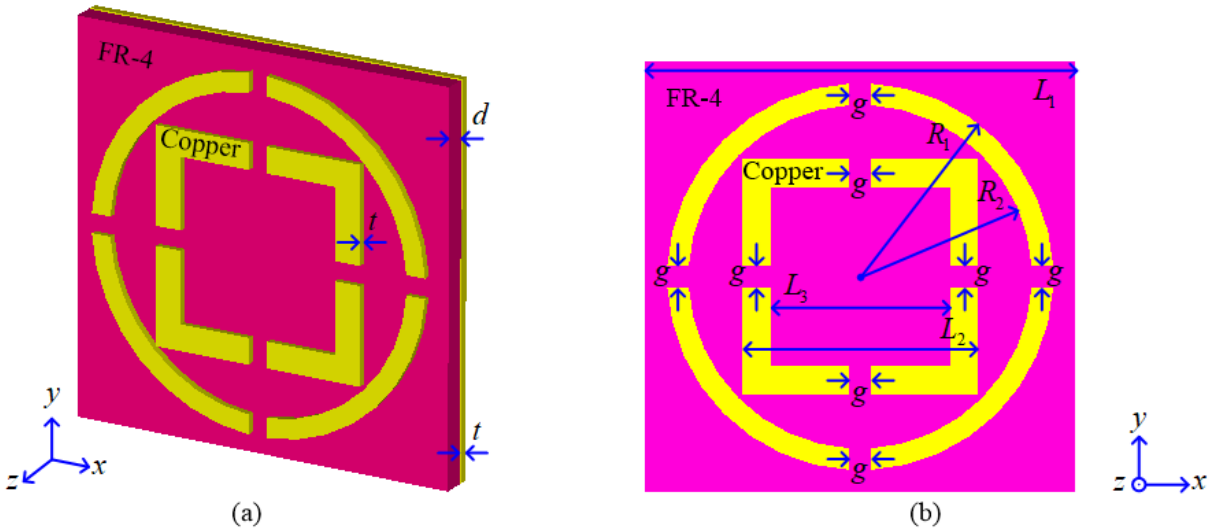

Figure 1. Material structure and dimension representations along with the suggested MM absorber's (a) 3D and (b) front view

The absorption coefficient (A) is calculated using the unitary property. This property is expressed by the following equation [8].

$$|S_{11}|^2 + |S_{21}|^2 = 1 \tag{1}$$

Here, |•| defines the magnitude of '•', S_{11} represents the reflection coefficient, and S_{21} represents the transmission coefficient. Due to the ground plane in the suggested MM absorber structure in Figure 1, S_{21} is zero across the entire frequency range [9]. However, this is only possible if the structure is lossless [10]. Since the MM absorber structure considered in the suggested structure is not lossless, A can be calculated as follows [10, 11].

$$A = 1 - |S_{11}|^2 - |S_{21}|^2 \tag{2}$$

For the lossless case, since $S_{21} = 0$, the equation for A becomes as follows.

$$A = 1 - |S_{11}|^2 \tag{3}$$

It is necessary to convert the S_{11} and S_{21} coefficients given in dB to linear form, that is, to calculate their magnitude. This process is carried out as follows.

$$|S_{11}| = 10^{(S_{11}/20)} \text{ and } |S_{21}| = 10^{(S_{21}/20)} \tag{4}$$

3. SIMULATIONS

The reflection and transmission coefficient analysis to evaluate the absorption performance of the suggested MM absorber was performed using Computer Simulation Technology (CST) Studio Suite, a high-performance 3D EM analysis software package for the design, analysis, and optimization of EM components and systems. The boundary conditions for the suggested MM absorber design in Figure 1 have been selected as shown in Figure 2.

Simulations were carried out for the suggested MM absorber in the microwave Ku- and K-bands under normal incidence (0°) in the frequency domain under the boundary conditions specified in Figure 2. Reflection and transmission coefficients in dB and amplitude are given in Figure 3(a) and 3(b), respectively.

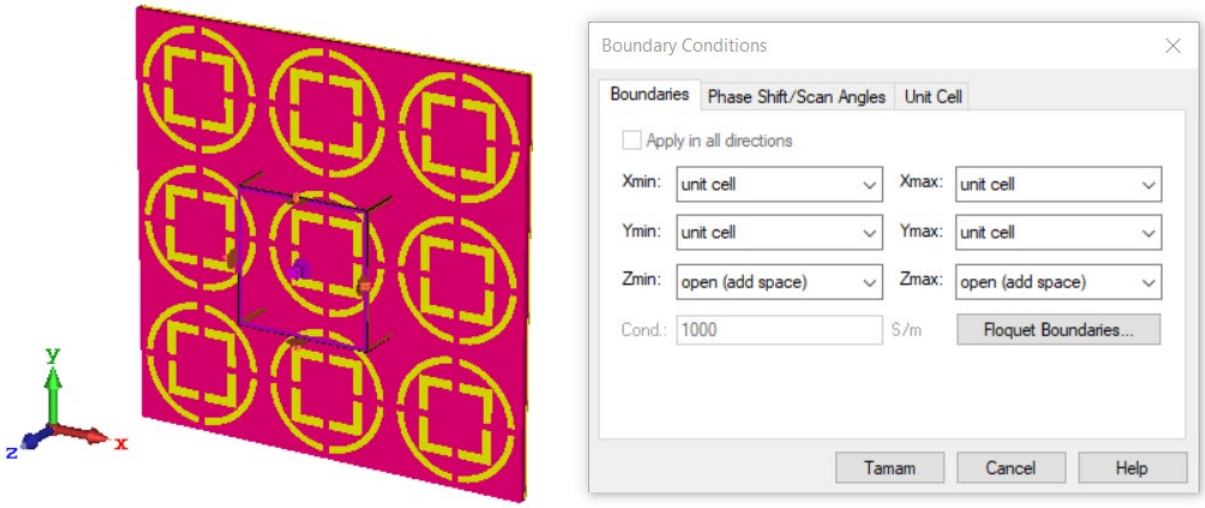

Figure 2. Boundary conditions for the suggested MM absorber design

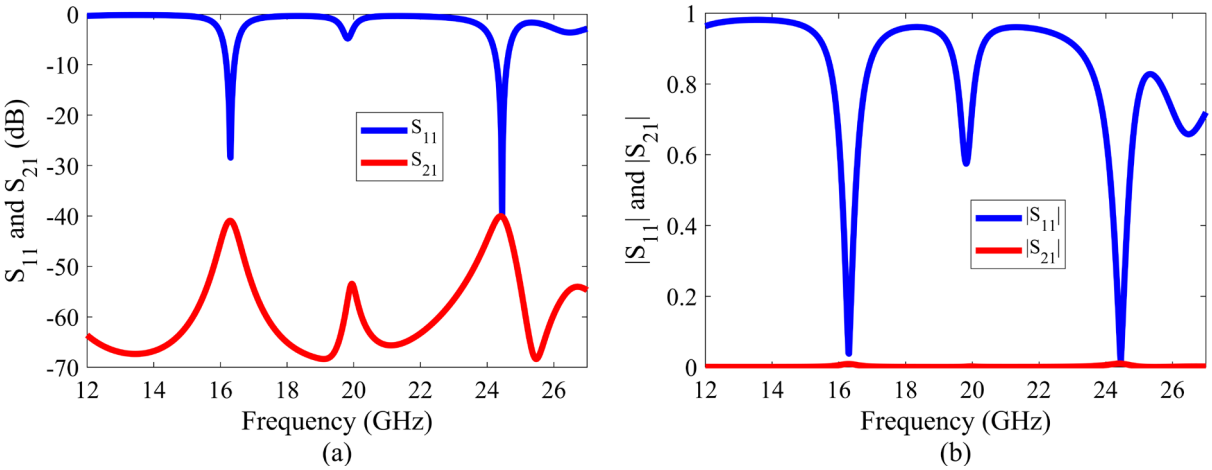

Figure 3. (a) Reflection and transmission coefficients in dB (S_{11} and S_{21}, respectively) and (b) amplitude ($|S_{11}|$ and $|S_{21}|$, respectively)

When Figure 3(a) is examined, it is seen that the lowest reflection coefficients (S_{11}) are –28.419 dB at the 16.305 GHz frequency point in the microwave Ku-band and –39.731 dB at the 24.45 GHz frequency point in the microwave K-band. The highest transmission coefficients (S_{21}) at the specified frequency points are –40.958 dB and –40.119 dB, respectively. It should also be noted that the S_{21} value is less than –41 dB at every frequency point in the microwave Ku- and K-bands. Figure 3(b) shows the linearized values of the reflection and transmission coefficients. When Figure 3(b) is examined, it is seen that the lowest reflection coefficient magnitude $(|S_{11}|)$ is 0.038 and 0.01 at the 16.305 GHz and 24.45 GHz frequency points in the microwave Ku- and K-bands, respectively, and the transmission coefficient magnitude $(|S_{21}|)$ is approximately equal to zero at each frequency point. For the suggested MM absorber, absorption coefficients were calculated in the microwave Ku- and K-bands from Equation (2) based on the reflection and transmission coefficients given in Figure 3 and plotted against frequency and given in Figure 4.

When Figure 4 is examined, it is seen that the suggested MM absorber offers an absorption coefficient (ratio) of 0.9985 (99.85%) at the 16.305 GHz frequency point in the microwave Ku-band and 0.9993 (99.93%) at the 24.45 GHz frequency point in the microwave K-band. In addition, the suggested MM absorber offers absorption ratios of 66.98% and 56.72%, respectively, at the frequency points of 19.815 GHz and 26.505 GHz in the microwave K-band and since the absorption ratios are less than 90%, the absorption at this points is not taken into consideration. As a result, the absorber we suggest provides a high absorption rate (over 99%) at two frequency points (16.305 GHz and 24.45 GHz) in two bands (microwave Ku- and K-bands).

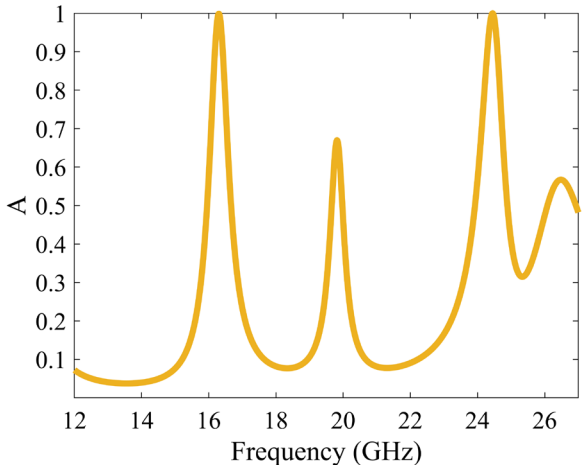

Figure 4. Absorption coefficient of the suggested MM absorber

Additionally, the effect of dielectric substrate thickness on absorption will be examined in this section. Therefore, simulations were performed for the suggested MM absorber by varying the FR-4 dielectric substrate thickness between d = 0.8–1.2 mm with values of 0.1 mm. The magnitude of the reflection and transmission coefficients obtained from these simulations and the absorption ratios calculated from these values are plotted against frequency and presented in Figures 5(a)–5(c), respectively.

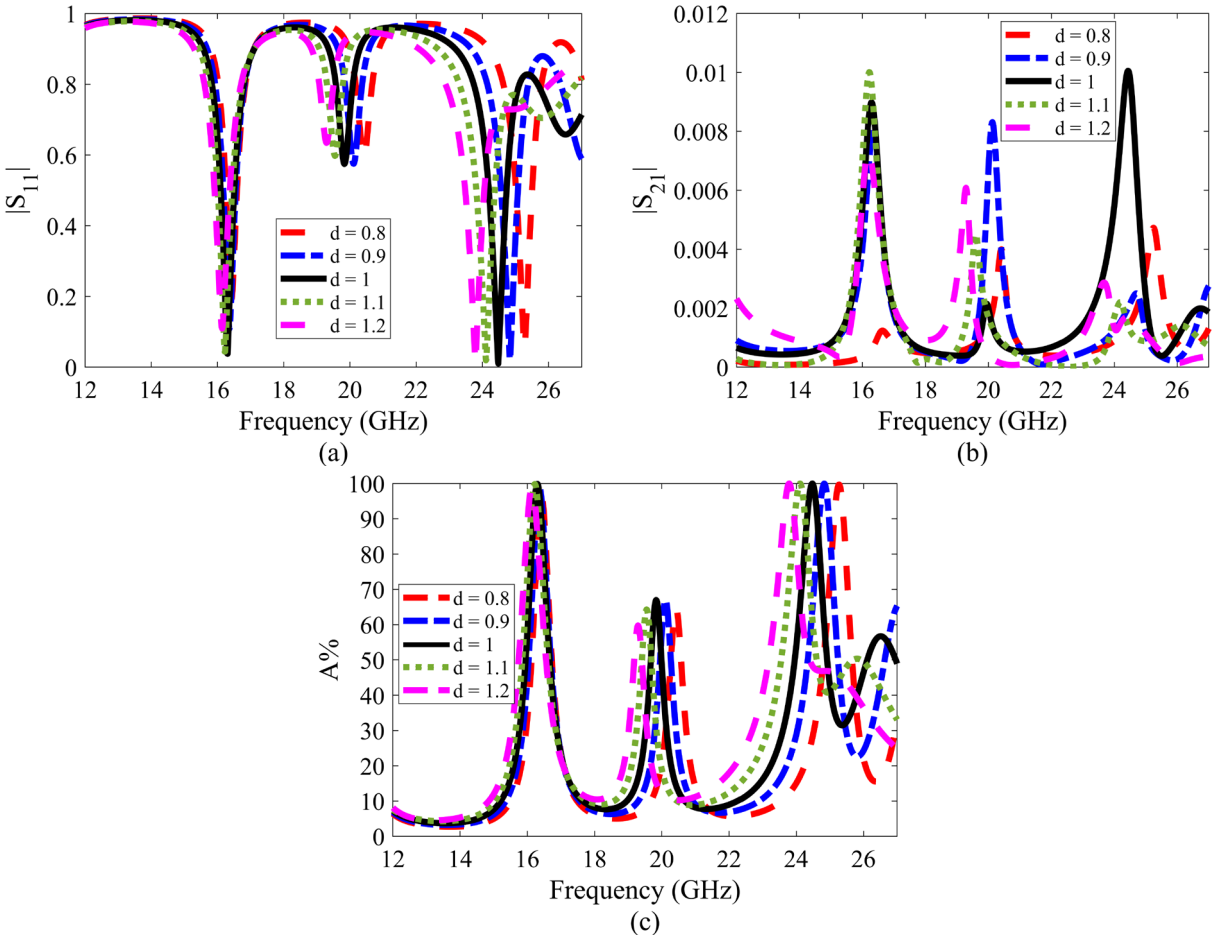

Figure 5. Simulated (a) $|S_{11}|$ and (b) $|S_{21}|$ coefficients for the suggested MM absorber by varying the FR-4 dielectric substrate thickness d = 0.8–1.2 mm with values of 0.1 mm and the absorption ratios (A%) calculated from these values.

When the magnitudes of the reflection and transmission coefficients are examined from Figures 5(a) and 5(b), respectively, it is seen that as the substrate thickness increases, the lowest $|S_{11}|$ value frequency point shifts to the

left and the $|S_{21}|$ value are less than 0.01 at all frequency points in the microwave Ku- and K-bands. When the absorption ratios calculated from the $|S_{11}|$ and $|S_{21}|$ values in Figure 5(c) are examined, it is seen that the frequency points showing absorption ratios around 99% (and more) shift to the left with increasing substrate thickness, but the high absorption ratio value is maintained as the substrate thickness changes.

4. CONCLUSION

In this study, a dual-band MM absorber design consisting of a inner-nested SRR structure on a grounded FR-4 dielectric substrate is suggested. The geometric parameters for the suggested structure have been optimized to exhibit nearly 100% absorption in the microwave Ku- and K-bands. The FR-4 dielectric substrate used in the design is only 1 mm thick. This thickness makes thin to the design. Additionally, the suggested MM absorber has a compact structure and can be adjusted to provide a high absorption rate at different frequency points/bands by changing parameters (e.g., substrate thickness). As a result, the suggested MM absorber is a potentially guiding design for applications such as wireless communication, stealth technology, EM interference, and EM compatibility.

References

[1] W. J. Padilla, D. N. Basov, and D. R. Smith, "Negative refractive index metamaterials," *Mater. Today*, vol. 9, no. 7–8, pp. 28–35, Jul.–Aug. 2006.

[2] J. B. Sun and J. Zhou, "Metamaterials: The art in materials science," *Eng.*, vol. 44, pp. 145–161, Jan. 2025.

[3] Y. I. Abdulkarim, A. Mohanty, O. P. Acharya, B. Appasani, M. S. Khan, S. K. Mohapatra, et. al., "A review on metamaterial absorbers: Microwave to optical," *Front. Phys.*, vol. 10, art. no. 893791, Apr. 2022.

[4] I. N. Idrus, M. R. I. Faruque, S. Abdullah, M. U. Khandaker, N. Tamam, and A. Sulieman, "An oval-square shaped split ring resonator based left-handed metamaterial for satellite communications and radar applications," *Micromachines*, vol. 13, no. 4, art. no. 578, Apr. 2022.

[5] S. Hannan, M. T. Islam, M. R. I. Faruque, M. E. H. Chowdhury, and F. Musharavati, "Angle-insensitive co-polarized metamaterial absorber based on equivalent circuit analysis for dual band WiFi applications," *Sci. Rep.*, vol. 11, no. 1, art. no. 13791, Jul. 2021.

[6] B. X. Wang, C. Y. Xu, and F. W. Pi, "Review of broadband metamaterial Absorbers: From principles, design strategies, and tunable properties to functional applications," *Adv. Funct. Mater.*, vol. 33, no. 14, Apr. 2023.

[7] H. Y. Zheng, T. S. Pham, L. Y. Chen, and Y. P. Lee, "Metamaterial perfect absorbers for controlling bandwidth: Single-peak/multiple-peaks/tailored-band/broadband," *Cryst.*, vol. 14, no. 1, art. no. 19, Jan. 2024.

[8] W. C. Zhou, P. H. Wang, N. Wang, W. Jiang, X. C. Dong, and S. Hu, "Microwave metamaterial absorber based on multiple square ring structures," *AIP Adv.*, vol. 5, no. 11, art. no. 117109, Nov. 2015.

[9] S. Kalraiya, M. Ameen, R. K. Chaudhary, and R. K. Gangwar, "Compact ultrathin conformal metamaterial dual-band absorber for curved surfaces," *Int. J. RF Microwave Comput. Aided Eng.*, vol. 29, no. 12, art. no. e21929, Dec. 2019.

[10] Y. I. Abdulkarim, F. O. Alkurt, H. N. Awl, F. F. Muhammadsharif, M. Bakir, S. Dalgac, et al., "An ultrathin and dual band metamaterial perfect absorber based on ZnSe for the polarization-independent in terahertz range," *Results Phys.*, vol. 26, art. no. 104344, Jul. 2021.

[11] M. J. Hossain, N. Mubashsara, R. Khan, M. A. Matin, P. Sarigiannidis, and S. K. Goudos, "Design of an ultra-thin metamaterial absorber with machine learning-assisted absorption prediction," *IEEE Trans. Artif. Intell.*, vol. 6, no. 10, pp. 2630–2644, Oct. 2025.

2nd International Conference on Multidisciplinary Sciences and Technological Developments (ICMUSTED 2025)

December 12-15, 2025

Discriminating Natural Modes from Defect Signatures in Rolling Bearings Through Hybrid Vibration Modelling

Azeddine Ratni[1], Ali Damou[1], Djamel Benazzouz[1], Mohamed Tsebia[2]

[1]Solid Mechanics and Systems Laboratory, University of Boumerdes, Boumerdes, Algeria
[2]Signals and Systems Laboratory, University of Boumerdes, Boumerdes, Algeria
Corresponding author: Azeddine Ratni (a.ratni@univ-boumerdes.dz)

Abstract

The reliability of rotating machinery is a key factor in the performance of electromechanical and mechatronic systems, including those used in renewable energy, aerospace, and industrial automation. This study presents a hybrid method combining dynamic modelling and signal analysis to distinguish between natural vibrations caused by internal clearances in rolling bearings and vibrations generated by structural defects. A mass-spring-damper model is developed to describe the dynamic behaviour of the bearing components, resulting in a system of differential equations that represent the intrinsic vibrational characteristics. Fault scenarios are simulated by applying external excitation forces that reproduce typical bearing defects. Time-domain techniques are applied to separate natural responses from those induced by faults. In parallel, frequency-domain analysis using the complete mathematical formulation of the Fourier Transform reveals clear spectral differences between healthy and damaged bearings. This combined approach enables accurate identification of mechanical defects and enhances the effectiveness of condition monitoring. The method can be applied to various types of rotating machinery and contributes to early fault detection, improved maintenance strategies, and increased operational reliability. The proposed method focuses on the discrimination of natural vibrational modes from defect-related signatures in rolling bearings, enabling targeted and early-stage fault diagnosis.

Keywords: Fault diagnosis, Rolling bearings, Signal processing, Dynamic modelling, Natural vibration modes

2nd International Conference on Multidisciplinary Sciences and Technological Developments (ICMUSTED 2025)

December 12-15, 2025

Quantitative Structure–Toxicity Relationship Prediction of Ionic Liquid Toxicity Using an GWO-Optimized Support Vector Machine

Hayet Abdellatif[1], Maamer Laidi[1], Cherif Si-Moussa[1], Widad Benmouloud[1], Imane Euldji[1]

[1]Laboratory of Biomaterials and Transport Phenomena, Department of Process Engineering, Faculty of Technology, Yahia Fares University of Medea, Medea, Algeria
Corresponding author: Hayet Abdellatif (e-mail: hayet.abd44@gmail.com)

Abstract

Ionic liquids (ILs) are considered a promising alternative to traditional organic solvents and have attracted considerable scientific attention due to their unique physicochemical properties, including non-flammability, extremely low vapor pressure and melting point, high solvation capacity, and minimal volatility, making them appealing for various green chemistry applications. However, despite their advantages, several studies have demonstrated that ILs can exert toxic effects on aquatic and terrestrial ecosystems, which highlights the importance of assessing and predicting their toxicity to ensure their safe and sustainable use in industrial and environmental contexts. In this study, a quantitative structure–toxicity relationship (QSTR) approach was applied to predict the toxicity (logEC50) of 134 ILs. Chemical structures were represented using SMILES notations obtained from the PubChem database, and molecular descriptors were calculated using AlvaDesc software. From the initial 5666 molecular descriptors, the 11 most informative descriptors were selected using a genetic algorithm (GA). A hybrid predictive model based on the grey wolf optimizer and support vector machine (GWO-SVM) was then developed. The dataset was randomly divided into 80% for training and 20% for testing using MATLAB to validate the model and prevent overfitting. The GWO-SVM model demonstrated excellent predictive performance, with root mean square error (RMSE), R, and R^2 values of 0.0174, 0.9997, and 0.9995 for the training set, and 0.0118, 0.9999, and 0.9998 for the test set, respectively, indicating a strong generalization ability and high accuracy in toxicity prediction. These findings confirm the efficiency of the GWO-SVM QSTR model in capturing complex structure–toxicity relationships of ILs and highlight its potential as a reliable decision-support tool for the safe design and selection of environmentally benign ionic liquids.

Keywords: Ionic liquids, Quantitative structure–toxicity relationship, Grey wolf optimizer, Support vector machine, Toxicity prediction, Molecular descriptors

2nd International Conference on Multidisciplinary Sciences and Technological Developments (ICMUSTED 2025)

December 12-15, 2025

Bibliometric Analysis of AI-Driven Energy Harvesting and Prediction in Resource-Constrained IoT and Edge Systems

Sami Acik[1,2], Selahattin Kosunalp[3], Mustafa Tasci[3]

[1]Department of Electrical Electronics Engineering, Faculty of Engineering and Natural Sciences, Gaziantep Islam Science and Technology University, Gaziantep, Türkiye
[2]Department of Electrical-Electronics Engineering, Institute of Postgraduate Education, Bandirma Onyedi Eylul University, Bandirma-Balıkesir, Türkiye
[3]Department of Computer Technologies, Gonen Vocatioal School, Bandirma Onyedi Eylul University, Bandırma-Balıkesir, Türkiye
Corresponding author: Selahattin Kosunalp (e-mail: skosunalp@bandirma.edu.tr)

Abstract

This paper presents a comprehensive bibliometric and predictive analysis of research on artificial intelligence (AI)-driven energy harvesting and energy prediction in resource-constrained Internet of Things (IoT) and edge systems. Using data retrieved from the Web of Science database covering 2015–2024, the study examines the evolution of publication trends, influential authors, collaboration networks, and thematic focuses within this rapidly growing field. The analysis reveals a substantial rise in research activity after 2019, driven by increasing demand for sustainable and intelligent energy management in IoT environments. Keyword co-occurrence and citation mapping indicate dominant themes such as lightweight neural models, hybrid forecasting architectures, and optimization techniques for low-power devices. In addition to conventional bibliometric mapping, the study employs machine learning models—linear regression (LR) and support vector regression (SVR)—to forecast future research directions, demonstrating sustained growth in publication output. The findings highlight key interdisciplinary linkages between AI, renewable energy, and edge computing, offering strategic insights for future research and development of efficient, AI-based energy solutions for resource-limited IoT ecosystems.

Keywords: Energy harvesting, IoT, Resource-constrained devices, Deep learning and machine learning, Bibliometric analysis

1. INTRODUCTION

The ubiquitous proliferation of Internet of Things (IoT) devices has transformed various sectors, enabling unprecedented levels of connectivity and data collection [1]. However, the continued operation of these devices, especially in remote or autonomous settings, faces substantial power supply challenges. Many IoT nodes are characterized by small battery capacities, necessitating frequent replacements or recharging, which limits their widespread adoption and scalability [2–4]. Overcoming these energy constraints is fundamental for realizing the full potential of IoT ecosystems, particularly in resource-limited environments and at the network edge.

Energy harvesting (EH) emerges as a compelling solution to power these devices by converting ambient energy sources—such as solar, thermal, kinetic, and radio-frequency—into usable electrical energy [5]. However, the inherent intermittency and variability of harvested energy sources present significant obstacles to reliable system operation [3]. To mitigate these issues, artificial intelligence (AI) and machine learning (ML) techniques have become instrumental in intelligently managing and predicting energy availability [5]. AI-driven approaches offer the capacity to optimize energy allocation, forecast energy yield, and adapt device behaviour based on predicted energy availability and application requirements [6–10].

The integration of AI with EH for resource-constrained IoT and edge systems represents a dynamic and expanding research area [11–15]. Given the rapid advancements in both AI methodologies and EH technologies, a systematic overview of the scholarly discourse becomes increasingly valuable. This analysis presents a comprehensive bibliometric investigation of the scientific literature concerning AI-driven EH and prediction within resource-constrained IoT and edge computing contexts. The objective is to map the intellectual structure of this interdisciplinary field, identify publication trends, discern key research themes, highlight influential authors and journals, and characterize international collaboration patterns. By performing this quantitative assessment, this

work aims to provide a structured understanding of the field's evolution and to delineate strategic directions for future inquiry.

The investigation spans publications from 2015 to 2024, focusing on the interplay of EH, energy prediction, and solar energy in the context of IoT and edge devices, specifically examining the application of deep learning and ML techniques. This structured approach facilitates a robust understanding of the trajectory and intellectual landscape of this critical research domain. The primary aim of this paper is to conduct a comprehensive bibliometric analysis of research related to EH, energy prediction, and AI-based optimization in resource-constrained IoT and edge systems. Data were collected from a leading academic database Web of Science (WoS) covering the period from 2015 to 2024. By combining bibliometric techniques with ML-based predictive analytics, this study not only explores past and present research trends but also anticipates potential future directions in this rapidly evolving field.

Through this approach, the study aims to:

- Identify the most influential authors, studies, and institutions shaping the landscape of AI-driven energy harvesting research,
- Map the collaborative and citation networks, emphasizing international partnerships and interdisciplinary intersections among IoT, edge computing, and renewable energy domains,
- Highlight the key thematic areas and knowledge gaps, such as lightweight AI architectures, hybrid forecasting models, and adaptive energy management strategies for low-power devices,
- Predict emerging research trajectories using ML models such as linear regression (LR) and support vector regression (SVR) to forecast publication growth and thematic evolution.

This paper contributes to the body of knowledge by providing a holistic and data-driven overview of AI-enhanced energy management research within the context of IoT and edge systems. By leveraging both bibliometric and predictive analyses, the findings not only illuminate current research hotspots but also guide future priorities, collaborations, and policy development for sustainable and intelligent energy solutions.

2. PLATFORM OVERVIEW AND ANALYTICAL FRAMEWORK

This study utilizes BiBLoX, a Flask-based web platform designed to automate bibliometric analysis and ML–driven trend forecasting in scientific research [16]. BiBLoX, as a recently-proposed platform, integrates three essential modules—data acquisition, bibliometric analysis, and ML prediction—within a unified Python ecosystem, providing researchers with both retrospective and predictive insights into publication and citation dynamics. BiBLoX employs a three-layer architecture comprising a user-interactive front end, a Flask-based analytical back end, and a structured data layer supported by MySQL or PostgreSQL.

- The front end enables users to enter search parameters (keywords, title strings, or year ranges) and to visualize analytical outputs through interactive dashboards.
- The back end orchestrates data retrieval, preprocessing, and analysis tasks. It automatically collects publication data from WoS, Scopus, and TR Dizin, employing application programming interface (API) connections and web-scraping mechanisms (e.g., Selenium) to ensure broad data coverage.
- The data layer handles cleaned and standardized metadata—such as author names, institutions, journal titles, citation counts, and keywords—using transformation techniques like string normalization and Levenshtein-based author matching to reduce redundancy and ambiguity.

Once data are retrieved, BiBLoX performs an integrated set of bibliometric evaluations:

- Co-authorship analysis to construct collaboration networks and identify influential authors and institutions using graph-theoretical measures (e.g., degree centrality, betweenness).
- Citation analysis to determine the most cited publications, journals, and countries, complemented by H-index and G-index computation.
- Keyword co-occurrence and word frequency analysis for mapping thematic trends, represented through word clouds and temporal evolution charts.
- Temporal trend analysis that visualizes annual publication and citation growth.

Visualization libraries such as Plotly, Matplotlib, and D3.js are integrated into BiBLoX to produce interactive and publication-ready graphics. To extend conventional bibliometrics toward forecasting, BiBLoX incorporates ML

models—specifically LR, SVR, and decision tree (DT) algorithms—to predict future publication and citation trajectories.

Feature variables include year, citation count, number of authors, journal impact factor, and subject category. Models are trained on historical data (e.g., 2015–2022) and validated on recent years (e.g., 2023–2024), with performance evaluated using mean squared error (MSE), root mean squared error (RMSE), mean absolute error (MAE), and the R-squared (R^2) metrics. The SVR model typically yields the highest predictive accuracy, capturing nonlinear patterns in scientific growth.

Compared to conventional tools such as VOSviewer, Bibliometrix, SciMAT, and Gephi, BiBLoX uniquely provides:

- Automated data retrieval from multiple databases without manual import,
- Integrated web-based environment accessible via Flask, and
- Dual analytical capability, combining bibliometric mapping and ML prediction within a single framework.

Thus, BiBLoX bridges the gap between descriptive bibliometric mapping and predictive analytics, enabling dynamic assessment of both the historical structure and future evolution of research domains.

3. RESULTS

The bibliometric analysis of 362 publications from 2015 to 2024 revealed distinct trends and characteristics of research activity in AI-driven EH and prediction for resource-constrained IoT and edge systems. The subsequent subsections detail the findings across various analytical dimensions.

Figure 1 presents the annual publication count that demonstrates a clear trajectory of increasing research interest. Starting with a single publication in 2015, the volume rose gradually to 6 in 2017 and 3 in 2018. A notable acceleration occurred in 2019 with 22 publications, followed by 30 in 2020, 47 in 2021, and 51 in 2022. The most recent years show continued expansion, with 59 publications in 2023 and a substantial 82 publications by 2024. This sharp increase post-2019 indicates a significant and sustained growth in scholarly output, reflecting the escalating academic and industrial interest in intelligent energy management for constrained IoT environments. The total number of publications within the defined period reached 362, underscoring the dynamic nature of this interdisciplinary field.

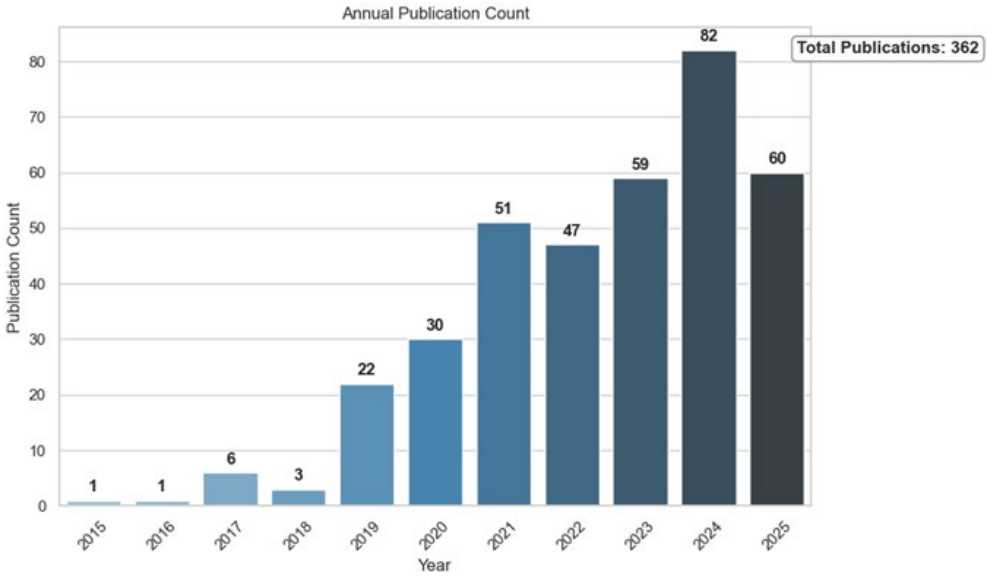

Figure 1. The number of publications per year

The annual citation trend presents a more complex picture. Citations remained relatively low from 2015 (approximately 10) to 2018 (around 117) as shown in Figure 2. A pronounced peak in citations was observed in 2019, reaching 2963. Following this peak, a consistent decline in annual citations was recorded: 937 in 2020, 727 in 2021, 397 in 2022, 237 in 2023, and approximately 100 by 2024. This pattern suggests a period of high impact for foundational works around 2019, with more recent publications still accumulating citations. The bubble chart

illustrating years by citation count visually reinforces this, with the largest bubble corresponding to 2019, and subsequent years showing progressively smaller bubbles, indicating fewer citations per year.

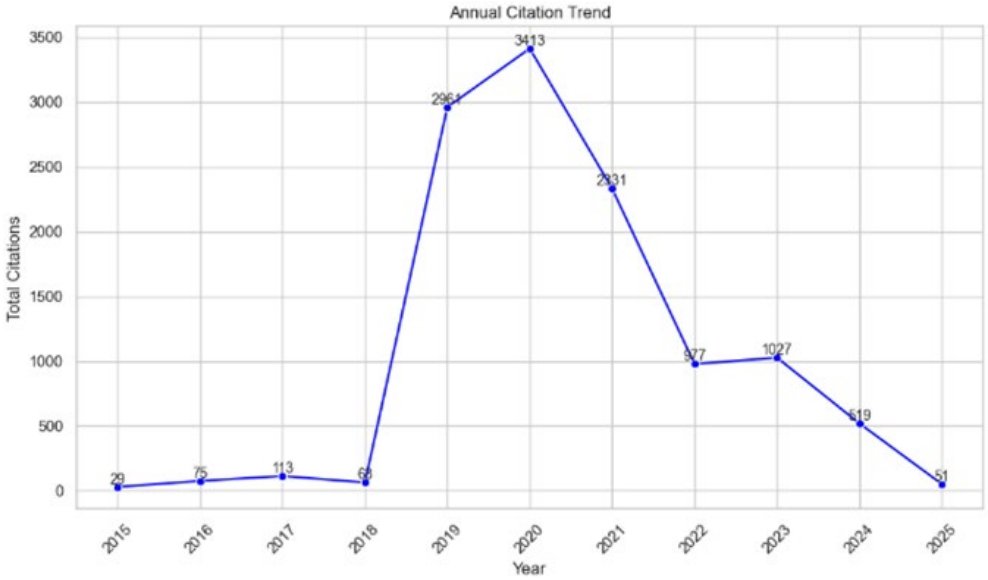

Figure 2. The number of citations per year

Figure 3 shows the future publication predictions using both LR and SVR models, suggesting a continued upward trend in publication volume. Both models predict around 82 publications for 2025, aligning with the observed growth. Conversely, the annual citation trend and prediction (Figure 4, conceptual placement), which was presented in Turkish as "Yillik Atif Sayisi Trendi ve Tahmini," projects a continued decrease in annual citations from the 2019 peak, extending into 2025. This divergence between publication growth and citation decline merits further investigation in the discussion section.

Figure 3. The number of predicted publications per year

Figure 4 presents the most frequent terms in keywords in recent research trends. It highlights that EH is the most dominant keyword with 106 occurrences, followed by IoT (95) and ML (82), showing a strong emphasis on sustainable and intelligent technologies. The mid-tier terms such as deep learning and AI further emphasize the growing integration of data-driven methods into IoT and energy-based systems. Lower-frequency keywords like solar energy, edge computing, and triboelectric nanogenerator suggest specialized areas of application within broader smart technology research. Overall, the chart reflects the convergence of renewable energy systems and AI as a central focus in contemporary academic and industrial studies.

Figure 4. The most frequent terms

Figure 5 illustrates the distribution of research outputs across major scientific journals. It is evident that IEEE Access leads significantly with 22 publications, highlighting its popularity as a multidisciplinary and open-access platform for emerging technologies. Following it, the IEEE Internet of Things Journal with 15 publications and Nano Energy with 11 publications indicate a strong research focus on smart, energy-efficient, and nanotechnology-driven systems. Journals like Sensors, Chemical Engineering Journal, and Energies also show considerable contributions, reflecting the intersection of sensor technology, energy systems, and material science. Lower but notable publication counts in Advanced Functional Materials, Electronics, IEEE Sensors Journal, and Sustainability suggest diversified yet interconnected areas of study. Overall, the chart underscores the dominance of IEEE-affiliated and energy-related journals in disseminating cutting-edge research in IoT, nanotechnology, and sustainable energy systems.

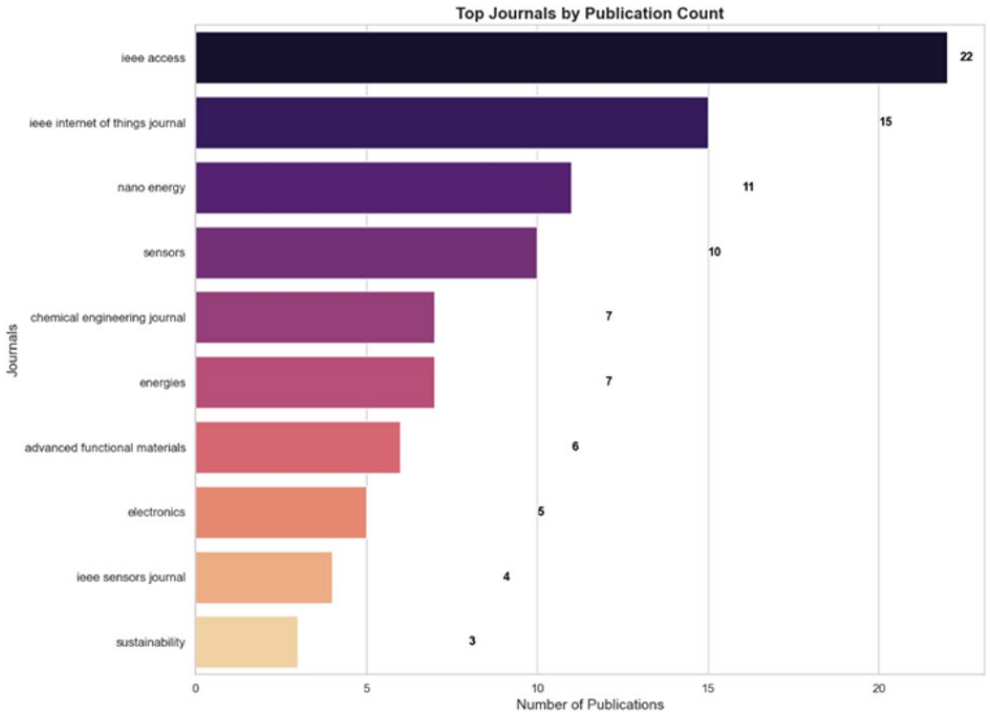

Figure 5. Top journals by publication count

4. CONCLUSION

This study provides a comprehensive bibliometric and predictive analysis of AI-driven EH and energy prediction research within resource-constrained IoT and edge computing systems. By examining publications from 2015 to 2024, the results reveal a significant rise in research interest, particularly after 2019, reflecting the accelerating convergence of AI and sustainable energy management. The analysis highlights key themes, including lightweight deep learning architectures, hybrid forecasting models, and optimization strategies for low-power devices, while identifying major contributing countries, institutions, and journals shaping the field. ML–based prediction models

such as LR and SVR indicate a sustained upward trajectory in future publication trends, underscoring the growing relevance of this domain. Overall, the findings emphasize the strategic importance of integrating AI with EH technologies to enable self-sustaining, intelligent, and efficient IoT ecosystems, offering valuable insights for researchers, practitioners, and policymakers aiming to advance next-generation energy-aware systems.

References

[1] Y. Wang, J. Chen, and M. Li, "Deep reinforcement learning for adaptive energy management in IoT devices with intermittent harvesting," *IEEE Transactions on Green Communications and Networking*, vol. 6, no. 3, pp. 1234–1245, 2022.

[2] Q. Zhang, P. Liu, and S. Yang, "A hybrid forecasting model for solar energy generation in edge computing environments using CNN-LSTM," *Applied Energy*, vol. 287, art. No. 116523, 2021.

[3] H. Li and J. Kim, "Machine learning-based energy prediction for wireless sensor networks with diverse harvesting sources," *Sensors*, vol. 20, no. 15, art. no. 4150, 2020.

[4] X. Liu, B. Sun, and J. Chen, "Lightweight federated learning for energy-efficient anomaly detection in IoT edge devices," *IEEE Internet of Things Journal*, vol. 10, no. 7, art. no. 6123–6134, 2023.

[5] L. Yang, Y. Wang, and Q. Zhang, "AI-driven power management strategies for triboelectric nanogenerator-powered IoT nodes," *Nano Energy*, vol. 60, pp. 789–798, 2019.

[6] H. Sun and J. Lee, "Optimization of energy harvesting and data transmission in cognitive radio IoT networks using deep learning," *IEEE Access*, vol. 10, pp. 101234–101245, 2022.

[7] M. Chen, T. Xu, and Y. Liu, "Energy-efficient deep learning inference on edge devices: A pruning approach for CNNs," *Journal of Parallel and Distributed Computing*, vol. 158, pp. 112–124, 2021.

[8] T. Xu, S. Kim, and J. Li, "Reinforcement learning for adaptive scheduling in energy harvesting IoT systems," *Energies*, vol. 13, no. 20, art. no. 5402, 2020.

[9] H. Kim and L. Wang, "A comprehensive review of AI applications for energy management in smart grid and IoT systems," *Renewable and Sustainable Energy Reviews*, vol. 175, art. no. 113115, 2023.

[10] S. Lee and D. Park, "Dynamic energy budgeting for self-powered IoT devices using imitation learning," *IEEE Transactions on Mobile Computing*, vol. 21, no. 11, pp. 3845–3858, 2022.

[11] K. Gai, H. Wu, and Y. Wu, "An energy-aware adaptive pruning scheme for CNNs on resource-constrained edge devices," *IEEE Internet of Things Journal*, vol. 8, no. 10, pp. 8089–8099, 2021.

[12] J. Panand L. Cai, "Machine learning for optimal RF energy harvesting placement in IoT environments," *Sensors*, vol. 20, no. 14, art. no. 3881, 2020.

[13] Y. Gao and Y. Chen, "EH-Edge: An energy harvesting-driven cloud-edge-end device collaborative IoT platform for online failure prediction," *IEEE Transactions on Industrial Electronics*, vol. 70, no. 11, pp. 11626–11637, 2023.

[14] P. Kumar and R. Singh, "A review on machine learning algorithms for energy harvesting IoT networks," *Journal of Network and Computer Applications*, vol. 199, art. no. 103304, 2022.

[15] N. Bhatia and V. Sharma, "Sustainable AI: Lightweight models for renewable energy systems," *Renewable and Sustainable Energy Reviews*, vol. 189, art. no. 113941, 2024.

[16] K. Kesgin and D. Ozer, "BiBLoX: A flask-based automatic bibliometrics and machine learning system for scientific trend prediction," *Authorea Preprint*, 2025.

2nd International Conference on Multidisciplinary Sciences and Technological Developments (ICMUSTED 2025)

December 12-15, 2025

Numerical Analysis of the Seismic Bearing Capacity of Offshore Shallow Skirted Foundations on Sand Using the Pseudo-Static Approach

Alaoua Bouaicha[1]

[1]Scientific and Technical Research Center on Arid Regions, Mohamed Khider University, 07000 Biskra, Algeria
Corresponding author: Alaoua Bouaicha (e-mail: alaoua.bouaicha@univ-biskra.dz)

Abstract

The seismic stability of offshore shallow foundations is a major concern in the design of marine and coastal infrastructures, where strong ground motions can significantly affect the load-bearing performance. Among the various foundation systems, skirted shallow foundations have shown great potential due to their ability to enhance bearing capacity and limit settlements by mobilizing additional lateral soil resistance. This study presents a detailed numerical investigation of the seismic bearing capacity of a strip skirted foundation resting on sandy soil, based on the pseudo-static approach. The analyses were carried out using Finite Element Limit Analysis (FELA), which allows for an accurate evaluation of ultimate loads while ensuring rigorous consideration of soil failure mechanisms. The effects of three main parameters—embedment depth (Ds), internal friction angle of sand (φ), and horizontal seismic coefficient (kh)—were systematically examined. Results indicate that increasing the embedment ratio significantly improves the seismic bearing capacity, while higher values of kh reduce it due to the additional inertial forces. The inclusion of vertical skirts leads to a pronounced increase in the bearing capacity ratio (BCR), confirming their beneficial role in enhancing the seismic performance of offshore foundations. Furthermore, the comparison with previously published results demonstrates the validity and consistency of the present findings. This study contributes to a better understanding of the seismic response of skirted foundations on sandy soils and provides useful insights for the optimal design of offshore energy, bridge, and port structures subjected to earthquake loading.

Keywords: Bearing capacity, Skirted foundation, Finite element limit analysis (FELA), Pseudo-static approach, Embedment depth

2nd International Conference on Multidisciplinary Sciences and Technological Developments (ICMUSTED 2025)

December 12-15, 2025

Leveraging Large Language Models for Transport-Triggered Architecture Processor Design

Latif Akcay[1]

[1]Department of Computer Engineering, Erzurum Technical University, Erzurum, Türkiye
Corresponding author: Latif Akcay (e-mail: latif.akcay@erzurum.edu.tr)

Abstract

Recently, the use of large language models (LLMs) to aid hardware design and implementation has become a popular research topic. This study uses the state-of-the-art Gemini 3 Pro model to develop application-specific processor hardware, investigating the suitability of such models for assisting with hardware design tasks. Transport triggered architectures (TTAs) stand out among application-specific instruction-set processors due to their high flexibility and scalability. However, designing processors with this architecture requires a high degree of domain-specific software and hardware expertise. Furthermore, manually implementing interconnection networks and hazard handling logic is particularly complex and error prone. Therefore, achieving efficiency by using LLMs that can execute these processes would be highly beneficial for designers. Nevertheless, the hardware code for TTA processors is less widespread than that for traditional processors, and the amount of data available for artificial intelligence (AI) training is limited. In this context, a simple 32-bit processor was designed using an iterative and conversational prompting strategy. This architecture features a fully connected four-bus interconnect, custom functional units (arithmetic logic unit (ALU), multiplier and shifter), and a hazard-free register file access mechanism. Tests were also performed to prove the functionality of the design, and the hardware was synthesised for use with field-programmable gate arrays (FPGAs). This paper presents a summary of the entire process, highlighting current capabilities and key shortcomings, and discussing future actions to guide similar studies. It also concludes that LLMs do not replace the hardware engineer yet, but rather efficiently accelerate the test, design, verification, implementation and documentation cycles.

Keywords: LLM-aided hardware design, AI-assisted hardware design, Application-specific processor design, Transport-triggered architecture, Prompt engineering

1. INTRODUCTION

As electronic devices become more diverse and smaller, the number and complexity of tasks assigned to them is also increasing significantly. Furthermore, designing these systems to consume less energy is paramount. These requirements are prompting designers to develop application-specific processor models that are much more efficient. The stagnation of Moore's Law and the end of Dennard scaling also necessitate a paradigm shift in computing hardware development. This shift involves moving away from general-purpose processors and towards domain-specific architectures (DSAs) and application-specific instruction-set processors (ASIPs) [1]. In order to meet rising performance expectations while delivering a solution that is more efficient and lower in R&D costs, designers are implementing custom hardware accelerators on field-programmable gate arrays (FPGAs). However, the considerable expertise, significant experience and often lengthy development times required to create such systems using traditional hardware design methods remain the most significant obstacles [2].

Among the various ASIP architectures, the transport triggered architecture (TTA) stands out as a highly flexible alternative to traditional very long instruction word (VLIW) or reduced instruction set computing (RISC) designs [3]. In a TTA processor, computation occurs as a side effect of data movement between functional units (FUs) [4]. The interconnection network is exposed to the programmer, and an operation is triggered when data reaches a special trigger port. This philosophy simplifies the design of the control unit, as no complex instruction decoding stage is needed [5]. Another advantage of this approach is that the register file access rate decreases dramatically as the data is moved to the FU, where it will be processed next. Despite all these architectural advantages, the implementation of a TTA processor with traditional methods becomes significantly more difficult due to the increase in the number and complexity of FUs and transport buses.

While large language models (LLMs), trained with very large data sets, usher in a new era in automation in many areas, they also have a significant opportunity to demonstrate a similar effect in the field of hardware and software

development [6]. While it's not entirely accurate to claim that they can yet achieve fully automated, reliable implementation, it's at least possible to say that they can be quite helpful to designers, especially in these labour-intensive processes [7].

In this paper, we investigate the potential of an LLM-aided methodology for designing and implementing a simple 32-bit TTA processor. While hardware description language (HDL) code for conventionally designed processors is widely available, code for processors developed using relatively new methods, such as TTA, is much less readily available. LLMs are less trained on such designs, and consequently, producing a TTA processor's hardware is much more challenging than that of a conventional processor. In contrast to conventional code-generation tasks, a collaborative workflow is demonstrated, whereby the LLM functions as the primary register transfer level (RTL) author, while the human designer assumes the role of verifier and prompt engineer. The resulting design was verified through simulations and successfully synthesized for an Artix-7 FPGA [8]. Although there are some interesting papers in the literature that include processor core designs developed leveraging artificial intelligence assistance, there is no other study yet for TTA processors.

The remainder of this paper is organized as follows: Section 2 provides a fundamental background on TTA and demonstrates the processor model targeted to be generated with the prompting strategy preferred in the study. The following Section 3 discusses the simulation and synthesis results of the generated design, which is the outcome of the present study. Finally, the paper is concluded in Section 4, along with the remarks for future studies.

2. MATERIAL AND METHOD

2.1. Transport-Triggered Architecture

In traditional VLIW architectures, instructions explicitly dictate the operations of the FUs. By contrast, in TTA, instructions merely define how data is transferred from source units to destination units. The computation process then occurs because of this data movement. The TTA structure essentially consists of two basic types of units: transport buses and FUs. FUs are independent units containing either basic arithmetic operations or custom operations defined by the designer. Transport buses form the interconnection between the instruction memory and the FUs, and control the transfer of data under the control unit's direction. Figure 1 shows the units and connection structure of a classic TTA processor.

The TTA architecture offers designers a highly flexible, scalable and modular structure during the ASIP development process and is a freely licensed development method. Additionally, the customized parallel computing (CPC) group at Tampere University provides a free and open-source TTA processor development environment called OpenASIP [9].

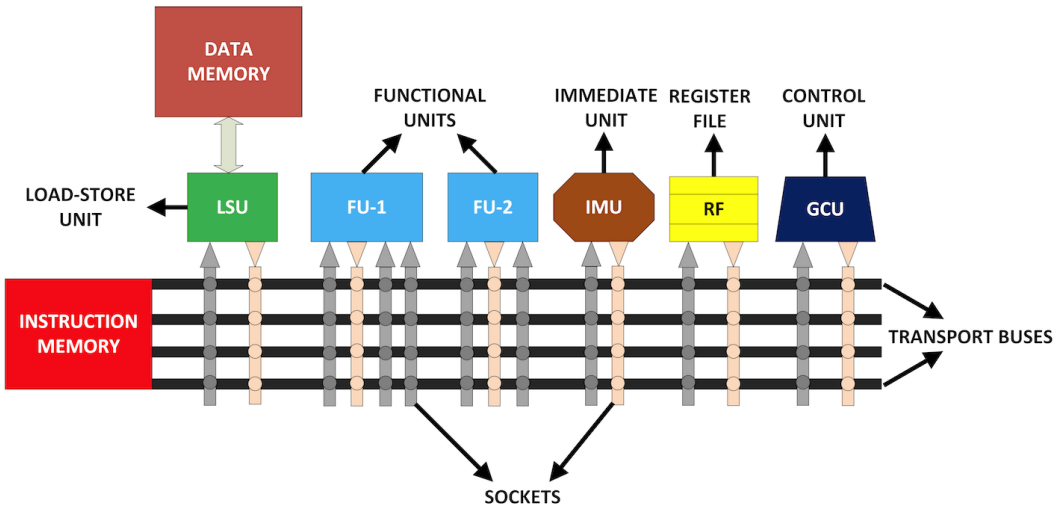

Figure 1. Block structure of a conventional TTA processor

2.1. Prompting Strategy

The design methodology employed in this study was initiated with a structured, role-based, and zero-shot prompt presented to the Gemini 3 Pro. The initial prompt is reproduced verbatim in Figure 2. The architecture (TTA), target hardware (Nexys4DDR development board [10]), and data path constraints were clearly defined within the

prompt. This minimized the risk of hallucination and allowed the model to generate synthesizable HDL code. While this initial formal specification ensures the modularity of the design, during the conversion of the theoretical design to practical Verilog code, it was observed that the model struggled with timing accuracy and signal prioritization, particularly those inherent to the TTA architecture.

The most common errors encountered during the code generation process were identified as being either synchronization losses between hardware identifiers (IDs) and software (read-only memory (ROM)) HEX codes, or the omission of the forwarding logic required to capture data within the same cycle in the arithmetic logic unit (ALU) operation. The most critical issue identified was the failure to assign priority to "immediate" values among data paths during the writing process to the Register File. Furthermore, errors such as the incorporation of logical corrections (e.g. register write signals) into the code but the forgetting to physically connect these signals to the module ports clearly demonstrated the importance of human oversight.

In this context, the design process evolved from a one-way code generation to an iterative debugging cycle based on simulation feedback. The simulation waveforms and error logs provided by the author served as a framework for the model to identify and rectify abstract logic errors, leading to the identification of concrete connection problems. This collaborative effort evidently demonstrates that LLMs have the potential to act as competent "digital architects" in designing complex processor architectures. However, it is important to note that they require human guidance and a rigorous verification process for ensuring bit-exact accuracy and hardware synthesizability.

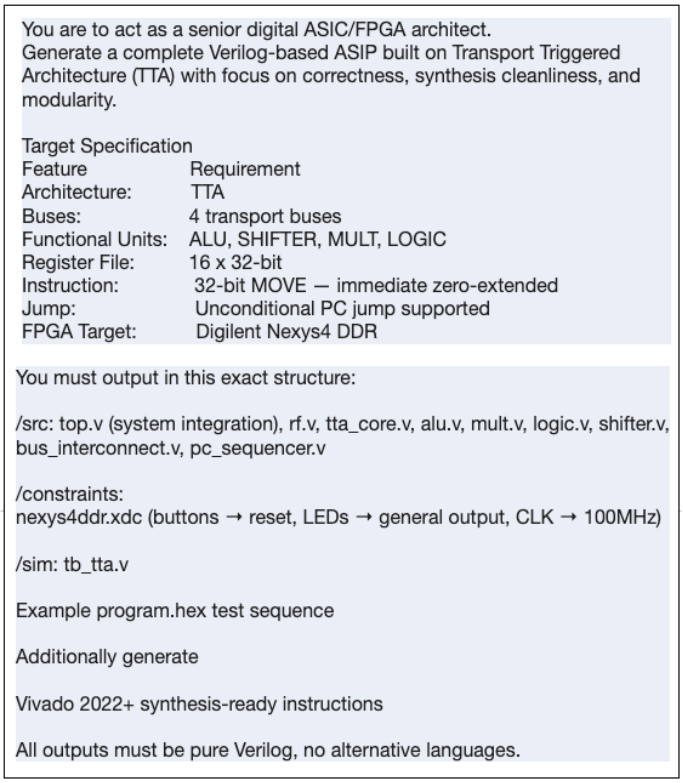
You are to act as a senior digital ASIC/FPGA architect.
Generate a complete Verilog-based ASIP built on Transport Triggered Architecture (TTA) with focus on correctness, synthesis cleanliness, and modularity.

Target Specification

Feature	Requirement
Architecture:	TTA
Buses:	4 transport buses
Functional Units:	ALU, SHIFTER, MULT, LOGIC
Register File:	16 x 32-bit
Instruction:	32-bit MOVE — immediate zero-extended
Jump:	Unconditional PC jump supported
FPGA Target:	Digilent Nexys4 DDR

You must output in this exact structure:

/src: top.v (system integration), rf.v, tta_core.v, alu.v, mult.v, logic.v, shifter.v, bus_interconnect.v, pc_sequencer.v

/constraints:
nexys4ddr.xdc (buttons → reset, LEDs → general output, CLK → 100MHz)

/sim: tb_tta.v

Example program.hex test sequence

Additionally generate

Vivado 2022+ synthesis-ready instructions

All outputs must be pure Verilog, no alternative languages.

Figure 2. Structured zero-shot prompting for automated TTA processor design

3. EXPERIMENTAL RESULTS

An intensive simulation process was conducted to test the functional accuracy of the 32-bit TTA processor, which was produced as a result of a mutual debugging process carried out with the Gemini 3 Pro LLM. Figure 3 shows a portion of the simulation waveform, which successfully tested a full instruction set encompassing instantaneous value loading, register file operations, and ALU, multiplier, shifter, and logic units.

Following the verification phase, the design was synthesized using the Xilinx Vivado [11] tool for the Digilent Nexys4 DDR platform. The synthesized circuit demonstrated the low hardware cost and high efficiency of the TTA architecture using only 613 LUTs, 464 Flip-Flops, and 3 digital signal processing (DSP) slices. Even though no timing optimizations or pipelining improvements were used on the design by the Vivado tool, the processor was able to reach a maximum operating frequency (F_{max}) of 92 MHz. This demonstrates that the artificial intelligence (AI)-generated RTL code is not only functionally correct but also optimized enough to run close to

the system clock speed on standard FPGA fabrics. While the model demonstrated high success in creating standard modules, it failed to produce error-free code, particularly in cases such as bus contention, write priorities, and cyclic signal timings, and required extensive feedback for correction. This study focused on hardware design and excluded the automated generation of a software toolchain, such as an assembler or compiler, that would facilitate processor programmability.

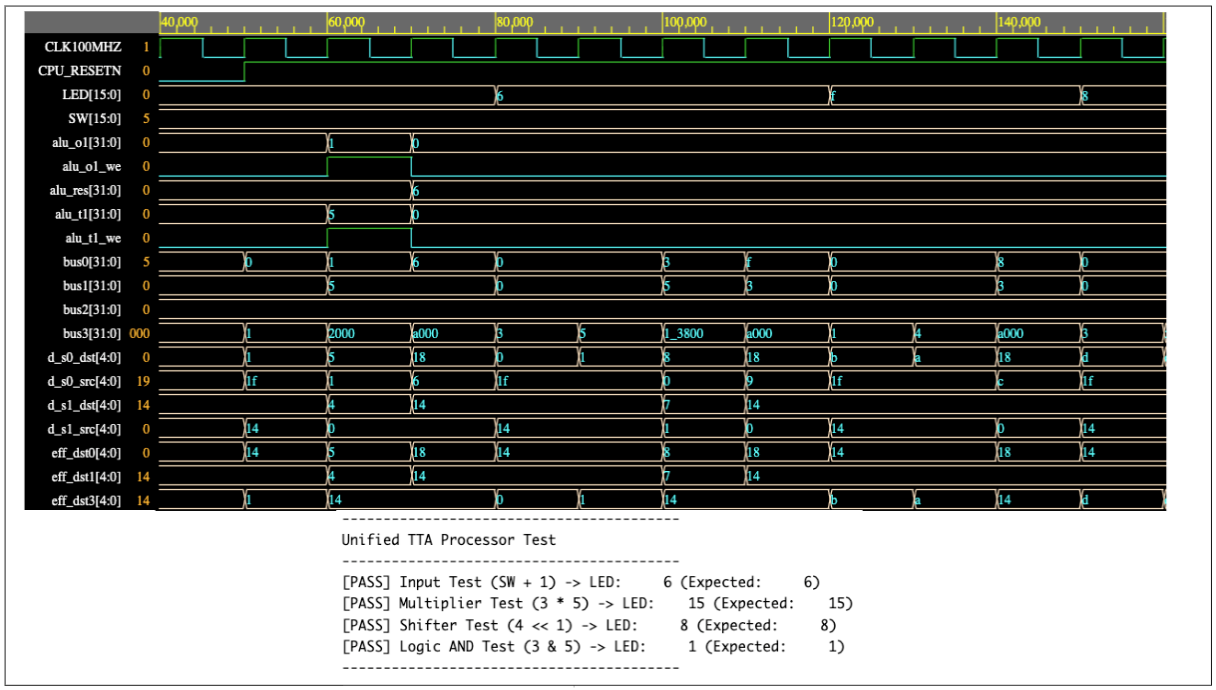

Figure 3. Simulation waveform and terminal output of the resulting TTA processor

4. CONCLUSION

LLM-assisted hardware design and implementation has become prominent in recent years as a new method for electronic design automation (EDA). This study aimed to generate the necessary constraint codes for a TTA processor hardware, testbench, and FPGA implementation using the Gemini 3 Pro LLM. To achieve this, a structured and detailed prompt strategy that highlighted the model's strengths employed first. Simulation and synthesis errors were then fed back into the model, leading to an iterative debugging process. As a result, a core capable of performing basic functions was achieved without any human intervention. While this study demonstrated the feasibility of LLM-assisted hardware design, it also clearly demonstrated that the process relies on robust human-AI collaboration rather than full automation. The limited availability of open-source sample code for TTA processors reduces the likelihood of models being successful in such architectures. Therefore, future studies aimed at addressing this lack of data could significantly contribute to the literature.

Acknowledgments

In this study, the LLM Gemini 3 Pro was utilized for hardware design and implementation of a TTA-based processor. The LLM was used as research subjects for comparative HDL code generation, not as co-authors or content generators for this manuscript.

References

[1] J. L. Hennessy and D. A. Patterson, "A new golden age for computer architecture," *Commun. ACM*, vol. 62, no. 2, pp. 48–60, Feb. 2019. doi: 10.1145/3282307

[2] H. Esmaeilzadeh, E. Blem, R. St. Amant, K. Sankaralingam, and D. Burger, "Dark silicon and the end of multicore scaling," in *Proc. 38th Annu. Int. Symp. Comput. Archit. (ISCA)*, San Jose, CA, USA, 2011, pp. 365–376. doi: 10.1145/2000064.2000108

[3] H. Corporaal, *Microprocessor Architectures: From VLIW to TTA*. Chichester, U.K.: John Wiley & Sons, 1997.

[4] L. Akcay and B. O. Yalcin, "Lightweight ASIP design for lattice-based post-quantum cryptography

algorithms," *Arabian Journal for Science and Engineering*, vol. 50, pp. 835–849, 2025. doi: 10.1007/s13369-024-08976-w

[5] L. Akcay and B. O. Yalcin, "Analysing the potential of transport triggered architecture for lattice-based cryptography algorithms," *International Journal of Embedded Systems*, vol. 15, no. 5, pp. 404–420, 2022. doi: 10.1504/IJES.2022.127164

[6] S. Thakur, B. Ahmad, H. Pearce, B. Tan, B. Dolan-Gavitt, R. Karri, et al., "VeriGen: A large language model for verilog code generation," *ACM Trans. Des. Autom. Electron. Syst.*, vol. 29, no. 3, art. no. 46, May 2024. doi: 10.1145/3643664

[7] M. Liu, T.-D. Ne, R. Kirby, C. Cheng, N. Pinckney, R. Liang, et al., "ChipNeMo: Domain-adapted LLMs for chip design," *arXiv*, 2023. doi: 10.48550/arXiv.2311.00176

[8] Xilinx Inc., "Artix-7 FPGAs data sheet: DC and AC switching characteristics," DS181 (v1.25), San Jose, CA, USA, 2018.

[9] P. Jääskeläinen, V. Guzma, A. Cilio, J. Takala ve H. Berg, "HW/SW co-design toolset for customization of exposed datapath processors," in *Computing Platforms for Software-Defined Radio*, W. Hussain, J. Nurmi, J. Isoaho, and F. Garzia, Eds. Cham, Switzerland: Springer, 2017, pp. 147–164. doi: 10.1007/978-3-319-49679-5_8

[10] Digilent, Inc., *Nexys4 DDR FPGA Board Reference Manual*, Rev. C, Sept. 11, 2014. [Online]. Available: https://digilent.com/reference/_media/nexys4-ddr:nexys4ddr_rm.pdf

[11] Xilinx, *Vivado Design Suite*, White Paper WP416, Rev. 1.1, Jun. 22, 2012. [Online]. Available: https://docs.amd.com/v/u/en-US/wp416-Vivado-Design-Suite

2nd International Conference on Multidisciplinary Sciences and Technological Developments (ICMUSTED 2025)

December 12-15, 2025

Evaluating the Role of Plant Growth-Promoting Rhizobacteria Strains in Boosting the Nutritional Quality of *Trifolium Alexandrinum*

Yousra Debbah[1], Mohamed Bencherchali[1], Saida Messgo-Moumene[1]

[1]Department of Biotechnology and Agroecology, University of Saad Dahleb, Blida, Algeria
Corresponding author: Yousra Debbah (e-mail: debbah_yousra@univ-blida.dz)

Abstract

Trifolium alexandrinum L. is a key forage legume valued for its high palatability, digestibility, and rich nutritional profile, making it essential for improving livestock performance, milk yield, and overall farm productivity. Enhancing its nutritive quality is therefore a priority in sustainable livestock production systems. Conventional fertilization practices, although effective in increasing biomass, can contribute to soil degradation, nutrient imbalance, and environmental risks. In contrast, plant growth-promoting rhizobacteria (PGPR) offer a sustainable alternative, enhancing plant nutrition, stimulating growth, and improving soil fertility through eco-friendly mechanisms. The present study aimed to evaluate the effects of two strains, BT1 and BT2, on the nutritional composition of *Trifolium alexandrinum* at the flowering stage under open-field conditions. The experiment followed a randomized design with five replications per treatment. Seeds were primed before sowing, and 20 mL of each bacterial suspension was applied at the early vegetative stage. At flowering, plant samples were harvested and analysed for crude protein, crude fibre, dry matter, and ash content using standard laboratory methods. The strain's application significantly influenced the nutritional parameters of *Trifolium alexandrinum*. Crude protein, a key indicator of forage quality, increased in both inoculated treatments, reaching 17.27% in BT1 and 17.22% in BT2, compared with 16.05% in the control, confirming the capacity of PGPR to enhance nitrogen assimilation. Crude fibre showed slight variation across treatments, with values of 26.81% (BT1), 26.52% (BT2), and 26.13% (control), indicating stable cell wall development. Ash content, representing the mineral fraction, was highest in BT1 (11.54%), followed by the control (11.23%) and BT2 (11.04%). Overall, strain BT1 demonstrated the greatest improvement in nutritional quality, increasing protein and mineral levels. These findings highlight the potential of PGPR as effective biofertilizers that increase forage value, support livestock health, and contribute to environmentally sustainable agricultural systems.

Keywords: *Trifolium alexandrinum*, Plant growth-promoting rhizobacteria (PGPR), Nutritional quality, Forage enhancement

2nd International Conference on Multidisciplinary Sciences and Technological Developments (ICMUSTED 2025)

December 12-15, 2025

Sustainable Utilization of *Mentha Pulegium* by-Products: From Cellulose Microfibers to Fermentable Sugars

Fatma Bhiri[1], Feriel Lessig[1], Amir Bouallegue[2], Samira Abidi[1], Aida Ben Hassen Trabelsi[1]

[1]Laboratory of Wind Energy Management and Waste Energy Recovery. Research and Technology Center of Energy, Technopark of Borj-Cedria, 2050 Hammam Lif, Tunisia
[2]Laboratory of Food Oral Processing, School of Food Science and Biotechnology, Zhejiang Gongshang University, 310018 Hangzhou, China
Corresponding author: Fatma Bhiri (e-mail: fatmabhiri@gmail.com)

Abstract

Hydrodistillation by-products represent a significant source of underutilized biomass with potential environmental challenges if not valorized. Investigating these wastes, particularly from *Mentha pulegium*, is essential for recovering value-added compounds and enhancing sustainable resource utilization. This study explores the extraction of cellulose microfibers from hydrodistillation by-products of *Mentha pulegium* for subsequent hydrolysis into fermentable sugars suitable for second-generation bioethanol production. Mechanical and chemical treatments were applied to disrupt the lignocellulosic biomass structure and remove non-cellulosic components. Optimization of alkaline treatment using 2% NaOH achieved a cellulose yield of 96.31%. A bleaching step with sodium chlorite further purified the fibers by removing residual lignin. Structural and morphological changes were analyzed by colorimetry, scanning electron microscope (SEM), Fourier transform infrared spectroscopy (FT-IR), and X-ray diffraction (XRD), confirming effective removal of lignin and hemicelluloses and high crystallinity of the isolated microfibers. Chemical hydrolysis of the extracted cellulose microfibers demonstrated the feasibility of using *Mentha pulegium* by-products as raw materials for producing sugars applicable in renewable energy fields, particularly for bioethanol production.

Keywords: Hydrodistillation by-products, *Mentha pulegium*, Cellulose microfibers, Fermentable Sugars, Bioethanol production

2nd International Conference on Multidisciplinary Sciences and Technological Developments (ICMUSTED 2025)

December 12-15, 2025

Unlocking Aromatic Potential: Tripartite Rhizosphere Interactions Steer Metabolism for Stable Essential Oil Biosynthesis in Citronella Grass

Ferota Larasati[1], Sudiarso Sudiarso[2], Nunun Barunawati[3]

[1]Agronomy Department, Brawijaya University, Malang, Indonesia
Corresponding author: Ferota Larasati (e-mail: ferotalarasati20@gmail.com)

Abstract

The production and quality of essential oils in aromatic plants such as citronella grass (*Cymbopogon nardus* L.) depend not only on genetic factors but are also profoundly determined by complex dynamics within the rhizosphere. This study aims to bridge a critical knowledge gap by unveiling the synergistic tripartite interaction between nutrient availability, soil microorganisms, and plant physiology in enhancing secondary metabolite biosynthesis. The experimental analyses indicate that the integrated application of organic fertilizer and specific rhizobacteria inoculation significantly enhanced rhizosphere health, resulting in a 40% increase in plant biomass and a substantial reshaping of the plant's metabolic profile. Essential oil yield resulted in 2.3%, directly correlated with optimized nutrient uptake. Specifically, the citronellal content increased by 10% compared to the treatment with rhizobacteria, while citronellol and geraniol levels remained stable. Soil analysis demonstrated a 63% increase in phosphorus and 72% increase in potassium availability, with exchangeable calcium, magnesium, and sodium reaching 25.32, 14.28, and 1.43 cmol(+)kg^{-1}, respectively. These findings reveal a crucial mechanism where optimal nutrient conditions promote efficient resource allocation, enabling plants to build a strong metabolic foundation for stable production of key aromatic compounds rather than triggering stress responses. The results provide both a sustainable cultivation strategy for citronella grass and a novel framework for manipulating rhizosphere ecosystems to engineer aromatic plant quality at the metabolic level.

Keywords: *Cymbopogon nardus*, Monoterpene, Tripartite interaction, Organic manure, Soil fertility

2nd International Conference on Multidisciplinary Sciences and Technological Developments (ICMUSTED 2025)

December 12-15, 2025

Potential of Plant Waste Ash Supplemented Culture Media for in Vitro Microtuber Induction in *Solanum Tuberosum* L.

Amina Belguendouz[1], Benamar Benmahioul[2]

[1]Department of Agronomic Sciences, Institute of Natural and Life Sciences, Nour Bachir University Center of El Bayadh, 32000 El Bayadh, Algeria
[2]Department of Forest Resources, Faculty of Natural and Life Sciences and Earth and Universe Sciences, University of Tlemcen Abou Bekr Belkaid, Tlemcen, Algeria
Corresponding author: Amina Belguendouz (e-mail: amna.war@gmail.com)

Abstract

This study explores the feasibility of incorporating plant waste–derived ash into culture media to support *in vitro* regeneration and microtuber formation in two potato cultivars, *Solanum tuberosum* L. cultivars. *Desiree* and *Spunta*. The findings demonstrate the successful regeneration of complete plantlets via the induction of both caulogenic and rhizogenic pathways, with organogenesis strongly influenced by the mineral constituents of the ash-enriched media. Meristematic explants displayed high organogenic competence, underscoring their importance for efficient micropropagation and the production of genetically stable, pathogen-free plants. Microtuber formation was assessed using hormone-free Murashige and Skoog (MS) medium and MS medium supplemented with naphthaleneacetic acid (NAA), under three photoperiod regimes. The results revealed that hormone-free MS medium primarily promoted vegetative growth, whereas the addition of NAA markedly enhanced both the initiation and enlargement of microtubers. Photoperiod also played a decisive role in tuberization: cultures exposed to 8 h and 16 h of light generated larger and heavier microtubers compared with those maintained in continuous darkness. Overall, the study provides evidence that plant waste ash can be effectively integrated into tissue-culture systems as a sustainable alternative for in vitro propagation and microtuber production in potato.

Keywords: *Solanum tuberosum* L., Cultivars, Plant waste ash, Organogenesis, Micropropagation, Microtuber formation

2nd International Conference on Multidisciplinary Sciences and Technological Developments (ICMUSTED 2025)

December 12-15, 2025

Effects of Activated Charcoal Supplementation on in Vitro Microtuber Production and Quality in Potato

Amina Belguendouz[1], Benamar Benmahioul[2]

[1]Department of Agronomic Sciences, Institute of Natural and Life Sciences, Nour Bachir University Center of El Bayadh, 32000 El Bayadh, Algeria
[2]Department of Forest Resources, Faculty of Natural and Life Sciences and Earth and Universe Sciences, University of Tlemcen Abou Bekr Belkaid, Tlemcen, Algeria
Corresponding author: Amina Belguendouz (e-mail: amna.war@gmail.com)

Abstract

This study investigates the influence of activated charcoal (AC) on optimizing *in vitro* microtuberization in two potato (*Solanum tuberosum* L.) cultivars *Spunta* and *Desiree*. Using semi-solid and liquid Murashige and Skoog (MS) media supplemented with different AC concentrations, the results show that AC markedly improves key morphological parameters of developing microtubers. In *Spunta*, semi-solid MS medium yielded the highest-quality microtubers, with mean diameter and weight reaching 1.36 cm and 1.18 g, respectively, whereas liquid media increased microtuber number but reduced overall size and biomass. For Desiree, the most favorable microtuber traits (1.04 cm, 1.06 g) were obtained at 2 $g \cdot L^{-1}$ AC, while *Spunta* exhibited optimal performance at 10 $g \cdot L^{-1}$ AC (1.16 cm, 0.94 g). These outcomes highlight the pivotal role of AC in enhancing microtuber quality and underscore its relevance as a selection criterion in pre-basic seed potato production systems designed for direct field deployment.

Keywords: *Solanum tuberosum* L., Cultivar selection, Tissue culture, Seed tuber quality, Microtuber induction

2nd International Conference on Multidisciplinary Sciences and Technological Developments (ICMUSTED 2025)

December 12-15, 2025

Lignocellulosic Biomass Valorization for Biogas Production

Samira Abidi[1], Arwa Masrouhi[1,2], Fatma Bhiri[1], Aida Ben Hassen Trabelsi[1]

[1]Laboratory of Wind Energy Management and Waste Energy Recovery, Research and Technology Center of Energy, 2050 Tunis, Tunisia
[2]Higher institute of Applied Sciences and of Technology of Mahdia, Tunisia
Corresponding author: Samira Abidi (e-mail: samira.abidi@crten.mesrs.tn)

Abstract

Energy and useful materials can be produced by applying biological and thermal conversion processes such as anaerobic digestion and pyrolysis. Pyrolysis has been used mostly for the conversion of biomass to bio-crude and biochar, a stable form of nearly pure carbon that has application in many agricultural and environmental applications. The use of biochar as an adjuvant to stabilize the anaerobic digestion process has been extensively documented in the literature. We studied the effects that biochar has on the biomethane potential (BMP) during anaerobic digestion of citrus waste under mesophilic conditions (37 ºC). Lemon peel waste (LPW) was pyrolyzed in a laboratory fixed-bed reactor at a final temperature of 500 °C with an incremental heating rate of 10 °C/min, under an nitrogen atmosphere to produce biochar. The substrate to inoculum (S/I) ratio is the ratio of the amount of substrate to the amount of inoculum used, and it is a crucial parameter in anaerobic digestion processes. A series of experiments aimed at determining the ideal circumstances for anaerobic digestion (such as the quantity of biochar and the ratio (S/I)) and the impact of each factor on the studied responses were determined. The Nemrod software, a tool for simulating experiment matrices, has determined the ideal conditions for the two factors under investigation to maximize the responses. These are approximately 5.25 mg/L of biochar for factor X1 (biochar quantity) and 0.4 for factor X2, the substrate to inoculum ratio (S/I). Under ideal conditions, the percentage of chemical oxygen demand (DCO) absorption is 27.71%, the percentage of total organic carbon (TOC) absorption is 68.56 %, and the maximum percentage of methane (CH_4) produced is 14.33%. More research is needed to understand the complex interactions between biochar type, dosage, substrate characteristics, and process parameters for large-scale commercial applications.

Keywords: Anaerobic digestion, Biochar, Lignocellulosic biomass, Biochemical pathways

Nanoencapsulation of Polyphenols from Native *Schinus Molle* and Non-Native Fruits for Sustainable Plant Growth Promotion

Matias Aguilar[1,2,3], Jorge Montanari[1,2,3], Luciano Gabbarini[1,2,3]

[1]Laboratory of Nanosystems for Biotechnological Applications, National University of Hurlingham, 1688 Buenos Aires, Argentina
[2]National Council for Scientific and Technical Research, Buenos Aires, Argentina.
[3]Scientific Research Commission of the Province of Buenos Aires, 1900 La Plata, Argentina
Corresponding author: Matias Aguilar (e-mail: matiasfab.aguilar@gmail.com)

Abstract

Polyphenols (PFs) are recognized as powerful biostimulants, capable of improving plant growth by enhancing nutrient absorption, regulating development, and protecting against oxidative stress. However, their widespread application is severely limited by rapid environmental degradation, requiring high doses that can negatively affect the rhizosphere microbiome. This research approaches this limitation by developing a sustainable bio-input through the extraction and nanoencapsulation of PF from native *Schinus molle* (Aguaribay) and non-native blueberries. The aim of this work is the achievement of a stable and controlled-release system, which is critical for avoiding negative impacts on the rhizosphere, considering that *Schinus molle* is a co-evolved native species. Our methodology involves comprehensive characterization of the extracted PF, their subsequent encapsulation into lipid nanostructured carriers, and testing of their release kinetics and biostimulant activity. Preliminary results confirm successful extraction via a green chemistry approach (ethanolic solution). Total PF content, measured by the Folin-Ciocalteu method, showed a result of 0.819 mg EAC/g sample on a fresh basis. Antioxidant capacity was also determined by the 2,2-diphenyl-1-picrylhydrazyl (DPPH) method, and the sample has been stored at 4°C to evaluate stability kinetics. The core innovation is utilizing nanoencapsulation to reduce the effective dosage while extending biological activity, therefore preserving the integrity of the soil microbiome. This strategy is a possible solution by formulating next-generation, environmentally sound biostimulants tailored for controlled delivery.

Keywords: Nanoencapsulation, Polyphenols, Biostimulant

2nd International Conference on Multidisciplinary Sciences and Technological Developments (ICMUSTED 2025)

December 12-15, 2025

Nurses' Perceptions of Spirituality and Spiritual Care: A Cross-Sectional Study in Kabul, Afghanistan

Farzana Mortazavi[1], Hatice Sutcu[1]

[1]Faculty of Health Sciences, Cyprus International University, Nicosia, Turkish Republic of Northern Cyprus
Corresponding author: Hatice Sutcu (e-mail: hsutcu@ciu.edu.tr)

Abstract

This study aimed to explore nurses' perceptions of spirituality and spiritual care in Kabul, Afghanistan, and examine their association with socio-demographic and professional characteristics. A cross-sectional design involving 193 nurses from public and private hospitals was adopted. Data were collected using a socio-demographic questionnaire and the Spirituality and Spiritual Care Rating Scale. The majority of nurses were female (53.4%), aged 20–29 (51.8%), and married (63.7%). Most participants held a bachelor's degree (51.8%) and reported income matching their expenses (69.4%). A significant proportion (82.9%) reported no health problems. Professionally, 38.3% had 1–5 years of experience, and 58.5% worked in private hospitals. Intensive care units (13.0%) and maternity wards (16.1%) employed the highest proportions of nurses. Only 14.5% had completed specialized spiritual care training. Nurses associate spirituality with providing emotional support, respecting dignity, privacy, and cultural beliefs, while also fostering hope and inner peace. Spirituality was not perceived as limited to religious worship (1.32 ± 1.11), while kindness, empathy, and reconciliation were highly valued in spiritual care (3.26 ± 0.74). Scale scores were significantly higher among women, older nurses, and those with greater education or experience ($p < 0.001$). Nurses working in intensive care units and private hospitals had higher scores compared to their counterparts in public hospitals ($p < 0.05$). Interestingly, nurses with no spiritual care training scored higher than those who received training ($p < 0.001$). Nurses in Kabul recognize spirituality and spiritual care as integral to holistic care. However, gaps in training and varying perceptions highlight the need for structured educational programs to enhance the delivery of spiritual care in clinical practice.

Keywords: Spiritual care, Nursing, Holistic care, Spirituality

The Knowledge and Attitudes of Iranian Nurses About Pain Management

Elahe Mohammadian[1], Hatice Sutcu[2], Fatemeh Bahramnezhad[3]

[1]Faculty of Health Sciences, Cyprus Aydin University, Kyrenia, Turkish Republic of Northern Cyprus
[2] Faculty of Health Sciences, Cyprus International University, Nicosia, Turkish Republic of Northern Cyprus
[3]Nursing and Midwifery Care Research Centre, Tehran University of Medical Sciences, Tehran, Iran
Corresponding author: Hatice Sutcu (e-mail: hsutcu@ciu.edu.tr)

Abstract

Pain management is a significant aspect of patient care. Numerous studies have highlighted the fact that nurses have knowledge gaps regarding this issue. For this reason, this study aims to evaluate the pain management knowledge, attitudes, and practices of Iranian nurses in hospitals in Tehran, Iran. By using the knowledge and attitude survey regarding pain tool developed by Betty Ferrell (2014), this study also examines how demographic factors can impact their performance in care units. The results confirm that the level of education is the strongest factor that affects knowledge scores (PhD holders: 13.53 ± 4.74, and Master's degree holders: 13.02 ± 4.72). Our gender-based analysis indicates that male participants scored significantly higher (11.74 ± 4.33) compared to female participants (10.71 ± 4.02). In terms of age groups, our findings revealed that participants aged 20-29 demonstrated the highest scores (11.70 ± 4.29), while those aged 30-39 showed the lowest (10.38 ± 3.99). Full-time experienced nurses and night shift nurses exhibited higher scores of pain management knowledge (nurses with 16 or more years of experience showed higher scores: 16.92 ± 4.46). Analysing performance also revealed that nurses in general struggled to manage pain. In conclusion, enhancing pain management techniques in nursing practice needs a multidimensional approach that encompasses training and education, technical support, and professional growth. Bridging the gaps between theory and practice will enhance both patient care and nurses' level of confidence in carrying out one of the most significant aspects of healthcare.

Keywords: Pain management, Nursing, Attitudes, Education, Knowledge

Exploring the Interplay Between Sulpiride and Physical Activity: Health Sciences Perspectives

Hassina Fisli[1], Mohamed Lyamine Chelaghmia[2]

[1]Laboratory of Applied Chemistry, Material Sciences Department, 8 May 1945 Guelma University, Guelma, Algeria
[2]Materials Analysis and Engineering Laboratory, Process Engineering Department, 8 May 1945 Guelma University, Guelma, Algeria
Corresponding author: Hassina Fisli (e-mail: fislihassina24@gmail.com)

Abstract

The relationship between pharmacological treatments and physical activity has emerged as a central issue in health sciences, given its significant implications for patients' overall well-being. Sulpiride, an antipsychotic belonging to the substituted benzamides family, is characterized by dopaminergic antagonist and antidepressant properties. It is widely prescribed for the treatment of psychiatric disorders such as schizophrenia, dysthymia, and certain psychosomatic conditions. However, its pharmacological profile can markedly influence patients' physical and psychological health, particularly by affecting their ability to engage in regular exercise. From a clinical standpoint, sulpiride may cause side effects such as sedation, weight gain, or motor disturbances, which can restrict physical performance and reduce adherence to physical activity. These consequences highlight the need for careful monitoring and individualized treatment plans. Conversely, when appropriately adapted, physical activity can serve as an effective therapeutic adjunct: it enhances mood, supports metabolic balance, prevents cardiovascular complications, and improves overall quality of life. Particular attention should be devoted to vulnerable populations, especially individuals suffering from psychiatric disorders, in order to ensure that exercise practices remain both safe and beneficial. Future research should focus on interdisciplinary strategies that integrate pharmacology, psychology, and sport sciences to optimize clinical and psychosocial outcomes. Examining the reciprocal interaction between sulpiride and physical activity thus opens new perspectives for more patient-centered care and promotes global well-being.

Keywords: Sulpiride, Physical activity, Psychiatric disorders, Pharmacological treatment, Health sciences

2nd International Conference on Multidisciplinary Sciences and Technological Developments (ICMUSTED 2025)

December 12-15, 2025

Personalized Nutrition and Food Design

Ali Khalfa[1,2], Azzeddine Senouci[1], Djahira Hamed[1], Mounir Chihab[1], Sofiane Bouazza[3], Bensalah Fatima[1], Farid Bennabi[4]

[1]Department of Agri-Food, Faculty of Science and Technology, University of Ain Temouchent, Ain Temouchent, Algeria
[2]Laboratory of Applied Hydrology and Environment, Ain Temouchent, Algeria
[3]Department of Biology, Faculty of Natural and Life Sciences, University of Djillali Liabes, Sidi Bel Abbes, Algeria
[4]Department of Biology, Faculty of Science and Technology, University of Ain Temouchent, Ain Temouchent, Algeria
Corresponding author: Ali Khalfa (e-mail: ali.khalfa@univ-temouchent.edu.dz)

Abstract

Personalized nutrition and food design are emerging as innovative approaches to improve individual health outcomes. This study aims to evaluate the application of personalized nutrition in the development of tailored food products adapted to specific metabolic and lifestyle profiles. A cohort of 120 adult participants was recruited and assessed through dietary surveys, genetic markers, and metabolic profiling. The data were analyzed using IBM SPSS version 28 and expressed as mean and standard deviation. The mean difference was presented at a 95% confidence interval, and machine learning algorithms were employed to generate individualized dietary recommendations. Based on these recommendations, a set of personalized food prototypes, including snacks and functional beverages, was developed and tested. The prototypes were evaluated for nutritional quality, palatability, and consumer acceptance through sensory analysis and structured questionnaires. Additionally, changes in health indicators such as glycemic response, lipid profile, body mass index, and digestive comfort were monitored over a 6-week intervention period. Preliminary findings suggest that participants who consumed personalized food products showed improved glycemic control, reduced cholesterol levels, and reported higher levels of satiety and overall satisfaction compared to those following generalized dietary advice. This study also revealed important challenges, such as the need to balance nutritional optimization with affordability and convenience, which are key factors influencing consumer adoption. Furthermore, the integration of artificial intelligence demonstrated strong potential for translating complex biological data into practical dietary solutions, while also highlighting the importance of user-friendly tools to guide decision-making. Overall, the results underline the promise of personalized nutrition as a strategy for chronic disease prevention and health promotion. By combining advanced data analysis with innovative food design, this work demonstrates how tailored dietary interventions can offer both scientific and practical value, paving the way for more sustainable and individualized approaches to nutrition and wellness.

Keywords: Personalized nutrition, Food design, Dietary, Recommendations, Consumer acceptance

2nd International Conference on Multidisciplinary Sciences and Technological Developments (ICMUSTED 2025)

December 12-15, 2025

Antibacterial Activity of Lactic Acid Bacteria Strains on Uropathogens

Djamila Amamra[1], Fadela Chougrani[1], Mansouria Belhocine[1], Abdelkader El-Amine Dahou[1]

[1]Laboratory of Animal Production Sciences and Technologies, Faculty of Natural and Life Sciences, University of Mostaganem, Algeria
Corresponding author: Djamila Amamra (e-mail: djamila.amamra.etu@univ-mosta.dz)

Abstract

Lactic acid bacteria have been used for centuries due to their beneficial effects as antibacterial agents in human health, especially to combat urinary tract infections. To this end, we worked on various isolates of dairy origin which underwent preliminary identification. They were then tested for their antagonistic effect against hospital-acquired *Staphylococcus aureus* and *Pseudomonas aeruginosa* using well diffusion method. Ten isolates were selected (6 bacilli and 4 cocci) based on their antibacterial power. These lactic strains showed strong inhibitory activity against both pathogenic strains. The inhibition appeared as a clear zone around the inhibitory strain with varying diameters (between 10 and 20 mm), due to the production of inhibitory substances excreted outside the cell. The various treatments performed using the well diffusion method allowed us to conclude that the identified strains are inhibitory due to the production of organic acids and bacteriocins.

Keywords: Lactic acid bacteria, Dairy origin, Urinary tract infection, Antibacterial activity

2nd International Conference on Multidisciplinary Sciences and Technological Developments (ICMUSTED 2025)

December 12-15, 2025

Synthesis, Structural Elucidation, and Molecular Modeling Studies of 1,2,4-Triazolo-1,5-Benzodiazepine Diastereoisomers as Promising Anti-Ebola Candidates

Marouane Ait Lahcen[1], Nouhaila Ait Lahcen[1], Saad Zekri[1], Samir Hmaimou[1], Mohamed Adardour[1], Ismail Hdoufane[1], Driss Cherqaoui[1,2], Abdesselam Baouid[1]

[1]Molecular Chemistry Laboratory, Department of Chemistry, Semlalia Faculty of Sciences, Cadi Ayyad University, Marrakech, Morocco
[2]Sustainable Materials Research Center (SUSMAT-RC), University of Mohammed VI Polytechnic, 43150 Benguerir, Morocco
Corresponding author: Marouane Ait Lahcen (e-mail: mar.aitlahcen@gmail.com)

Abstract

In this work, we report the synthesis of 1,2,4-triazolo-1,5-benzodiazepine diastereoisomers and their comprehensive evaluation through molecular docking studies, which revealed promising inhibitory potential against the Ebola virus. The synthesized compounds were fully characterized using ^{1}H and ^{13}C NMR spectroscopy, along with high-resolution mass spectrometry (HRMS). Notably, one compound was successfully crystallized, and its molecular structure was unambiguously confirmed by single-crystal X-ray diffraction, providing definitive stereochemical insights. Furthermore, molecular docking and molecular dynamics simulations demonstrated strong binding affinities of these diastereoisomers toward the target viral protein, highlighting their potential as anti-Ebola agents. Overall, these results indicate that the synthesized molecules could serve as valuable leads for the development of new therapeutic candidates against the Ebola virus.

Keywords: 1,2,4-triazolo-1,5-Benzodiazepine, X-ray, Molecular docking, Molecular dynamics, Ebola virus

2nd International Conference on Multidisciplinary Sciences and Technological Developments (ICMUSTED 2025)

December 12-15, 2025

Detection of Multi-Drug-Resistant Extended Spectrum β-Lactamase Producing *Enterobacteriaceae* in Patients with Urinary Tract Infection

Anfal Kara[1], Naouel Boussoualim[1], Feryal Belfihadj[1], Meriem Elkolli[1]

[1]Laboratory of Applied Biochemistry, University of Setif, Setif, Algeria
Corresponding author: Anfal Kara (karaanfel98@gmail.com)

Abstract

It is estimated that there are about 150 million urinary tract infections (UTIs) per annum worldwide. The most common etiological agent in UTIs is *Enterobacteriaceae*; data shows that there is an increasing resistance among UTI pathogens to conventional drugs, *Enterobacteriaceae* have the ability to hydrolyze oxyimino-cephalosporins and monobactams. The prevalence of this group limited the use of β-lactam antibiotics as treatment. This study aimed to determine the prevalence of the extended spectrum of β-lactamases (ESBL) and their resistance profile in urinary tract infection by a reference method of the Kirby Bauer diffusion in Mueller Hinton agar. 100 urine samples were processed for culture and antimicrobial sensitivity testing; identification by using microbiological, biochemical tests and analytical profile index (API) 20E. ESBL were screened by a phenotypic method. ESBL production was detected in 25% of samples, 72% was *Escherichia coli*, 20% was *Klebsiella*, and 8% was *Proteus*; The ESBL-producing strains were significantly resistant to imipenem (100%), ticarcillin and piperacillin (88%), nitrofurantoin (84%); the combination ticarcillin + clavulanic acid and ceftazidime (80%) show also a high rate of acquired resistance. The study found high resistance to broad-spectrum antibiotics like cefotaxime (64%), cephalexin (60%), cotrimoxazole (56%), cefixime (52%), aztreonam (48%), ofloxacin (48%) which are commonly used to treat UTIs. Moderate resistance was observed against several antibiotics, including ciprofloxacin (40%), nalidixic acid, and the combination ticarcillin + tazobactam (36%), cefepime (36%), cefoxitin (28%), chloramphenicol (24%). While resistance to many antibiotics was high, there was relatively lower resistance to certain antibiotics like gentamycin (16%), and tobramycin (4%). This study underscores the growing issue of antibiotic resistance in UTIs, with ESBL-producing bacteria becoming increasingly common and difficult to treat with conventional antibiotics. It emphasizes the importance of responsible antibiotic use, monitoring resistance patterns, and exploring alternative treatment options to address this emerging public health concern.

Keywords: Multi-drug-resistant, Urinary tract infection, *Enterobacteriaceae*, ESBL-producing strains, Antibiotic resistance

2nd International Conference on Multidisciplinary Sciences and Technological Developments (ICMUSTED 2025)

December 12-15, 2025

Examining the Satisfaction Levels of Patients with Nursing Care in the Internal Medicine Ward

Cigdem Koc[1], Halise Coskun[2]

[1]Famagusta State Hospital, Famagusta, Turkish Republic of Northern Cyprus
[2]Faculty of Health Sciences, Eastern Mediterranean University, Famagusta, Turkish Republic of Northern Cyprus
Corresponding author: Halise Coskun (e-mail: halise.coskun@emu.edu.tr)

Abstract

Patient satisfaction with the concept of quality, which is becoming increasingly important in healthcare services, has significant importance in evaluating health services. This research was conducted as a descriptive and cross-sectional study to determine the satisfaction levels of patients with nursing care.The study was conducted with 85 patients who were hospitalized at least 2 nights in the internal medicine wards of Famagusta State Hospital and voluntarily accepted to participate in the study.While collecting research data, the patient descriptive characteristics form and the Newcastle Nursing Care Satisfaction Scale were used. Patients participating in the study; 47.06% of them were primary school students, of whom 35.29% were 50-65 years old, 52.94% were male graduates, 71.76% of the males were married, 32.94% of them are not working in a job. It was determined that the patients included in the study received the highest score on the 9th item, "Nurses' helpfulness," in the Newcastle Nursing Care Satisfaction Scale, and obtained an average of 4.60 points. The lowest score was given to the 15th item of the scale, 'Nurses listen to your worries and concerns' with an average of 4.02 points. Considering these findings, suggestions were made to the nurses working in the internal medicine service that it would lead to more effective care by providing more explanations to patients and approaching them with greater care and attention to their concerns and worries.

Keywords: Nursing, Nursing care, Patient satisfaction

2nd International Conference on Multidisciplinary Sciences and Technological Developments (ICMUSTED 2025)

December 12-15, 2025

Impact of Child-Centered Empowerment on Lifestyle Behaviors in Children with Leukemia

Pouran Varvani Farahani[1], Candan Ozturk[2], Aziz Eghbali[3], Atefeh Rezapoor[3]

[1]Faculty of Health Sciences, Cyprus International University, Nicosia, Turkish Republic of Northern Cyprus
[2]Faculty of Nursing, Near East University, Nicosia, Turkish Republic of Northern Cyprus
[3]Clinical Research Development Center of Aliasghar Hospital, Iran University of medical sciences, Tehran, Iran
Corresponding author: Pouran Varvani Farahani (e-mail: pfarahani@ciu.edu.tr)

Abstract

Leukemia and its treatment can significantly disrupt the lifestyle and well-being of children. This study evaluated the effect of a child-centered empowerment model on the lifestyle of children with leukemia. This double-blind randomized clinical trial was conducted on 46 school-aged children (7–13 years) diagnosed with leukemia and admitted to an oncology clinic. Participants were randomly assigned to intervention and control groups (n = 23). The intervention group received the family-centered empowerment model, consisting of four dimensions: perceived threat (severity and sensitivity), self-efficacy, educational participation, and evaluation, while the control group received routine care. Data were collected using demographic, lifestyle, and empowerment questionnaires. The lifestyle questionnaire assessed five domains: nutrition, sleep, physical activity, physical health, and stress. Data were analyzed using SPSS version 25 with paired and independent t-tests and descriptive statistics. A p-value of < 0.05 was considered statistically significant. Before the intervention, there was no significant difference in lifestyle scores between the experimental group (61.7 ± 4.7) and the control group (59.8 ± 4.2) ($p = 0.159$). After the intervention, a significant difference was observed, with the experimental group scoring higher (78.8 ± 8.1) compared with the control group (59.7 ± 4.2) ($p \leq 0.001$). Implementing child-centered empowerment is feasible and effective for improving the lifestyle of children with leukemia. Child-centered empowerment can be integrated into pediatric oncology care as a supportive, non-invasive strategy to enhance coping, promote healthier daily habits, and improve overall well-being in children with leukemia.

Keywords: Patient empowerment, Family, Life style, Leukemia, Children

2nd International Conference on Multidisciplinary Sciences and Technological Developments (ICMUSTED 2025)

December 12-15, 2025

Identification of Potent Sulfonamide Derivatives Targeting MMP2 through Pharmacophore Ligand-Based Modeling

Saad Zekri[1], Nouhaila Ait Lahcen[1], Adnane Ait Lahcen[1], Wissal Liman[2], Ismail Hdoufane[1], Driss Cherqaoui[1,3]

[1]Molecular Chemistry Laboratory, Department of Chemistry, Faculty of Sciences Semlalia, Cadi Ayyad University, 40000 Marrakech, Morocco
[2]Bioinformatics Laboratory, College of Computing, University Mohammed VI Polytechnic, Morocco
[3]Sustainable Materials Research Center (SUSMAT-RC), University of Mohammed VI Polytechnic, 43150 Benguerir, Morocco
Corresponding author: Saad Zekri (e-mail: s.zekri.ced@uca.ac.ma)

Abstract

Matrix metalloproteinase 2 (MMP2) is a zinc dependent endopeptidase involved in extracellular matrix remodeling and plays a pivotal role in tumor invasion and metastasis. Given its association with cancer progression, MMP2 has emerged as a promising therapeutic target. however, the lack of selective inhibitors has hindered clinical success. In this study, we employed an integrated computational strategy to identify potential MMP2 inhibitors. A ligand-based pharmacophore model was developed from a dataset of sulfonamide derivatives with reported inhibitory activity. The model was rigorously validated using a decoy screening approach and statistical metrics, including receiver operating characteristic-area under the curve (ROC-AUC), enrichment factor, and Goodness of Hit score, demonstrating strong predictive power. The validated model was subsequently applied to screen a Food and Drug Administration (FDA) approved drug library to explore repurposing opportunities. Selected hits were further evaluated through molecular docking, which revealed favorable binding affinities and key interactions within the active site of MMP2. To confirm binding stability under physiological conditions, molecular dynamics simulations were performed on both apo and ligand bound systems, followed by trajectory analysis. The combined results highlight several FDA approved candidates with potential inhibitory activity against MMP-2. This work provides valuable insights into the design of selective MMP2 inhibitors and establishes a foundation for further optimization and experimental validation.

Keywords: MMP-2 inhibitors, Pharmacophore modeling, Drug repurposing, Molecular docking, Molecular dynamics simulations

2nd International Conference on Multidisciplinary Sciences and Technological Developments (ICMUSTED 2025)

December 12-15, 2025

Valorization of Moroccan Medicinal Biodiversity as a Source of Novel Antileishmanial Agents

Mohammed-Yassine Takzima[1], Mohamed Echchakery[1,2], Mohamed Hafidi[1], Loubna El Fels[1]

[1]Laboratory of Water Sciences, Microbial Biotechnologies, and Natural Resources Sustainability, Unit of Microbial Biotechnologies, Agrosciences, and Environment, Faculty of Sciences-Semlalia, University Cadi Ayyad, 40000 Marrakech, Morocco
[2]Laboratory of Health Sciences and Technologies, Epidemiology and Biomedical Unit, Hassan Premier University, Higher Institute of Health Sciences, Settat, Morocco
Corresponding author: Mohammed-Yassine Takzima (e-mail: mohammed.takzima@gmail.com)

Abstract

Leishmaniasis is a parasitic disease that remains a persistent health challenge in Morocco, especially in its cutaneous form. In many rural regions, limited access to conventional treatments has encouraged the continued reliance on traditional medicine, where local biodiversity provides essential therapeutic resources. Communities widely use Moroccan medicinal and aromatic plants to manage symptoms of leishmaniasis through decoctions, infusions, poultices, and topical applications. This review compiles ethnopharmacological knowledge and field reports on the use of Moroccan plants in traditional practices against leishmaniasis. These practices demonstrate the strong link between cultural heritage and the sustainable use of natural resources. The case of leishmaniasis illustrates how biodiversity-based practices continue to contribute to community health resilience and provide a valuable foundation for future research and innovation.

Keywords: Biodiversity, Leishmaniasis, Ethnopharmacology, Traditional medicine, Morocco

2nd International Conference on Multidisciplinary Sciences and Technological Developments (ICMUSTED 2025)

December 12-15, 2025

Epidemiological Profile and Phenotypic Characterization of Aminoglycoside-Resistant Clinical Strains in the Setif Region

Iman Krache[1], Anfal Kara[2], Naouel Boussoualim[1], Zineb Daoudi[2], Noussaiba Douadi[2], Fatma Gridi[2]

[1]Laboratory of Applied Biochemistry, Department of Biochemistry, Ferhat Abbas University of Setif 1, Setif, Algeria
[2]Laboratory of Applied Microbiology, Department of Microbiology, Ferhat Abbas University of Setif 1, Setif, Algeria
Corresponding author: Imane Krache (e-mail: doussakr@yahoo.fr)

Abstract

This study examined 135 aminoglycoside-resistant bacterial strains collected in Setif between 2021 and 2023. Antibiotic susceptibility testing was performed according to the Clinical and Laboratory Standard Institute (CLSI) standards, and phenotypic assays evaluated virulence through biofilm and enzyme production. Statistical analysis was carried out using Statistical Package for the Social Sciences (SPSS). The findings revealed a predominance of resistance among women (55.6%) and adults (68.1%), with urinary tract infections being the most frequent (76.3%). *Escherichia coli* was the leading isolate (40.7%). High resistance levels were recorded for amoxicillin (83%), amoxicillin–clavulanic acid (80%), cephalexin (74.8%), cefixime (71.1%), trimethoprim–sulfamethoxazole (74.8%), and gentamicin (72.6%). Chloramphenicol (53.3%), imipenem (47.4%), and amikacin (47.4%) showed moderate susceptibility. Multidrug resistance involving seven antibiotics was observed in 25.6% of strains, with notable cross-resistance between gentamicin and β-lactams. Most isolates exhibited low biofilm production (62.96%), while enzymatic activity varied among strains. These results emphasize the alarming spread of aminoglycoside resistance and the need for strengthened antibiotic stewardship programs in the Setif region.

Keywords: Aminoglycoside resistance, Clinical isolates, Epidemiology, Multidrug resistance, Virulence factors

2nd International Conference on Multidisciplinary Sciences and Technological Developments (ICMUSTED 2025)

December 12-15, 2025

Anti-Bacterial and Anti-Inflammatory Activities of the Mucus of the Snail *Helix Aspersa* Muller

Imene Yahla[1]

[1]Laboratory of Beneficial Miciroorganisms, Functional Food and Health, Abdelhamid Ibn Badis University of Mostaganem, Mostaganem, Algeria
Corresponding author: Imene Yahla (e-mail: imene.yahla@univ-mosta.dz)

Abstract

The mucus of the snail *Helix aspersa* muller in used in many pharmacologic products. The objective of the present study is to explore the antimicrobial, antioxidant, and anti-inflammatory properties of the mucus of the snail *Helix aspersa* muller from the region of Mostaganem, Algeria. The antimicrobial activity was tested against 07 pathogenic microorganisms: *Bacillus cereus*, *Bacillus subtilis*, *Candida albicans*, *Escherichia coli*, *Pseudomonas aeruginosa*, *Staphylococcus aureus*, and *Salmonella typhi*. Besides, the anti- inflammatory activity was evaluated by the inhibition of protein denaturation. The obtained results show an antibacterial activity demonstrated by the following diameters in descending order, with *Candida albicans* (09 ± 00.00 millimeters mm), *Bacillus subtilis*, *Staphylococcus aureus*, *Salmonella typhi* (08 ± 00.00 mm).No antimicrobial activity was noted against strains *Bacillus cereus*, *Pseudomonas aeruginosa*, and *Escherichia coli*. In addition, anti-inflammatory activity results show that *Helix aspersa* muller snail mucus is able to control autoantigen production through inhibition of protein denaturation. The denaturation inhibitory activity of bovine serum albumin (BSA) can be attributed to the presence of different bioactive compounds found in mucus. These results suggest the possibility of using *Helix aspersa* muller snail mucus as a treatment for certain infections of bacterial origin or even certain fungal infections and even anti-inflammatory treatment.

Keywords: Mucus, *Helix aspersa* muller, Antibacterial activity, Anti-inflammatory activity

2nd International Conference on Multidisciplinary Sciences and Technological Developments (ICMUSTED 2025)

December 12-15, 2025

Computer-Aided Drug Discovery of Novel Ebola Virus Glycoprotein Inhibitors: Integrating QSAR, Fragment-Based Design, and Molecular Dynamics

Nouhaila Ait Lahcen[1], Wissal Liman[1,2], Saad Zekri[1], Mehdi Oubahmane[1], Ismail Hdoufane[1], Mohammed Mater Alanazi[4], Mohamed Maatallah[1], Driss Cherqaoui[1,3]

[1]Department of Chemistry, Cadi Ayyad University, Marrakech, Morocco
[2]College of Computing, University Mohammed VI Polytechnic, Benguerir, Morocco
[3]Sustainable Materials Research Center, University of Mohammed VI Polytechnic, Benguerir, Morocco
[4]Department of Pharmaceutical Chemistry, College of Pharmacy, King Saud University, 11671 Riyadh, Saudi Arabia
Corresponding author: Nouhaila Ait Lahcen (e-mail: nouhaila.aitlahcen@ced.uca.ma)

Abstract

Ebola virus disease remains a critical global health threat, with no approved small-molecule therapeutics available to date. The Ebola virus glycoprotein (EBOV-GP), essential for mediating host cell entry, represents a highly attractive target for antiviral drug development. In this study, we implemented an integrated computer-aided drug discovery workflow to identify novel EBOV-GP inhibitors. Our approach began with the construction of a robust and predictive quantitative structure-activity relationship model (QSAR), trained on a curated dataset of known active compounds against EBOV-GP. The validated model was then employed to screen over 15,000 virtual molecules generated via fragment-based design strategies, using three structurally diverse lead scaffolds. High-performing candidates were prioritized based on predicted activity and molecular docking scores. Subsequent absorption, distribution, metabolism, excretion, and toxicity (ADMET) filtering confirmed their favorable drug-likeness and pharmacokinetic profiles. The top-ranked compounds were subjected to extensive 150 ns molecular dynamics (MD) simulations, revealing stable interactions within the EBOV-GP binding pocket. Molecular mechanics/generalized born surface area (MM/GBSA) binding free energy calculations further supported their strong affinity for the target site. This study highlights the power of combining QSAR modeling, fragment-based molecular design, virtual screening, ADMET profiling, and MD simulations to accelerate the discovery of potent and safe anti-Ebola agents. The most promising hits identified herein represent compelling candidates for future in vitro and in vivo validation.

Keywords: QSAR models, EBOV-GP inhibitors, Molecular docking, Molecular dynamics, MM/GBSA binding free

2nd International Conference on Multidisciplinary Sciences and Technological Developments (ICMUSTED 2025)

December 12-15, 2025

Biopolymeric Films of HEC/PAADDA Crosslinked with Glutaraldehyde as Controlled Release Systems of Tannic Acid for Antitumoral and Wound Healing Applications

Isabela Viudes Rossatto Ferrarezi[1], Ingrid Cristine de Sousa Everton[1], Júlia Monteiro Fernandes[2], Luca Kiichi Suzuki Trancolin[1], Lucas Gomes Nascimento[3], Marcos Elias da Silva Almeida[1], Maria Carolina Rodrigues Garcia[4], Mariana Aparecida Vieira[5], Weslley Aparecido Vicente Luiz[1], William Capellari Fumegali[1]

[1]Experimental Pathology, State University of Londrina, Londrina, Brazil
[2]Nursing, Planalto University Center of the Federal District, Marília, Brazil
[3]Medicine, Lusíada University Center, Santos, Brazil
[4]Nursing and Medicine, University of Marilia, Marília, Brazil
[5]Nursing, Higher Education Faculty of the Interior of São Paulo, Marília, Brazil
Corresponding author: Isabela Viudes Rossatto Ferrarezi (e-mail: isabelavrossatto@gmail.com)

Abstract

The combination of biocompatible polymers crosslinked with glutaraldehyde (GLU)enables controlled tannic acid (TA) release, enhancing its stability and therapeutic potential in wound healing and cancer treatment. These systems offer improved mechanical strength, antimicrobial activity, and sustained drug delivery, though further studies are needed to validate their physicochemical and biological performance for clinical application. The objective of this study is to theoretically evaluate the potential of biopolymeric films composed of 2-hydroxyethylcellulose (HEC)/ poly(acrylamide-co-diallyldimethylammonium chloride) (PAADDA) crosslinked with GLU as controlled release systems for TA, assessing their possible applications in antitumor and wound-healing contexts to support the design of future experimental investigations. The methodology described in the literature highlights the development of polymer-based delivery systems designed to overcome the limitations of TA, such as rapid degradation and low bioavailability. By encapsulating TA within polymeric matrices, hydrogels, or films, researchers achieved controlled and sustained release, protecting the compound from oxidation and enhancing its therapeutic performance. These methods demonstrated effectiveness in wound healing by promoting tissue regeneration and reducing oxidative stress, and in cancer treatment by inhibiting angiogenesis and inducing apoptosis in tumor cells. The results from the literature indicate that TA, a plant-derived polyphenol with strong antioxidant, anti-inflammatory, antimicrobial, and antitumor properties, faces limitations due to rapid degradation and low bioavailability. To address these challenges, polymer-based delivery systems such as hydrogels and films have been developed to enable controlled release and maintain its biological activity. These systems have shown encouraging outcomes in wound healing by promoting tissue regeneration and in cancer therapy through the inhibition of angiogenesis and the induction of apoptosis.

Keywords: Drug liberation, Drug screening assays, Antitumor, Glutaral, Wound healing

1. INTRODUCTION

The pursuit of innovative materials is a constant priority in medical science and technology, and polymeric membranes stand out for their versatility and impact, including applications in tissue engineering, prosthetics, medical devices, and diagnostics. They are highly adaptable, enabling significant advances in drug delivery systems, diagnostic devices, and biosensors, while offering biocompatibility and safety for use in human tissues [1].

The selection of 2-hydroxyethylcellulose (HEC) and poly(acrylamide-co-diallyldimethylammonium chloride) (PAADDA) membranes was motivated by the need for an efficient and sustainable solution for developing biomedical materials with adjustable properties. HEC/PAADDA films crosslinked with glutaraldehyde (GLU) are materials of great interest in the pharmaceutical and biotechnological fields, formed by chemical bonding between HEC and PAADDA polymer chains using GLU, resulting in a stable and functional matrix [2].

HEC is a cellulose derivative widely used in pharmaceutical, cosmetic, and industrial applications due to its hydrophilicity and biocompatibility, while PAADDA is a cationic copolymer with antimicrobial properties, often employed in medical and cosmetic formulations. The combination of HEC/PAADDA crosslinked with GLU provides enhanced mechanical and chemical properties, making it ideal for use in controlled drug delivery systems [3, 4].

The crosslinking of HEC/PAADDA polymers with GLU results in a three-dimensional structure capable of encapsulating bioactive compounds and releasing them in a controlled manner over time, a desirable behavior in therapeutic systems since it maintains constant concentrations of the active agent, reduces adverse effects, and improves treatment adherence [5].

Tannic acid (TA) is a natural polyphenol with well-recognized antioxidant, antimicrobial, anti-inflammatory, and antitumor properties, making it a bioactive molecule of great pharmaceutical value [1–6]. Recent studies demonstrate its potential to inhibit tumor cell proliferation and modulate signaling pathways associated with cell survival, such as phosphatidylinositol 3-kinase/protein kinase B (PI3K/Akt) and mitogen-activated protein kinase (MAPK), granting it relevance in antitumor and wound-healing therapies [7].

The use of renewable-source polymers, such as HEC, contributes to environmental sustainability by replacing non-biodegradable synthetic materials. These biopolymeric films provide eco-friendly and low-impact alternatives aligned with the demand for green and sustainable technologies [1].

Skin cancer, including melanoma and squamous cell carcinoma, represents a growing public health concern due to its high incidence and metastatic potential. Conventional treatments often involve surgery, radiotherapy, and topical chemotherapy; however, these approaches may result in systemic side effects and difficulty maintaining local therapeutic concentrations. Controlled release systems offer a promising solution by enabling localized and sustained delivery of therapeutic agents, minimizing side effects, and improving treatment efficacy [8].

The crosslinking of HEC/PAADDA polymers with GLU forms a three-dimensional matrix capable of encapsulating and releasing therapeutic agents in a controlled manner, modulating release kinetics, improving local tissue adhesion, protecting the active compound, and reducing systemic adverse effects, making it ideal for controlled drug delivery applications [9].

The controlled release system based on HEC/PAADDA crosslinked with GLU and incorporated with TA has potential for integration into smart dressings and tissue regeneration scaffolds. It can also be combined with biosensors or stimulus-responsive release technologies, such as pH, temperature, or tumor microenvironment responsiveness, offering an innovative approach to the treatment of oncological lesions [10].

Despite the advances achieved, few studies investigate the specific combination of HEC/PAADDA crosslinked with GLU and TA for antitumor and wound-healing applications. It is necessary to evaluate the physicochemical properties, release kinetics, and biological compatibility of this system in preclinical models to establish its efficacy and safety for clinical use [11].

Therefore, the present study aims to evaluate, in a speculative manner, the potential of biopolymeric films composed of HEC/PAADDA crosslinked with GLU as controlled release systems for TA, examining the theoretical feasibility of their application in antitumor and wound-healing contexts, with the purpose of supporting the design of future experimental investigations.

2. MATERIAL AND METHOD

This study is characterized as an exploratory-descriptive research with a qualitative and quantitative approach, as it allows for the observation, description, and analysis of a phenomenon, as well as the exploration of its dimensions, manifestations, and interrelated components [12]. The main reagents employed were PAADDA at a concentration of 10% weight/volume, HEC, GLU, and TA. All compounds were commercially obtained from Merck® without any prior purification or chemical modification, thus preserving the original properties provided by the manufacturer. Additional materials included distilled water produced by a simple distillation system, magnetic stirring hot plates, an oven, and standard laboratory glassware. This research follows an exploratory-descriptive design with a qualitative-quantitative approach. The methodological framework was structured based on the study by Marques [13], which is an experimental investigation employing quantitative methods of data analysis and integration of scientific literature to examine the potential of GLU-crosslinked HEC/PAADDA films. The quantitative approach was applied to describe and analyze experimental data obtained from previous studies,

while the qualitative component was used due to the exploratory nature of the research and the integration of findings from the scientific literature. This qualitative aspect enabled a comprehensive understanding of the relationships among structure, properties, and biomedical applicability of the materials, contributing to a more holistic and interpretative analysis. The dosages and calculations adopted were based on well-established academic protocols that employ equivalent methodologies for the preparation and characterization of hybrid polymeric films. Therefore, the study aims to provide a robust theoretical foundation to guide the design of future experimental investigations.

The films composed of HEC and PAADDA were prepared by dissolving precise mass quantities (g) of each polymer in distilled water. The HEC/PAADDA ratios were set at 70/30, 50/50, and 30/70 (%), using GLU as a crosslinking agent at a concentration of 0.2 $mol \cdot L^{-1}$. The mixtures were magnetically stirred at room temperature for 1 hour and then cast into suitable containers for drying in an oven at 40 °C (±1 °C) for 24 hours until complete solvent evaporation. This procedure, known as the solvent casting or evaporation method, enabled the formation of homogeneous films, which were subsequently subjected to physicochemical and structural characterization. The resulting films were characterized through various analyses to evaluate their properties and behavior for potential biomedical applications. Thickness was measured in triplicate using a precision micrometer (0.001 mm). Solubility and swelling degree were determined from mass variation after immersion in distilled water. Optical properties and color parameters (L*, a*, b*) were analyzed by ultraviolet-visible (UV-Vis) spectrophotometry in the 200–800 nm range and by colorimetry. Structural characterization was performed using Fourier-transform infrared spectroscopy (FTIR) in the range of 4000–400 cm^{-1} for identification of functional groups, and X-ray diffraction (XRD) between 3° and 60° with Cu radiation to determine crystallinity. Thermal stability was assessed by thermogravimetric analysis (TGA) in the range of 25–600 °C under a nitrogen atmosphere with a heating rate of 10 $°C \cdot min^{-1}$. Electrical properties were determined by electrochemical impedance spectroscopy (EIS) within the frequency range of 1 Hz to 1 MHz, with an amplitude of 5 mV at 25 °C. The surface morphology of the films was examined by scanning electron microscopy (SEM), enabling the observation of their structure and homogeneity. Together, these analyses provided a detailed evaluation of the physicochemical, thermal, and morphological properties of the films, offering important insights into their potential performance and biomedical applicability.

The adsorption kinetics of TA onto the HEC/PAADDA films with ratios of 30/70, 50/50, and 70/30 (%) were theoretically evaluated based on experimental parameters reported in the literature. In similar studies, 0.1 g of the film was immersed in 25 mL of an aqueous TA solution (6.11×10^{-6} $mol \cdot L^{-1}$, pH 6) under agitation at 150 rpm and 25 °C. At specific time intervals, aliquots of the supernatant were analyzed by UV-Vis spectrophotometry (λ = 274 nm) to estimate the variation in TA concentration. The incorporation percentage (%I) was calculated according to Equation (1):

$$\%I = \frac{C_i - C_t}{C_i} \times 100 \quad (1)$$

Where C_i is the initial concentration of TA ($mol \cdot L^{-1}$), and C_t is the concentration at time t ($mol \cdot L^{-1}$). Following the systematization and analysis of the aforementioned steps, an exploratory approach will be conducted to theoretically evaluate the feasibility of the films as controlled-release systems for TA in both antitumor and wound-healing contexts, thereby supporting the design of future experimental studies.

3. RESULTS

The characterization of the films is an essential step to understand their physical, chemical, and structural properties. In the case of HEC/PAADDA films crosslinked with GLU, this analysis involves various instrumental techniques, such as FTIR, XRD, TGA, EIS, and SEM. These procedures allow the identification of molecular composition, evaluation of thermal stability, determination of crystallinity degree, and examination of the surface morphology of the materials. The knowledge obtained from these analyses is crucial to correlate the structural characteristics of the films with their performance as controlled release systems for TA in aqueous media. The graph shown below (Figure 1) details the solubility of the crosslinked films at HEC/PAADDA ratios of 30/70(%), 50/50(%), and 70/30(%), all measured at room temperature and pH = 6. The data indicate that the film with a 30/70(%) HEC/PAADDA ratio reached a solubility of 50%, the 50/50(%) film 27%, and the 70/30(%) film 30%. These results show that a higher proportion of PAADDA is associated with increased solubility of the films.

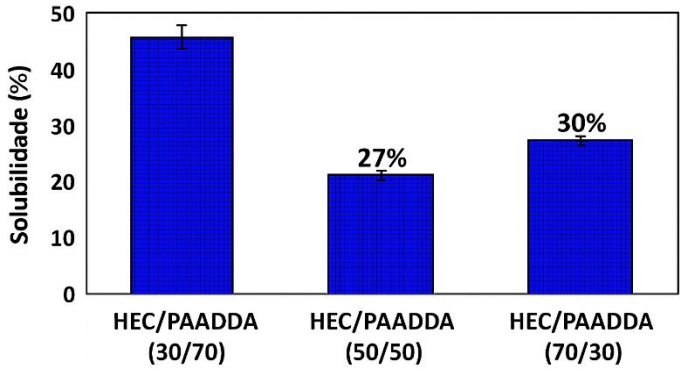

Figure 1. Film solubility

HEC/PAADDA films with ratios of 30/70(%), 50/50(%), and 70/30(%) were analyzed for their swelling degree, which represents the percentage increase relative to the initial mass of the film when exposed to an aqueous environment. The graph shown in Figure 2 demonstrates that the HEC/PAADDA 30/70(%) film reached a swelling degree of 500%, the 50/50(%) film reached 200%, and the 70/30(%) film reached 80%. These results reveal a significant difference in the swelling capacity according to the proportion of PAADDA in the film.

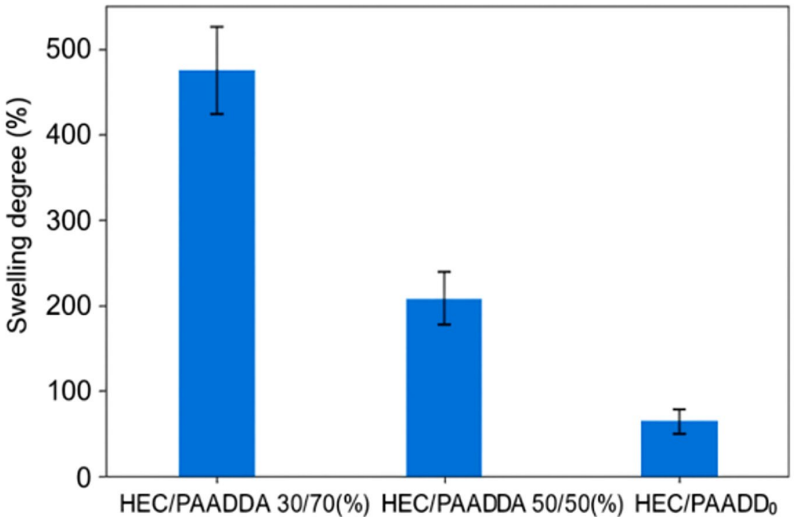

Figure 2. Degree of swelling

The HEC and PAADDA films were evaluated in different proportions (30/70%, 50/50%, and 70/30%) after the crosslinking process with GLU, aiming to understand how variations in composition influence their optical and physicochemical properties. Figure 3 presents the UV-Vis spectra of the produced films, showing that the pure PAADDA film exhibited the highest transmittance, around 90% at 600 nm (visible region), followed by the HEC film, with approximately 80% at the same wavelength. For the HEC/PAADDA blends, the transmittance at 600 nm followed the trend 70/30 > 50/50 > 30/70, with approximate values of 78%, 70%, and 55%, respectively. This reduction in transparency with the increasing PAADDA fraction indicates the formation of amorphous and heterogeneous regions that intensify light scattering. The lower transparency observed in the HEC/PAADDA 30/70 film may be associated with its higher solubility and swelling capacity. Solubility data showed that the HEC/PAADDA 30/70(%) film exhibited the highest value, reaching approximately 50%, followed by the 50/50(%) and 70/30(%) films, with 27% and 30%, respectively. Similarly, the swelling degree displayed a directly proportional behavior, reaching 500% for the 30/70(%) film, 200% for the 50/50(%), and 80% for the 70/30(%). These results demonstrate that a higher proportion of PAADDA promotes water absorption and structural expansion of the films, which in turn negatively affects their transparency. Thus, a direct correlation between the optical and physicochemical properties is observed: as the PAADDA content increases, solubility and swelling also increase, generating microirregularities that reduce optical transmittance. Furthermore, all HEC/PAADDA films showed lower transmittance values in the 250 nm range (UV region) compared to pure HEC, suggesting potential application as a barrier against ultraviolet radiation (Figure 3).

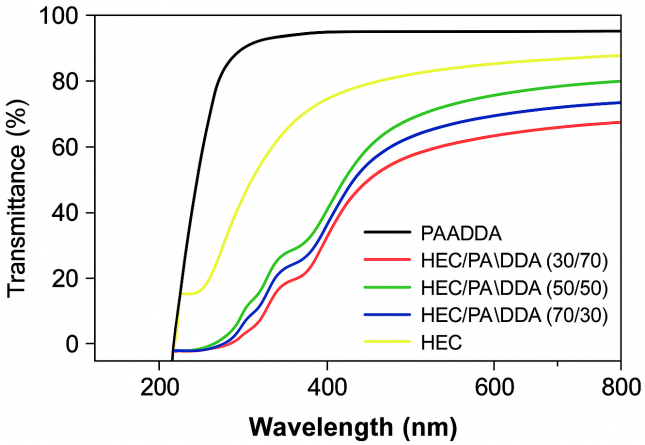

Figure 3. Optical and physicochemical properties of HEC/PAADDA films with different composition ratios

In Figure 4, the pure PAADDA film exhibited the highest luminosity (L = 89.10), indicating a lighter coloration with a slight tendency toward bluish and greenish tones (negative a and b values). The pure HEC film, on the other hand, also showed high luminosity (L = 88.70), but with slightly positive a and b values, revealing a subtle yellowish hue. In the HEC/PAADDA blends, a gradual darkening trend was observed with increasing HEC content, consistent with the reduction in transmittance previously discussed. For the HEC/PAADDA (30/70) film, the luminosity was L = 84.20, with a slightly yellow tone (b = 34.50). In the 50/50 blend, the color became more intense, with L = 78.60 and a perceptible increase in a and b values, indicating the appearance of warmer tones. The 70/30 blend showed the lowest luminosity (L = 73.40) and high a (12.50) and b (56.90) values, representing a pronounced yellowish-reddish coloration, consistent with the higher HEC content and the reduction in optical transparency described in the UV-Vis spectra. These results confirm that increasing the HEC fraction enhances warm tones and reduces luminosity, whereas pure PAADDA provides greater clarity and a bluish-greenish tendency. Such chromatic variations reflect the structural and optical differences previously observed in solubility, swelling, and transmittance analyses, demonstrating coherence between the physicochemical parameters and the visual properties of the films (Figure 4).

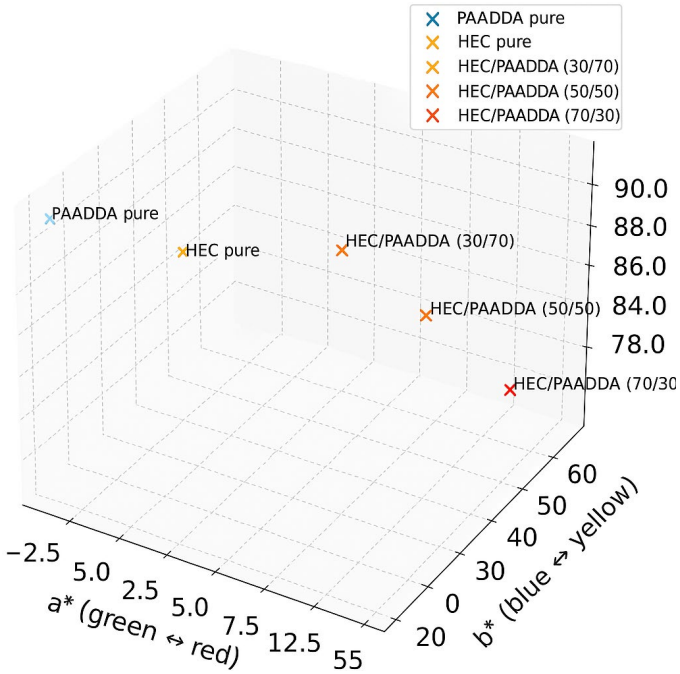

Figure 4. CIELAB colorimetric diagram of the HEC/PAADDA samples

The FTIR spectra were obtained for pure PAADDA films, pure HEC films, and their HEC/PAADDA blends in different proportions. The spectra of the pure materials reveal the main characteristic bands of each polymer. The spectrum of pure PAADDA exhibits a broad band in the region of 3400–3200 cm^{-1}, attributed to the stretching vibrations of N–H groups and the possible presence of hydrogen bonds. Bands located near 1650 cm^{-1} and 1600 cm^{-1} are associated with the stretching vibrations of the carbonyl group (C=O) and the deformation of the NH

group, respectively, which are typical of amide structures. On the other hand, the spectrum of pure HEC shows an intense broad band between 3600–3300 cm^{-1}, corresponding to the stretching vibrations of hydroxyl groups (O–H), which is characteristic of the cellulosic structure and indicative of strong hydrogen bonding interactions. The bands around 2900 cm^{-1} correspond to the stretching of methylene groups (CH_2), while the region between 1050–1100 cm^{-1} is attributed to the stretching of C–O–C groups, associated with the glycosidic structure of the cellulose main chain. Table 1 shows the FTIR spectra of HEC/PAADDA blends with proportions of 30/70, 50/50, and 70/30. It is observed that as the HEC fraction increases, the O–H band becomes broader, and the intensity of the N–H bands around 3400 cm^{-1} decreases, suggesting the formation of intermolecular hydrogen bonds between the hydroxyl groups of HEC and the amide groups of PAADDA. Moreover, a slight shift of the C=O band (1650 cm^{-1}) toward lower wavenumbers is observed, reinforcing the hypothesis of chemical interactions and the possible formation of cross-links between the polymer chains. These spectral variations confirm that the progressive incorporation of HEC modifies the chemical environment of the PAADDA chains, enhancing hydrophilic interactions and contributing to structural and morphological changes in the films. Therefore, the FTIR results are consistent with the previously discussed physicochemical and optical analyses, evidencing partial compatibility between the polymers and the influence of HEC content on the final structure of the films (Table 1).

Table 1. Main bands and interpretations of the FTIR spectra of HEC, PAADDA films, and their blends

Sample	Region/Wavenumber (cm^{-1})	Band Assignment	Interpretation/Remarks
Pure PAADDA	3400-3200	N-H stretching and hydrogen bonding	Broad band indicating the presence of amide groups and possible intermolecular interactions.
	1650	Carbonyl (C=O0 stretching	Typical of amide groups; the band shifts in blends, suggesting chemical interaction.
	1600	N–H group deformation	Associated with the amide structure of the PAADDA chain.
Pure HEC	3600-3300	O–H (hydroxyl) stretching	Broad and intense band characteristic of the cellulosic structure and strong hydrogen bonding.
	2900	C–H (CH_2 groups) stretching	Indicates the presence of methylene groups in the chain.
	1050-1100	C–O–C stretching	Related to the glycosidic structure of HEC.
HEC/PAADDA Blend (30/70, 50/50, 70/30)	~ 3400	O–H and N–H	Band broadening and reduction in N–H intensity with increasing HEC fraction, indicating intermolecular hydrogen bonding between HEC and PAADDA.
	~1650 (slight shift to lower wavenumbers)	C=O	Shift confirms chemical interaction and possible formation of cross-links between polymer chains.
	1050–1100	C–O–C	Remains present, but with variations in intensity depending on the HEC proportion
General Analysis	-	-	The incorporation of HEC alters the chemical environment of PAADDA, enhancing hydrophilic interactions and promoting partial compatibility between the polymers.

Table 2 presents the TGA results of the films, showing that all samples exhibit a similar thermal behavior throughout the heating process. The first mass loss, occurring between approximately 30 °C and 150 °C, is attributed to the evaporation of physically adsorbed water or residual moisture present in the films. The second stage of mass loss, observed between about 200 °C and 500 °C, corresponds to the thermal decomposition of the polymeric components, indicating the breakdown of the main polymer chains. This two-step degradation profile suggests that the films possess good thermal stability up to around 200 °C, after which polymer degradation becomes more pronounced.

Table 2. TGA of the films

Characteristic	Details	Temperature Range (°C)	Attribution
General behavior	All curves exhibit similar thermal behavior	N/A	N/A
First mass loss	Moderate mass loss	30–150	Evaporation of adsorbed free water
Second mass loss	Additional mass losses observed	≈ 200–500	Thermal decomposition of the polymers

N/A: Not applicable

3.1. EIS

The DC conductivity values obtained showed that the blend films are less conductive than the pure HEC and PAADDA polymers. The conductivity (σ) depends on the charge carrier density (n) and charge carrier mobility (μ). The value of n is associated with the dipoles present in the HEC and PAADDA polymers, while μ is directly related to the crystallinity of the polymer chains, which can either facilitate or hinder charge mobility. The EIS results are consistent with the XRD findings. The higher conductivity of PAADDA can be explained by its amorphous structure, which facilitates charge mobility along the polymer chain, resulting in higher σ values. In contrast, HEC exhibits lower conductivity due to its semicrystalline structure, as evidenced in its diffractogram. Regarding the HEC/PAADDA blends, the σ values were the lowest among all samples, indicating that crosslinking with GLU reduces polymer chain mobility and, consequently, electrical conductivity.

3.2. SEM

The SEM images revealed that the crosslinked HEC/PAADDA blend films present phase separations leading to the formation of pores within the films. This porous morphology supports the films' swelling capacity and highlights their potential advantages for applications as adsorptive membranes.

3.3. TA Adsorption Study

The study of TA adsorption on HEC/PAADDA films crosslinked with GLU is essential for assessing the efficiency and capacity of these materials in controlled release systems for bioactive substances. Adsorption kinetics were investigated for different HEC/PAADDA ratios (30/70, 50/50, and 70/30 (%)) using 0.1 g of film in an aqueous TA solution (6.11×10^{-6} mol·L^{-1}) at pH 6 and 25 °C, under constant agitation at 150 rpm. Residual TA concentrations were monitored by UV-Vis spectrophotometry at λ = 274 nm, enabling the calculation of incorporation efficiency over time. This methodology allows for a detailed evaluation of the interaction between the polymers and TA, revealing the influence of different HEC/PAADDA ratios on the adsorption capacity of the films. The results provide relevant insights into adsorption efficiency and the potential applicability of these films in controlled drug release systems, contributing to the development of optimized devices for pharmaceutical and biomedical applications.

3.4. Adsorption Kinetics

The kinetic analysis of TA adsorption by HEC/PAADDA films demonstrated that the polymeric composition significantly influences the adsorption efficiency and mechanism. The film with the highest PAADDA content (30/70%) exhibited the greatest adsorption capacity, reaching approximately 58% incorporation and equilibrium after 40 minutes, indicating a higher affinity between the cationic groups of PAADDA and TA. The intermediate composition (50/50%) showed faster adsorption kinetics, achieving 45% incorporation and equilibrium within 21 minutes, representing a good balance between rate and efficiency. In contrast, the film with the highest HEC

content (70/30%) presented the lowest adsorption capacity, reaching equilibrium in just 7 minutes with low incorporation, likely due to the reduced availability of active cationic sites. Among the applied kinetic models, the pseudo-second-order model provided the best fit ($R^2 > 0.98$ for all compositions), indicating that the process is predominantly controlled by chemical interactions. The pseudo-first-order model showed moderate fits ($R^2 = 0.902$ and 0.92 for 30/70% and 50/50%, respectively) and was unsatisfactory for 70/30% ($R^2 = 0.40$). The intraparticle diffusion model indicated that diffusion is not the predominant rate-limiting factor. Therefore, the results confirm that increasing the PAADDA fraction enhances TA adsorption, and that the 50/50% composition offers the most balanced performance, making it the most promising for controlled release systems of bioactive compounds and purification processes.

3.5. General Discussion

The characterization of HEC/PAADDA films crosslinked with GLU revealed properties favorable for their application in controlled release systems of active substances. Crosslinking increased the hydrophobicity and thermal stability of the films while reducing their solubility in aqueous media. Films with higher HEC content exhibited lower swelling capacity and greater thermal stability, whereas those richer in PAADDA showed higher TA adsorption capacity. The FTIR, XRD, TGA, EIS, and SEM analyses confirmed the formation of crosslinks, enhanced crystallinity, and improved electrochemical performance of the materials. The pseudo-second-order kinetic model best described the adsorption process, particularly for the 50/50% composition, which demonstrated the best balance between efficiency and adsorption time. In summary, the results demonstrate that varying the proportions of HEC and PAADDA allows tuning of structural, optical, and adsorption properties, making these films promising candidates for pharmaceutical, biomedical, and UV-protective barrier applications.

3.6. Synthesis of What the Literature Shows About TA and Delivery Systems

TA is a hydrolyzable polyphenol widely recognized for its antioxidant, antimicrobial, anti-inflammatory, wound-healing, and antitumor properties, as demonstrated in *in vitro* and preclinical studies. Its anticancer activity involves multiple mechanisms, including inhibition of cell proliferation, induction of apoptosis, and modulation of matrix metalloproteinases (MMPs) and angiogenesis. Therefore, ensuring the maintenance of TA's bioactivity after its incorporation into polymeric matrices is not only plausible but essential for therapeutic efficacy [7]. Polyphenol-based polymeric systems, such as hydrogels and films containing TA, have been extensively studied and shown to provide controlled and pH-dependent release, a desirable feature for applications in slightly acidic environments, such as the tumor microenvironment and healing wounds. The polymerization process and the degree of crosslinking are key determinants of retention, stability, and release kinetics of the bioactive compound [14].

In tumor models, TA has demonstrated antitumor and antiangiogenic effects by inhibiting the expression of VEGF, COX-2, and the metalloproteinases MMP-2 and MMP-9, as well as by reducing the polarization of M2-type macrophages, which promote tumor progression [15]. Polymeric films and hydrogels have been widely used as controlled-release systems for bioactive compounds, since features such as matrix structure, swelling degree, porosity, crosslinking level, and molecular interactions between the active compound and the polymer, including chemical adsorption and electrostatic affinity, directly influence the release kinetics. In the case of TA, studies indicate that its incorporation into polymeric matrices provides protection against degradation, promotes sustained release, and enhances topical application, thus expanding its therapeutic potential across different biological contexts [16].

In antitumor contexts, the sustained release of TA has been identified as a key factor in maintaining a stable therapeutic concentration within the tumor microenvironment, contributing to the inhibition of angiogenesis, MMP activity, and the induction of cell apoptosis. In wound-healing applications, the controlled release of this compound has been associated with maintaining a favorable moist environment, enhancing exudate absorption, and stimulating cell proliferation, while preventing sudden releases that could lead to local toxicity or accelerated elimination of the bioactive agent.

3.7. Mapping Between Film Properties and Expected Release Mechanisms

The following section relates the presented results (solubility, swelling, transmittance, TA adsorption, FTIR/crosslinking) to the requirements for effective controlled release (Table 3).

Table 3. Mapping between film properties and expected release mechanisms

Film Property	Observed Result	Implication for Controlled Release of TA
Solubility: 30/70 ≈ 50%; 50/50 ≈ 27%; 70/30 ≈ 30%	Higher solubility for the formulation with more PAADDA (30/70)	High solubility → risk of rapid "burst" release or even matrix dissolution. For sustained release, moderate-to-low solubility is desired. Therefore, 50/50 or 70/30 formulations are more promising for prolonged release.
Swelling: 30/70 ≈ 500%; 50/50 ≈ 200%; 70/30 ≈ 80%	Films richer in PAADDA absorb more water and swell significantly	High swelling facilitates water infiltration and TA diffusion, favoring faster release. For prolonged controlled release, lower swelling (as in 70/30) supports slower release, though it also depends on TA adsorption and matrix crosslinking.
TA Adsorption: 30/70 → ~ 58% incorporation in ~ 40 min; 50/50 → ~ 45% in 21 min; 70/30 → low loading in 7 min	Higher PAADDA content resulted in greater incorporation; intermediate ratio provided balance	Higher PAADDA content resulted in greater incorporation; intermediate ratio provided balance
Crosslinking and Polymer–TA Interactions (FTIR: C=O band shift, H-bond formation)	Evidence of chemical interactions between HEC and PAADDA, and crosslinking with GLU	Chemical interactions and crosslinking reduce chain mobility, slowing TA diffusion and favoring controlled release. This compensates for swelling and solubility effects.
Morphology/Porosity (SEM: phase separation, pore formation in films	Porosity observed leading to high swelling and rapid adsorption	Porosity favors initial diffusion, possibly causing a "burst" effect. For more controlled release, smaller pores or a denser matrix would be advantageous.
Conductivity/Chain Mobility (EIS: crosslinked films show lower conductivity)	Crosslinking limits chain mobility, resulting in lower conductivity	Reduced mobility indicates slower molecular diffusion, which favors sustained release.

Based on the mapping, it is possible to identify which aspects are supported by the experimental data and which remain potentially viable but dependent on further optimization. The films' high TA adsorption capacity, as evidenced by the approximately 58% incorporation observed for the HEC/PAADDA 30/70 ratio, demonstrates that the polymeric matrix has strong potential to efficiently encapsulate the bioactive molecule, fulfilling one of the fundamental prerequisites for its application in controlled release systems. The presence of chemical interactions and crosslinking bonds within the matrix, confirmed by FTIR and EIS analyses, indicates that the films possess a stable structure, an essential characteristic to ensure the integrity of the material until the moment of active compound release. This structural stability contributes to maintaining the physicochemical properties of the films and controlling the diffusion rate of TA over time. Furthermore, the variations observed in swelling and solubility parameters among the different HEC and PAADDA ratios demonstrate that the material's structural and functional properties can be tuned by modifying its composition. This ability to modulate the physicochemical behavior of the films reinforces their technical feasibility for the development of adjustable release systems, making them adaptable for different therapeutic applications such as antitumor and wound-healing treatments. Although the results indicate promising potential for HEC/PAADDA films as controlled release systems, some aspects still require optimization. For applications demanding prolonged release, the material should exhibit low solubility and reduced swelling capacity to prevent excessively rapid TA release or premature matrix dissolution. In this context, the 30/70 formulation, despite its high adsorption efficiency, may pose a risk of immediate "burst release" or structural fragmentation, compromising control over the diffusion process. The high porosity and

significant swelling observed in this formulation could favor an abrupt initial release, which is not always desirable in therapeutic contexts such as antitumor or wound-healing treatments, where maintaining constant levels of the active agent is crucial for efficacy and safety. Therefore, balancing adsorption capacity with structural stability must be optimized, possibly through adjustments in the HEC/PAADDA ratio or the degree of crosslinking with GLU. Another aspect that remains to be developed is the absence of data on the kinetic release profile of TA, such as cumulative release curves over time, as well as on the preservation of its biological activity after release. These parameters are critical for confirming the system's therapeutic efficacy and should be addressed in subsequent experimental stages. Moreover, for antitumor applications, the system's feasibility depends not only on achieving controlled release but also on ensuring targeted delivery to the tumor tissue, maintaining TA stability within the tumor microenvironment, and confirming the polymer matrix's biocompatibility with surrounding healthy cells. These complementary parameters are essential to establish the suitability of HEC/PAADDA films for safe and localized therapies. Based on these considerations, it can be stated that GLU-crosslinked HEC/PAADDA films demonstrate theoretical viability as controlled release systems for TA, provided that specific parameters (particularly polymer ratio, crosslinking degree, and control of porosity/swelling) are optimized to ensure appropriate release behavior. Notably, the 50/50 formulation stands out as the most promising candidate for controlled release due to its balanced adsorption capacity and kinetic profile. For antitumor and wound-healing applications, this matrix exhibits strong potential but requires further experimentation to confirm its release profile, biocompatibility, and therapeutic activity.

3.8. Specifications for Application Contexts

In the antitumor context, the primary requirement for a drug delivery system is that TA be released locally within the tumor microenvironment, maintaining an effective concentration for a prolonged period, sufficient to inhibit VEGF-mediated angiogenesis, reduce MMP-2 and MMP-9 expression, and induce apoptosis. Evidence published by MDPI indicates that TA exhibits significant antitumor effects, including the downregulation of MMP-2, MMP-9, COX-2, and VEGF in different experimental models [15]. Recent studies by Wang [17] reinforce these findings, demonstrating that TA exerts anticancer effects in several cancer cell lines, including urothelial carcinoma, by inhibiting the PI3K/Akt signaling pathway, reducing Akt phosphorylation, and decreasing the expression of pluripotency markers such as SOX2, OCT4, and NANOG. These results highlight the compound's ability to modulate key signaling pathways involved in tumor cell survival and proliferation, supporting its use in targeted therapy delivery systems. In this context, the polymeric matrix must exhibit structural stability after application, avoiding rapid dissolution and allowing gradual, controlled release of the compound. Based on the obtained results, it can be inferred that formulations with lower swelling and solubility tend to promote this behavior, contributing to more sustained TA release. Among the evaluated ratios, the 70/30 composition shows indications of slower release, although it incorporates a smaller amount of TA, suggesting that a balance between loading capacity and release control is necessary. The 50/50 formulation, in contrast, appears to offer a more advantageous intermediate profile, combining adequate structural stability with satisfactory bioactive incorporation efficiency. The tumor microenvironment, typically characterized by a slightly acidic pH around 6.5, should also be considered. Since TA adsorption was studied at pH 6, there is evidence that the matrix could respond favorably under these conditions, promoting controlled release at the target site. Exploring this pH-sensitive behavior could further enhance the potential of the matrix for targeted antitumor therapies [18].

3.9. Wound Healing Context

In the context of wound healing, the controlled release of TA plays an important role by promoting a balanced inflammatory response, stimulating fibroblast proliferation and collagen deposition, and exerting antimicrobial and antioxidant effects. For this type of application, the polymeric matrix must allow adequate absorption of exudates, maintain a moist environment favorable to tissue repair, and enable safe and non-traumatic removal after use [16]. TA is a polyphenol widely recognized for its antioxidant, anti-inflammatory, antimicrobial, wound-healing, and antitumor properties. Additionally, it exhibits photoprotective effects, shielding fibroblasts from UVB-induced damage by reducing reactive oxygen species formation and inhibiting the expression of MMP-1, an enzyme associated with extracellular matrix degradation [16]. These findings reinforce TA as a promising molecule not only for its antioxidant potential but also for its antitumor and regenerative effects. Therefore, its incorporation into controlled release systems is particularly relevant for contexts such as oncological wounds, radiodermatitis, or post-surgical reconstruction, where it is necessary to control inflammation, promote tissue regeneration, and prevent local recurrence.

Based on the results obtained in this study, it can be inferred that matrices with moderate to high swelling may offer an advantage, as they enable greater wound fluid absorption, a desirable feature in bioactive dressings. In this regard, the 30/70 composition showed the highest degree of swelling, indicating potential for use as a tannic

acid-releasing dressing. However, this behavior may also increase the risk of accelerated matrix degradation or excessively rapid compound release, suggesting that additional adjustments, such as increasing the degree of crosslinking, may be required to ensure a more gradual and sustained release. Similar systems have been described by Ali [19], who developed films based on chitosan, carboxymethylcellulose, and tannic acid, achieving approximately 90% compound release within 24 hours and favorable results in wound healing. These findings reinforce that the films developed in this study, due to their high swelling capacity and good bioactive incorporation, show promising potential for application as active wound dressings with controlled release properties.

3.10. Future Experimental Requirements to Validate Viability

Based on this theoretical framework, it is possible to outline experimental studies aimed at deepening the understanding of the behavior and applicability of the developed films. A first step involves determining the TA release profile for each polymeric proportion (30/70, 50/50, and 70/30) using simulated media that represent different physiological conditions: pH 7.4 for healthy tissues and blood, pH 6.5 for the tumor microenvironment, and pH between 7.0 and 8.0 for wound sites. This evaluation will allow identification of how pH influences the release kinetics of the bioactive compound. Another important aspect is adjusting the degree of crosslinking with GLU to modulate the solubility and swelling properties of the matrix. This step aims to achieve a balance between structural stability and controlled release capacity. Additionally, it is recommended to assess the biological activity of the released TA by evaluating its cytotoxicity in relevant tumor cell lines, as well as its effects on fibroblast and keratinocyte migration and viability, essential parameters for wound-healing applications. The structural stability of the films, before and after the release process, should be analyzed through techniques such as SEM and FTIR to confirm matrix integrity during use. It is also essential to evaluate the biocompatibility and hemocompatibility of the formulations without TA, ensuring safety and suitability for biomedical applications. Finally, the application of kinetic models, such as Higuchi and Korsmeyer–Peppas, may help determine the predominant release mechanisms, whether diffusion-controlled, matrix relaxation-controlled, or a combination of both. For potential antitumor applications, in vivo or ex vivo studies are recommended to investigate the local release and tissue distribution of TA, thereby consolidating the feasibility of the proposed systems.

4. CONCLUSION

The results presented in this study indicate that the biopolymeric matrix composed of HEC and PAADDA, crosslinked with GLU, exhibits suitable physicochemical and structural properties to function as a controlled release system for TA. The analyses demonstrated the efficiency of bioactive compound incorporation, the structural stability provided by crosslinking, and the ability to modulate characteristics such as solubility, swelling, and porosity, allowing the matrix behavior to be adjusted according to the intended therapeutic application. The theoretical feasibility observed reinforces the potential of these films for both antitumor and wound-healing applications. In the oncological context, structural stability and sustained TA release are essential to maintain effective therapeutic concentrations within the tumor microenvironment, promoting antiangiogenic, antiproliferative, and pro-apoptotic effects. In wound-healing scenarios, greater swelling capacity and exudate absorption favor the maintenance of a moist environment, inflammation control, and tissue regeneration. Among the formulations evaluated, the 50/50 proportion stands out as the most balanced condition for controlled release systems, combining adequate TA incorporation with satisfactory structural stability, making it promising for general therapeutic applications. The 30/70 formulation, in turn, appears more suitable for use in bioactive dressings due to its higher swelling degree and faster release—features desirable for accelerating tissue repair. Conversely, the 70/30 and 50/50 compositions show greater potential for antitumor applications due to their lower solubility and slower release profiles, enabling localized and sustained bioactive action. However, experimental validation of these findings is essential. *In vitro* and *in vivo* assays evaluating release kinetics, biocompatibility, selective cytotoxicity, and maintenance of TA bioactivity are crucial steps for confirming the applicability of the developed systems. Conducting these studies will consolidate understanding of the release mechanisms involved and optimize formulation conditions for each intended use.

In summary, the crosslinked HEC/PAADDA films constitute a versatile and tunable platform for the controlled release of bioactive compounds, offering promising foundations for the development of advanced therapeutic systems applicable both in localized oncological treatments and in next-generation bioactive dressings, thus contributing to the advancement of sustainable and multifunctional biomedical technologies.

References

[1] P. Confferri, C. T. Moraes, B. M. E. R. Gonçalves, and R. M. C. Santana. “Influence of tannic acid addition

on biodegradable films of isolated soy protein," in *Proceedings of the 15th Brazilian Congress of Polymers (15th CBPOL)*, Bento Gonçalves, RS, 2019, vol. 15, no. 1, pp. 1171–1175.
[2] C. A. de S. Melo, R. J. Domingues, and A B. Lima. "Development of gels and drug stability," *R. Health and Life Collection*, vol. 22, no. 1, pp. 1–53, 2018.
[3] M. E. E. Consendey, G. G. Celestino, A. L. Shiguihara, and J. Amim Junior. "Preparation and characterization of PVP/PAADDA blends," *Brazilian Journal of Development*, Curitiba, vol. 7, no. 10, pp. 95067–95080, 2021.
[4] R. B. W. Evaristo. "Materials obtained from cellulose: origin, synthesis and applications," *Virtual Journal of Chemistry*, vol. 15, no. 6, pp. 1154–1162, 2022.
[5] R. F. Silva and L. Pogacnik, "Polyphenols from food and natural products: Neuroprotection and safety," *Antioxidants*, vol. 9, art. no. 61, 2020.
[6] S. M. Kumara, A. M. Sayeed, and S. U. Rani, "Antimicrobial properties of plant essential oils against human pathogens and their mode of action: An updated review," *Evidence-Based Complementary and Alternative Medicine*, vol. 2016, art. no. 3012462, 2016.
[7] K. Huang, H. Liu, H. Zhang, X. Zhang, H. Jiang, X. Liu, and X. Wang, "Tannic acid: A link between metallic elements and biomedical applications," *Coordination Chemistry Reviews*, vol. 548, no. 2, art. no. 217193, 2026. doi: 10.1016/j.ccr.2025.217193
[8] L. A. Jadhav and S. K. Mandlik, "Nanocarriers in skin cancer treatment: Emerging drug delivery systems," *Nanomedicine Journal*, vol. 5, no. 2, pp. 45–60, 2024. doi: 10.1016/j.ntm.2024.100068
[9] E. Bahramzadeh, E. Yilmaz, S. Sheidaei, and R. Nosrati, "Glutaraldehyde-cross-linked chitosan-graft-poly(N-hydroxyethyl acrylamide) films: Synthesis, characterization, and biomedical applications," *Journal of Biomedical Materials Research Part B: Applied Biomaterials*, vol. 113, no. 4, pp. 789–799, 2025. doi: 10.1016/j.ijbiomac.2025.146343
[10] A. Korel, A. Samokhin, E. Zemlyakova, A. Pestov, E. Blinova, and M. Zelikman. "A carboxyethylchitosan gel cross-linked with glutaraldehyde as a candidate carrier for biomedical applications," *Gels*, vol. 9, no. 9, pp. 756–772, 2023. doi: 10.3390/gels9090756
[11] S. Adepu and S. Ramakrishna, "Controlled drug delivery systems: Current status and future perspectives," *Journal of Controlled Release*, vol. 331, no. 1, pp. 1–22, 2021. doi: 10.3390/molecules26195905
[12] F. de N. C. dos S. Cordeiro, H. P. Cordeiro, L. O. A. D. Pinto, C. C. I. Sefer, E. V. Santos-Lobato, and L. T. de Mendonça, "Descriptive exploratory qualitative studies: A bibliometric study," *Brazilian Journal of Health Review*, Curitiba, vol. 6, no. 3, pp. 11670–11681, 2023. doi: 10.34119/bjhrv6n3-259
[13] J. Marques, C. M. Duarte, A. L. Shiguahara, and J. A. Júnior, "Characterization and application of HEC/PAADDA films cross-linked with glutaraldehyde," in *Proceedings of the Giulio Massarani Scientific, Technological, Artistic and Cultural Initiation Conference*, Rio de Janeiro, RJ: UFRJ, 2021.
[14] Z. Li, Z. Chen, H. Chen, K. Chen, W. Tao, X. K. Ouyang, L. Mei, and X. Zeng, "Polyphenol-based hydrogels: Pyramid evolution from crosslinked structures to biomedical applications and the reverse design," *Bioactive Materials*, vol. 17, pp. 49–70, Feb. 2022. doi: 10.1016/j.bioactmat.2022.01.038
[15] N. Oršolić, M. Kunštić, and M. Jazvinšćak Jembrek, "Antitumor and antiangiogenic effect of tannic acid in the advanced stage of Ehrlich ascites tumor in mice," *International Journal of Molecular Sciences*, vol. 26, no. 18, art. no. 9070, 2025. doi: 10.3390/ijms26189070
[16] I. Guimarães, R. Costa, S. Madureira, S. Borges, A. L. Oliveira, M. Pintado, and S. Baptista-Silva, "Tannic acid tailored-made microsystems for wound infection," *International Journal of Molecular Sciences*, vol. 24, no. 5, art. no. 4826, 2023. doi: 10.3390/ijms24054826
[17] M. Wang, L. He, and P. Yan, "Integrated network pharmacology, molecular docking and experimental validation to investigate the mechanism of tannic acid in nasopharyngeal cancer," *Scientific Reports*, vol. 15, no. 1, p. 5645, Feb. 2025. doi: 10.1038/s41598-025-90211-z
[18] C. Chen, T. Ma, W. Tang, X. Wang, Y. Wang, J. Zhuang, Y. Zhu, and P. Wang, "Reversibly-regulated drug release using poly(tannic acid) fabricated nanocarriers for reduced secondary side effects in tumor therapy," *Nanoscale Horizons*, vol. 5, no. 6, pp. 986–998, 2020. doi: 10.1039/d0nh00032a
[19] M. Ali, S. Ullah, and S. Ullah. "Innovative biopolymers composite based thin film for wound healing applications," *Scientific Reports*, vol. 14, art. no. 27415, 2024. doi: 10.1038/s41598-024-79121-8

2nd International Conference on Multidisciplinary Sciences and Technological Developments (ICMUSTED 2025)

December 12-15, 2025

Infertility Among Women in Tebessa (Northeastern Algeria): Anthropometric and Biological Risk Determinants

Khalida Abla[1], Nassima Toumi-Halaimia[1], Sawssane Ziani[1], Ines Benamer[1], Asma Kraidia[1]

[1]Applied Biology Department, Echahid Cheikh Larbi Tebessi University, Tebessa, Algeria
Corresponding author: Khalida Abla (e-mail: khalida.abla@univ-tebessa.dz)

Abstract

In 2010, the World Health Organization estimated that there were 48.5 million infertile couples globally. This study aims to identify risk factors linked to female infertility in Tebessa. Through a random selection process, we selected 180 adults, specifically married women of childbearing age whose partners did not exhibit any signs of fertility problems. The findings indicate that there is no significant correlation between the age of a woman at the time of her marriage or her current age and her inability to conceive a child. The results also show that the primary risk factors for infertility are being overweight, which is typically characterized by android fat distribution, and having gained weight since childhood or adolescence. It was found that spontaneous miscarriages, oligomenorrhea, anovulation, and polycystic ovary syndrome are significantly associated with infertility with a significant degree. Obesity impairs the fertility of women by causing reproductive abnormalities and ovulation disorders, which ultimately leads to a decrease in fertility.

Keywords: Infertility, Normal period to conception, Risk factors, Obesity women

2nd International Conference on Multidisciplinary Sciences and Technological Developments (ICMUSTED 2025)

December 12-15, 2025

Impact of Traditional Phytotherapy on Hematological Parameters and Chemotherapy Tolerance in Breast Cancer Patients: A Case-Control Study in Tebessa, Algeria

Khalida Abla[1], Nassima Toumi-Halaimia[1], Sawssane Ziani[1]

[1]Applied Biology Department, Echahid Cheikh Larbi Tebessi University, Tebessa, Algeria
Corresponding author: Khalida Abla (e-mail: khalida.abla@univ-tebessa.dz)

Abstract

This study aims to evaluate the impact of complementary phytotherapy on hematological parameters and chemotherapy tolerance in breast cancer patients. A cross-sectional case-control study was conducted among 200 women, divided into two groups: Women receiving combined chemotherapy and phytotherapy (100 participants) and women receiving chemotherapy alone (100 participants). Data collection included hematological parameters, tumor characteristics, phytotherapeutic practices, and chemotherapy-related side effects. Statistical analyses were performed using student's test and the chi-square test. The most frequently used medicinal plants were ephedra alata, artemisia herba-alba, and nigella sativa. Women receiving both chemotherapy and phytotherapy showed significantly better hematological profiles, with reduced erythropenia, lower frequency of anemia, decreased leukopenia, and reduced neutropenia. Chemotherapy tolerance was also improved, with significant reductions in nausea, appetite loss, and dry mouth. The duration of chemotherapy side effects was significantly shorter in women combining both treatments. These findings suggest that complementary phytotherapy may contribute to preserving hematological balance and improving tolerance to chemotherapy, supporting further investigation into its integration in oncology care.

Keywords: Breast cancer, Phytotherapy, Chemotherapy, Hematological parameters, Traditional medicine

2nd International Conference on Multidisciplinary Sciences and Technological Developments (ICMUSTED 2025)

December 12-15, 2025

Effects of Twin Hearts Meditation Versus Mandala Coloring on Practical Examination Anxiety in Undergraduate Nursing Students

Pouran Varvani Farahani[1], Samineh Esmailzadeh[2], Precious Chisom Uzoeghelu[1], Hatice Sutcu[1]

[1]Faculty of Health Sciences, Cyprus International University, Nicosia, Turkish Republic of Northern Cyprus
[2]Faculty of Nursing, Near East University, Near East Boulevard, Nicosia, Turkish Republic of Northern Cyprus
Corresponding author: Pouran Varvani Farahani (e-mail: pfarahani@ciu.edu.tr)

Abstract

Nursing students frequently experience high levels of exam anxiety, which negatively affects academic performance and overall well-being. Mandala coloring and Twin Hearts Meditation are complementary interventions that may help reduce anxiety. This study aimed to compare the effects of these two interventions on exam anxiety among nursing students. This randomized clinical trial was conducted on 100 nursing students. Participants were randomly assigned into two groups: The mandala coloring group (n = 50) and the twin hearts meditation group (n = 50). The interventions were delivered immediately prior to a practical examination. Exam anxiety levels were assessed before and after the intervention using the Spielberger state-trait anxiety inventory (STAI). Data were analyzed using SPSS version 25, applying paired and independent t-tests, with $P < 0.05$ considered statistically significant. There were no statistically significant differences in sociodemographic characteristics or pre-intervention anxiety scores between the two groups ($P > 0.05$). Following the intervention, the mean exam anxiety score in the mandala coloring group decreased significantly from 61.90 ± 16.0 to 45.50 ± 6.57 ($P \leq 0.001$). The twin hearts meditation group also showed a significant reduction in anxiety, from 67.52 ± 17.24 to 62.78 ± 17.33 ($P \leq 0.001$). However, independent t-test analysis revealed that the reduction in anxiety was significantly greater in the mandala coloring group compared to the meditation group ($P \leq 0.001$). Both mandala coloring and twin hearts meditation were effective in reducing exam anxiety among nursing students, with mandala coloring demonstrating greater efficacy.

Keywords: Mandala coloring, Meditation, Exam anxiety, Nursing students, Complementary therapies, Mental health

2nd International Conference on Multidisciplinary Sciences and Technological Developments (ICMUSTED 2025)

December 12-15, 2025

Body Image Perception Among Women After Mastectomy

Mohamed Khalyfa[1,2], Mohammed-Yassine Takzima[3], Imane Bettane[4], Youssef El Allam[2], Aya Ait Benaim[1]

[1]High Institute of Nursing and Health Techniques, Safi, Morocco
[2]Laboratory of Health Sciences and Technologies, Higher Institute of Health Sciences, Hassan First University, Settat, Morocco
[3]Laboratory of Water Sciences, Microbial Biotechnologies, and Natural Resources Sustainability, Unit of Microbial Biotechnologies, Agrosciences, and Environment, Faculty of Sciences-Semlalia, Cadi Ayyad University, Marrakech, Morocco
[4]Bioscience and Health Research Laboratory, Community Medicine and Public Health Department, Faculty of Medicine, Cadi Ayyad University, Marrakech, Morocco
Corresponding author: Mohamed Khalyfa (e-mail: mohamed.khalyfa.doc@uhp.ac.ma)

Abstract

Mastectomy, as a primary treatment for breast cancer, has profound effects not only on women's physical health but also on their body image and emotional well-being. In cultural contexts such as Morocco, where femininity and motherhood are closely tied to bodily integrity, the psychological and social repercussions of breast loss are particularly significant. This quantitative study was conducted among 40 women who underwent mastectomy, using a structured questionnaire to assess physical, psychological, and socio-cultural factors influencing their perception of body image. The findings reveal that 83% of participants associated breast loss with a loss of femininity, 77% reported dissatisfaction with body symmetry, and over 60% avoided mirrors or social interactions. Furthermore, 30% showed moderate to severe anxiety-depressive symptoms, while 54% felt less attractive and 58% were dissatisfied with surgical scars. These impacts were further aggravated by factors such as economic precarity, illiteracy, and lack of family support. The study emphasizes the urgent need for integrated care models that incorporate psychological counseling, culturally sensitive education, and support networks to facilitate post-mastectomy adjustment. A multidisciplinary approach is essential to restore self-esteem, improve mental health outcomes, and promote full social reintegration for women affected by breast cancer.

Keywords: Mastectomy, Body image, Breast cancer, Psychological distress, Moroccan women

2nd International Conference on Multidisciplinary Sciences and Technological Developments (ICMUSTED 2025)

December 12-15, 2025

In Silico Prediction of the Biological Activity of New Oxazole Derivatives

Nadia Hadhoum[1], Nassim Haddouche[1], Yasmine Hannachi[1], Sabine Herbi[1]

[1]Departmentof Pharmacy, Mouloud Mammeri University of Tizi-Ouzou, Tizi Ouzou, Algeria
Corresponding author: Nadia Hadhoum (e-mail: nadia_hadhoum@yahoo.fr)

Abstract

As part of the development of new anti- inflammatory agents, our work focuses on the design of a series of novel oxazole-derived molecules. A basic chemical structure was proposed based on results from the structure-activity relationships of marketed molecules. Thirty molecules were thus proposed with the aim of improving the anti-COX-2 activity of celecoxib while increasing selectivity towards the latter. The ionization state of the compounds was predicted, followed by an in silico molecular docking study to evaluate the interactions between the compounds of this new series and the COX-1 and COX-2 enzymes. Among them, molecule number thirty exhibits an affinity comparable to that of celecoxib, a selective non- steroidal anti-inflammatory drug (NSAID) targeting COX-2, while molecule twenty-eight shows interactions with key amino acids of the active site. Furthermore, in silico studies were conducted to predict the physicochemical, pharmacokinetic, and toxicological properties of the compounds., including their ability to cross the blood-brain barrier and gastrointestinal absorption. Finally, the chemical reactivity of the proposed molecules was evaluated using density functional theory (DFT), allowing analysis of frontier orbitals and calculation of reactivity descriptors.

Keywords: Anti-inflammatory, oxazole, docking, Chemical absorption, distribution, metabolism, excretion, and toxicity (ADMET), DFT

2nd International Conference on Multidisciplinary Sciences and Technological Developments (ICMUSTED 2025)

December 12-15, 2025

Circular Economic Model in the Hotel Industry for the Optimization of Solid and Recyclable Waste: Case Study of the City of Essaouira, Morocco

Assala Loukili[1], Mohamed Hafidi[1], El Hassan El Mouden[2], Abdallah Nassour[3], Nour-El Houda Chaher[3], Loubna El Fels[1,4]

[1]Unit of Microbial Biotechnologies, Agrosciences, and Environment, Laboratory of Water Sciences, Microbial Biotechnologies, and Natural Resources Sustainability, Faculty of Sciences-Semlalia, Cadi Ayyad University, Marrakesh, Morocco
[2]Laboratory of Water, Biodiversity and Climate Change, Faculty of Science-Semlalia, Cadi Ayyad University, Marrakech, Morocco
[3]Department of Waste and Resource Management, Rostock University, 18051 Rostock, Germany
[4]Sustainable Materials Research Center (SUSMAT-RC), University Mohamed VI Polytechnic (UM6P), Benguerir, Morocco
Corresponding author: Assala Loukili (e-mail: assalaloukili@gmail.com)

Abstract

This study examines solid waste management practices in the hotel industry in Essaouira, Morocco, a coastal tourist center under increasing environmental pressure. Data was collected from 19 hotels, enabling statistical and qualitative assessments of waste production and management performance. Hotels were classified into three categories: (1) those with no waste management system, (2) those without a formal system but attempting to reduce plastic use, and (3) those implementing structured systems incorporating source separation, recycling, and composting. The results show that hotels in category 3 achieve significantly better environmental outcomes and operational efficiency, confirming trends observed in international research on sustainable tourism. Despite municipal efforts to promote environmentally friendly practices, limitations remain in terms of infrastructure availability and regulatory enforcement. The study provides targeted recommendations to help hotel managers improve their waste reduction strategies and highlights the need to strengthen institutional frameworks in order to consolidate sustainability across the sector. Overall, the findings underscore the importance of adopting proactive and integrated approaches to waste management to ensure the long-term environmental and economic resilience of tourism activities in Essaouira, Morocco.

Keywords: Solid waste, Recycling, Source separation, Sustainability, Environmental regulations

2nd International Conference on Multidisciplinary Sciences and Technological Developments (ICMUSTED 2025)

December 12-15, 2025

Food Safety and Microbial Control

Ali Khalfa[1,2], Azzeddine Senouci[1], Djahira Hamed[1], Mounir Chihab[1], Sofiane Bouazza[3], Bensalah Fatima[1], Farid Bennabi[4]

[1]Department of Agri-Food, Faculty of Science and Technology, University of Ain Temouchent, Ain Temouchent, Algeria
[2]Laboratory of Applied Hydrology and Environment, Ain Temouchent, Algeria
[3]Department of Biology, Faculty of Natural and Life Sciences, University of Djillali Liabes, Sidi Bel Abbes, Algeria
[4]Department of Biology, Faculty of Science and Technology, University of Ain Temouchent, Ain Temouchent, Algeria
Corresponding author: Ali Khalfa (e-mail: ali.khalfa@univ-temouchent.edu.dz)

Abstract

Food safety is a growing concern due to the frequent occurrence of foodborne illnesses linked to microbial contamination. Contaminated food products not only cause acute gastrointestinal infections but also contribute to long-term health complications and economic losses. This study aims to evaluate the microbiological quality of commonly consumed food products collected from local markets and small food outlets, where sanitary conditions are often insufficient. A total of 40 samples, including dairy products, meat, and ready-to-eat foods, were analyzed using standard microbiological techniques. Total viable counts, coliforms, and the presence of common foodborne pathogens such as *Escherichia coli* and *Staphylococcus aureus* were investigated. In addition, basic hygiene practices during food handling, storage conditions, and packaging were observed and recorded. The data were analyzed using IBM SPSS version 28 and expressed as mean and standard deviation, with mean differences presented at a 95% confidence interval. The results revealed that more than half of the samples exceeded acceptable microbial limits, particularly in ready-to-eat foods sold under inadequate hygienic conditions. *Escherichia coli* was detected in several meat and dairy products, suggesting possible fecal contamination along the supply chain, while *Staphylococcus aureus* was associated with poor handling practices and lack of personal hygiene among food vendors. Statistical analysis confirmed significant differences in contamination levels between properly packaged products and those sold in open-air conditions. These findings highlight the urgent need for improved hygiene practices, stricter monitoring of food sold in local markets, and enforcement of safety standards. Low-cost interventions, such as training programs for food handlers, proper storage facilities, and the adoption of simple microbial control measures, could significantly reduce health risks. Raising public awareness and strengthening local inspection systems are essential steps to enhance consumer safety and restore trust in the food supply chain.

Keywords: Food safety, Microbial contamination, Hygiene practices, Local markets, Foodborne pathogens

Knowledge of Leishmaniasis: A Comparative Review of Morocco and Ethiopia

Mohammed-Yassine Takzima[1], Mohamed Echchakery[1,2], Mohamed Hafidi[1], Loubna El Fels[1]

[1]Laboratory of Water Sciences, Microbial Biotechnologies, and Natural Resources Sustainability, Unit of Microbial Biotechnologies, Agrosciences, and Environment, Faculty of Sciences-Semlalia, Cadi Ayyad University, Marrakech, Morocco
[2]Laboratory of Health Sciences and Technologies, Epidemiology and Biomedical Unit, Higher Institute of Health Sciences, Hassan Premier University, Settat, Morocco
Corresponding author: Mohammed-Yassine Takzima (e-mail: mohammed.takzima@gmail.com)

Abstract

Leishmaniasis is a neglected tropical disease that continues to pose a serious public health concern in endemic regions such as Morocco and Ethiopia. Caused by protozoan parasites of the Leishmania genus, the disease primarily appears as visceral or cutaneous forms. Despite its burden, it remains underdiagnosed and poorly managed due to limited healthcare access and low public awareness. This review examines how demographic, socioeconomic, cultural, and health-related factors influence knowledge and prevention practices. A particular focus is placed on comparing studies conducted in Morocco and Ethiopia. Relevant articles published between 1956 and 2024 were reviewed using the preferred reporting items for systematic reviews and meta-analyses (PRISMA) framework and data from Scopus and Web of Science. The findings reveal significant gaps in knowledge across both countries, especially regarding sandflies as disease vectors. In several Ethiopian districts, fewer than a quarter of respondents recognized sandflies as the cause of cutaneous leishmaniasis. In Morocco, a large proportion of respondents were unaware of transmission modes, and many believed bites were unavoidable. Reliance on traditional medicine was high in both contexts, often preferred over modern treatment. Even among healthcare professionals, particularly in rural Moroccan settings, knowledge gaps were evident due to a lack of training and information. Education emerged as the most influential factor in improving knowledge and prevention behavior. Populations with higher education levels and longer residency in endemic areas showed greater awareness. Community involvement was also noted as a potential driver for improved prevention practices. In conclusion, efforts to control leishmaniasis in endemic settings like Morocco and Ethiopia must prioritize health education, professional training, and culturally tailored outreach. Addressing these knowledge gaps is essential to enhancing prevention and reducing transmission.

Keywords: Leishmaniasis, Knowledge, Awareness, Morocco, Ethiopia

2nd International Conference on Multidisciplinary Sciences and Technological Developments (ICMUSTED 2025)

December 12-15, 2025

Chemical Profiling and Neuroprotective Activity in Elaeagnaceae Leaves

Rayene Bouaita[1], Randa Djemil[1], Samira Bouahlit[1], Saber Boutellaa[2], Chourouk Babouche[1], Zineb Bouamrane[2]

[1]Laboratory of Biotechnology, Water, Environment and Health, Department of Molecular and Cellular Biology, University of Abbes Laghrour Khenchela, Algeria
[2]Laboratory of Sciences and Materials, Department of Biochemistry, University of Abdelhafid Boussouf, Mila, Algeria
Corresponding author: Bouaita Rayene (e-mail: bouaita.rayene@univ-khenchela.dz)

Abstract

Alzheimer is a progressive neurodegenerative disorder characterized by memory impairment. Inflammation plays a major role in the pathogenesis of this disease, leading to neuronal damage through chronic activation of inflammatory pathways. Natural anti-inflammatory agents have attracted increasing interest due to their ability to modulate neuroinflammatory responses and exert neuroprotective effects. This study evaluates the neuroprotective potential of plant extract from the elaeagnaceae family collected in Eastern Algeria, by assessing their inhibitory activity against butyrylcholinesterase (BChE), one of the key enzyme involved in alzheimer. The leaves were extracted by maceration to obtain an ethyl acetat extract. The chemical composition of the extract was determined using high-performance liquid chromatography (HPLC), allowing the identification and quantification of major bioactive compounds. The anti-inflammatory activity was evaluated using the bovine serum albumin (BSA) assay, showing significant activity for the ethyl acetate extract 53.52 ± 0.49% compared to diclofenac 89.57 ± 1.69 % at a concentration of 1000 µg/mL. Enzyme inhibition assays revealed that the extract inhibited BChE with a value of inhibitory concentration 50% (IC_{50}) = 325.16 ± 46.30 µg/mL compared to galantamine IC_{50} = 34.75 ± 1.99 µg/ml. The presence of phenolic and flavonoid compounds showed a strong correlation with both anti-inflammatory and cholinesterase inhibitory activities. These findings suggest that elaeagnaceae extract may represent a promising natural therapeutic approach to attenuate neuroinflammation, and cholinergic dysfunction associated with alzheimer's disease. Further in vivo studies are required to confirm these neuroprotective effects and to evaluate their potential clinical applications.

Keywords: Neurodegenerative diseases, Enzyme inhibition, Elaeagnaceae, Bioactive compounds, Anti-inflammatory effect

2nd International Conference on Multidisciplinary Sciences and Technological Developments (ICMUSTED 2025)

December 12-15, 2025

Nickel Sulfate Induced Hepatotoxicity Mediated Through Reactive Oxygen Species Generation and Impairing the Antioxidant Defense in Albino Rats

Mohamed Khiari[1], Youcef Bougoutaia[2], Nadjette Bourafa[1], Zine Kechrid[3]

[1]Department of Biology, University of Souk Ahras, Souk Ahras, Algeria
[2]Department of Biology, University of Djelfa, Djelfa, Algeria
[3]Department of Biochemestry, University of Annaba, Annaba, Algeria
Corresponding author: Mohamed Khiari (e-mail: mohamedkhiari@yahoo.fr)

Abstract

The rapid development of technology has exposed man and his environment to a number of exotic metals. Nickel (Ni) is one of the most metal pollutants, and it is seriously threatening our ecosystem and human health. This experimental study was designed to investigate nickel-induced hepatotoxicity in albino rats. Twenty-one adult rats were divided into two groups of seven animals each group. The first group was used as a control and received saline solution while the second was administered with nickel sulfate (2.0 mg/100 g, intraperitonially) simultaneously on alternate days. Body weight gain was recorded regularly. After 21 consecutive days, cellular functions were evaluated by biochemical and oxidative stress markers. The nickel sulfate decreased body weight gain. Nickel treatment produced also oxidative injury characterized by an increase in glucose concentration, enzymes markers activities, and bilirubin concentrations. Simultaneously, liver glutathione level (GSH) and catalase activity were diminished. These results are further substantiated with obviously changes in hepato-histoarchithecture. This work warrants careful assessment of nickel sulfate (NiSO4) before their commercial and industrial applications.

Keywords: Nickel, Hepatotoxicity, Oxidative stress, Rats

A Green Nanotechnology Approach: Rice Husk-Derived Carbon Quantum Dots (CQDs) for Sustainable Applications

Mohd Hafizuddin Ab Ghani[1], Siti Hajar Othman[1], Siti Zulaika Razali[1], Mohd Ali Mat Nong[1], Josephine Liew Ying Chyi[1], Nishata Royan Rajendran Royan[2], Chen Ruey Shan[3], Johari Abdu Rahim[4]

[1]Institute of Nanoscience and Nanotechnology, Universiti Putra Malaysia, Serdang, Malaysia
[2]School of Engineering, University of Wollongong Malaysia (UOW), Shah Alam, Malaysia
[3]Department of Applied Physics, Faculty of Science and Technology, Bangi, Malaysia
[4]Joema Malaysia Global, Besut, Malaysia
Corresponding author: Mohd Hafizuddin Ab Ghani (e-mail: m_hafizuddin@upm.edu.my)

Abstract

The imperative for green chemistry necessitates the sustainable of agricultural waste into high-value functional materials. This study highlights an environmentally conscious and economically viable strategy for synthesizing highly fluorescent carbon quantum dots (CQDs) from rice husk (RH), a globally abundant lignocellulosic residue. The synthesis of CQDs from the abundant agricultural waste RH represents a significant advancement in sustainable materials science. The RH-derived CQDs are highly versatile due to their functionalized surfaces, enabling them to be applied across several critical sustainable domains, including environmental monitoring where they function as highly sensitive fluorescent nanosensors for heavy metal ions and antibiotics, and environmental remediation through the adsorptive removal of organic pollutants. Furthermore, they show great promise in agri-tech, enhancing key metrics like seed germination and root growth, as well as in energy applications as efficient components in photocatalysis and optoelectronic devices.

Keywords: Green Nanotechnology, Rice husk, Carbon quantum dots, Agricultural waste, Advanced material

2nd International Conference on Multidisciplinary Sciences and Technological Developments (ICMUSTED 2025)

December 12-15, 2025

Biochar Amendment and PGPR Inoculation Improve Growth, Nutrient Uptake, and Soil Fertility in Millet

Asma Dahani[1], Elmostapha Outamamat[1], Khalid Oufdou[1], Loubna El Fels[1]

[1]Unit of Microbial Biotechnologies, Agrosciences, and Environment, Laboratory of Water Sciences, Microbial Biotechnologies, and Natural Resources Sustainability, Faculty of Sciences-Semlalia, University Cadi Ayyad, 40000 Marrakech, Morocco

Corresponding author: Asma Dahani (e-mail: asmadahani@gmail.com)

Abstract

The degradation of soils and the loss of fertility pose significant challenges for sustainable cereal cultivation, especially in arid and semi-arid regions. Reliance on chemical fertilizers has intensified soil deterioration and environmental impacts, highlighting the necessity for sustainable and eco-friendly agricultural practices. Biochar addition and inoculation with plant Growth-Promoting rhizobacteria (PGPR) have gained attention as strategies to simultaneously enhance soil quality and crop performance. This study investigated the combined effects of biochar and a bacterial consortium on millet (*Pennisetum glaucum L.*) growth and soil fertility. Soils were amended with biochar and inoculated with a consortium including Actinobacteria *(A4)* and bacteria (*B1)*. Plant growth indicators, including height, root and shoot biomass, along with physiological traits such as chlorophyll content and photosynthetic efficiency, were recorded. Soil physicochemical properties were also analyzed to evaluate improvements in fertility. The findings revealed a pronounced synergistic effect between biochar and PGPR treatments. Millet plants receiving the combined amendment showed significant improvements, with growth increasing by 91% and biomass by 110% relative to the untreated control. Nutrient uptake was markedly enhanced, accompanied by notable gains in soil fertility indicators: organic matter increased by 88.23%, available phosphorus by 6.94%, and total nitrogen by 36.38%. These results highlight that the integration of biochar and PGPR inoculation provides an effective and sustainable strategy to enhance millet productivity and rehabilitate soil health, contributing to more resilient agroecosystems in arid and semi-arid regions.

Keywords: Degraded Soil, PGPR, Fertilizer, Millet, Plant development, Biochar

Mapping the Physico-Chemical and Microbiological Characteristics of Olive Mill Wastewater Across Morocco: Advancing a Waste-to-Resource Circular Strategy

Oumaima Dahbane[1], Mohamed Hafidi[2], Mohammed Rhazi[3], Youness Bouhia[1]

[1]Unit of Microbial Biotechnologies, Agrosciences, and Environment, Laboratory of Water Sciences, Microbial Biotechnologies, and Natural Resources Sustainability, Faculty of Sciences Semlalia, University Cadi Ayyad, 40000 Marrakech, Morocco
[2]African Sustainable Agriculture Research Institute (ASARI), Mohammed VI Polytechnic University (UM6P), 70000 Layoune, Morocco
[3]Interdisciplinary Laboratory in Bio-Resources, Environment and Materials, Higher Normal School, Cadi Ayyad University, 40000 Marrakesh, Morocco
Corresponding author: Oumaima Dahbane (e-mail: o.dahbane.ced@uca.ac.ma)

Abstract

Olive mill wastewater (OMWW) represents one of the most challenging environmental pollutants in Mediterranean olive-producing countries due to its high organic load and phytotoxic compounds. Morocco, ranked among the top global olive oil producers, generates large volumes of OMWW every extraction season, yet limited data exist on the variability in its characteristics according to processing practices and regional agro-ecological conditions. In this study, OMWW samples were collected from five major olive-oil-producing regions in Morocco during the 2024–2025 extraction campaign. A comprehensive physicochemical and microbiological characterization was carried out to identify the key factors influencing OMWW composition. The analyses included pH, electrical conductivity, total organic carbon, chemical oxygen demand (COD), biological oxygen demand (BOD), polyphenol concentrations, and solid content. Microbiological assessment comprised total aerobic mesophilic bacteria counts and fungi, and isolation of culturable strains for further investigation. The results revealed substantial variability among regions, highlighting the influence of olive cultivar, climate, and extraction systems (two-phase vs. three-phase) on OMWW quality. Higher COD, polyphenols, and acidity were generally linked to three-phase systems, while two-phase systems resulted in more concentrated organic loads due to reduced water consumption. Microbial diversity also varied, indicating different potentials for biological valorization depending on local operating conditions. This dataset provides the first step toward mapping OMWW quality indicators across Moroccan production basins, offering valuable insight for national strategies on waste valorization and environmental protection. Understanding regional variability is essential for designing tailored management approaches, such as composting, anaerobic digestion, and soil amendment; thereby promoting the circular integration of OMWW into sustainable agriculture. Our findings support improved decision-making for both environmental agencies and the olive-oil sector, contributing to responsible waste management in alignment with circular economy goals.

Keywords: Olive mill wastewater, Physicochemical and microbiological characterization, Regional variability, Morocco, Sustainable waste management

2nd International Conference on Multidisciplinary Sciences and Technological Developments (ICMUSTED 2025)

December 12-15, 2025

Key Scoring Models Used for Performance Evaluation of Employees: A Systemic Review and Its Applicability in the Albanian Banking Sector

Sllavka Kurti[1], Katerina Vasili[1]

[1]Department of Management, University of Tirana, Tirana, Albania
Corresponding author: Katerina Vasili (e-mail: katerinavasili01@gmail.com)

Abstract

Every manager, despite the industry has the responsibility to assess and evaluate the employee's performance. However, this process is often based on incomplete and subjective information about an employee's contributions, whether as an individual or as part of a team. Therefore, it impacts the employee's development, motivation affecting the organizational performance in general. This challenge becomes even more critical in environments with high employee turnover, where managerial decisions regarding performance assessments, identification of improvement areas, and delivery of constructive feedback play a vital role in retaining talent, sustaining staff motivation, and enhancing organizational outcomes. This article aims to identify and compare the main models used in the employee performance evaluation process that include scoring and other objective forms of measurement of the performance. By taking into consideration recent developments in technology as well as previous existing scoring models, it would be beneficiary to assess and compare the benefits and suitability for using these models in different industries. Furthermore, this article has explored through semi structured interviews the current performance evaluation models of the back-office employees in the Albanian banking sector, aiming to determine if there is any methodology or approach towards performance evaluation in the back office and whether it uses objective information to assess employee performance. There have been considered models such as multi criteria decision making approach, fuzzy approach, behaviorally anchored rating scale (BARS), graphic rating scale and weighted point systems. The characteristics of these methods are evaluated and compared to each other in order to determine their main strengths, weaknesses and suitability in assessing back-office employees. This comparison should assist future research regarding performance evaluation practices. Thus, this exploratory comparative study aims to give a perspective and a reference for further research and implementation of scoring models that are based on measurable and objective indicators, making the decision of managers easier and further impact on the staff retention and overall organizational performance.

Keywords: Performance appraisal, Scoring models, Fuzzy approach, Multi-criteria decision making, BARS

1. INTRODUCTION

In most industries, particularly those in the service sector, human resources (HRs) constitute the organization's most valuable assets. High-performing organizations recognize the diversity, capabilities, and potential of their workforce as key sources of competitive advantage. Within this context, performance evaluation becomes a critical managerial function, as it directly influences the effective utilization and development of HRs. In creating and implementing an appraisal system, management must determine what the performance appraisal system will be used for and then decide on the process to implement the system. The methods selected and the instruments used to implement them are crucial in determining whether the organization manages its performance successfully [1]. Employee performance is an essential part of this analysis, as they influence or participate in all the activities carried out within companies [2]. Performance evaluation is central to personnel management within organizations, with objectives that span from diagnosing performance gaps to conducting comprehensive assessments of employee contributions. These evaluations are paramount in decision making regarding bonuses, dismissals, or development of skills [3]. According to Poddar and Chattopadhyay predicting employee performance and productivity is essential for organizational success [4]. High-performing personnel contribute substantially to attaining companies' objectives, boosting performance, and productivity, and upholding a competitive edge in the marketplace. Nevertheless, conventional performance assessment approaches frequently depend on subjective evaluation, which can be impacted by inconsistent standards, individual biases, and limited data. Choi and Choi assert that these shortcomings hamper companies from making accurate predictions regarding workers' performance and inhibit their capability to make informed choices concerning talent management and resource allocation [5]. Therefore, it is of utmost importance for a more data-driven approach to employee performance prediction. Shortcomings in traditional performance assessment techniques have become apparent

over time. Subjective assessments, such as supervisor annual performance appraisals or ratings, lack objectivity and may not take into consideration all relevant components impacting employee performance [6]. Furthermore, these methods frequently suffer from biases, encompassing leniency or halo implications, where a comprehensive impression of an employee impacts ratings across distinct performance dimensions. Such biases can lead to inaccurate evaluation and misalignment between actual performance and perceived performance [7].

On the other hand, scoring models offer a more objective, quantitative approach that provides managers with more realistic and consistent results during the performance evaluation process. However, certain qualitative aspects must still be considered, particularly those related to an employee's potential and characteristics that may fall outside the scope of scoring models. Considering that the scoring models evaluate only certain aspects of the employee performance, they tend to leave out some important aspects of it. While some models tend to be more holistic, each one presents specific advantages and disadvantages that organizations must consider during implementation, to avoid any biases or malfunctions in the overall appraisal process which could lead to negative organizational consequences. In the era of artificial intelligence, there have been further integration of these models into systems that provide real time feedback, objective analysis, and also provide predictive insights regarding performance appraisal. However, the machine learning techniques are based on these traditional forms of evaluation, and are further developed by additional data collected. Therefore they are left out of the scope of this study, in order to focus on the main characteristics of the main scoring techniques.

2. LITERATURE REVIEW

As organizations aim to monitor the job performance of their employees through systematic evaluation processes, high-performing individuals are generally recognized and rewarded, while lower-performing employees may be subject to remedial measures. There is no element in performance appraisal that is more important than an impartial and accurate appraisal of his/ her contribution. Unfortunately, despite all advancements in research and technology the number of organizations using an effective performance appraisal system is limited [8].

Performance appraisal systems need to be effective in improving or sustaining employee performance, otherwise they are a tremendous waste of time and money spends on development and implementation. Although most organizations have adopted methods for appraisal, their effectiveness is still a matter of concern.

There has been vast research on the performance evaluation field, while the quantitative methods have been developed mostly in the recent years [1]. In overall performance evaluation is characterized by a thorough analysis of the employee and of his/her respective performance in the job position. This process plays an important role for the company to identify problems or disruptions, including problems in supervision and adaptation of people in their positions lack of motivation of employees, and failure to take advantage of skills [9]. To provide these various benefits, performance evaluation must be correctly applied, and the use of efficient techniques and tools for each scenario is important [2].

However, many organizations do not use the systematic way to evaluate the performance of their employees that makes the evaluation method inconsistent and often inefficient. Therefore, developing a systemic approach is necessary as well as regular use of the methodology use in order to have the adequate data and regularly updated information for each employee. Yet organizations must use a set of indicators to determine the performance of an employee, which makes the process complex and criteria changes depending on the job process and industry [1]. Despite the importance of the qualitative analysis of certain factors of the employee performance, it is still necessary to enhance the decision making through structured data in accordance with the organizational priorities, predefined by the employer or the manager through certain models that come in handy whenever defining the methodology to be used in the performance evaluation. Certainly, there are multiple scoring models that can be considered by organizations when defining the methodology to be used for performance evaluation. The selected criteria are also based on the industry and certain job-related specifics in each institution. On this study there are considered several main scoring models well-known and used worldwide by organizations.

2.1. Multicriteria Decision Analysis

The multi-criteria decision-making (MCDM) strategies have been used for the evaluation of employee performance taking into account various criteria. Over the past years, numerous quantitative and subjective methodologies have developed. However, the research [10] and [11] provide ample evidence of the significance of staff performance evaluation and its connection to the performance of the company. The use of MCDM methods provides tools able to support the decision-making process through recommendation of actions to the one responsible for making decisions [12]. It is a technique that combines the output of alternatives with a variety of

conflicting, qualitative, or quantitative parameters, resulting in a consensus-based solution [13]. When applied to performance evaluation, these methods prove to be significant in identifying points of improvement, enabling development of skills in personnel in the organizations [14].

The multi criteria decision approach (MCDA) methods are necessary whenever certain aspects to be evaluated have different metrics and use different criteria. The MCDA methods clarify the subjectivity that is present in any decision process. The objectives are combined through the subjective evaluation of the decision maker, who incorporate his preferences into the model. The MCDM includes itself different methods that can be applied depending on the context and decision-making needs. Ishizaka propose three main groups of MCDA methods such as the full aggregation approach, outranking approach and the goal, aspiration, or reference level approach [15].

Concretely, in the full aggregation approach, each criterion has a score and these are then synthesized into a global score, thus assuming compensation among them. In the outranking approach, there is no compensation, but there may be incomparability among the criteria. In this approach, two options may have the same score, but their behavior may be different and therefore incomparable. And lastly in the Goal or reference level approach method are identified the alternatives based on their closeness to a defined reference [2].

The analytic hierarchy process (AHP) and technique for order preference by similarity to ideal solution (TOPSIS) methods are both applied to problems of classification and choice, and they are very popular in the MCDA [16]. The TOPSIS method has a goal, aspiration, or reference level approach, in which the alternatives are compared to the solution understood to be ideal. In contrast, the AHP has a full aggregation approach, generating a score from pair-by-pair comparisons among the alternatives. [17] indicate that one of the advantages of the AHP is admitting subjectivity as an intrinsic part of the decision-making process. According to [18], TOPSIS stands out through its adjustment to problems with a large number of criteria and alternatives, especially with quantitative criteria [19].

2.2. Fuzzy Logic

Fuzzy logic uses approximation rather than exact reasoning, due to the human nature in reasoning being of an approximate nature. This method has been applied to several performance appraisal systems and it is based on the multi-criteria assessment that deals with imprecision, and subjectivity in evaluating performance by assigning degrees to linguistic variables. It allows for approximate reasoning, enabling systems to incorporate expert knowledge and human-like inference to evaluate complex systems where precise mathematical models are difficult to define, leading to more flexible performance assessments [20]. This methodology is a good model for a transparent and fair multi-criteria performance evaluation in different organizations [21].

When applying fuzzy set theory to fuzzy group decision support system, it assists the decision maker to make better decisions and recommendations under different circumstances and alternatives. The multifactorial evaluation model is proposed for the application of the fuzzy logic theory to a decision-making process in information, decision, and control systems. The reviewed works on fuzzy approach support the fuzzy logic theory as a conceptual framework for use in the development of the performance appraisal system because fuzzy logic theory allows performance appraisal system to be developed by using fuzzy variables and relationships [22].

Fuzzy logic helps to find the performance index of an individual if the company's performance data and rating based on judgment are available and reduce subjectivity. The whole process of using the Fuzzy approach uses three main steps that are non-linear using a set of input data to generate a scaled output, providing a means to represent uncertainties, and deals with problems in a vague environment of perception of things and human thinking [22]. These steps include the Fuzzification, using membership function to graphically describe situation in environment, where a set of input data are gathered and converted to a fuzzy data set using fuzzy linguistic variables, fuzzy linguistic terms and membership functions. The membership states all information contained in a fuzzy set. Membership functions of fuzzy sets must be precisely defined in respect of function type and function parameters. Both the parameters and shape of the membership functions strongly influence the accuracy. Furthermore, rules are evaluated, these systems use "if-then" rules, similar to human reasoning, to connect these fuzzy variables. The last step is defuzzification, generating output data or actual results, the resulting fuzzy output is mapped using the membership functions.

The fuzzy logic theory has been applied in various fields with keywords "performance," "evaluation," "severity," "possibility," "importance," and "satisfaction," but their meaning varies with the situations [23]. A fuzzy set contains elements that have varying degrees of membership in the set. This fuzzy logic theory transforms linguistic variables into fuzzy sets to replace the crisp sets. The values of linguistic variables are not just numbers, but verbal

variables or sentences in a natural or artificial language. The fuzzy concept is very useful in complicated situations to be appropriately described by quantitative expressions.

2.3. Behaviorally Anchored Rating Scale (BARS)

BARS stands, a tool that assesses employee performance by linking specific behavioral examples to different levels on a rating scale and focuses on traits for progressive performance [24]. It is not random that the BARS method has remained resilient throughout the course of time and continues to be researched still. The literature on best practices in performance appraisal continues to suggest the use of a behavioral anchor format, particularly the BARS method, and the discussion involving its resiliency should provide some insights into why it is recommended. However, there are several issues which need to be addressed if this method is to do well in the future, such as its limitations, challenges, and an existing research gap [25].

The BARS method combines both the work behavior of an employee with the personal traits [26], focusing on employee traits such as devotion, work processes, and employee work efficiency, emphasizing the quality and quantity of work and employee behavior at work [25]. In this method, the vertical behavior scale for each work indicator consists of 5-10 and each dimension is arranged based on an anchor [25].

When using BARS method for assessing employee performance, the input of HRs specialists, supervisors and employees is essential in determining the anchor for the indictors which will be given an assessment ranging from 1-5 on each anchor. The indicators are extracted from the aspects that affect the job performed by the employee such attendance, collaboration, innovation, automation of processes, compliance, responsibility, etc. Anchor itself is a detailed description of a person's behavior that shows performance on each indicator criterion. The anchor criteria in question are a person's attitude or behavior that reflects himself in doing a job to produce performance for the organization or company [27]. Rating is an assessment described in the form of numbers, ranging from 1 (very high), 2 (high), 3 (sufficient), 4 (low), and 5 (very low) [25].

Despite job-related specifics, BARS method usually consists of five to ten vertical scales. Scales represent a certain aspect of the performance that is important for doing the job accordingly. Additionally, each scale is anchored to at least five critical events that reflect highly effective to highly ineffective job behaviors relevant to the aspect under consideration [28]. Scale values are assigned to the critical incidents, which correspond to the approximate degree of effectiveness with the highly effective behavior being assigned the highest value on the scale. The major performance dimensions for a job and the critical incidents for each dimension are identified through job analysis by future scale users (e.g., employees actually performing the job and their managers), who are expected to be thoroughly knowledgeable about the job [29]. In developing critical incidents, the emphasis is on incorporating job related behaviors that are observable and reflect various levels of desirable performance [27].

However, using BARS for assessing employee performance, requires continuous updates as there are continuous changes required for different job positions throughout time as well as a well-defined assessment process based on the analysis of the individual employee [27]. In the BARS method, development is usually carried out by people who are experts and know the work and requirements in the field of HRs, resulting in more accurate job performance. Furthermore, the result generated from the assessment is used for giving feedback to employees, therefore the existence of critical events will make it easier for ratings to be assessed. Critical incidents generally start from 5-10 into performance dimensions that are related to each other [27]. They are used in the scale should be considered carefully for their relevance to the position being assessed, so that the standard of assessment will be clear [25].

The BARS method is widely used for a long period of time as it is a reliable source, including the perspective of different appraisers. By anchoring scales to concrete behaviors, BARS minimizes the subjective interpretations that can occur with traditional appraisal methods, while employees gain a clearer understanding of what constitutes good, average, or poor performance through detailed behavioral examples [30].

2.4. Graphic Rating Scale

Graphical rating scales are the most frequently utilized method for performance reviews in most enterprises [31]. This method is included in the method that is easy to develop and easy to modify if it is necessary to change the criteria that become the assessment material [32]. In this aspect, a graphic rating scale involves a performance appraisal evaluation checklist. A graphic rating scale as an appraisal method, often lists the key behavioral traits needed for the job including communication, teamwork, attentive towards details, etc. Managers evaluate the employees based on numerical or descriptive scales. The scale contains clear labels, such as numbers (1 to 5) or

short phrases (“Exceeds expectations,” “Meets expectations,” “Needs improvement”). The rating of employees, makes it easier to determine how someone is performing in each area and compare employees across the board [32].

The graphic rating scales use in different industries ensures the managers and employers that they are making informed decision regarding employee performance including here rewards and salary increases, promotions, identification of areas for training as well as improvement plans for each employe. They also enable the collection of quantitative and objective data to the HR managers especially to skills related to their job position and responsibilities [32]. This method assess performance continuously and is a straightforward way for managers to assess employees and identify their strong qualities or the areas that need improvement. Rating scales are more flexible, not only to measure attitudes but can also be used to measure respondents’ perceptions of environmental phenomena, such as scales to measure social status, economy, knowledge, abilities, and others [33].

In order to implement graphic rating scale as a method for performance evaluation is important to evaluate job-related criteria that is paired with certain performance values, while same as in BARS method a scale is used to rate scores for each attribute. The scale consists of specific responses, such as “Unlikely,” “Hard to say,” or “Likely”, while the evaluator selects the option that best reflects the employee’s behavior or performance. However, the scale should be considered carefully as it may not capture the importance of certain traits or behaviors for specific roles, leading to an incomplete assessment.

Graphic rating scales can change and adopt to different roles within an organization, completing the needs in different areas that need an objective evaluation method. The scales can also vary appearance, based on the specific condition of different structures and departments in the organization. Common formats include numerical rating scale, color-coded rating scale, often corresponding with traffic light scale or word or comment-based rating scale can be used [34].

2.5. Weighted Point Systems

The last method chosen is the weighted point system. As it is already noted, throughout time there have been developed different methodologies using different criteria, in order to fit in an inclusive model, the results of unbiased evaluation of employee performance.

HR managers and supervisors use weighted averages in HRs performance appraisals to evaluate all aspects of an employee’s performance with respect to the importance each factor has to the business. and these weights may not be equally aligned across companies or even industries. However, companies understand that all performance factors are not equally important and use weighted averages in HRs performance appraisals to obtain a better, more-rounded picture of the employee and his or her successes and failures.

Weighting can be used to emphasize the performance elements an organization considers most important for each position.

3. METHODOLOGY

This study adopts a comparative qualitative methodology to identify and analyze the main models used in employee performance evaluation, with a particular focus on scoring techniques and other objective measurement approaches. The research first examines existing models discussed in the literature, including MCDM, fuzzy approaches, BARS, graphic rating scales, and weighted point systems. These models were assessed and compared based on their methodological characteristics, degree of objectivity, and applicability across different industries, taking into account recent technological advancements that influence performance measurement practices.

To complement the theoretical analysis, the study also investigates the current performance evaluation methods applied in the Albanian banking sector, specifically for back-office employees. This empirical component is based on 36 semi-structured interviews conducted with HRs professionals and employees across five major banks operating in the country. The interviews aimed to determine whether structured methodologies are used for back-office performance evaluation and to what extent objective criteria inform these assessments. The qualitative data were analyzed thematically and revealed that banks primarily rely on managerial feedback, with limited use of objective scoring models such as a Likert-scale weighted point system in one bank and 360-degree feedback in another. These findings were then compared with the theoretical models to evaluate their strengths, weaknesses, and suitability for back-office roles in the banking industry.

4. COMPARISON BETWEEN MODELS

In comparing among models, it is essential to previously determine the applicability of the model considering the industry, the ability to measure processes, the organizational culture, and other factors related to the expected outcomes. In the following assessment of main strengths and weaknesses of each model are considered under their applicability in the banking system and more specifically in the back-office employees. Below is made a summary of the main methods identified by the literature noting the key strengths and weaknesses of each model.

Table 1. Fuzzy approach

Fuzzy Approach	
Strengths	Weaknesses
The structure of fuzzy logic systems is understandable and straightforward Fuzzy logic uses approximation rather than exact reasoning, due to the human nature in reasoning being of an approximate nature. Fuzzy systems are suitable for uncertain or approximate reasoning, especially for the system with a mathematical model that is difficult to derive. Fuzzy logic allows decision making with estimated values under incomplete or uncertain information. Fuzzy logic makes a prediction method to predict a future event.	When creating a fuzzy system, deciding on the membership function and basic rules is challenging. The flaws in the rules decided, might generate unacceptable results. The use of fuzzy logic may become an obstacle to the verification of system reliability, while it might have imprecision, and vagueness, but not uncertainty [35]. Requires tuning of membership functions Fuzzy Logic control may not scale well to large or complex problems.

Table 2. BARS

BARS	
Strengths	Weaknesses
The BARS method combines both the work behavior of an employee with the personal trait The BARS development process appears to be flexible The process utilized in developing BARS tends to ensure that covers the entire performance domain of a job and include all major job dimensions based on an extensive job analysis The BARS instrument is developed by the actual users and appraisers and appraisees themselves The involvement of employees in the BARS development process should instill a strong sense of fairness among the employees [29].	The implementation of BARS method can be challenging and time-consuming as it requires significant effort to develop specific behavior descriptions for each performance criterion. In organizations that have a large number of roles and the job description of employees are changing fast, makes it difficult to implement BARS. Also, BARS is not fit for all types of jobs and roles as it is based on observable traits that are specific. Some aspects of performance, such as creativity or problem-solving, may be difficult to evaluate using BARS.

Table 3. Graphic rating scales

Graphic Rating Scales	
Strengths	Weaknesses
This method ensures the identification of trends and developments of the employee performance in the organization. It makes it easier for the manager to identify the top performing employees and areas of improvement or that need more training. Using uniform option to evaluate every employee makes it more objective to assess them accordingly as it would be with detailed descriptive feedback. The implementation if graphic rating scales is easier compared to other methodologies as certain aspects under assessment are applicable across roles in the organization.	The interpretation of the scales is different for different employees and managers as some of the managers would see some aspects as granted for the job and some others as a skill to be appreciated. One of the most common biases of this method is the “halo effect,” which highlight only certain aspects that are very strong points for an employee leaving out some very important details related to doing the job. Employees can have certain strengths and areas for improvement that don’t fit into the established criteria. Averaging data where an employee that scores extreme ends is valued the same as the one that scores average.

Table 4. Weighed point systems

Weighed Point Systems	
Strengths	Weaknesses
The weighed point system makes subjective data measurable as it returns information into scores. The scoring system provides a clear and measurable performance, leading to an easier decision-making and communication of the progress to the employee. The model is flexible and can be adapted to different roles, departments, or types of goods and services.	The system is still subjective because the weights and scoring criteria are set by people and can be influenced by biases. The implementation of it for a certain role might not be applicable across positions within organization. When the scoring systems are used to rate employees and evaluate them in general, it leads to higher level of competition within the department, leading to a potential non-functional team.

As presented above, each of the methods faces certain challenges especially for its implementation, while some other methods are considered as rather simpler, while the results can have large biases. However, one of the main points identified in performance evaluation research is that the subjectivity is present despite the method. The assessment of each job position and determining key performance indicators is generally a difficult task that cannot avoid the subjectivity, as well as it cannot reach to the full extent the job position, otherwise the methodology would be too specific and too hard to be used and assessed by all the interested parties.

However, certain methods are more applicable than others. For instance, the BARS is among the most widely used methodologies for performance evaluation and has been adopted across many industries for decades. Despite its popularity, it requires considerable time and effort to develop and implement effectively. On the other hand, graphic rating scales are easy to use but they leave out significant information that is necessary for the evaluator. Despite all the advantages and disadvantages of each methodology, they still ensure that the institution has some objective and preset ways of assessing the performance of their main assets in the organization and whether they are performing accordingly or additional training or motivation is needed.

In the banking sector, assessing the performance of back-office employees remains a significant challenge, as job descriptions and organizational structures are continually evolving in response to market pressures, technological advancements, and increasing regulatory requirements. Thus, the performance evaluation of employees often remains to simple feedback from the manager and 360 degrees feedback including other employee's perspective. Yet, with the technology advancements it is expected that these institutions implement methods like fuzzy approach or BARS to have a more realistic and objective approach towards their main assets, as well as reduce turnover in the experienced employees.

As highlighted in the literature and the comparison among methods the most sophisticated methods used for performance appraisal are Bars and Fuzzy approach as part of the multi criteria decision making method. On the other hand, graphic rating scales and weighted point systems can also be used as they are easily implemented, while they risk on creating very competitive and toxic environments. This challenge risks on creating non functional teams and thus less cooperating departments, leading to potential exposure of the way of doing business, while the front-office employees that often strongly rely on the processes performed in the back might be exposed to non-functional teams, therefore non-supportive processes.

5. CURRENT LANDSCAPE OF THE ALBANIAN BANKING SECTOR

Currently the Albanian market is facing significant issues with the lack of HRs and specialized workforce, the Albanian banking sector has also been affected by these developments, facing a very high turnover of employees, being one of the main topics discussed by the Central Bank as well as main economy forums in the country. However, as pointed out through 36 semi structured interviews with HRs and employees of five of the banks operating in the country it was noted that the methodologies applied by the banks are mainly related to feedback given by the manager for the employee, 365 degree feedback in one of the banks and a weighted point system consisting on 5 general questions rated in a Likert scale, where the manager gave the opinion on the performance of the employee based on the group of question that was rather not specific.

Table 6. Five general questions rated in a Likert scale

Banks	Employees of HR	Back-Office Employees	Front Office Employees	Have Worked in Front and Back Office	Average Experience in Banking
5	6	12	10	8	6.8 years

From the HR employees it was noted that the main focus in evaluating performance is on the front-office employees, which reward system is based on bonuses, therefore their performance is measured in a more structured way, defining a set of objectives and targets to be measured generally in a quarter, that in proportion of its completeness the reward is given. Further, for the back-office employees, it is more difficult to generalize the key performance indicators (KPIs) as the tasks performed are different for each job position, therefore little to no standardization exists. The general way of evaluating performance is based on the direct feedback from the manager, while for the bank that has implemented the 365 degrees feedback it is also considered the self-evaluation as well as the feedback requested by other employees that directly collaborate with the employee whose performance is being evaluated. Despite the efforts, the evaluation remains at a qualitative and descriptive level, where there is no measurable information that has been documented overtime in order to determine the progress, involvements in the development process and overall performance of the employees.

In one of the banks, it is noted a general group effort to standardize the KPIs to be used in evaluating employees, however there are several difficulties faced especially related to the measurement of jobs, and the resistance of the managers towards the changes in methodologies. When asked about the automation of process in the HRs department, the HRs professionals, have assessed that the current department structures have a certain workload that generally doesn't allow the necessary time to assess and ameliorate the processes, while the automation of processes is narrowed to systems that generally gather the general employee information and calculation of leaves and salaries.

As mentioned above in one of the banks it is implemented a 365-degree system where employees do the self-assessment, the managers and other employees give an assessment, regarding a set of general questions regarding work attitude, cooperation and technical skills. This software doesn't make assessments regarding the performance, it gathers the qualitative information on the employee, to be further processed by the manager and the HR department before giving the final assessment to the employee. One of the smaller banks in the market uses general Microsoft Office templates to assess employee performance, given to managers and requested to complete the performance details based on a Likert scale for a 5-question template, followed by a qualitative assessment of the evaluation for each question.

When the employees of the back-office are asked about the overall evaluation process, their general point of view is that the evaluation followed by a reward often follows a certain pattern and it is followed by material and tangible rewards once in a few years, while the relationship with the manager is often determined as a factor that affects significantly the frequency of the evaluation, while the feedback assessment is repetitive at least on yearly basis in all the banks taken into consideration. The feedback is often focused on whether positive or negative results throughout the years based on the material outcome. However, there is little to no key indicators to be measures and assessed as the weight is often not set in any of the models used by the banks. These developments lead to the approach of the employees that often the change of the job position from one bank to another will lead to better financial evaluation and their worth would be fairly appreciated. On the opposite, the employees that often stay stable in their job position are dissatisfied from their employer while the evaluation is often remaining to their appreciation by the colleagues and the manager, often not followed by a financial reward.

This tendency remains to both front and back-office employees, leading to a higher turnover rate into the banking system in general, especially in the recent years. As for the front office employees, they do consider the variable bonus rate received above the preset salary as a tool of evaluating their performance on quarterly and yearly basis. The additional benefits attributed to the standard financial package also serve as a motivation tool to perform and exceed their targeted performance. On the other hand, the target and objective setting for the back-office employees is often not clear, while some job descriptions overlap, leading to different expectations form the employees and the managers. As described by the most senior employees, the training of new and internship employees often is not considered on the daily load, leading to negative feedback received often by the managers, while the workload is maintained for a considerable amount of time by senior employees as the training period is usually long and requires adequate training and time for the new employees to work independently. Additionally, the staff turnover is a leading cause for the remaining employees to require improvement conditions and financial packages as the senior employees have the additional workload caused by the leaving employees and training of the new staff

Another very important insight is given by the employees interviewed that have shifted from working in the front to working in back-office, where the approach towards the evaluation is different, depending on their job position, however, related to the evaluation in the back-office position it is noted that often there is no quantitative analysis of the performance and the evaluation is made at lesser frequencies compared to the evaluation in the front office. Yet, defining of the quantitative measures is challenging and requests a lot of effort to standardize and put the adequate weights that will fit their perception or the manager's. Respectively, both front and back office in banking

have their differences in the nature of the jobs performed, the tasks requested by each employee and the approach towards measurable performance is different. Nevertheless, in some of the banks, employee's performance is evaluated under the same set of questions completed by the managers in the form of feedback or in a short form of Likert Scale questions associated with descriptive feedback to reason the choice for the employee.

One important takeaway from the interviews is that the automation and implementation of software or supporting tools to assess employees, keep track of their progress and their needs for training, for banks is still out of their schedules and that it is often not considered by HR managers or senior managers, while the main challenge is still considered recruitment and onboarding of experienced employees, while the high turnover is often considered as part of a developing market tendency. However, considering the increasing ageing population in the country and emigration leading to a potential brain drain in the country, it is necessary to address the issue of high turnover rates and performance appraisal in the correct way, in order to retain staff within the institution and the market as well. The issue is raised as well by the Central Bank, where the high turnover rates of senior employees have led to a significant loss in the knowledge related to historic events of the institutions and the know-how expertise they had within the organization.

Lastly, the overall perception of the all interviews is that there is a notable discrepancy between the tools used and the desirable methods, however there is little to no effort to make progress throughout these issues. For some of the banks that are part of the international European groups some effort is noted as throughout Balkan economies, the challenge of retaining employees has been present throughout time, while finding experienced employees in the market is being another challenge that requires attention and measures taken in time in order to avoid potential lack of skills within the company or significantly higher costs faced by the banks related to it.

6. CONCLUSIONS AND SUGGESTIONS

Through this article were identified the main scoring models that can be used to evaluate objectively the employee performance in various industry and additionally detect the main strengths and weaknesses for each method. Through this assessment it was pointed out that each of the models faces certain challenges to be implemented and it requires a very well thought process in advance regarding main components that are necessary for the role as well as the behavior and qualities of the employees.

Despite that none of the models leaves out the subjectivity in the process, through formalizing the key objectives and indicators to be evaluated for all the employees continuously, ensures the objectivity in the performance evaluation process. This objectivity often is a base for informed decisions of the management and timely identification of areas for improvement or that need more training.

Through market analysis of the Albanian banking sector and the interviews performed with HR and other employees highlighted the necessity of performing more structured evaluation of employee performance. As some of the banks apply certain forms of performance evaluation, they are mainly focused on subjective input of the manager in forms of feedback, rated questions associated with certain justifications for the choice, however no structured information regarding main aspects of the job and the behavior of the employee are assessed related to key performance indicators.

Additionally, there is limited effort towards automatizing of HR processes in general including performance appraisal. While some banks are trying to make automation at group level, there is little focus on the performance appraisal as well as some resistance that might be faced from managers due to changes in methodologies.

As for the most suitable scoring models to use in performance appraisal of back-office employees, it is noted that implementing BARS or fuzzy approach might lead to more effective and objective evaluation and will make it easier to identify the areas for improvement, despite their difficulties in implementing and making additional effort in identifying the KPIs. On the other hand, both graphic rating scales and weighed point averages are easier to implement and return the subjective information into scored results in order to remove a part of the biases that exist from pure feedback. Yet, they do face challenges when applicable to back-office positions as the results attributed for each role are different and there is little to no similarity between job descriptions among departments. This would require additional assessment and make the evaluation method not standardized.

References

[1] I. Ahmed, I. Sultana, S. K. Paul, and A. Azeem, "Employee performance evaluation: A fuzzy approach," *International Journal of Productivity and Performance Management*, vol. 62, no. 7, pp. 718–734, 2013.

[2] J. Miranda, T. Amaral, A. Amaral, and F. Amaral, “Multicriteria decision model for employee performance evaluation,” *Revista de Carreiras e Pessoas*, vol. 14, no. 1, pp. 33–59, 2024.
[3] H. A. Hijazi, “The impact of applying good governance principles on job satisfaction among public sector employees in Jordan,” *Open Journal of Business and Management*, vol. 9, no. 1, pp. 1–31, 2015.
[4] A. Poddar and S. Chattopadhyay, “A proposed theory for predicting employee performance using machine learning,” in *Interdisciplinary Research in Technology and Management*, S. Chakrabarti, R. Nath, P. K. Banerji, S. Datta, S. Poddar, and M. Gangopadhyaya, Eds. London: CRC Press., 2021.
[5] Y. Choi, M. Choi, M. Oh, and S. Kim, “Service robots in hotels: Understanding the service quality perceptions of human-robot interactio,” *Journal of Hospitality Marketing & Management*, pp. 613–635, 2020.
[6] F. Fallucchi, M. Coladangelo, G. Giuliano, and E. W. D. Luca, “Predicting employee attrition using machine learning techniques,” *Computers*, vol. 9, no. 4, art. no. 86, 2020.
[7] M. D. R. Hassan, R. K. Ray, and F. R. Chowdhury, “Employee performance prediction: An integrated approach of business analytics and machine learning,” *Journal of Business and Management Studies*, vol. 6, no. 1, pp. 215–219, 2024.
[8] P. W. Team, *Performance Appraisal and Organizational Performance (A Survey of Selected Banks in PH)*, Project Clue, 2025.
[9] C. Gil, *Gestão de Pessoas: Enfoque nos Papéis Profissionais*, 2014.
[10] M. Kilduff, R. Angelmar, and A. Mehra, “Top management-team diversity and firm performance: Examining the role of cognitions,” *Academy of Management Journal*, vol. 11, no. 1, pp. 21–34, 2025.
[11] M. Higgs, U. Plewnia, and J. Ploch, *Influence of Team Composition on Team Performance and Dependence on Task Complexity*, Henley Management College, 2003.
[12] C. F. S. Gomes and H. G. Costa, “Using prospective vision and multi-criteria decision analysis with scenario planning,” *Relat. Pesqui. Eng. Prod.*, 2013.
[13] U. Zaremba, “Does the industry matter? Airline bankruptcy prediction,” in *Proceedings of the Springer Conference*, 2019.
[14] F. C. Zamcopé, L. Ensslin, S. R. Ensslin, and A. Dutrs, “Modelo para avaliar o desempenho de operadores logísticos: Um estudo de caso na indústria têxtil,” *Gestão & Produção*, 2010.
[15] P. Ishizaka and A. Nemery, *Multi-Criteria Decision Analysis: Methods and Software*, John Wiley & Sons, 2013.
[16] M. Cinelli, M. Kadziński, M. Gonzalez, and R. Słowiński, “How to support the application of multiple criteria decision analysis? Let us start with a comprehensive taxonomy,” *Omega*, 2020.
[17] L. V. Lemos, M. A. L. Freitas, and A. S. Tenório, “Método AHP: Emprego no financiamento do fluxo de caixa de uma companhia de saneamento básico,” *Revista de Administração de Roraima-RARR*, vol. 9, no. 2, pp. 157–174, 2019.
[18] L. C. R. Carpinetti and J. F. R. Lima, “A comparison between TOPSIS and fuzzy-TOPSIS methods in supporting multi-criteria decision-making for supplier selection,” *Applied Soft Computing*, 2015.
[19] L. Wang, Y. Ali, S. Nazir, and M. Niazi, “ISA evaluation framework for security of internet of health things system using AHP-TOPSIS methods,” *IEEE Access*, vol. 8, pp. 152316–152332, 2020.
[20] R. C. Jing, C. H. Cheng and L. S. Chen, “A fuzzy-based military officer performance appraisal system,” *Applied Soft Computing*, 2007.
[21] C. Moon, J. Lee, C. Jeong, J. Lee, S. Park, and S. Lim, “An implementation case for the performance appraisal and promotion ranking,” in *IEEE International Conference on Systems, Man and Cybernetics*, 2007.
[22] C. Ardil, “Applying fuzzy logic theory to performance management,” in *2nd World Conference on Technology, Innovation and Entrepreneurship*, Istanbul, Turkey, 2017, pp. 153–161.
[23] R. S. Yadav and V. P. Singh, “Modeling academic performance evaluation using soft computing techniques: A fuzzy logic approach,” *International Journal on Computer Science and Engineering*, vol. 3, no. 2, pp. 676–686, 2011.
[24] B. J. Waithanje and E. N. Mandere, “Influence of behavioral anchored rating scales on employee performance at Kenya Commercial Bank,” *The International Journal of Business & Management*, vol. 8, no. 9, 2020.
[25] O. Y. A. Sari, K. Satriawan, and A. Hartiati, “Analysis of employee performance appraisal using the behaviorally anchored rating scale method at CV. BBC,” *American International Journal of Business Management*, vol. 7, no. 8, pp. 218–225, 2024.
[26] G. Dessler, *Human Resource Management*, 13th ed., Boston, MA, USA: Pearson Education, 2013.
[27] J. A. Carpini, S. K. Parker, and M. A. Griffin, “A look back and a leap forward: a review and synthesis of the individual work performance literature,” *Academy of Management Annals*, vol. 11, no. 2, 2017.
[28] G. Bohlander and S. Snell, *Managing Human Resources*, Boston, MA, USA: Cengage Learning, 2012.

[29] S. C. Debnath, B. B. Lee, and S. Tandon, "Fifty years and going strong: What makes behaviorally anchored rating scales so perennial as an appraisal method?," *International Journal of Business and Social Science*, vol. 6, no. 2, pp. 16–25, 2015.
[30] PwC, *PwC's Global Compliance Survey*, Ireland, PwC, 2025.
[31] A. Woods, "Subjective adjustments to objective performance measures: The influence of prior performance," *Accounting, Organizations and Society*, vol. 37, no. 6, pp. 403–425, 2012.
[32] K. Anugrah and I.Ujianto, "Employee assessment applications using the graphic rating scale and profile matching methods at XYZ University," *Journal of Development Research*, vol. 5, no. 2, 2021.
[33] M. Darmanto, S. Sulistiowati, and J. Lemantara, "Design and construction of an application for feasibility analysis of establishing Indomaret using the analytical hierarchy process method and graphic rating scale for CV Sigma Sukses Kreasi," *Journal of Accounting Information Systems and Computers*, 2016.
[34] S. Jay, *Graphic Rating Scale: Pros, Cons, Examples, and Best Practices*, *AIHR*, 2025.
[35] M. Masoumi, S. Hossani, F. Dehghani, and A. Masoumi, "The challenges and advantages of fuzzy systems applications," *A Preprint*, 2020.

2nd International Conference on Multidisciplinary Sciences and Technological Developments (ICMUSTED 2025)

December 12-15, 2025

Albania's Perspective in Fighting High-Level Corruption Compared to Bulgaria, Before the Technical Closing of EU Accession Negotiations

Anila Shehi[1]

[1]Department of Public Law, University of Tirana, Tirana, Albania
Corresponding author: Anila Shehi (e-mail: adollani@gmail.com)

Abstract

Reflecting Albania's aspiration to complete the technical negotiation process by the end of 2027, Albania currently demonstrates stronger progress in tackling high-level corruption compared to Bulgaria two to three years before completing its technical negotiations. The comparison is made with Bulgaria, which (together with Romania), is one of the second-to-last two states that joined the European Union (EU). In the context of EU's enlargement, in addition to the fight against corruption and organized crime, a special attention is dedicated to the corruption of high-ranking officials. The demands that EU is putting on Albania, are giving a pushing force to the special investigative entities. Based on several statistics and international reports, it is generally perceived that the corruption risk in Albania is very high, mostly consisting of the misuse of state resources. In a comparative perspective, the corruption in Bulgaria was addressed more generally, as "serious corruption" or "widespread corruption" and there was a lack of a track record at the high-level. The concept of "high-level corruption" for Bulgaria first appeared clearly in the European Commission's reports after the technical closing of the negotiations. The objective of this research is to analyse the comparison between Albania's and Bulgaria's level of effective efforts to detect high-level corruption, two to three years before the technical closing of negotiations. Albania's position (42) in Corruption Perceptions Index, as candidate country, reflects recent improvements. Bulgaria's position (43) in Corruption Perceptions Index reflects that despite being an EU Member State since 2007, indicates that it continues face challenges related to state capture and weak accountability. The similarity in their rankings, despite their different statuses, suggests that EU membership alone does not automatically ensure progress in reducing corruption.

Keywords: High-level corruption, Negotiations, Officials, EU accession

1. INTRODUCTION

European Union (EU) goal is to promote peace, its values and the well-being of its citizens. With this in mind, EU aims to offer freedom, security and justice without internal borders, sustainable development based on balanced economic growth and price stability, a highly competitive market economy with full employment and social progress, and environmental protection; to fight social exclusion and discrimination, promote scientific and technological progress, enhance economic, social and territorial cohesion and solidarity among member countries, respect its rich cultural and linguistic diversity, establish an economic and monetary union whose currency is the euro [1]. The rule of law, democracy and fundamental rights are the foundation for the EU's work to foster peace, prosperity, competitiveness, social cohesion and stability across the continent.

Albania is going through a complex and dynamic process specifically regarding the fight against high-level corruption. In Albania, there are encouraging initial results of the Special Structure against Corruption and Organized Crime (SPAK) and SPAK courts. The number of persons investigated, prosecuted, and convicted for corruption charges has been increasing over the past years [2]. Media, civil society, academia and the community in overall, have special attention on the upcoming developments with respect to the detection of major corruption scandals. Although few in number, opposition individuals and investigative media is providing substantial support to SPAK.

The objective of this research is to analyse the comparison between Albania's and Bulgaria's (as Bulgaria, together with Romania, were the second-to-last countries to join the EU) level of effective efforts to detect high-level corruption as a major factor that impacts the progress of the negotiations process.

Referring to Marta Kos' aspiration that the technical negotiation process for Albania could be finished by end of 2027, is Albania on the same path, as Bulgaria was two to three years before the technical closing of negotiations?

What do both countries have in common with respect to the challenges and results in fighting against high-level corruption?

This study is prepared based on qualitative analysis of legislation, institutional reports (such as SPAK's annual reports, EC's Rule of Law reports, Corruption Perceptions Index by Transparency International), case studies of high-level corruption proceedings, and policy documents.

1.1. Albania

Albania, as an EU candidate country, has officially launched accession negotiations in March 2020 and started the technical accession negotiations in July 2022. Albania has shown a strong and firm political commitment leading to the opening of negotiations on 6 clusters. Albania opened the first cluster, cluster 1 "Fundamentals" on 15 October 2024 and opened the last one, cluster 5 "Resources, Agriculture and Cohesion" on 17 November 2025. Albania successfully opened all six clusters within 13 months.

Nowadays Albania is experiencing major transformation to consolidate a sustainable Rule of Law. It is facing multidimensional challenges to meet the European requirements towards the EU accession, as its final goal. The European Commission highlights in the 2025 Communication on EU Enlargement Policy that Albania continued to make progress in reforms under the fundamentals cluster, in particular on the comprehensive justice reform and with the completion of the vetting process in first instance, further good results by the Special Structure against Corruption and Organized Crime (SPAK) in anti-corruption cases, active international cooperation against organised crime and capacity development for financial investigations [3].

Despite the good progress in reforms, the perception among experts and business executives is that the level of corruption is high. Corruption in Albania is prevalent in most areas of public and business life, including in all branches of central and local government and institutions. The most vulnerable sectors are public infrastructure, cadastre and property rights, customs, tax administration, education, health, public procurement, Public–Private Partnership contracts, etc. [4]. The first major corruption scandal investigated in Albania is the "Fraud in a Public Tender for Sterilization Equipment," in 2020, which consisted in a €100 million contract for the sterilization of surgical equipment in public hospitals [5]. The second major corruption scandal is the "Incinerator Scandal." It consisted in the construction and operation of three incinerators (two of which have not yet been built), all given to the same group of people, creating virtually a monopoly. The Albanian incinerators were created from no demand, no requirement, and no official proposal. It all started with a request from a newly set up company, with no capital or experience. The three concession contracts for the construction of incinerators have cost Albanian taxpayers €72 million until June 2020, while they have all failed to provide the expected services [6].

Currently in Albania, numerous high-ranking officials are serving prison sentences, but the highest-level officials among them are the mayor of Tirana, Erion Veliaj (in 2025) and former President of Albania Ilir Meta (in 2024), both arrested on charges of money laundering and corruption. Most recently, public attention is highly focused on the investigations against the Deputy Prime Minister and Minister of Infrastructure and Energy Belinda Balluku, to whom SPAK has issued an order banning her on leaving the country, as well assuspended her from all her governmental duties. The fight against corruption of high-ranking officials, although it has produced encouraging results, remains a significant challenge for strengthening the rule of law in Albania.

1.2. Bulgaria

Bulgaria opened the negotiations in February 2000, closed the technical ones in 2004 and became an EU Member State in 2007. Bulgaria has gone through a long fight against corruption process.

In the Bulgarian society, the poverty of Bulgaria is repeated again and again [7]. Based on the 2000 Regular Report on Bulgaria's Progress Towards Accession, corruption scandals have been widely reported in the press. The Parliament rejected a motion of no confidence against the government for implementing a policy of corruption and covering up its real-time manifestations. Whilst allegations of corruption were rife, it was difficult to obtain substantial and reliable information on how the judicial system was dealing with corruption cases. Some information on bribery cases was available, but it was not possible to obtain clear figures for corruption-related cases [8].

Referring to 2001 Regular Report on Bulgaria's Progress Towards Accession, corruption was a very serious problem in Bulgaria. Customs, the police, university teachers, business community, public sector officials who had close contact with the public and the judiciary were perceived to be among the most corrupt professions.

Corruption was considered as one of the main problems facing Bulgarian society.[9] The phenomenon of corruption remained widespread even one year later as is evidenced in the 2002 Regular Report on Bulgaria's Progress. The public ranked corruption as one of the most serious problems facing the country. Customs, occupations linked to the judicial system, tax officials, parliamentarians, police and ministry officials were perceived to be among the most corrupt groups [10].

With the advancement of the accession process, political corruption gradually shifted from privatization and illegal trafficking to the spheres of concessions, public procurement, and the use of EU funds. An alarming trend has been the effort by government institutions to mask reluctance and incapability for coherent action against political corruption [11]. While Bulgaria and Romania are good performers regarding the transposition of EU law, they have not managed to overcome structural shortcomings of their law enforcement structures, pointing to problems at the later stages of the implementation process [12]. The prolonged situation of corruption led to the eruption of public protests on December 1, 2025.

Tens of thousands of people demonstrated against the 2026 budget and called for the government to step down. This is the biggest protest the Balkan country has seen for years. The protesters chanted "Resignation!" and projected the words "Resign" and "Mafia" onto the government buildings around the square and held two large banners saying: "Generation Z is coming" and "Young Bulgaria without the mafia." Protesters want the government to keep their promise to withdraw the 2026 budget, which proposed steeper taxes on dividends and a hike in social security contributions. They are also angry about public sector corruption and are calling for the resignation of the minority coalition government of Rosen Zhelyazkov. Bulgaria, with a population of 6.4 million people, is one of the most corrupt countries in the EU. Youth is protesting "all the arrogance" shown by the country's leaders and "all the lawlessness". President Rumen Radev, called for the government to step down. Critics are concerned about the economic impact of the budget in a country that is ranked as one of the poorest in the EU. They are also worried that greater flows to the public sector will further entrench graft. The protests come as the Balkan country prepares to adopt the European common currency, the Euro, on January 1, 2026. The president of the European Central Bank, Christine Lagarde, warned last month that that inflation may jump when Bulgaria joins the Eurozone [13].

3. RESULTS

In the pre-accession years, the Regular Reports (2000-2003) on Bulgaria's Progress Towards Accession emphasize that corruption is very serious, yet they do not cite any convictions of high-level officials. Corruption in Bulgaria was addressed more generally, as "serious corruption" or "widespread corruption" and there is a lack of a track record at the high-level. The concept of "high-level corruption" for Bulgaria first appeared clearly in the European Commission's reports after the technical closing of the negotiations. In Albania's case, the situation is different. Given that the fight against corruption is fundamental in every report submitted to the European Commission, the track record of high-level official cases constitutes, among other things, a concrete indicator of the performance and success of the law enforcement agencies and special investigative entities.

Bulgaria's Corruption Perceptions Index 2023 (three years before the closing of technical negotiations), score is 3.9/10. [14] Bulgaria's Corruption Perceptions Index 2024 score is 43/100 [15]. Albania's Corruption Perceptions Index 2024 score is 42/100 [15]. It is very significant that Bulgaria as an EU Member State, scores in 2024 almost identically to Albania as a candidate country.

The Corruption Perceptions Index scores for 2024 show that Albania (42/100) and Bulgaria (43/100) have very similar levels of perceived public-sector corruption. Both countries score below the Corruption Perceptions Index midpoint (50/100), which means that they perform below the EU average and that corruption is still considered a serious and widespread problem in each country.

Bulgaria is ranked slightly higher (76th) than Albania (80th), but the difference of four positions in a group of 180 countries is quite insignificant. It reflects that both countries have the same overall performance level in anti-corruption assessments.

4. CONCLUSION

Despite the different status, nowadays, Albania and Bulgaria are facing same challenges related to integrity, rule of law, transparency, and anti-corruption enforcement. Even though Albania has incurred major corruption scandals from high-ranking officials, the fruitful engagement of the Special Anti-Corruption Structure and Anti-Corruption and Organised Crime courts, is rebuilding trust among the public and giving hope for a democratic

governance. Albania, unlike Bulgaria, is advancing the fight against corruption through a considerable number of concrete cases involving high-level officials implicated in corruption affairs. Although it still has a long way to go before joining the EU, law enforcement agencies are showing firm commitment in combating corruption and encouraging results despite the difficulties they are facing, such as political influence, shortage of administrative staff and limited financial means. Albania's position (42) in Corruption Perceptions Index, as candidate country, reflects recent improvements. Bulgaria's position (43) reflects that despite being an EU Member State since 2007, it continues to be affected by state capture and weak accountability.

The similarity in their rankings, despite their different statuses, suggests that EU membership alone does not automatically ensure progress in reducing corruption. Albania's achievements increase the trust of EU institutions in fulfilment of its obligations within a reasonable time, thereby accelerating the country's accession timeline to the EU. Based on this research, Albania demonstrates strong prospects for fulfilling Marta Kos' aspiration that the technical negotiation process for Albania could be finished toward the end of 2027.

References

[1] European Union. *Aims and values* [Online]. Available: https://european-union.europa.eu/principles-countries-history/principles-and-values/aims-and-values_en

[2] European Commission. (2024, Jul. 24). *Albania 2024 report* [Online]. Available: https://commission.europa.eu/document/download/0154dce1-5026-45de-8b37-e3d56eff7925_en?filename=59_1_58088_coun_chap_albania_al.pdf

[3] European Commission. (2025, Nov. 4). *Communication on EU enlargement policy* [Online]. Available: https://enlargement.ec.europa.eu/document/download/eb69a890-40d6-4696-801e-612d51709fdd_en?filename=2025%20Communication%20on%20EU%20Enlargement%20Policy.pdf

[4] European Commission. (2023, Jul. 20). *Screening report Albania* [Online]. Available: https://enlargement.ec.europa.eu/document/download/b83313ef-48c5-4bef-9f00-f5d66509572e_en?filename=AL%20Cluster_1%20Draft%20screening%20report_external%20version.pdf

[5] F. Sinoruka. (2023, Aug. 17). *Albania arrests former deputy minister over dubious surgical equipment concession* [Online]. Available: https://balkaninsight.com/2023/08/17/albania-arrests-former-deputy-minister-over-dubious-surgical-equipment-concession/

[6] Exit. (2020, Oct. 12). *Exit explains: Albania's three waste incinerators* [Online]. Available: https://exit.al/en/2020/10/12/exit-explains-albanias-three-waste-incinerators/

[7] N. Veselinova. (2020, Oct.). "The European Union and Bulgaria – Geographical thoughts," *Eastern Academic Journal* [Online], no. 1, pp. 11–17. Available: https://www.e-acadjournal.org/article-20-1-2.html

[8] European Commission. (2000, Nov. 23) *Bulgaria Regular Report 2000* [Online]. Available: https://enlargement.ec.europa.eu/bulgaria-regular-report-2000_en

[9] European Commission (2001, Nov. 27) *Bulgaria regular report 2001* [Online]. Available: https://enlargement.ec.europa.eu/bulgaria-regular-report-2001_en

[10] European Commission (2002, Jun. 19) *Bulgaria regular report* [Online]. Available: https://enlargement.ec.europa.eu/bulgaria-regular-report-2002_en

[11] Center for the Study of Democracy, "On the eve of EU accession: Anti-corruption reforms in Bulgaria," Corruption Assessment Report 2005/2006, 2006. [Online]. Available: https://www.files.ethz.ch/isn/28943/3.pdf

[12] F. Schimmelfennig and F. Trauner (2009). "Post-accession compliance in the EU's new member states," *European Integration Online Papers* [Online]. vol. 13, special no. 2. Available: https://eiop.or.at/eiop/texte/EIoP_2009_SpecIssue_2.pdf?utm_source=chatgpt.com

[13] Deutsche Welle. (2025, Dec. 2). *Bulgaria sees biggest protest in years* [Online]. Available: https://www.dw.com/en/bulgaria-sees-biggest-protest-in-years/a-74975871

[14] Transparency International, "Corruption perceptions index 2001," 2001. [Online]. Available: https://www.transparency.org/en/cpi/2001

[15] Transparency International, "Corruption perceptions index 2024," 2024 [Online]. Available: https://www.transparency.org/en/cpi/2024

2nd International Conference on Multidisciplinary Sciences and Technological Developments (ICMUSTED 2025)

December 12-15, 2025

Exploratory Factor Analysis of Mobile Application Usage Among Youth Associations in Malaysia

Mohd Hazlami Jusoh[1], Noor Aisyah Abdul Aziz[1], Mohd Yusri Ibrahim[2]

[1]Centre for Fundamental and Continuing Education, Universiti Malaysia Terengganu, Terengganu, Malaysia
[2]Faculty of Business, Economics and Social Development, Universiti Malaysia Terengganu, Terengganu, Malaysia
Corresponding author: Mohd Hazlami Jusoh (e-mail: mohdhazlamijusoh@gmail.com)

Abstract

Utilisation of mobile applications has become increasingly prominent among the youth generation in digital eras. The role of mobile applications as sophisticated tools facilitates youth connecting and interacting to share information and communicate within organisations virtually. This study aims to validate and measure the instrument of mobile application usage among youth associations members. The instruments for assessing mobile application usage comprise two constructs: the perception of use and the perceived usefulness of mobile applications. A total of 401 youth association members in Terengganu, Malaysia, were involved as respondents through questionnaire distribution. The quantitative data were analysed using Statistical Package for the Social Sciences (SPSS) software, including a reliability coefficient test and exploratory factor analysis (EFA). The reliability coefficient (Cronbach's alpha) of mobile application usage was found to be 0.954. The results from the EFA procedure indicated the value of the measure of sampling adequacy (MSA) for Kaiser-Meyer-Olkin (KMO) (0.944) is accepted when the value is greater than 0.50 and the Bartlett's test of sphericity (BTS) is significant (chi square 5275.916, $p < 0.05$). The result from the total variance explained suggests two factors from the EFA procedure showed eigenvalues greater than 1.0 and contributed 71.636%. No items were excluded, and all 15 items were accepted when the values of the loading factor obtained were between 0.676 and 0.837, greater than 0.5. This study successfully validates and measures the items for the instrument of mobile application usage among youth association members in Terengganu, Malaysia. These findings offer youth in enhancing and empowering organisational leadership through digital interaction and identify further research areas.

Keywords: Mobile application usage, Youth associations, Digital interaction, Exploratory factor analysis

2nd International Conference on Multidisciplinary Sciences and Technological Developments (ICMUSTED 2025)

December 12-15, 2025

Understanding the Role of AI Literacy in Work Engagement: The Mediating Effects of Job Crafting and Job Insecurity, and the Moderating Role of Regulatory Focus

Ali Jan Shayiq[1], Ipek Mete Tonge[1]

[1]Business School, Ankara Yildirim Beyazit University, Ankara, Türkiye
Corresponding author: Ali Jan Shayiq (e-mail: ali.shayiq13@gmail.com)

Abstract

As artificial intelligence (AI) increasingly transforms contemporary workplaces, understanding how employees adapt to AI-driven changes has become a crucial organizational priority. While AI offers substantial benefits—such as efficiency and innovation—it may simultaneously create psychological strain and job insecurity among employees with lower levels of AI literacy. Grounded in the job demands–resources (JD–R) model and regulatory focus theory, this study examines how AI literacy influences work engagement through the mediating roles of job crafting and job insecurity, and whether promotion and prevention regulatory foci moderate these relationships. AI literacy, conceptualized as a multifaceted personal resource encompassing understanding, evaluating, and effectively using AI technologies, is expected to encourage proactive behaviors such as job crafting while reducing perceived threats associated with job insecurity. Employees who possess higher AI literacy are more likely to reframe AI as a developmental opportunity rather than a workplace threat, thereby enhancing adaptive responses. Conversely, low AI literacy may heighten uncertainty and reduce engagement. This study also investigates how individuals with promotion or prevention orientations differentially interpret AI-related changes, shaping the effects of AI literacy on psychological and behavioral outcomes. This quantitative cross-sectional study will recruit employed adults across diverse sectors in Türkiye using an online survey. Validated measurement tools—including the Meta-AI Literacy Scale, job crafting scale, job insecurity scale, and work engagement scale—will be administered to a target sample of approximately 395 participants. Data will be analyzed using structural equation modeling and moderated mediation techniques. By clarifying the mechanisms linking AI literacy to employee engagement, this research aims to provide strategic insights for organizations designing AI-focused training programs, promoting adaptive work behaviors, and supporting employee well-being in technologically evolving environments.

Keywords: Artificial intelligence literacy, Work engagement, Job crafting, Job insecurity, Regulatory focus

2nd International Conference on Multidisciplinary Sciences and Technological Developments (ICMUSTED 2025)

December 12-15, 2025

Scientific Integrity in the Era of Artificial Intelligence: Current Knowledge and Challenges for Nursing Education – A Narrative Review

Imane Bettane[1], Mohammed-Yassine Takzima[2], Mohamed Khalyfa[3]

[1]Bioscience and Health Research Laboratory, Community Medicine and Public Health Department, Faculty of Medicine, Cadi Ayyad University, Marrakech, Morocco
[2]Laboratory of Water Sciences, Microbial Biotechnologies, and Natural Resources Sustainability, Unit of Microbial Biotechnologies, Agrosciences, and Environment, Faculty of Sciences-Semlalia, Cadi Ayyad University, Marrakech, Morocco
[3]Laboratory of Health Sciences and Technologies, Higher Institute of Health Sciences, Hassan First University, Settat, Morocco
Corresponding author: Mohammed-Yassine Takzima (e-mail: mohammed.takzima@gmail.com)

Abstract

Artificial intelligence (AI) is profoundly transforming research and teaching methods in health sciences. While these tools offer immense potential for innovation and support, they also raise new ethical questions regarding scientific rigor, transparency, and accountability. Understanding the implications of AI for scientific integrity has therefore become essential, particularly in the training of nursing students, who represent future contributors to research and evidence-based practice. This narrative review examines the current state of knowledge regarding the relationship between scientific integrity and artificial intelligence, identifying the primary challenges, risks, and opportunities for integrating these dimensions into nursing education. A narrative literature review was conducted using major international databases in health, education, and technology (PubMed, Cumulative Index to Nursing and Allied Health Literature (CINAHL), Scopus, European Research Infrastructure Consortium (ERIC)). Studies published between 2015 and 2025 were selected based on their thematic relevance, conceptual rigor, and contribution to reflections on scientific integrity and the use of AI in nursing education. Findings highlight that AI is redefining the principles of scientific integrity, creating risks of opacity, bias, and automated plagiarism, while also offering potential for pedagogical innovation and the development of ethical reasoning. Nursing curricula must therefore integrate critical and digital literacy skills to ensure the responsible use of these technologies. The integration of AI in research calls for a reconfiguration of the principles of scientific integrity, grounded in transparency, shared responsibility, and critical training of researchers to ensure the responsible and informed use of AI in the production and application of knowledge.

Keywords: Artificial intelligence, Scientific integrity, Ethics, Nursing education, Narrative review

2nd International Conference on Multidisciplinary Sciences and Technological Developments (ICMUSTED 2025)

December 12-15, 2025

The Challenges Encountered by Science Teachers in Utilizing Laboratory Facilities

Ulas Kubat[1]

[1]Department of Curriculum and Instruction, University of Minnesota, St. Paul, USA
Corresponding author: Ulas Kubat (e-mail: ulaskubat@)yahoo.com)

Abstract

The objective of this study is to identify the challenges encountered by science teachers in utilizing laboratory facilities. Laboratories hold significant importance in science education, serving as critical environments for achieving learning outcomes through firsthand student engagement or instructional demonstrations. Science teachers endeavor to incorporate laboratories into the teaching-learning process to the extent permitted by available resources. The effective use of laboratories contributes to the development of students' research, problem-solving, and logical reasoning skills. By providing an experiential learning setting, laboratories stimulate student interest and curiosity, thereby facilitating more durable knowledge acquisition. Furthermore, well-implemented laboratory practices support the enhancement of students' problem-solving abilities and psychomotor skills. In accordance with this objective, data were collected via semi-structured interviews conducted with 26 science teachers. Analysis of the interview findings revealed that laboratory conditions in schools are largely inadequate. Additionally, teachers reported that overcrowded classrooms hinder the effective utilization of laboratory facilities. Due to safety concerns, teachers often resort to demonstrating experiments themselves rather than having students perform hands-on activities. Moreover, respondents indicated that a lack of materials and equipment in laboratories frequently prevents the conduction of certain experiments

Keyword: Science education, Science teacher, Laboratory

2nd International Conference on Multidisciplinary Sciences and Technological Developments (ICMUSTED 2025)

December 12-15, 2025

The Chronotopes of Racialized Experience in Toni Morrison's *The Bluest Eye*

Tulay Dagoglu[1]

[1]Department of English Language and Literature, Istanbul Aydin University, Istanbul, Türkiye
Corresponding author: Tulay Dagoglu (e-mail: tulaydagoglu@aydin.edu.tr)

Abstract

Toni Morrison's *The Bluest Eye* (1970) has been the focus of numerous critical studies exploring race, beauty, and identity; however, the ways in which time and space shape human experience within the narrative remain unexamined. Drawing on Mikhail Bakhtin's concept of the chronotope, the deep interrelation of temporal and spatial relations that gives form and meaning to narrative, this study reinterprets Morrison's novel through the lens of racialized experience and the psychic confinement of Black subjectivity. Bakhtin emphasizes that time and space in literature are intrinsically connected, forming the ground of representation from which narrative events and social meanings emerge. The chronotope thus operates as a form-shaping ideology that constructs experience by linking temporal rhythms with spatial settings to define historical, social, and biographical relations. In *The Bluest Eye*, Bakhtin's minor chronotopes such as the "Parlor," "Road," "Threshold," and "Provincial Town" define the racialized conditions of mobility, belonging, and visibility. These temporal–spatial structures expose how psychic confinement, displacement, and social hierarchy characterize lived experience and subjectivity under racial oppression. Time takes on a cyclical yet immobilized rhythm, as the novel's seasonal structure functions ironically to delineate not renewal but the progressive worsening of trauma and decay, whereas space, whether domestic, communal, or segregated, holds the imprint of exclusion. Together, these chronotopes fashion Morrison's narrative as a meditation on how race structures the very conditions of temporality and spatial belonging in twentieth-century America.

Keywords: *The Bluest Eye*, Bakhtin, Chronotopes, Racial oppression

2nd International Conference on Multidisciplinary Sciences and Technological Developments (ICMUSTED 2025)

December 12-15, 2025

Challenge of Ancient Regimes Toward the Republic: Example of Napoleon Bonaparte

Erdal Aydin[1]

[1]Political Science and Public Administration, Duzce University, Duzce, Türkiye
Corresponding author: Erdal Aydin (e-mail: erdalaydin@duzce.edu.tr)

Abstract

We have many revolutions in the world political history. It is well known and accepted that human civilizations go back to almost seven thousand years. Early civilizations appeared in the Mesopotamia located among famous two rivers, Tigris and Euphrates. It was not spontaneous that early human communities preferred and set up a great land fed by rivers and led amazing fertilized agricultures as well water for surviving life. Human beings have great potentials in many areas. It's not like other beings. Let's look any species of animals. They may have some special abilities but it's stable and fixed. On the other hand human beings may carry thousands of abilities and skills. That's why we have many faculties, disciplines, arts, sports and so on. Indeed civilizations based on two important parameters. One is accumulation of past experiences that guide us. The second is exchange of knowledge, culture and innovations. Politic as master of arts for Aristotle led and guide these civilizations. Human beings as political actors may have disposals over the geography, animals, forests as well as humans. Of course this great potential and freedom may be very good as well as harmful. After renaissance and reforms French Revolution had been one of the great case in the human history. It let famous three slogans which are freedoms, equalities and liberties. Napoleon Bonaparte was a great commander and political leader who challenged the French Republic. He declared emperor twice but finally not succeed. His capacity and authority actually was output of the conjectural period of the France. Army and most of society supported his dreams. He represented real power of absolute supporters of ancient regimes. Comparing Reich of Germans, Republic defeated the dignity and imagination of ancient regimes in the France.

Keywords: Napoleon Bonaparte, Republics, Ancient regimes, Revolutions

2nd International Conference on Multidisciplinary Sciences and Technological Developments (ICMUSTED 2025)

December 12-15, 2025

Structural, Photocatalytic, and Dielectric Properties of ZnO-Phosphate Glass-Ceramics

Chaima Assamadi[1], Nourdine El Binna[1], Mohamed El Masloumi[1,2], Abdelaziz El Abiad[1], Hakima Aouad[1]

[1]Department of Chemistry, Cadi Ayyad University, Marrakech, Morocco
[2]Department of Chemistry, Sultan Moulay Slimane University, Beni Mellal, Morocco
Corresponding author: Chaima Assamadi (e-mail: assamadi.chaima.uca@gmail.com)

Abstract

The uncontrolled release of synthetic dyes such as methylene blue (MB), methyl orange (MO), and methyl red (MR) represents a serious environmental challenge due to their high stability and toxicity. Heterogeneous photocatalysis is widely regarded as an efficient approach for degrading these persistent pollutants. Zinc oxide (ZnO), with its wide band gap, strong oxidation potential, and low cost, is a promising candidate. However, its practical use as a powder is limited by recovery and stability issues. To overcome these drawbacks, phosphate-based glass-ceramics were developed incorporating ZnO as a crystalline phase. Structural flexibility within the phosphate network enables Zn^{2+} incorporation and ZnO crystallization during heat treatment, enhancing photocatalytic performance under ultraviyole (UV)–visible light by improving charge separation and dye adsorption. Beyond photocatalysis, ZnO incorporation significantly influences the dielectric response of the glass-ceramics. Dielectric studies reveal that ZnO addition modifies polarization mechanisms, leading to higher permittivity values and a transition from insulating to more conductive behavior at low frequencies. This dual functionality positions ZnO-phosphate glass-ceramics as multifunctional materials with potential applications not only in wastewater treatment but also in electronic devices requiring tailored dielectric properties.

Keywords: ZnO, Phosphate glass-ceramics, Photocatalysis, Dielectric properties, Dye degradation, Wastewater treatment

2nd International Conference on Multidisciplinary Sciences and Technological Developments (ICMUSTED 2025)

December 12-15, 2025

Structural and Optical Characterization of Cellulose Acetate/ZnO Nanocomposite Films

Asmaa Bessaad[1], Badreddine Toubal[1]

[1]Material Science Department, University of Algiers 1 (Benyoucef Benkhedda), Algiers, Algeria
Corresponding author: Asmaa Bessaad (e-mail: a.bessaad@univ-alger.dz)

Abstract

In this study, cellulose acetate (CA), a biodegradable polymer derived from renewable cellulose, was doped with zinc oxide (ZnO) nanoparticles to enhance its structural, optical, and morphological properties. The CA/ZnO composite films were prepared by a solution casting method with different ZnO concentrations to optimize the nanoparticle dispersion and polymer interaction. The structural analysis by fourier transform infrared spectroscopy (FTIR) confirmed the presence of strong intermolecular interactions between ZnO and the hydroxyl and carbonyl groups of cellulose acetate, indicating partial coordination bonding. X-ray diffraction (XRD) patterns revealed the semi-crystalline nature of the composites, with distinct diffraction peaks corresponding to ZnO crystallites embedded within the polymer matrix. Scanning electron microscopy (SEM) images showed a uniform distribution of ZnO nanoparticles at lower concentrations, while higher loadings led to slight agglomeration on the film surface. Optical characterization using ultraviolet (UV)–visible spectroscopy demonstrated that the incorporation of ZnO increased the absorption intensity in the UV region and slightly widened the optical band gap from 3.82 eV to 3.95 eV, suggesting improved transparency and potential for UV-blocking applications. Thermal analysis indicated an enhancement in the thermal stability of the doped films compared to pure cellulose acetate. The improved physicochemical properties highlight the synergistic effect between ZnO nanoparticles and the polymeric matrix. Overall, the CA/ZnO nanocomposite films exhibit promising features for use in biodegradable packaging, photocatalytic systems, and optical coatings, combining environmental sustainability with functional performance.

Keywords: Cellulose acetate, ZnO nanoparticles, Composite films, Characterization, Optical properties

2nd International Conference on Multidisciplinary Sciences and Technological Developments (ICMUSTED 2025)

December 12-15, 2025

Wide-Angle Quad-Band Metamaterial-Based Absorber Operating in Microwave Bands

Yunus Kaya[1], Ugur Cem Hasar[2]

[1]Department of Electronics and Automation, Bayburt University, 69010 Bayburt, Türkiye
[2]Department of Electrical and Electronics Engineering, Gaziantep University, 27310 Gaziantep, Türkiye
Corresponding author: Yunus Kaya (e-mail: ykaya@bayburt.edu.tr)

Abstract

In this study, a quad-band metamaterial (MM) absorber is suggested. The unit cell of the suggested MM absorber structure contains a metallic (copper) metasurface (MS) consisting of two square shaped ring resonators with a split in one arm on the top surface of a single-layer FR-4 dielectric substrate. The numerical analysis of the designed MM absorber structure was performed in CST Studio Suite, a simulation software based on the finite integration technique (FIT). The suggested MM-based absorber provides nearly 100% absorption across four different frequency bands (microwave S-, C-, Ku-, and K-bands (2–4 GHz, 4–8 GHz, 12–18 GHz, and 18–27 GHz, respectively)) at four resonance frequencies (2.365 GHz, 4.95 GHz, 12.3 GHz, and 18.61 GHz). Thanks to its designed MS structure, the suggested absorber exhibits good stability (with an absorption rate of over 80%) for transverse electric (TE) mode waves under polarization angle up to 30° and oblique incidence up to 60°.

Keywords: Metamaterial absorber, Quad-band, Wide-angle

1. INTRODUCTION

Today, the demand for the development of suitable materials and procedures to reduce the effects of electromagnetic (EM) waves is increasing day by day [1]. This demand led to the introduction of the concept of absorber [2]. An absorber is a block of material used to absorb part of a particle's energy [3]. Research on absorbers is rapidly increasing due to their applications in many fields such as medical imaging, signal absorption, invisibility, sensors, and antennas [4, 5]. Some classic examples of EM absorbers include the Dallenbach, Salisbury, and Jaumann absorbers [6]. However, these traditional absorbers are unsuitable for many practical applications due to their bulky dimensions and design complexity [7, 8]. Therefore, in order to meet the need for simple and compact absorbers, the research focus has shifted to metamaterial (MM) absorbers [9]. MMs, which are unnatural materials with different electromagnetic (EM) behaviors, have found a wide range of applications in recent years. One of these, MM-based absorbers, are attracting significant interest due to their high absorption performance, thin layers, and low cost [10]. These MM-based absorbers can trap or absorb an incident EM wave at specific points of the device depending on their operating bandwidths and consequently convert the EM wave into heat [11].

In this study, an MM-based absorber designed on a single-layer and easily accessible FR-4 dielectric substrate is presented, which offers 99.71%, 99.81%, 99.95%, and 99.97% absorption rates, respectively, at frequencies of 2.365 GHz, 4.95 GHz, 12.3 GHz, and 18.61 GHz, respectively, in microwave S-, C-, Ku-, and K-bands (2–4 GHz, 4–8 GHz, 12–18 GHz, and 18–27 GHz, respectively). Additionally, the suggested MM absorber, thanks to its designed structure, exhibits good stability (with an absorption rate of over 80%) for transverse electric (TE) mode waves, both in terms of polarization angle (up to 30°) and under oblique incidence (up to 60°).

2. SUGGESTED MM-BASED ABSORBER DESIGN

The suggested quad-band MM-based absorber design was implemented using CST Studio Suite, a high-performance EM analysis software program based on the finite integration technique (FIT). The suggested unit cell design is shown in Figure 1. The designed unit cell is designed to achieve high absorption in four different microwave bands (S-, C-, Ku-, and K-bands). This absorber design consists of top, middle, and bottom layers, as shown in Figure 1. An FR-4 dielectric substrate with a relative dielectric constant of 4.3 and a loss tangent of 0.025 is used in the middle layer. The top layer consists of copper resonators with a conductivity of 5.8×10^7 S/m, while the bottom layer consists of the same copper ground plane. Figure 1(a) shows the front view of the suggested absorber unit cell, while Figure 1(b) shows the thicknesses of the layers (resonators, substrate, and

ground) of the suggested absorber unit cell in three-dimensional (3D). The top surface of the suggested structure consists of two square rings with a split on one arm. The dimensions of the MM absorber unit cell shown in Figure 1 are given in mm in Table 1. These final unit cell dimensions have been optimized to achieve the best results (high absorption rate, quad-band absorber, and wide-angle).

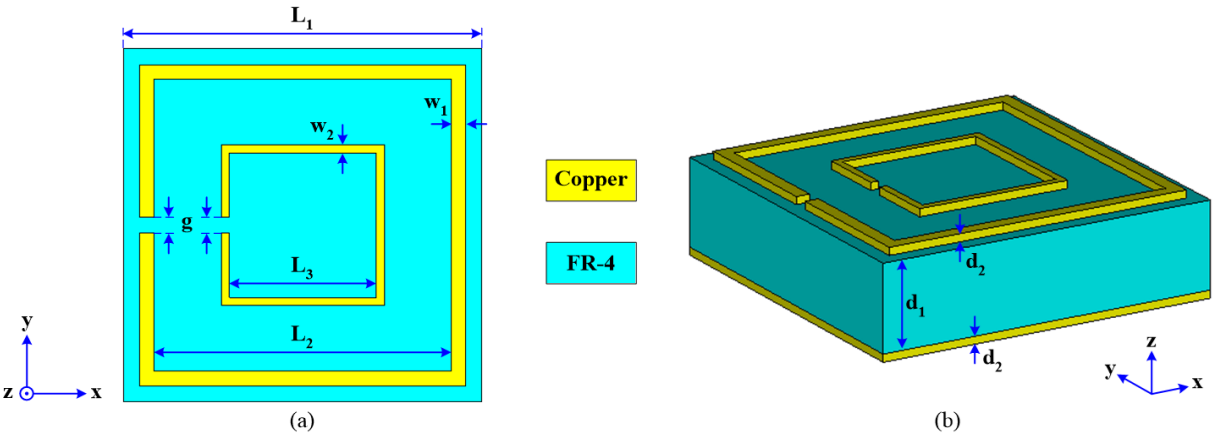

Figure 1. (a) Front view and (b) 3D layer thickness representation of the suggested absorber unit cell

Table 1. Suggested MM-based absorber unit cell dimensions in mm

L_1	L_2	L_3	w_1	w_2	g	d_1	d_2
11	9.1	4.5	0.45	0.25	0.5	2.8	0.035

3. SIMULATION RESULTS

For numerical analysis, boundary conditions in CST Studio Suite were selected as "unit cell" along the x- and y-axes and "open (add space)" along the z-axis. Accordingly, the absorption (A) for the suggested MM-based absorber is calculated as follows from the simulations to be performed [2, 10, 11].

$$A = 1 - T - R \tag{1}$$

Here, T and R denote transmission and reflection, respectively, and are defined as follows [12].

$$T = |S_{21}|^2 = \left[\frac{(1-r_0)^2 \left(1-e^{i2nk_0d}\right)}{1-r_0^2 e^{i2nk_0d}} \right]^2 \tag{2}$$

$$R = |S_{11}|^2 = \left[\frac{r_0 \left(1-e^{i2nk_0d}\right)}{1-r_0^2 e^{i2nk_0d}} \right]^2 \tag{3}$$

Here, $|S_{21}|$ and $|S_{11}|$ represent the transmitted and reflected power respectively, while Z is the impedance and $r_0 = (Z-1)/(Z+1)$. Additionally, n is the refractive index, k_0 is the wave number of the incident wave in free space, and d is the length of the slab.

When Equation (1) is examined, it is seen that if the reflected and transmitted power is minimized (to zero), absorption can be maximized (to 100% absorption) [2, 10–12]. As shown in Figure 1, for the suggested absorber, since the bottom layer, i.e., the ground plane, is made of copper, there is no transmitted power, i.e., $|S_{21}| = 0$ and therefore $T = 0$ [2, 10–12]. Therefore, Equation (1) takes the following form.

$$A = 1 - R = 1 - |S_{11}|^2 \tag{4}$$

However, this is only valid when the structure is lossless. This is not possible in real-time applications [13]. The suggested structure was simulated in the 0–24 GHz frequency range using the CST Studio Suite EM simulation

program. The transmitted and reflected powers obtained from the simulation ($|S_{21}|$ and $|S_{11}|$, respectively) and the absorption values (A) calculated from these simulation data using Equation (1) are shown in Figure 2 versus frequency. From Figure 2(a), it can be seen that the $|S_{21}|$ value for the suggested structure is 0.054, 0.043, 0.021, and 0.017, respectively, at the resonance frequencies of 2.365 GHz (in the microwave S frequency band), 4.95 GHz (in the microwave C frequency band), 12.3 GHz (in the microwave Ku frequency band), and 18.61 GHz (in the microwave K frequency band) and the $|S_{11}|$ value is zero in the entire simulated frequency range. From Figure 2(b), it can be seen that the suggested structure offers a quad-band MM absorber performance with an absorption values (rates) of 0.9971 (99.71%), 0.9981 (99.81%), 0.9995 (99.95%), and 0.9997 (99.97%), respectively, at four resonant frequencies of 2.365 GHz, 4.95 GHz, 12.3 GHz, and 18.61 GHz, respectively, in the microwave S-, C-, Ku- and K-bands.

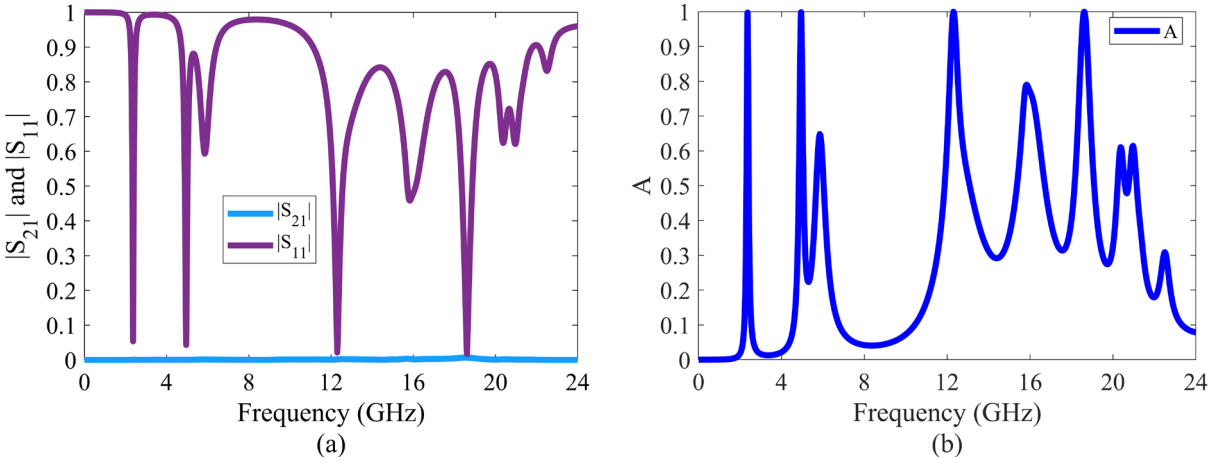

Figure 2. (a) Transmitted and reflected powers ($|S_{21}|$ and $|S_{11}|$, respectively) simulated in CST Studio Suite for the suggested MM-based absorber, and (b) calculated absorption value (A).

The suggested structure was examined for different polarization angles (ϕ = 0°, 10°, 20°, and 30°) under normal incidence (θ = 0°) for TE mode waves. The absorption values calculated from the simulated $|S_{21}|$ and $|S_{11}|$ values for different polarization angles are shown in Figure 3(a). When Figure 3(a) is examined, the suggested MM-absorber structure shows an absorption rate of over 80% at the specified frequency points for a polarization angle of up to 30° under normal incidence. Secondly, the suggested structure was investigated under oblique incidence (θ = 0°, 20°, 40° and 60°) for TE mode waves. The absorption values calculated from the simulated $|S_{21}|$ and $|S_{11}|$ values under different oblique incidence angles are shown in Figure 3(b). When Figure 3(b) is examined, the suggested MM-absorber structure shows an absorption rate of over 80% at the specified frequency points up to 60° under oblique incidence. These results also indicate that the suggested MM-absorber structure exhibits good stability under both polarization angle and oblique incidence (up to 30° for ϕ and up to 60° for θ).

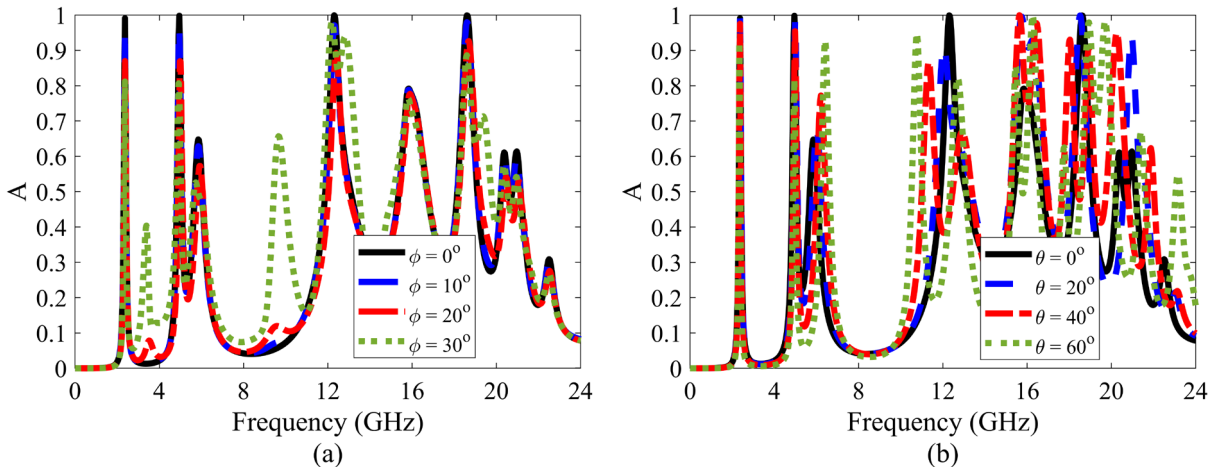

Figure 3. For the TE mode waves, the absorption values obtained for (a) different polarization angles (ϕ = 0°, 10°, 20°, and 30°) under normal incidence (θ = 0°) and (b) oblique incidence (θ = 0°, 20°, 40°, and 60°)

4. CONCLUSION

In our study, an MM-based absorber was designed that exhibits high absorption performance in four bands with absorption values (rates) of 0.9971 (99.71%), 0.9981 (99.81%), 0.9995 (99.95%), and 0.9997 (99.97%), respectively, at four resonance frequencies of 2.365 GHz, 4.95 GHz, 12.3 GHz, and 18.61 GHz, respectively, in the microwave S-, C-, Ku-, and K-bands. Additionally, the suggested absorber can provide wide-angle absorption under both polarization angle and oblique incidence (up to 30° for ϕ and up to 60° for θ). MM absorber consisting of two square-shaped ring copper patches with a slit on one arm printed on a 2.8 mm thick FR-4 dielectric substrate with full copper lamination on the bottom plane can be easily realized.

References

[1] S. Akram, M. Ashraf, A. Javid, H. A. Abid, S. Ahmad, Y. Nawab, et al., "Recent advances in electromagnetic interference (EMI) shielding textiles: A comprehensive review," *Synth. Met.*, vol. 294, art. no. 117305, Apr. 2023.

[2] Z. Q. Du, J. G. Liang, T. Cai, G. M. Wang, T. W. Deng, and B. R. Wu, "Designing an ultra-thin and wideband low-frequency absorber based on lumped resistance," *Opt. Express*, vol. 30, no. 2, pp. 914–925, Jan. 2022.

[3] X. J. Liu, F. Xia, M. Wang, J. Liang, and M. J. Yun, "Working mechanism and progress of electromagnetic metamaterial perfect absorber," *Photonics*, vol. 10, no. 2, art. no. 205, Feb. 2023.

[4] S. Jorwal, A. Dubey, R. Gupta, and S. Agarwal, "A review: Advancement in metamaterial based RF and microwave absorbers," *Sens. Actuators A-Phys.*, vol. 354, art. no. 114283, May 2023.

[5] A. Parveen, A. Irshad, M. Um-e-Kalsoom, M. N. U. Shah, D. Tyagi, M. Alam, et al., "A review on advancing electromagnetic wave absorption in metamaterials: Progress, challenges, theoretical background, and advanced technological applications," *Adv. Mater. Technol.*, vol. 10, no. 20, Oct. 2025.

[6] F. Costa, A. Monorchio, and G. Manara, "Theory, design and perspectives of electromagnetic wave absorbers," *IEEE Electromagn. Compat. Mag.*, vol. 5, no. 2, pp. 67–74, Aug. 2016.

[7] Q. A. Alsulami, S. Wageh, A. A. Al-Ghamdi, R. M. H. Bilal, and M. A. Saeed, "A tunable and wearable dual-band metamaterial absorber based on polyethylene terephthalate (PET) substrate for sensing applications," *Polym.*, vol. 14, no. 21, art. no. 4503, Nov. 2022.

[8] G. W. Duan, J. Schalch, X. G. Zhao, A. B. Li, C. X. Chen, R. D. Averitt, et al., "A survey of theoretical models for terahertz electromagnetic metamaterial absorbers," *Sens. Actuators A-Phys.*, vol. 287, pp. 21-28, Mar. 2019.

[9] Y. Q. Zhang, W. J. Zhou, X. F. Qin, Q. Zhao, Y. X. Chen, X. Y. Zhang, et al., "Broadband tunable terahertz near-perfect absorber enabled by rotationally symmetric single-layer graphene: A theoretical study," *Phys. Lett. A*, vol. 546, art. no. 130502, Jun. 2025.

[10] Q. Zhou, B. Xue, S. Y. Gu, F. Ye, X. M. Fan, and W. Y. Duan, "Ultra broadband electromagnetic wave absorbing and scattering properties of flexible sandwich cylindrical water-based metamaterials," *Results Phys.*, vol. 38, art. no. 105587, Jul. 2022.

[11] R. Rahad, A. M. Mohsin, M. B. H. Bhuian, and M. M. Rahman, "Graphene-metamaterial based tunable broadband polarization ınsensitive absorber for terahertz antenna design," *IEEE Access*, vol. 12, pp. 48654–48667, 2024.

[12] S. Gangula, M. Vinukonda, and N. Rao, "Polarization ınsensitive absorber with ıncreased bandwidth using multilayer metamaterial," *Int. J. Electron. Commun. Eng.*, vol. 14, no. 8, pp. 246–250, 220.

[13] C. M. Watts, X. L. Liu, and W. J. Padilla, "Metamaterial electromagnetic wave absorbers," *Adv. Mater.*, vol. 24, no. 23, pp. OP98–OP120, Jun. 2012.

2nd International Conference on Multidisciplinary Sciences and Technological Developments (ICMUSTED 2025)

December 12-15, 2025

Enhanced Activation of Peroxymonosulfate by a Mixed Oxide Co_2O_4-Fe_2O_3 for Sunset Yellow Dye Removal

Djedjiga Bousalah[1,2], Hanane Zazoua[1], Amel Boudjemaa[1], Khaldoun Bachari[1], Nahed Dokhan[2], Mohamed Zine Messaoud-Boureghda[3], Fayrouz Benhaoua[2]

[1]Scientific and Technical Research Center for Physico-Chemical Analyses, 42004 Bou-Ismail, Algeria
[2]Materials Processes and Environment Research Unit, M'hamed Bougara University, Boumerdes, Algeria
[3]Food Technology Research Laboratory, M'hamed Bougara University, Boumerdes, Algeria
Corresponding author: Djedjiga Bousalah (e-mail: bousalahdj2015@gmail.com)

Abstract

This research investigated the application of a mixed oxide Co_2O_4-Fe_2O_3, for the activation of peroxymonosulfate (PMS) in the degradation of sunset yellow (SY) dye in aqueous medium. The catalyst was characterized using various techniques including X-ray diffraction (XRD), scanning electron microscopy coupled with energy-dispersive X-ray spectroscopy (SEM-EDX), the Brunauer-Emmett-Teller (BET) method and Fourier transform infrared (FTIR) spectroscopy. Complete elimination (100 %) of SY was achieved within in 90 min under optimal conditions: initial dye concentration = 50 mg/L, Peroxymonosulfate concentration = 0.4 mM, pH = 7, catalyst dose = 0.1g/L, and temperature = 20 °C, with a first-order rate constant (k) of 0.02372 min^{-1}. Radical quenching experiments using tert-butyl alcohol and methanol revealed that $SO_4^{\bullet -}$ and $^{\bullet}OH$ were generated during PMS activation process by Co_2O_4-Fe_2O_3 with ($SO_4^{\bullet -}$) playing the dominant role in the degradation process. Furthermore, the composite successfully activated PMS for SY degradation over three consecutive catalytic cycles without any significant loss of activity. Under the same optimal conditions, the rate constants were 0.03462 and 0.02372 min^{-1} for the photocatalytic and catalytic systems, respectively, indicating that light irradiation had no significant effect on the reaction rate.

Keywords: Co_2O_4-Fe_2O_3, Peroxymonosulfate (PMS), Sulfate radicals, Sunset yellow, Catalytic oxidation

2nd International Conference on Multidisciplinary Sciences and Technological Developments (ICMUSTED 2025)

December 12-15, 2025

Applications of MEMS Sensors and Micropneumatics in Automated Systems

Goran Čubrić[1], Ivana Salopek Čubrić[2]

[1]Department of Clothing Technology, University of Zagreb Faculty of Textile Technology, Zagreb, Croatia
[2]Department of Textile Design and Management, University of Zagreb Faculty of Textile Technology, Zagreb, Croatia
Corresponding author: Goran Čubrić (goran.cubric@ttf.unizg.hr)

Abstract

Micro-electro-mechanical systems (MEMS) integrate electronic and mechanical components at the microscale. They are characterized by high precision, low energy consumption, and the ability to be embedded in limited spaces. In the textile and clothing industry, MEMS are primarily used as sensors, while the role of actuators remains limited due to low generated forces and unfavorable operating conditions. A key application is the control of relative humidity during yarn spinning. Humidity directly affects fiber strength, elasticity, and static charge. MEMS sensors enable precise measurement and regulation, improving yarn quality and process efficiency. Another important area is the detection of thread breakage in weaving. Accelerometers placed on warp sheets detect acceleration changes, allowing non-contact break detection. This reduces downtime and increases productivity. MEMS technology also supports the development of smart and intelligent clothing. Integrated sensors monitor environmental conditions and biological signals, enabling adaptive and interactive garments. Alongside MEMS, micropneumatics is being developed. Miniaturized pneumatic elements act as actuators in clothing, for example, to adjust thermal insulation via air chambers. Artificial pneumatic muscles are also being explored. These flexible actuators can be embedded in gloves or garments to assist movement, particularly for elderly or mobility-impaired users. In production processes, micropneumatics automates sewing, cutting, and material handling, increasing precision and efficiency. The integration of MEMS and micropneumatics represents a significant step toward smart, functional, and highly automated textile systems.

Keywords: Sensors, MEMS, Micropneumatics, Industry, Automation

2nd International Conference on Multidisciplinary Sciences and Technological Developments (ICMUSTED 2025)

December 12-15, 2025

First-Principles Investigation of ABX_3 Perovskites: Structural and Functional Properties for Spintronic Applications

Saadiya Benatmane[1,2]

[1]Faculty of Sciences and Technology, Department of Science and Technology, Abdelhamid Ibn Badis University, 27000 Mostaganem, Algeria
[2]Laboratory of Modelling and Simulation of Materials Science, Djillali Liabes University of Sidi Bel-Abbes, 22000 Sidi Bel-Abbes, Algeria
Corresponding author: Saadiya Benatmane (e-mail: saadia.benotmane@univ-mosta.dz)

Abstract

This study presents a comprehensive first-principles investigation of the structural, elastic, electronic, magnetic, and optical properties of cubic nitride perovskites $BaCaN_3$ and $BaSrN_3$. Calculations were performed using the WIEN2k code based on the full-potential linearized augmented plane wave (FP-LAPW) method within the framework of density functional theory (DFT). Both the generalized gradient approximation of Perdew-Burke-Ernzerhof (GGA-PBE) and the modified Becke–Johnson (mBJ) potential were employed to accurately describe the electronic structure. The equilibrium structural parameters were obtained by fitting the Birch–Murnaghan equation of state, confirming the stability of both compounds in their cubic phase at the ground state. Elastic constants, calculated via the IRelast package, reveal that both $BaCaN_3$ and $BaSrN_3$ are mechanically stable, ductile, and elastically anisotropic. These results are further supported by the computed Pugh's ratio and Poisson's ratio. The electronic band structure indicates that both compounds exhibit half-metallic behavior, with metallic character in one spin channel and semiconducting behavior in the other. A direct band gap was observed in the spin-down channel, with values of 4.28 eV and 3.81 eV for $BaCaN_3$ and $BaSrN_3$, respectively, and 6.31 eV and 6.42 eV using mBJ. Density of states (DOS) and partial DOS analyses reveal that the N-2p orbitals dominate near the Fermi level. The total magnetic moment was found to be an integer value of 5 μB for both compounds, confirming their half-metallic ferromagnetic nature. The magnetism mainly originates from the spin polarization of nitrogen p-electrons. Finally, the calculated optical properties, including the frequency-dependent refractive index n(ω) and extinction coefficient k(ω), provide additional insight into the potential of $BaCaN_3$ and $BaSrN_3$ for spintronic and optoelectronic applications.

Keywords: Perovskites, Elastic properties, Optical properties, Density functional theory, Energy gap

2nd International Conference on Multidisciplinary Sciences and Technological Developments (ICMUSTED 2025)

December 12-15, 2025

Multimodal Large Language Models and Image Processing: A Bibliometric and Network Analysis for the Period 2023–2025

Adem Korkmaz[1], Selma Bulut[2]

[1]Department of Computer Technologies, Bandirma Onyedi Eylul University, Bandirma, Türkiye
[2]Department of Computer Technologies, Kirklareli University, Kirklareli, Türkiye
Corresponding author: Adem Korkmaz (e-mail: ademkorkmaz@bandirma.edu.tr)

Abstract

This study presents a comprehensive bibliometric and network analysis of 1,067 unique English-language articles published between 2023 and 2025 in the Web of Science and Scopus databases, systematically mapping the intersection of multimodal large language models (MM-LLMs) and image processing. Using a unified dataset constructed through digital object identifier (DOI)-based merging and deduplication, the analysis first examines annual publication trends, distribution across application domains, author collaboration networks, and the co-occurrence structure of author keywords. The findings reveal a marked increase in multimodal LLM research, particularly in 2025, indicating rapid growth of the field over a relatively short period. The application-domain analysis shows that the highest concentration of output is in medical imaging and healthcare applications, followed by general-purpose vision–language tasks and safety-critical domains such as autonomous driving, remote sensing, industrial inspection, and robotics. The keyword co-occurrence network demonstrates that the concepts of "large language models," "multimodal large language models," "deep learning," and "computer vision" occupy central positions in the network, with task- and domain-oriented terms clustering around this core. The co-authorship analysis further indicates that scientific output is concentrated mainly around a few dominant research groups, that there are relatively few bridge authors connecting clusters, and that the collaboration structure still exhibits a fragmented pattern. Overall, the results provide a holistic picture of the current state of the multimodal LLM–image processing literature and make visible both mature and relatively underexplored thematic areas for future research.

Keywords: Multimodal large language models, Image processing, Bibliometric analysis, Keyword co-occurrence, Co-authorship network

1. INTRODUCTION

Large language models (LLMs) have rapidly evolved from text-only systems into general-purpose reasoning engines that achieve near-human-level performance on a wide range of tasks, from professional exams to complex coding and mathematical problem-solving [1, 2]. The introduction of GPT-4, a large-scale multimodal model that accepts both image and text inputs, marked a critical inflection point, demonstrating that the same generative backbone can interpret visual content, answer questions about images, and support complex decision-making pipelines [1]. In parallel, domain commentaries in medicine and imaging have begun to position LLMs and their multimodal extensions as a new infrastructure layer for clinical and scientific workflows [2].

Building on these advances, multimodal large language models (MLLMs) integrate vision encoders with robust LLM backbones to process and reason over heterogeneous data such as images, text, video, and other sensory inputs [3, 4]. Recent surveys highlight that MLLLMs typically adopt modular architectures that bridge pretrained visual and textual components via projection layers or cross-attention, and that they are increasingly trained with instruction-following objectives on large-scale image–text corpora [3,4]. Wu et al. provide an early taxonomy of multimodal architectures, training strategies, and evaluation protocols, emphasizing the role of LLMs as a "reasoning core" over unified multimodal representations [3]. Yin et al. further argue that MLLMs, exemplified by GPT-4V, may represent a plausible path toward more general artificial intelligence, given their emergent abilities in story writing from images, optical character recognition (OCR)-free mathematical reasoning, and cross-domain transfer [4].

These conceptual developments are grounded in concrete model families. Flamingo, introduced by DeepMind, demonstrated that a single visual language model can achieve state-of-the-art few-shot performance across diverse vision–language tasks by coupling frozen vision and language backbones through a lightweight cross-attention

layer [5]. Large language and vision assistant (LLaVA) extended the idea to instruction tuning: by pairing a CLIP-like vision encoder with a Vicuna-based LLM and training on GPT-4-generated multimodal instruction data, LLaVA achieves impressive open-ended visual dialogue and strong performance on benchmarks such as ScienceQA [6]. Such models typify a broader trend in which multimodal instruction tuning and alignment techniques initially developed for text-only LLMs are being adapted to vision–language settings.

The impact of MLLMs is noticeable in safety-critical image-based domains. In healthcare, multimodal models that combine clinical text with radiological images are being explored for automated report generation, visual question answering, triage support, and interactive decision assistance [7]. Recent reviews in radiology and medical imaging emphasize that MLLMs can integrate heterogeneous inputs, including two-dimensional (2D) radiographs, three-dimensional (3D) computerized tomography (CT)/magnetic resonance imaging (MRI), free-text clinical notes, and structured metadata, within a single reasoning framework, enabling more holistic analyses than traditional unimodal systems [8]. Concrete implementations, such as chest X-ray (CXR)-LLaVA, demonstrate that domain-adapted MLLMs can detect key findings on chest X-rays and generate radiology reports with higher clinical fidelity than general-purpose models [9].

Beyond medicine, similar patterns are emerging in other high-stakes application areas. In autonomous driving, DriveGPT4 leverages multimodal LLMs to jointly interpret multi-frame video streams, explain vehicle actions in natural language, and predict low-level control signals in an end-to-end fashion, thereby combining perception, planning, and explanation in a single interpretable pipeline [10]. In remote sensing, EarthGPT is a universal MLLM tailored to multi-sensor satellite imagery, unifying scene classification, image captioning, visual question answering, and grounding tasks across optical, SAR, and infrared modalities through conversational interfaces [11]. These examples illustrate how multimodal LLMs are reshaping the landscape of computer vision by framing classical perception problems as components of interactive, language-mediated systems.

At the same time, early empirical evaluations in clinical and diagnostic contexts reveal substantial limitations and risks. Benchmarking studies comparing multimodal artificial intelligence (AI) systems with human experts on medical image challenges report that current models can match or exceed average human accuracy on some tasks, yet remain sensitive to distribution shifts, incomplete inputs, and prompt variations [12]. Reviews in medical imaging and radiology highlight unresolved issues around hallucinated findings, lack of transparency in decision paths, data scarcity for high-quality multimodal training sets, and the computational costs of deploying large models in real-world workflows [8]. These concerns reinforce the need for systematic mapping of where and how MLLMs are being deployed, which tasks and domains are most mature, and where critical research gaps remain.

A growing body of survey work has begun to address parts of this agenda. Technical overviews synthesize architectural taxonomies, training paradigms, and benchmark suites for general-purpose MLLMs [3, 4]. Domain-focused reviews in healthcare discuss use cases such as medical report generation and visual question answering, as well as regulatory and ethical implications [7, 8, 13]. However, existing surveys largely adopt a narrative or exemplar-based approach; they do not systematically quantify the evolution of the field in terms of publication trends, co-authorship structures, or topic clusters over the period in which MLLMs have rapidly proliferated (2023–2025). In particular, there is a lack of bibliometric work that jointly (i) maps the intellectual structure of multimodal LLM research at the intersection of text and images, and (ii) links this structure to application domains such as medical imaging, autonomous driving, robotics, industrial inspection, and remote sensing.

2. MATERIAL AND METHOD

This study was designed as a descriptive bibliometric analysis and conceptual mapping of the academic literature on multimodal large language models (MM-LLMs) and image processing published between 2023 and 2025. The aim is to identify (i) publication volume and temporal trends systematically, (ii) distribution across application domains, (iii) key concepts and research themes, (iv) the structure of collaborations, and (v) the most influential works.

The literature search was conducted in two major citation databases: Web of Science Core Collection (WoS) and Scopus. In both databases, the search strategy focused on capturing multimodal LLMs and their use in image processing tasks.

In WoS, the search was carried out in the Author Keywords field using query combinations of the following type:

- “multimodal” OR “multi-modal” OR “vision-language model” OR “vision language model”
- “large language model*” OR LLM* OR “foundation model*” OR “generative AI”

- “image caption*”, “visual question answering”, “VQA”, “visual grounding”, “text-to-image”, “image generation”

These terms were combined using AND/OR operators, and the search results were restricted to the years 2023–2025. In Scopus, a similar conceptual scope was targeted in the keywords field, and the same key terms were used with appropriate logical operators. In both databases, the following filters were applied:

- Document type: “article” only (peer-reviewed journal articles),
- Language: English,
- Year range: 2023–2025.

After applying the inclusion and exclusion criteria, 707 articles were retrieved from WoS and 858 from Scopus. The retrieved records were evaluated according to the following criteria: studies were included if they (i) were peer-reviewed journal articles published between 2023 and 2025 in English, (ii) involved a multimodal or vision–language model using at least two modalities (text + image), and (iii) reported an experimental evaluation on a task directly related to image processing (e.g., visual question answering (VQA), image captioning, visual grounding, text-to-image generation, image classification/segmentation, etc.). Conference papers, book chapters, editorials, opinion pieces, short notes, and records available only in abstract form were excluded, as were studies that considered only unimodal LLMs (text-only) or unimodal visual models (image-only) without text–image integration, and papers that mentioned MM-LLMs only conceptually without reporting experimental or applied results. These filters were used directly in the database interfaces wherever possible, and subsequently, titles and abstracts were screened to remove additional out-of-scope records.

2.1. Record Integration and Digital Object Identifier (DOI)-Based De-Duplication

The records retrieved from WoS and Scopus were integrated using a DOI-based merging approach to construct a single study universe. The following steps were applied to the DOI fields in both databases:

- DOI normalization: Leading and trailing whitespaces were removed; prefixes such as https://doi.org/, http://doi.org/, and doi: were stripped; and all characters were converted to lowercase to create a standardized DOI field (DOI_norm).
- Removal of invalid and missing DOIs: Records with empty or invalid DOI fields were excluded from the analysis.
- Within-database de-duplication: In each of the WoS and Scopus files, duplicate entries with the same DOI were identified, and only a single record was retained for each DOI.
- Cross-database de-duplication and merging: Scopus was taken as the reference source in terms of standardization of bibliometric fields. For each DOI, the Scopus record was prioritized, and WoS records with the same DOI were treated as duplicates. For DOIs present in WoS but absent in Scopus, the corresponding WoS records were transformed to match the Scopus field structure (authors, title, year, journal name, abstract, keywords, etc.) and then added to the dataset.

As a result of this process, records from the two databases were de-duplicated at the DOI level, yielding a master dataset of 1,067 unique articles. This dataset was exported in comma-separated values (CSV) format and used as the primary data source for subsequent bibliometric analyses.

2.2. Bibliometric Analysis

Descriptive bibliometric analyses were conducted on the unified dataset. First, the number of publications was analyzed by year (2023, 2024, 2025) and by distribution across application domains. Application domains were determined through a rule-based classification of article titles, abstracts, and author keywords. Based on characteristic key phrases appearing in the text, the following categories were defined:

- Medical/Healthcare (medical imaging, clinical applications),
- Autonomous Driving/Transportation,
- Remote Sensing,
- Industrial/Manufacturing,
- Robotics,
- General Vision/AI (general vision–language tasks without a specific domain), and
- Other/Unspecified (studies that do not specify a clear application domain).

The automatic assignments were manually checked and corrected for ambiguous or borderline cases. To examine author productivity, names in the Authors field formatted as Surname, I. were parsed, the total number of publications was calculated for each author label, and the most prolific author clusters were identified. To assess citation impact, the "Cited by" field from Scopus was used to rank the most highly cited works.

2.3. Network Analyses: Keyword Co-Occurrence and Co-Authorship

To examine the conceptual structure and collaboration networks, two primary network analyses were conducted using VOSviewer (v1.6.x):

Co-occurrence analysis of author keywords:

- Unit of analysis: Author keywords,
- Inclusion threshold: Keywords occurring at least 3 times,
- Counting method: Complete counting,
- Normalization: Association strength metric (VOSviewer default), and
- Clustering: Thematic clusters automatically identified using the visualization of similarities (VOS) clustering algorithm.

This analysis visualized the central position of core concepts such as "large language models", "multimodal large language models", "deep learning", and "computer vision" within the network, along with task/application-related terms associated with them, thereby revealing the field's conceptual map.

2.4. Co-Authorship Network Analysis

- Unit of analysis: Authors,
- Inclusion threshold: authors with at least one publication and 1 citation,
- Counting method and normalization: VOSviewer default settings, and
- Clustering: VOS clustering algorithm.

This network was used to visualize the leading research groups in the literature, the intensity of collaboration within and between these groups, and the authors who act as bridges between clusters.

2.5. Ethical Considerations

This study was conducted exclusively on bibliographic metadata obtained from open academic databases and does not involve any individual participant data or personal data. Therefore, no procedures requiring ethics committee approval were undertaken. Nevertheless, all analyses were carried out in accordance with the terms of use of the respective databases and with general principles of research ethics.

3. RESULTS

3.1. Overall Publication Profile and Temporal Trends

The unified dataset constructed after DOI-based de-duplication of records from the WoS and Scopus databases consists of 1,067 unique articles. This dataset covers English-language journal articles published between 2023 and 2025.

Based on Scopus metadata, the yearly distribution shown in Figure 1 indicates that nine articles were published in 2023, 124 in 2024, and 725 in 2025. This pattern reveals that the literature at the intersection of multimodal large language models and image processing has grown extremely rapidly in a very short period. While a limited number of proof-of-concept studies represent 2023, publication volume increased substantially in 2024, and 2025 witnessed a pronounced "explosion" of both methodological and application-oriented work. A similar upward trend is observed in WoS, which is likewise restricted to the 2023–2025 period, indicating that multimodal LLM research has quickly become one of the field's central topics.

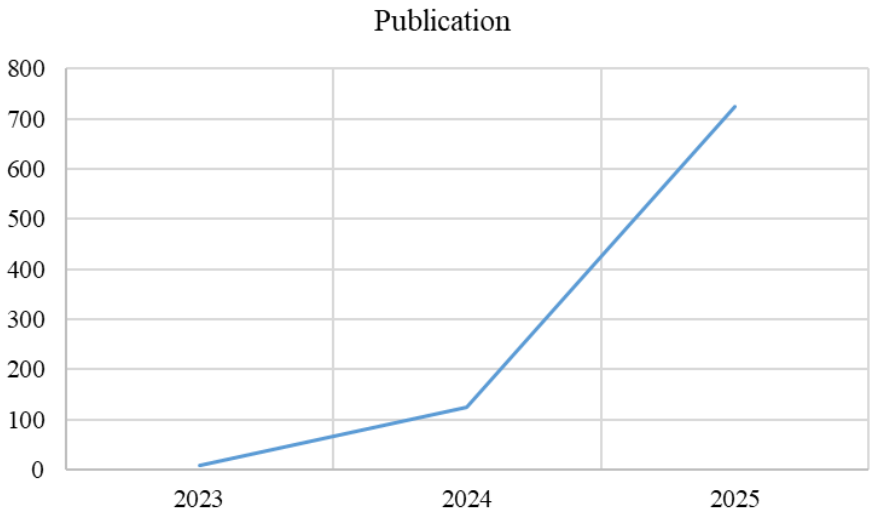

Figure 1. Number of publications by year

3.2. Publication Distribution by Application Domain

The rule-based classification of article titles, abstracts, and keywords indicates that multimodal LLM-based image processing studies span several application domains. The domain-based distribution of the 1,067 articles is approximately as follows:

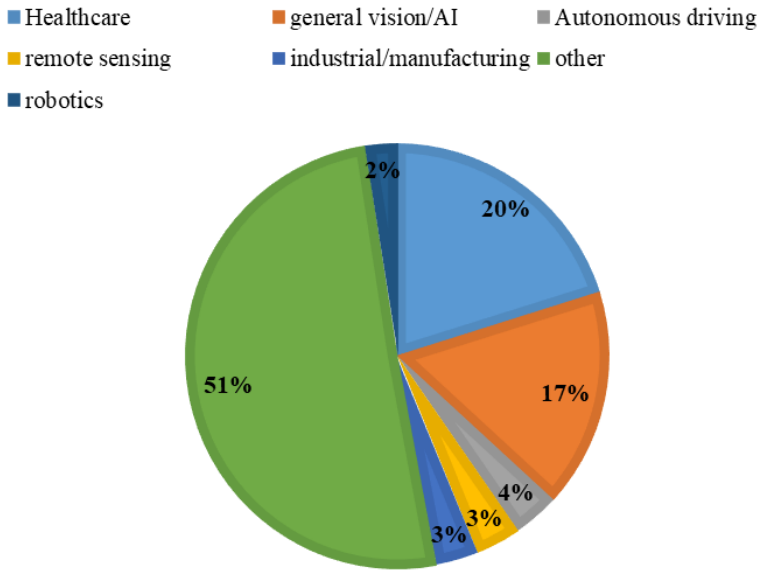

Figure 2. Publication distribution by application domain

As shown in Figure 2, when the distribution of the 1,067 articles at the intersection of multimodal large language models and image processing is examined by application domain, it is observed that the most significant share belongs to the medical imaging and healthcare field; the Medical/Healthcare category, with 215 articles, accounts for approximately 20.1% of the total. This is followed by the general vision/AI category, which primarily includes general-purpose vision–language tasks conducted on datasets such as COCO and Visual Genome, with 178 articles (16.7%). Among safety-critical application areas, there are 38 articles (3.6%) in the Autonomous Driving/Transportation category, 37 articles (3.5%) in remote sensing (remote sensing, satellite/aerial imagery), 34 articles (3.2%) in the Industrial/Manufacturing category focusing on industrial inspection and production processes, and 26 articles (2.4%) in Robotics. The remaining 539 articles (50.5%) are grouped under the other/unspecified category, comprising studies whose titles, abstracts, and keywords do not clearly indicate a specific application domain or remain at a very general level.

There are several possible reasons for this high proportion. First, given that multimodal LLM research is still a relatively new field, a substantial portion of the work focuses on core methodological developments (new architectures, training techniques, evaluation protocols). Such studies aim to improve general capabilities rather

than target a specific application context and therefore may not carry an explicit "application domain" label [3,4]. Second, many studies investigate general visual understanding tasks (VQA, image captioning) on broad, diverse datasets without explicitly linking them to a particular sector, such as automotive or healthcare. Third, some research is interdisciplinary or exploratory in nature and may not yet be described using a standardized application-domain terminology. This can be seen as a reflection of the field's dynamic and rapidly evolving nature. In future work, a more detailed content analysis of the studies in this broad category would help identify emerging sub-themes.

The General Vision/AI category encompasses studies that focus primarily on VQA, image captioning, visual grounding, and text-to-image generation tasks on general-purpose datasets such as COCO and Visual Genome, and that do not bear a label associated with any specific application domain. Fields such as autonomous driving, remote sensing, industrial quality control, and robotics, while smaller in number, stand out as niche subdomains that are safety-critical and have high-risk, high-impact potential. The high proportion of the Other/Unspecified category indicates that many methodological or theory-oriented studies do not define a clear application context.

3.3. Conceptual Structure: Co-Occurrence of Author Keywords

Figure 3 depicts the co-occurrence network constructed from author keywords that appear at least three times. Nodes represent keywords, node size reflects frequency of occurrence, and colors indicate thematic clusters identified by the VOSviewer clustering algorithm.

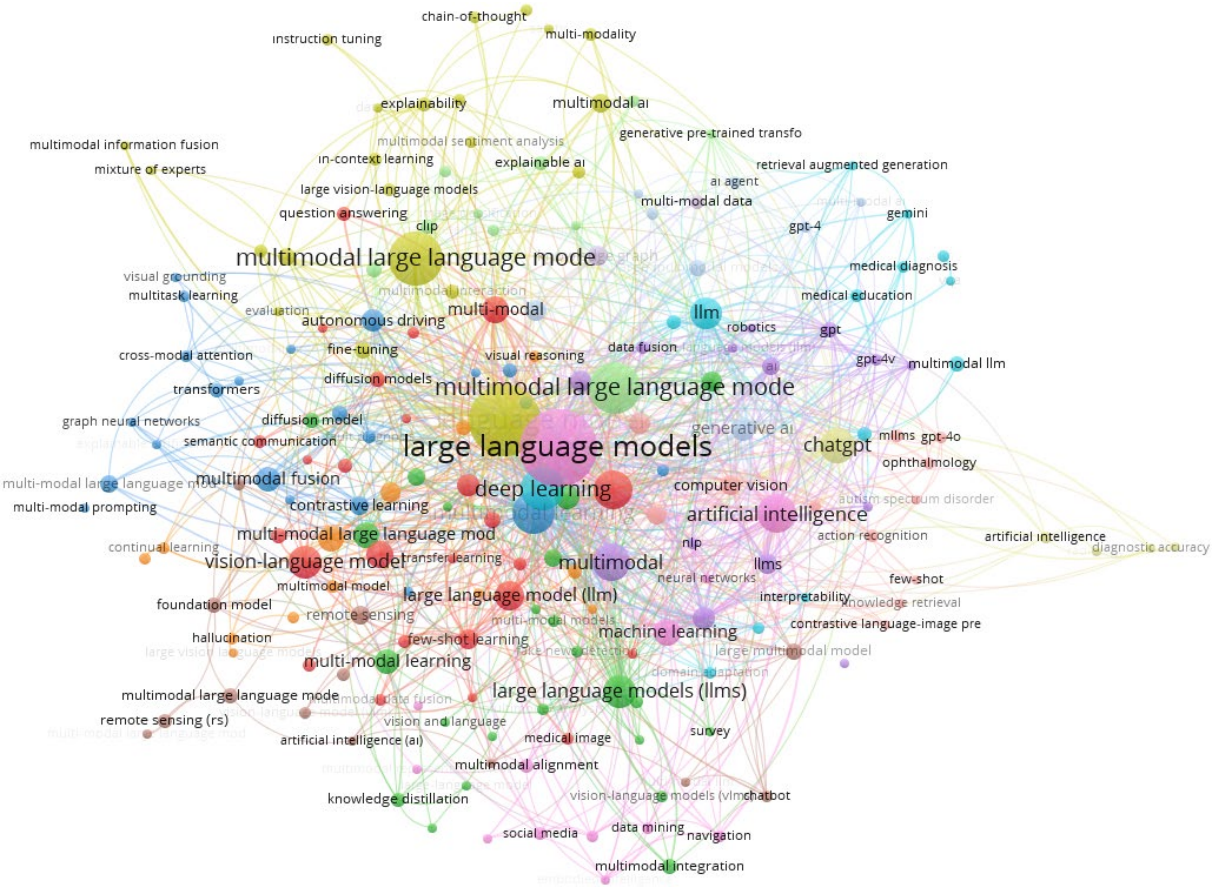

Figure 3. Co-occurrence network of author keywords (Minimum frequency: 3 keywords)

At the center of the network, the largest nodes correspond to "large language models," "multimodal large language models," and closely related terms such as "deep learning," "artificial intelligence," and "computer vision." The high frequency of these concepts and their dense connections with many other terms indicate that a substantial portion of the literature is still organized around an LLM-centered multimodal paradigm.

Around this central core, numerous subclusters, each represented by a different color, emerge. Within these clusters:

- On one side, architecture- and methodology-oriented terms such as “vision-language models”, “multimodal learning”, and “foundation models”,
- On another, concepts denoting specific tasks such as VQA, image captioning, visual grounding, and text-to-image generation,
- As well as smaller nodes reflecting application domains such as medical imaging, autonomous driving, and remote sensing, are observed.

Moving from the center toward the periphery, the keywords become more niche and task- or domain-specific. This structure suggests that the literature is characterized by both a broad shared core (LLMs + multimodal learning) and diversification into multiple application-focused directions; accordingly, the research ecosystem exhibits diversity both horizontally (across different tasks and domains) and vertically (deepening within specific areas).

3.4. Collaboration Structure: Co-Authorship Network

Figure 4 presents the co-authorship network constructed among authors who meet the threshold of at least one publication and one citation. Nodes represent authors, edges denote co-authorship relations, and colors indicate collaboration clusters.

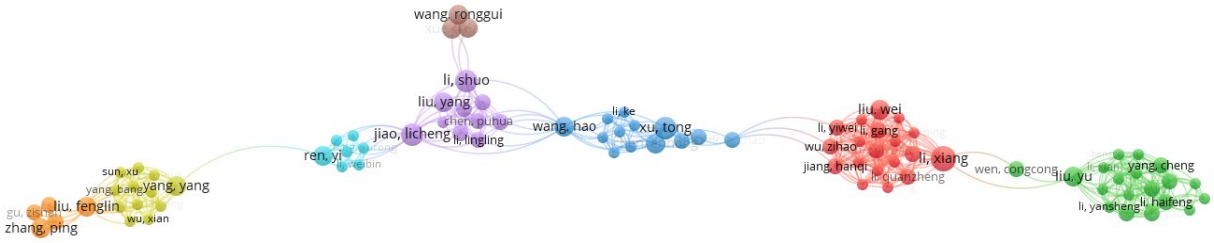

Figure 4. Co-authorship of authors (1 publication and 1 citation)

The overall structure of the network reveals several relatively distinct, strong research groups in the literature. The red and green clusters on the right-hand side represent core teams with dense internal connections and multiple joint publications; these typically correspond to groups within the same institution or national network and engage in regular collaboration. The yellow and orange clusters on the left-hand side correspond to smaller but similarly locally focused research groups.

There appear to be relatively few “bridge” authors between clusters; some nodes located in the central part of the network connect multiple clusters. These authors act as intermediary agents who contribute to the network's integration by collaborating both within their own groups and with external groups. Nevertheless, the overall structure remains fragmented and group-based, suggesting that large-scale, continuous, and multi-center international collaborations remain limited. This indicates that, in the future, increased inter-cluster collaboration could further strengthen the circulation of knowledge across disciplines and geographies.

The co-authorship network analysis thus shows that the collaboration structure in the field is markedly fragmented and clustered around a few dominant research groups. This fragmented structure can be interpreted as an indicator that the intersection of multimodal LLMs and image processing is still an emerging and maturing research area. In new and rapidly developing fields, collaborations typically first form within existing laboratories, institutions, or strong national networks, and inter-cluster bridge connections emerge over time [14]. The limited number of bridge authors observed in the present analysis may indicate that knowledge and methodological approaches have not yet fully diffused across different research communities. While this may constrain the potential for interdisciplinary innovation, it may also slow the development of synergistic approaches to problems in various application areas (e.g., medicine and autonomous driving). As the field matures, fostering stronger cross-cluster collaborations through conferences, shared datasets, and benchmark initiatives will be critical for accelerating innovation and reducing methodological redundancy [15].

3.5. Most Prolific Authors and Most Influential Studies

The author productivity analysis was conducted using names in the authors field formatted as Surname, I. As a result, different individuals sharing the same surname–initial combination may be grouped under a single label; the findings should therefore be interpreted with this limitation in mind. Within this framework, the most frequently occurring author labels include “Li, Y.” (38 publications), “Wang, Y.” (37), “Zhang, Y.” (28), and “Li,

Z.", "Li, J.", and "Liu, Y." (27 publications each). This pattern reflects the intensive contribution of the research ecosystem in China and surrounding regions to the multimodal LLM and image processing literature.

An examination of the most highly cited studies using the "Cited by" field in Scopus shows that specific themes have achieved substantial impact within a short period of time. Among the top 10 articles, prominent topics include:

- LLM-based end-to-end driving models in autonomous driving (e.g., DriveGPT4),
- multimodal LLM applications in healthcare (chest radiography, pathology images, multimodal LLM surveys in medicine),
- multimodal models developed for remote sensing and Earth observation (e.g., EarthGPT),
- ChatGPT and exam security, and
- comprehensive evaluations of the multimodal capabilities of GPT-4o.

These findings indicate that multimodal LLMs are rapidly assuming a central role—both in research interest and in citation impact — in data-intensive and safety-critical domains such as healthcare, autonomous driving, and remote sensing.

4. CONCLUSION

In this study, the intersection of multimodal large language models (MM-LLMs) and image processing was mapped, both bibliometrically and conceptually, using 1,067 unique articles compiled from WoS and Scopus between 2023 and 2025. The findings show that the transition from text-centric LLMs to multimodal, vision–language architectures, exemplified by GPT-4 and similar models, represents not only a conceptual but also a dramatic quantitative shift in publication volume and topic diversity [1, 3, 4]. In particular, the surge in publications observed in 2025 indicates that multimodal LLMs have moved beyond being a niche research topic and have become a central component of the computer vision and artificial intelligence literature.

An examination of domain distribution reveals that MM-LLM–based image processing studies are most densely clustered in medical imaging and healthcare, followed by general-purpose vision–language tasks and safety-critical applications such as autonomous driving, remote sensing, industrial inspection, and robotics. This result is consistent with recent work discussing the potential role of MLLMs in medical imaging and clinical workflows [2, 7, 8]. In particular, medical MLLM applications, such as CXR-LLaVA, developed for chest radiography, pathology images, and clinical report generation, substantiate the medical focus identified in our analysis with concrete examples [8, 9]. Similarly, the way DriveGPT4 unifies the perception–decision–action pipeline in autonomous driving within a single, explainable multimodal chain [10] and EarthGPT's integration of multi-sensor remote sensing data with language interfaces [11] aligns with the autonomous systems and remote sensing clusters observed in the literature.

The co-occurrence analysis of author keywords showed that concepts such as "large language models," "multimodal large language models," "deep learning," and "computer vision" occupy central positions in the network and are densely connected to numerous task and application terms. This structure is consistent with Wu et al.'s taxonomy, which positions multimodal LLMs as a "central reasoning core" operating over visual and textual representations [3], and with Yin et al.'s assessment that frames multimodal LLMs as a possible intermediate step toward more general intelligence [4]. The co-authorship network, in turn, demonstrated that scientific output is concentrated mainly around a few dominant research groups and geographically defined clusters, that there are relatively few authors acting as bridges across clusters, and that a fully global, densely connected collaboration network has not yet emerged.

This study complements existing technical and domain-focused surveys [3, 4, 7, 8, 13] by adding a bibliometric perspective. While current surveys and domain reviews primarily provide in-depth discussions of architectures, training strategies, and benchmark suites through exemplar model families such as Flamingo and LLaVA [5, 6], the present study systematically characterizes the quantitative evolution of the field, topic clusters, collaboration structures, and highly cited core works over the same period. In doing so, it situates the opportunities and risks highlighted in studies on multimodal AI in medical imaging [2, 7–9], autonomous driving [10], remote sensing [11], and clinical diagnosis evaluation [12] within a broader publication universe.

Nevertheless, the study has several limitations. First, the analysis is restricted to WoS and Scopus, excluding other databases and grey literature. Second, only English-language journal articles with DOIs were included, which may limit the representation of linguistic and regional diversity. Third, the application-domain and task classifications

were derived using a rule-based approach that relied on titles, abstracts, and keywords, without deep analysis of full-text content. Finally, performance indicators and error types were not quantitatively synthesized at a meta-analytic level; instead, conceptual and thematic trends were foregrounded.

Several concrete directions emerge for future work. First, as seen in evaluation and comparison studies on the clinical performance of multimodal AI in medical imaging and diagnosis [2, 8, 12], systematic task-level meta-analyses of different MLLMs (e.g., for VQA, report generation, segmentation) would help delineate capability boundaries more objectively. Second, there is a need for more domain-specific, mixed-methods research (e.g., in radiology, pathology, and autonomous driving) that jointly examines critical risks such as hallucination, bias, explainability, and data privacy [2, 7, 8, 12] within real-world workflows and regulatory frameworks. Third, longitudinal bibliometric analyses extending beyond 2025 could track the diffusion dynamics of new MLLM families (e.g., lighter-weight, energy-efficient, domain-specialized models) [3, 4] and shed light on the transition from "single large models" to multi-model, ecosystem-based solutions.

In conclusion, this study provides an integrated framework that characterizes the position and evolution of multimodal large language models in image processing, using bibliometric and network analysis tools. This framework offers an evidence-based reference point for technical and domain-focused surveys to build upon. It makes visible to policymakers, research funders, and practitioners which tasks and application domains have reached relative maturity and which still contain substantial research gaps. In doing so, it helps shape the multimodal LLM research agenda in a more balanced, reliable, and socially responsible manner.

References

[1] OpenAI, J. Achiam, S. Adler, S. Agarwal, L, Ahmad, I. Akkaya, et. al., "GPT-4 Technical Report," *arXiv Preprint*, 2023. doi: 10.48550/arXiv.2303.08774

[2] T. J. Bradshaw, X. Tie, J. Warner, B. Nett, A. B. Holbrook, and B. M. Kinsella, "Large language models and large multimodal models in medical imaging: A primer for physicians," *J. Nucl. Med.*, vol. 66, no. 2, pp. 173–181, Feb. 2025. doi: 10.2967/jnumed.124.268072

[3] J. Wu, W. Gan, Z. Chen, S. Wan, and P. S. Yu, "Multimodal large language models: A survey," *arXiv Preprint*, 2023. doi: 10.48550/arXiv.2311.13165

[4] S. Yin, C. Fu, S. Zhao, K. Li, X. Sun, T. Xu, at. Al., "A survey on multimodal large language models," *Natl. Sci. Rev.*, vol. 11, no. 12, art. no. nwae403, 2024. doi: 10.1093/nsr/nwae403

[5] J.-B. Alayrac, J. Donahue, P. Luc, A. Miech, I. Barr, Y. Hasson, et al., "Flamingo: A visual language model for few-shot learning," in *Advances in Neural Information Processing Systems 35 (NeurIPS 2022)*, 2022.

[6] H. Liu, C. Li, Q. Wu, and Y. J. Lee, "Visual instruction tuning," in *Advances in Neural Information Processing Systems 36 (NeurIPS 2023)*, 2023.

[7] R. AlSaad, A. Abd-Alrazaq, S. Boughorbel, A. Ahmed, M.-A. Renault, R. Damseh, and J. Sheikh, "Multimodal large language models in health care: Applications, challenges, and future outlook," *J. Med. Internet Res.*, vol. 26, art. no. e59505, 2024. doi: 10.2196/59505

[8] Y. Nam, D. Y. Kim, S. Kyung, J. Seo, J. M. Song, and J. Kwon, "Multimodal large language models in medical imaging: Current state and future directions," *Korean J. Radiol.*, vol. 26, no. 10, pp. 900–923, Oct. 2025. doi: 10.3348/kjr. 2025.0599

[9] S. Lee, J. Youn, H. Kim, M. Kim, and S. H. Yoon, "CXR-LLaVA: A multimodal large language model for interpreting chest X-ray images," *arXiv Preprint*, 2023. doi: 10.48550/arXiv.2310.18341

[10] Z. Xu, Y. Zhang, E. Xie, Z. Zhao, Y. Guo, and K.-Y. K. Wong, "DriveGPT4: Interpretable end-to-end autonomous driving via large language model," *IEEE Robot. Autom. Lett.*, vol. 9, no. 10, pp. 8186–8193, 2024. doi: 10.1109/LRA.2024.3440097

[11] W. Zhang, M. Cai, T. Zhang, Y. Zhuang, and X. Mao, "EarthGPT: A universal multi-modal large language model for multi-sensor image comprehension in the remote sensing domain," *IEEE Trans. Geosci. Remote Sens.*, vol. 62, art. no. 5917820, 2024. doi: 10.1109/TGRS.2024.3409624

[12] R. Kaczmarczyk, T. I. Wilhelm, R. Martin, and J. Roos, "Evaluating multimodal AI in medical diagnostics," *NPJ Digit. Med.*, vol. 7, no. 1, art. no. 205, Aug. 2024. doi: 10.1038/s41746-024-01208-3

[13] Z. Yi, T. Xiao, and M. V. Albert, "A survey on multimodal large language models in radiology for report generation and visual question answering," *Information*, vol. 16, no. 2, art. no. 136, 2025. doi: 10.3390/info 16020136

[14] S. Milojević, "Principles of scientific research team formation and evolution," *Proc. Natl. Acad. Sci.*, vol. 111, no. 11, pp. 3984–3989, Mar. 2014. doi: 10.1073/pnas. 1309723111

[15] M. F. W. Festing, "The collaborative era in science: Governing the network," *Sci. Public Policy*, vol. 48, no. 4, pp. 589–601, Aug. 2021. doi: 10.1093/scipol/scab026

2nd International Conference on Multidisciplinary Sciences and Technological Developments (ICMUSTED 2025)

December 12-15, 2025

Exploring the Thermoelectric Potential of Perchalcogenoborates via DFT-Based Analysis

Fatima Garadi[1], Ahmed Al-Amin Ben Kamri[2], Ben Messaoud Chikh Lakdar[2]

[1]Laboratory of Materials for the Application and Valorization of Renewable Energies, Material Science Department, Amar Telidji University, Laghouat, Algeria
[2]Materials Physics Laboratory, Material Science Department, Amar Telidji University, Laghouat, Algeria
Corresponding author: Fatima Garadi (e-mail: f.garadi@lagh-univ.dz)

Abstract

Perchalcogenoborates, a promising subclass of chalcogenometallates, have recently garnered increasing attention for their potential in energy conversion technologies, particularly in thermoelectric applications. These materials combine the chemical versatility and structural diversity of group 13 elements with the favorable electrical and thermal characteristics of chalcogenides. Such a combination results in low lattice thermal conductivity, tunable electronic band structures, and potential for high thermoelectric efficiency. Despite these advantages, the exploration of perchalcogenoborates for thermoelectric applications remains relatively limited, with most previous studies focused on their optical functionalities. In this work, we employ first-principles calculations based on density functional theory (DFT) to investigate the structural, electronic, and mechanical properties of a representative perchalcogenoborate compound. The calculated elastic constants confirm mechanical stability, while the electronic band structure indicates a moderate band gap conducive to optimized charge carrier transport. Furthermore, the density of states analysis reveals the hybridization effects between the chalcogen and boron orbitals, which can influence carrier mobility and thermal transport. These intrinsic properties suggest that perchalcogenoborates may offer an attractive balance between electrical conductivity and suppressed thermal conductivity—key criteria for achieving a high thermoelectric figure of merit (ZT). The findings from this theoretical investigation provide valuable insights into the fundamental characteristics of perchalcogenoborates and support their potential as emerging materials for efficient thermoelectric energy conversion. Further studies, including phonon transport and doping effects, could help in tailoring their properties for practical device applications.

Keywords: Perchalcogenoborates, Thermoelectric materials, Density functional theory (DFT), Electronic structure

TITLE	Proceedings Book of the 2nd International Conference on Multidisciplinary Sciences and Technological Developments (ICMUSTED 2025)
ISSUED IN	Erzurum, Türkiye
ISSUED BY	Ertual Akademi
EDITION	First, Pages XLI + 453
ISBN	978-625-7960-84-7